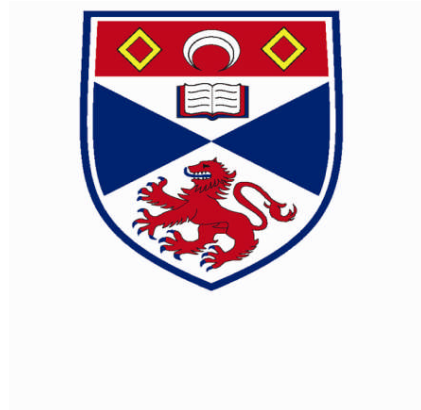


Dynamics of the British Ice Sheet and Prevailing Hydrographic Conditions for the last 175,000 years:

An investigation of marine sediment core MD04-2822
from the Rockall Trough



Fiona Danielle Hibbert

School of Geography and Geosciences
University of St Andrews

Submitted to the University of St Andrews for the degree of
Doctor of Philosophy

For my parents, Maureen and Daniel

This study presents a stratigraphic investigation of the marine sediment core MD04-2822 from the Rockall Trough (56° 50.54' N, 11° 22.96' W; 2344 m water depth). This core is currently the only available high resolution record for the calibration of Late Quaternary sedimentary sequences of the British (Hebridean) margin. It therefore offers an unprecedented archive of changing sedimentological and climatological conditions for the last 175,000 years. The high resolution, multi-proxy records have enabled surface and deep water conditions within the Rockall Trough to be reconstructed. In addition, the fluctuating nature of ice-rafted debris (IRD) inputs to the MD04-2822 site allowed a first order attempt of BIS dynamics for the entirety of the last glacial period (i.e. from the demise of the last interglacial to the decay of the Devensian/Weichselian ice sheet) as well as the majority of the penultimate (Saalian/MIS 6) glaciation.

Sediment core MD04-2822 is ideally located to capture the dynamics of the British Ice Sheet (BIS) via a continuous record of IRD and fine-grained terrigenous inputs. Fundamental to this is the construction of a robust chronology. This was achieved via: the correlation of the benthic $\delta^{18}\text{O}$ record to a global $\delta^{18}\text{O}$ stack (SPECMAP); the correlation of the surface proxies (% *N. pachyderma* (sinistral) and XRF Ca) to the Greenland $\delta^{18}\text{O}$ and Antarctic methane ice core records; and radiocarbon dating. This chronology was validated using both radiocarbon dating and tephra horizons. An evaluation of the event stratigraphy approach used in the construction of the MD04-2822 chronology is presented.

The marine record provides a valuable archive of past ice sheet dynamics as much terrestrial evidence is removed or obscured by subsequent ice sheet oscillations. MD04-2822 provides the first direct evidence for the expansion of the BIS onto the Hebridean Margin during MIS 6 (thereby confirming previous long-range seismic correlations).

The continuous sedimentation at MD04-2822 enabled the first insights into the early dynamics of the last BIS. Increases in IRD and fine grained terrigenous material delivered to the MD04-2822 at ca. 72 kyr represent the first significant delivery of material from the BIS across the continental shelf to the core site. The BIS would therefore have attained a marine calving margin by this time. A multi-proxy investigation of provenance was undertaken, however, unequivocal provenance determinations remain problematic. The location of the core suggests the proximal BIS as the most likely source of terrigenous inputs.

The expanded nature of the MD04-2822 sediments during the penultimate deglacial (Termination II) provide the first details of BIS dynamics for this period: the interplay of large inputs of freshwater from the decay of the Saalian (MIS 6) ice sheets (including the BIS) upon the surface and deep water circulation of the North Atlantic is investigated. In addition, sub-orbital climatic variability is documented at this location throughout the last interglacial (MIS 5e) and appears to be an intrinsic feature of the both N.E. Atlantic surface and deep water circulation of the last 175 kyr.

ACKNOWLEDGEMENTS

I would like to thank a number of people for their support, guidance and expertise which has helped me to see this PhD to completion, in particular: my parents, Kevin and many family and friends who have been tireless in their support and encouragement. I also wish to thank and acknowledge the support of my supervisors Bill Austin, Bob Gatliff, Melanie Leng, John Walden and Richard Holmes who have provided guidance and enthusiasm, as well as many fruitful discussions regarding marine mud, IRD and forams. I have also benefited greatly from discussions with many within the British Geological Survey as well as the School of Geography and Geosciences– thank you.

I would also like to thank the University of St Andrews and the British Geological Survey for providing funding for this study.

In addition, I would like to thank and acknowledge the contributions of:

The captain and crew of the R.V. Marion Dufresne; the R.S. Discovery and BGS staff for the extraction of the cores used in this study; Guy Rothwell and Belinda (BOSCORF); Melanie Leng and Hilary Sloane (NIGL, BGS Keyworth); Charlotte Bryant (NERC RCL); Ian Millar (NIGL, BGS Keyworth); Angus, Donald and Chris (FEEA, University of St Andrews).

CHAPTER 1: Introduction

1. Introduction and Rationale:	1
1.1. The NW sector of the last British Ice Sheet	2
1.2. Summary	5
2. Background:	6
2.1. MD04-2822 site location and offshore stratigraphy	7
2.2. Modern hydrography of the North Atlantic	8
2.2.1 Glacial hydrography	8
2.3. Glaciomarine deposition: Calving, IRD and meltwater	9
2.3. Summary	13
3. Aims and Objectives	14
3.1. Research Questions	14
4. Thesis Overview	14

CHAPTER 2: Materials and Methods

1. Site Location and Core Retrieval:	17
2. Core Logging and Lithological description	17
2.1. Core Logs	17
2.2. Overview of MD04-2822 stratigraphy	20
2.2. Sediment physical properties	21
3. Sampling	23
4. Multi-elemental X-ray fluorescence (XRF) core scanning	25
5. Calculation of Linear Sedimentation Rate (LSR):	27
6. Hydrographic reconstructions	28
6.1. Faunal and IRD counts	28
6.2. Stable Isotope measurements ($\delta^{18}\text{O}$ and $\delta^{13}\text{C}$)	29
6.3. Palaeotemperature reconstruction	31
7. IRD Inputs	32
7.1. Calculation of IRD flux	32
8. IRD Provenance	33
8.1. Lithological characterisation of IRD grains	33
8.1.1. Major element geochemistry of tephra horizons	34
8.2. Radiogenic Isotope Analysis (Pb, Nd, Sr)	37
8.3. Other Proxies for Terrigenous Inputs	38
8.3.1. Magnetic Susceptibility	38
8.3.2. XRF Si/Sr, Fe/Ca and Ca/Sr	38
9. Age control	40
9.1. AMS ^{14}C dating	40

CHAPTER 3: Chronostratigraphy

1. Orbital tuning of the benthic stable isotope record	43
1.1. Astronomical forcing of Global Ice Volumes (SPECMAP and LR04)	44
1.2. Radiometric Age Constraints on benthic $\delta^{18}\text{O}$ stacks	45
1.3. Influences upon the benthic $\delta^{18}\text{O}$	46
1.3.1. Synchronicity of $\delta^{18}\text{O}$ responses	46
1.3.2. Influence of hydrographic variations on $\delta^{18}\text{O}$ (inter- and intra-basin)	47
1.3.3. Assumptions, resolution and discrepancies	47
1.4. Other limitations	48
1.4.1. Tuning to SPECMAP and LR04	49
2. Greenland ice core tuning to surface proxies	52
2.1. Dansgaard-Oeschger (D/O) events within ice and marine records	52

2.2. Greenland Ice core Chronologies	53
2.2.1. Assumption of synchronicity within the tuning approach.....	56
2.2.2. Pacing of the D/O events.....	56
2.3. Tuning to the NGRIP $\delta^{18}\text{O}$ record (ss09sea timescale).....	58
2.3.1. Estimate of temporal uncertainty of surface proxy tuning.....	59
3. Atmospheric methane concentration tuning of surface proxies	62
3.1. Tuning to EPICA Dome C methane record.....	63
3.2. Test of tuning to Antarctic methane record.....	63
4. Composite Age model for MD04-2822	68
5. Independent checks of age model construction	71
5.1. Tephra isochrones	71
5.1.1. Age estimates for NAAZ II.....	71
5.2. Testing the MD04-2822-NGRIP tuning with AMS ^{14}C dating.....	72
5.2.1. Stratigraphic Integrity and Sample Selection.....	73
5.2.2. Analytical Limits for the Precision of Radiocarbon Measurements	74
5.2.3. Marine radiocarbon reservoir effect.....	77
5.2.4. Calibration:.....	78
5.2.5. Radiocarbon Age-Models:	79
5.2.6. Application of radiocarbon dating to MD04-2822 – A test of tuning.....	81
6. Comparison to the ‘regional stratotype’	85

CHAPTER 4: An Evaluation of the Event Stratigraphy Approach in Marine Sediments

1. Background	89
2. Advantages of Event Stratigraphies	92
2.1. Age control.....	92
2.2. Formation of local event stratigraphies: Rockall Trough (ca. 0 to 200 kyr)	92
2.3. ‘Replication’ – insights into BIS dynamics.....	95
2.4. Assessing the geographical expression of events.....	97
2.4.1. Characterisation of the NEA-GS3b warming event	100
2.4.2. The influence of bioturbation, productivity, terrigenous inputs and meltwater	102
2.4.3. Event stratigraphies and geographic expression of events – NEA-GS3b	103
3. Assumptions and disadvantages of event stratigraphies	104
3.1. Resolution	104
3.1.1. Practical: bioturbation, sedimentation rates and sampling	104
3.1.2. Methodological: radiocarbon and ice core uncertainties.....	105
3.2. Assumption of linear sedimentation between tie-points	106
3.3. Assumption of synchronicity	107
3.3.1. Synchronicity between climate archives	107
3.3.2. Assumption that all events are recorded within all archives	110
3.3.3. Assessment of leads and lags	110
4. The INTIMATE protocols	111
4.1. Application of the INTIMATE protocol to marine records	112
4.1.1. Comparison of palaeoenvironmental events to the regional stratotype.....	116
4.1.2. Validation of Radiocarbon age model- Tephrochronology.....	116
5. Conclusions	118

CHAPTER 5: The correction of core ‘over-sampling’

1. Background	121
2. Material and Methods:	123
3. Lithostratigraphy	124
4. Chronostratigraphy	124

5. The over-sampling problem and correction using a gravity core	122
5.1. Creation of a 'spliced' linear sedimentation rate	122
6. Other possible explanations	125
7. Summary and Conclusions	129

CHAPTER 6: The Last and Penultimate Glacial Cycles in the MD04-2822 record

1. Methods	131
2. Ice-rafted deposition over the last 175 kyr	132
2.1. Hydrological conditions – Surface waters.....	136
2.2. Hydrological conditions – Bottom waters.....	136
3. Comparison of the last and penultimate glaciations within MD04-2822.....	140
3.1. BIS dynamics inferred from MD04-2822 within a regional context	141
3.1.1. The MD04-2822 MIS 6 record.....	141
3.1.2. The MD04-2822 MIS 2/3 record	144
3.2. Comparison of the last two glacial intervals within MD04-2822	146
4. Comparison of the Last and Penultimate Deglaciations	149
4.1. Deglacial history	149
4.1.1. Termination I.....	149
4.1.2. Termination II	158
4.2. Comparison of Terminations I and II within MD04-2822	163
5. Conclusions	164

CHAPTER 7: Surface and deep water during the last interglacial (MIS 5e)

1. Background	167
2. The last interglacial as recorded within MD04-2822.....	170
2.1. Termination II	170
2.2. MIS 5e benthic $\delta^{18}\text{O}$ plateau	172
2.3. Benthic $\delta^{13}\text{C}$ during the interglacial	173
2.4. Surface proxies.....	173
3. Age Control for the last interglacial	177
4. Discussion	178
4.1. Termination II	178
4.2. The MIS 5e benthic $\delta^{18}\text{O}$ plateau	180
4.3. Benthic $\delta^{13}\text{C}$ changes: reflections on changes to AMOC through the last interglacial.....	185
4.4. Surface Conditions	188
4.4.1. Early MIS 5e (Termination II)	189
4.4.2. Surface water conditions - the <i>N. pachyderma</i> (sinistral) plateau.....	191
4.4.3. Comparison to other North Atlantic Records.....	192
4.4.4. Reconciling the Surface Hydrology of the Last Interglacial:.....	196
5. Summary and Conclusions	199

CHAPTER 8: Glacial Inception

1. Background	203
2. Regional Evidence of Glacial Inception after the Last Interglacial	204
2.1. North Atlantic records of ice sheet activity during MIS 5	205
2.2. Regional Evidence for the Evolution of Ice Sheet Growth after the Last Interglacial	208
2.2.1. NW European evidence.....	210
2.2.2. British evidence for the early history of the Weichselian/Devensian BIS	212
2.3. Summary	214

3. Events recorded at the MD04-2822 core site.....	216
3.1. MIS 5 and MIS 4 – Glacial Inception	216
3.2. Early Dynamics of the BIS.....	222
3.2.1. IRD lithological characterisations	222
3.2.2. Radiogenic isotope analysis of MD04-2822 bulk sediment.....	226
3.2.3. Age estimate for the early Weichselian BIS expansion	235
3.3. Summary and Conclusions.....	237
4. Overview.....	238

CHAPTER 9: Conclusions and Future Prospects

1. Chronology.....	241
1.1. Correction of Coring Artefacts.....	242
2. British Ice Sheet Activity	242
2.1. MIS 6.....	243
2.2. Termination II	243
2.3. Early history of the BIS after the Last Interglacial	244
2.4. MIS 3 and MIS 2.....	244
3. Millennial-scale variability of hydrographic conditions	245
4. Provenance	245
5. Reflections on the future potential of the MD04-2822 archive.....	245
6. Publications	247

APPENDICIES

REFERENCES

CHAPTER 1: Introduction

Figure 1.1: LGM limits of the last BIS:..... 5
Figure 1.2: Bathymetric setting of MD04-2822 6
Figure 1.3: Seismo-stratigraphy of MD04-2822 7
Figure 1.4: Modern Circulation 9
Figure 1.5: A schematic of the main processes contributing to glaciomarine sedimentation (adapted from Dowdeswell 1987). 10

CHAPTER 2: Materials and Methods

Figure 2.1: MD04-2822 Summary lithological Log.....19
Figure 2.2: Turbidite identification using magnetic properties of the sediments.20
Figure 2.3: Summary Stratigraphy for MD04-282221
Figure 2.4: Schematic of sampling and analytical procedures carried out on MD04-2822.24
Figure 2.5: Illustration of the fidelity of 1 cm and 2 mm XRF core scanning26
Figure 2.6: Photograph to illustrate some visual lithological characterisations35
Figure 2.7: XRF core scanning Ca/Sr records39

CHAPTER 3: Chronostratigraphy

Figure 3.1: MD04-2822 benthic $\delta^{18}\text{O}$ on the SPECMAP timescale.....50
Figure 3.2: Correlation of NGRIP $\delta^{18}\text{O}$ record and MD04-2822 surface proxies.....60
Figure 3.3: Age depth models - tuning to the NGRIP $\delta^{18}\text{O}$ record and benthic $\delta^{18}\text{O}$ stacks.....61
Figure 3.4: Tuning to the Antarctic EDC methane record..... .64
Figure 3.5: Age depth models based upon the tuning to the EDC methane record..... 65
Figure 3.6: Age depth models based upon the tuning to methane record for the last glacial period..... 65
Figure 3.7: Millennial scale events within both the Greenland and Antarctic ice cores 66
Figure 3.8: Compound age model. 69
Figure 3.9: MD04-2822 planktonic foraminifera abundance, % *N. pachyderma* (sinistral) and stratigraphical position of radiocarbon dating intervals..... 75
Figure 3.10: Age-depth models for MD04-2822..... 80
Figure 3.11: Testing of tuning to Greenland ice core $\delta^{18}\text{O}$ using radiocarbon dating 84
Figure 3.12: Comparison of tuned ages to NGRIP (GICC05 timescale)..... 86

CHAPTER 4: An Evaluation of the Event Stratigraphy Approach in Marine Sediments

Figure 4.1: Map of core locations mentioned in this chapter..93
Figure 4.2: Local event stratigraphy.....94
Figure 4.3: Comparison of IRD records for MD04-2822, MD95-2006 and ODP 980.96
Figure 4.4: Local event stratigraphy – GS3.....99
Figure 4.5: GS3 event stratigraphy on age (tuned to NGRIP on the GICC05 timescale).101
Figure 4.6: Concentration of rhyolitic tephra and % *N. pachyderma* (sinistral).....109
Figure 4.7: Stratigraphic position of radiocarbon dating intervals.113
Figure 4.8: MD04-2822 % *N. pachyderma* (sinistral), planktonic foraminiferal concentration and number of planktonic foraminifers counted in analysis113
Figure 4.9: Age-depth models based upon tuning to NGRIP $\delta^{18}\text{O}$ (GICC05 timescale).....114

CHAPTER 5: The correction of core ‘over-sampling’

Figure 5.1: Schematic of three possible coring scenarios (adapted from Skinner and McCave 2003) 122
Figure 5.2: GEOTEK magnetic susceptibility records..... 125
Figure 5.3: NGRIP $\delta^{18}\text{O}$ record on the GICC05 timescale and the age model determined for MD04-2822..125

Figure 5.4: Magnetic Susceptibility records.....	124
Figure 5.5 Calculated IRD flux for MD04-2822:	124

CHAPTER 6: The Last and Penultimate Glacial Cycles in the MD04-2822 record

Figure 6.1: MD04-2822 IRD flux, June insolation and global sea level.....	133
Figure 6.2: Terrigenous proxies for MD04-2822.	134
Figure 6.3: Proxy records for MD04-2822	137
Figure 6.4: MD04-2822 benthic (<i>C. wuellerstorfi</i>) $\delta^{18}\text{O}$ and $\delta^{13}\text{C}$	139
Figure 6.5: Location map.....	140
Figure 6.6: Linear sedimentation rate and IRD flux.....	144
Figure 6.7: Isopach map of Rockall Trough sediment thickness.....	147
Figure 6.8: MD04-2822 terrigenous proxies.	153
Figure 6.9: Summary figure for Termination I at MD04-2822..	154
Figure 6.10: Mapped and modelled limits for the Younger Dryas glaciation of Scotland.....	157
Figure 6.11: Summary figure of MD04-2822 proxies for Termination II	160

CHAPTER 7: Surface and deep water during the last interglacial (MIS 5e)

Figure 7.1: MD04-2822 proxies on depth for the Termination II, MIS 5e and MIS 5d.....	171
Figure 7.2: MD04-2822 surface proxies.....	175
Figure 7.3: Reconstructed SSTs and seawater $\delta^{18}\text{O}$	176
Figure 7.4: Age control for MIS 5e in MD04-2822	178
Figure 7.5: MD04-2822 proxies for the last interglacial on age.....	182
Figure 7.6: MD04-2822 proxy records on age	190
Figure 7.7: Comparison of benthic and surface proxies between MD04-2822 and ODP 980. 195	
Figure 7.8: North Atlantic surface circulation. (modern; early and late MIS 5e; ‘climatic optimum’).....	197
Figure 7.9: Summary figure for MD04-2822 Termination II and MIS 5e proxies on age.	200

CHAPTER 8: Glacial Inception

Figure 8.1: Principle locations mentioned in the text.....	204
Figure 8.2: Proxy records for ODP 980 (from Oppo et al 2006).....	206
Figure 8.3: Simplified lithostratigraphy for the Clyde and Argyshire Basins describing the Devensian ice sheet growth (Finlayson et al 2010).....	213
Figure 8.4: Reconstruction of the European Weichselian ice sheets extent (Svendsen et al 2004)	215
Figure 8.5: Spatial distribution of C events.	217
Figure 8.6: Interglacial-glacial transition for MD04-2822..	218
Figure 8.7: Benthic $\delta^{13}\text{C}$ and IRD flux (on a logarithmic scale).	219
Figure 8.8: Relative sea level reconstruction, the % <i>N. pachyderma</i> (sinistral) and IRD flux for MD04-2822.	221
Figure 8.9: MD04-2822 hydrological conditions and IRD lithological characterisations.....	223
Figure 8.10: MD04-2822 hydrographic and terrigenous proxies (MIS4).....	225
Figure 8.11: Bulk sediment analyses for MD04-2822 - radiogenic isotopes and modelled BIS source component.....	227
Figure 8.12: Sr and $\epsilon_{\text{Nd}}(0)$ analyses for MD04-2822 plotted within the fields of Grousset et al (2001).	229
Figure 8.13: (a) $^{143}\text{Nd}/^{144}\text{Nd}$ versus $1/[\text{Nd}]$ and (b) $^{87}\text{Sr}/^{86}\text{Sr}$ versus $1/[\text{Sr}]$	230
Figure 8.14: Greenland Stadial 9 and H4 in MD95-2006 and MD04-2822.	232
Figure 8.15: Treeigenous inputs, lithological characterisations and radiogenic isotopes.....	233
Figure 8.16: Summary figure: MD04-2822 radiogenic anlayses, magnetic un-mixing model (<i>C. Peters, unpublished data</i>) and terrigenous inputs (IRD etc.) with surface hydrography....	234
Figure 8.17: MD04-2822 hydrological proxies and terrigenous inputs presented on age.....	236

ABBREVIATIONS

AAIW	Antarctic Intermediate Water
AADW	Antarctic Deep Water
AMS	Accelerator mass spectrometry
AMOC	Atlantic Meridional Overturning Circulation
b2k	Years before 2000
BGS	British Geological Survey
BIS	British Ice Sheet
BKIS	Barents-Kara Ice Sheet
BOSCORF	British Ocean Sediment Core Research Facility
BTIP	British Tertiary Igneous Province
BMAR	Bulk mass accumulation rate
D/O	Dansgaard-Oeschger cycle
Dfc	Dark finely crystalline i.e. 'diagnostic' BIS lithic grains
FEEA	Facility for Earth and Environmental Analysis
FMAZ II	Faeroe Marine Ash Zone II (a.k.a. Fugloyarbanki tephra)
<i>G. bulloides</i>	<i>Globerigina bulloides</i>
GIS	Greenland Interstadial
GS	Greenland Stadial
GNAIW	Glacial North Atlantic Intermediate Water
H (event)	Heinrich Event
IRD	Ice rafted debris
[IRD]	IRD concentration
ISOW	Iceland-Scotland Overflow Water
kyr	10 ³ years
LIS	Laurentide Ice Sheet
LGM	Last Glacial Maximum
LSR	Linear sedimentation rate
LSW	Labrador Sea Water
MIS	Marine Isotope Stage
MOW	Mediterranean Overflow Water
<i>N. pachyderma</i> (sinistral)	<i>Neogloboquadrina pachyderma</i> (sinistral)
NAAZ I or NAAZ II	North Atlantic Ash Zone I or II respectively
NAC	North Atlantic Current
NADW	North Atlantic Deep Water
NEEM	North Greenland Eemian Ice Drilling (http://neem.nbi.ku.dk)
NERC RCL	NERC Radiocarbon Laboratory, East Kilbride
NIGL	NERC Isotope Geosciences Laboratory, BGS Keyworth
pMC	Percentage modern carbon (AMS ¹⁴ C determinations)
psu	Practical salinity unit
RPI	Relative geomagnetic palaeointensity
RSL	Relative sea level
SAMS	Scottish Association for Marine Sciences, Oban
SST	Sea surface temperature
SUERC	Scottish Universities Environment Research Centre AMS Facility, East Kilbride
THC	Thermohaline Circulation

CHAPTER 1: Introduction and Background

This thesis presents proxy data from the marine sediment core MD04-2822 recovered from the Rockall Trough (56° 50.54' N, 11° 22.96' W, 2344 m water depth). This high resolution record provides the first insights into the early history of the last British Ice Sheet (BIS) as well as confirming the presence of a BIS during the penultimate glacial. An evaluation of both ice sheet dynamics and hydrographic conditions documented within the proxy records of MD04-2822 are presented for the last ~175,000 years.

This chapter provides a general overview of the rationale and background to this study. Detailed reviews of the appropriate literature, as well as discussions of both the evidence for glacial activity and the proxies investigated are to be found within the later chapters of the thesis. Only a brief background to the study is given here.

1. Introduction and Rationale:

The Earth's climate system, on a variety of timescales, is governed by interconnected forcing mechanisms, one important component of which is the interaction between the cryosphere and ocean systems. Ice-rafted debris (IRD) within marine sediments of the North Atlantic provides an important archive of glacial activity on adjacent landmasses and attests to the activity of multiple calving ice margins during the last glacial cycle. IRD records therefore provide a means to reconstruct ice sheet dynamics and their interaction with the climate system, providing evidence of both the source of the ice and the location of melting (e.g. Ruddiman 1977, Bond and Lotti 1995).

While the importance of the orbital (Milankovitch) changes in insolation were largely established from the deep-sea oxygen isotope record of global ice volume (Broecker and van Donk 1970, Imbrie et al 1984), the histories of individual ice sheets have been far more difficult to establish. Indeed, superimposed on these long-term changes are climate oscillations operating at suborbital or millennial timescales that cannot be accounted for solely by orbital variations. A large body of evidence has emerged over the past two decades for suborbital scale changes in marine, ice core and terrestrial records. Most prominent are the Dansgaard–Oeschger (D/O) cycles first documented in Greenland ice core records (e.g. Dansgaard et al 1982): abrupt climate transitions over Greenland with rapid warming spanning a few decades followed by gradual cooling over a few hundred to thousand years. Such rapid oscillations are now widely documented for both the Northern and Southern Hemisphere ice core records with counterparts widely seen in marine records (e.g. Bond et al 1993).

Groupings of D/O cycles during the last glacial period display longer-term cooling trends – the Bond cycles – which culminate with rapid warming events. The coldest of the D/O events within the Bond cycles, immediately prior to the rapid warming transition, coincide with surges in Northern Hemisphere ice sheets, releasing large volumes of debris-laden icebergs into the North Atlantic, termed Heinrich events (H) (Heinrich 1988, Broecker et al 1992, Hemming 2004). Such large-scale destabilisation of the Laurentide Ice Sheet appears to have hindered the formation of North Atlantic Deep Water (NADW), effectively reducing the Atlantic Meridional Overturning

Circulation (AMOC) (Heinrich 1988, Bond et al 1992, 1993, Broecker 1994, Ganopolski and Rahmstorf 2001). The imprint of these massive iceberg calving events, IRD layers rich in detrital dolomitic carbonate, is now well documented within North Atlantic marine records.

IRD events in the North Atlantic are in addition, found to recur on millennial-scale periodicities – intervals far shorter than the pacing of Heinrich Events. Owing to the strong link between the position of the oceanic polar front and extent of sea ice, IRD can be used as a tracer of both ice sheet activity and sea ice extent. Detailed lithic investigations of North Atlantic IRD have enabled complex histories of the Northern Hemisphere ice sheets to be teased from the marine record (e.g. Bond and Lotti 1995, Bond et al 1997b, 1999). These high-latitude North Atlantic IRD variations and associated oscillations in surface water conditions, i.e. the position of the polar front, have in turn been correlated in detail to Greenland air temperatures (e.g. Bond et al 1993, Fronval et al 1995, Elliot et al 1998). The forcing mechanisms that drive these IRD events on quasi-1500 a periodicities include internal ice sheet instabilities, changes in ocean circulation, fluctuations in sea level and variations in solar parameters (see, for example, reviews by Alley and Clark 1999, Rahmstorf, 2003).

The marine record of ice rafting and related climate proxies often proves advantageous in investigations of longer-term regional ice sheet histories; on land continuous records with evidence of multiple ice sheet advances are frequently removed or masked by subsequent oscillations. The relative contributions of individual ice sheets may also be deduced from detailed analysis of lithic material; characteristic or diagnostic lithic types within the IRD signal can reveal the ice sheet dynamics of their source region or even individual ice streams (Scourse et al 2000). For the British Ice Sheet (BIS), current high-resolution records detailing ice sheet dynamics extend only to the Marine Isotope Stage (MIS) 4/3 transition at ca. 60 kyr (e.g. Wilson et al 2002, Peck et al 2007, Peters et al 2008). The MD04-2822 record, presented in this study, offers the opportunity to replicate and extend these records through the entirety of the last glacial cycle, the last interglacial and into the penultimate glacial.

Current understanding of the evolution, extent and demise of the last BIS is based upon both terrestrial and marine records, although opinions vary as to the extent and geometry of the last BIS. A brief overview is given here with emphasis given to the NW sector of the BIS.

1.1. The NW sector of the last British Ice Sheet

Records of the last BIS, *inter alia* offshore moraines, tunnel valleys, mega-scale glacial lineations, sediment cores, seismic data, landform evidence, e.g. trimlines and cosmogenic dating, are most ‘complete’ for the post-Last Glacial Maximum (LGM) interval of the glacial cycle. Evidence for the timing of the onset and subsequent geometry of glaciation remains extremely limited. Recurrent glacial advances across the continental shelf through MIS 12 to MIS 2 are inferred from seismic reflection profiles for the Hebridean, Western Shetland and North Sea shelves (e.g. Cameron et al 1987, Sejrup et al 1991, 1994, 2005, Stoker et al 1993, 1994, Gatliff et al 1994, Holmes 1997) and it has been speculated that the last BIS was ‘a long-lived feature

that probably existed for most of the Devensian as a highly mobile and sensitive ice sheet' (Bowen et al 2002).

Episodic ice rafting events for the last 50 to 60 kyr have been recorded in marine cores with the implication of repeated glacial advances during this period (e.g. Knutz et al 2001, 2002). Indeed, the periodic advances recorded within the marine record appear to be confirmed by clusters of terrestrial ^{36}Cl dates¹ indicating deglaciation events, which seem to be associated with Heinrich events (Stone et al 1998, Bowen et al 2002), with the BIS reaching its maximum extent as early as ca. 37 kyr and the coalescence of the BIS and Fennoscandian Ice Sheet (FIS) in the North Sea at ca. 40 kyr (Sejrup et al 2005, Bowen et al 2002).

In contrast, ice free conditions for much of mainland Scotland during MIS 3 have been inferred from organic-rich deposits and cosmogenic landform ages. Calibrated radiocarbon ages range from 31 to 38 cal. kyr BP from Tolsta Head, North Lewis (von Weymarn and Edwards 1973, Whittington and Hall 2002) and Sourlie, near Glasgow (Jardine et al 1988, Bos et al 2004) (Figure 1.1), while cosmogenic dates from Ireland (Bowen et al 2002) and six radiocarbon dates from Balglass close to the southern end of Loch Lomond infer a regional constraint of the onset of glaciation in Scotland to ca. 36.5 cal. kyr BP (Brown et al 2007) and suggest limited Scottish ice at 30 kyr (Hall et al 2003). Much of the onshore evidence therefore suggests ice-free conditions through most of MIS 3, with the initiation of the last BIS only subsequent to 35–32 kyr BP. The terrestrial and marine evidence therefore appears incompatible during MIS 3.

The maximum extent of the last major BIS glaciation remains poorly defined (e.g. Clark et al 2004b). Indeed the term 'Last Glacial Maximum' (LGM) ought to be employed with caution. The Environmental Processes of the Ice age: Land, Oceans, Glaciers (EPILOG) project recommends the use of 'LGM' for the period between 19 and 23 kyr (Mix et al 2001) and many place the BIS LGM at 18 to 24 kyr (Boulton et al 1991, Bowen et al 2002), while others have used the term to denote the period 25 to 35 kyr (Sejrup et al 2005, Carr et al 2006, Bradwell et al 2008) or in reference to the global ice volume maximum at 30 to 22 kyr determined from sea-level curves (e.g. Peltier and Fairbanks 2006).

The extension to of the BIS to its maximum limits was dependent upon both global and local influences. These local influences include: the degree of isostatic depression, the type of ice margin (marine terrestrial, grounded or shelving etc), variations in ice source regions and ice divides through time. Variation in these factors probably resulted in different sectors of the last BIS reaching its maximum extension at different times (Chiverrell and Thomas 2010).

¹ The reliability of these ages have been questioned: some of these dates are associated with very large errors and for most sites, based upon only one exposure age. Single ages are often associated with potential problems of nuclide inheritance and sampling uncertainties, more recent studies include a number of ages for each site in order to minimise such effects (e.g. Ballantyne 2010). The Bowen et al (2002) ages also appear inconsistent with both radiocarbon ages (e.g. McCabe and Clarke 2003) and ^{10}Be exposure ages (Ballantyne et al 2007) suggesting extension of the LGM Irish sector ice sheet offshore.

At its maximum, the last BIS was an expansive continental shelf glaciation (Figure 1.1), inferred from offshore stratigraphy, geomorphology and seismic data, with some evidence for the coalescence of the BIS and FIS in the North Sea (Stoker et al 1993, 1994, Hall et al 2003, Sejrup et al 2005, Bradwell et al 2007, 2008) although not all sectors of the ice reached their maximum extent at the same time (e.g. Chiverrell and Thomas 2010, McCarroll et al 2010). Similarly, more extensive dimensions, possibly extending far onto the continental shelf, for the LGM limits in western Ireland is emerging (e.g. King et al 1998, Sejrup et al 2005, Thomas and Chiverrell 2006, Ballantyne et al 2008, McCabe 2008, Ballantyne 2010) than the traditional onshore extent (e.g. Warren 1991, Bowen et al 2002) (Figure 1.1). Alternatively Bowen et al (2002) propose the most extensive Devensian glaciation is placed at a point between the last interglacial (MIS 5e) and ca. 37 kyr with ice covering the entirety of Scotland and Ireland; however, scant evidence is offered for this interpretation. Within this interpretation, the LGM BIS (ca. 22 kyr) is generally seen as but one of a number of BIS glacial advances since the last interglacial.

Two principal models of activity for the last BIS are therefore proposed (Figure 1.1):

1. the relatively small and mobile BIS spanning much of the last glacial cycle with maximum extent being reached prior to ca. 37.5 kyr with multiple advances and deglaciation events; or
2. that of a largely ice-free MIS 3, initiation post ca. 35 kyr, with ice advance after ca. 34 to 32 kyr, extensive shelf edge glaciation at ca. 30 to 25 kyr, sea-level induced reorganisation and the final decay by melting rather than calving at a stable margin situated close to the present coastline.

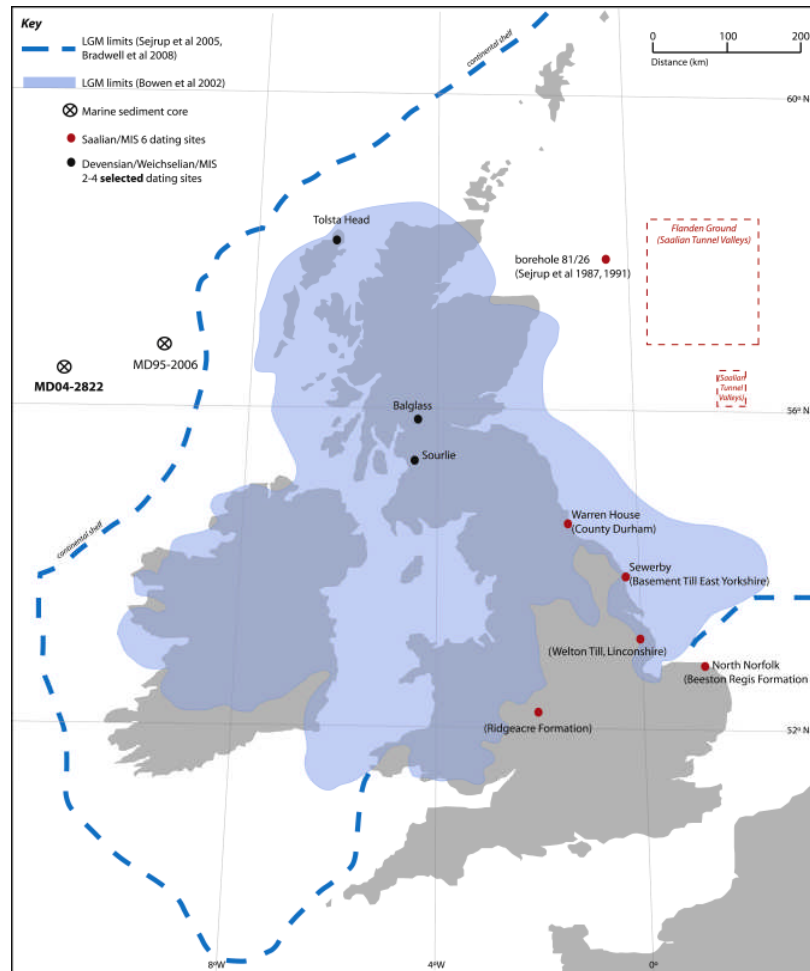
Evidence for major glaciation of northwestern Britain prior to the Devensian/Weichselian is very limited, in part due to the potential modification or removal by subsequent ice sheet oscillations. However, seismic reflection profiles from the Hebridean margin suggest significant expansions of the BIS during each of the main glacial stages (MIS 2, 4, 6 etc.) (Stoker et al 1994); although the resolution and continuity of seismic data, together with inadequate age control, preclude the clear distinction of individual advances between MIS 4 and 2 (Sejrup et al 2005).

Within MIS 6 (correlated with the Saalian glacial period; e.g. see Lee et al 2010), BIS activity has been documented within the North Sea basin (Sejrup et al 1987, Carr 2004) with limited and ambiguous terrestrial evidence (Figure 1.1), for which differing chronological and stratigraphical interpretations are offered for the same data (e.g. Lee et al 2010, discussed in chapter 6). Indeed the speculated expansion of the BIS onto the northwestern Scottish margin during MIS 6 (e.g. Sejrup et al 2005) is inferred only from long-range correlations with the North Sea succession (Holmes 1997).

Well-dated, high-resolution IRD records which 'tie-in' to the existing seismic stratigraphy from this margin extend only to ca. 50 to 60 kyr (Knutz et al 2001, 2002, Wilson and Austin 2002, Peters et al 2008). Scant evidence is available documenting the early glacial history of the last BIS (i.e. subsequent to the last interglacial), and this often proves difficult to interpret due to its fragmentary nature and problematic age

control. However, a recent re-evaluation of terrestrial deposits in NW Scotland (Buchan; Gemmell et al 2007) tentatively suggests a major BIS glaciation within MIS 4 (ca. 59 to 71 kyr) (discussed in chapter 8).

Figure 1.1: LGM limits of the last BIS: dashed line gives the approximate position of the LGM limits proposed by Sejrup et al (2005), Bradwell et al (2008), whilst the blue shaded area are the limits proposed by Bowen et al (2002). Marine sediment cores are indicated by the open circles with black cross. Selected dating sites mentioned within the thesis are given by black filled dots for the last BIS, red filled dots for the penultimate (MIS 6) glaciation.



1.2. Summary

The nascent history of the last BIS (Devensian/Weichselian) is largely unknown, with the previous (MIS 6/Saalian) glacial cycle even less well documented, due to: the removal or obfuscation of terrestrial evidence; the limited temporal extension of current high resolution marine sediment cores; and potentially problematic age control.

Existing data support the assertion that the proximity of MD04-2822 to the northwestern European glaciated margin makes this site ideal to capture the IRD signals for the last glacial cycle of the northeast Atlantic region and the BIS in

particular (cf. marine sediment core MD95-2006 from the Barra Fan; e.g. Knutz et al 2001, Wilson et al 2002, Peters et al 2008). In addition, as the temporal span of the MD04-2822 sediments far extends beyond current high resolution records (ca. 60 kyr), the early history of the NW sector of the last BIS, as well as the previous BIS, and their interaction with the climate system may be unravelled from this continuous record through the apposite use of proxy data.

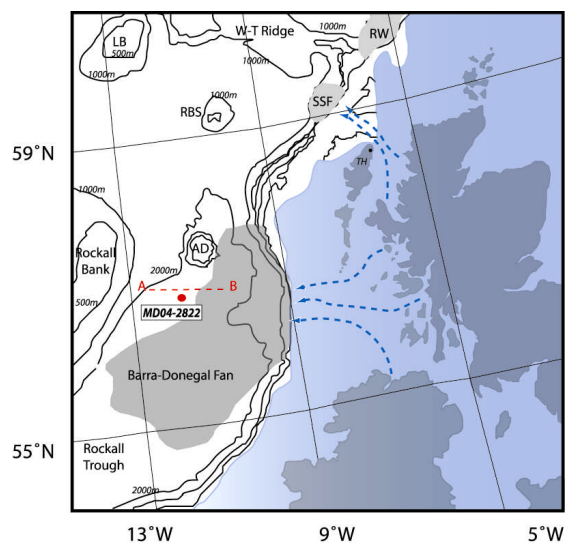
2. Background:

This study concentrates upon BIS dynamics and hydrographic proxy records (both surface and deep water) preserved within the MD04-2822 marine sediment core for the last ~175 kyr. The following section outlines in brief the modern and glacial hydrographic conditions within the North Atlantic as well an overview of glaciomarine sedimentation and IRD.

2.1. MD04-2822 site location

Giant piston core MD04-2822 was recovered by the RV Marion Dufresne from the Rockall Trough (56° 50.540 N, 11° 22.960 W; 2344 m water depth, recovered in 2004). The site is located on the distal margin of the Barra Fan complex (Figure 1.2). The Barra Fan is the most southerly developed glaciogenic fan on the northwestern European continental margin (Knutz et al 2001) and comprises debris flow lobes and glaciomarine sediments fed by Pleistocene ice streams (Stoker 1995). The Barra Fan and Donegal Fan together form the largest sediment depocentre off northwestern Britain (Armishaw et al 2000).

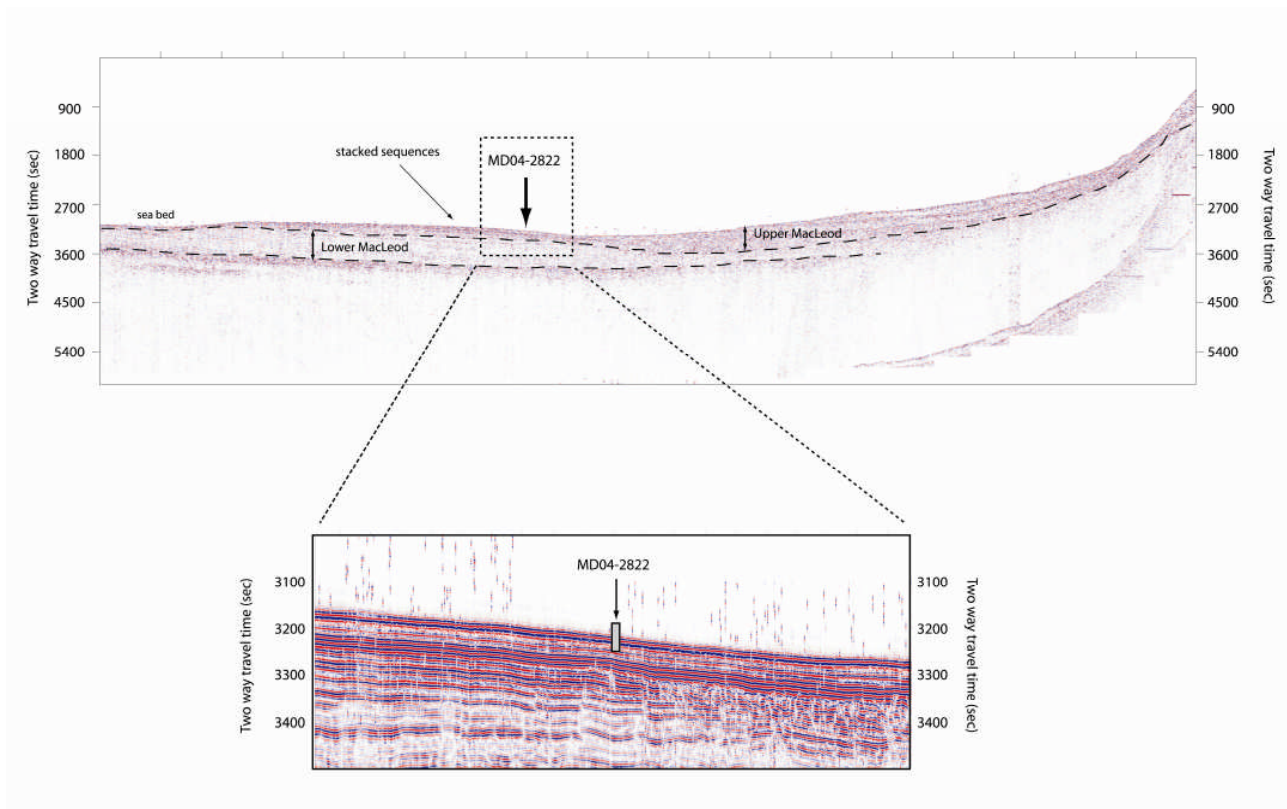
Figure 1.2: Bathymetric setting of MD04-2822 including the maximum extent and major ice streams (dashed blue lines) of the last British Ice Sheet (adapted from Sejrup et al 2005, Bradwell et al 2008), trough mouth fans (Barra-Donegal Fan; SSF, Sula Sgeir Fan; RW, Rona Wedge) and other bathymetric features (Rockall Bank; AD, Anton Dohrn; RBS, Rosemary Bank Seabight; LB, Lousy Bank; W-T Ridge, Wyville-Thompson Ridge. Location of seismic line BGS1992_56-1 is given by the dashed black line (Figure 1.3).



The offshore stratigraphy of the region has been widely studied (e.g. Stoker 1995, Howe 1995, Knutz et al 2002) and the Barra Fan is a region where debris flows, turbidites, contourites as well as hemipelagic sedimentation contribute to the depositional sequences. Three seismostratigraphic units have been identified for the Hebridean Slope (Stoker et al 1994): the Lower MacLeod, a Pliocene to mid Pleistocene slope to basin floor deposit; the Upper MacLeod, a mid to upper Pleistocene glaciogenic deposit; and the MacAulay, an upper Pleistocene to Holocene slope to basin floor, distal glaciomarine drape.

From seismic line BGS_1992_56-1 (Figure 1.3), the Lower and Upper MacLeod units may be discerned with stacked seismic sequences at the MD04-2822 location. This broad sheeted drift deposit can clearly be seen in the lower panel (zoom-in) of Figure 1.3.

Figure 1.3: Seismo-stratigraphy of MD04-2822 core site with inferred seismostratigraphical units (after Holmes 1992, Stoker 1994); seismic line BGS_1992_56-1 (Sparker)



Based upon the available seismic data (Figure 1.3), MD04-2822 was recovered from the distal margins of the Barra Fan (in a region away from debris flows associated with this fan). The core is well placed to investigate the dynamics of the former BIS as the region was fed by ice-streams during the last glacial period (Sejrup et al 2005, Bradwell et al 2008), however the site is unaffected by debris flows or thick turbidite sequences (c.f. MD95-2006; Peters et al 2008, Knutz et al 2002, Wilson and Austin 2002) (Figure 1.3). A detailed lithological consideration of MD04-2822 can be found in chapter 2.

2.2. Modern hydrography

At present the bottom current regime within the Rockall Trough comprises a mix of NADW flowing at depths of 2–3 km (McCartney 1992), Labrador Sea Water (LSW), which enters from the southwest at depths of 1–2 km, and the intermittent supply of Iceland-Scotland Overflow Water (ISOW) across the Wyville–Thompson Ridge (Lee and Ellet 1965, Ellet and Roberts 1973, Dickson and Kidd 1986, van Aken 2000). Overflow of deep water from the Nordic Seas across the Wyville-Thomson Ridge into the Rockall Trough, forms a strong southwesterly flow along the western side of the deepest portions of the Rockall Trough. A component of this flow influences the MD04-2822 site through (re)circulation as a cyclonic gyre (New and Smythe-Wright 2001).

Present-day surface water conditions are primarily influenced by the North Atlantic Current (NAC) and the East North Atlantic Water which flows northeast along the continental shelf at a depth of 500 to 1,200 m. The core of the modern NAC branches into two major northeastward flows within the North East Atlantic, one through the Iceland Basin and the other through the Rockall Trough; these form the major northward pathways of Atlantic Water in the northern North Atlantic (Fratantoni 2001). The latter begins as a shelf-edge current above the Irish-Scottish continental shelf. Within the Nordic Seas, the two branch structure remains, with Atlantic Water confined to a 200-600 km wide wedge (Orvik and Niiler 2002).

The Rockall Trough region is therefore a conduit by which warm, saline waters are supplied to the Nordic Seas, and upon losing heat to the atmosphere, these waters eventually comprise the cold, fresh southward flowing deep water (Holliday et al 2000). This inflow of Atlantic waters around the Faeroe Islands sees the warmest flow concentrated to the east of the islands and the British Isles (Orvik and Niiler 2002) (Figure 1.4). The polar front i.e. the ‘boundary’ between polar and subpolar waters, currently lies far to the north of the core site, however during the last glacial, the polar front was repeatedly located far to the south, off the Iberian Margin (e.g. Ruddiman and McIntyre 1981, de Abreu et al 2003).

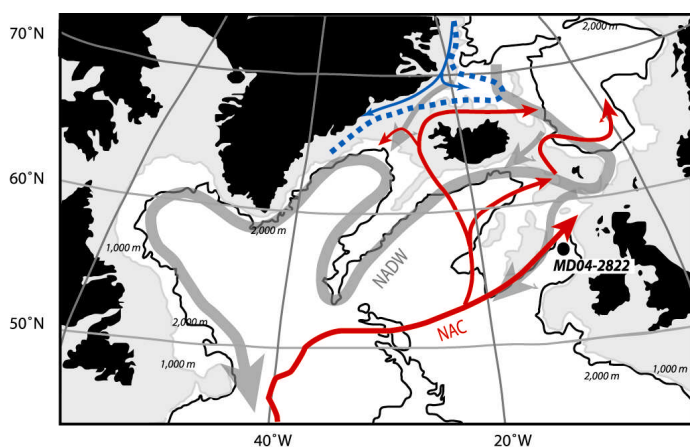
2.2.1. *Glacial hydrography of the North Atlantic*

During glacial intervals, convection in the North Atlantic changed from NADW formation in the Nordic Seas to an intermediate mode in the northern North Atlantic (Glacial North Atlantic Intermediate Water (GNAIW)) (e.g. Boyle and Keigwin 1989, Bertram et al 1995, Venz et al 1999, McManus et al 2004, Meland et al 2008, Lynch-Stieglitz et al 2007). This may have produced a meta-stable state of convection that was susceptible to small perturbations in the freshwater budget of the North Atlantic (Ganopolski and Rahmstorf 2001) and the disruption of AMOC (e.g. Broecker 1992, 1994). AMOC disruption led to a reduction in inter-hemispheric heat ‘piracy’ and accounts for the cold stadial intervals recorded in the Greenland ice cores, and their Southern Hemisphere warming counterparts (e.g. Blunier and Brook 2001) i.e. the ‘bipolar seesaw’ (Broecker et al 1990, Stoker 1998).

During the last glacial, the site of deep convection was located to the south compared to present; cold surface waters became more buoyant as evaporation reduced (Duplessy et al 1988) but the resulting water mass (GNAIW) was of insufficient

density to sink into the deep North Atlantic, instead this water bathed depths of 1000 to 2000 m (Venz et al 1999). Other studies suggest that GNAIW sank to depths of ~2.3 km (Boyle and Keigwin 1987, Zahn et al 1987, Oppo and Lehman 1993), or the presence of an additional water mass at intermediate depths (2-3 km) (i.e. neither GNAIW or glacial Antarctic (AABW), nor mixing of the two) but water mass derived from sustained formation of a deep water component in the Norwegian Greenland Seas² (Yu et al 2008). During the last glaciation, the proximity of Rockall Bank to the area of GNAIW has been speculated (Venz et al 1999).

Figure 1.4: Modern principal deep and surface circulation patterns of the North Atlantic (after Hansen and Østerhus 2000). Red arrows give the approximate position of warm surface currents, blue cold surface currents (dashed blue line gives the approximate position of the modern polar front). Dark grey arrows give the approximate position of deep water currents.



2.3. Glaciomarine deposition: Calving, IRD and meltwater

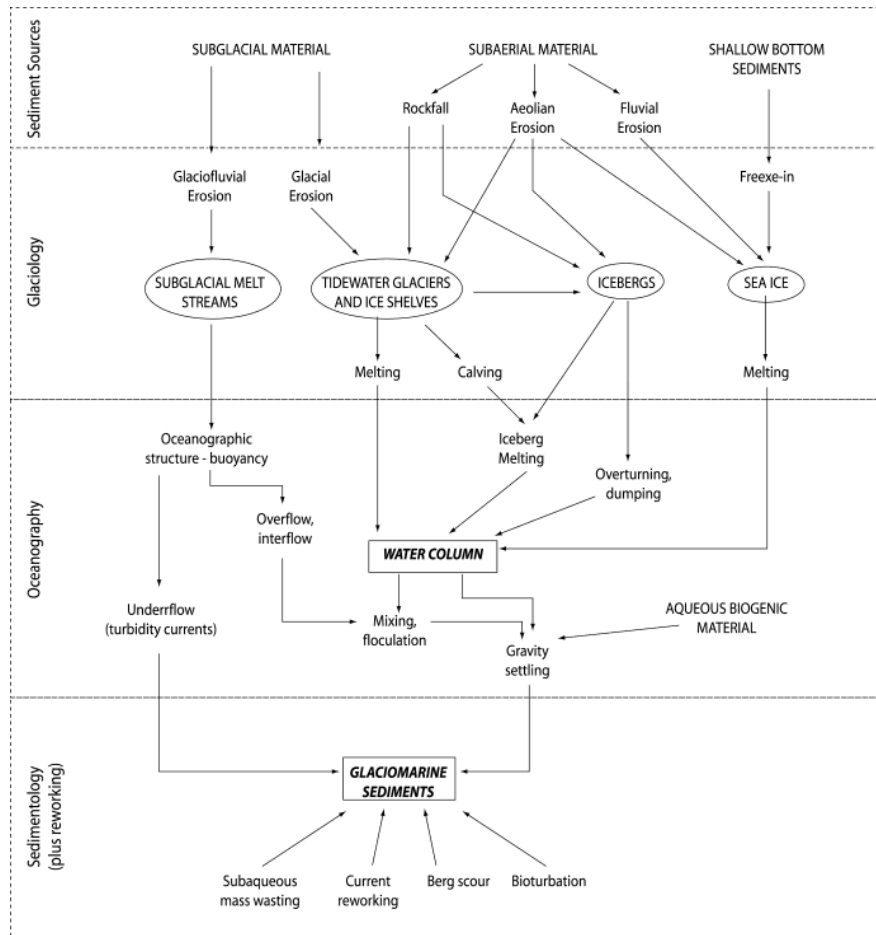
Glaciomarine sedimentation occurs in a range of environmental settings that may be, in general, related to climatic conditions; for example, present day ‘warm’ settings of the tidewater glaciers of Alaska and the Chilean fjordlands to ‘coldest’ air and water temperatures of East Antarctica (Dowdeswell et al 1998). At present, deposition from glaciers or ice sheets in relatively warm and moist conditions is mainly from meltwater plumes (e.g. Svalbard, Alaska; Powell 1984), whilst in colder environments with lower precipitation, deposition is mainly via ice-rafting with a smaller component by sea ice (e.g. East Antarctica and East Greenland) (Dowdeswell et al 1998). A schematic of the main processes by which sediments are transferred to the marine environment is given in Figure 1.5. The type of glaciomarine deposit varies with distance from the ice front. For example, a diamicton³ lithofacie may be deposited beneath floating ice shelves, gravity flows etc, whilst further from the ice

² Production of deep water during glacials is also thought to be dependent upon the extent of sea ice cover within the Nordic Seas (Kellogg 1980). The presence of extensive sea ice cover prevents the advection of warm salty waters to these high latitudes. However, seasonal (i.e. summer) ice free conditions in the Nordic Seas during glacial conditions would have enabled some degree of convection to occur (e.g. Hebbeln et al 1994).

³ These are very poorly sorted sediments.

front deposition is of a marine outwash mud comprised of glacial flour and minor amounts of coarse grains (Powell 1981).

Figure 1.5: A schematic of the main processes contributing to glaciomarine sedimentation (adapted from Dowdeswell 1987).



Calving and meltwater (at an oceanic margin) is known to be responsible for the majority of mass loss in contemporary ice sheets (e.g. Reeh 1968, Paterson 1994). Icebergs have the capacity to transport entrained material large distances from the point at which they were calved and in exceptional cases this may be as great as several thousands of kilometres (e.g. Ruddiman and McIntyre 1981, Ruddiman and Wright 1987, Heinrich 1988). Present day studies of icebergs indicate that entrained sediments comprise a very small fraction of the total ice calved, although modern icebergs may not be direct analogues due the differences in the availability of material within the glacial system (Andrews 2000). The amount of material entrained within the glacier ice is dependent upon where it is located within the ice mass: subglacial ice is often associated with high sediment loads; supraglacial ice is variable in entrained material; whilst englacial ice (which forms the bulk of the ice mass) is also variable but typically has low sediment concentrations (e.g. Dowdeswell 1986, Dowdeswell and Murray 1990). The sediment content of icebergs is generally poorly sorted and heterogeneous in grain size (Dowdeswell and Dowdeswell 1989).

The composition of sediment deposited by calved icebergs reflects a ‘characteristic half-distance’ of 50 to 100 km (Clark 1987) and IRD records in proximal locations are dominated by the adjacent ice stream source (Scourse et al 2009).

Extensive ice sheets in full glacial conditions are characterised by major fast flowing outlet glaciers and ice streams, which produce large numbers of icebergs. However, for extensive floating ice tongues (e.g. some present N and NE Greenland outlet glaciers) basal melting may occur (e.g. Rignot 1996, van der Veen 2002); thus debris may be released prior to iceberg calving (Dowdeswell et al 1998). The importance of ice streaming is suggested by present studies of the Antarctic Ice Sheet; ~ 90 % of all ice and sediment discharged from this ice sheet originated within ice streams (Bently and Giovinetto 1991, Bamber et al 2000). Modelling studies suggest dynamic ice streaming behaviour was a feature of the former BIS (e.g. Boulton and Hagdron 2006, Hubbard et al 2009) and accords with much of the geological evidence⁴ (e.g. Bradwell et al 2008).

The rate (and location) of sediment release from an iceberg is dependent upon the velocity of the iceberg, rate of melting, position of the debris within the iceberg and the number of overturning events (Syvitski et al 1987). In addition, factors of *inter alia*, the velocity of the iceberg, the temperature difference between the iceberg and the surrounding water, air temperatures, net radiation and erosion by wave action also contribute to the decay of a calved iceberg (Andrews 2000). The presence of widespread sea ice may potentially limit the transport of calved icebergs and restrict deposition near the outlet terminus (e.g. Syvitski et al 1996). Modelling studies illustrate the dominance of climatological factors (prevailing wind patterns and ocean currents) in determining the trajectories of calved icebergs (e.g. Bigg et al 1996, 1997, Death et al 2006). During intervals of maximum ice extent onto the continental shelf, icebergs would largely be forced to track across the deep ocean (Dowdeswell et al 1995).

IRD within marine sediments is conventionally thought of as grains >150 µm, although other grain sizes have been used⁵. Gwiazda et al (1996) suggest that ‘no mechanism other than ice rafting can account for delivery of grains this large’ within marine sediments. However, within ‘typical’ glacial sediments, the sand fraction (i.e. 63 to 2,000 µm) is the least represented and is dominated primarily by clays (<63 µm) (Drewry 1986, Andrews 2000) although the exact size ranges are strongly influenced by crystal configuration and rock weaknesses (Slatt and Eyles 1981). The use of sand sized particles to indicate ice sheet-ocean interactions is a matter of convention within the palaeoceanographic community i.e. it ‘represents an operationally simple parameter to define and measure, not because the processes are well understood!’ (Andrews 2000).

The sand content of marine sediments is governed by: sand inputs, sedimentation accumulation rates and the transfer of sand by contour currents or the winnowing of

⁴ For example, the mega-scale lineations of the Witch Ground (North Sea; Graham et al 2007) and Minch (Stoker and Bradwell 2005, Bradwell et al 2007) as well as landform evidence (e.g. Gollidge and Stoker 2006, Merritt et al 2003, Gordon and Sutherland 1993).

⁵ Ruddiman (1977) used >200 µm in the spatial distribution maps of the North Atlantic during the last glacial period, Heinrich (1988) used grains >180 µm, whilst grain sizes as low as >63 µm have been used to infer ice rafted deposition (e.g. Revel et al 1996).

fine material. The sortable silt (10 to 63 μm) fraction in particular is susceptible to changes in the strength of bottom currents (e.g. McCave et al 1995, McCave and Hall 2006). Silt sized particle may also be delivered by wind, meltwater plumes, resuspension by bottom currents, iceberg ploughing and sea ice. The dominance of the <63 μm size fraction has been used by some to suggest that this size fraction is the most representative of source provenance (Hemming et al 1998, Grousset et al 1993), even though a variety of transport mechanisms may be invoked.

In order to minimise the effect of random sediment delivery upon variations in the IRD content of marine sediments, IRD flux is calculated (Ruddiman 1977, see chapter 2, *Materials and Methods*). Changes in the IRD flux to a site may reflect differing scenarios including: i) an increase in iceberg flux with constant sediment content and melt rate; ii) a change in the sediment concentration for constant iceberg flux and melt rate; or iii) a change in the location of the zone of melting due to surface and sub-surface temperature changes (Andrews 2000). In addition, increased IRD flux may result from either ice sheet advance or decay (McCabe and Clark 1998, Clarke et al 1999) and is dependent upon the presence of a marine margin; the rate of iceberg calving; the debris content of icebergs; the rate of iceberg melting; and the strength, direction and heat content of surface currents over the core site.

Glacial meltwater also contains high sediment concentrations. Some of this material is deposited as the plume rises if grains are sufficiently large, otherwise entrained material is carried to surface, or depth at which the plume become neutrally buoyant, at which point the plume spreads out laterally and grains settle out of this horizontally spreading gravity current. These may be captured by surface currents and spread over large areas and with fine-grained material settling out in ice-distal areas (e.g. Boulton 1990). Modern tidewater glacier turbid plumes extend for less than 80 km from the coast. By contrast, Late Pleistocene Labrador Slope plumes extended almost 200 km in parallel and 130 km perpendicular to the continental shelf⁶ (Hesse et al 1997, Hesse and Khodabakhsh 2006).

Sea ice may also transport variable amounts of fine grained sediment to the deep ocean (e.g. Nürnberg et al 1994). Sediments may be incorporated by: surface fine grained aeolian; coarse grained rockfalls; storms; ice-keels in direct contact with sediment (in very shallow water); coarse grains incorporated via 'anchor-ice' formation and 'basal freeze-on' (Dowdeswell et al 1998, Scourse et al 2009, M. Stoker, *pers. comm.*). Modern studies within the polar North Atlantic suggest highly variable debris content and grain sizes within individual floes, although material is generally fine grained as freezing of turbid sea water and aeolian inputs incorporate mainly silts and clays (Nürnberg et al 1994, Dowdeswell et al 1998). Deposition of this material occurs in a similar manner to that for glacier derived debris, i.e. meltout, dumping or overturning, making assessment of the contribution of sea ice problematic (Dowdeswell et al 1998). Indeed a sea ice transport mechanism is invoked for several Late Quaternary tephra horizons (e.g. Austin et al 1995, 2004).

⁶ These modern examples are relatively small tidewater glaciers; Hesse et al (1997) liken the Pleistocene outlets to the size of the modern Yellow or Mississippi rivers where meltwater plumes extend for hundreds of kilometres across continental shelves (McCave 1972, Wright et al 1988).

Within this study, reference is made to both the IRD ($>150\ \mu\text{m}$) and the bulk sediment record (principally via XRF core scanning, see chapter 2, *Materials and Methods*) in order to attempt a reconstruction of ice sheet dynamics and terrigenous inputs.

The study of sediments from proximal depositional settings ($< 100\ \text{km}$ from the glacier margins; Andrews and Principato 2002) often proves advantageous in reconstructions of ice sheet dynamics, in that records are generally high resolution (and counterbalance, to an extent, the smoothing effects of bioturbation) and offer the potential of correlating events to terrestrial evidence. However, the variety of depositional process may complicate interpretation. For example, disturbance on the continental shelf may produce turbidites, potentially scouring away some of the sedimentary record. The position of MD04-2822 within the Rockall Trough, dominated by primarily hemipelagic sedimentation, minimises the potential of sampling non-conformable sequences; it is of course subject to bioturbation and potential bottom current reworking of fine material, although the calculation of IRD fluxes minimises this potential bias of IRD concentration.

2.4. Summary

The BIS can be thought of as sensitive to climatic changes owing to its extreme maritime position (e.g. Eyles and McCabe 1989, Boulton 1990). Thus MD04-2822 is ideally positioned to capture both the changing water mass characteristics of the northeast Atlantic and the dynamics of the proximal BIS ice sheet, through the incorporation of terrigenous material (IRD and fine grained) for the last $\sim 175\ \text{kyr}$.

3. Aims and Objectives

MD04-2822 provides the high resolution material for the calibration of Late Quaternary Hebridean Margin sedimentary sequences (e.g. Holmes 1997, Fyfe et al 1993, Stoker et al 1993) due to its far greater temporal extension than current high resolution records for this margin (e.g. Wilson et al 2002, Peck et al 2007, Peters et al 2008). In addition, MD04-2822 presents a unique opportunity to investigate the dynamics of the last BIS through a complete glacial cycle, from fully interglacial to glacial conditions.

In order to accomplish the aim outlined above, a detailed stratigraphic investigation of the MD04-2822 sediments will be undertaken with the following objectives in mind:

- The construction of a robust chronostratigraphy for the core and from this:
 - the calculation of the flux of material (i.e. terrigenous inputs, IRD) to the core site through time;
 - establish the pattern of delivery of BIS derived material to the MD04-2822 site for the last ~175 kyr and;
 - to determine the nature (if any) of ice-ocean-climate interactions at the MD04-2822 site via proxy records of environmental change.

In accomplishing the above, the following research questions, arising from the contemporary scientific theory and evidence on the Late Quaternary British Ice Sheet will be addressed.

3.1. Research Questions

Regarding the dynamics of the BIS and prevailing hydrographic conditions for the last ~175 kyr, as recorded within the MD04-2822 sediments, the following research questions will be addressed (Table 1).

4. Thesis Overview

The layout of this thesis is described within the Table of Contents. With regard to this structure, the principal aim of this thesis, i.e. the construction of a robust chronology for the MD04-2822 sediments is outlined in chapter 3, with an evaluation of the event stratigraphy approach used to construct the MD04-2822 chronostratigraphy contained within chapter 4. The principal scientific findings regarding the dynamics of the BIS during the last two glacial periods, and the intervening interglacial, are presented in chapters 6, 7 and 8. Chapter 2 outlines the materials and methods used for this study. Chapter 5 presents an example of coring artefacts and its correction using MD04-2822 as an example. A final summary chapter details the main scientific findings of this work and the significance of these within the context of ice-ocean-climate interactions. The thesis concludes with some reflections on possible future work arising from this study.

Table 1: Research Questions

Topic	Related Research Questions
1. BIS Activity	
<p>(a) <i>The penultimate glacial (MIS 6):</i> There is limited evidence currently available to suggest BIS activity within MIS.</p> <p>The penultimate deglacial is largely unknown.</p>	<ul style="list-style-type: none"> • Is there any offshore evidence for the NW sector of the BIS during MIS 6? • If so what is the behaviour of the MIS 6 BIS and what is the relationship to climate variability? • What is the nature of Termination II at the MD04-2822 core site? • Was there a ‘Younger Dryas/GS1’ type event at MD04-2822 during the penultimate deglaciation? • How does Termination II compare to records of the last deglacial from the same core?
<p>(b) <i>The last glacial cycle</i> Scant evidence currently available relating to the earliest history of the last BIS.</p> <p>Disparity between marine and terrestrial records of BIS activity during MIS 3.</p>	<ul style="list-style-type: none"> • When is the first offshore evidence for the initiation of the last BIS within MD04-2822? • Was MIS 3 ‘largely’ ice free (e.g. Hall et al 2003)? • Given the disparity between the terrestrial and marine evidence during MIS 3, when was the last BIS of a sufficient size to deliver material to the MD04-2822 core site?
2. Hydrographic Conditions	
<p>(a) <i>The penultimate glacial (MIS 6):</i> Millennial-scale climate variability has been widely documented for the last glacial period e.g. the D/O cycles documented within both ice and marine records (e.g. Bond et al 1993).</p>	<ul style="list-style-type: none"> • What were the surface and deep water conditions at MD04-2822 during the penultimate glacial? • What influence (if any) did the penultimate BIS have upon surface water conditions? • Is there any evidence for millennial-scale surface water temperature variations (analogous to the D/O cycles) within MIS 6?
<p>(b) <i>The last interglacial (MIS 5e):</i> Contrasting views of the last interglacial within the NE Atlantic are offered (e.g. McManus et al 2002, Oppo et al 2001).</p>	<ul style="list-style-type: none"> • Was the last interglacial ‘stable’ at the MD04-2822 core site (as documented by water mass proxies) as suggested by Oppo et al (1997), McManus et al (2002)? • Is there any evidence for sub-orbital surface or deep water variability during the last interglacial?

CHAPTER 2: Materials and Methods

Investigation into the dynamics of the last two major cycles of the Late Quaternary British Ice Sheet (BIS) activity was undertaken primarily on the giant piston core MD04-2822, with limited complimentary work on the gravity core +56-12/15 CS taken at the same location. Methods of collection for these cores, and analyses undertaken are briefly described.

1. Site Location and Core Retrieval:

The giant piston core MD04-2822 was collected in 2004 by the R.V. *Marion Dufresene* from the Rockall Trough (56° 50.54' N, 11° 22.96' W, ~38 m recovery) at a present water depth of 2,344 m. The core was cut into 1.5 m sections, split lengthways and passed through a GEOTEK multi-sensor core logging system. The following measurements were undertaken at 1 cm intervals: sediment thickness; P-wave amplitude; P-wave velocity; density; magnetic susceptibility; impedance and fractional porosity (section 0, this chapter; figure 2.1). The archive portion is stored at the British Ocean Sediment Core Research Facility (BOSCORF), Southampton, the working half is stored at ~4 °C at the School of Geography and Geosciences, University of St Andrews.

The gravity core +56-12/15 CS (56.8423 °N, 11.3827 °W, 3.95 m recovery) was recovered on the 15th of September 2009 by the R.R.V. *Discovery*. The plastic liner tube was cut into ~1 m lengths and sealed on the ship. The lengths were split in half lengthways, allowing examination and description of the core at BGS Loanhead and the University of St Andrews. GEOTEK multi-sensor core logging was carried out at the Scottish Association for Marine Science (SAMS, Scottish Marine Institute, Oban, Argyll). Both the archive and working sections are currently on loan to the University of St Andrews from the British Geological Survey and are in cold storage at ~4 °C.

2. Core Logging and Lithological description

Both MD04-2822 and +56-12/15 CS were described from detailed visual examination of the cleaned core surface. Lithological and structural features as well as any bioturbation traces were noted. Sediment composition (i.e. clay, silt, sand) was estimated and colour was determined using the Munsell soil colour charts. A summary lithological log is presented in Figure 2.1.

2.1. Core Logs

Based on detailed core logs (Appendix A₁), physical properties (Appendix A₂) and XRF core scan data (see section 4, this chapter), sedimentation for both MD04-2822 and +56-12/15 CS is considered to be continuous with no obvious hiatuses observed. There is, however, a gap in MD04-2822 of approximately 20 cm at a depth of 16.5 m; this is thought to be an artefact of piston core retrieval (i.e. 'pull-apart') as the sediments are cohesive and display no signs of disturbance or inflow.

Four major lithological units are identified in sediment core MD04-2822 based upon sediment structure, composition, colour, magnetic susceptibility and XRF Ca content (Figure 2.1, Appendix A₁, A₂, A₃).

- **Unit A** (0–2.8 m): Light in colour, silty-clay, high calcium content and foraminifera (>150mm) abundance with low magnetic susceptibility.
- **Unit B** (2.8–23.2 m): Dark grey-brown in colouration, clayey silt with some sand in the lower portion, generally low calcium content and foraminifera abundance, low weight percentage (by mass) >63 µm and episodic high magnetic susceptibility.
- **Unit C** (23.2–25.5 m): Light in colour, clay-silt-sand with high calcium and foraminifera content with low magnetic susceptibility.
- **Unit D** (25.5–37.7 m): Dark grey-brown in colour, generally silty-clay in composition, low calcium content with fluctuating foraminiferal abundance and episodic high magnetic susceptibility.

Using a facies approach, an initial analysis of the depositional history may be made (Figure 2.1). This suggests two episodes of glacio-marine deposition (units B and D) interspersed with countourite and hemipelagic sedimentation. Within units B and D, there are episodic high magnetic susceptibility that correspond to thin (<1 cm) silt laminae. These silt laminae are often indistinct ('whispy') in appearance, although some display sharp bottom contacts and a slight fining upwards. These are interpreted as distal (or low concentration) turbidites (c.f. Stow and Bowen 1980); intervals of silt laminae are marked in Figure 2.1. During sampling, any suspected turbidite layers were avoided.

Turbidite layers are well documented for the neighbouring core MD95-2006 (these were especially evident within the >63 µm processed residues); these have also been distinguished using magnetic parameters (Peters et al 2008). Similar magnetic analyses were undertaken for the 16.5 to 30 m interval of MD04-2822 (Figure 2.2). When plotted against the MD95-2006 data, few intervals fall within the turbidite envelope defined by Peters et al (2008), although suspected turbidites (as distinguished from magnetic parameters occur at: 16.6 to 16.8m, 17.7 to 18.2 m, 18.4 m and 18.6 m (C. Peters, *unpublished data*). This confirms the visual lithological assessment made of these sections of the core during logging (Appendix A₁).

Distinct bioturbation tracks are infrequent and not a prominent feature of the record (although zoophycus burrows were evident at ~19.5 to 21.5 m and ~25 m); these were avoided during sampling. However, traces of bioturbation were evident throughout the core as mottling (of course, very bioturbated sediments may appear homogenous in character).

Small dropstones were noted on the cut surface of the core (both archive and working section), notably within lithological units B and D (Figure 2.1); a large dropstone (~0.5 cm x 0.5 cm) was recorded at 16.93 m.

Figure 2.1: Summary MD04-2822 lithological log, units, facies and depositional interpretation. A detailed sedimentological log, sediment physical properties and sediment photograph may be found in Appendix A₁, A₂ and A₃ respectively).

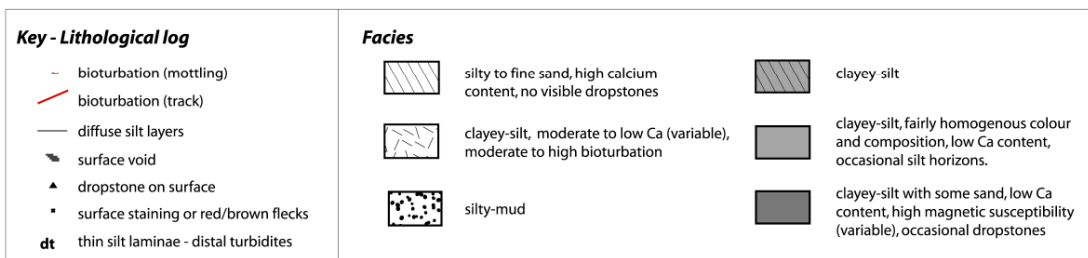
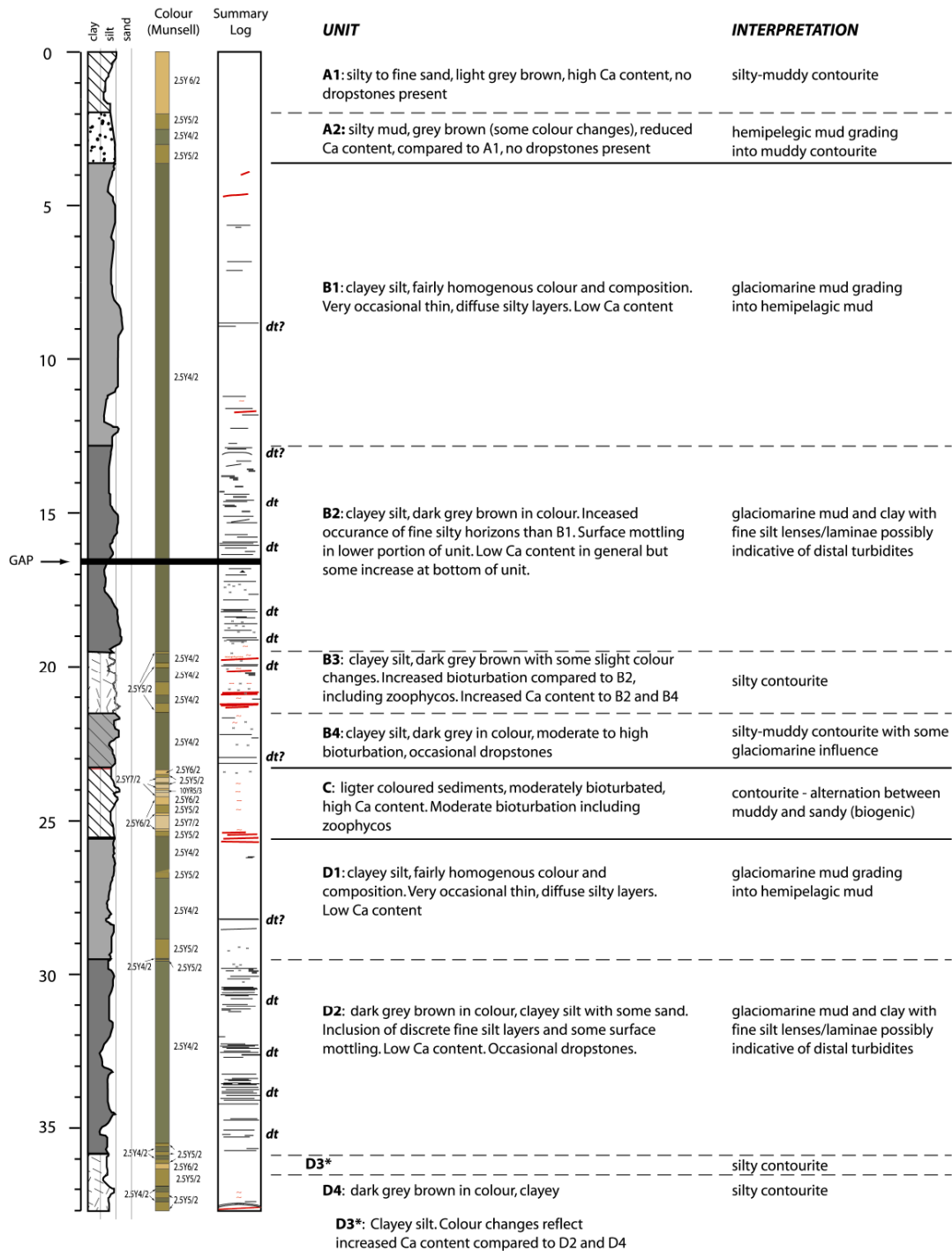
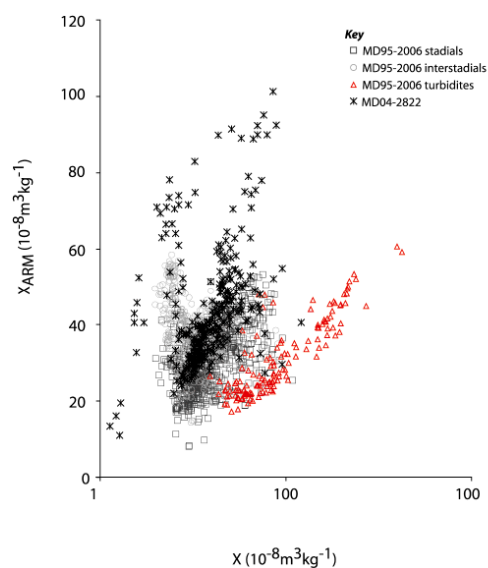


Figure 2.2: ARM versus X for stadial, interstadial and turbidite samples for core MD95-2006 following plotting method of Kissel (2005) (Peters et al 2008) and the same parameters for MD04-2822 for interval 16.5 to 30 m (black crosses; C. Peters, *unpublished data*). The MD95-2006 turbidite samples given in red.



2.2. Stratigraphy – Overview

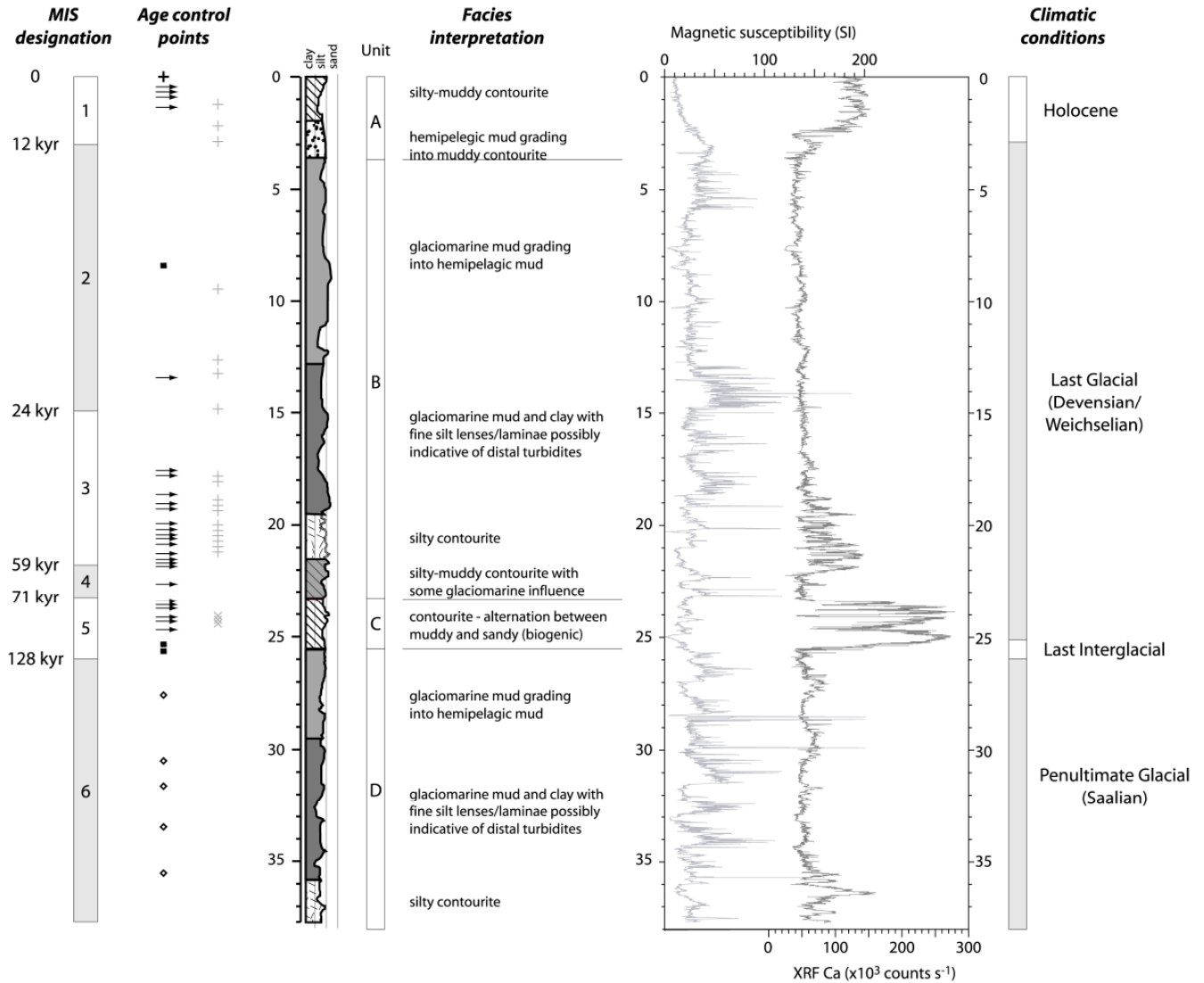
The stratigraphy (and chronostratigraphy) is outlined here in brief, in order to place the sampling and analytical procedures within context (detailed in subsequent sections of this chapter) (Figure 2.3). This is intended as a brief synopsis; a detailed consideration of chronological control for the core can be found within chapter 3. Age control was achieved via: correlation of the MD04-2822 benthic $\delta^{18}\text{O}$ record to SPECMAP (Pisias et al 1984, Martinson et al 1987); the correlation of surface water proxies (% *N. pachyderma* (sinistral) and XRF Ca) to the Greenland $\delta^{18}\text{O}$ ice core record (NGRIP members 2004); tuning of surface proxies to the Antarctic ice core methane record (EPICA Dome C; Parrenin et al 2007, Loulergue et al 2008) and; radiocarbon dating of the core top.

The lowermost unit (unit D) of the core is predominately clay-silt and is inferred to be dominated by glaciomarine sedimentation; dropstones and thin silt lenses/laminae (associated with high magnetic susceptibility and interpreted as distal turbidites) are evident. This unit is correlated to MIS 6 and the penultimate (Saalian) glaciation (Figure 2.3).

Unit C is a contourite correlated to MIS 5, with the last interglacial (MIS 5e, ca. 123 kyr) placed at approximately 25.5 m. MIS 5 is clearly evident in the record as an interval of high Ca content (Figure 2.3).

Unit B grades from silty contourite to primarily glaciomarine sedimentation and is correlated to MIS 4 to MIS 2 inclusive (i.e. the last glacial interval). Episodic high magnetic susceptibility is associated with thin silt laminae and interpreted as distal turbidites (Figure 2.3). Unit A is mainly a silty/muddy contourite with high calcium and low magnetic susceptibility. This is correlated to the Holocene (Figure 2.3).

Figure 2.3: Summary stratigraphy for MD04-2822. MIS designations and age estimates are after Imbrie et al (1984). Age control points are those used in the construction of the MD04-2822 chronology (chapter 3). Facies are those detailed in Figure 2.1. Further explanation of how age control was obtained for the core may be found in chapter 3.



Key (chronostratigraphic tie-points):

- correlation of benthic $\delta^{18}\text{O}$ to global stack (SPECMAP)
- surface proxy tuning to Greenland $\delta^{18}\text{O}$ ice core record
- ◇ surface proxy tuning to Antarctic ice core methane record
- + radiocarbon dating
- × radiocarbon dating (background correction)

2.3. Sediment physical properties (GEOTEK multi-sensor core scanning)

Both cores were passed through a GEOTEK multi-sensor core logger. The physical properties of MD04-2822 (Appendix A₂) were measured onboard ship, whilst +56-1215 CS were determined at SAMS, Oban, approximately 2 months after collection but only a couple of days after splitting.

The GEOTEK system enables detailed, down-core, non-destructive analyses discussed below (Appendix A₂). Manufacturer typical accuracies are given within Table 2.1.

Table 2.1: GEOTEK quoted typical accuracies
(GEOTEK manual; www.geotek.co.uk/sites/default/files/manual.pdf)

	Typical accuracy
Core motion (linear precision)	0.1 mm
Gamma density	$\pm 0.01 \text{ g cc}^{-1}$
P-wave velocity	$\pm 5 \text{ m s}^{-1}$
Electrical resistivity	$\pm 0.2 \text{ ohm}$
Magnetic susceptibility	$\pm 5 \%$

Magnetic susceptibility varies as a function of mineral content allowing inferences of changing sediment provenance or diagenetic environment to be made, as well as correlation to nearby cores (see chapter 5). The profile for MD04-2822 is highly variable with high values at 5-7 m, 13-15 m, 18-19 m, 28-31 m and 32-34 m.

Gamma density was measured by the attenuation of a beam of gamma radiation. In saturated sediments the gamma density (or GRAPE¹) varies with sediment type and tends to increase down-core with compaction and de-watering of sediments. Gamma density is a record of bulk density and may be used as an indicator of lithological and porosity changes. This parameter for MD04-2822 is fairly uniform downcore with some slight increase in values consistent with compaction and dewatering of the sediments. A notable feature of low values is evident at 7 to 8 m.

Electrical resistivity/impedance is measured using a matched pair of inductive coils that simultaneously measure the resistivity of both the core and the free air; this differential measurement provides stable determination of resistivity. Electrical resistivity varies mostly with changes in pore water salinity but also varies as a function of sediment porosity and permeability. The impedance profile is very similar to the density profile for MD04-2822, probably reflecting a decrease in porosity downcore.

P-wave velocity is the travel time of a compressional wave pulse and is measured across the core. Ultrasonic pulses are transmitted and received by a pair of rolling transducers. P-wave velocity is primarily a function of density or porosity in unconsolidated sediments but increases rapidly in consolidated sediments. This parameter is highly variable within MD04-2822, varying as a function of sediment porosity.

¹ Gamma Ray Attenuation Porosity Elevator, after Evans (1965) who used the technique to estimate porosity.

3. Sampling

Only MD04-2822 has been sampled to date. The working half of MD04-2822 was lithologically described (Figure 2.1), sampled and processed at the University of St Andrews. Initial sampling was 1cm slices at a depth increments of 10 cm for the entire core length. Material in contact with the plastic liner was removed to minimise any effects of ‘smearing’ (Austin 1994).

Each sample was weighed, freeze dried and weighed once more to allow a calculation of water content (wet mass – dry mass). The sample was then wet sieved at >63 µm and dried at 40 °C to prevent (further) fractionation of stable isotopes within the calcium carbonate of foraminifera shells. The percentage (by mass) of the sample > 63 µm was then be calculated. A schematic of the different analyses undertaken is given in Figure 2.4.

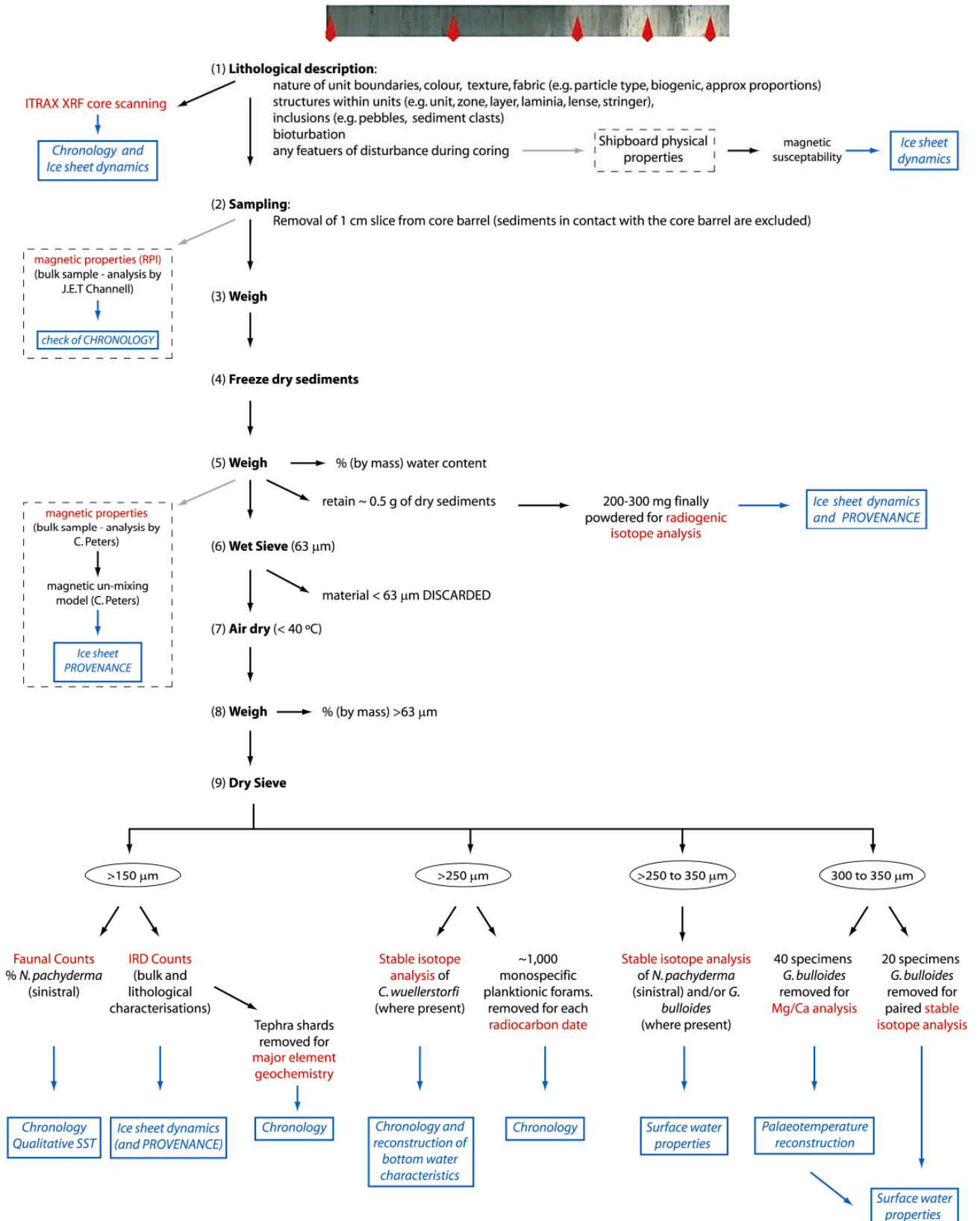
From the initial stratigraphy, lithological interpretation and subsequent age control, additional high resolution sampling was undertaken for intervals of interest (Table 2.2).

Table 2.2: Depths and resolution of additional sampling for MD04-2822.

Depth interval (cm)	Time interval	Rationale	Resolution	Chapter
0-1 to 50-51 cm	Holocene	Comparison to MIS 5e	5 cm	7
	Greenland Stadial (GS) 3 (Fugloyarbanki tephra)	Confirmation of the stratigraphy of GS 3		4
2003-2004 to 2021-2022 cm	Greenland Stadial 9 and Heinrich event 4	Stratigraphy of GS9 and analogy of a ‘small’ BIS for MIS 4	2 cm	8
2150-2151 cm to 2170-2171 cm	North Atlantic Ash Zone II	Confirmation of chronostratigraphy	1cm	3
2220-2221 cm to 2340-2341 cm	MIS 3/4 transition, MIS 4 and MIS 5a	Investigation of early history of the BIS (provenance of IRD)	2 cm	6 and 8
Selected intervals 2350-2351 cm to 2464-2465 cm	MIS 5 cold ‘C’ events (e.g. McManus et al 2002)/ Greenland Stadials 20 to 26 inclusive	Correlation to other North Atlantic sea surface records and investigation of early BIS dynamics	2 cm	6 and 8
2490-2491 to 2560-2561cm	MIS 5d/5e transition, MIS 5e, Termination II	Detailed investigation of Termination II	2 cm	6 and 8

CHAPTER 2:
Materials and Methods

Figure 2.4: Schematic of sampling and analytical procedures carried out on the MD04-2822 sediments. Text in red are the analytical techniques used whilst those in blue indicate what the results of those procedures were use for in this thesis. All work was carried out by F. Hibbert except those within the dashed boxes.



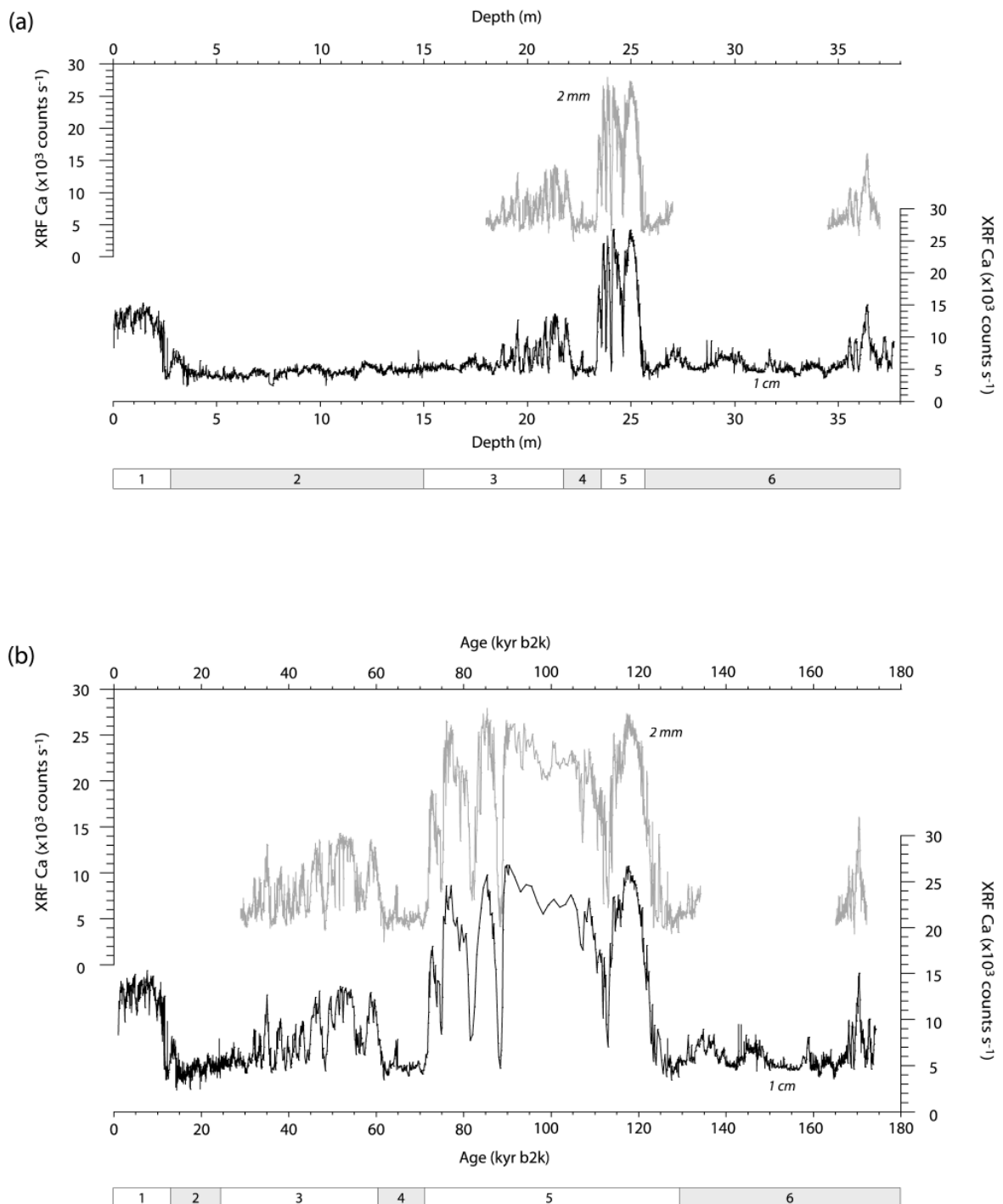
4. Multi-elemental X-ray fluorescence (XRF) core scanning, ITRAX™

The multi-function core scanning instrument (ITRAX™) enables optical, radiographic and elemental variations for sediment cores to be attained in a non-destructive manner and provide a useful means of core characterisation. They describe basic, unambiguous sample properties and high quality, high resolution geochemical data. These elemental and other sedimentological variations can then be used to infer environmental, sedimentological and diagenetic changes (Croudace et al 2006) as well as possible sediment provenance (Rothwell et al 2006). The ITRAX records are also invaluable in guiding further detailed destructive sampling (Rothwell 2006).

The ITRAX™ core scanning was undertaken at BOSCORF, Southampton, UK (2007) by F. Hibbert. The archive sections of MD04-2822 were logged (visual description) and prepared by cleaning the surface of the sections with a glass slide to ensure a clean, flat surface. This was loaded into the ITRAX core scanner: the scanner consists of an optical in line camera that operates in line with the stepper motor movement (to progress the core through the scanner), a flat beam x-ray scanner and micro x-ray fluorescence detection system. For XRF analysis, measurement is at 45° to the incident x-ray beam using a Si drift x-ray detector and digital signal processing provides energy-dispersive spectrometry.

The X-rays for irradiating the core are generated by a 3kW Mo X-ray tube operating at 30 kV and 30 mA. The elemental XRF parameters were set, adjusted and refined. A count time of 40 s with step size of 1 cm was used (with some limited 2 mm replication, the fidelity of which is illustrated in Figure 2.5). The elemental peak areas are roughly proportional to the concentrations of major and trace elements present within the sediments (Rothwell et al., 2006; Thomson et al., 2006) although the ITRAX geochemical data should be considered as semi-quantitative in nature and caution exercised in their interpretation (Croudace et al 2006). The x-ray radiography was disabled for all 1 cm step size core scanning as the radiographs would be of insufficient resolution to determine any structural features.

Figure 2.5: ITRAX XRF 1cm and 2 mm Ca profiles for MD04-2822 (a) on depth (grey – 2mm resolution; black 1 cm resolution); (b) on age (compound, see chapter 3) (grey – 2mm resolution; black 1 cm resolution). MIS designations after Imbrie et al (1984). The reader is directed to Figure 2.3 for an overview of the stratigraphy (and chronology) of the MD04-2822 sediments.



5. Calculation of Linear Sedimentation Rate (LSR):

Linear sedimentation rates may be determined from the dimensions of the sediment core once an age model for the core has been achieved i.e. the amount of sediment deposited within a specified time interval. This is vital for the calculation of fluxes of material deposited at the MD04-2822 site (e.g. IRD flux).

The upper portions of piston cores are susceptible to over-sampling due to piston movement during coring, whilst gravity cores are prone to sediment under-sampling in their lowermost portions. The effects are typically associated with the upper portions (~10 m) of piston and lower sections (~4 m) of gravity cores respectively (Skinner and McCave 2003). This distortion of sediment dimensions and hence dimensionally derived linear sedimentation rates, may lead to erroneous calculations of sediment fluxes.

Lithological examination of MD04-2822 did not present any obvious features of over-sampling, however once IRD fluxes had been calculated², unexpectedly high IRD flux rates during the Younger Dryas/ Greenland Stadial (GS) 1 (i.e. greater than those calculated for the Last Glacial Maximum), pointed to the possibility of an over-estimation of the linear sedimentation rate for the upper section of MD04-2822. The recovery in September 2009 of a gravity core from the same location, provided an opportunity to investigate this further (see chapter 5, *Correction of core 'over-sampling'*).

Gravity core +56-12/15 CS (from the same location as MD04-2822) is considered a facsimile of the upper over-sampled sections of the piston core MD04-2822. The two cores were correlated using their magnetic susceptibility records, which enabled the chronology of MD04-2822 (age tie points only) to be translated onto the gravity core. From this, a 'corrected', spliced linear sedimentation rate was calculated and applied to the upper section of the piston core (see chapter 5 for further details).

² IRD Flux = IRD concentration * Linear sedimentation rate * dry bulk density (see section 7.1) and any errors within estimates of the sedimentation rate will be carried forward into any calculation of IRD flux (see chapter 5)

6. Hydrographic reconstructions

6.1. Faunal and IRD counts

The percentage abundance of the planktonic foraminifera *N. pachyderma* (sinistral) has been used extensively for the reconstruction of glacial-interglacial conditions within the North Atlantic (Ericson 1959, CLIMAP 1976, Bond et al 1993) utilising the reciprocal faunal abundance variation with temperature/water mass variations (e.g. Ericson 1959, CLIMAP 1976, Bé and Tolderlund 1971). The left coiling *N. pachyderma* (sinistral) morphospecies is dominant in the modern cold northern latitudes (< 7°C) and is used as an indicator of the position of the polar front i.e. the transition between polar and subpolar water masses (Bé and Tolderlund 1971, Johannessen et al 1994, Pflaumann et al 1996, 2003).

The relative abundance of *N. pachyderma* (sinistral) was used to construct the chronology of the core (via correlation to the Greenland and Antarctic ice cores; chapter 3) as well as a proxy for sea surface temperatures (i.e. high % *N. pachyderma* (sinistral) is associated with polar conditions, low % *N. pachyderma* (sinistral) with sub-polar conditions) and the movement of the polar front. IRD counts were converted to IRD flux and used as a proxy of ice sheet dynamics.

The relative abundance of the planktonic, polar species of foraminifera *Neogloboquadrina pachyderma* (sinistral), a semi-quantitative proxy for sea surface temperatures (SST) in the North Atlantic region (Bond et al., 1993; Johannessen et al., 1994) and total IRD concentration, was determined from the >150 µm size fraction. Counts were a minimum of 300 for both total planktonic foraminifera and IRD (all analyses undertaken by F. Hibbert).

Samples of very high abundances of foraminifera and/or IRD were progressively split in half until sufficient to spread evenly across a picking tray. Squares within the picking tray were sampled at random and all foraminifera and/or IRD grains in each square were counted until a minimum of 300 was achieved.

$$\text{Total number of grains in split} = \frac{\text{total number grains counted}}{\text{number of squares counted}} * 42$$

(42 is the total number of squares within the picking tray)

$$\text{Total number of grains within sample} = \text{total number grains in split} * 2^{\text{number of splits}}$$

$$\text{Concentration (grains or foraminifera g}^{-1}\text{)} = \frac{\text{Total number of grains in sample}}{\text{dry weight of sediment processed}}$$

6.2. Stable Isotope measurements ($\delta^{18}\text{O}$ and $\delta^{13}\text{C}$)

For oxygen isotopes, there are three principle influences upon the $\delta^{18}\text{O}$ composition of the mineral precipitated:

1. The water temperature at which the mineral is precipitated (δT) (Emiliani 1955, 1971, Shackleton 1967, 1974).
2. The $\delta^{18}\text{O}$ of the water in which the mineral is precipitated ($\delta^{18}\text{O}_{\text{water}}$) and is determined by both global (variation in global ice volumes ($\Delta\delta_{GIV}$); Shackleton 1967, Fairbanks 1989, Waelbroeck et al 2002) and local influences ($\Delta\delta_{\text{Local}}$). These local influences include: the balance between evaporation and precipitation; inputs of low $\delta^{18}\text{O}$ freshwater (e.g. meltwater of river); sea ice³ with resulting seasonal fluctuations (Strain and Tan 1993, Dokken and Jansen 1999) and; advection and mixing of waters from different source areas (Weiss et al 1979, Fairbanks 1982, Parrein and Potter 1984, Kipphut 1990, Frew et al 1995).
3. Vital effects including: ontogenic effects (e.g. Spero and Lee 1996, Kroon and Darling 1995), symbiotic photosynthesis effects (e.g. Spero and Lee 1993, Spero et al 1997), respiration effects (e.g. Lane and Doyle 1956, Grossman 1987), gametogenic effects (e.g. Bé 1980, Bemis et al 1998) and the effect of changes in $[\text{CO}_2^*]$ (e.g. Spero et al 1997, Bemis et al 1998, Bijma et al 1999).

Therefore:

$$\Delta\delta^{18}\text{O}_{\text{Mineral}} = \Delta\delta^{18}\text{O}_{\text{Water}} + \Delta\delta T \quad (1)$$

$$\Delta\delta^{18}\text{O}_{\text{Mineral}} = (\Delta\delta_{GIV} + \Delta\delta_{\text{Local}}) + \Delta\delta T + \text{Vital} \quad (2)$$

The $\delta^{18}\text{O}$ of the benthic foraminifera *C. wuellerstorfi* was used to construct the age model for MD04-2822 (chapter 3) as well as a first order approximation of global ice volumes. The $\delta^{13}\text{C}$ of the same species may be used to construct bottom water properties. This taxonomic group reliably records deep water properties (Curry and Oppo 2005) although the epibenthic *C. wuellerstorfi* does not calcify in isotopic equilibrium with bottom water but in a constant 1:1 relationship (Mackensen and Bickert 1999). Accordingly *C. wuellerstorfi* values are often adjusted by 0.64 ‰ to place them on a *Uvigerina* equivalent scale (Shackleton and Opdyke 1973). It has also, been suggested that *C. wuellerstorfi* secretes calcite close to isotopic equilibrium of seawater $\delta^{18}\text{O}$ (Bemis et al 1998). No correction has been applied to the values obtained for MD04-2822 samples. The reader is directed to chapter 3, *Chronostratigraphy*, for a full discussion of influences upon the benthic $\delta^{18}\text{O}$ isotope signal.

³ Newly formed sea ice is enriched by $\sim 2.57 \pm 0.10$ ‰ relative to sea water $\delta^{18}\text{O}$ (Macdonald et al 1995) and presents seasonal fluctuations in local $\delta^{18}\text{O}$ of sea water with melting and formation of sea ice (cf. Strain and Tan 1993). Increases in surface salinity with brine rejection during sea ice formation may lead to convection and the transport of surface waters to the ocean interior (Rohling and Bigg 1998, Dokken and Jansen 1999).

Benthic $\delta^{13}\text{C}$ carries an imprint of the nutrient content of deep water masses (Shackleton 1977, Duplessy et al 1984) and may be used for the reconstruction of bottom water circulation through time (e.g. Curry et al 1998, Mackensen et al 2001, Curry and Oppo 2005). Species specific vital effects and microhabitat effects may produce deviations from the $\delta^{13}\text{C}_{\text{DIC}}$ of bottom waters (e.g. review by Mackensen 2008).

The $\delta^{18}\text{O}$ of planktonic foraminifera may be used to reconstruct the $\delta^{18}\text{O}$ of the water in which they calcified and thus allow temperature and salinity changes of the surface ocean to be discerned.

N. pachyderma (sinistral) calcifies below the surface at depths up to 200 m (Bauch et al 1997) during summer within its ecological range (Bé and Tolderlund 1971, Reynolds and Thunell 1986) but may calcify outside of the summer at the upper extent of its range (Schmidt and Mulitza 2002, King and Howard 2005). *N. pachyderma* (sinistral) is commonly used for isotopic measurements of surface waters of high and mid-latitudes during glacial intervals (e.g. Bond et al 1993, Fronval et al 1995, Lackschewitz et al 1998, Elliot et al 1998, van Kreveld et al 2000).

G. bulloides is a shallow dwelling planktonic foraminifera with calcification at ~ 30 m depth (Schiebel et al 1997, Barker and Elderfield 2002, Hillaire-Marcel and Bilodeau 2000) and is associated with the spring bloom (Ganssen and Kroon 2000, Chapman 2010). *G. bulloides* is found in modern subpolar waters of the North Atlantic (Bé and Tolderlund 1971, Johannessen et al 1994, Carstens et al 1997). When sufficient numbers of this species was present, they were also picked for stable isotope analyses in order to provide, when compared with $\delta^{18}\text{O}$ of *N. pachyderma* (sinistral), information upon surface water stratification.

A conventional light microscope was used to select foraminifera for stable isotope analysis at the NERC Isotope Geosciences Laboratory (NIGL), BGS Keyworth and Facility for Earth and Environmental Analysis (FEEA), University of St Andrews. The samples were dry sieved at >250 to 350 μm and 30 monospecific individuals of the planktonic foraminifera *N. pachyderma* (sinistral) and *Globigerina bulloides* were selected for each depth interval. Where present at >250 μm , the epibenthic species *Cibicidoides wuellerstorfi* was also picked for stable isotope analysis. In addition, 20 *G. bulloides* individuals from the 300 to 355 μm size fraction were removed for stable isotope analysis from the same intervals as samples for Mg/Ca analysis (i.e. paired measurements). All analyses were undertaken by F. Hibbert.

Analytical precision of $\delta^{18}\text{O}$ and $\delta^{13}\text{C}$ (1σ) is <0.08‰ (NIGL), 0.07 ‰ (FEEA), with respect to both ratios and is reported on the Vienna Pee Dee Belemnite (VPDB) scale through the NBS standards and working laboratory standard (Carrara Marble for both laboratories). The values obtained for *C. wuellerstorfi* have not been corrected for disequilibrium effects (e.g. Shackleton and Opdyke, 1973).

Repeats of planktonic isotopes from the same interval, although not from a homogenised sample aliquot, show fairly close correspondence for both NIGL and FEEA. The percentage error in the values obtained are greater for $\delta^{13}\text{C}$ than for $\delta^{18}\text{O}$ (Appendix B₁). This may be due to incomplete cleaning and/or the inadvertent inclusion of organic material within the chambers of the foraminifera. The average

percentage error is similar for both planktonic (*N. pachyderma* (sinistral) and *G. bulloides*) as for the benthic *C. wuellerstorfi*.

In order to investigate the main processes influencing $\delta^{18}\text{O}$, specific analytical strategies have been adopted, e.g. using monospecific records picked from a narrow size range in order to minimise vital effects. The use of Mg/Ca analysis enables temperature effects to be constrained for selected paired isotope and Mg/Ca analyses (MIS 5e and Holocene samples; see chapter 7).

6.3. Palaeotemperature reconstruction (Mg/Ca analysis of planktonic foraminifera)

The use of foraminiferal Mg/Ca ratio utilises the thermodynamic control upon the substitution of Mg^{2+} for Ca^{2+} within the shell matrix during calcification. This substitution is related to the temperature of the surrounding waters, with the Mg/Ca ratio increasing exponentially with increasing temperature (e.g. Lea et al 1999, Barker et al 2005). This is based upon the assumption that the Mg/Ca content of the open ocean is constant over glacial-interglacial timescales (Barker et al 2005). Mg/Ca ratios determinations have become a well established method for the reconstruction of past ocean temperatures (e.g. Barker and Elderfield 2002, Eggins et al 2003, Cléroux et al 2008, Thornalley et al 2009). A palaeotemperature record was generated for both MIS 5e (the last interglacial; chapter 7) and a portion of the Holocene within MD04-2822 (chapter 7). All analyses were undertaken by F. Hibbert.

For Mg/Ca determinations, 40 *G. bulloides* individuals (300 to 355 μm) were picked under a conventional light microscope for the depth intervals 2510.5 to 2560.5 cm (inclusive) at 2cm resolution, 2490.5 cm to 2510.5 cm (inclusive) at 5cm resolution and 2450.5 cm to 2490.5 cm (inclusive) at 10cm resolution. These were cleaned following the procedure of Barker et al (2003); foraminiferal tests were gently broken by crushing between two glass slides; clay removal via centrifuging and minimum settling technique using ultra pure water followed by methanol; boiling with alkali buffered 1% H_2O_2 removed any organic material; coarse grained silicates were removed manually under a microscope and finally a dilute acid leach (0.001 M HNO_3).

Once cleaned, samples were dissolved in nitric acid (0.075 M) and diluted to a fixed Ca concentration of 60 to 100 ppm within 250 μl solution. Analyses were carried out on a Varion Vista ICP-AES at the University of East Anglia in February 2008 and February 2009. Analytical precision of 0.02 mmol/mol (relative standard deviation of 0.49 %) was determined from replicate runs of a standard solution. When this is calculated with respect to temperature, the mean standard deviation is 0.05m $^\circ\text{C}$, however, the uncertainty associated with the conversion to temperature (conservative estimates of 1 $^\circ\text{C}$) are far in excess of the intra-sample variation.

Conversion of concentration to temperature estimates was undertaken using the palaeotemperature equation of Elderfield and Ganssen (2000):

$$\text{Mg} / \text{Ca} = 0.72 \times e^{(0.1 \times T)}$$

where,

T is temperature in $^\circ\text{C}$

Analysis of procedural blanks indicates that Mg leaching from vials and/or laboratory contamination was minimal. Aluminium concentrations of each sample were monitored to ensure effective removal of clay contaminants had been achieved; samples with detectable Al concentrations were discarded.

Attempts were made to run replicate analyses, however, only a limited number were successful (Appendix B₂).

7. IRD Inputs

7.1. Calculation of IRD flux

The calculation of IRD flux ensures that changes to the IRD content of sediments is not just the result of random sediment delivery (Ruddiman 1977). IRD flux is considered in preference to IRD concentration because the latter may be influenced by ‘dilution’ of the IRD signal to the site by increased fine fraction terrigenous material transported during episodes of increased ice sheet activity/cold climatic conditions i.e. during stadials. High IRD inputs are anticipated for the LGM and have been demonstrated for the neighbouring core MD95- 2006 (Knutz et al 2001), located 83 km from MD04-2822. However, due to high inputs of primarily fine fraction terrigenous materials, the contribution of elevated amounts of ice-rafted material during the LGM are masked for MD04-2822. The proximity of MD04-2822 to an actively glaciated margin highlights the difficulty of interpreting IRD concentration signals and reinforces the necessity for a robust chronology in order to calculate IRD flux.

IRD concentration, [IRD] (grains >150 μm per gram dry sediment) (see above), was converted to IRD flux ($\text{grains cm}^{-2} \text{ kyr}^{-1}$) using the bulk mass accumulation rate (BMAR) calculated from the linear sedimentation rate (LSR) derived from the MD04-2822 age model (for detailed explanation of age model construction, please see chapter 3, *Chronostratigraphy*).

$$\text{IRD flux} = \text{BMAR} * [\text{IRD}]$$

where,

$$\text{BMAR} = \text{LSR} * \rho_{\text{DB}}$$

Linear sedimentation rates (LSR) are estimated from the dimensions of the piston core whilst the dry bulk density (ρ_{DB}) is estimated from wet and dry sediment mass and corrected for salt content (assuming sediment particle and pore water densities of 2650 and 1025 kg m^{-3} and pore water salinity of 35 g kg^{-1}).

$$\text{Wet weight (+ salt water)} = x \text{ (g)}$$

$$\text{Dry weight (+ salt)} = y \text{ (g)}$$

$$\text{Weight of sediment - salt (Y)} = x - (0.035*y)$$

assuming a salinity of 35 $\text{g kg}^{-1} = 0.035$

Dry mud volume = $Y/2.65$
assuming a sediment density of 2.65 g cm^{-3}

Fluid volume = $(x-y)/1.025$
assuming a water density of 1.025 g cm^{-3}

Wet sample volume = dry mud volume + fluid volume
Hence;

Dry bulk density = $(Y)/$ wet sample volume

Bulk mass accumulation rate (BMAR) = LSR * ρ_{DB}

IRD flux = BMAR * IRD concentration

8. IRD Provenance

8.1. Lithological characterisation of IRD grains

Visual lithological characterisations of IRD grains ($> 150 \mu\text{m}$) has been used to determine possible source regions for some lithic grain types, these in turn may be used to derive ice sheet or ice stream dynamics from ambient sediment influxes. For example: peak concentrations of detrital carbonate (of assumed North American origin) are used to define Heinrich events and the dynamics of the Laurentide Ice Sheet (e.g. Bond et al 1992); peak concentrations of tephra shards derived from Icelandic volcanic eruptions may facilitate correlation of palaeoenvironmental records and enable reconstructions of palaeoceanographic conditions (e.g. Lacasse et al 1996); within the Rockall Trough, basalt grains have been used to determine the dynamics of the British Ice Sheet as these grains are thought to derive from the British Tertiary Igneous Province (BTIP) (Knutz et al 2001, 2007).

For locations proximal to ice sheets or ice streams, such as MD04-2822, the 'bulk'/ambient IRD signal will derive, in the main, from that proximal ice sheet or ice stream (Scourse et al 2009, Peck et al 2007). Both 'bulk' (i.e. total IRD flux to the core site) and lithic characterisation are considered within this study. Lithological characterisations were used in chapter 8 as a means whereby the provenance of IRD delivered to the site could be investigated. In addition, lithological characterisation enabled the detection of tephra layers (e.g. North Atlantic Ash Zone (NAAZ) I and II which was subsequently confirmed by major element geochemical analysis, section 8.1.1) which served as a check of the MD04-2822 chronology (chapter 3). In addition, Heinrich Event 4 was identified by the presence of detrital carbonate (chapter 8). All analyses were undertaken by F. Hibbert.

Visual lithological characterisation of IRD grains ($>150 \mu\text{m}$) was undertaken using a conventional light microscope; a minimum count of 300 grains was used to characterise: quartz; hematite stained quartz (any visible staining on the grain when viewed under the microscope); dark finely crystalline (e.g. basalt, presumed BTIP

origin Knutz et al., 2001, 2007); volcanic glass (tephra); black glass (obsidian); pumice; crystalline rock fragments; mica; detrital carbonate (sugary dolomitic carbonate, grey and chalky) and other (Figure 2.6).

Table 2.3 details lithological characterisations used to infer IRD provenance within the North Atlantic. However, the similar geological histories circum-North Atlantic can and does leave similar IRD 'signatures' within the sediments. For example, dark volcanic lithics may be derived from igneous sources both to the immediate east (British Tertiary Igneous Province) and west (e.g. Rockall Bank, Anton Dohrn) of the MD04-2822 core site or indeed to farther afield (e.g. the Faeroe Islands). A reduction of 120 m sea level around the LGM (e.g. Peltier and Fairbanks 2006), could also have resulted in basal freeze-on of volcanic material, derived from the Rockall Bank, to sea ice, pack ice or icebergs (M. Stocker, pers. comm., Hibbert et al 2010, Scourse et al 2009). The relative contribution of basalt derived from sources to the immediate west of the core site is difficult to quantify.

The significance of a western source and the influence of post-depositional erosion/transport by bottom currents remain undetermined for MD04-2822 but are thought to be minor contributing factors in the total flux of IRD.

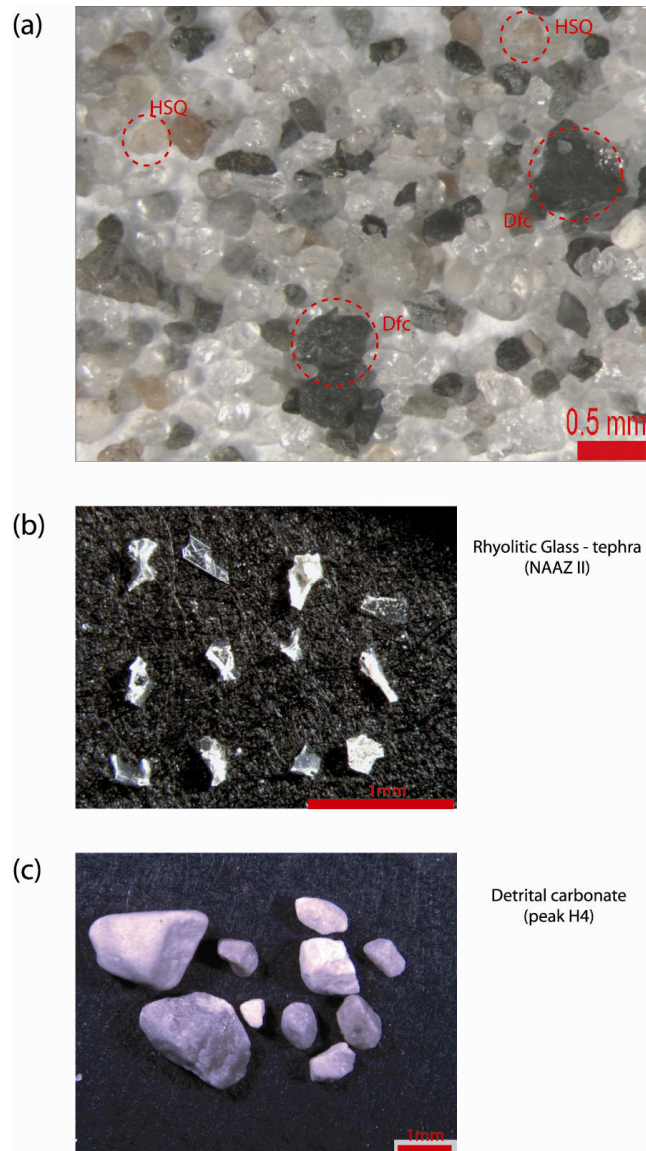
8.1.1. Major element geochemistry of tephra horizons

Major element geochemistry of tephra shards facilitates the correlation with well characterised tephra horizons within other records (marine, terrestrial or ice core). Tephra horizons common to both the Greenland ice cores and marine sediments may also be used as chronostratigraphical tie-points (see chapter 3), however this requires that any tephra horizon be confirmed as originating from the same geochemical population (e.g. Austin et al 2004). As such, major element geochemistry was undertaken for tephra horizons identified within MD04-2822. All analyses were undertaken by F. Hibbert (Appendix B₃).

Tephra shards were selected using a conventional light microscope; shards for geochemical analysis were selected from either the greater than 250 μm or the 150 to 250 μm size range. These were mounted onto double sided tape and embedded in clear AralditeTM, allowed to harden and polished. The sample blocks were then evaporated-carbon vacuum-coated.

Major element analyses were carried out using an electron microprobe at FEEA, University of St Andrews, and expressed as oxide percentages. A JEOL JXA8600 electron microprobe was operated using an accelerating voltage of 15 kV, beam current of 10nA and spot size of 5 μm . Primary calibrations were established using a combination of synthetic oxides, pure metals and well characterised minerals. Secondary rhyolitic and basaltic glass standards (TB1G, Lipari, BCR2G, S-OBS, A-THO and A-ALK) were routinely analysed and used to assess sample stability. Published data for Lipari (Hunt and Hill, 1996) and TB1G (Potts et al., 2002) glasses and values of these standards acquired at FEEA are listed in Appendix B₃. Only totals greater than 95% are used in the characterisation of the tephra shards.

Figure 2.6: Photograph to illustrate some visual lithological characterisations used in this study. (a) A typical glacial >150 μm sample (2810-2811 cm), red dashed circle highlight haematite stained quartz (HSQ) grains and 'dark finely crystalline' (Dfc) grains. Quartz dominates IRD throughout the core (<150 μm). (b) rhyolitic tephra grains from the abundance maxima of North Atlantic Ash Zone II (NAAZ II) (2163-2164 cm), note the characteristic 'bubble-wall' morphology. (c) detrital carbonate grains from the peak of Heinrich event 4 (2015-2016 cm), note their characteristic 'sugary' appearance.



CHAPTER 2:
Materials and Methods

Table 2.3: Lithological indicators of provenance and associated source regions (after Peck et al 2007)

Lithology	Proposed source	References	Ice sheet
'bulk' IRD flux at core locations proximal to ice stream	Proximal ice source	Scourse et al 2009, Peck et al 2007	n/a
Detrital carbonate/Dolomitic carbonate	Hudson Bay	Bond et al 1992, Andrews and Tedesco 1992	LIS
	Baffin Bay	Andrews 1988, Andrews and Tedesco 1992, Parnell et al 2007	LIS
Hornblende grains (Paleoproterozoic ages)	North American igneous provinces	Hemming et al 1998	LIS
	NW Scotland	Peck et al 2007	BIS?
Haematite stained grains	Gulf of St Lawrence E. Greenland	Bond and Lotti 1995 van Kreveld et al 2000, St John et al 2004	LIS? E. Greenland?
	British Isles	Peck et al 2007	BIS?
Obsidian (black glass) Pumice Basalt	Icelandic volcanic province	e.g. Bond and Lotti 1995, Lackschewitz and Wallrabe-Adams 1997	Iceland
	British Tertiary Province	Basalt only – Knutz et al 2001, Knutz et al 2007, Hibbert et al 2010	BIS
	Offshore sources - Rockall Bank/Anton Dohrn/Wyville-Thompson Ridge	M Stoker (pers. comm.), Hibbert et al 2010, Scourse et al 2009	n/a
	Faeroe Islands Greenland	Basalt - Knutz (pers. comm.), Knutz et al (submitted)	Greenland
Tephra	Icelandic eruptions	e.g. Lacasse et al 1996, Hafliðason et al 2000, Austin et al 1995, 2004, Peters et al 2010	Icelandic
<i>'Typical' BIS assemblage</i>			
Basalt	British Tertiary Province	Knutz et al 2001, Hibbert et al 2010	BIS
Pale-dark brown/grey limestone	Irish Carboniferous formations	Knutz et al 2001, Sevastopulo 1981	BIS
Shale		Knutz et al 2001	BIS
Black limestone		Knutz et al 2001	BIS
Chalk		Cretaceous Upper Campian	Celtic Sea – Scourse et al 2000 Irish Sea ice stream – Scourse et al 2000, Peck et al 2006 North Sea (via Norwegian Channel Ice Stream) – Sejrup et al 2005
Schist/Mica	Scottish metamorphic provinces?	Celtic Sea – Scourse et al 2000 Peck et al 2007	BIS

8.2. Radiogenic Isotope Analysis (Pb, Nd, Sr)

Radiogenic isotope may be used to determine provenance of sediments and IRD delivered to marine sediments (e.g. Hemming 2004, Grousset et al 2001). Analyses may be plotted within source end-member fields (whole rock compositions of circum-Atlantic exposed basement rocks; or IRD from sources proximal to the former North Atlantic ice streams e.g. Grousset et al 2001, Jeandel et al 2007). The dominant composition of the sediment falls along the mixing line of two or more end members.

Studies of the distances distinct/'diagnostic' lithic types are transported from the ice margin indicate concentrations of the distinct mineralogy decreases exponentially with increasing distance from the ice margin. An approximate 'half-distance' of a few tens of kilometres is proposed (Clark 1987). Therefore the products of basal glacial erosion delivered to the deep ocean within approximately 50 to 100 km should reflect rock types of that ice stream. The isotopic composition of carbonate free sediments provides a geochemical fingerprint of potential source areas i.e. the discrimination of young, radiogenic inputs (e.g. from Iceland) from ancient, un-radiogenic inputs (such as those from beneath the Laurentide Ice Sheet) (e.g. Snoeckx et al 1999, Grousset et al 2001). However, Farmer et al (2003) note that using strontium and neodymium isotopes alone may be unable to discriminate between European and Canadian-shield derived material.

Radiogenic isotope analyses were used in a multi-proxy investigation into the early history of the last BIS (chapter 8). Sample preparation was undertaken by F. Hibbert, with analysis by facility staff at NIGL.

Bulk sediment analysis of the radiogenic isotopes of Pb, Sr and Nd were undertaken at NIGL. Samples were analysed from: 2003-2004 cm to 2025-2026 cm (Heinrich event 4 (H4), approximate 2 cm resolution); and 2219-2220 cm to 2384-2385 cm intervals (MIS 4, approximate 5 cm resolution). Approximately 200 - 300 mg of sample material was finely powdered prior to submission to NIGL.

All reagents used were either double-quartz distilled, with the exception of the acetic acid, which was Romil uPA ultrapure reagent.

Samples were weighed into clean Savillex teflon beakers and leached with a few millilitres of 10 % acetic acid to remove carbonate material. Samples were then dried, reweighed, and spiked with ^{84}Sr and ^{150}Nd tracers prior to dissolution using HF/HNO₃. A further millilitre of HNO₃ was added to break down any fluorides present and then 6M HCl was used to convert the samples to chloride form. Finally, the samples were converted to bromide form using 1ml of 1M HBr, and taken up in a further 1 ml of HBr in preparation for column chemistry.

Pb was separated using Dowex AG-1x8 anion exchange resin in disposable polypropylene columns. Matrix elements (including Sr and Nd) were eluted from the column in 1M HBr, and collected for further processing. Pb was collected in 6M HCl, dried down with a little 16M HNO₃ to drive off excess bromine, and taken up in 2 % HNO₃ in preparation for mass spectrometry.

The matrix fraction containing Sr and Nd was dried down with a few drops of HNO₃, again to drive off excess bromine. The sample was then taken up in 2.5M HCl, and

passed through a column containing Dowex AG50x8 cation exchange resin, allowing collection of a clean Sr fraction. The light rare-earth fraction was stripped from the column using 6M HCl. The Sr fraction was dried down in preparation for mass spectrometry. The rare-earth fraction was dried down then taken up in 0.2M HCl in preparation for Nd separation. Nd was separated using Eichrom LN-SPEC resin in a Biorad polypropylene column.

Pb was analysed on a Nu-Plasma HR mass spectrometer using Tl-doping to monitor for instrumental mass bias. A secondary normalisation to the NBS981 values of Thirlwall (2000) was applied. Sr was loaded on single Re filaments using a TaO activator and analysed on a Thermo-Electron Triton mass spectrometer using a dynamic multicollection algorithm. Instrumental mass bias was corrected using a $^{86}\text{Sr}/^{88}\text{Sr}$ value of 0.1197. 24 analyses of the NBS987 standard gave a value of 0.710254 ± 0.000006 (1σ). Nd was also analysed on a Thermo-electron Triton mass spectrometer using dynamic multicollection on a double Ta-Re filament assembly. Instrumental mass bias was corrected using a $^{146}\text{Nd}/^{144}\text{Nd}$ ratio of 0.7219. Twelve analyses of the La Jolla standard gave a value of 0.511848 ± 0.000006 (1σ).

Analytical values obtained may be found in Appendix B₄.

8.3. Other Proxies for Terrigenous Inputs

8.3.1. *Magnetic Susceptibility*

Bulk sediment analysis of magnetic susceptibility may be used as a proxy for terrigenous inputs as this varies as a function of mineral content, with high terrigenous inputs resulting (in general) in high magnetic susceptibility. The magnetic susceptibility used throughout this thesis was obtained on board ship at the time of core collection.

8.3.2. *XRF Si/Sr, Fe/Ca and Ca/Sr*

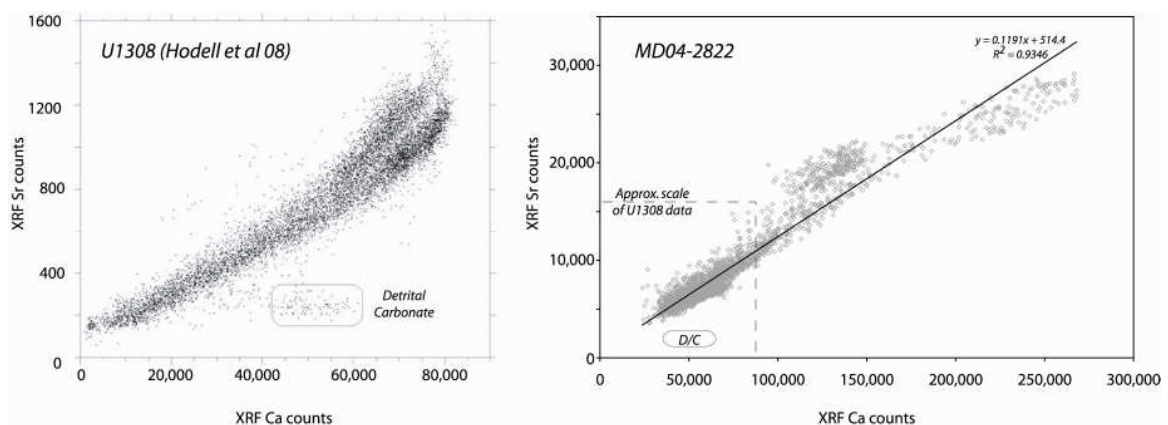
The XRF Si/Sr record determined from ITRAX core scanning (section 4, this chapter) identifies intervals high in detrital silicate minerals as well as lithogenous clay minerals. Si/Sr has been used by Hodell et al (2008) to identify intervals rich in detrital silicate minerals (e.g. quartz and feldspar); these intervals are inferred as enhanced deposition of terrigenous material within the MD04-2822 record. Alternatively, increased Si/Sr may result from decreased biogenic inputs. The Fe/Ca record, in conjunction with Si/Sr, is also employed as a proxy for terrigenous inputs, in particular lithogenous clay minerals (e.g. illite, chlorite, kaolinite). Fe and Al are important constituents of many clay minerals and were measured during core scanning. Whilst the Al record closely matches both Si/Sr and Fe/Ca, the counts per second are rather low (<200 per second; Ca >30,000 per second) and so the latter two proxies are preferred. Fe is ratio-ed with Ca; increased terrigenous or alternatively decreased biogenic inputs result in elevated Fe/Ca values.

XRF core scanning (e.g. Hodell et al 2008) has been used to detect Heinrich Events within sediments using the ratio of calcium to strontium (Ca/Sr). Ca and Sr are strongly correlated and covary over glacial-interglacial cycles, reflecting changes in

the biogenic carbonate of the sediments (Figure 2.7). The Heinrich Events are discernable when biogenic carbonate is low and detrital carbonate high; biogenic calcite has a greater Sr concentration than inorganic calcite or dolomite (Hodell et al 2008). However, it appears that either the amount of detrital carbonate delivered to the site was insufficient to be detected during core scanning and/or high biogenic carbonate productivity masks any detrital carbonate deposition.

XRF core scanning of MD04-2822 produces far greater counts of both Ca and Sr than those for open ocean site U1308⁴ (Hodell et al 2008) suggesting that higher sedimentation rates⁵ coupled with high biogenic carbonate content for MD04-2822 may account for the difference between the cores. Only at ~ 2015.5 cm is there a clear peak in Ca/Sr. Subsequent lithological characterisation confirms this as Heinrich Event 4 (see chapter 4).

Figure 2.7: XRF core scanning Ca/Sr records for U1308 (eastern North Atlantic; Hodell et al 2008) and MD04-2822. Note the difference in scale between the two records. D/C = detrital carbonate envelope of Hodell et al 2008.



⁴ This is a reoccupation of DSDP 609 which has been used extensively to define Heinrich Events as well correlating Heinrich Events to the Greenland ice cores (e.g. Broecker et al 1992, Bond et al 1992, 1993)

⁵ As a first approximation, the average sedimentation rate for MD04-2822 is ~ 21 cm kyr⁻¹ (based upon a core length of 38 m and a time interval of 175 kyr); U1308 has an average of ~ 6 cm kyr⁻¹ (11.54 m equates to 191 kyr)

9. Age control

Chapter 3, *Chronostratigraphy*, details the methods used to achieve age control for the MD04-2822 core. The correlation of the benthic $\delta^{18}\text{O}$ (section 6.2) to a global $\delta^{18}\text{O}$ stack (SPECMAP; Pisias et al 1984, Martinson et al 1987) as well as the correlation of surface water proxies (% *N. pachyderma* (sinistral), section 6.1 and XRF Ca, section 4) to the Greenland $\delta^{18}\text{O}$ (NGRIP; NGRIP members 2004) and Antarctic methane ice core records (Parrenin et al 2007, Loulergue et al 2008) were used to determine the age model for the MD04-2822 sediments. In addition, tephrochronology (method of preparation for geochemical analysis is outlined above, section 8.1.1) and radiocarbon dating of monospecific planktonic foraminifera was used. The methodology for the latter is detailed below. All samples were prepared by F. Hibbert with age determinations carried out at the Scottish Universities Environment Research Centre (SUERC) AMS Facility.

9.1. AMS ^{14}C dating

A conventional light microscope was used to pick approximately 1,000 monospecific planktonic foraminifera (one *N. pachyderma* (sinistral) and five *G. bulloides*) of > 250 μm mesh size. Where possible, intervals of species abundance maxima were chosen for dating (i.e. dating of *G. bulloides* during intervals of low % *N. pachyderma* (sinistral)) in order to reduce the effects of mixing within the sediments (Bard et al 1987, 2004). A total of 24 monospecific samples, of 1,000 specimens of >250 μm mesh size whose weight ranged between 8 and 27 mg were analysed. For all but two *N. pachyderma* (sinistral) samples, analyses were carried out on the subpolar species *G. bulloides*.

Accelerator mass spectrometry (AMS) ^{14}C dating was performed at the Scottish Universities Environment Research Centre (SUERC) AMS Facility, East Kilbride, with preparation of the samples to graphite undertaken at the NERC Radiocarbon Laboratory (NERC RCL). Included for analysis were four samples from MIS 5 (2410–2411 cm, 2420–2421 cm and two samples from 2430– 2431 cm); these samples should be beyond the limits of the radiocarbon method and any observed sample ^{14}C activity would therefore be attributable to post-depositional processes, for example, contamination⁶. This background ^{14}C measurement should be similar for all the analysed samples from the core as the material has undergone the same sample handling. The conventional radiocarbon dates were calibrated using the Marine09 calibration curve (Reimer et al 2009) (using OxCal 4.1; Bronk Ramsey 2009).

Further consideration of radiocarbon dating of marine material (including calibration and the marine reservoir effect) can be found within chapter 3 (section 5.2). Details of the radiocarbon dating interval are given in table Table 2.4.

⁶ Samples of MIS 5 age (i.e. beyond the range of the radiocarbon method) were used as an additional procedural blank in order to assess contamination; results from the ‘dating’ of these MIS 5 samples were included in the background estimates of the laboratory – see chapter 3 for a full discussion.

Table 2.4: Conventional and calibrated radiocarbon dates for MD04-2822. Radiocarbon age determinations were calibrated using the Marine09 calibration curve (Reimer et al 2009) within the OxCal (version 4.1, Bronk Ramsey 2009) programme. No additional local marine reservoir correction was added prior to calibration.

Depth	Species	Conventional ¹⁴ C Age ± 1σ error		Calibrated Age (yrs BP) (Marine09; Reimer et al 2009)				Mid-point of 95.4 % probability distribution ± 1 standard deviation		
				68.2 % probability distribution		95.4 % probability distribution		yrs BP	yrs b2k	1 s.d.
0.5	<i>G. bulloides</i>	1,350	35	941	851	971	788	879	929	92
210.5	<i>G. bulloides</i>	9,552	39	10,490	10,370	10,520	10,280	10,400	10,450	120
310.5	<i>G. bulloides</i>	12,472	39	13,979	13,841	14,040	13,780	13,910	13,960	130
390.5	<i>G. bulloides</i>	10,145	40	11,190	11,131	11,216	11,101	11,159	11,209	58
950.5	<i>N. pachyderma</i> (sinistral)	17,200	70	20,147	19,616	20,261	19,579	19,920	19,970	341
1270.5	<i>G. bulloides</i>	19,635	85	23,142	22,620	23,370	22,512	22,941	22,991	429
1310.5	<i>G. bulloides</i>	19,830	62	23,440	22,980	23,510	22,665	23,088	23,138	423
1490.5	<i>N. pachyderma</i> (sinistral)	21,015	70	24,780	24,440	24,946	24,340	24,643	24,693	303
1750.5	<i>G. bulloides</i>	24,639	109	29,326	28,837	29,435	28,575	29,005	29,055	430
1790.5	<i>G. bulloides</i>	25,495	100	30,198	29,756	30,262	29,558	29,910	29,960	352
1800.5	<i>G. bulloides</i>	25,225	108	29,843	29,445	30,162	29,413	29,788	29,838	375
1890.5	<i>G. bulloides</i>	29,315	167	33,891	33,108	34,437	32,979	33,708	33,758	729
1921.5	<i>G. bulloides</i>	30,058	184	34,684	34,100	34,765	33,675	34,220	34,270	545
1950.5	<i>G. bulloides</i>	31,661	221	36,266	35,315	36,406	35,120	35,763	35,813	643
2000.5	<i>G. bulloides</i>	34,171	299	39,059	38,056	39,462	37,513	38,488	38,538	975
2020.5	<i>G. bulloides</i>	34,609	312	39,541	38,711	40,238	38,540	39,389	39,439	849
2040.5	<i>G. bulloides</i>	36,251	446	41,479	40,619	41,885	40,070	40,978	41,028	908
2060.5	<i>G. bulloides</i>	38,876	617	43,326	42,361	43,995	42,016	43,005	43,055	990
2090.5	<i>G. bulloides</i>	41,664	869	45,539	44,298	46,345	43,564	44,954	45,004	1391
2112.5	<i>G. bulloides</i>	44,792	1325	48,920	46,336	<i>Out of range</i>	45,837	n/a	n/a	n/a

CHAPTER 3¹: Chronostratigraphy

Age control for the MD04-2822 record has been primarily achieved via an event stratigraphy approach encompassing the following methods:

1. tuning of the benthic $\delta^{18}\text{O}$ record to globally averaged benthic stacks;
2. tuning of the surface proxies to the Greenland ice core $\delta^{18}\text{O}$ record;
3. tuning of the surface proxies to the Antarctic methane record;
4. tephrochronology and
5. radiocarbon dating.

Details of these methods are outlined in this chapter. An evaluation of the event stratigraphy approach is given in chapter 4, with reference to examples from the MD04-2822 sediment core.

The reader will note that several age models have been constructed for certain portions of the MD04-2822 record. These all follow an event stratigraphy approach but the choice of tuning ‘target’ is governed by the temporal scale under investigation. These different age models are more fully outlined in the appropriate section of the thesis. For instance, the initial MD04-2822 stratigraphy was placed on an age model using all the methods outlined above, whereas within chapter 7 (MIS 5e) the age model was constructed using the matching of the MD04-2822 benthic $\delta^{18}\text{O}$ record to radiometrically determined ages for sea level stillstands (after Shackleton et al 2002). The reasons for adopting a different tuning ‘target’ are set out in the appropriate section. The following chapter focuses on the construction of the age model for the entire MD04-2822 core and evaluates the proxy records used.

1. Orbital tuning of the benthic stable isotope record

Marine Isotope Stages (MIS) were first identified by Emiliani (1955) and have been used consistently for over fifty years as a means of age control within marine sediments. The $\delta^{18}\text{O}$ of foraminiferal calcite ($\delta^{18}\text{O}_{\text{Mineral}}$) is a function of temperature (T) and $\delta^{18}\text{O}$ of the water ($\delta^{18}\text{O}_{\text{Water}}$) in which the calcite formed (equation 1) and is therefore intimately linked to the global hydrological cycle, primarily as a function of the global ice volume and salinity (equation 2):

$$\Delta\delta^{18}\text{O}_{\text{Mineral}} = \Delta\delta^{18}\text{O}_{\text{Water}} + \Delta\delta T \quad (1)$$

$$\Delta\delta^{18}\text{O}_{\text{Mineral}} = (\Delta\delta_{\text{GIV}} + \Delta\delta_{\text{Local}}) + \Delta\delta T \quad (2)$$

Shackleton (1967) demonstrated the correlation between the benthic $\delta^{18}\text{O}$ and global ice volume: this relationship has allowed the global sea-level signal to be distinguished and marine records to be aligned on a common timescale.

¹ This chapter forms the basis of the chronostratigraphy section of *Hibbert FD*, Austin WEN, Leng MJ, Gatliff RW. 2010. British Ice Sheet dynamics inferred from North Atlantic ice-rafted debris records spanning the last 175 000 years. *Journal of Quaternary Science* 25(4): 461–482 doi. 10.1002/jqs.1331

The creation of globally averaged stacks of benthic foraminiferal $\delta^{18}\text{O}$ provide reference features that facilitate correlation and improve the signal-to-noise ratio within the climate signal (Lisiecki and Raymo 2005) as well as facilitating age control. These stacks (e.g. Imbrie et al 1984, Lisiecki and Raymo 2005) assume changes in benthic $\delta^{18}\text{O}$ are synchronous both within and between ocean basins.

MIS stratigraphies commonly utilise either astronomical forcing to underpin the global $\delta^{18}\text{O}$ stack (e.g. Martinson et al 1987) or radiometric dating of fossil sea level markers such as coral terraces (e.g. Broecker and van Donk 1970, Shackleton et al 2002). A brief review of these approaches is given in the following sections.

1.1. Astronomical forcing of Global Ice Volumes (SPECMAP and LR04)

The stack of Pisias et al (1984) is an averaged record of seven benthic records and forms the basis of the widely used SPECMAP stacks. SPECMAP consists of two chronologies: the high-resolution 0–300 kyr timescale of Martinson et al. (1987) and the longer timescale, extending to 800 kyr, of Imbrie et al (1984). The shorter-term, higher-resolution timescale of Martinson et al (1987) was chosen for the age model tuning of MD04-2822 and so only this age model is discussed further.

The SPECMAP age model (Martinson et al 1987) is based upon orbital parameters: the astronomical forcing of ice ages via variations in seasonal and latitudinal insolation (e.g. Croll 1864; Milankovitch 1941; Broecker and van Donk 1970; Hays et al 1976). This orbitally forced age model was transferred to the stacked isotope stratigraphy of Pisias et al (1984) via a mapping function; the transfer was assumed to maintain the integrity of the original and the final error envelope has an average error of ± 5000 years (Martinson et al 1987). Recent U/Th dating of corals suggests this may be an overestimation of error (Thompson and Goldstein 2006).

Both the SPECMAP stack and age model are based upon relatively few records. Since their publication, increasing numbers of long, high-resolution benthic $\delta^{18}\text{O}$ records have become available. This, in conjunction with the call for a palaeoceanographic ‘type section’ (e.g. Alley 2003), has prompted the construction of other stacks: *inter alia* Shackleton (1995), Karner et al (2002), Huybers and Wunsch (2004) and Lisiecki and Raymo (2005).

Due to the relatively large number of Atlantic cores used in their stack, the benthic $\delta^{18}\text{O}$ record of MD04-2822 was compared to the high resolution LR04 stack (Lisiecki and Raymo 2005). The age model for the LR04 stack differs from SPECMAP in that it is not solely constrained by orbital parameters. The stack was aligned to a simple model of ice volume alongside average sedimentation rates. However, this is not effective for the youngest portion of the stack where uncompact, sometimes ‘oversampled’, sediments may distort sedimentation rates² (e.g. Skinner and McCave, 2003). The radiocarbon dated benthic $\delta^{18}\text{O}$ record of Waelbroeck et al (2001) has been used for the 0–22 kyr portion and the Shackleton et al (2000) high-resolution Iberian margin planktonic $\delta^{18}\text{O}$ record, tuned to the $\delta^{18}\text{O}$ Greenland ice core, as age control for

² For an example of this phenomenon from the MD04-2822 record and a means of correcting for this coring artefact, the reader is directed to chapter 5.

the 22–120 kyr portion of the LR04 stack. These age control points have been anchored by the U/Th-dated age of 130 kyr for Termination II of Bard et al (1990) and Stein et al (1993). Whilst this stack offers increased resolution, age control beyond ca. 130 kyr is primarily derived from astronomical parameters. Errors are estimated to be ~4kyr for the 0 to 1 Myr portion of the stack (Liseicki and Raymo 2005).

1.2. Radiometric Age Constraints on benthic $\delta^{18}\text{O}$ stacks

The benthic $\delta^{18}\text{O}$ record may also be used as a proxy for global sea level (Shackleton, 1967); therefore U/Th-dated sea-level reconstructions from coral terraces can and should provide useful constraints for $\delta^{18}\text{O}$ events within orbital tuned age models such as SPECMAP. Recent improvements in precision and accuracy of U/Th coral terrace age determinations by thermal ionisation mass spectrometry (TIMS) mean that errors associated with this technique have been reduced from around $\pm 6,000$ to $\pm 1,000$ years. These dating improvements has been used to challenge (e.g. Winograd et al 1992; Henderson and Slowey 2000; Gallup et al 2002) the orbitally derived ages of Martinson et al (1987).

For example, a key constraint of both the SPECMAP timescale of Martinson et al (1987) and the LR04 age model (Liseicki and Raymo 2005) is the timing of the MIS 6/5 transition; respectively 129.8 kyr \pm 3,050 years (Martinson et al 1987, their Table 2) and 130 kyr for LR04 (from Bard et al 1990, Stein et al 1993; Liseicki and Raymo 2005). Recent work utilising radiometric U/Th dating of coral terraces and sea level estimates provide additional constraints on Termination II that suggest older ages than the orbitally derived SPECMAP age for this climatic marker: for example, 140 kyr (Winograd et al 1992), 135 kyr (Henderson and Slowey 2000), 132 kyr (Shackleton et al 2002).

Many U/Th age determinations assume a closed system, whereby there is no loss or gain of U and Th except by radioactive decay in the coral since death. The assumption can sometimes produce unreliable age estimates (e.g. Gallup et al 1994) and an open system, where U-series daughters are redistributed, can occur. The work of Thompson and Goldstein (2006) attempted to address the problems of published closed-system equations by recalculating assuming an open system and a relatively continuous record of sea-level change was produced for the last 240 kyr.

In addition, the authors identified U/Th ages that correspond to the Pisias et al (1984) benthic $\delta^{18}\text{O}$ stack; these therefore can be used as tie-points for a $\delta^{18}\text{O}$ stratigraphy independent of orbital tuning. The form of these two records is striking and the average difference in the age determinations between the Thompson and Goldstein (2006) and Martinson et al (1987) timescales is 1,100 years; however, divergence in the chronologies at the transition from the end of MIS 3 to the LGM and the MIS 7/6 boundary do occur. As discussed above, these authors suggest SPECMAP error estimates of $\pm 5,000$ years to be an overestimation. The validity of this approach is still debated; Hearty et al (2007), point out that the sea level curve produced by Thompson and Goldstein (2006) does not resemble any geologically derived sea level (for MIS 5e) and suggest that their corrected ages display a ‘systematic diagenetic shift rather than a temporal correction’

However the direct conversion of benthic $\delta^{18}\text{O}$ to global ice volumes and sea level is problematic for two reasons. Firstly, the $\delta^{18}\text{O}$ of the foraminiferal shell is a product of both the $\delta^{18}\text{O}$ of the seawater and a thermodynamic fractionation component that is a function of calcification temperature (Epstein et al 1953, Shackleton 1974). Secondly, the $\delta^{18}\text{O}$ of seawater is a function of the mean ocean $\delta^{18}\text{O}$, which reflects continental ice volumes and the average $\delta^{18}\text{O}$ of continental ice, as well as local hydrological effects (e.g. Labeyrie et al 1987, Skinner and Shackleton 2005). These are discussed further in the following section.

1.3. Influences upon the benthic $\delta^{18}\text{O}$

The utility of benthic $\delta^{18}\text{O}$ as a stratigraphic tool and concerns regarding implicit assumptions of the $\delta^{18}\text{O}$ response to both astronomical forcing and local influences e.g. hydrographic conditions have lead some to question our ability to use the benthic $\delta^{18}\text{O}$ stratigraphy at sub-orbital timescales. These include: variations between ocean basins (Skinner and Shackleton 2005); that benthic $\delta^{18}\text{O}$ need not scale consistently with sea level change (e.g. Skinner and Shackleton 2005); the influence of local hydrographic changes (e.g. Labeyrie et al 1987).

1.3.1. Synchronicity of $\delta^{18}\text{O}$ responses

Changes in benthic $\delta^{18}\text{O}$ are assumed to be synchronous across ocean basins within $\delta^{18}\text{O}$ stacks (e.g. Imbrie et al 1984, Lisiecki and Raymo 2005). The validity of this assumption appears to be corroborated by observations for the Last Glacial Maximum (LGM) where radiocarbon ages of aligned stack $\delta^{18}\text{O}$ features agree to within $\sim 1,000$ years³ (Duplessy et al 1991); i.e. if changes are asynchronous, then there should be significant age uncertainties for age models based upon benthic $\delta^{18}\text{O}$ alignment.

However, Skinner and Shackleton (2005) reveal a significant lag (~ 4 kyr) in the response of $\delta^{18}\text{O}$ in the Pacific compared to the Atlantic and argue that these age discrepancies are a product of late temperature increases in the Pacific, as well as millennial scale hydrographic changes in the Atlantic. Lisiecki and Raymo (2009) also demonstrate that large changes in the benthic $\delta^{18}\text{O}$ (e.g. across terminations), are indeed diachronous between the Atlantic and the Pacific. A significant temporal difference has also been identified in the rate of transfer between the two oceans in modelling studies (e.g. Wunsch and Heinbach 2008).

These large discrepancies in the timing of benthic $\delta^{18}\text{O}$ changes could produce significant age model errors when based upon alignment to a stack or in using the benthic $\delta^{18}\text{O}$ record as a proxy for global ice volume changes (Skinner and Shackleton 2005, Lisiecki and Raymo 2009). Whilst seawater $\delta^{18}\text{O}$ changes are not synchronous at millennial timescale (e.g. Skinner and Shackleton 2005), oceanic mean $\delta^{18}\text{O}$ will represent global ice volume changes over longer timescales (multi-millennial), and an individual benthic $\delta^{18}\text{O}$ record will record both global glacio-eustatic changes as well as local hydrographical changes (temperature and deep water $\delta^{18}\text{O}$) (Skinner and Shackleton 2006) which may lead to possible ‘over-

³ This is comparable to the approximate mixing time of the ocean ($\sim 1,000$ years).

printing' by local influences on the global ice volume signal i.e. deep water temperature and salinity changes (e.g. Duplessy et al 2007).

1.3.2. *Influence of hydrographic variations on $\delta^{18}\text{O}$ (inter- and intra-basin)*

In aligning benthic $\delta^{18}\text{O}$ records to the global stacks, changes in deep water temperatures have the potential to produce significant offsets between records (see equations 1 and 2). Local hydrographic conditions may influence a benthic $\delta^{18}\text{O}$ record by, for example, the influence of brine formation (e.g. Dokken and Jansen 1999) and changes deep ocean temperatures (e.g. Skinner and Shackleton 2005). Deep water temperature changes are especially important across terminations in the North Atlantic where temperature and salinity changes account for more than half the observed glacial-interglacial change in benthic $\delta^{18}\text{O}$ (Shrag et al 1996, Adkins et al 2002). Furthermore, benthic $\delta^{18}\text{O}$ changes within the same oceanic basin may also produce asynchronous responses, with rapid transmission to intermediate depths and an additional ~1,500 years for the 'signal' to reach deep water sites (Labeyrie et al 2005, Waelbroeck et al 2006).

Such diachronous changes in benthic $\delta^{18}\text{O}$ also have important implications for the use of the benthic $\delta^{18}\text{O}$ as a proxy for global ice volume changes. The timing of benthic $\delta^{18}\text{O}$ change across terminations may differ significantly from ice volumes or sea level changes due to local hydrographic changes and/or delays in meltwater reaching the deep Pacific (Skinner and Shackleton 2005). Indeed, at many North Atlantic sites, benthic $\delta^{18}\text{O}$ may significantly lead global ice volume changes due to early changes in hydrographic conditions (Skinner and Shackleton 2006, Waelbroeck et al 2008).

It has been suggested that Atlantic benthic $\delta^{18}\text{O}$ leads global ice volume changes during Terminations I and II (Skinner and Shackleton 2006, Waelbroeck et al 2008) with consistently different amplitudes of $\delta^{18}\text{O}$ change between basins for the last 5 terminations (Lisiecki and Raymo 2009). Amplitudes of isotopic stage and sub-stages are slightly larger in the Atlantic than the Pacific (Zahn and Mix 1991, Waelbroeck et al 2002) possibly due to the larger temperature and salinity changes (Shrag et al 1996, Adkins et al 2002) associated with changes in hydrographic conditions (Skinner and Shackleton 2005).

Therefore, aligning benthic $\delta^{18}\text{O}$ records from different oceanic basins or at different depths within the same basin, may produce age model errors of several thousand years; Lisiecki and Raymo (2009) estimate termination mid-points may differ by as much as 4 kyr between the Atlantic and Pacific and that 'termination mid-points make particularly poor stratigraphical tie-points'. Such age uncertainties vary between terminations due to differing ice volumes at the glacial maximum and/or differing insolation forcing (e.g. Parrenin and Paillard 2003). As a consequence, Lisiecki and Raymo (2009) also assign similar uncertainties (~ 4 kyr) to the use of benthic $\delta^{18}\text{O}$ as a proxy of global ice volume changes across terminations.

1.3.3. *Assumptions, resolution and discrepancies in age of orbitally derived age models*

The assumption of simplistic, smooth response to changing insolation was questioned by Shackleton et al (2002). An underlying hypothesis within the Martinson et al (1987) timescale is the assumption of a smoothly varying response of palaeoclimate

records to changes in insolation, whilst a phase lag between forcing and response is implicit in insolation-driven ice-sheet models (Imbrie and Imbrie, 1980). This is believed to be particularly problematic for the last interglacial where such assumptions prohibit estimates of the duration of an extended interval (i.e. the MIS 5e plateau) when northern ice volumes were ‘static’⁴ at a size no greater than present (Shackleton et al 2002).

Problems of resolution and use on short(er) i.e. millennial timescales of the global $\delta^{18}\text{O}$ stacks are noted within (e.g. Shackleton et al 2003, Skinner and Shackleton 2005, 2006). In particular for the Middle Pleistocene, resolution is typically 50 kyr whilst most major climatic and palaeoenvironmental units are typically in the order of 10 kyr (i.e. half a precession cycle) rather than half an eccentricity cycle (~ 50 kyr) (Shackleton et al 2003).

Considerable discrepancies exist between the orbitally derived ages of key events, such as Termination II, when compared to U/Th dated coral terraces (e.g. Thompson and Goldstein 2006). Whilst lags between the Pacific and Atlantic (e.g. Skinner and Shackleton 2005) point to uncertainties in the timing of events (~4 kyr) during Terminations and therefore making the mid-point of a termination a ‘particularly poor stratigraphic tie-point’ (Lisiecki and Raymo 2010). Whilst there is a reasonable degree of consistency between many estimates of the mid-point of Termination II, considerable debate remains as to the robustness of this chronostratigraphical marker in benthic $\delta^{18}\text{O}$ records.

1.4. Other limitations

A major limitation to the successful tuning of the benthic $\delta^{18}\text{O}$ record of MD04-2822 is the quality of the benthic record itself through certain stratigraphic intervals. The abundance of *C. wuellerstorfi* is highly variable, with very low numbers within portions of MIS 2 and 6.

As outlined above, influences on deep-water $\delta^{18}\text{O}$ are potentially complex. At intermediate water depths in the northeast Atlantic, an important influence on benthic $\delta^{18}\text{O}$ is the formation of deep-water brines, whereby sea-ice-derived brines and their $\delta^{18}\text{O}$ signature are transferred to the deep ocean. Dickson et al (2008) postulate for MD95-2006 a core located approximately 83 km away from MD04-2822 at a similar water depth, millennial-scale changes in benthic $\delta^{18}\text{O}$ through MIS 3 are related at least in part to the formation of low salinity, deep-water brines. Indeed these changes in the benthic $\delta^{18}\text{O}$ possess not only a component of local brine formation (i.e. on the Hebridean Shelf) but are perhaps indicative of wider regional processes linked to Nordic Sea overflow routes into the North Atlantic (Dokken and Jansen 1999; van Kreveld et al 2000).

Despite these limitations, the close correspondence between the results of the independent tuning of the benthic $\delta^{18}\text{O}$ record to the two orbitally based SPECMAP and LR04 age models, in addition to the U/Th-dated benthic stack features of Thompson

⁴ ‘Static’ is taken by the authors to include ± 10 m relative sea level change

and Goldstein (2006), provide an initial, albeit imprecisely correlated chronology from which further refinements can be made.

1.4.1. Tuning of MD04-2822 benthic $\delta^{18}\text{O}$ to SPECMAP and LR04

The tuning of the MD04-2822 *Cibicides wuellerstorfi* $\delta^{18}\text{O}$ record for MD04-2822 to the global stacks was undertaken by visually matching stratigraphical features common to both. For example, some of the features identified by Pisias et al (1984) could be identified in the MD04-2822 record (Figure 3.1). These could then be assigned ages using the age model of Martinson et al (1987). Depths intermediary to the tie- points were assigned ages via linear interpolation between tie- points. The same approach was used for the LR04 stack (Lisiecki and Raymo 2005). The resulting age models, using both these using targets, are given in Figure 3.1; tie-point are given in Appendix C₁.

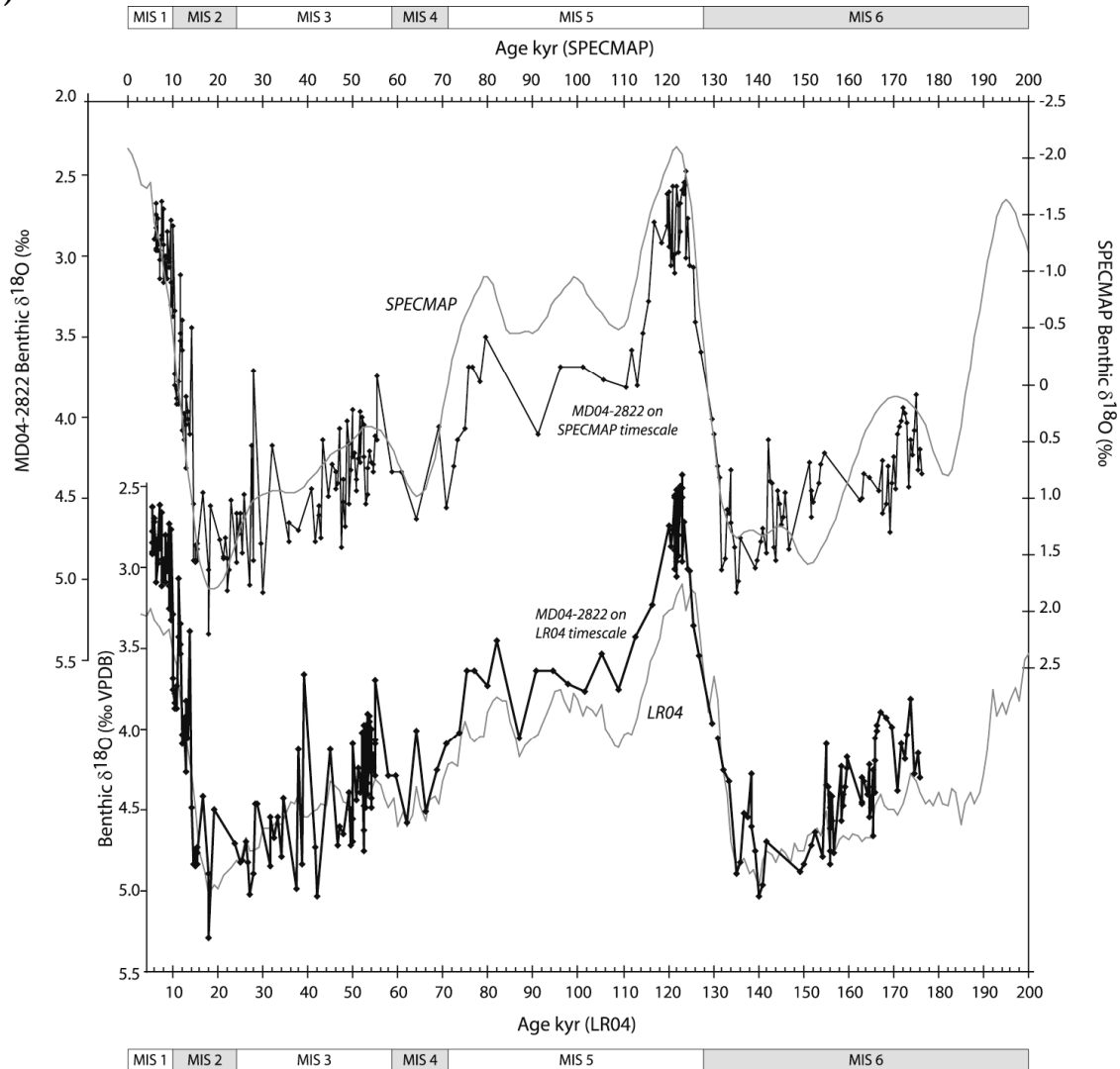
The independent tuning to both SPECMAP and LR04 compare favourably; the most marked differences are within the older portion of the record (MIS 6) where alternative correlations are possible. The increased variance of the LR04 age model may allow greater confidence in assigning tie-points. Intermediary depths as well as core top and bottom estimates were also obtained by linear interpolation between tie-points.

The Thompson and Goldstein (2006) ‘corrected’ radiometric ages were correlated to the SPECMAP isotope features of Pisias et al (1984) and where appropriate, these have been plotted alongside the benthic tuned age-depth models (Figure 3.1B). These ages mainly fall within the error estimates for the tie-points using both the SPECMAP and LR04 stacks. However, the veracity of these ‘corrected’ ages remains contentious (e.g. Hearty et al 2007).

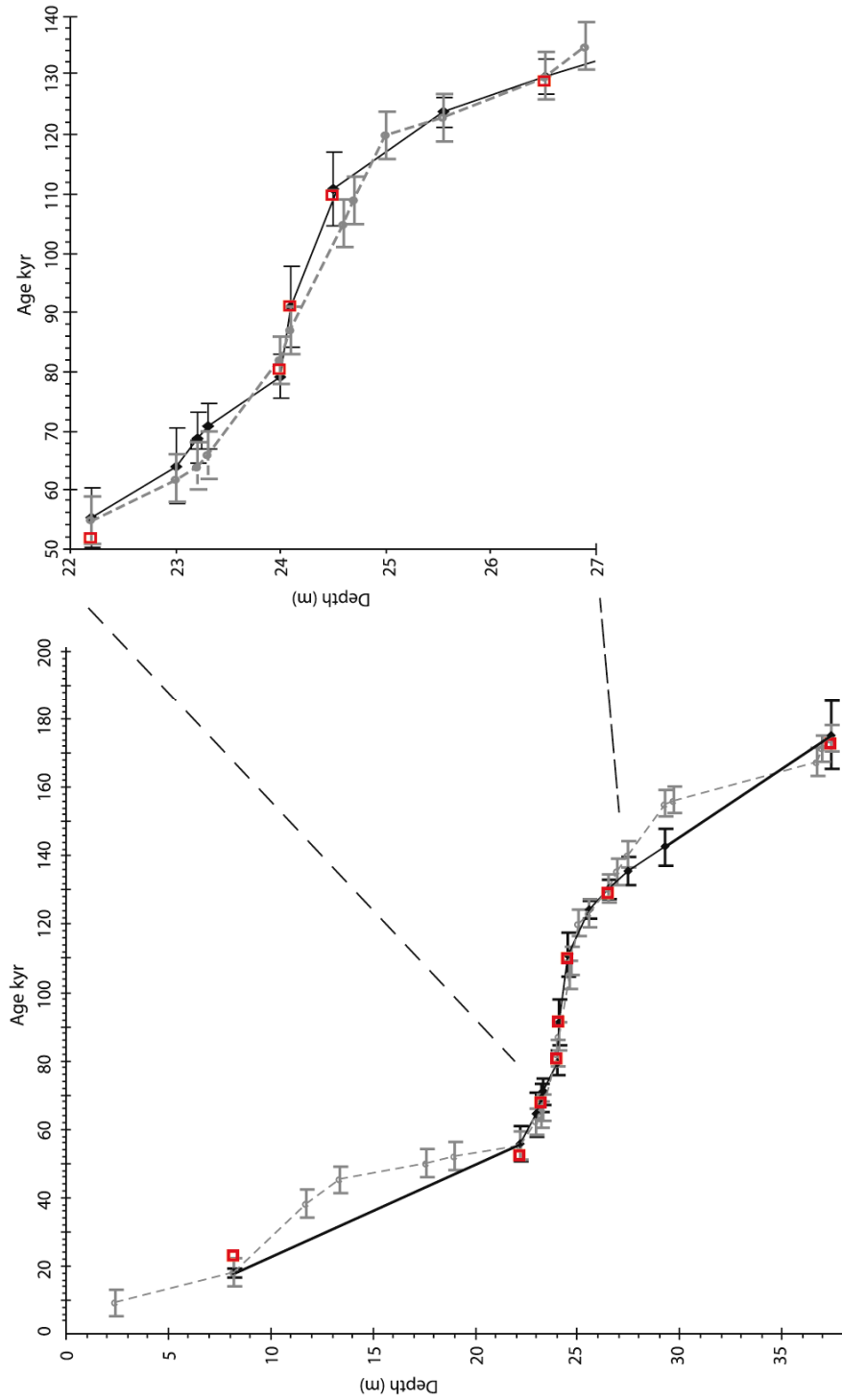
CHAPTER 3:
Chronostratigraphy

Figure 3.1: a) top MD04-2822 benthic $\delta^{18}\text{O}$ on the SPECMAP (Martinson et al 1987) timescale (black) and the SPECMAP stack (grey), bottom MD04-2822 benthic $\delta^{18}\text{O}$ on the LR04 timescale (black) and the LR04 stack (Lisecki and Raymo 2005). MIS designations are after Imbrie et al (1984).
b) Age-depth models resulting from benthic tuning (opposite).

(a)



(b) Age-depth models resulting from benthic tuning: SPECMAP tuned-black filled diamonds; LR04 stack grey dashed lines; red open boxes are the Thompson and Goldstein (2006) radiometric ages for isotope features identified by Pisias et al (1984). Error estimates for SPECMAP are those given in Martinson et al (1987), error estimates for the LR04 are ~4 kyr (Lisieck and Raymo 2005), 2σ error estimates for the Thompson and Goldstein (2006) fall within the symbol. Right panel is an enlargement of the 22-27 m (~50-140 kyr) portion.



2. Greenland ice core tuning to surface proxies

The surface water proxies for MD04-2822 present a fairly complete record in contrast to the somewhat patchy the benthic $\delta^{18}\text{O}$ record. As such, the MD04-2822 age model was refined by additional, independent tuning. Instead of a globally averaged stack, the surface water proxies are tuned to the NGRIP (ss09sea timescale) $\delta^{18}\text{O}$ ice record (NGRIP members 2004).

2.1. Dansgaard-Oeschger (D/O) events within the Greenland ice and marine sediment records

A conspicuous feature common to both the Greenland $\delta^{18}\text{O}$ ice core records (e.g. GISP2, GRIP, NGRIP) and the surface proxies of MD04-2822 is the presence of a series of abrupt millennial-scale climate oscillations, the Dansgaard–Oeschger (D/O) events first recognised in the Greenland ice cores (e.g. Dansgaard et al 1993) and subsequently in North Atlantic marine sediment cores (e.g. Bond et al 1993; Bond and Lotti 1995). The approach of tuning marine and Greenland records, using the D/O features common to both, assumes the synchronicity of change in surface waters and atmospheric temperature changes over Greenland (e.g. Bond et al 1993; Shackleton et al 2000). The Greenland $\delta^{18}\text{O}$ ice core records (NGRIP on the ss09sea timescale, NGRIP members 2004), while currently extending to only ca.123 kyr, do provide high-resolution, well-dated records with which the MD04-2822 surface water proxies may be correlated.

The D/O events typically begin with an abrupt warming in Greenland of ~ 5 to 10 °C over a few decades (or less) followed by a gradual cooling over several hundred or thousand years. The cooling phase often ends with an abrupt cooling into stadial conditions (Dansgaard et al 1993). The D/O events have been linked to changes in thermohaline circulation, which together with atmospheric circulation, may account for the global expression of these events (Keigwin et al 1994, Voelker 2002, Clark et al 2002).

Mechanisms explaining the DO events include: thermohaline circulation bistability (Broecker et al 1985); oscillations in the volume transport of the thermohaline circulation (i.e. the bi-polar see-saw of Broecker et al 1990); switching between two modes of thermohaline circulation with freshwater forcing (e.g. Alley et al 2001, Ganopolski and Rahmstorf 2001); latitudinal shifts of convection in the North Atlantic ocean (Rahmstorf 1994); stochastic resonance (Gammaitoni et al 1998; Alley et al 2001, Ganopolski and Rahmstorf 2002); solar forcing mechanisms (Denton and Karlen 1973; Bond et al 2001; Braun et al. 2005) and; sea-ice growth within a ‘cold’ climate and a corresponding weakening of thermohaline overturning (Loving and Vallis 2005).

2.2. Greenland Ice core Chronologies

Currently there are three⁵ Greenland ice core records regularly used as means of age control within marine sediment sequences; GISP2 (75.2°N, 38.3°W), GRIP (75.2°N, 37.3°W) and NorthGRIP (hereafter referred to as NGRIP, 75.1°N, 42.3°W). The following section briefly details each ice core, in particular their chronologies. The strong similarities, in general, between the $\delta^{18}\text{O}$ records of the different ice cores suggests that the dominant influence was regional climate change and that differences in detail are most likely due to basal deformation and/or geographical gradients in atmospheric isotope ratios (Johnsen et al 2001, Rasmussen et al 2008).

The GISP2 ice core chronology is based upon annual layer counting, with age uncertainties estimated at $\pm 2\%$ to 40 kyr (beyond which counting uncertainties become much more significant at ± 5 to 10%) (Meese et al 1997). The GRIP timescale (Johnsen et al 1995) is based on layer counting to 15 kyr BP and glaciological modelling for the older portion, similarly the ss09sea timescale developed by Johnsen et al (2001) is a combination of layer counting and glaciological modelling. The ss09sea timescale has subsequently been transferred to the NGRIP $\delta^{18}\text{O}$ record (NGRIP members 2004). The GRIP and GISP2 ice core records (and chronologies) compare favourably to one another in the main; a 3 kyr age difference is evident at ca. 50 kyr (Svensson et al 2006).

Recently the DYE-3, GRIP and NGRIP ice cores have been dated in parallel by annual layer counting as part of the Greenland Ice Core Chronology 2005 (GICC05) project (Andersen et al 2006, Rasmussen et al 2006, Svensson et al 2006, 2008, Vinther et al 2006), which has allowed the synchronisation of records on a common timescale. GICC05 now extends to 60 kyr, incorporating Greenland Interstadial 17 (Svensson et al 2008). The ss09sea timescale compares reasonably well throughout with GICC05 (0–60 kyr), resulting in a maximum age difference of 900 years; only in the 18–26 kyr and 48–60 kyr intervals does the age difference exceed 500 years. The differences may be due to errors in the counted timescale, deviations from the modelled behaviour in the $\delta^{18}\text{O}$ -accumulation relationship within the ss09sea timescale, or a combination of these. The GICC05 age scale incorporates explicit age uncertainty estimates: 1% within the Holocene and 5% within the glacial portion (Svensson et al 2008).

The Greenland ice cores and their associated chronologies are taken to represent the current best estimate of North Atlantic palaeoclimate event stratigraphy (Skinner 2008, Lowe et al 2008, Southon 2004). Comparison between the Greenland ice core records (and their age models) to other climate archives (e.g. marine) with independent age control 'should' confirm the regional event stratigraphy and chronology of events.

Shackleton et al (2004) utilised the paired coral radiometric and ^{14}C age determinations (Fairbanks et al 2005) as age control for the planktonic isotope record of MD95-2042 (Iberian Margin, 37°48'N, 10°10' W) which closely resembles the

⁵ Other ice cores have been drilled (Camp Century, Dye-3, Renland) from varying locations in Greenland however the three specified above have been the core most commonly used as a tuning 'target' for marine sediment cores. The NEEM (North Greenland Eemian Ice Core Drilling <http://nbi.ku.dk>) project is currently underway to recover ice from the last interglacial.

GRIP $\delta^{18}\text{O}$ record. The close correspondence of the planktonic isotope record and the GRIP $\delta^{18}\text{O}$ enabled the radiometric ages for the D/O events, identified in both records, to be transferred to the Greenland ice core (the GRIP.SFCP04 timescale). This timescale sought to provide an 'absolute' calibration of the Greenland ice core records in an attempt to reconcile stratigraphic integration of ice, marine and speleothem records with absolute age control. The resulting age model (GRIP.SFCP04) suggests older (up to 1.2 kyr) ages for the onset of the D/O events when compared to the age models of GRIP (Johnsen et al 2001), GISP2 (Meese et al 1997) and NGRIP (both the ss09sea, NGRIP members 2004; and the GICC05 timescale, Andersen et al 2006) (Shackleton et al 2004, Svensson et al 2006).

Svensson et al (2006) suggest that either the GICC05 timescale contains errors in the number of annual layers (too few GIS 1 to 3, too many GIS 3 to 8) or that the GRIP.SFCP04 age of GIS 3 is too old. An alternative proposed by Skinner (2008) is that between GIS 2 and 8, marine reservoir corrections for the Iberian margin radiocarbon dates⁶ (see Shackleton et al 2004, Bard et al 2004) are too conservative *and* that the GICC05 timescale is 'missing time'. In effect, an increase radiocarbon marine reservoir for the Iberian margin cannot account for the entirety of the age differences between SFCP04-GRIP, speleothem and GICC05 age scales (as proposed by Svensson et al 2008) between ~24 and 38 ka BP. Although, when correlated with speleothem records (Hulu Cave, Boutavera Cave; Wang et al 2001, 2006) the age differences fall within the maximum counting error for the GICC05 timescale. A combination of 'missing' annual layer counts and variations in the marine reservoir effects is currently proposed to account for the age discrepancies between the GICC05 age scale and other radiometrically determined age scales (Skinner 2008).

The NGRIP ice core is now regarded by many as a standard reference core (e.g. Lowe et al 2008, Wolff et al 2009) as, 'it is complete and continuous through the entire glacial' and 'it has the most complete multi-parameter layer-counted dating⁷ over the last 60 ka' (Svensson et al 2008). The NGRIP $\delta^{18}\text{O}$ record was chosen as the tuning 'target' for MD04-2822 in preference to the GRIP and GISP2 profiles owing to the inferred lack of disturbance within the oldest sections of the NGRIP ice core (NGRIP members 2004). Ice folding and flow, close to the bedrock, are thought to limit the usefulness of basal data from the GRIP and GISP2 ice records (Alley et al 1995). The ss09sea timescale (Johnsen et al 2001, NGRIP members 2004) for the NGRIP $\delta^{18}\text{O}$ record is used as this is the sole chronology that spans the entire ca. 123 kyr currently available within the Greenland ice cores and provides continuity of tuning 'target'. However, this chronology relies upon glaciological modelling as well as layer counting, unlike the GICC05 timescale which is solely based upon layer counting (Andersen et al 2006; Rasmussen et al 2006, Svensson et al 2006, 2008; Vinther et al 2006).

⁶ The marine reservoir age of 500 ± 100 years is applied to the radiocarbon age determinations of MD95-2042 by Shackleton et al 2004. For the same core, Bard et al (1987, 2004a,b) applied a 400 year reservoir age to MD95-2042 samples, Bard (2004a) used a 500 year correction whilst archaeological samples on the Iberian coast yielded reservoir ages in excess of 600 years (Monges Soares (1993). This region currently experiences upwelling, thereby increasing the marine reservoir effect.

⁷ On the NGRIP GICC05 timescale

The chronology for the climatic events for the Last Termination, as recommended by the INTIMATE group (Lowe et al 2008) as the ‘regional stratotype’ for the synchronisation of palaeoenvironmental records within the North Atlantic region, is based upon the mid-point of the $\delta^{18}\text{O}$ within the NGRIP, GRIP and GISP2 records (on the GICC05 timescale). However, as noted by Lowe et al (2008), the task of assigning the timing of these events can be ‘an ambiguous task’. The age estimates contained with the INTIMATE protocol (Lowe et al 2008) are to be regarded as *preliminary*.

In addition to the subjective nature of assigning the transition of the rapid D/O events within the ice records, when used to obtain age control for marine sediments via tuning, the $\delta^{18}\text{O}$ rather than the deuterium excess is used as the ‘tuning target’, which is the ‘clearest indicator of climate change’ (Lowe et al 2008). The deuterium record reflects major reorganisations of the atmospheric circulation which are generally followed by more gradual changes in temperature (as reflected in the $\delta^{18}\text{O}$ record). For example, at the end of the Younger Dryas (GS 1), the abrupt change in deuterium excess occurred over ~20 years or less, whilst the temperature change occurred over ~50 years (Dansgaard et al 1989, Jouzel et al 2005).

The deuterium excess parameter is largely influenced by conditions prevailing in the oceanic moisture source which provide the polar precipitation (Craig and Gordon 1965, Merlivat and Jouzel 1979, Jouzel et al 2007). However, all factors influencing the record can not adequately be accounted for, for example, variations in the isotopic content of surface waters due to large iceberg discharges (Jouzel et al 2007), although this effect is thought to be minor as areas most influenced by large iceberg discharges would also experience lowered evaporation (Roche and Paillard 2005). The contribution of large, local temperature changes to the deuterium excess record, rather than solely changes in the source of precipitation, cannot be excluded from reconstructions (Jouzel et al 2007, Landis et al 2005). Additionally, the effect of seasonality upon precipitation delivered to Greenland, due to atmospheric circulation changes (resulting from e.g. the Laurentide ice sheet) as well as extended sea ice cover within the North Atlantic, is an important factor previously underestimated in attempts to reconstruct temperature records on the glacial-interglacial timescales from the deuterium excess records, leading to wide discrepancies in the reconstructions (Jouzel et al 2007). The Greenland ice core deuterium excess records have a clear affinity with the D/O events (Jouzel et al 2007) first identified within the ice core $\delta^{18}\text{O}$ records (e.g. Dansgaard et al 1993), as well as marine sediment cores (e.g. Bond et al 1993).

Whilst the $\delta^{18}\text{O}$ record of the rapid warming of the D/O events has generally been preferred⁸ for the translation of age to marine sediment cores, a large body of evidence now exists to suggest that the relationship between the $\delta^{18}\text{O}$ of the ice core record and temperature is not straightforward (Wolff et al 2009); the translation of isotopic change to temperature is variable in time, probably due to changes in the spatial distribution of precipitation (Jouzel et al 2003; Krinner and Werner 2003). The ‘missing years’ proposed by Skinner may be accounted for in part by difficulties in

⁸ The $\delta^{18}\text{O}$ record reflects temperature changes over Greenland, whilst the marine proxy records (e.g. % *N. pachyderma* (sinistral)) used in correlations are linked to sea surface temperature changes.

discerning annual layers at the height of the last glaciation when accumulation rates over Greenland are low (Andersen et al 2006).

While the refinement of the Greenland chronologies such as the GICC05 timescale with its well-defined uncertainty estimates presents certain advantages, and the problems associated with glaciologically modelled chronologies well documented (i.e. the non linear relationship between $\delta^{18}\text{O}$ and Greenland temperatures), for consistency the NGRIP ss09sea timescale is used as the tuning 'target' for the entire stratigraphy because this record remains the sole Greenland timescale extending to ca. 123 kyr.

2.2.1. Assumption of synchronicity within the tuning approach

Tuning marine and Greenland records, using the D-O features common to both, assumes the synchronicity of change in surface waters, as recorded by proxy records and atmospheric temperature changes over Greenland (e.g. Bond et al 1993; Shackleton et al 2000). The assumption of regional synchronicity of events with Greenland has recently been questioned on a decadal to multi-centennial scale (see Blaauw et al 2010). The authors highlight large dating errors which preclude firm inferences as to the regional synchronicity of a French lake record (Wohlfarth et al 2008) to the Greenland ice cores. Indeed, long-distance correlations, based on matching of climate records, often pre-suppose synchronicity for which no independent evidence is offered (e.g. Wunsch, 2006). However, key chronostratigraphical intervals have been tested using well characterised tephra horizons, present in both the Greenland ice cores and marine sedimentary sequences (e.g. the stratigraphical position and timing of North Atlantic Ash Zones I and II) (see Austin and Abbott 2010, Austin et al 2004, Austin et al 1995, Peters et al 2009). The assumption of synchronicity seems to hold for these investigated intervals within North East Atlantic marine and the Greenland ice cores. For example, the stratigraphical position of the rhyolitic (II-RHY-I) North Atlantic Ash Zone II tephra horizon on the cooling limb of Greenland Interstadial 15 within both the Greenland $\delta^{18}\text{O}$ ice core record and the marine *N. pachyderma* (sinistral) records suggests the synchronicity of these events within the North Atlantic (Austin et al 2004; for further discussion of the assumed synchronicity of marine and ice core records, the reader is directed to chapter 4).

The event stratigraphy approach is not dependent upon key stratigraphic markers such as tephra horizons, although the presence of tephra may significantly reduce uncertainty associated with the visual matching of records. However, events are still presumed to be synchronous; although convincing, NAAZ II can only securely confirm this relationship for GIS 15. The placement of this tephra layer upon the cooling limb of GIS 15 within both the Greenland ice core records and marine sediment cores, is highly suggestive of synchronicity but at present scant evidence is available for other portions of the record to allow a full assessment of the validity of this assumption for the entire glacial. Further research utilising other tephra layers and/or archives would further clarify this issue.

2.2.2. Pacing of the D/O events

The apparent consistency of the timing (~1,500 years) of the D/O events within the Greenland ice core records prompted Rahmstorf (2003) to suggest that they may be

though of as a 'precise clock'. The pacing of the D/O events on a quasi-1,500 year cycle, however, remains debated.

The abrupt warming events within the Greenland ice cores have been found to have periodicities of ~1500 years; Grootes and Stuvier (1997) found prominent peaks within the GISP2 ice core with a period of 1,470 years with other preferred intervals of 3,000 and 4,500 years (Alley et al 2001a, b) i.e. multiples of the quasi-1,500 year period in which 'a beat or two is skipped' (Rahmstorf 2003). Changes in the latitude of NADW formation (i.e. a state change in thermohaline circulation in the North Atlantic) triggered by variations in the freshwater budget of the Nordic Seas may precipitate such events requiring only a very small forcing (not necessarily major ice sheet instability) (Ganopolski and Rahmstorf 2001). The D/O events can be thought of as a switching within the system between two modes of operation with some threshold. As this 'threshold process' is not a strictly a periodical process, a random component (i.e. noise) may enable stochastic resonance to occur (Gammaitoni et al 1998) with the result that not every variation in AMOC results in a D/O type event (Ganopolski and Rahmstorf 2002). An alternative explanation is that the events are 'noise' induced (e.g. Ditlevsen et al 2007, Wunsch 2006). The underlying mechanism remains elusive with both variations in external i.e. solar forcing (e.g. Bond et al 2001, Braun et al 2005) or internal oscillations of the climate system (Broecker et al 1990) proposed.

The quasi-1,470 year period was first noted within the layer counted GISP2 record (Grootes and Stuvier 1997) but this peak was not significant within the GRIP ice core record on the ss09sea timescale (Ditlevsen et al 2005). Analysis of the NGRIP $\delta^{18}\text{O}$ record (NGRIP members 2004) on the GICC05 timescale (Andersen et al 2006, Rasmussen et al 2006, Svensson et al 2006, 2008; Vinther et al 2006), found the recurrence times to be indistinguishable from a random occurrence (Ditlevsen et al 2007). These authors suggest that this is also the case for the GISP2 $\delta^{18}\text{O}$ record and that the D/O events are probably noise induced. However, Shulz (2002) proposed that the onset of the D/O cycles within GISP2 varied by 20 % (± 294 years) around the 1,470 year period but the applicability of the methodology employed has recently been questioned (Braun et al 2010). Rahmstorf (2003) found within the layer counted GISP2 (Meese et al 1997) the 1,470 period to be stable to within a few percent; 12 % for 23 cycles at a 95% confidence interval. This apparent regular timing is suggestive of a periodic forcing, for example, solar forcing or the combinations of several periodic forcings (e.g. Braun et al 2005). However, this hypothesis does not appear consistent with the phase relation between the ^{10}Be (a proxy for solar activity) and $\delta^{18}\text{O}$ (a proxy for Greenland climate) GRIP records (Muscheler and Beer 2006).

The presence of a periodic recurrence of the D/O events remains uncertain. The presence or absence of a periodic 'beating' has implications as to the underlying cause. A periodic recurrence suggests an external origin whilst a non-periodic recurrence may indicate an internal climate mechanism (Ditlevsen et al 2007).

2.3. Tuning of MD04-2822 surface proxies to the NGRIP $\delta^{18}\text{O}$ record (ss09sea timescale)

The Greenland ice core and MD04-2822 surface records were matched using the millennial-scale oscillations (D/O cycles) of the Greenland $\delta^{18}\text{O}$ ice core record, in particular the characteristic rapid warming transitions into D/O events. These features are prominent in the MD04-2822 surface water proxies of percentage abundance of the planktonic foraminifera *N. pachyderma* (sinistral) and XRF core-scanning calcium profile.

The percentage abundance of *N. pachyderma* (sinistral) can be employed as a semi-quantitative measure of sea surface temperature and indicator of the position of the polar front (e.g. Bond et al 1993), while the XRF calcium record obtained by ITRAX core scanning is thought to be primarily driven by biogenic calcium carbonate (Rothwell et al 2006, Crowdace et al 2006). These two surface water proxies are used in conjunction in order to minimise the possibility of ‘mis-tuning’ the records as a result of differences in sampling resolution. The percentage *N. pachyderma* (sinistral) record was sampled every 10 cm⁹; this is of insufficient resolution to resolve the details of all the D/O cycles, most notably within MIS 2 and 3. In contrast, the XRF calcium record has a minimum resolution of 1 cm¹⁰. The similarities between the surface proxies and the NGRIP $\delta^{18}\text{O}$ records are striking, particularly the portion relating to MIS 3, 4 and 5 (Figure 3.2). However, the tuning of the records appears to break down within the LGM until the Younger Dryas/Greenland Stadial 1, due to the absence of pronounced D/O cycles and the dilution of the XRF Ca record with increased terrigenous inputs from an actively glaciated margin. By combining the *N. pachyderma* (sinistral) record with the ITRAX calcium record, the tuning to NGRIP $\delta^{18}\text{O}$ can be optimised.

The rapid transitions into the D/O events were identified and the mid-point of the transition used as a tie-point between the NGRIP $\delta^{18}\text{O}$ record and MD04-2822 (cf. Shackleton et al 2000; Austin et al 2004). Once the tie-points had been assigned, intermediary depth age control was achieved by linear interpolation. Example correlations between the surface proxy data of MD04-2822 and the NGRIP $\delta^{18}\text{O}$ record (ss09sea timescale) are given in Figure 3.2. Tie-points used in the construction of the NGRIP tuned record are given in Appendix C₂.

For the Holocene interval, the correlation was based upon millennial- scale ‘cycles’ observed in the XRF calcium record because the distinct, abrupt D/O events seen in *N. pachyderma* (sinistral) throughout the glacial interval are highly attenuated. However, the same coupling of the atmospheric conditions over Greenland and surface water conditions in the North Atlantic is assumed to persist across the last glacial transition into the Holocene (Bond et al 1997a) and the MD04-2822 calcium data appear to confirm this observation. The ss09sea age scale is relatively imprecise for the Last Termination (Svensson et al 2008, Lowe et al 2008); it is partially modelled rather than layer counted (Svensson et al 2006) and age uncertainties are not quantified (Blockley et al 2004 estimate ss09sea age uncertainties to be at least centennial in

⁹ Additional 1, 2 and 5 cm sampling undertaken within some portions of the core

¹⁰ ITRAX resolution is 2 mm for 18 to 27 m and 34.5 to 37 m of MD04-2822.

magnitude). The advantages of using the NGRIP (GICC05 timescale record) include multi-parameter layer-counted dating for the last 60 kyr and a quantified uncertainty estimate (Andersen et al 2006, Svensson et al 2006, 2008). Chapter 6 concerns the last termination and the NGRIP $\delta^{18}\text{O}$ (GICC05 timescale) is used in preference as the tuning target.

Little age difference is seen between the tuning of the MD04-2822 proxies to the NGRIP $\delta^{18}\text{O}$ record using the ss09sea and GICC05 timescales, indeed the ss09sea timescale tuning falls within the age uncertainties (i.e. the max. counting error) for the GICC05 timescale (Figure 3.3).

When the tuning of the surface proxies to NGRIP $\delta^{18}\text{O}$ (on both the ss09sea and GICC05 timescale) is compared to the benthic tuning to SPECMAP and LR04, the age-depth models compare favourably apart from 8 to 20 m (~ 20 to 60 kyr b2k) where the benthic tuning gives considerably older ages. This is due in part to the difficult task of tuning the patchy benthic record as alternative benthic $\delta^{18}\text{O}$ correlations are possible through this interval (Figure 3.3).

2.3.1. *Estimate of temporal uncertainty of surface proxy tuning*

At present no robust estimate of the age uncertainty associated with the tuning of surface proxies to the Greenland ice core is available. The *a priori* assumption of the synchronicity of events within different palaeo-archives may not hold in all instances (see e.g. Blaauw et al 2010 and comment by Austin and Abbott 2010) and the vagaries of visual matching ('wobble-matching') may impede the consistent correlation of the different records by different workers. Additionally, there is some suggestion that all variations within the sub-polar marine environment may not be registered within the Greenland ice cores (e.g. subtle variations in sea surface temperatures experienced within the sub-polar North Atlantic may not be recorded within the Greenland $\delta^{18}\text{O}$ signal; please see chapter 4).

The stratigraphical position of the mid-point of the transition into the interstadial within the MD04-2822 proxy records can be difficult to position due to the effects of bioturbation and the resolution of the proxy data. Intermediary points (i.e. those between the tie-points) are determined by linear interpolation between those points. Whilst expedient, this may not reflect the 'true' sedimentation; the variable sedimentation through the record can not be accounted for between tie-points.

The ice core chronological uncertainties are only part of the total age error for the tuning to Greenland (for example the often problematic designation of annual layers, gas versus ice age; e.g. Scwander et al 1997). The GICC05 timescale attempts to quantify this (i.e. the maximum counting error) but no such estimates are currently available for the ss09sea timescale. Worth remembering is the cautionary tone struck by Skinner (2008), 'a given chronostratigraphy is best viewed as a hypothesis'.

Figure 3.2: A) NGRIP $\delta^{18}O$ record on the ss09sea timescale (NGRIP members 2004); B) MD04-2822 ITRAX XRF Ca profile and C) % *N. pachyderma* (sinistral). Example correlations given by dashed grey line. Vertical red line denoted the stratigraphical position of NAAZ II within both the NGRIP $\delta^{18}O$ and MD04-2822 records.

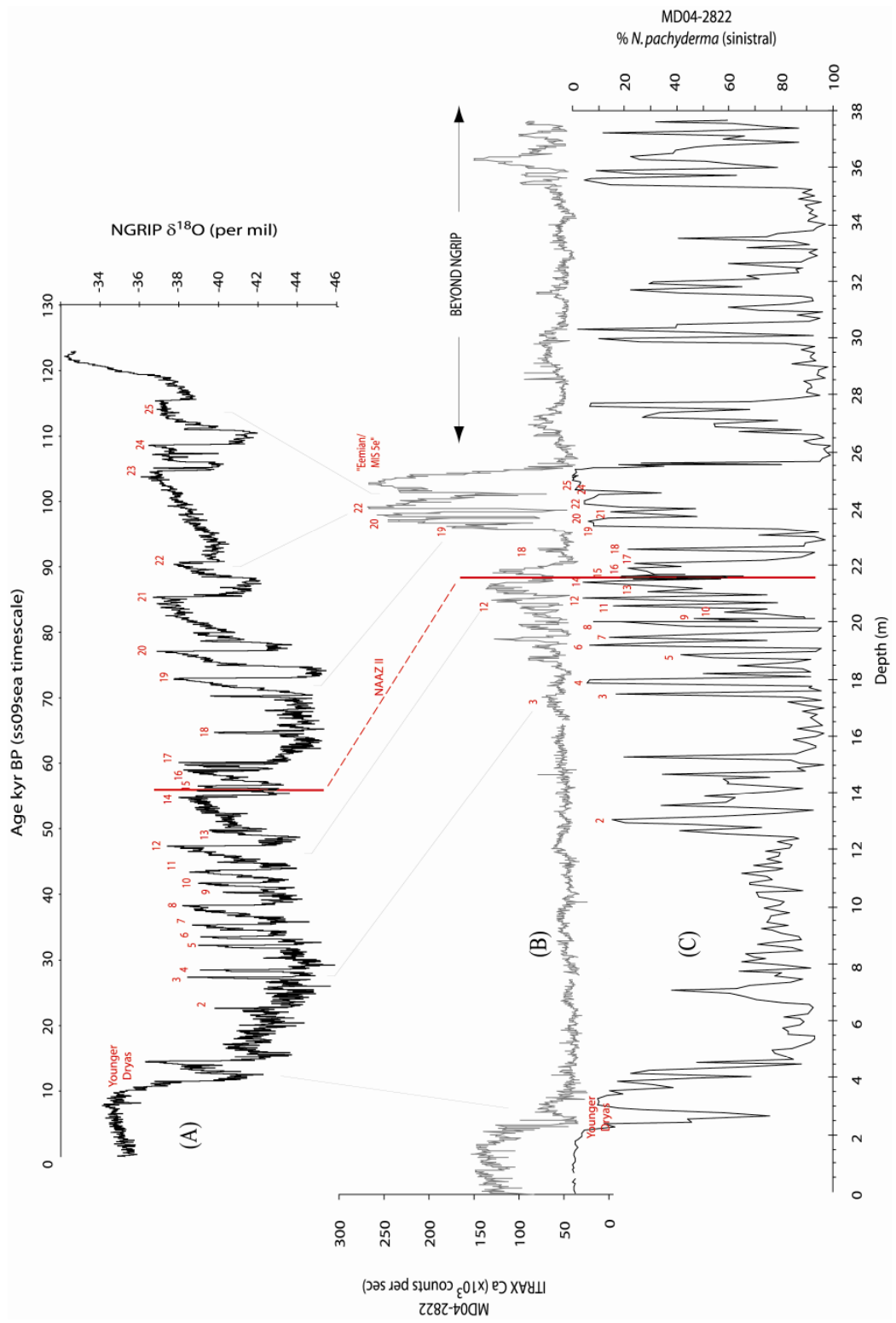
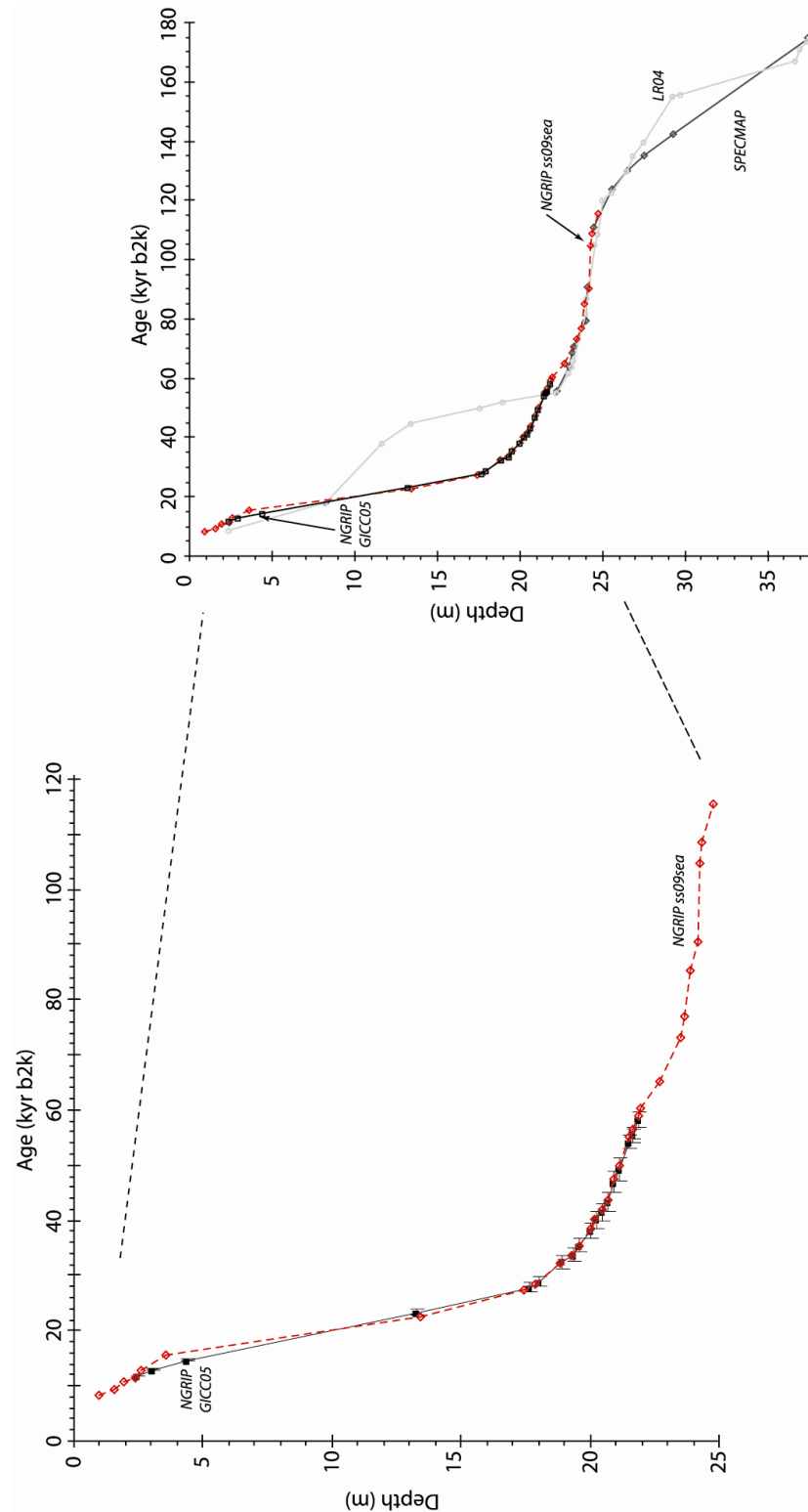


Figure 3.3: Age depth models based upon the independent tuning of MD04-2822 surface proxies to the NGRIP $\delta^{18}\text{O}$ record on both the ss09sea timescale (Johnsen et al 2001, NGRIP members 2004; red triangles, dashed line) and GICC05 timescale (0 to 60 kyr, Andersen et al 2006; Svensson et al 2006, 2008; Vinther et al 2006, black filled squares and solid line). Comparison to the tuning of MD04-2822 benthic $\delta^{18}\text{O}$ to the global stacks (SPECMAP and LR04).



3. Atmospheric methane concentration tuning of surface proxies

Atmospheric methane concentration records from both the Greenland and Antarctic ice cores have been used to synchronise records of climate between the two hemispheres (e.g. Blunier and Brook 2001). The rapid mixing time of methane between the hemispheres (~1 yr) allows the large-scale changes in concentration to be considered as essentially synchronous (Blunier and Brook 2001). Ice core methane concentration therefore provides a tool whereby the Greenland and Antarctic records have been synchronised and by which the coupling of climate variability between the two hemispheres has been demonstrated, notably the one-to-one coupling of the Antarctic warm events to the Greenland D/O events via the bipolar seesaw mechanism (EPICA members 2006). Thus millennial-scale variability is seen not only in Northern Hemisphere records (e.g. Johnsen et al 2001, NGRIP members 2004) but also within Antarctic methane records (Petit et al 1999, Jouzel et al 2007, Loulergue et al 2008). Loulergue et al (2008) have recently demonstrated that the millennial-scale changes in the EPICA Dome C record methane concentrations, associated with the Antarctic $\delta^{18}\text{O}$ isotopic maxima (Blunier and Brook 2001, Delmotte et al 2004, Spahni et al 2005), are ubiquitous through the last eight glacial cycles.

The relationship between millennial-scale atmospheric temperature changes over Greenland and sea surface temperature change within the North Atlantic has been firmly established (e.g. Bond et al 1993, Shackleton et al 2000) and this relationship is a means by which age control is achieved for many marine records (e.g. Shackleton et al 2000, Austin et al 2004). As discussed above, the construction of the MD04-2822 chronology utilised this approach as far back as ca. 123 kyr; beyond this time limit there are currently no reliable Northern Hemisphere ice core records available. However, temperature changes over Greenland, as recorded in the $\delta^{18}\text{O}$ ice core records, show striking similarities to their methane concentrations. Blunier et al (2007) have shown that inter-hemispheric comparison of methane records enables a millennial-scale, low-resolution comparison of Antarctic and Greenland temperatures. In essence, methane synchronisation allows for the reliable comparison of millennial-scale climate variations between the hemispheres. As such, the Antarctic methane record is used as a means by which further age control may be achieved for MD04-2822 beyond the current limits of the Greenland ice core chronologies. The high-resolution Antarctic methane records can, in effect, act as a proxy for inter-hemispheric, millennial-scale temperature fluctuations back through time (Delmotte et al 2004, Loulergue et al 2008). The high-resolution EPICA Dome C (EDC) ice core methane record of Loulergue et al (2008) is used as a proxy for Northern Hemisphere temperature fluctuations beyond 123 kyr in refining the initial, benthic $\delta^{18}\text{O}$ tuned age model.

The age scale used for the EDC methane data is the EDC3 timescale (Parrenin et al 2007); this shows good agreement, in general, with the Vostok records of the last 450 kyr, Dome Fuji records (Parrenin et al 2007), as well as the composite Greenland records (EPICA members 2006, Blunier et al 2007) and the composite benthic $\delta^{18}\text{O}$ LR04 stack of Lisiecki and Raymo (2005). Indeed, the comparison to the LR04 record is striking; age differences between the independently derived timescales do not exceed 6 kyr and for the last 400 kyr these are particularly small, ranging between 1.5 and 3 kyr (Figure 3.5).

3.1. Tuning of MD04-2822 surface proxies to EPICA Dome C methane record (EDC3 timescale)

The EDC methane record was used as the MIS 6 tuning 'target' for the surface ocean proxies of MD04-2822. Assuming changes in methane concentrations to be synchronous between the hemispheres and utilising the established synchronous relationship between Greenland air temperatures and North Atlantic sea surface temperatures, warm sea surface conditions (i.e. low percentages of *N. pachyderma* (sinistral)) at the core site are correlated with peaks in global methane concentration documented in the EDC record. This event stratigraphy allows tie-points to be assigned and the translation of ice core ages to the marine record. Age control between these tie-points was achieved via linear interpolation (Figure 3.4). Whilst additional correlations between the two records may be possible, only large variations in both the SST of the North Atlantic and in Antarctic methane concentrations are used in the age model.

The MD04-2822 record has only been tuned to the EDC methane record beyond Termination II. The reasons for this are twofold: firstly, subsequent to the last interglacial Greenland ice core records are available and provide a more direct means by which age assignments may be made; secondly, based upon the synchronisation of the Greenland and Antarctic methane records, synchronisation uncertainties are at their largest between the two records immediately post Termination II (Blunier et al 2007). The results of the tuning are illustrated in Figure 3.4. Beyond the limits of Greenland ice core tuning, the independent results obtained from the orbital tuning, i.e. the matching of the benthic $\delta^{18}\text{O}$ record to the global reference curve and the matching of sea surface temperature proxies to Antarctic methane records, are generally in good agreement Figure 3.5.

3.2. Test of tuning to Antarctic methane record

If the tuning of the MD04-2822 surface proxies to the EDC Antarctic methane record is reasonable i.e. that Antarctic methane concentration may be considered an global proxy for inter-hemispheric temperature fluctuations (Delmotte et al 2004, Loulergue et al 2008) (despite the enormous geographical separation of these two climate archives), we should be able to obtain age determinations for the last glacial cycle using this method that are fairly consistent with Greenland ice core-tuned ages. The Antarctic record methane record for the last glacial was not used in the construction of the final age model due to the availability of the much more proximal Greenland ice core records containing tephra isochrones common to both ice and marine sediment cores. Instead, tuning to the Antarctic methane record for the last glacial period was attempted as a test of methodology.

The age-depth model generated using tuning to Antarctic methane records for the last glacial compare very favourably with those generated by more conventional tuning 'targets' (. However, when plotted against the NGRIP $\delta^{18}\text{O}$ record (ss09sea), the timing of the transitions into the interstadials of the D/O events varies. This inter-hemispheric variation in the timing of millennial scale climate variability has been demonstrated between the ice core $\delta^{18}\text{O}$ records. Warming in Antarctica (as recorded by $\delta^{18}\text{O}$) occurs prior to their Greenland counterparts (Blunier et al 1998, Blunier and Brook 2001, EPICA members 2006, Blunier et al 2007, Ahn and Brook 2007, 2008 – their figure 1 reproduced as Figure 3.7 below) when the ice cores are synchronised using 'long-lived' atmospheric gases such as methane (Figure 3.7).

Figure 3.4: Tuning of surface proxies (a) XRF Ca and (b) % *N. pachyderma* (sinistral) to (c) the Antarctic EDC methane record (Loulergue et al 2008) on the EDC3 timescale (Parrenin et al 2007). Correlation of sea surface warming and increases in methane concentration (a proxy for inter-hemispheric temperature fluctuations) are given by numbers 1 to 5 and grey lines. Correlation was only undertaken beyond Termination II (heavy black line denotes portion of the EDC methane record used for tuning).

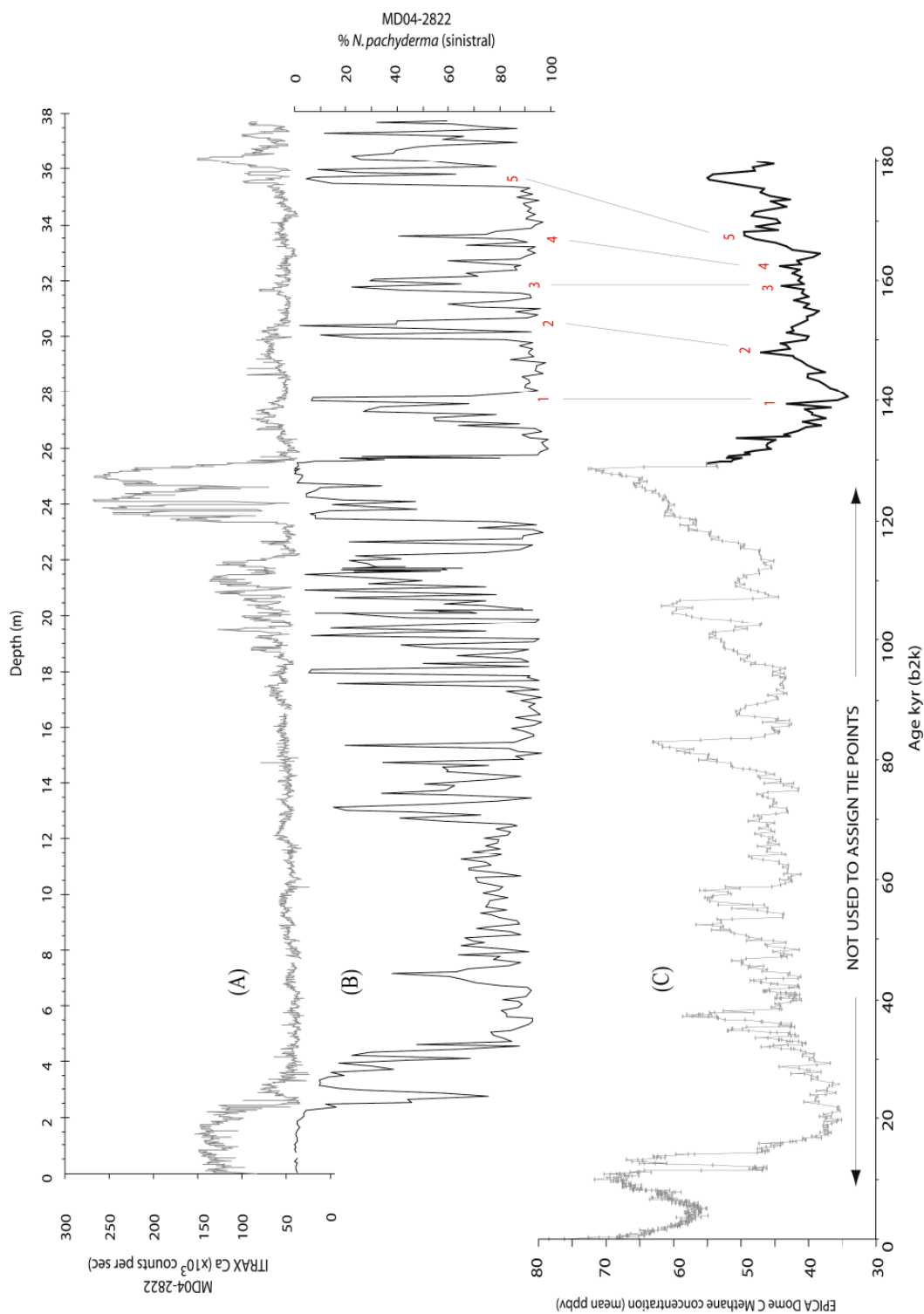


Figure 3.5: Age depth models based upon the tuning of the surface proxies to the EDC methane record (red) and other tuning methods (SPECMAP grey open diamonds; LR04 grey open circles; NGRIP $\delta^{18}\text{O}$ ss09sea black filled squares).

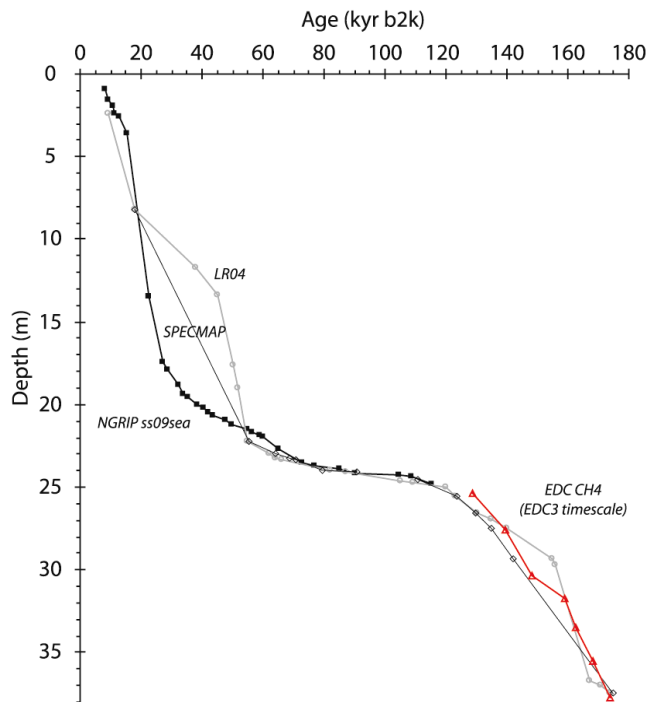


Figure 3.6: Age depth models based upon the tuning of surface proxies to the EDC methane record (red) for the entirety of the last glacial period. Also shown are the age models derived from tuning of the MD04-2822 proxies to SPECMAP, LR04 and NGRIP $\delta^{18}\text{O}$ on the ss09sea timescale.

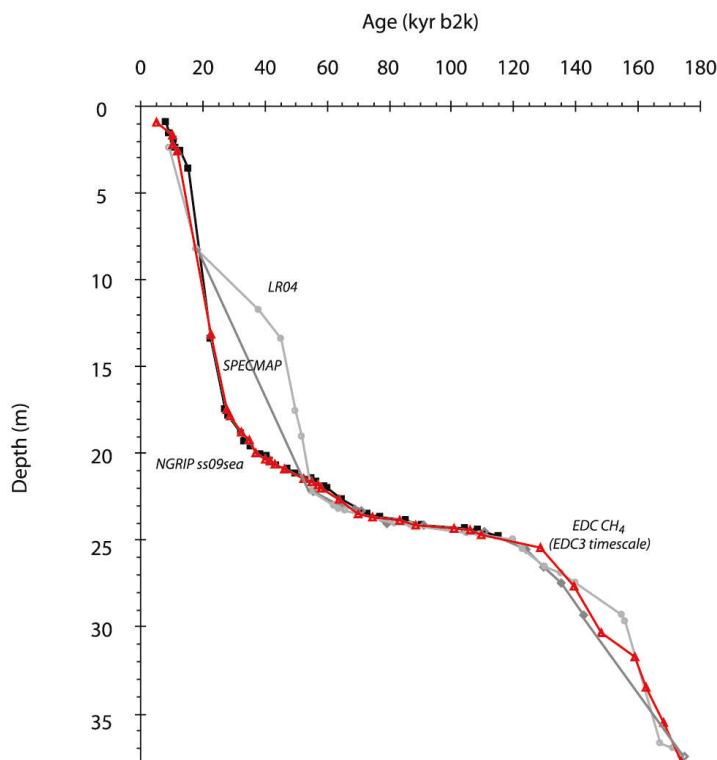


Figure 3.7: Millennial scale events within both the Greenland and Antarctic ice cores (reproduced from Ahn and Brook 2008): (a) Greenland ice core $\delta^{18}\text{O}$; (b) Antarctic ice core $\delta^{18}\text{O}$; (c) atmospheric CO_2 and (d) atmospheric methane.

IMAGE REMOVED - COPYRIGHT PROTECTED
(see original reference in caption above)

An explanation for the asynchronous timing of events between the poles invokes changes in AMOC; a reduction in AMOC results in a cooling of the northern hemisphere and warming in the south – the ‘bi-polar see-saw’ of Broecker (1998) whereby if production of dense water is reduced in one hemisphere, an increase in the other hemisphere would occur. The millennial-scale events in Antarctica are thought to be initiated by inputs of freshwater into the North Atlantic, thereby weakening AMOC and warming in Antarctica (e.g. Blunier et al 1998, Ganopolski and Rahmstorf 2001, Stocker and Johnsen 2003).

Some question the role of AMOC (e.g. Steig 2006) citing the current minor role of AMOC within the heat budget of the polar regions with the atmosphere compensating any oceanic changes (e.g. Wunsch 2006) and the ‘not very convincing’ evidence for the role of freshwater inputs into the North Atlantic (Steig 2006). Troggweiler and Lea (2010) recently proposed these discrepancies in the timing of events between the hemispheres resulted from a colder North Atlantic causing the Inter Tropical Convergence Zone (ITCZ) and Trade winds to move from their usual position. This in turn forced the movement of the southern hemisphere westerlies to the north of the Antarctic Circumpolar Current. As upwelling is reduced and no longer acts to move warm(er¹¹) water northwards away from the Antarctic continent, a warming is experienced in Antarctica.

The asynchrony of temperature changes between the hemispheres through the last glacial, does not however, prevent the use of the Antarctic methane record as a tuning ‘target’ within MIS 6. The rapid mixing time between hemispheres (thereby

¹¹ As the upwelled water moves northwards, it takes up solar heat (which without upwelling acts to warm Antarctica) and carries this heat across the equator to the North Atlantic (Crowley 1992)

providing a global signal) as well as this short life time, enables large variations in this gas to be distinguished almost immediately within either hemisphere. The synchronisation uncertainty for these records is estimated at approximately 200 to 800 years¹² (Blunier et al 2007, EPICA members 2006). Additionally, the pole to pole gradient of methane is only a few percent as the lifetime of the gas is only approximately ten times the exchange rate between the hemispheres. The short lifetime does, however, mean that changes in the production/destruction rates would be almost immediately evident in the global methane record and the D/O events are associated with large variations in methane over a short time (Blunier et al 2007). The EDML time series comparison with NGRIP (EPICA members 2006) and subsequent spectral comparison of the two records shows a 'significant relationship' on timescales of a few centuries for the period 20 to 90 kyr with a consistent 'out-of-phase' temperature relationship. The strong linear relationship between the warming in Antarctica and the duration of the following warming in Greenland has been linked by the authors as reflecting the duration of reduced AMOC and hence the amount of heat retained by the Southern Ocean.

An age model for the last glacial section of the MD04-2822 record was constructed using the Antarctic methane record (EPICA Dome C on the EDC3 timescale) as the tuning 'target', although this is *not* used in the final age model for the core. This compares favourably to that achieved by more conventional ice core tuning i.e. to the Greenland $\delta^{18}\text{O}$ record and therefore provides us with some confidence that ages derived for MIS 6 are reasonable. At present these age determinations cannot be comprehensively tested, although the close correspondence of the magnetic palaeointensity record for MD04-2822 to the global stack is reassuring (JET Channell, *pers. comm.*).

¹² Uncertainty comprises: the gas versus ice age for both cores as well as the uncertainty of the match between the two cores which is mainly determined by the resolution of the records; the concentration and inter-hemispheric gradient of methane (Blunier et al 2007).

4. Composite Age model for MD04-2822

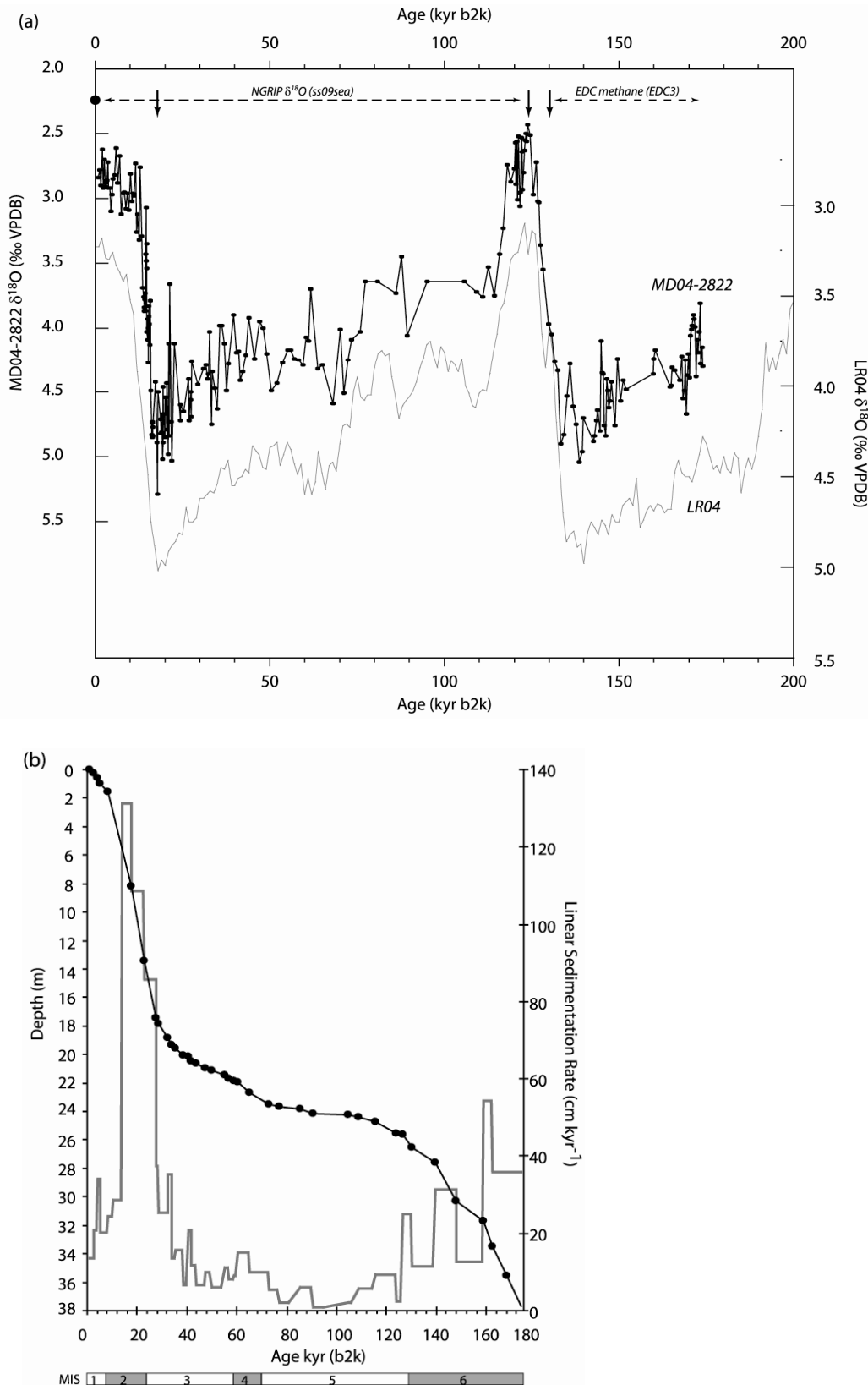
Following the independent tuning of both the benthic $\delta^{18}\text{O}$ and surface proxies (% *N. pachyderma* (sinistral) and XRF calcium records) to the tuning ‘targets’ outlined in the previous sections, a final age model for the entire MD04-2822 record was achieved using a combination of these methods. The tie-points used in this composite chronology are given in Table 3.1.

The age control for MD04-2822 is therefore a composite record comprising of:

1. a core top age was obtained by ^{14}C dating;
2. surface proxies tuned to the ss09sea timescale of Greenland $\delta^{18}\text{O}$ variation (NGRIP members 2004) for the last glacial (0 to ca.123.8 kyr);
3. tuning of the benthic $\delta^{18}\text{O}$ to the SPECMAP (Martinson et al 1987) record for MIS 5e and Termination II (123.8–130 kyr) and finally,
4. the tuning of the surface proxies to the EDC Antarctic methane record (Parrenin et al 2007, Louergue et al 2008) for the oldest section (130 to ca.168 kyr).

The resulting age depth model for MD04-2822 highlights the variable nature of deposition at this core site; sedimentation increases during MIS 6 and the latter stages of MIS 3 and into MIS 2, whilst sedimentation rates are generally low during the ‘warmer’ intervals of the MD04-2822 record i.e. the last interglacial and the Holocene. The large increases in linear sedimentation rate (calculated by linear interpolation between tie-points) during MIS 6 and especially MIS 2 reflect the increased inputs of terrigenous material, most likely from the proximal British Ice Sheet.

Figure 3.8: (a) MD04-2822 benthic $\delta^{18}\text{O}$ record on the compound age model (black) plotted with the LR04 stack (on its own age model - grey, Lisieck and Raymo 2005) for comparison. Black filled circle give the position of the ^{14}C core top date, dashed black lines indicate surface proxy tuning to Greenland (NGRIP $\delta^{18}\text{O}$ on the ss09sea timescale) and to Antarctic methane (EPICA Dome C, EDC3 timescale), arrows give the position of the benthic $\delta^{18}\text{O}$ tuning points to the SPECMAP benthic $\delta^{18}\text{O}$ stack. (b) Compound age-depth model for MD04-2822 with the calculated sedimentation rates.



CHAPTER 3:
Chronostratigraphy

Table 3.1: Chronostratigraphic tie –points used in the construction of the compound age model the MD04-2822 record. Tuning target timescale used is given in brackets.

Event	Age (yrs b2k)	MD04-2822 Depth (cm)	Source
core top	930	0.5	Calibrated AMS ^{14}C date
	2,500	22.012	Surface proxy tuning to NGRIP $\delta^{18}\text{O}$ (ss09sea)
	4,125	55.905	Surface proxy tuning to NGRIP $\delta^{18}\text{O}$ (ss09sea)
	5,275	95.005	Surface proxy tuning to NGRIP $\delta^{18}\text{O}$ (ss09sea)
	8,175	153.904	Surface proxy tuning to NGRIP $\delta^{18}\text{O}$ (ss09sea)
MIS 2.2*	17,850	820.5	Benthic $\delta^{18}\text{O}$ tuning to SPECMAP (Martinson et al 1987) isotopic maxima
Trans. into GIS 2	22,675	1344.905	Surface proxy tuning to NGRIP $\delta^{18}\text{O}$ (ss09sea)
Trans. into GIS 3	27,375	1747.009	Surface proxy tuning to NGRIP $\delta^{18}\text{O}$ (ss09sea)
Trans. into GIS 4	28,475	1788.900	Surface proxy tuning to NGRIP $\delta^{18}\text{O}$ (ss09sea)
Trans. into GIS 5	32,300	1884.905	Surface proxy tuning to NGRIP $\delta^{18}\text{O}$ (ss09sea)
Trans. into GIS 6	33,650	1932.405	Surface proxy tuning to NGRIP $\delta^{18}\text{O}$ (ss09sea)
Trans. into GIS 7	35,450	1956.905	Surface proxy tuning to NGRIP $\delta^{18}\text{O}$ (ss09sea)
Trans. into GIS 8	38,400	2002.905	Surface proxy tuning to NGRIP $\delta^{18}\text{O}$ (ss09sea)
Trans. into GIS 9	40,375	2015.905	Surface proxy tuning to NGRIP $\delta^{18}\text{O}$ (ss09sea)
Trans. into GIS 10	41,800	2045.405	Surface proxy tuning to NGRIP $\delta^{18}\text{O}$ (ss09sea)
Trans. into GIS 11	43,650	2067.405	Surface proxy tuning to NGRIP $\delta^{18}\text{O}$ (ss09sea)
Trans. into GIS 12	47,450	2092.905	Surface proxy tuning to NGRIP $\delta^{18}\text{O}$ (ss09sea)
Trans. into GIS 13	49,850	2116.904	Surface proxy tuning to NGRIP $\delta^{18}\text{O}$ (ss09sea)
Trans. into GIS 14	54,950	2148.404	Surface proxy tuning to NGRIP $\delta^{18}\text{O}$ (ss09sea)
Trans. into GIS 15	56,600	2166.905	Surface proxy tuning to NGRIP $\delta^{18}\text{O}$ (ss09sea)
Trans. into GIS 16	59,100	2187.405	Surface proxy tuning to NGRIP $\delta^{18}\text{O}$ (ss09sea)
Trans. into GIS 17	60,250	2197.905	Surface proxy tuning to NGRIP $\delta^{18}\text{O}$ (ss09sea)
Trans. into GIS 18	65,000	2269.404	Surface proxy tuning to NGRIP $\delta^{18}\text{O}$ (ss09sea)
Trans. into GIS 19	73,050	2348.405	Surface proxy tuning to NGRIP $\delta^{18}\text{O}$ (ss09sea)
Trans. into GIS 20	77,100	2369.905	Surface proxy tuning to NGRIP $\delta^{18}\text{O}$ (ss09sea)
Trans. into GIS 21	85,350	2386.905	Surface proxy tuning to NGRIP $\delta^{18}\text{O}$ (ss09sea)
Trans. into GIS 22	90,400	2416.904	Surface proxy tuning to NGRIP $\delta^{18}\text{O}$ (ss09sea)
Trans. into GIS 23	104,550	2427.904	Surface proxy tuning to NGRIP $\delta^{18}\text{O}$ (ss09sea)
Trans. into GIS 24	108,600	2436.904	Surface proxy tuning to NGRIP $\delta^{18}\text{O}$ (ss09sea)
Trans. into GIS 25	115,400	2476.905	Surface proxy tuning to NGRIP $\delta^{18}\text{O}$ (ss09sea)
MIS 5.5.1*	123,820	2554.5	Benthic $\delta^{18}\text{O}$ tuning to SPECMAP (MIS 5e – isotopic minima)
	126,320	2560.5	Benthic $\delta^{18}\text{O}$ tuning to EDC methane (after Loulergue et al 08)
MIS 6.0 (T II)*	130,000	2652.5	Benthic tuning – mid-point of transition i.e. Termination II
	139,455	2760.5	Surface proxy tuning to EDC methane (EDC 3)
	148,084	3030.5	Surface proxy tuning to EDC methane (EDC 3)
	159,048	3170.5	Surface proxy tuning to EDC methane (EDC 3)
	162,371	3350.5	Surface proxy tuning to EDC methane (EDC 3)
	168,061	3554.5	Surface proxy tuning to EDC methane (EDC 3)
core base	174,030	3768.5	Interpolation

* stack of Pisias et al 1984, timescale of Martinson et al 1987

5. Independent checks of age model construction

Skinner (2008) suggests that ‘a given chronostratigraphy is best viewed as a hypothesis’. In order to assess the validity of the MD04-2822 compound age model (presented above) two independent checks have been applied: tephrochronology and radiocarbon dating.

5.1. Tephra isochrones

The presence of tephra horizons within ice, marine and terrestrial records provides a means by which such records may be linked. If the ages of such horizons are known from one climate archive (e.g. ice cores), tephra may provide an additional, independent age control tie-point within other palaeoclimate archives (e.g. marine sediment cores). These tephra horizons (e.g. NAAZ I and II) are not used within the compound age model, instead the presence of such events serves as an independent check of the validity of the MD04-2822 age model.

An initial test of the tuning of the surface proxies to the NGRIP $\delta^{18}\text{O}$ record (ss09sea timescale) was the prediction of key independent stratigraphical markers. The presence of chronostratigraphic tephra marker horizons, North Atlantic Ash Zones (NAAZ) I and II (Ruddiman and Glover 1972, 1982), known to be present within both Greenland ice cores (Grönvold et al 1995; Zielinski et al 1997) and deep marine sediments (e.g. Kvamme et al 1989; Lacasse et al 1996), provide potential ‘anchors’ between the MD04-2822 and NGRIP records.

The sediment core was sub-sampled at high resolution (1 cm contiguous intervals) about the predicted positions and two distinctive rhyolitic tephra horizons, centred about 270cm and 2163.5cm, respectively, were found. Correlation of these tephra horizons to NAAZ I and II was determined by shard morphology and confirmed by major element geochemical analysis (Appendix B₃).

The positions of NAAZ I and II provide ‘anchors’ between the Greenland $\delta^{18}\text{O}$ and MD04-2822 records, thereby confirming the event stratigraphy and tuning (Figure 3.2). Ages were not assigned to these tephra horizons; instead they were used to confirm the event stratigraphy of the core *in sensu lato*. Age estimates for these tephra horizons based upon the compound chronology are presented in Table 3.2.

5.1.1. Age estimates for NAAZ II derived from the various tuning approaches

NAAZ II has recently been identified in the NGRIP ice core and an age estimate obtained using the GICC05 timescale (Svennson et al 2008). Table 3.2 and Table 3.6 give the estimated age for this event based upon tuning to the different tuning ‘targets’. All estimates for this depth i.e. the maximum abundance of rhyolitic shards, were found to be within the error estimates of the GICC05 age (although the SPECMAP estimate is slightly outside the uncertainty estimate).

The confirmation of the presence of NAAZ II, although not used as a tie-point in the chronostratigraphy, was incorporated into other age models (e.g. the Fugloyarbanki tephra within GS 3 was used as a chronostratigraphic tie-point in chapter 4).

Table 3.2: Age estimates for chronostratigraphic tephra horizons. Age estimates for MD04-2822 are based upon the compound age model.

	MD04-2822		NGRIP (GICC05)		Radiometric		
	Depth (cm)	Age (compound age model, yrs b2k)	Age $\pm 1 \sigma$ (yrs b2k)	Reference	Age $\pm 1 \sigma$ (yrs b2k)	Method	Reference
NAAZ I (Vedde Ash)	270.5	12,572	12,171 \pm 57	Rasmussen et al 2006	10,380 \pm 65 (10.4-10.3 ^{14}C kyr BP)	radiocarbon	Rasmussen et al 2007 (Björck et al 1992, Birks et al 1996)
NAAZ I (I-THOL-2)	290.5	13,269	n/a	n/a			Björck et al 1992
NAAZ II (II-RHY-1)	2163.5	56,296	55,380 \pm 1,184	Svensson et al 2008	54,550 \pm 2,000	Ar/Ar	Sigurdsson et al 1998, Lacasse and Grabe-Schönberg 2001)

Tephra horizons within the MD04-2822 sediments support the tuning of the surface proxy records to the Greenland ice core (NGRIP on the ss09sea timescale) for the last glacial. The continuing identification and characterisation of tephra layers (e.g. the NEEM ice core project to capture undisturbed ice from the last interglacial) within both the marine and ice core records should facilitate both the correlation of these records as well as age control.

5.2. Testing the MD04-2822-NGRIP tuning with AMS ^{14}C dating

The designation of GIS events within the MD04-2822 record was further tested by AMS ^{14}C dating. Whilst the tuning to the NGRIP $\delta^{18}\text{O}$ record (ss09sea timescale; Johnsen et al 2001, NGRIP members 2004) is an established method for gaining age control for marine sediments (c.f. Shackleton et al 2000), there is a clear danger of ‘mis-tuning’ the generally low resolution (10 cm) MD04-2822 % *N. pachyderma* (sinistral) record to the Greenland ice core, without recourse to some independent age control. The radiocarbon method, even taking into account the inherent uncertainties in the correction and calibration of radiocarbon dates, was used as a cross reference by which tuning may be validated.

An initial 6 ‘range-finder’ dates were followed by an additional 18 analyses, of which four were of MIS 5 age (i.e. beyond the dating limits of the radiocarbon method) in order to provide a procedural blank of the same provenance and handling as the unknown samples to be dated. In general, *G. bulloides* was preferred for radiocarbon dating in order to reduce some of the uncertainties, both temporal and spatial, of the regional component of the marine reservoir effect. Subpolar water masses are typically advected northwards from lower latitudes and are, on average, well exchanges with atmospheric carbon dioxide (e.g. Austin et al 1995). Sample selection considerations and uncertainties associated with the radiocarbon method within the marine environment are discussed in the following sections.

5.2.1. *Stratigraphic Integrity and Sample Selection*

The manner and conditions in which marine samples for radiocarbon dating have been deposited and subsequently handled may influence age determinations. Samples will, to a greater or lesser extent, have been affected by physical and/or chemical alteration depending upon the setting within which the sample has been transported and/or deposited (Lowe and Walker 2000). Care is needed in both evaluating any depositional history and sample preparation prior to submission to a radiocarbon dating facility. Indeed, ^{14}C dating relies upon assumptions including ‘that the foraminifera analysed represent coherent, in-situ assemblages’ (Austin 1994) and that ‘constituent carbon in each dated horizon is contemporaneous with the time of sediment accumulation’ which may not always be the case as ‘no sediment horizon is a closed system’ (Lowe et al 2007). Lowe and Walker (2000) assert that the consideration of the depositional history of a sample is amongst the most important factor in determining a radiocarbon age as ‘attempts to correct for other potential influences...can only result in spurious levels of precision if the geological integrity of the samples remains in question’.

Complicating factors in sampling procedures include contamination during coring, sediment storage, sub-sampling and activities prior to submission. During extraction of sediment cores, a downward smearing of sediments may occur, sidewall contamination, the manifestation of which will be a ‘smoothing’, for example, of faunal or depositional changes (Austin 1994). This may be minimised through an apposite sampling strategy; the outermost portion of sediment i.e. that in contact with the core barrel, should be avoided in order to minimise any contamination that occurred during recovery of the core. Inappropriate sample storage and processing may also result in the contamination of samples.

Large (>150 μm) planktonic foraminifera are preferred for AMS ^{14}C age determinations. Such large sized foraminifera are less prone to current redistribution than finer sediments and ^{14}C ages may be directly related to other palaeoceanographic data derived from foraminifera such as $\delta^{18}\text{O}$ and $\delta^{13}\text{C}$ (Brown et al 2000). All samples submitted for radiocarbon dating were > 150 μm with all *G. bulloides* samples > 250 μm . Monospecific samples are selected from abundance maxima in order to maximise stratigraphic integrity of the intervals (Bard et al 2000, 2004, Waelbroeck et al 2001).

Bard et al (1987, 2004) advocate picking foraminifera for dating from abundance maxima in order to minimise bioturbation biases; picking from an abundance minimum may result in an unreliable age determination as foraminiferal shells may have been transported from intervals of higher abundance levels above (or below) the dated interval. The intervals for dating were, in the main, from high abundance levels of the particular species chosen for dating, either *N. pachyderma* (sinistral) or *G. bulloides* (Figure 3.9). *G. bulloides* dates were selected, in the main, from within the Greenland Interstadial (GIS) events where this species is dominant.

For interstadial portions of the core, samples of *G. bulloides* were preferred to *N. pachyderma* (sinistral) for the process of radiocarbon dating, in order to minimise

local marine reservoir effects¹³ upon age determinations (see section 5.2.3 below for discussion of the marine reservoir effect) and due to the generally higher abundances of *G. bulloides* within the MD04-2822 record (Figure 3.9).

Within the modern ocean environment, this species is typically found close to the surface (Bé and Tolderlund 1971) and is subject to a negligible marine reservoir effect (e.g. Austin et al 1995)¹⁴. During stadials however, the corresponding high percentage abundance of *N. pachyderma* (sinistral) require that samples of this species (a modern polar species occupying a greater depth range, both surface and subsurface; Bé and Tolderlund 1971) are used for dating purposes. Unfortunately the use of *N. pachyderma* (sinistral) increases the uncertainty of age estimates due to the possibility of increased marine reservoir effects during stadials (e.g. Reimer et al 2009). Caution should therefore be exercised when comparing radiocarbon ages for the two species. Each would experience different hydrological conditions, with respect to the heterogeneous nature of ¹⁴C within both the lateral and vertical structure of the ocean (Ascough et al 2007) and in terms of the influence of meltwater on ocean-atmosphere exchange. The core site is located at relatively high latitudes, where marine reservoir ages are thought to be large and variable (Bard et al 2004a).

5.2.2. Analytical Limits for the Precision of Radiocarbon Measurements

Key to the determination of a radiocarbon date is an assessment of the sources of error associated with background ¹⁴C, pre-treatment (if any) of foraminifera samples, graphitisation and sample contamination considerations. For AMS ¹⁴C dating, limits upon the precision include the performance of the equipment and the purity of the targets prepared (Lowe and Walker 2000).

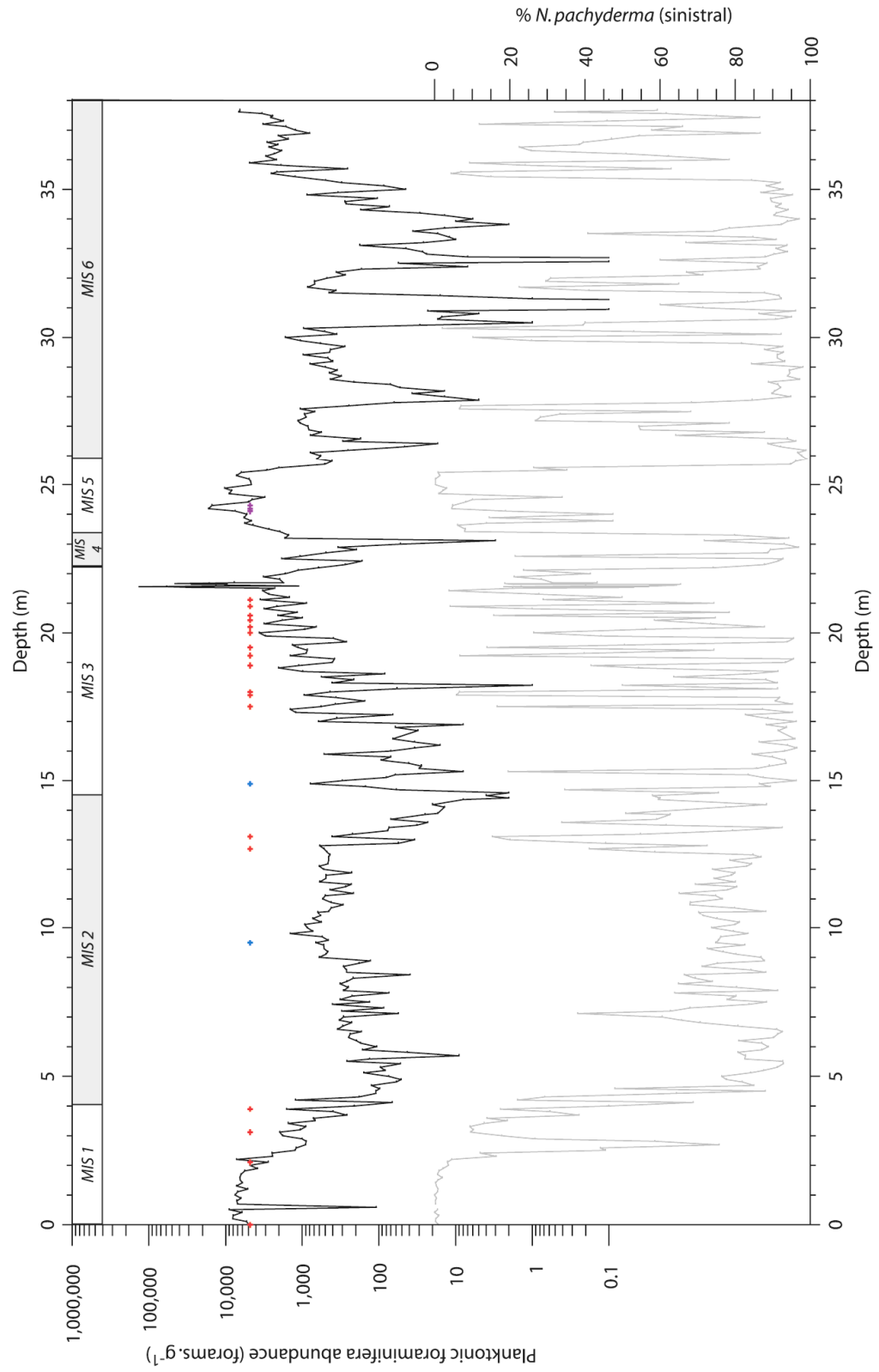
Measurement of background values during radiocarbon age determinations tend to display a scatter of around one third of their value; this is subsequently incorporated into an age determination increasing uncertainty (e.g. Nadeau et al 1997, 2001, Schleicher et al 1998). Reductions in errors associated with background levels would therefore result in improved radiocarbon determination.

In addition to AMS background, a low ¹⁴C concentration procedural blank is prerequisite for the analysis of very old, i.e. those approaching the limits of radiocarbon dating, or very small samples (Schleicher et al 1998). Blank values describe the ¹⁴C added to the sample during different processing steps within the laboratory. The preparation of blanks follows procedures for unknown samples i.e. graphitisation and target pressing. The blanks commonly utilised in background estimation for radiocarbon determinations are either the minerals Icelandic double spar or IAEA C1 Carrara marble (Nadeau et al 2001).

¹³ The marine reservoir effect is an offset in the ¹⁴C age between contemporaneous organisms from the terrestrial and marine environments – see section 5.2.3, this chapter for further discussion.

¹⁴ The global average marine reservoir age, R(t) of surface waters is ~405 yrs (Reimer et al 2009). Modern estimates of local deviations (ΔR) from the global average (R(t)) marine reservoir age of surface waters is estimated as $\Delta R \sim 14$ years for the Hebridean Shelf, with a regional average of British waters of 17 ± 14 years. Western Scotland is estimated to experience a modern ΔR of 6 years (n=5). Average ΔR : western Norway is 40 years; SW Norway is 5 years (n=16) and; 75 years for Iceland (n=6) (Reimer and Reimer 2010)

Figure 3.9: MD04-2822 abundance of planktonic foraminifera (black), the % *N. pachyderma* (sinistral) record (grey) and stratigraphical position of radiocarbon dating intervals (red – *G. bulloides*, blue – *N. pachyderma* (sinistral) and purple *MIS 5 G. bulloides*). Note the logarithmic scale for the abundance of planktonic foraminifera.



The use of mineral background material in the evaluation of the age of biogenic carbonates, especially for older samples, is inadequate (e.g. Nadeau et al 2001). These authors demonstrate that the apparent ages of biogenic samples are younger than those for mineral samples and suggest that to accurately assess the age of older samples, i.e. those greater than 30 ka, background material of the same species and of the same provenance as the unknown samples is used as a procedural blank. The cause of the discrepancy between mineral and biogenic determinations remains, as yet, imperfectly understood. It has been suggested that the crystal structure of the shells and the defects within them may be responsible for the younger apparent age (Lownestam and Weiner 1989). If no material of the same provenance is available, generic biogenic material such as mixed foraminifera could be used.

Fortuitously, MD04-2822 extends beyond the radiocarbon method which enabled samples from MIS 5 (> 90 to 100 kyr) to be included with each batch of samples for radiocarbon analysis in order to quantify background ^{14}C with material comparable to samples used for chronological control. These samples were taken from very abundant planktonic foraminifera, primarily *G. bulloides*, intervals at depths of 2410–2411 cm, 2420–2421 cm and two samples from 2430–2431 cm. The ^{14}C enrichment (expressed as the percent modern carbon) and conventional radiocarbon age for these samples is given in Table 3.3, no background correction has been applied to the MIS 5 samples. This background ^{14}C measurement should be similar for all the analysed samples from the core as the material has undergone the same sample handling.

Table 3.3: Background determinations for MD04-2822. No background correction is applied to the foraminifera samples. Mean background and associated standard deviation of the MIS 5 samples of 0.43 ± 0.05 was applied to samples above a depth of 2021-2022 cm within the core.

Depth (cm)	Publication Code	Species	^{14}C enrichment (% modern $\pm 1\sigma$)	Conventional Radiocarbon Age (yrs BP $\pm 1\sigma$)
2410-2411 †	SUERC-17743	<i>G. bulloides</i>	0.45 \pm 0.01	43,354 \pm 183
2420-2421 †	SUERC-17744	<i>G. bulloides</i>	0.37 \pm 0.01	44,915 \pm 189
2430-2430 †	SUERC-17745	<i>G. bulloides</i>	0.46 \pm 0.01	43,162 \pm 149
2430-2430	SUERC-13847	<i>G. bulloides</i>		47,800 \pm 1,400
Procedural blank – Iceland spar calcite *	n/a	n/a	0.35 \pm 0.01	n/a
Procedural blank – graphite *	n/a	n/a	0.26 \pm 0.01	n/a

* analysed at same time as first three samples (SUERC 17743, 17744, 17745)

† SUERC graphite background slightly elevated (0.26%MC) compared to normal (~ 0.15 % modern carbon (pMC) C. Bryant, *pers. comm.*)

Schleicher et al (1998) using mixed foraminifera (>100 kyr) and ‘no measurable ^{14}C concentration’ obtained values of 0.38 ± 0.07 % modern carbon with a mean of 0.14 % modern carbon for Carrara marble. This difference was attributed to contamination of the Eemian foraminifera samples. Similar differences between mineral and organic background materials was found by Gulliksen and Thomas (1992) where figures of 0.32 % modern carbon for foraminiferal material can be contrasted to 0.18 % modern carbon for the mineral Icelandic double spar.

It should be remembered that the quoted analytical precision ‘should not be regarded as indicative of the accuracy of the estimates’ as precision does not necessarily indicate the reliability of the date (Lowe et al 2007). Additionally the uncertainty associated with radiocarbon determinations (and subsequent calibration) may limit the temporal resolution of the sediment sequence dated. For example, Telford et al (2004a) demonstrate that to achieve centennial resolution through the Holocene, 24 dated horizons are needed to reduce the statistical noise. The MD04-2822 record has far lower resolution due to the much longer timescale and the relatively few dates. However, as the radiocarbon ages are not the basis for the age model, rather a check, this concern is not considered significant.

5.2.3. *Marine radiocarbon reservoir effect*

The marine radiocarbon reservoir effect is the offset between contemporaneous material derived from the atmospheric and oceanic reservoirs of ^{14}C and is both spatially and temporally variable. Variations in marine reservoir effect change as a function of local oceanographical and climatological variables including temperature, wind speed, sea ice and location of upwelling zones (e.g. Stocker and Wright 1996, Kovanen and Easterbrook 2002, Merlivat and Memery 1983, Austin et al 1995, Voelker et al 1998, Waelbroeck et al 2001, Eiriksson et al 2004).

Large changes in the marine reservoir effect are known for the North Atlantic (e.g. Austin et al 1995, Voelker et al 1998, Waelbroeck et al 2001, Eiriksson et al 2004) induced by *inter alia*, changes in ocean circulation, the presence of meltwater/sea ice impeding the atmospheric-ocean exchange and the incorporation of ‘old’ carbon derived from the melting of ice sheets (e.g. Domack et al 1989).

The marine reservoir effect has also been shown to be variable through time, and related to atmospheric variations in ^{14}C , linked to climate changes as well as geomagnetic and solar magnetic field intensities (e.g. the Laschamp or Mono Lake excursions). Such variations in the marine reservoir effect are difficult to constrain over the full range of the radiocarbon method. The Younger Dryas (GS1) event however, provides a useful illustration of these variations during an interval of abrupt climate change within the North Atlantic region. Austin et al (1995) demonstrated a change in the local marine reservoir effect in a core from the Hebridean margin, with an increase of ~700 years at the time of deposition of the Vedde Ash tephra layer. This seems to have been subsequently confirmed by the modelling study of Singarayer et al (2008). Large changes in the marine reservoir effect have also been observed during the Heinrich Events (Voelker et al 2000, Sarnthein et al 2007).

During interstadial events, surface hydrological conditions are thought to be similar to present with no significant additional reservoir contribution (Austin et al 1995). However, during stadials, surface conditions were very different from present. The polar front was located to the south of the core sites and the proximity of these core locations to actively glaciated margins also increases the likelihood of meltwater inhibiting ocean-atmosphere exchange. Both of these phenomena are associated with significant increases in marine reservoir effect. It would seem reasonable that the marine reservoir effect for stadial samples should be increased but the difficulty of establishing such values, both spatially and temporally, is recognised. Indeed,

relatively small spatial differences (<50 km apart) may result in variations in ΔR (Ascough et al 2007). In modern polar waters, ΔR values range from ~400 to 800 years (Reimer and Reimer 2010). This may be a conservative estimate of local variations in reservoir effect during stadial events. As the assessment of the marine reservoir effect through time is unsatisfactory, the ^{14}C dates were calibrated using only the global average incorporated into the Marine09 calibration curve (Reimer et al 2009).

5.2.4. Calibration:

Calibration frequently introduces additional error which, in combination with stratigraphic errors, reduces the precision of the age determination substantially. However, calibration does provide more realistic uncertainty ranges (Lowe et al 2007). Calibration archives should, *sensu stricto*, have an absolutely determined chronology (e.g. dendrochronology) for carbon derived directly from the archive in question (e.g. the atmosphere), however, there are currently none available prior to ca. 12.5 kyr, and the provision of a marine calibration prior to this date has been problematic (Reimer et al 2009). The Marine09 calibration curve uses an ocean-atmosphere diffusion box model to calculate values for the 0 to 12.5 cal. BP (as in the Marine04 curve; Oeschger et al 1975, Stuvier and Braziunas 1993, Hughen et al 2004b). From 12.5 to 50 cal BP, the atmospheric IntCal09 curve, which is derived from marine data which include a 'questionable' constant marine reservoir correction of 405 years (Reimer et al 2009).

Radiocarbon age determinations are Gaussian in structure however the probability distributions resulting from calibration curves are non-Gaussian (Bennett 1994, Lowe et al 2007). The calibration curves are statistically complex and reflect sudden variations in atmospheric radiocarbon content, which is not yet fully understood (e.g. Taylor et al 1992). The use of Bayesian probability approach in age-depth models presents several advantages, *inter alia*: no data is excluded until analysis is complete; outcomes are not influenced by the operator as age determinations are treated independently and; they use standardised routines for the integration of complex non-Gaussian probability distributions of the calibrated data (Lowe et al 2008, Bronk Ramsey 2009).

Commonly a method for generating a point estimate of a calibrated date uses the intercept (mean, median) based methods. Such estimates are found to exhibit 'undesirable behaviour' as they are highly sensitive to the mean of the radiocarbon date and adjustments to the calibration curve (Telford et al 2004a). These authors highlight that 'no single value can adequately describe the complex shape of a calibrated radiocarbon probability density function and wherever possible this full distribution should be used'.

It must be remembered, however, that the age-depth relationships of radiocarbon dates may only be reliably established if those dates are calibrated. For the MD04-2822 samples, no additional ΔR was added during calibration, despite the unlikely assumption of constant spatial and temporal variation in marine reservoir effect. The application of an average global marine reservoir age during calibration is rather simplistic; indeed, the IntCal Working Group (Reimer et al 2009) convey a strong warning to the marine community that the 'user must decide whether large reservoir

changes are likely to affect their chronology and provide their own estimates of reservoir changes and uncertainties' in using the Marine09 calibration curve.

The reported MD04-2822 conventional radiocarbon ages were converted to calendar ages using OxCal 4.1 programme (Bronk Ramsey 2009) (see section 5.2.5 below).

5.2.5. Radiocarbon Age-Models:

Age-depth models produced from calibrated radiocarbon dates in their most simplistic form join the mean values of individual dates and assume a linear sedimentation rate (in some instances, 'outliers' may be ignored¹⁵). Other models (e.g. polynomial regression, splines etc) may be applied to radiocarbon data with the different approaches giving different results depending upon the model applied in relation to both the age at a particular depth and the uncertainty associated with that estimate (e.g. Bennett 1994, Telford et al 2004b). The more simplistic approaches underestimate the statistical limitations of the data with the assumption of linear sedimentation rate unlikely, especially during intervals of pronounced climatic changes. Indeed, the more widely spaced the dated horizons the more questionable is this approach (Lowe et al 2007). Additionally, if the radiocarbon dates are expressed in terms of their 1σ uncertainties, then the 'true' age of approximately a third of age estimates will lie outside these error estimates, therefore joining the mean values is 'highly questionable' (Lowe et al 2007). Bronk Ramsey (2008, 2009) advocates the use of Bayesian analysis of radiocarbon estimates and the use of deposition models in order to refine chronologies with the incorporation of information regarding depositional process due to the 'imprecision of individual calibrated radiocarbon determinations' when considered in an age-depth model.

Three aspects of radiocarbon dating have led to the development of such statistical analysis methods: many depositional sequences require the consideration of large numbers of radiocarbon determinations; radiocarbon determinations are the measurement of an isotope ratio and their interpretation requires the statistical analysis using calibration curves and; once calibrated, radiocarbon dates have probability density functions that are not normally distributed (Bronk Ramsey 2009). The most widely used approach is Bayesian statistics (Buck et al 1991, Christen et al 1995, Bronk Ramsey 2008, 2009) and these have been incorporated into calibration software (e.g. OxCal; Bronk Ramsey 1995, 2001, 2009). OxCal (version 4.1; Bronk Ramsey 2009) has been used for the calibration of MD04-2822 radiocarbon determinations. A depositional model (Bronk Ramsey 2008) incorporated into this software, was used in order to include stratigraphical information within the *prior model*¹⁶ so that the age-depth model takes into account both the deposition model used and the radiocarbon age determinations.

The validity of any such age-depth model is dependent upon the number of age estimates obtained, the temporal resolution to which those events are resolved and the

¹⁵ Lowe et al (2007) highlight that the exclusion of apparent outliers on the basis that they do not 'fit' the age-depth model is invalid if the ages are plotted on the ¹⁴C timescale as this timescale is not linear. Calibrated radiocarbon estimates are unusual in producing complicated likelihood distributions; most dating methods a normal (Gaussian) distribution may be used (Bronk Ramsey 2008)

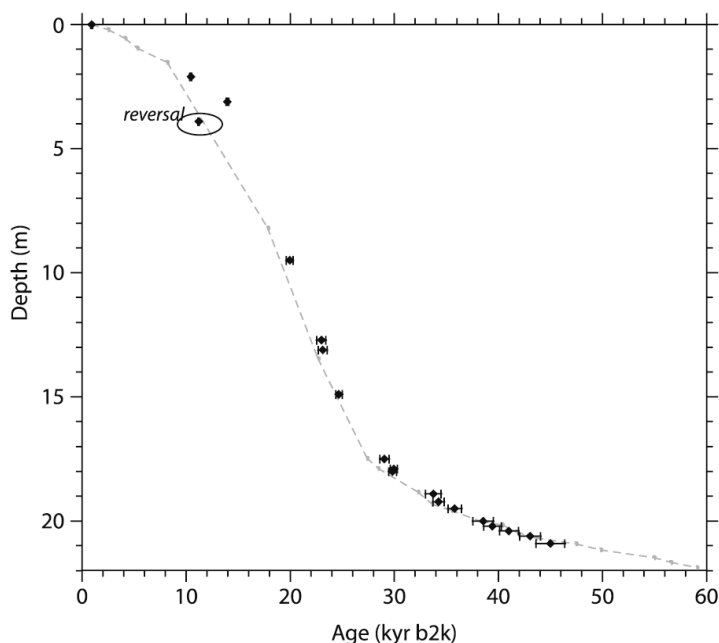
¹⁶ *Prior model*: this is in essence the information we have of the sedimentary system before the set of radiocarbon measurements.

complexity of the sedimentation rate (Telford et al 2004b, Lowe et al 2007). For radiocarbon dating, centennial resolution is difficult to achieve even within the Holocene (Telford et al 2004a,b); for the last termination, ‘true’ errors are frequently millennial in magnitude (Lowe et al 2007). Telford et al (2004b) propose that age estimates for palaeoenvironmental events are better constrained by dating immediately ‘and unambiguously’, above and below the event, than by age-depth models. As uncertainty will increase when comparing between sites, these authors suggest that time-parallel markers such as tephra and geomagnetic stratigraphy be used. The use of tephrochronology is strongly urged by the INTIMATE group (e.g. Lowe et al 2001, 2008) as a means by which radiocarbon age models may be validated.

For MD04-2822, a relatively low number of dates are available for the time interval considered, but the mean age difference between those calibrated ^{14}C dates is greater than the error range of the individual dates. Therefore this is held to be a valid age-depth model for the sediment core, but that this age model is ‘crude’ at best (c.f. Lowe et al 2007) although highly indicative. An age-depth model has been constructed from the calibrated radiocarbon dates (Figure 3.10). In using the calibrated radiocarbon ages as a check of the tuning to the Greenland ice core (NGRIP $\delta^{18}\text{O}$, ss09sea timescale), and the close correspondence between the two independent age-depth models (Figure 3.10), the MD04-2822 age-depth model does not appear to be affected by ‘mis-tuning’ between the ice and marine sediment cores.

The calibrated radiocarbon ages do perform, however, a vital role in confirming the correlation of the D/O events between the marine and ice core records. The procedure for this is described in the following section.

Figure 3.10: Age-depth models from MD04-2822: grey dashed line is the finalised compound age model; black diamonds ($\pm 1\sigma$) calibrated radiocarbon ages. Radiocarbon dates were calibrated via the OxCal programme (version 4.1) (Bronk Ramsey 2009) using the Marine09 calibration curve (Reimer et al 2009) with no additional ΔR added to the global average of 405 years implicit in the calibration curve. Note reversal in radiocarbon age determinations at 390.5 cm



5.2.6. Application of radiocarbon dating to MD04-2822 – test of tuning

All reported ^{14}C and calibrated ages for MD04-2822 are given in Table 3.4. Radiocarbon age determinations were calibrated using a deposition model (*P_sequence*; Bronk Ramsey 2008) within the OxCal (version 4.1) programme (Bronk Ramsey 2009). No additional regional marine reservoir effect was added to the global marine average incorporated within the Marine09 calibration curve (Reimer et al 2009). As most of the analyses were carried out on *G. bulloides* within interstadial events, the assumption of a constant reservoir effect, with no additional local component, is not unreasonable. Austin et al (1995) propose that for a core of similar latitude, surface water interstadial conditions may be considered similar to present.

As a means of testing tuning to the Greenland ice core $\delta^{18}\text{O}$ record (section 2, above), the calibrated radiocarbon determination for each of the interstadial events are compared to the tuned ages for the same depth interval (Table 3.5, Figure 3.11). The calibrated radiocarbon dates (in yrs b2k) were compared to the tuned (NGRIP $\delta^{18}\text{O}$ on the GICC05 timescale) ages derived for the same interval. The GICC05 timescale was chosen in preference to the compound chronology ages for two reasons: firstly, the ages for the interstadial events have been determined via layer counting and includes an uncertainty estimate (termed the maximum counting error) and; secondly, estimates for the duration of the interstadial events are available for most interstadial events thereby allowing to evaluate if the radiocarbon date falls within the interstadial (see Wolff et al 2009, Lowe et al 2008).

The calibrated radiocarbon dates do, in general, permit the discrimination of the interstadial or stadial event dated, when used in conjunction with proxy and stratigraphic information (e.g. where the abundance of *N. pachyderma* (sinistral) are low for a dated horizon i.e. an interstadial, a stadial designation based solely on calibrated radiocarbon ages is unrealistic) (Table 3.6, Figure 3.11). A prominent reversal in the calibrated radiocarbon ages is evident at 390-391 cm; this may be due to problems with contamination. For the two *N. pachyderma* (sinistral) dates, despite the unlikely assumption of a similar local reservoir effect as interstadials, these also fall within the expected stadial event based upon the tuning of surface proxies to the Greenland ice core record.

Most of the calibrated radiocarbon dates are older than their equivalent tuned ages for the same depth interval. This may reflect an increased local reservoir effect and/or differences between the construction of the radiocarbon calibration age model and the Greenland ice core chronology (c.f. Skinner 2008). Contamination may account for the younger radiocarbon age than tuned age during GS 9 and GIS 12. Contamination of the samples is a concern, particularly acute for older samples, where any ^{14}C contamination may have a disproportionate effect upon the age determination. Unfortunately, it was not possible to undertake any additional cleaning of the MD04-2822 samples, other than with de-ionised water, prior to submission. Etching of the outer ~20 % of the shells may have reduced the impact of any adsorbed CO_2 as well as removing any non-contemporaneous fines (or e.g. coccoliths) (c.f. Heier-Neilsen et al 1995) in conjunction with reference and blank considerations (see section 5.2.2, this chapter).

CHAPTER 3:
Chronostratigraphy

Using both the calibrated radiocarbon dates and stratigraphic/proxy information (e.g. % *N. pachyderma* (sinistral)), gives confidence that the tuning to the Greenland ice core (NGRIP $\delta^{18}\text{O}$, ss09sea timescale) is unaffected by ‘mis-tuning’ between the two records.

Table 3.4: Conventional and calibrated radiocarbon dates for MD04-2822. Radiocarbon age determinations were calibrated using the Marine09 calibration curve (Reimer et al 2009) within the OxCal (version 4.1, Bronk Ramsey 2009) programme. No additional local marine reservoir correction was added prior to calibration.

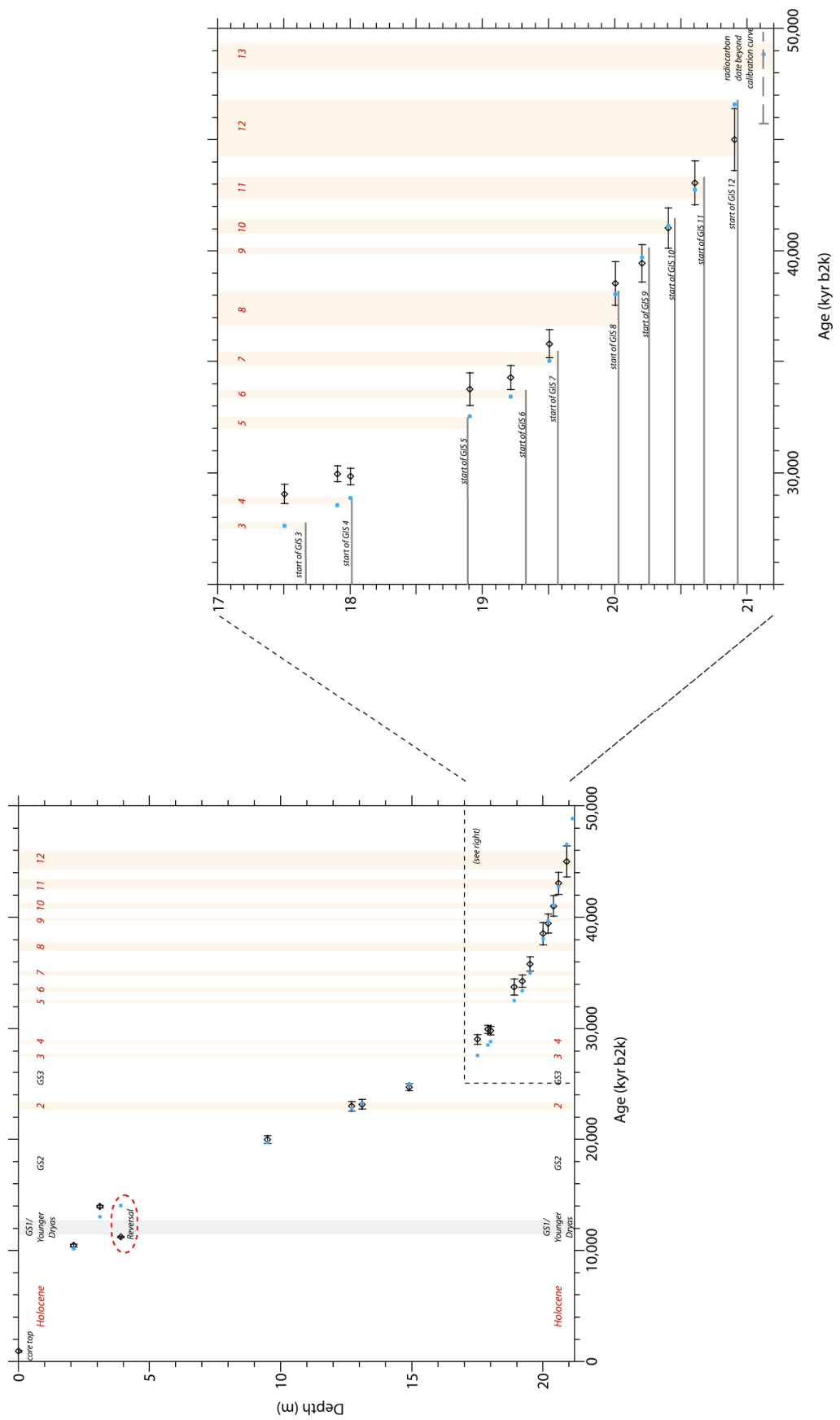
Depth	Conventional ^{14}C Age $\pm 1\sigma$ error		Calibrated Age (yrs BP) (Marine09; Reimer et al 2009)				Mid-point of 95.4 % probability distribution ± 1 standard deviation		
			68.2 % probability distribution		95.4 % probability distribution		yrs BP	yrs b2k	1 s.d.
0.5	1,350	35	941	851	971	788	879	929	92
210.5	9,552	39	10,490	10,370	10,520	10,280	10,400	10,450	120
310.5	12,472	39	13,979	13,841	14,040	13,780	13,910	13,960	130
390.5	10,145	40	11,190	11,131	11,216	11,101	11,159	11,209	58
950.5	17,200	70	20,147	19,616	20,261	19,579	19,920	19,970	341
1270.5	19,635	85	23,142	22,620	23,370	22,512	22,941	22,991	429
1310.5	19,830	62	23,440	22,980	23,510	22,665	23,088	23,138	423
1490.5	21,015	70	24,780	24,440	24,946	24,340	24,643	24,693	303
1750.5	24,639	109	29,326	28,837	29,435	28,575	29,005	29,055	430
1790.5	25,495	100	30,198	29,756	30,262	29,558	29,910	29,960	352
1800.5	25,225	108	29,843	29,445	30,162	29,413	29,788	29,838	375
1890.5	29,315	167	33,891	33,108	34,437	32,979	33,708	33,758	729
1921.5	30,058	184	34,684	34,100	34,765	33,675	34,220	34,270	545
1950.5	31,661	221	36,266	35,315	36,406	35,120	35,763	35,813	643
2000.5	34,171	299	39,059	38,056	39,462	37,513	38,488	38,538	975
2020.5	34,609	312	39,541	38,711	40,238	38,540	39,389	39,439	849
2040.5	36,251	446	41,479	40,619	41,885	40,070	40,978	41,028	908
2060.5	38,876	617	43,326	42,361	43,995	42,016	43,005	43,055	990
2090.5	41,664	869	45,539	44,298	46,345	43,564	44,954	45,004	1391
2112.5	44,792	1325	48,920	46,336	<i>Out of range</i>	45,837	n/a	n/a	n/a

Please note – the calibrated ages presented here differ slightly from those within Hibbert et al (2010). The ages presented here were obtained using the updated Marine09 calibration curve whereas Hibbert et al (2010) used the Marine04 calibration curve available at the time of publication..

Table 3.5: Comparison of calibrated radiocarbon dates (Marine09 calibration curve used; Reimer et al 2009) to the corresponding tuned ages (GICC05 timescale) for the same interval. Age estimates for the start of the NGRIP $\delta^{18}O$ features is also given (see table 2 within Wolff et al 2009, table 1 within Lowe et al 2008).

Depth (cm)	Tuned stratigraphic position	Calibrated ^{14}C Age (95.4 % probability distribution) yrs BP		Stratigraphic position confirmed by ^{14}C dating?	Age start of interval (GICC05 timescale) yrs b2k	Age est. Reference
0.5	n/a (core top)	971	788	n/a	n/a	n/a
210.5	End of Younger Dryas	10,520	10,280	Yes	11,703	Rasmussen et al (2006)
310.5	Start of Younger Dryas	14,040	13,780	Yes	12,896	Rasmussen et al (2006)
390.5	Uncertain - GIS 1c?	11,216	11,101	Reversal	13,954	Andersen et al (2006)
950.5	GS2	20,261	19,579	Yes	22,900	Andersen et al (2006)
1270.5	Warming immediately post GIS 2	23,370	22,512	Yes	n/a	n/a
1310.5	GIS 2	23,510	22,665	Yes	23,340	Andersen et al (2006)
1490.5	GS3	24,946	24,340	Yes	27,540	Andersen et al (2006)
1750.5	GIS 3	29,435	28,575	No – Older than GS3 but could also be GIS 4	27,780	Andersen et al (2006)
1790.5	GIS 4 (towards end)	30,262	29,558	Yes – Older the GIS 4 but younger than GIS 5	28,900	Andersen et al (2006)
1800.5	GIS 4 (near start)	30,162	29,413	Yes - Older than GIS 4 but younger than GIS 5	28,900	Andersen et al (2006)
1890.5	GIS 5 (peak GIS indistinct within % Nps)	34,437	32,979	Yes - Older than GIS 6 but younger than GIS 5	32,500	Andersen et al (2006)
1921.5	GIS 6	34,765	33,675	Yes - Older than GIS 4 but younger than GIS 6	33,740	Andersen et al (2006)
1950.5	GIS 7	36,406	35,120	Yes - Older than GIS 7 but younger than GIS 8	35,480	Andersen et al (2006)
2000.5	GIS 8	39,462	37,513	Yes - Older than GIS 8 but younger than GIS 9	38,220	Andersen et al (2006)
2020.5	GS 9	40,238	38,540	Yes		Andersen et al (2006)
2040.5	GIS 10	41,885	40,070	Yes	41,460	Andersen et al (2006)
2060.5	GIS 11	43,995	42,016	Yes	43,340	Svensson et al (2008)
2090.5	GIS 12	46,345	43,564	Yes	46,860	Svensson et al (2008)
2112.5	GIS 13	<i>Out of range</i>	45,837	Outside calibration range	49,280	Svensson et al (2008)

Figure 3.11: Testing of tuning to Greenland ice core $\delta^{18}\text{O}$ using radiocarbon dating. Calibrated radiocarbon dates (black open diamonds); corresponding tuned age for same depth interval (blue filled circle). Pink filled vertical bars give the position of the Greenland interstadial events and their approximate duration (see Wolff et al 2009, Lowe et al 2008); GIS numbering given in red. Horizontal black lines indicate the stratigraphic position of the start of the GIS.



6. Comparison to the ‘regional stratotype’ (NGRIP $\delta^{18}\text{O}$ on the GICC05 timescale) (after INTIMATE protocol, Lowe et al 2008)

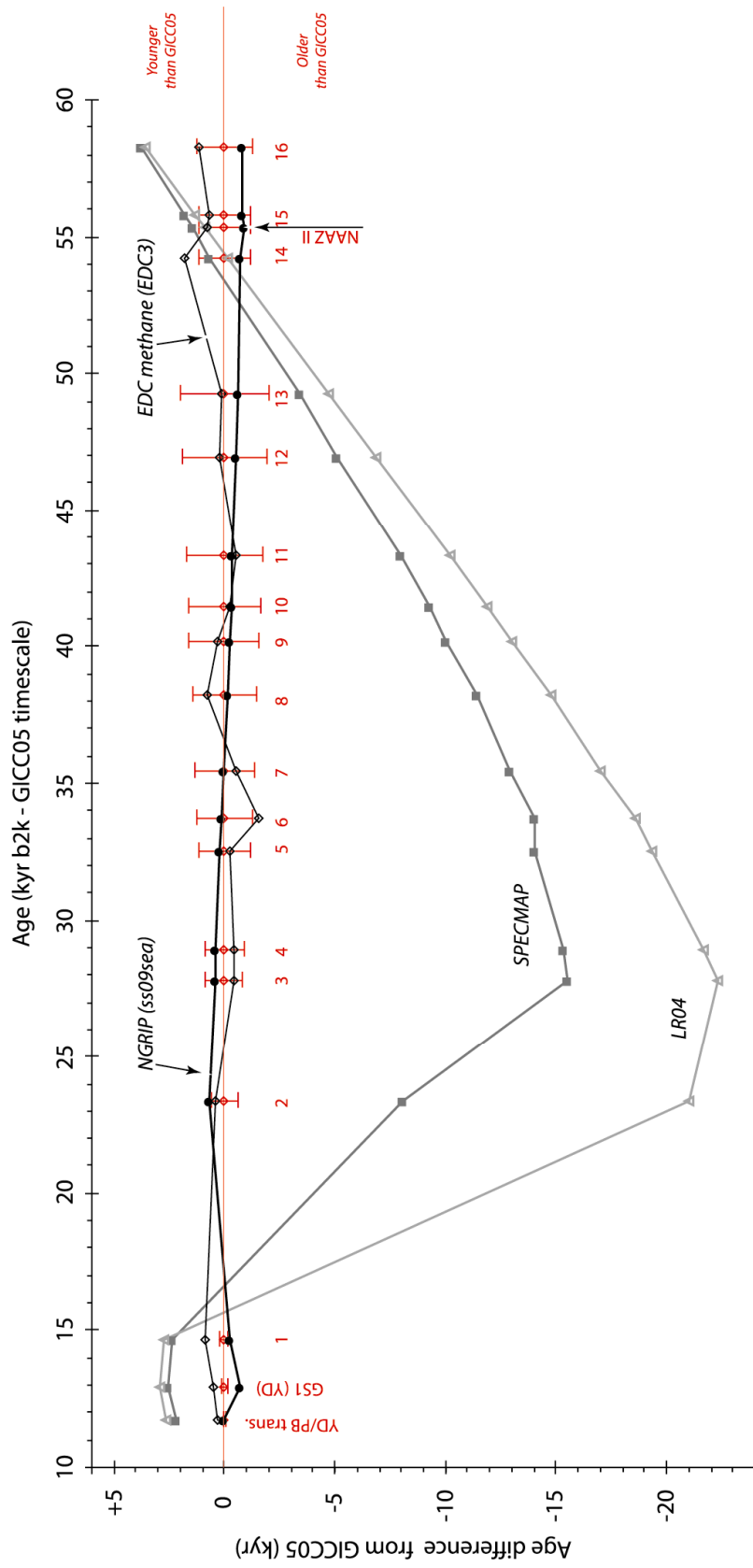
As a further test of tuning (using all the above mentioned tuning ‘targets’), the ages determined from these independent tuning methods are compared to those of the GICC05 timescale as this has become a reference core for both event stratigraphy and timing of the last glacial events (e.g. Lowe et al 2008). The ages for the transitions into the interstadials within the GICC05 timescale are used as a ‘standard’ by which the other tuning methods (benthic stacks, tuning to Greenland, tuning to Antarctica) may be compared (i.e. GICC05 age – other tuning method age) (Table 3.6, Figure 3.12).

Table 3.6: Comparison of age of the transition into the Greenland Interstadials (NGRIP GICC05 timescale) compared to the tuned (SPECMAP, LR04, NGRIP ss09sea and Antarctic methane) ages. Δ Age = GICC05 age minus age for same depth derived from the other listed tuning techniques; positive numbers denote ages younger than GICC05, negative values indicate age estimates older than GICC05. (YD=Younger Dryas, PB=Preboreal). Age estimates for tephra layer NAAZ II are given in bold.

	GICC05 age (yr b2k)	Error	MD04- 2822 depth cm	SPECMAP age	Δ Age (yr)	LR04 age	Δ Age (yr)	NGRIP ss09sea age (yr b2k)	Δ Age (yr)	Antarctic CH ₄ age (yr b2k)	Δ Age (yr)
YD/PB transition	11,703	50	245.5	9,541	2,162	9,078	2,625	11,700	3	11,423	280
GS1 (YD)	12,896	138	300.5	10,335	2,561	9,931	2,965	13,617	-721	12,418	478
GIS 1e	14,692	186	440.5	12,359	2,333	11,948	2,744	14,956	-264	13,852	840
2	23,340	596	1325.5	31,413	-8,073	44,382	-21,042	22,675	665	22,939	402
3	27,780	832	1766.509	43,257	-15,477	50,086	-22,306	27,375	405	28,246	-466
4	28,900	898	1801.4565	44,196	-15,296	50,585	-21,685	28,475	425	29,316	-416
5	32,500	1,132	1888.905	46,544	-14,044	51,834	-19,334	32,300	200	32,723	-223
6	33,740	1,286	1932.905	47,726	-13,986	52,304	-18,564	33,650	90	35,307	-1,567
7	35,480	1,321	1956.905	48,371	-12,891	52,529	-17,049	35,450	30	36,001	-521
8	38,220	1,449	2002.905	49,606	-11,386	52,960	-14,740	38,400	-180	37,449	771
9	40,160	1,580	2025.905	50,224	-10,064	53,176	-13,016	40,375	-215	39,854	306
10	41,460	1,633	2045.405	50,747	-9,287	53,358	-11,898	41,800	-340	41,748	-288
11	43,340	1,736	2067.405	51,338	-7,998	53,565	-10,225	43,650	-310	43,844	-504
12	46,920	1,915	2092.905	52,023	-5,103	53,804	-6,884	47,450	-530	46,656	264
13	49,280	2,031	2116.904	52,668	-3,388	54,029	-4,749	49,850	-570	49,114	166
14	54,220	1,150	2148.408	53,514	706	54,324	-104	54,950	-730	52,400	1,820
NAAZ II*	55,380	1,184	2163.5	53,919	1,461	54,466	914	56,296	-916	54,632	748
15	55,800	1,196	2166.905	54,011	1,789	54,498	1,302	56,600	-800	55,135	665
16	58,280	1,256	2187.405	54,561	3,719	54,690	3,590	59,100	-820	57,139	1,141

*For comparison a radiometric age for NAAZ II of 54.5 ± 2 kyr was obtained by Ar-Ar dating (Sigurdsson et al 1998, Lacasse and Garbe-Schönberg 2001)

Figure 3.12: Comparison of tuned ages (SPECMAP, Martinson et al 1987, grey filled circles; LR04, Lisiecki and Raymo 2005, grey open triangles; NGRIP ss09sea, NGRIP members 2004, black filled circles and; Antarctic (EPICA Dome C) methane, Parrenin et al 2007, black open diamonds) for the transitions into the Greenland Interstadials 1 to 16 on the NGRIP GICC05 timescale. The NGRIP GICC05 age estimates, uncertainties and numbering are given in red.



The tuning of the surface proxies to the Greenland ice cores agree very well (within the age uncertainty estimates of the GICC05 timescales. Also apparent is the close correspondence of the surface tuning to the Antarctic methane record. The age estimates generally fall within the GICC05 uncertainties; exceptions are the transition into GIS 1 (654 years younger than the GICC05 error envelope), GIS 6 (281 years older than the uncertainty window) and GIS 14 (670 years younger than the GICC05 error envelope). In contrast the tuning of benthic $\delta^{18}\text{O}$ to the global stacks (SPECMAP and LR04) produce age estimates that are considerably older; the LR04 estimates are greater than their SPECMAP equivalents. The patchy nature and generally low resolution of the benthic record, in addition to possible alternative correlations within some sections (most notably the last glacial) may be responsible for the large age offsets when compared with the surface tuning approaches. Difficulties associated with the benthic $\delta^{18}\text{O}$ tuning method, e.g. deep water temperature change ‘over-printing’ the global signal, would further add to uncertainties. These effects would be greatest during the climate transitions that underpin the surface proxy tuning methods.

The close comparison of the surface tuning approaches lends confidence to the matching of the surface proxies to Antarctic methane within MIS 6. However, there is currently no way in which to test the ‘hypothetical’ age model within MIS 6. One technique that may provide some insight in the future is relative geomagnetic palaeointensity.

Relative geomagnetic palaeointensity (RPI) offers a measurable proxy that is global in nature and devoid of environmental influences, as such, an independent marine chronology could eventually eliminate difficulties inherent in oxygen isotope stratigraphy (Channell et al 2009) including the phase lag between forcing and response implicit in insolation-driven ice-sheet models (Imbrie and Imbrie, 1980) and the assumption that $\delta^{18}\text{O}$ is purely a glacial ice volume signal (Skinner and Shackleton 2005). In the future, utilising a paired RPI and benthic $\delta^{18}\text{O}$ records could facilitate correlation of Greenland and Antarctic ice cores to marine sediment cores via $^{10}\text{Be}/^9\text{Be}$ data (Channell et al 2009) as geomagnetic field intensity is a control on cosmogenic nuclide production (Channell et al 2008).

For MD04-2822 the close correspondence of the RPI record (JET Channell, *unpublished data*) on its finalised age model to the PISO-1500 stack¹⁷ (Channell et al 2008, 2009) (JET Channell, *pers comm.*) lends independent support for the MD04-2822 age-depth model, particularly within MIS 6.

¹⁷ PISO-1500 stack is a combined relative geomagnetic palaeointensity and benthic isotope stack and provides a template for the correlation marine sediment RPI records (Channell et al 2009). It should be noted, however, the PISO-1500 stack is low resolution compared to the MD04-2822 data (JET Channell, *unpublished data*). The age model for the stack is based upon benthic $\delta^{18}\text{O}$ record of U1308 (Gardar Drift; Hodell and Curtis 2008, Hodell et al 2008, 2009, Channell et al 2008) which is aligned the LR04 benthic $\delta^{18}\text{O}$ stack (Lisiecki and Raymo 2005), thus some of the difficulties of using benthic $\delta^{18}\text{O}$ remain.

CHAPTER 4¹: An Evaluation of the Event Stratigraphy Approach in Marine Sediments

This chapter reviews and evaluates the event stratigraphy approach, in particular with respect to chronological control of marine sediments. The event stratigraphy approach is used extensively within palaeoceanography as a means of age control (e.g. the correlation of marine proxy records to the Greenland $\delta^{18}\text{O}$ ice core records; chapter 3). This chapter sets out the advantages and disadvantages of this technique using two examples from the MD04-2822 record as a means by which the utility and limitations may be illustrated. The examples are: i) the formation of a local event stratigraphy ('replication') and ii) the subdivision of Greenland Stadial (GS) 3.

The correlation of marine palaeoenvironmental events within the North Atlantic, and on a common timescale, is essential in assessing the spatial and temporal variation of such events and thus inform our understanding or causal relationships within the climate system. Records of common climatic and environmental events recorded within sediment successions (or other archives such as ice), have enabled event stratigraphies to be established on varying timescales, resolutions and geographic coverage. This approach has been widely utilised within Quaternary investigations; indeed, such an approach is advocated by the INTIMATE² group.

An event stratigraphy approach enables different proxy records to be linked together via the covariation of their individual events using, for example, 'wobble-matching'. Indeed, age control of marine sediment sequences often utilises the correlation of an initial event stratigraphy to a global $\delta^{18}\text{O}$ stack (e.g. Pisias et al 1984, Imbrie et al 1984, Martinson et al 1987) or the Greenland ice cores (e.g. Shackleton et al 2000). The INTIMATE group (Lowe et al 2008), recently recommended a protocol for the correlation of palaeoenvironmental events within the North Atlantic. This codification draws upon the widely adopted and established event stratigraphy approach. It stresses the importance of a local stratigraphic definition of events, with their timing and duration determined by an independent method, radiocarbon for example, prior to correlation to the Greenland ice cores and the validation of such correlations via, for example, tephrochronology (Lowe et al 2008).

The compound chronology for MD04-2822 (chapter 3) utilises event stratigraphy, however, it varies subtly from that recommended by Lowe et al (2008) in that it is reliant upon tuning to the Greenland ice core (NGRIP $\delta^{18}\text{O}$ on the ss09sea timescale; NGRIP members 2004), for the interval ca. 0 to 123 kyr, and tuning to the EPICA Dome C methane record (Loulergue et al 2008) on the EDC 3 timescale (Parrenin et al 2007) within MIS 6, for primary age control. In contrast to the INTIMATE approach, independent age control (radiocarbon dating and tephrochronology) served

¹ Work on GS3 has been accepted for publication in *Quaternary Science Reviews*; Austin WEN, **Hibbert FD**, Rasmussen SO, Peters C, Abbott PM, Bryant CL The synchronisation of palaeoclimatic events in the North Atlantic region during Greenland Stadial 3. In addition, some material has been incorporated into Austin WEN and **Hibbert FD**. Tracing Time in the Ocean: A brief review of chronological constraints in marine event-based stratigraphies within the same issue. All material within this chapter is the sole work of F. Hibbert.

² INTIMATE: INTegration of Ice-core, MARine and TERrestrial records of the North Atlantic is a project within the INQUA Palaeoclimate Commission.

as invaluable checks of the tuning. Stratigraphical information such as the position of tephra layers, provided *a priori* bounds in the placement of tie-points between the MD04-2822 record and the Greenland ice core.

This chapter aims to evaluate the event stratigraphy approach using examples from the MD04-2822 record. A brief background of the use of event stratigraphy within palaeoenvironmental investigations is given. Examples from the Rockall Trough and for four cores from the NE Atlantic during Greenland Stadial (GS) 3 illustrate some of the advantages of an event stratigraphy approach. Finally, an evaluation of event stratigraphy, the assumptions therein and particular problems arising from its application within marine environments is offered, in light of the examples presented.

1. Background: Event Stratigraphies

Event stratigraphies have been used extensively within palaeoenvironmental investigations. These often prove advantageous in allowing records to be linked based upon common events. Indeed, early work on the reconstruction of the limits of the British Ice Sheet (BIS) during the last glaciation were based upon the correlation of glacial units and drift mapping (e.g. Wright 1913, 1937, Charlesworth 1928, 1929, 1957) and is continued today in careful mapping and other palaeoenvironmental investigations of both the extent and timing of the last BIS. Indeed, current evidence for a Hebridean shelf edge glaciation during MIS 6 (other than this study) is based upon the long-range correlation of seismic reflection data (Holmes 1997).

Additionally, using an event stratigraphy may permit the transferral of age control to an individual record and this age control need not be conditional upon well constrained ages of that individual record. For example, correlating a marine record to a benthic $\delta^{18}\text{O}$ stack allows the transfer of the stack chronology to the sediment sequence. Alternatively many marine sediment sequences in the North Atlantic utilise the presence of prominent sea surface warming events within the last glacial (the D/O events) to correlate to the well dated Greenland ice cores. The ice core ages may then be transferred to the marine sediments.

Age control can also be obtained for marine sediments independent of an event stratigraphy e.g. via radiocarbon, however, this may not always be practical (i.e. where foraminifera numbers are low) or possible (e.g. beyond the limits of the radiocarbon method or funding constraints). In addition, the radiocarbon method is associated with a number of uncertainties within the marine environment such as the variable local marine reservoir effect. As such, using the Greenland ice core chronologies often proves an expedient and highly effective means of age control. Employing an event stratigraphy allows for the correlation of events within sedimentary sequences, even in the absence of precise age control. The reasons for the change in proxies need not be fully understood for a common event stratigraphy to be confirmed or for transfer age control (Knight 2003).

Event stratigraphies may also provide invaluable information regarding local or regional influences upon a sedimentary record, enabling an assessment of the representative nature of an individual record. If such event stratigraphies have robust,

independent (i.e. non-transferred) age constraints, they may provide insights into the both the timing of climatic events and the phasing of those events.

If several archives contain the same event stratigraphy (e.g. Greenland ice cores, marine sediments, speleothems), there should in principal, be a consistent chronology for those events. Skinner (2008) demonstrated that the independent age control of several archives (containing the same event stratigraphy) deviated subtly from one another and suggested that this enabled inferences regarding absolute age control, radiometric calibration (including marine reservoir effects) and the initial stratigraphic correlations to be drawn (see chapter 3, *Chronostratigraphy*).

However, there are a number of difficulties associated with event stratigraphies including: climate archive resolution, which is dependent upon sedimentation rate and preservation (Shackleton et al 2000); dating control (e.g. Lowe et al 2001, Blaauw et al 2010) and; how different depositional environments record the climate signal (Knight 2003). Indeed, some proxies are more sensitive to specific types of change (e.g. temperature) than others (Hoek and Bohncke 2001). Such differences may result in a regionally synchronous event appearing lagged in phasing due to the differing response times of archives (Knight 2003). Alternatively, 'time-transgressive' (asynchronous) events may appear synchronous within low resolution records (Seilacher 1991). These concerns (dating control, assumption of synchronicity etc) will be addressed in the following sections of this chapter, with reference to examples from the MD04-2822 record

A partial solution to some of these concerns has been the convention of using rapid climate events as tie-points between records (Wohlfarth et al 1993, Shackleton et al 2000, Lowe et al 2001, Austin et al 2004). These rapid events may be thought of as rapid 'jumps' between quasi-stable states (e.g. Alley et al 1999, Broecker 2000) and occur as discrete events within sedimentary records (Seilacher 1991, Geldsetzer and Nowland 1993, Knight 2003). The most widely used is the transitions into the D/O events which are prevalent in the many palaeoenvironmental records of the last glacial.

A potential major disadvantage of utilising an event stratigraphy approach is the assumption that all climate changes will be recorded within all proxy records and that all records may be correlated to one another (Knight 2003). This assumption may be reasonable at some scales, for example, the pervasive quasi-1,500 year 'cycle' (e.g. Alley et al 2001) within the North Atlantic. An expression of this 'cycle' are the prominent warming features (Dansgaard-Oeschger (D/O) events) first identified within the Greenland ice cores (Dansgaard et al 1992) which are also evident within marine cores (e.g. Bond et al 1993, Bond and Lotti 1995). The rapid warming into the D/O events, which occur over relatively short time intervals (e.g. Lang et al 1999), may be used to tie the records together and allow the transfer of the well constrained ice core ages to the marine sediment core. Tuning marine and Greenland records, using the D/O features common to both, assumes the synchronicity of change in surface waters and atmospheric temperature changes over Greenland (e.g. Bond et al 1993; Shackleton et al 2000). The % *N. pachyderma* (sinistral) proxy record has been used extensively within the NE Atlantic to construct age models for marine sediment cores, via tuning to the well dated Greenland ice cores. This 'matching' of the D/O events between records does, however, prevent an assessment of any leads or lags within the

climate system which is a key consideration in attempting to understand the mechanisms of palaeoenvironmental change.

The following sections provide examples of the advantages of the event stratigraphy approach as: (i) a means of 'replication' thereby enabling assessment of local versus regional influences to be made and; (ii) a means whereby age control may be achieved and the geographic expression of events may be determined.

2. Advantages of Event Stratigraphies

2.1. Age control

One advantage of using this approach is the ability to transfer ages from one record to another if both contain the same event stratigraphy. This is a common means by which age control is achieved for marine sediments; events may be correlated from an individual record to a benthic $\delta^{18}\text{O}$ stack or to the Greenland ice core records and the chronology transferred. This is the means by which age control for the MD04-2822 core was obtained (see chapter 3, *Chronostratigraphy*). Event stratigraphy may also facilitate the correlation of events even in the absence of robust age control (e.g. the correlation of seismic reflection profiles)

2.2. Formation of local event stratigraphies: Rockall Trough (ca. 0 to 200 kyr)

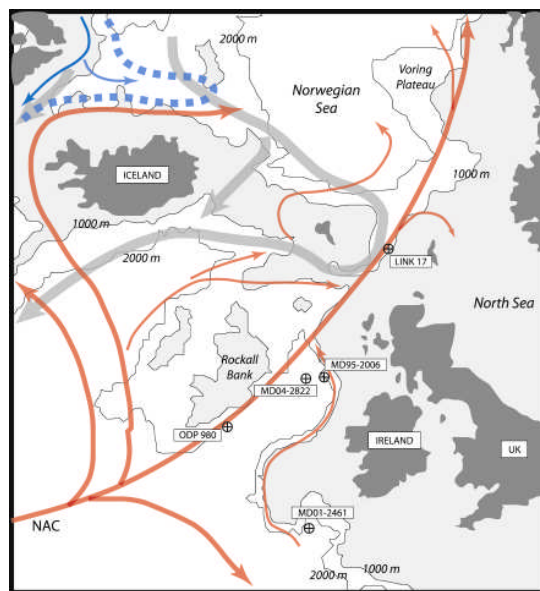
As noted above, event stratigraphy may be fruitfully employed even where no robust age model is available. This approach has long been used within Quaternary investigations (e.g. Wright 1913, Charlesworth 1928). A local event stratigraphy may enable an evaluation of the representative nature of a feature contained within an individual record. Whilst it is not strictly replication, it aids interpretation of proxy records, particularly if also accompanied by a robust age model for that event stratigraphy. In the following example, three marine sediment cores are correlated based upon climatic 'events'; once aligned, a local event history may be unravelled based upon these events.

A Rockall Trough event stratigraphy was constructed on a local (basin) scale by comparing MD04-2822 with the high resolution piston core MD95-2006 (Barra Fan; 57°0.1.82'N; 10°03.48'W, 2120 m) and ODP 980 (55°29'N, 14°42'W, 2179 m) (Figure 4.1). These cores are at a similar water depth, approximately 240 km apart and well characterised (e.g. Knutz et al 2001, 2002, Wilson and Austin 2002, Dickson et al 2008, McManus et al 1994, 2002, Oppo et al 2006, Channell and Raymo 2003). MD95-2006 and ODP 980 are approximately 83 km and 240 km respectively from the MD04-2822 core site and this should enable regional features to be identified.

Marine sediment cores MD04-2822 and MD95-2006, in particular, afford a rare opportunity for the replication of marine proxy records within the last glacial period. These cores are located approximately 83 km apart, to the west of the former NW BIS. Replication within palaeoceanography is limited, due to the cost (time and expenditure) of obtaining material and generating proxy records. However, it is essential in assessing the representative nature of any record and the contribution of local versus regional influences.

The benthic $\delta^{18}\text{O}$ of MD04-2822 and ODP 980 are shown in (Figure 4.2– note only the uppermost portion of the ODP 980 record is shown³) and show remarkable similarities to one another and to the benthic $\delta^{18}\text{O}$ stacks (e.g. SPECMAP and LR04). The large shift in $\delta^{18}\text{O}$ associated with the transition from MIS 7 to MIS 6 is absent within MD04-2822, however the transition from MIS 6 into MIS 5 and MIS 2 into MIS 1 are very clear from the benthic $\delta^{18}\text{O}$. The proximity of these cores and their similar water depths allows the benthic $\delta^{18}\text{O}$ to be thought of as essentially time parallel events as local influences on the benthic $\delta^{18}\text{O}$ would be similar for both cores⁴ (see chapter 3, *Chronostratigraphy*, for a discussion on the influences on benthic $\delta^{18}\text{O}$ that may produce offsets in the benthic $\delta^{18}\text{O}$ record).

Figure 4.1: Map of core locations mentioned in this chapter. Red arrows indicate the approximate positions of modern warm surface currents, blue cold surface current and grey arrows the position of deep water flow. Dashed thick blue line gives the position of the modern polar front (after Hansen and Østerhus 2000).



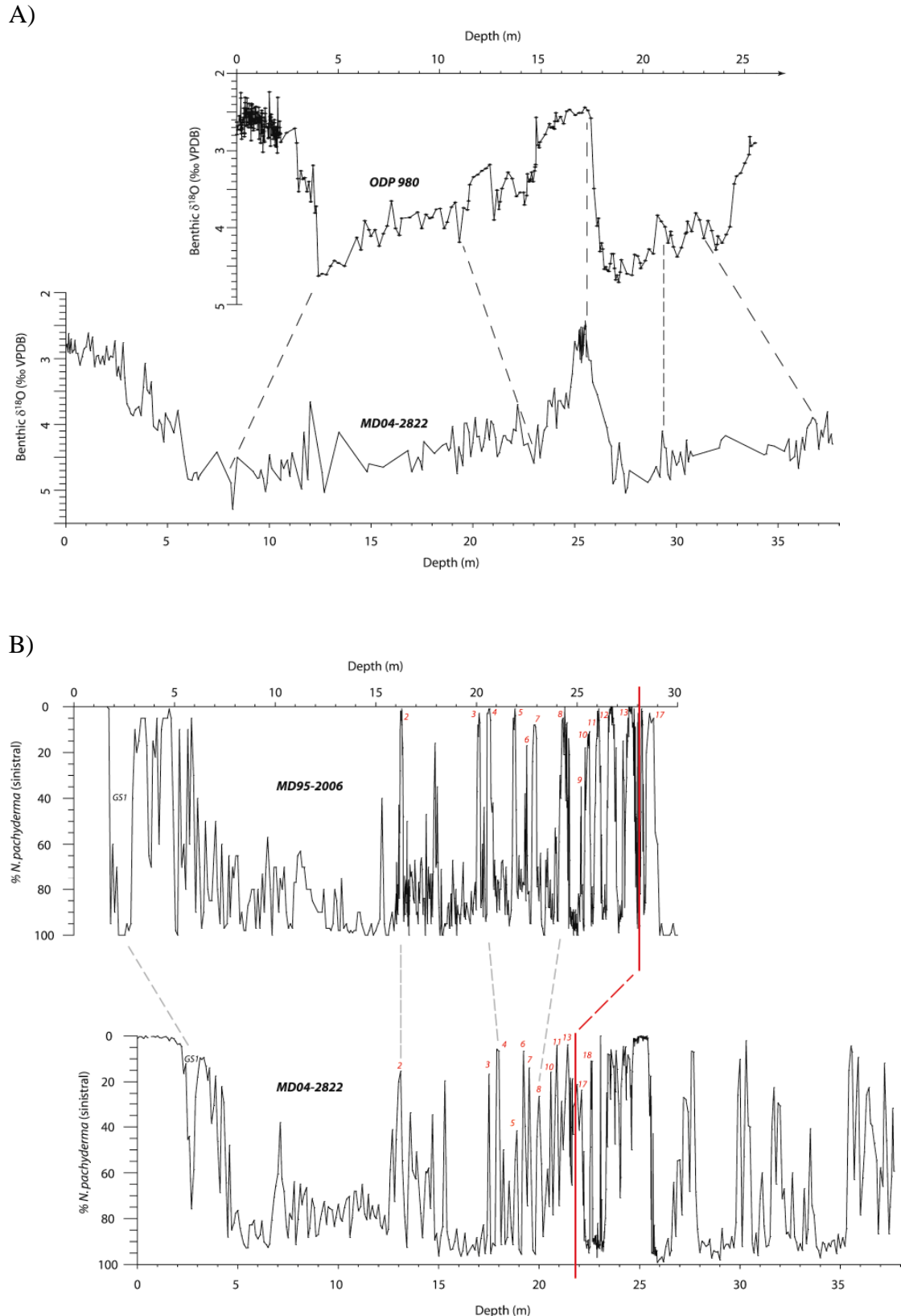
In the second example (panel b in Figure 4.2), the % *N. pachyderma* (sinistral) is the basis of the event stratigraphy. The migration of the polar front may be deduced from this proxy as this species occurs as a near monospecific assemblage north of the polar front (Bé 1977). Additionally, this proxy provides a well established semi-quantitative sea surface temperature (SST) record (e.g. Bond et al 1993, Dickson et al 2008). For MD04-2822 and MD95-2006, surface warming events (the D/O events) are conspicuous; due to the higher sampling resolution of MD95-2006 these events are more clearly defined. The use of the XRF Ca record with its much increased resolution, in conjunction with the % *N. pachyderma* (sinistral) record, of MD04-2822 enables the secure correlation to the D/O events (see chapter 3, *Chronostratigraphy*), therefore the Greenland ice core numbering scheme is confidently ascribed to each of these events for both cores.

³ ODP 980 extends to ~1.2 Ma

⁴ Deep water circulation within the Rockall Trough is dominated by NADW which flows along the western margin and the eastern margin as a cyclonic gyre possibly adding some degree complexity to the mixing of water masses within the Rockall Trough.

CHAPTER 4:
An Evaluation of the Event Stratigraphy Approach in Marine Sediments

Figure 4.2: Local event stratigraphy; each record is presented on its own depth scales (note depths are scaled to one another), example correlations are given by grey dashed lines A) benthic $\delta^{18}\text{O}$ records of MD04-2822 and ODP 980 (e.g. McManus et al 1994, 2001, Oppo et al 2001, Flower et al 2000) (note ODP 980 is shown only to 25 m). B) % *N. pachyderma* (sinistral) records for MD04-2822 and MD95-2006 (e.g. Wilson et al 2002, Dickson et al 2008, Leigh 2005). Red numbers give the GIS number and the stratigraphic position of peak abundance of the rhyolitic component (II-RHY-1) of NAAZ II.



Surface and deep water hydrographic events common to all three records can be identified for the last ~ 175 kyr; this forms the basis of the Rockall Trough event stratigraphy within which it would be possible to transfer the MD04-2822 compound age model to both MD95-2006 and ODP 980 and *vice versa*. However, in ‘synchronising’ the records, it is no longer possible to assess the phasing of the events between the records. This may be remedied if the events were to be independently dated, however, uncertainties associated with independent age control (e.g. radiocarbon dating) may hinder the reliable estimate of any phasing (if indeed they exist).

2.3. ‘Replication’ – insights into BIS dynamics

The close proximity of the cores mentioned above and the correlation of events recorded within those sediments, form the basis of the Rockall Trough event stratigraphy presented above. From this, the patterns of IRD delivered to the Rockall Trough area in high resolution for the last 175 kyr may be evaluated. MD04-2822 provides a ‘bridge’ by which the high resolution but relatively short temporal span of core MD95-2006 may be compared with the much lower resolution but greater time span of core ODP 980 (Figure 4.3). A similar coherent latitudinal pattern of IRD delivery to sediment cores proximal to the last BIS for the last ca. 50kyr was also identified by Scourse et al (2009) from 6 marine sediment cores.

The records are similar but the magnitude of IRD events varies between the records. Such comparisons are however still subject to the uncertainties in the construction of the chronology applied to all cores. The variation in magnitude of IRD events between the cores may be due to the increasing distance from the marine margins of the BIS but also due to difference in depositional settings. Unfortunately, I was unable to convert the IRD concentration data for MD95-2006 and ODP 980 to IRD flux as the water content data needed for the calculation of dry bulk density (and thus bulk mass accumulation rate; see chapter 3, section 7.1) was unavailable; this is especially important for cores proximal to former ice margins where the input of IRD may be ‘diluted’ by inputs of fine grained terrigenous material. In addition, differences in the surface hydrography may have affected the pattern and/or timing of IRD delivered to the sites.

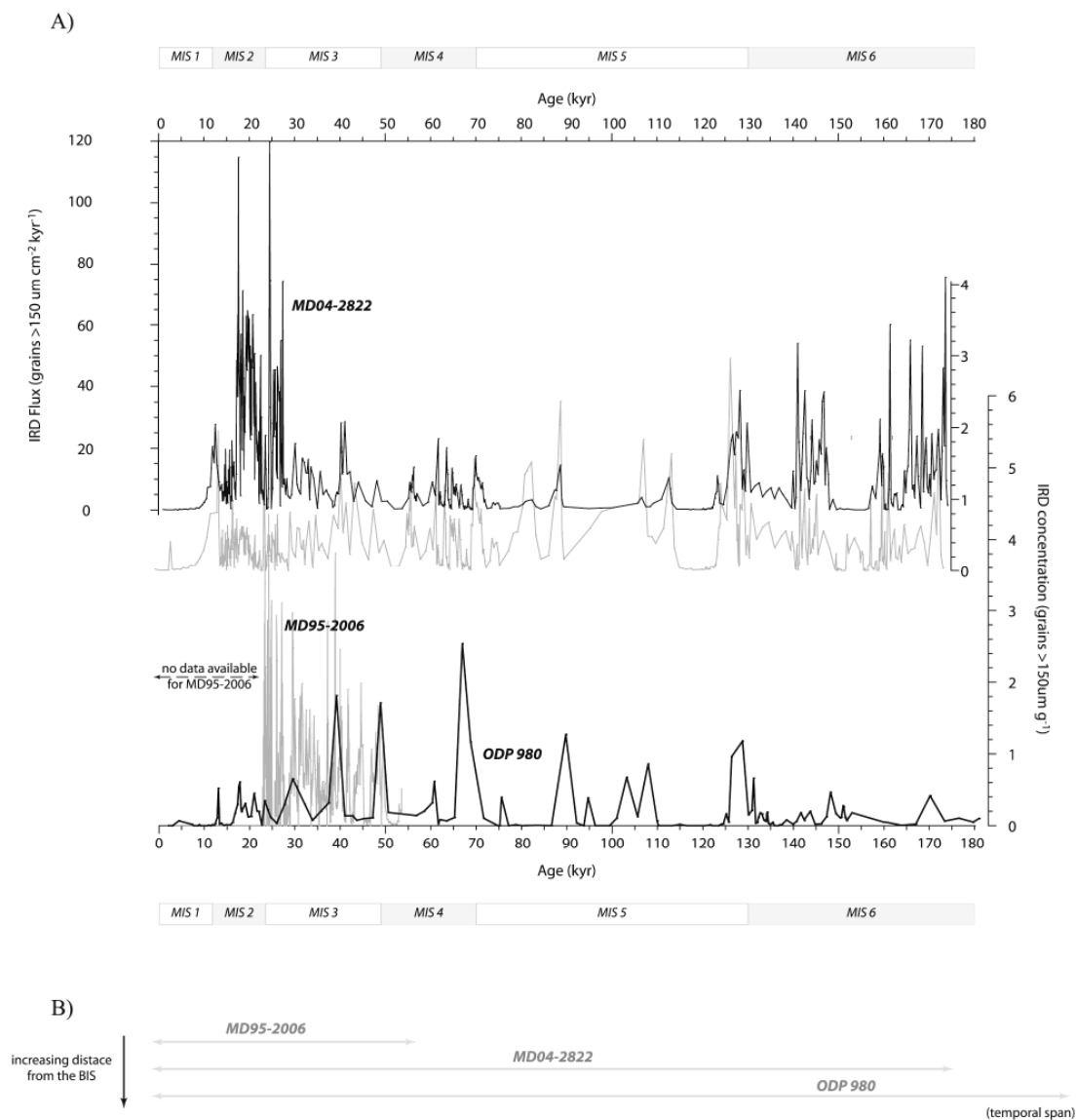
For the last glacial, the pattern of IRD delivery is very similar for MD04-2822 and MD95-2006 (Figure 4.3), with a pulse of IRD at ca. 50 and 40 kyr and sharp increase ca. 30 kyr reflecting the growth of the last BIS towards its maximum extent. These pulses in IRD deposition are also evident in ODP 980 although the magnitude of these events is different. This may reflect a ‘dilution’ of the ODP 980 record with increased fine grained terrigenous inputs and possible suppression of the surface productivity thereby reducing the biogenic component of the sediments, in the initial build-up of the last BIS.

A very large IRD peak is seen ca. 70 kyr in ODP 980 that is not seen in the MD04-2822 record, although there is a grouping of IRD events at this time. The more distal site (ODP 980) from the BIS marine margins during MIS 4, may have a disproportionately high IRD signal due to inhibition of surface productivity, and hence biogenic component of the sediments. Alternatively, the more proximal MD04-

2822 record may have an attenuated signal due to fine grained terrigenous inputs ‘diluting’ the IRD signal.

For the penultimate glacial, the pattern of IRD delivery is similar for MD04-2822 and ODP 980; the much reduced magnitude of the IRD signal at the ODP 980 site may reflect its location away from the BIS calving margins with most IRD released from icebergs before reaching the ODP 980 site.

Figure 4.3: A) IRD records for MD04-2822, MD95-2006 and ODP 980. Note that both IRD flux (upper panel) and IRD concentration (lower panel) are shown for MD04-2822. MIS designation after Imbrie et al (1984). B) schematic of the temporal resolution and distance from the former BIS.



The similarities evident between the records may aid any interpretation of the dynamics of former ice sheets in that they may provide a form of ‘replication’ which is often unavailable due to practical considerations. A consistent pattern of IRD delivery to the Rockall Trough for the three cores is evident, although interpretations are hampered as calculations of IRD flux for each core site are unavailable.

2.4. Assessing the geographical expression of events: An example from Greenland Stadial (GS)

The event stratigraphy approach may facilitate an assessment of the geographic expression of climatic events. For example, four marine cores were compared in order to investigate the spatial extent of a previously unidentified regional warming event interval within Greenland Stadial (GS) 3 (ca. 23.4 to 27.4 kyr b2k⁵) (Austin et al, *accepted*). A local event stratigraphy is used to correlate the cores to one another, which in turn is correlated to the NGRIP $\delta^{18}\text{O}$ record (NGRIP members 2004) and the NGRIP GICC05 timescale transferred to the marine sediments, in order to characterise this event. Correlation is based upon the identification of GIS 2, 3 and 4, as well as the Fugloyarbanki tephra (Faeroe Marine Ash Zone II) and Heinrich event 2, where present.

The four cores considered form a north-south transect from the Faeroe-Shetland Channel to the Porcupine Seabight (Figure 4.1, Table 4.1). All cores are primarily comprised of hemipelagic sediments with occasional dropstones (Hibbert et al 2010, Knutz et al 2001, Peck 2006, Rasmussen and Thomsen 2008). Turbidite layers have been identified within MD95-2006, particularly for the last glacial (e.g. Knutz et al 2002, Wilson et al 2002, Peters et al 2008).

Table 4.1: Location and water depth for cores investigated LINK 17, MD95-2006, MD04-2822 and MD01-2461 and relevant references.

Core	Location		Water depth (m)	Coring method	References
LINK 17	Eastern Faeroe-Shetland Channel	not available	1500	Piston core	Nielsen et al 2000 Rasmussen and Thomsen 2008
MD04-2822	Rockall Trough	56°50'N; 11°20'W	2344	Giant piston	Hibbert et al 2010
MD95-2006	Barra Fan	57°0.1.82'N; 10°03.48'W	2120	Giant piston	e.g. Kroon et al 2006, Knutz et al 2001, 2002a, Wilson et al 2002, Wilson and Austin 2002, Austin et al 2004, Peters et al 2008
MD01-2461	Porcupine Seabight	51°45'N; 13°25.90'W	1153	Giant piston	Peck et al 2006, 2007a, 2007b, Scourse et al 2009

The correlation of climatic events within the GIS 2 to GIS 4 ‘window’ was greatly aided by other proxy information, in addition to the % *N. pachyderma* (sinistral) for all cores. These included the presence of a basaltic tephra layer and an episode of very high IRD inputs (previously correlated to H2 for MD95-2006, LINK17 and MD01-2461). From Figure 4.4 and Table 4.2, a regional event stratigraphy was formulated. Of note is the warming event identified within all four cores within GIS 3 that is not associated with interstadials.

The Greenland ice core terminology has been adopted for the local event stratigraphy. The reasons for this are twofold: firstly, the MIS subdivision is of insufficient resolution for this interval and such proxy data unavailable for some of the cores; and secondly, the prominent D/O events are clearly present within both the marine and

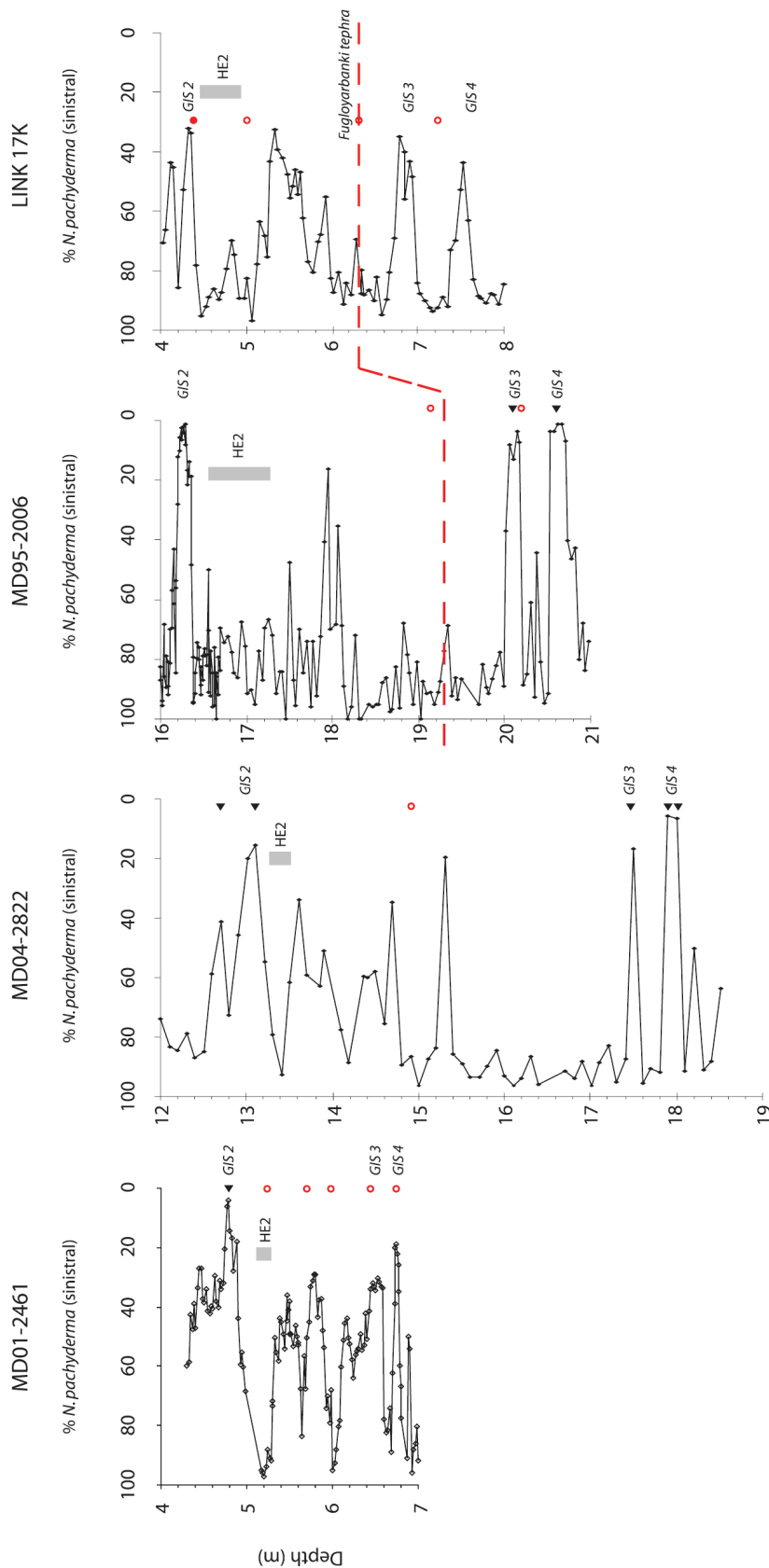
⁵ This age range is estimated from tuning the surface proxies to the NGRIP $\delta^{18}\text{O}$ record on the GICC05 timescale

Table 4.2: Local event stratigraphy and climatic correlation for MD04-2822, MD95-2006, LINK 17 and MD01-2461

Event	Climatic Correlation	Evidence for climatic correlation MD04-2822	Evidence for climatic correlation MD95-2006	Evidence for climatic correlation LINK 17 (Rasmussen and Thomsen 2008)	Evidence for climatic correlation MD01-2461 (Peck et al 2006, 2007a, 2007b)
Low % <i>N. pachyderma</i> (sin.)	GIS 4	<ul style="list-style-type: none"> • Sharp transition in and out • Radiocarbon dating (peak warming) 	Radiocarbon date	Stratigraphic position in relation to Fugloyarbanki tephra and HE 2	<ul style="list-style-type: none"> • Sharp transition in and out • Stratigraphic position between HE 2 and HE3
Low % <i>N. pachyderma</i> (sin.)	GIS 3	<ul style="list-style-type: none"> • Sharp transition in and out • Radiocarbon date (peak warming) 	Radiocarbon date	Stratigraphic position in relation to Fugloyarbanki tephra and HE 2	Stratigraphic position between HE 2 and HE3
Tephra	Fugloyarbanki (Faeroe Marine Ash Zone II)	n/a	Major element geochemical analysis of basaltic shards (C. Peters, unpublished data)	<ul style="list-style-type: none"> • Major element geochemistry (Wastegård et al 2006) • Stratigraphic correlation (Rasmussen and Thomsen 2008) to Fugloyarbanki tephra layer (geochemically confirmed) within other Faeroe cores (Rasmussen et al 2003, Wastegård et al 2006) 	n/a
High IRD content	Heinrich 2	<ul style="list-style-type: none"> • ITRAX Ca/Sr, environmental magnetics (C. Peters, unpublished data) • presence of detrital carbonate (but insufficient resolution to accurately position HE 2) 	<ul style="list-style-type: none"> • Lithic counts – elevated concentration of total lithics (Knutz et al 2001) • Environmental magnetic un-mixing model (C. Peters 2008)* • Lithological characterisation (Leigh 2006)* 	High IRD content	<ul style="list-style-type: none"> • Lithic counts – elevated concentration of total lithics • Lithological characterisation (see Peck et al 2007b)
Low % <i>N. pachyderma</i> (sin.)	unknown	Decreased % <i>N. pachyderma</i> (sinistral)	Decreased % <i>N. pachyderma</i> (sinistral)	Decreased % <i>N. pachyderma</i> (sinistral)	Decreased % <i>N. pachyderma</i> (sinistral)
Low % <i>N. pachyderma</i> (sin.)	GIS 2	<ul style="list-style-type: none"> • Sharp transition in and out • Radiocarbon date (peak warming) 	<ul style="list-style-type: none"> • Stratigraphic position of HE2 • Radiocarbon date (<i>Nps</i>) 	Stratigraphic position in relation to Fugloyarbanki tephra and HE 2	<ul style="list-style-type: none"> • Radiocarbon date • Stratigraphic position of HE2
Low % <i>N. pachyderma</i> (sin.)	Un-numbered warming immediately post GIS 2	<ul style="list-style-type: none"> • Sharp transition in and out • Radiocarbon date (peak warming) 	Sharp transition in and out stratigraphical position GIS 2	<ul style="list-style-type: none"> • Radiocarbon date (bivalve) • Sharp transition on and out, stratigraphic position HE 2 and GIS2 	Stratigraphical position of GIS 2

* Exact position of Heinrich Event 2 remains unresolved; this is attributed to a 'swamping' of the Laurentide carbonate signal by IRD originating from the proximal British Ice Sheet (Peters et al 2008). The high input of terrigenous material also obfuscates the exact location of HE 2 within MD04-2822.

Figure 4.4: Local event stratigraphy – GS3: % *N. pachyderma* (sinistral) records for MD01-2461 (Peck et al 2006, 2007a,b, Scourse et al 2009), MD04-2822, MD95-2006 (Wilson and Austin 2002, Austin et al 2004, Dickson et al 2008, Peters et al 2008) and LINK17 (Nielsen et al 2000, Rasmussen and Thomsen 2008) presented on their respective depth scales. Greenland Interstadial (GIS) events are marked. The stratigraphic position of radiocarbon dating intervals given by: black filled triangles (*G. bulloides*), open red circles (*N. pachyderma* (sinistral)) and red filled circle (unidentified bivalve). Depth of maximum abundance of basaltic tephra identified within MD95-2006 and LINK17 indicated by the dashed red line. The approximate position of Heinrich Event (HE) 2 is denoted by the filled grey boxes.



ice cores for this interval. As the warming event is currently recognised only within NE Atlantic marine cores (this study, Peck et al 2007, Rasmussen and Thomson 2008, Scourse et al 2009 and references therein) but not the wider Nordic Seas (e.g. Fronval et al 1995, Weinelt et al 2003), it would be inappropriate to sub-divide GS3 following only the scheme for the Greenland ice cores (cf. Lowe et al 2008). Instead, a prefix of North East Atlantic (NEA) is added. Based upon the regional event stratigraphy, a regional marine sub-division of GS3 is proposed. GIS 3 is followed by a cold interval in the NE Atlantic (NEA-GS3c⁶), then a warming with a restricted (i.e. spatially confined) northward retreat of the polar front (NEA-GS3b) and finally a cooling of surface waters (NEA-GS3a) prior to the warming transition into GIS 2.

The D/O events evident within the marine sediment records were correlated to the Greenland ice core records in order to obtain an estimate of the timing of the NEA-GS3b event. However, on comparison of the ice core and marine records, the NEA-GS3b warming event is absent from the NGRIP $\delta^{18}\text{O}$ record as well as marine records of the wider Nordic Seas.

The layer counted NGRIP $\delta^{18}\text{O}$ record on the GICC05 timescale (Andersen et al 2006, Rasmussen et al 2006, Svensson et al 2006, 2008, Vinther et al 2006) was used to obtain age control for the GS3 interval by tuning the surface proxies (% *N. pachyderma* (sinistral)) of all four cores to the Greenland ice core record using the transitions in (c.f. Shackleton et al 2000) and out⁷ of the well defined D/O events conspicuous within both, as well as the peak occurrence of the Fugloyarbanki tephra (where present⁸; Davies et al 2008). The tie-points and resulting age model are given in Appendix C₃ and Figure 4.5.

2.4.1. *Characterisation of the NEA-GS3b warming event*

The structure of the NEA-GS3 event when placed upon the same age scale is striking; within MD04-2822, MD95-2006 and LINK 17, the low % *N. pachyderma* (sinistral) represents the first significant warming post GIS 3, however, this relationship is less clear in MD01-2461 (Figure 4.5). Perhaps somewhat counter-intuitively, the warming event has a much wider manifestation (i.e. longer duration) in the most northerly of the cores (LINK 17). One might expect that this most northerly site would ‘see’ the warming into this event last, and the cooling out first; the progressive migration northwards (and subsequently southwards) of the polar front within GS3 should result in a ‘narrow’ (i.e. of shorter duration) warming peak compared to a more southerly core. However, using 40 % *N. pachyderma* (sinistral) abundance⁹, the duration of the interval is in line with MD04-2822 and MD95-2006.

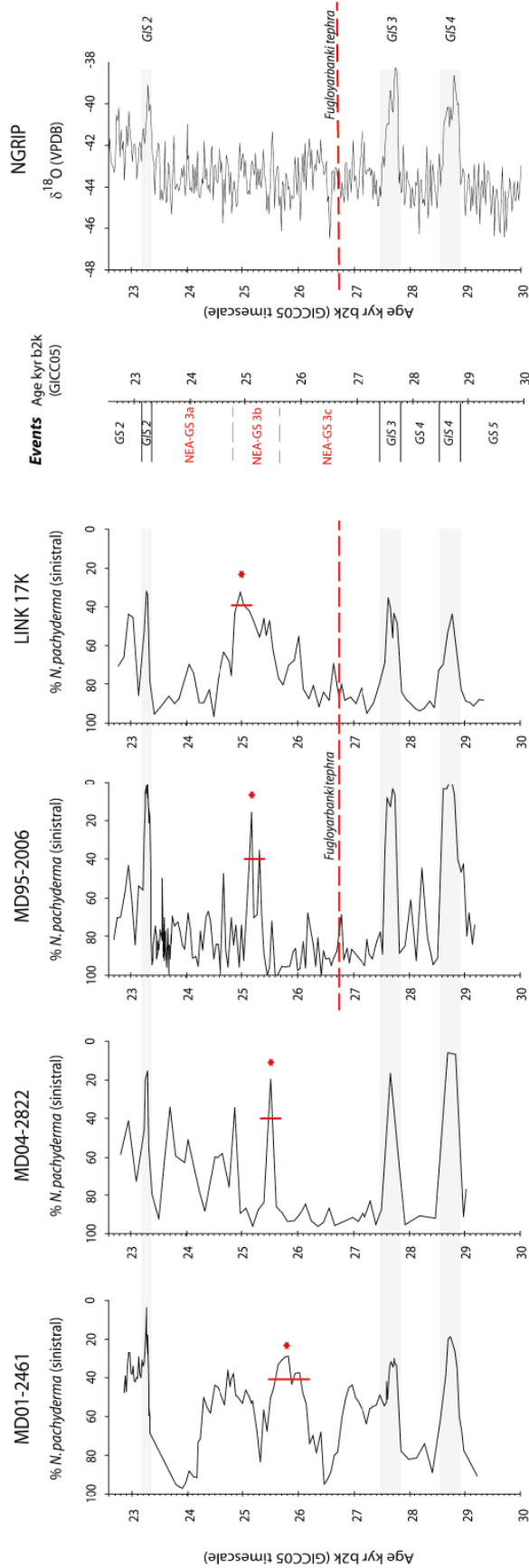
⁶ Note, the INTIMATE scheme numbers the sub-sections from the top downwards (c.f. Lowe et al 2008); this convention is followed for the proposed regional scheme for GS3.

⁷ The transitions out of the GIS are included in the GS3 age model as these are clearly identifiable within both the ice core and marine records.

⁸ Please note, the Fugloyarbanki tephra has been identified and geochemically characterised for MD95-2006 (C. Peters, unpublished data) and LINK 17 (Rasmussen and Thomsen 2008) only.

⁹ 40 % *N. pachyderma* (sinistral) was chosen as this reflects modern Arctic surface water faunal abundances at their lower limit (i.e. 90-40 % *N. pachyderma* (sinistral) hence the boundary between polar and sub-polar waters) (Bé and Tolderlund 1971, Johannessen et al 1994, Pflaumann et al 1996)

Figure 4.5: NGRIP $\delta^{18}\text{O}$ (GICC05 timescale) tuned age models for the % *N. pachyderma* (sinistral) records of MD01-2461, MD95-2006, MD04-2822 and LINK 17. The event stratigraphy for the four cores is outlined along with the approximate age for each sub-division. NGRIP $\delta^{18}\text{O}$ record is shown on the same GICC05 timescale. Horizontal grey shading indicates the position of interstadials 2, 3 and 4 whilst the position of the Fugloyarbanki tephra is denoted by the dashed horizontal red line. Red stars indicate the inferred maximum warmth for the warming event within Greenland Stadial 3, vertical red line indicates the 40 % abundance by which the NEA-GS3 subdivision is defined.



The 40 % ‘threshold’ value is used to evaluate the timing and duration of the NEA-GS3b event. The tuned age models give an estimated maximum duration of 1 kyr (ca. 26 to 25 kyr b2k) for the NEA-GS3b event. Whilst a later onset with increasing latitude for this event is discernable (Table 4.3), extreme caution should be exercised in interpreting this data. These age estimates are based upon a number of assumptions and estimates including: ice core age uncertainties (i.e. counting error associated with the timing of the interstadial/stadial transitions within the GICC05 timescale); stratigraphical uncertainties in the positioning of the transitions in to and out of the interstadials (within both the ice and marine cores); the assumption of a uniform sedimentation between these tie-points and; the use of linear interpolation over a lengthy period of time.

Table 4.3: Estimates derived from tuning to NGRIP (GICC05 timescale) for the timing of the onset (N. pachyderma (sin.) < 40%), peak warmth (lowest % N. pachyderma (sin.)) and end ((N. pachyderma (sin.) > 40%) of the warming event within Greenland Stadial 3 for cores LINK 17, MD95-2006, MD04-2822 and MD01-2461.

Core	Depth (cm) of peak warmth	Approx. age of onset of warming event (Nps < 40%) kyr b2k	Tuned Age for peak warmth yrs b2k	Approx. age for the end of warming event (Nps > 40%) kyr b2k	Approx. duration yrs of warming event (Nps < 40%)
LINK 17	533.5	25,131	24,971	24,880	250
MD04-2006	1794	25,400	25,175	25,130	270
MD04-2822	1530.5	25,650	25,508	25,340	210
MD01-2461	580.5	26,030	25,821	25,590	440

Post GIS 3, the four cores indicate sea surface conditions were cold (NEA-GS3c) with a subsequent migration of warm waters northwards into the NE Atlantic (NEA-GS3b). It is proposed that these warm waters did not penetrate far enough into higher s and thus were unable to influence air temperatures over Greenland during GS3 leading to a discrepancy in the event stratigraphies of Greenland and the NE Atlantic. The warm waters did, however, progress to the north of all core sites investigated resulting in a local GS3 warming (NEA-GS3b). The timing and duration of the NEA-GS3b event have been attempted but it must be remembered that the depths between the NGRIP tie points within the marine records are of assumed uniform deposition and this may not correspond to ‘true’ *in situ* deposition (i.e. the points in between the tie-points are ‘floating’ and may be ‘compressed’ or ‘expanded’ due to variations in depositional environment). Additionally, estimates are based upon linear interpolation over lengthy time periods.

2.4.2. *The influence of bioturbation, productivity, terrigenous inputs and meltwater*

The expression of the NEA-GS3b warming event within proxy records of the four cores reflects their latitude and the progression of the polar front northwards (or

southwards) with time. It may also be a product of: bioturbation; surface water productivity and; their differential depositional settings and proximity to actively glaciated margins with variable influx of both terrigenous material and meltwater.

The action of bioturbation, which can both attenuate and extend the depth distribution of a short-lived climatic event, must be remembered in consideration of all these sediment records.

Cold surface water conditions may inhibit the productivity of planktonic foraminifera thereby attenuating the biogenic component of the sediment record. For example, the peak warmth (*N. pachyderma* (sinistral) $\leq 40\%$) within LINK 17 is short in duration; the advection of warm waters to this latitude may have been weak and more spatially restricted than during the interstadials and could explain, in part, the differences in absolute values of % *N. pachyderma* (sinistral). Cold surface conditions may also inhibit calving and melting of icebergs from neighbouring glaciated margins. As such the transport of terrigenous material to the deep ocean could be reduced possibly contracting the terrigenous component of the sedimentary record.

Conversely, possible destabilisation of proximal glaciated marine margins may be triggered by an influx of warm waters to the NE Atlantic increasing sedimentation. The close proximity of MD04-2822 and especially MD95-2006 to the British Ice Sheet may have resulted in a large influx of terrigenous material to the sites masking the contribution of foraminiferal material to the sedimentary record. Additionally, meltwater from an actively glaciated margin may also act to impede foraminiferal abundances and thus the warming event may appear attenuated in comparison to other records.

MD01-2461 also exhibits a broad warming peak within GS3, perhaps as a function of the increased duration of the polar front to the north of this core site. There is a subsequent return to colder surface conditions followed by another broad warming peak in the MD01-2461 record. Additional warming event(s) are also seen in MD95-2006 and MD04-2822 and may be a manifestation of a fluctuating ('flickering') position of the polar front across the core sites in the latter stages of GS3.

2.4.3. *Event stratigraphies and geographic expression of events – NEA-GS3b*

The NEA-GS3b warming event has been identified as a local event; it is detected only within marine sediment cores of the NE Atlantic and is absent from the Greenland ice core records as well as marine sediment records of the wider Nordic Seas. The comparison of events via event stratigraphy has therefore enabled the geographic extent of this feature to be identified.

3. Assumptions and disadvantages of event stratigraphies

All event stratigraphies incorporate a number of assumptions, some potentially problematic including: the resolution of the archives or dating method; the assumption of linear sedimentation between the assigned tie-points and; the assumption of synchronicity. These were alluded to in the above examples but the following section discusses these in more detail.

3.1. Resolution

Shackleton et al (2000) raised concerns about the resolution of events within event stratigraphies; many events recorded within the Greenland ice cores are of short duration and as such, these events may only be recorded in marine sequences where accumulation rates are unusually high. Additionally, proxy records documenting such events may be severely biased, for example, a reduction in productivity during intervals such as the Heinrich events may result in disproportionately rare abundances of the microfossil studied. The construction of the MD04-2822 compound chronology was impeded by the very low abundance (or indeed total absence) of *C. wuellerstorfi* during glacial periods. This may be due to very high terrigenous inputs from a proximal glaciated margin 'diluting' or 'swamping' the fossil record. In addition to short duration, events within marine sediments may be 'missed' due to practical (e.g. sampling resolution) or methodological (e.g. limits of radiocarbon dating) constraints.

3.1.1. *Practical: bioturbation, sedimentation rates and sampling*

The resolution of the climate archives to be compared is an important consideration when transferring age control from one record to another. Bioturbation with marine sediments may 'smooth' the palaeoenvironmental record and, for example, make the positioning of tie-points more difficult by to 'extending' or attenuating events.

In conjunction with bioturbation, varying sedimentation rates may produce, for a series of hypothetically uniform duration events, a palaeoenvironmental record that appears to display events of varying resolution. For example, during episodes of high sedimentation, events may be captured in very high resolution, alternatively 'minor' events may be masked. Indeed, for MD04-2822, the distinctive Heinrich events are difficult to discern due to the high terrigenous inputs from a proximal BIS.

The choice of sampling strategy may also impact upon our ability to confidently assign events. An initial 10 cm resolution sampling strategy for MD04-2822 was expedient as I sought to obtain a record for the entire 38 m of this sediment core. However, this produced a relatively low resolution % *N. pachyderma* (sinistral) record for some portions of the core (i.e. those with lower rates of sedimentation) that made discerning the mid-point of the transitions into the D/O events difficult. Clearly this raises the distinct possibility of 'mis-tuning', i.e. events assigned to the wrong interstadial event. This is especially preoblematic where sedimentation rates and sampling resolution are low. However, in order to minimise this possibility, the % *N. pachyderma* (sinistral) and XRF Ca records were used in parallel to assign interstadial events, as well as using the calibrated radiocarbon ages of the interstadial events as a check of tuning (see chapter 3). A combination of increased sedimentation rates (due to closer proximity to a nascent BIS) and higher resolution sampling, means that the

D/O events within MIS 3 are more clearly evident in MD95-2006 than in the neighbouring MD04-2822 (Figure 4.2). In the GS3 example, the Fugloyarbanki tephra has yet to be identified within MD04-2822; the presence of this tephra layer within MD95-2006 would suggest that sea ice, by which this material probably was transported, also reached the MD04-2822 site. However, the current relatively low sampling resolution of the record means that it was 'missed' in sampling.

In the GS3 example presented above, radiocarbon dating was unable to provide a sufficiently robust age model (due to concerns regarding a temporally and spatially variable marine radiocarbon reservoir effect); it does, however, provide a powerful and vital screening tool. The use of the radiocarbon dates in this function also helps to mitigate the relatively low resolution of the % *N. pachyderma* (sinistral) record when used in conjunction with stratigraphical and proxy information. For example, if an interstadial event is dated (i.e. an event characterised by low % *N. pachyderma* (sinistral)), but the calibrated radiocarbon age was older than the interstadial assigned and younger than the next interstadial, we know that the event is not a stadial and we can therefore attribute the age offset to a combination of inadequate consideration of the local marine reservoir effect and differences between the ice core and calibration dataset chronologies. Initial interstadial designations may be confirmed therefore, using both the stratigraphic and age information in tandem.

3.1.2. *Methodological: limits of radiocarbon and uncertainties with the transfer of ice core chronologies*

For the MD04-2822 record, the limits of the radiocarbon dating method, restrict the use of this technique to interval of less than ~40 to 50 kyr. The Greenland ice cores currently extend only to ca. 123 kyr; although current drilling offers the possibility of a Greenland ice core record for the entire last interglacial (the NEEM project¹⁰). The benthic stacks extend over far longer timescales, however, the resolution of these is such that age control may be limited to only a few points within an extended timeframe, thereby limiting the temporal resolution of the resulting age model.

The errors associated with these dating techniques form part of the uncertainty within the tuned or transferred event stratigraphy. For the last 30 kyr of the GICC05 timescale, events may be resolved on annual or decadal scales, however, Lowe et al (2008) demonstrate that radiocarbon dating, for the same interval, is unable achieve such resolution due to the uncertainty associated with each determination.

Using the ice core chronologies (transferred by tuning to the marine sediment record) may resolve some events on a decadal scale, but the age uncertainty associated with the tie-point ages increases with the transfer to the marine sediment records due to e.g. bioturbation, the difficulty in determining the mid-point of the transition into the D/O event etc. Each of these should be kept in mind when interpreting the MD04-2822 record on any 'tuned' age model.

¹⁰ North Greenland Eemian Ice Core Drilling <http://neem.nbi.ku.dk>

3.2. Assumption of linear sedimentation between tie-points

This common assumption is implicit within many age models, including those produced for MD04-2822, although practical, it seems unfounded and rather unlikely. Glancing at the MD04-2822 core (see sediment photograph, chapter 2) and proxy records (e.g. Figure 4.2), it is evident that the MIS 5 interval (~60 kyr, 2-3 m of core) accounted for a far smaller portion of total sediment than the last glacial (MIS 4 to 2 inclusive; ~60 kyr, ~18 m of core) although the upper portion of the core has been affected by coring artefacts ('over-sampling'; see chapter 5). It is difficult to test whether this assumption is reasonable, although known chronostratigraphical markers may provide one means.

For the GS3 example, the presence of the Fugloyarbanki tephra within two of the cores, may elucidate variations in sedimentation rates with the application of differing tie-points. The GS3 local event stratigraphy was tuned to the Greenland ice core record using both the transitions in and out of the interstadial events. However, it is more usual to use just the transition into the interstadial as a tie-point as this occurs over short time periods and a sharp transition out of the interstadial event is not always clear within the Greenland ice core records. However, both the transitions into and out of interstadials 2 to 4 inclusive were clear in both the Greenland $\delta^{18}\text{O}$ and *N. pachyderma* (sinistral) records.

Comparison between the 'maximally' and 'minimally' tuned age models reveal insights regarding deposition. As such, the Fugloyarbanki has been omitted as a tie-point as means of investigating this assumption. The comparison produces age offsets for the intermediary depths, although sedimentation was still assumed to be linear between the tie-points. This offset was found to be greatest for core MD01-2461: ~465 years older for the transition out of GIS 3 using only the transitions into the interstadial as tie-points. However, the *N. pachyderma* (sinistral) record of MD01-2461 is difficult to interpret at this point and the choice of the mid-point of the transition out is rather subjective. For MD04-2822, the greatest difference was ~ 392 years for the transition out of GIS 4. Age offsets for MD95-2006 and LINK17 are smaller but also occur at the transition out of the interstadial events. These differences are unsurprising; changes in depositional environments within interstadials compared to stadials seem plausible if not probable, due to variations in surface water productivity (and thus biogenic inputs to sediments e.g. due to meltwater) which may be especially acute within fully glacial conditions.

Within GS3 itself, there appears to be very little variation in the age determined for intermediary depths for all the cores except MD01-2461. This may be a function of the number of tie-points within a given time period. For the GIS 4 to 3 interval, there are 4 tie-points within ~1.5 kyr; whereas for the GS3 interval, there are 4 (or 5 if the Fugloyarbanki tephra is present) tie-points within ~4.5 kyrs. The greater the number of tie-points, the closer approximation we are able to achieve of the 'true' sedimentation rates, assuming a variable rate of deposition between those tie-points. The assumption of linear sedimentation between the tie-points would seem, *prima facie*, to hold for the GS3 interval within these cores. For MD04-2822 and MD95-2006, age offsets of 1 to 3 years are observed between the highly and minimally tuned age models. The veracity of this cannot of course be determined; linear sedimentation may approximate an average of the 'true' sedimentation but this cannot be determined with any certainty using the above method.

3.3. Assumption of synchronicity

3.3.1. *Synchronicity between climate archives*

Using the rapid transitions into the D/O events conspicuous within the marine and ice cores as tie-points between the two environmental archives i.e. using an event stratigraphy approach facilitates age control for many marine sediment sequences including MD04-2822. This assumes the synchronicity of in air temperature over Greenland and North Atlantic sea surface temperature changes (c.f. Shackleton et al 2000). Whilst there need not be a full understanding of the mechanisms for change between proxy archives for an event stratigraphy to be employed (Knight 2003), there is a plausible causal mechanism linking these two archives involving thermohaline circulation. There is advection of warm, saline waters into high latitudes during the D/O events, and cooling of this water to form deep waters (thermohaline circulation) releases heat to the atmosphere and wider North Atlantic region. An expansion southwards of the polar front south during stadials is coincident with a reduction in the penetration of warm surface waters and thus a reduction in the heat released to the atmosphere.

Blaauw et al (2010) have recently questioned the assumption of synchronicity of the D/O events; they highlight large dating uncertainties which suggest that events within a French lake record (Wolfarth et al 2008) may not be synchronous with the events recorded in the Greenland ice cores. Additional diachronous climate shifts between records have also been observed for the Last Termination (e.g. Blockley et al 2004, Coope et al 1998).

The inclusion of tephra within several archives of environmental change (ice, marine, terrestrial) provides a means whereby the assumption of synchronicity may be tested. A tephra horizon may be thought of as ‘geologically instantaneous’; the delivery to the NE Atlantic marine sediments of primary air fall (onto sea ice) and subsequent transportation via surface circulation is thought to occur within decades (see Austin et al 2004). Indeed, based upon the stratigraphical position of the North Atlantic Ash Zone (NAAZ) II tephra layer on the ‘cooling’ limb of GIS 15 within both the marine and ice cores prompted Austin et al (2004) and Austin and Abbott (2010) to conclude that these D/O events are synchronous within the North Atlantic. It must be remembered that whilst strongly suggestive of synchronicity, this has been tested only for one of the D/O events in the marine and ice core records and at one location (MD95-2006; Barra Fan).

NAAZ II has also been identified (and confirmed via major element geochemistry) within MD04-2822 and MD01-2461 (Figure 4.6, Appendix B₃). The major element composition of the rhyolitic shards confirms all the shards are from the same population (II-RHY-I). The size distribution, for the peak occurrence of NAAZ II, within all three cores is remarkably similar and suggests deposition of this tephra layer was by the same mechanism (Austin et al 2004, Peck 2006, WEN Austin, *unpublished data*). The peak occurrence of the rhyolitic shards was used as the stratigraphical position of NAAZ II (Austin and Abbott 2010) due to concerns about stratigraphic separation (e.g. Wastegård et al 2006) of the different components of NAAZ II.

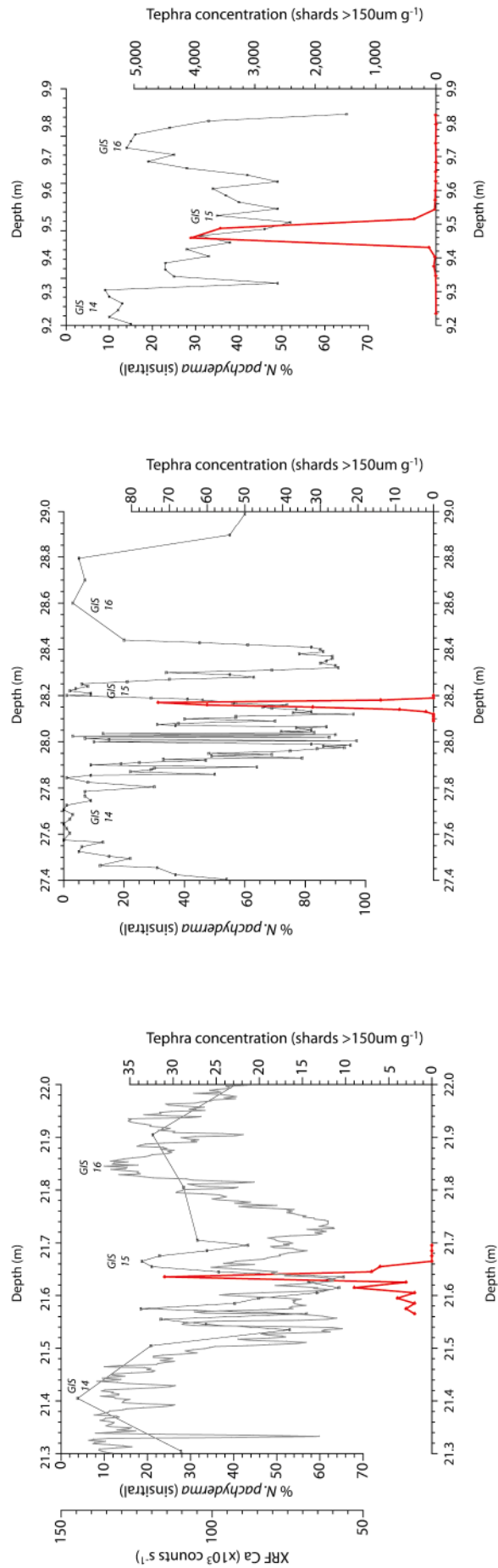
GIS 15 can be confidently discerned within MD04-2822 and MD95-2006, however, it is less clear in MD01-2461 (Figure 4.6). For MD04-2822 and MD95-2006, the peak rhyolitic tephra concentration clearly falls on the 'cooling-limb' of GIS 15. This is less evident within MD01-2461.

The concentration of the rhyolitic component within these three cores differs depending upon their latitude; peak concentrations for MD04-2822 and MD95-2006 are ~31 and 74 shards g⁻¹ respectively whereas in the more southerly MD01-2461, the concentration is > 4,000 shards g⁻¹ (Peck 2006). Whilst this event is recorded in all cores, the variation in the concentration of tephra hints at additional processes within the climate system, for example, the presence of sea ice or 'congestion' due to icebergs, which may have inhibited the transportation of tephra laden icebergs/sea ice to the MD04-2822 and MD95-2006 sites. Alternatively, clement surface water conditions at the MD01-2461 site may have led to the preferential melting of sea ice transporting the tephra at this site. The very similar size distributions for the peak occurrence of rhyolitic shards, and a lack of other volcanic grains at all three sites, as would be associated with entrainment of the tephra within icebergs, suggests these grains are primary airfall onto sea ice (Austin et al 2004; Peck 2006, WEN. Austin, *unpublished data*)

In the GS3 example, the presence of a basaltic tephra layer, the Fugloyarbanki/FMAZ II, aided the construction of the event stratigraphy. The stratigraphic position of this tephra layer within both N. Atlantic marine sediment cores (this study, Lackschewitz and Wallrabe-Adams 1997, Rasmussen et al 2003, Hafliðason et al 2000, Wastegård et al 2006) and the NGRIP ice core (Davies et al 2008) in a cold interval 'immediately' post GIS 3, would also seem to suggest that this volcanic event was recorded simultaneously within the two archives. Further testing of this assumption is required throughout the last glacial interval; tephrochronology may provide one such method. As the Fugloyarbanki (FMAZ II) and FMAZ III¹¹ tephra are currently the only tephra layers, apart from NAAZ II, identified in both marine and ice core records within MIS 2 and 3 (Davies et al 2008, Davies et al 2010), the testing of the synchronicity of events remains difficult.

¹¹ Faeroe Marine Ash Zone (FMAZ) III has been identified in marine cores (Rasmussen et al 2003, Wastegård et al 2006) and recently within the thermal peak of Greenland Interstadial 8 of the NGRIP ice core (Davies et al 2010). This layer has been given an age of 38,122 ± 723 yr b2k from the annually counted NGRIP record (GICC05 timescale) (Davies et al 2010).

Figure 4.6: Concentration of rhyolitic tephra (red line) within MD04-2822, MD95-2006 (Austin et al 2004) and MD01-2461 (Peck 2006) and % *N. pachyderma* (sinistral) records (black line) on their own depth scale. XRF Ca profile (grey line) is also shown for MD04-2822. GIS designations are given (according to original reference). Note different scales used for tephra concentration axes.



3.3.2. *Assumption that all events are recorded within all archives*

The GS3 example provides an illustration of both the merits and possible pitfalls of this assumption. The D/O events are clearly evident within both the marine and ice core archives of environmental change (Figure 4.5). However, the warming feature (NEA-GS3b) is only present in the marine records of the N.E. Atlantic; it is absent from the NGRIP $\delta^{18}\text{O}$ record and the marine records of the wider Nordic seas (e.g. Fronval et al 1995, Weinelt et al 2003). This event, whilst certainly forming part of the regional event stratigraphy, would not feature within a wider Atlantic/Nordic Seas or Greenland ice core event stratigraphy.

A restricted incursion of warm waters in the eastern Nordic Seas during GS3 (the NEA-GS3b event) is proposed to account for this discrepancy. During interstadials, warm waters penetrated into much of the Nordic Seas thereby influencing air temperatures over Greenland. However, during NEA-GS3b the incursion of warm waters into the Nordic Seas was insufficient to influence conditions over Greenland. The Greenland ice cores appear to record only the 'large' D/O events rather than more localised (i.e. NE Atlantic) sea surface warming. This is unsurprising as the D/O events are considered by many to represent a global phenomenon, with a S. hemisphere counterpart (e.g. Blunier and Brook 2001, Barker et al 2009) and therefore it seems reasonable that the events would be recorded in all climate archives. The assumption would therefore be reasonable for such large-scale climatic events. For GS3, the discrepancy highlighted between the climate archives, does enable regional events, as opposed to amphi-Atlantic, to be distinguished.

3.3.3. *Assessment of leads and lags*

By tuning records to the Greenland ice cores and assuming that the D/O events are synchronous, it is not possible to evaluate any leads or lags in the climate system. The GIS become 'fixed' in time i.e. 'regionally synchronous' and this precludes examination of the comparative timing/phasing of these events within a tuned chronostratigraphy. Interestingly, the GS3 warming event (NEA-GS3b) is positioned at subtly different points in the stadial (Figure 4.5) which may be as a consequence of the progressive movement northwards of the polar front during the stadial and/or an artefact of the deposition at each site.

If an independent age model was available i.e. one that has not been transferred, attempts to compare the timing of events contained within an event stratigraphy could be undertaken. This would provide a means whereby the assumption of synchronicity for these climatic events could be tested.

The protocol set out by the INTIMATE group (Lowe et al 2008), should facilitate just such comparison. It stresses the importance of an independent and validated age model, in assessing the degree of synchronicity of events.

4. The INTIMATE protocols (Lowe et al 2001, 2008):

One of the principal goals of the INTIMATE working group is the determination of the degree of synchronicity (or a-synchronicity) between atmospheric, marine, cryosphere and terrestrial archives of abrupt climate events. These common events form the basis of an event stratigraphy and independent age control (i.e. not derived via transferring from one record to another) may help unravel the phasing and mechanisms of these events. Limitations of current dating techniques have tended to inhibit the temporal resolution of the climatic event investigated and a precise order of events remains elusive for the last glacial-interglacial transition (Björck et al 1998, Walker et al 1999, Lowe et al 2001, 2008). Although the INTIMATE protocol currently extends only as far as ca. 30 kyr, the recommendations should be equally valid on longer timescales.

At present, INTIMATE recommends the construction of a local event stratigraphy with independent age control, which may then be compared to the regional stratotype in order to assess any lead/lags between the various climate archives for the same event (Lowe et al 2008). Currently, the NGRIP $\delta^{18}\text{O}$ record on the GICC05 timescale (Andersen et al 2006, Rasmussen et al 2006, Svensson et al 2006, 2008, Vinther et al 2006) is the preferred 'regional stratotype'. The NGRIP $\delta^{18}\text{O}$ record (on the GICC05 timescale) is recommended by the INTIMATE group as a regional stratotype appropriate to the North Atlantic for the following reasons: firstly, the GICC05 timescale has been achieved by annual layer counting for the last 60 kyr (Andersen et al 2006, Rasmussen et al 2006, Svensson et al 2006, 2008, Vinther et al 2006); secondly, the degree of uncertainty within the age model has been quantified; thirdly, there is increased stratigraphic resolution and; finally, the climatic events within the ice core records are resolvable on annual to decadal timescales. The GICC05 chronology also enables the duration of each event to be estimated (Lowe et al 2008, Wolff et al 2009). The GICC05 timescale is, therefore, held to provide 'significantly improved temporal resolution and precision' compared to other Greenland ice core timescales, but the ages should be considered 'preliminary' (Lowe et al 2008).

Whilst the GICC05 timescale represents an important advance, some difficulties remain; there are problems in the consistent application of criteria for determining annual layers and it should be noted that chronologies are rarely 'absolute' (Skinner 2008). A more detailed consideration of the GICC05 timescale for the NGRIP $\delta^{18}\text{O}$ record may be found within chapter 3 (*Chronostratigraphy*).

The INTIMATE protocols (e.g. Lowe et al 2001, 2008) also include guidance upon the use of radiocarbon dating as a means of independent age control. The degree to which a radiocarbon dated event stratigraphy may be deemed robust is associated with the several uncertainties which are dependent upon: the number of radiocarbon dates for a given sequence; sample selection and pre-treatment; sample and site specific factors, for example, the incorporation of 'old' carbon, the marine reservoir effect; analytical precision; calibration data sets and; often questionable assumptions made in age-depth models (i.e. linear sedimentation rates between dated horizons) (Lowe et al 2001, 2007, 2008). Additionally, INTIMATE recommends the validation of the independent (i.e. radiocarbon) chronologies for the local event stratigraphies via

tephrochronology or in exceptional circumstances, varved or laminated sequences and dendrochronology may provide such validation.

4.1. Application of the INTIMATE protocol to marine records

An attempt was made to use the INTIMATE protocol with respect to the GS3 example: identification of a local event stratigraphy (Figure 4.4); and the use of radiocarbon dating to attain an independent age model, although application to marine samples includes a number of uncertainties. The principle limitations include: the stratigraphic integrity of the samples; analytical precision; marine reservoir effects and; calibration procedures and assumptions used in age-depth models (e.g. Lowe et al 2008, 2007) (see chapter 3, section 5 for further discussion). The integrity of sample selection is stressed by Lowe et al (2008) in the construction of a radiocarbon age model.

In light of this, foraminifera were picked from abundance maxima in order to minimise bioturbation biases (Bard et al 1987, 2004a). For the MD04-2822 stratigraphy, and testing of the initial compound chronology, *G. bulloides* dates were selected in the main, from within GIS events where this species is dominant and planktonic foraminifera concentrations are high (Figure 4.7). However, the relatively low foraminiferal levels within GS3, thwarted attempts to directly constrain the NEA-GS3b warming event, via radiocarbon dating (Figure 4.8). However, several radiocarbon dates were obtained for each core investigated. Once calibrated these allow for the construction of an age model that is not dependent upon a transferred event chronology. This therefore, negates some of the concerns outlined above. However, intermediary ages are still determined by linear interpolation between the dated horizons.

The calibration of radiocarbon ages for the four cores used in the GS3 local event stratigraphy (Appendix C₃) was via the Marine09 calibration curve (Reimer et al 2009) using the OxCal programme (version 4.1; Bronk Ramsey 2009). Despite the unlikely scenario of a constant local marine reservoir effect, only the global average was incorporated into the calibration of the radiocarbon dates with no additional ΔR correction. A deposition model (and the Bayesian statistics utilised by the OxCal programme) was used in order to refine the radiocarbon chronology based upon stratigraphical information (see chapter 3, *Chronostratigraphy*). The calibrated radiocarbon ages and age-depth models for all four cores are given in Figure 4.9 and Appendix C₃.

For all four cores, there are notable differences in the calibrated ages determined using a deposition model (Bronk Ramsey 2008), where stratigraphical information is incorporated into the age model, and those calibrated individually (no additional model). However, the poor agreement of some of the modelled age determination must be noted (Appendix C₃).

Figure 4.7: Stratigraphic position of radiocarbon dating intervals (red *G. bulloides*, blue *N. pachyderma* (sinistral), % *N. pachyderma* (sinistral) (black line) and planktonic foraminifera concentration (grey dashed line). Red numbers indicate the Greenland Interstadial events tested by radiocarbon dating. Vertical dashed red line indicates the position of NAAZ II.

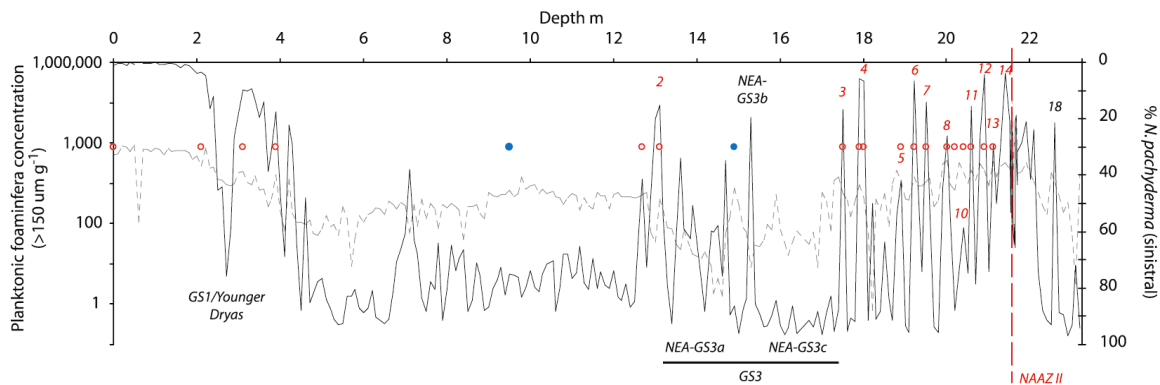


Figure 4.8: MD04-2822 % *N. pachyderma* (sinistral) (grey, bottom), planktonic foraminiferal concentration (middle) and number of planktonic foraminifers counted during assemblage counts (top). Pale grey vertical bars denote the stratigraphic positions of GIS 2, 3 and 4, pink shaded vertical bars highlight episodes of very low planktonic foraminiferal abundances and faunal counts. Stratigraphic position of radiocarbon dates given by crosses (red – *G. bulloides*; blue *N. pachyderma* (sinistral))

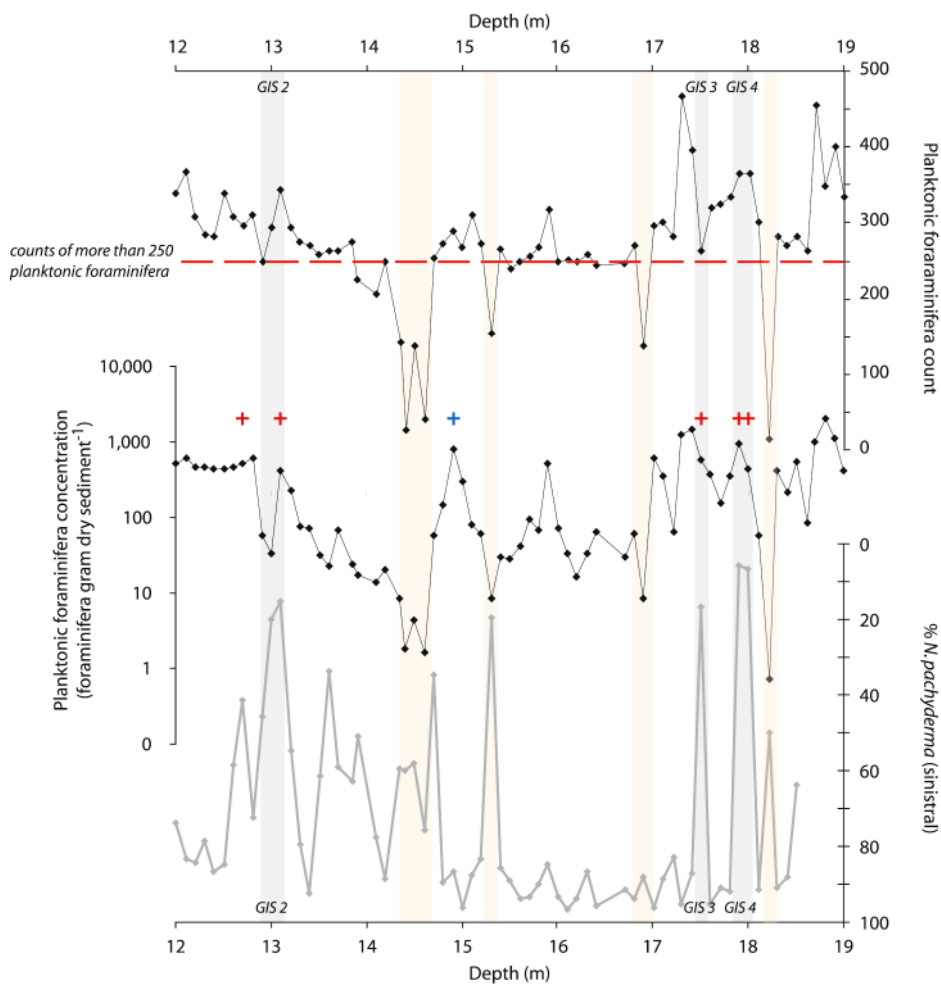
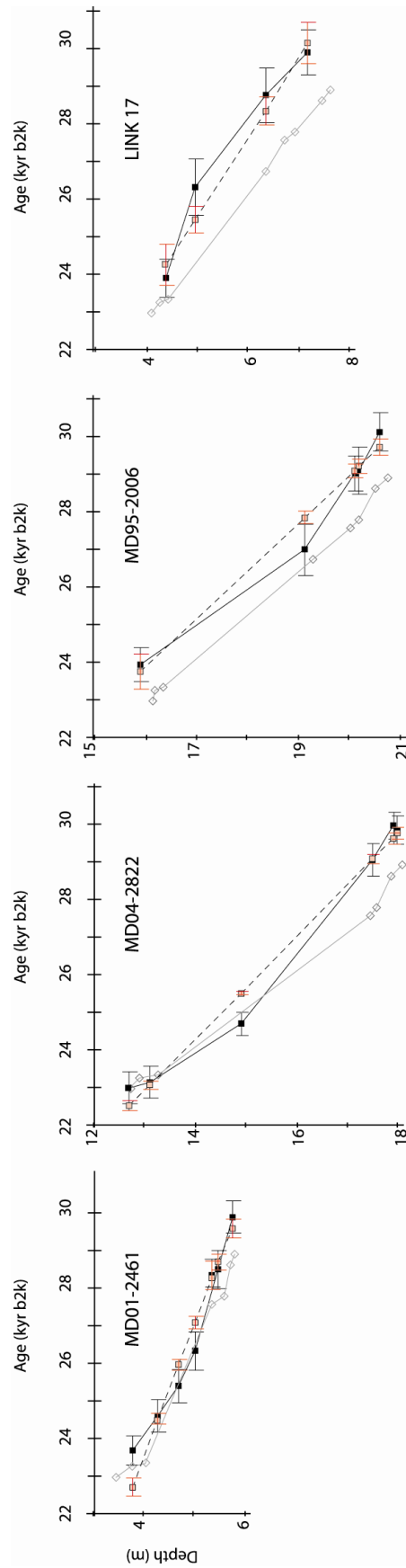


Figure 4.9: Age-depth models based upon tuning to NGRIP $\delta^{18}\text{O}$ (GIICC05 timescale), calibrated radiocarbon dates (black filled squares and solid line) and calibrated radiocarbon dates incorporating a deposition model (red filled squares and dashed line). All radiocarbon dates are shown as a mean of the probability distribution and 1 standard deviation. Radiocarbon dates are calibrated using the Marine09 calibration curve (Reimer et al 2009) within the OxCal software (version 4.1; Bronk Ramsey 2009). No local marine reservoir effect (ΔR) is added to the radiocarbon dates.



The age-depth models derived from the calibrated radiocarbon ages are, in general, older than those from tuning to the NGRIP $\delta^{18}\text{O}$ on the GICC05 timescale. This may reflect incomplete understanding of local marine reservoir effects for this time and location. Additionally, the age offset may reflect differences in the chronologies of the radiocarbon calibration curve and the layer counted Greenland ice core (c.f. Skinner 2008, Svensson et al 2006)¹². The temporal and spatial variation of the marine reservoir effect is documented for the modern ocean (e.g. see the database of Reimer and Reimer 2010) and some key intervals such as the Younger Dryas (e.g. Austin et al 1995, Singarayer et al 2008). Within the GS3 event stratigraphy (Figure 4.4); a radiocarbon date from LINK 17 (Faeroe-Shetland Channel) has been obtained for an interval of maximum abundance of basaltic tephra (confirmed as the Fugloyarbanki tephra layer by major element geochemical analysis). When this calibrated date (with no additional ΔR , only the global average, $R(t)$, incorporated within the Marine09 calibration curve) is compared to the NGRIP ice core age for this tephra horizon (on the GICC05 timescale - see Davies et al 2008), an age offset of ~1,600 years exists.

A substantial additional regional marine reservoir effect can therefore be inferred for this site at this point within GS3. Thus, the GS3 age models based solely upon radiocarbon dates include considerable uncertainties, particularly as: these cores are located at fairly mid-latitudes; stadial conditions and the reduction of the advection of exchanged surface water masses northwards; the proximity of the cores to an actively glaciated and calving margin and; the occurrence of seasonal sea ice (e.g. CLIMAP 1976, 1981, Shin et al 2003, Meland et al 2005) would all act to increase the local marine reservoir effect.

The NEA-GS3b warming event was not dated directly using radiocarbon. However, by linear interpolation between the calibrated radiocarbon dated intervals, an estimate of ~ 26 to 26.3 cal. kyr b2k for the peak warming was obtained. Using a 'limit' of 40 % *N. pachyderma* (sinistral), the NEA-GS3b event has an approximate duration from 26 to 26.6 cal. kyr b2k based upon the calibrated radiocarbon age models.

For the GS3 event stratigraphy, the use of radiocarbon dating proved insufficient to produce a robust age model due to several factors including: low foraminiferal abundances, low numbers of dates and the difficulty in adequately estimating the variation of the marine reservoir effect both spatially and temporally. The current radiocarbon age models are therefore associated with a large degree of uncertainty and are rather unsatisfactory for determining the timing and duration of the GS3 warming event. Reimer et al (2009) suggest that for sites such as MD04-2822, 'tuning to the Greenland ice cores and using tephra and paleomagnetic tie-points may provide a more meaningful timescale than calibrated ^{14}C ages'. Improvements in marine radiocarbon chronologies (e.g. stringent selection criteria and cleaning protocols, the incorporation of Bayesian statistics within calibration and age-depth modelling and

¹² The NGRIP **GICC05** timescale (Andersen et al 2006, Rasmussen et al 2006, Svensson et al 2006, 2008, Vinther et al 2006) is based upon annual layer counting to ca. 60 kyr (see chapter 3, *Chronostratigraphy*). The **IntCal09/Marine09** calibration curve however, is based upon: European tree ring chronologies spanning the last 12,594 yrs (datasets 1 to 7 - see references within Reimer et al 2009); both the varved (Hughen et al 2000, 2004a, b) and non-varved Cariaco Basin dataset (Hughen et al 2006); Iberian Margin-Hulu timescale record (Bard et al 2004b,c, Shackleton et al 2004) and; the independently dated coral records (Bard et al 1990, 1998, 2004a, Fairbanks et al 2005, Edwards et al 1993, Burr et al 1998, 2004, Cutler et al 2004). Full details of the datasets used may be found in the appendix within Reimer et al (2009).

ongoing attempts to constrain the marine reservoir effect) may enable robust independent age models to be constructed in the future, thereby facilitating the assessment of the degree of synchronicity between palaeoenvironmental events. However, the radiocarbon method is still dependent upon the availability of suitable material to be dated.

4.1.1. *Comparison of palaeoenvironmental events to the regional stratotype – NGRIP*

The next step in the INTIMATE protocol is the comparison of the local event stratigraphy and its independent age model to the regional stratotype. Currently the NGRIP $\delta^{18}\text{O}$ is recommended (Lowe et al 2008). This comparison should enable any discrepancies in the timing of correlated events to be determined (i.e. determination of any lead or lags in the climate system). However, the NEA-GS3b warming event is not contained within the Greenland ice core records and therefore cannot undertake this portion of the protocol as there is no obvious corresponding event within the NGRIP $\delta^{18}\text{O}$ record.

4.1.2. *Validation of Radiocarbon age model- Tephrochronology*

The final step in the INTIMATE protocol is that any correlations to the NGRIP $\delta^{18}\text{O}$ record should be validated using, for example, tephrochronology. Whilst the NEA-GS3b event is absent, the correlation of GIS 3 between the ice and marine sediment core cores is confirmed using the Fugloyarbanki tephra horizon. The presence of this tephra horizon also serves as a check of the radiocarbon age model.

The Fugloyarbanki/Faeroe Marine Ash Zone II (Wastegård et al 2006, Davies et al 2008) is the only other tephra, apart from NAAZ II, to have been identified within North Atlantic marine and Greenland ice core records within MIS 2 and MIS 3 (Davies et al 2008). Fortuitously for the GS3 event stratigraphy, this tephra layer has been identified in GS3 within the NGRIP ice core (Davies et al 2008) as well as several North Atlantic marine cores (Lackschewitz and Wallrabe-Adams 1997, Rasmussen et al 2003, Haflidason et al 2000, Wastegård et al 2006), suggesting a widespread distribution within the North Atlantic. This tephra layer has also been confirmed within the GS3 event stratigraphy; both MD95-2006 and LINK 17 have a distinctive basaltic tephra layer within NEA-GS3c, which has subsequently been confirmed by major element geochemical analysis (C. Peters, *unpublished data*, Austin et al *submitted*, Wastegård et al 2006). The stratigraphic position of this tephra layer in cores MD95-2006 and LINK 17 within a cold interval 'immediately' post GIS 3 agrees with both the ice core and other North Atlantic marine cores (see references above). Further, this tephra layer may be used to verify the GS3 radiocarbon age models.

The Fugloyarbanki tephra layer has recently been identified within the NGRIP ice core and has an age of $26,740 \pm 390$ years b2k (using the GICC05 timescale; Davies et al 2008). This event has been directly dated within LINK 17 (peak occurrence of this tephra layer is at 633 cm, see Appendix C₃ for conventional and calibrated age ranges). Once this conventional age has been calibrated the 95 % probability distribution suggests a slightly older age (median of probability distribution function for the deposition model is $28,290 \pm 372$ cal. yrs B.P.) than for the layer within the NGRIP ice core but comparable with the calibrated radiocarbon estimates ($27,721 \pm$

264 cal. yrs B.P.) for other marine cores if the two sigma uncertainty is considered¹³, although an offset of >1,500 years exists compared to the ice core age of Davies et al (2008). The radiocarbon age model for LINK 17 appears therefore to be corroborated by this tephra layer. However, this tephra horizon has not been identified within all cores. The GS3 radiocarbon age models remain relatively low resolution and the inherent difficulties associated with the method (e.g. unknown local marine reservoir variations) make these an imperfect estimation of the age-depth relationship within the cores.

The validation of correlation between marine and ice core records was key in constructing the compound chronology for the MD04-2822 sediment core. However, the success of this approach is dependent upon the resolution of the records and the presence of widely distributed and characterised tephra horizons within several climate archives (e.g. marine and ice cores).

At present, the INTIMATE protocol extends only for the last glacial-interglacial transition, for which there are numerous well characterised, widely distributed and temporally constrained tephra horizons (e.g. the Saksunarvatn, Vedde and Fugloyarbanki/Faeroe Marine Ash Zone II layers¹⁴; see e.g. Turney et al 2004, Lowe et al 2001, 2008). However, the number of these well defined tephra layers reported and characterised, decreases with increasing age. Again the assumption within event stratigraphies that all events are recorded within all archives, may not hold for tephra horizons. Past pathways of atmospheric circulation and sea ice may result in deposition of tephra events within confined geographical areas and perhaps not at all in other regions.

The Vedde Ash forms part of North Atlantic Ash Zone (NAAZ) I within marine environments, is widely dispersed geographically and provides a valuable means of correlation. It has been detected in lake sediments (Ireland to St Petersburg, Norway to Switzerland), marine sediments of the North East Atlantic as well as the Norwegian, Icelandic, Greenland and North Seas (Lowe et al 2008 and references therein). The Vedde Ash has previously been identified within a core from the St Kilda Basin (Austin et al 1995, Hunt et al 1995, Austin and Kroon 1996). However, whilst the presence of tephra was noted within the GS1/Younger Dryas interval of MD04-2822, this has yet to be characterised in detail (i.e. delineated into rhyolitic or basaltic components). Peters et al (2010) however, identified a basaltic component within this tephra horizon from magnetic parameters. This was subsequently confirmed visually and by major element geochemical analysis of a random selection of shards, as the basaltic component 1-TAB-1 of the Vedde Ash layer at a depth of 290-291 cm within MD04-2822. The peak concentration of rhyolitic shards within NAAZ I (the Vedde Ash) would need to be determined in order to use this as a

¹³ The Fugloyarbanki tephra has been directly dated within marine sediment cores and was given an estimated age range of 23,300 to 23,700 conventional ¹⁴C years BP (Wastegård et al 2006). This age range was then calibrated using the Fairbanks calibration curve (Fairbanks et al 2005) by Davies et al 2008 to give an estimated calendar age of 27,721 ± 264 cal. yrs B.P.

¹⁴ These tephra layers have been identified within the Greenland ice cores and their ages determined using the ice core chronologies e.g. the annual layer counted GICC05 timescale. These tephra layers are also known within marine sediments of the NE Atlantic (e.g. Austin et al 1995, Peters et al 2008, C.Peters unpublished data, Rasmussen and Thomsen 2008 S. Pyne-O'Donnell, unpublished data)

chronostratigraphic check of both the radiocarbon age model and tuning to the Greenland ice cores (c.f. Austin et al 1995, Austin and Abbott 2010).

However, the presence of NAAZ II has been identified and characterised within the MD04-2822 sediments. A peak occurrence of distinctive ‘bubble-walled’ rhyolitic tephra at 2163–2164 cm has been geochemically analysed; this layer can therefore be securely correlated to the II-RHY-1 component of NAAZ II (see Appendix B₃). This tephra layer does confirm the initial event stratigraphy at the limits of the radiocarbon method.

The radiocarbon derived age models for the GS3 event stratigraphy gives rise to GIS events that are consistently older than their counterparts in the Greenland ice core. Whilst this may be the case (diachronous changes are documented in some records e.g. Blockley et al 2004, Blaauw et al 2010), a more probable explanation is an imperfect understanding of the local marine reservoir effect (e.g. the large discrepancy between the calibrated radiocarbon age and ice core age for the Fugloyarbanki tephra). As such, the GS3 radiocarbon age model contains large uncertainties and the relatively few radiocarbon dated intervals, which render them insufficiently robust to evaluate the timing and duration of the NEA-GS3b warming event.

Within the marine environments, there are additional complications that limit the scope of the protocol set out by Lowe et al (2008). Perhaps most notable of these is the spatial and temporal variation in the marine reservoir effect. This, in conjunction with concerns regarding the selection of intervals for radiocarbon dating (i.e. the low planktonic foraminiferal abundances within the NEA-GS3b event), prevented a robust independent evaluation of the timing and duration of the NEA-GS3 warming event, as identified on a regional scale from the initial event stratigraphy. Additionally, the INTIMATE approach could not be implemented with respect to the NEA-GS3b event, even if an independent age estimate were obtained, as there is no analogous event within the Greenland ice core.

5. Conclusions

One of the primary advantages of the event stratigraphy approach, is the ability to assess the representative nature of an event and its geographic expression. These are both fundamental questions that should be considered within palaeoenvironmental research. Replication of records, within the strictest sense, is limited within palaeoceanography; building local or basin wide event stratigraphies is one means of addressing this difficulty.

Replication within palaeoceanography is very limited but applying an event stratigraphy may enable assessment of how representative a feature is locally (e.g. turbidites), regionally (e.g. the D/O warming events of the last glacial, or more localised SST changes) and indeed on an ocean basin scale (e.g. Heinrich events). In addition, it can also enable the geographic expression of a feature to be determined, as demonstrated by the GS3 example where the NEA-GS3b warming event is seen only within the N.E. Atlantic. These two features of the event stratigraphies allow a local or regional event history to be constructed, even in the absence of secure age control, although a robust age model greatly facilitates comparisons between

palaeoenvironmental archives as well as enabling the duration of events to be estimated.

Where age control is available (e.g. the benthic $\delta^{18}\text{O}$ stacks or the Greenland ice core chronologies), perhaps the most valuable function of an event stratigraphy approach is the ability to assign an age from an event without the need to directly date that event within each record. However, this is strongly dependent upon a well constrained and robust chronology. Radiocarbon has been suggested as a means of obtaining an independent age model for palaeoenvironmental records but this method is often fraught with difficulties within the marine environment. Tuning to the Greenland ice cores does, however, provide well constrained age estimates for events within marine sediments that extend beyond the scope of radiocarbon. However, assumptions of synchronicity and linear interpolation as well as dating uncertainties should be remembered in interpreting either radiocarbon or transferred ice core chronologies.

The assumptions implicit within both the application of an event stratigraphy (e.g. that all events are recorded in all records and that these events are synchronous) and the transferral of an age model from an event stratigraphy to an individual records (e.g. linear sedimentation between tie-points) remain problematic and require further testing, for example, further use of tephra isochrones may provide insights into the degree of synchronicity of events within different archives.

Event stratigraphies are invaluable in palaeoclimatic research, facilitating both age control and enabling the construction of local or regional event histories. The GS3 example demonstrates both of these. Whilst the INTIMATE protocol provides a sound means for correlation of events, as well as the assessment of any leads or lags in the climate system, it has proved difficult to obtain a sufficiently robust independent age model for the marine sediment sequences. Since the NEA-GS3b event is not evident with the Greenland ice cores $\delta^{18}\text{O}$ record the timing of the event between the two archives cannot be compared. The INTIMATE protocol holds some promise for the elucidation of the phasing of palaeoclimatic events that are currently assumed to be synchronous. In practise, the application to marine sediment sequences is however, hampered by limitations of the radiocarbon method (e.g. low foraminiferal abundances, unknown variations in the local marine reservoir effect). However, by employing a form of event stratigraphy (but not that of the INTIMATE protocol), a regional feature not previously identified with the Greenland ice cores, has been documented for the NE Atlantic.

CHAPTER 5:**The correction of core 'over-sampling': An example using giant piston core MD04-2822 and gravity core +56-12/15CS from the Rockall Trough.**

For palaeoceanographic studies, a primary aim during coring is the maintenance of stratigraphic and dimensional integrity of sediments in order to investigate depositional processes. The preservation of this stratigraphic 'truth' is essential when investigating depositional processes; sedimentation rates are often, although not exclusively, derived from the core dimensions (i.e. length of sediment recovered within a given timeframe). In practise, dimensional integrity is very difficult to achieve, due to the inherent problems of retrieving sediments from the deep ocean. One of the most pernicious effects of imperfect retrieval of sediments is over- or under-sampling, typically associated with the upper portions (<10 m) of piston and lower sections (>3 to 4 m) of gravity cores respectively. This distortion of sediment dimensions may lead to erroneous calculations of sediment fluxes. The effects of such over- or under-sampling may be very subtle so as to be un-noticeable during ordinary logging procedures; or extreme, instances of collapsed core liners and mid-core flow-in are reported (e.g. Bouma and Boerma 1968, McCoy 1985). The term over-sampling is used in preference to stretching as the latter would be associated with anomalously high porosities i.e. low densities and would require pore-water displacement (Széreméta et al 2004, Skinner and McCave 2003).

1. Background

Only a brief overview of coring techniques is offered here; for a full explanation, the reader is directed to the excellent review of Skinner and McCave (2003).

Over-sampling in piston cores is a result of movement within the core barrel of the piston, most likely due to cable recoil (McCoy 1985, Buckley 1994). As the cable accelerates upwards with rapid unloading at triggering, it pulls the piston with it. This creates a very low pressure within the core barrel as it moves downwards through the sediments. The potential extent of such piston recoil is determined by the water depth at the coring location and the whole weight of the coring equipment (Skinner and McCave 2003).

As an open barrel corer (piston or gravity) descends through sediments, an increasing (downward) vertical friction is exerted on the sediments below it (due to increasing material in the barrel and general increase in undrained shear strength of sediments with depth). With such piston movement, if the resulting negative pressure anomaly inside the core barrel (with respect to the sea floor pressure), is greater than the vertical friction stress, then a net upward (i.e. negative) pressure results below the descending corer. This exerts suction on the sediments ('syringe effect') leading to thickened or over-sampled sediments. The drop in pressure evolves as a function of time and develops independently of the downward friction stress; the sum of the opposing pressures varies throughout penetration leading to different down core effects (Skinner and McCave 2003) (Figure 5.1).

Based upon modelling, utilising principles of soil mechanics, Skinner and McCave (2003) demonstrated that imperfect piston coring does tend towards 'ideal' behaviour

i.e. no deformation of the sediments, at depths of 8 to 10 m in piston cores, as the cumulative friction stress within the corer and the reduced barrel pressure above the sediments caused by the moving piston, are balanced. Sediments below this point are essentially intact having suffered no over-sampling.

For gravity coring, many have noted the often shorter recovered length of sediments in relation to the penetration depth (Emery and Dietz 1941, Pratje 1952, Emery and Hülsemann 1964, Richards 1961, Lebel et al 1982, Blomqvist 1985, Buckley et al 1994). As stated above, the sediment column experiences an increasing downward frictional force as the core barrel descends which is imposed as a vertical stress on the sediments immediately below the corer at that point in the descent (Figure 5.1); this force is transferred through the sediment column as pore-fluid flow is too slow to dissipate it. This increasing internal friction will eventually be balanced by the increasing bearing capacity¹ of the sediments with depth (Skinner and McCave 2003).

Derived from their modelling study, Skinner and McCave (2003), illustrate that above the point where the cumulative downward friction is greater than the bearing capacity of the sediments, the sediments will enter the barrel while being subjected to increasing vertical stress. Conversely, below this point, *in situ* sediment thinning or under-sampling will occur. This point occurs at relatively shallow depths (~3 to 4 m) and accounts for the shortening of gravity cores commonly reported.

Figure 5.1: Schematic of three possible coring scenarios (from Skinner and McCave 2003, their figure 3): I) gravity coring; II) perfect piston coring (i.e. no piston acceleration); III) imperfect piston coring (acceleration of piston upwards).



Skinner and McCave (2003) concluded that 'the combination of a variety of core types will permit the best acquisition of the *in-situ* stratigraphic truth'. This chapter seeks to describe an application of a combined analysis of core types from the same location, in order to create a spliced sedimentation rate that more closely approximates the stratigraphic and dimensional 'truth'.

The giant piston core MD04-2822 displayed no obvious sign of over-sampling upon close visual inspection and lithological logging (chapter 2). However, upon calculation of IRD flux, an unexpectedly high value was obtained for the Younger Dryas (GS1) interval (~2-3 m core depth). The calculation of IRD flux from IRD concentrations

¹ Bearing capacity - this represents the force that the *in situ* sediments may support before failing completely causing sediment by-passing.

requires an estimation of the linear sedimentation rate, which is, in general, derived from the dimensions (and chronology) of the core. During the Younger Dryas/ GS 1 (ca. 11.7 to 12.9 kyr b2k; GICC05 timescale), IRD flux to the core site was calculated to be greater than those for the LGM². This seems counterintuitive; reconstructions of the last BIS propose far greater extent (and marine margins) for the LGM BIS (e.g. Hubbard et al 2009) than for the Younger Drays (Golledge et al 2008). Over-sampling during coring was thought to be responsible for an erroneous linear sedimentation rate (and hence IRD flux), although other possibilities are considered (section 6, this chapter).

Fortunately, the availability of a gravity core raised from the same location has enabled the degree of over-sampling within the upper portion of the piston core to be assessed and a 'corrected' sedimentation rate determined for the upper portion of piston core MD04-2822. The chapter demonstrates the utility of Skinner and McCave (2003) recommendation for combining coring techniques in order to obtain the best approximation of the '*in situ stratigraphic truth*'.

2. Material and Methods:

The giant piston core MD04-2822 was recovered from the Rockall Trough (56° 50.54' N, 11° 22.96' W; 2344 m water depth) by the R.V. *Marion Dufresne* in 2004. A gravity core, +56-12/15 CS, was recovered from approximately the same location by the R.R.V. *Discovery* in September 2009.

For the gravity core +56-12/15 CS, a total of 3.95 m was recovered whilst the penetration depth (as estimated from the mud-line on the outside of the core barrel) was the entire length of the 6 m core barrel used. This would equate to a recovery to penetration ratio of 0.66 (2dp). This compares favourably with ratios reported by Buckley et al (1994) (average of 0.67, 6 years of data); Richards et al (1961) (average of 0.7 from 20 cores); Emery and Hülsmann (1964) (average of 0.5 to 0.6, 29 cores).

Hvorslev (1949) proposed, that for soils, the 'undisturbed' length (L_s) for cohesive sediments could be predicted by;

$$L_s = 10 \text{ to } 20 * D_s$$

where,

D_s is the minimum diameter of the core barrel

For the gravity core +56-12/15CS, the diameter of the core liner was 150 mm; from the above equation, the predicted 'undisturbed' depth for this core would be at 1.5 to 3 m depth. Skinner and McCave (2003) suggest that this point would be at approximately 3 to 4 m for most gravity cores.

Both cores were analysed using a GEOTEK multi-sensor core logger. The physical properties of MD04-2822 were measured onboard ship, whilst for +56-12/15 CS, these were determined at the Scottish Association for Marine Science (SAMS, Scottish Marine Institute, Oban, Argyll) approximately 2 months after collection but only a couple of days after splitting. The GEOTEK system enables detailed, down-

² The LGM within this chapter uses the definition of EPILOG (Mix et al 2001): ca. 19 to 23 kyr.

core, non-destructive analyses of: gamma density; P-wave velocity; electrical resistivity and magnetic susceptibility. Only the magnetic susceptibility records for both cores are presented here (Figure 5.2).

The IRD concentration (grains $>150 \mu\text{m g}^{-1}$) has been determined for MD04-2822 with a minimum of 300 grains counted per sample using a conventional light microscope. This was converted to IRD flux using the method detailed in chapter 2:

$$\text{IRD flux} = \text{BMAR} * [\text{IRD}]$$

where,

$$\text{BMAR} = \text{LSR} * \rho\text{DB}.$$

The linear sedimentation rate (LSR) was determined from the core dimensions in combination with an age depth model (tuned to the NGRIP $\delta^{18}\text{O}$ record on the GICC05 timescale, section 4, this chapter and Appendix C₂).

3. Lithostratigraphy: MD04-2822 and +56-12/15 CS

Both cores have been visually examined and logged (chapter 2); sedimentation is interpreted as hemipelagic in nature. Visual inspection of the cores did not reveal any structures indicative of sediment disturbance. The magnetic susceptibility profiles obtained from the GEOTEK core scanning for both cores are presented in Figure 5.2. These show striking similarities and allow for the visual correlation of the two records. Difficulty was experienced in visually correlating upper 2 m of the piston core and 1 m of gravity core.

4. Chronostratigraphy – MD04-2822

Age control for MD04-2822 was achieved via tuning of the surface water proxy (% *N. pachyderma* (sinistral)) record to the NGRIP $\delta^{18}\text{O}$ record (GICC05 timescale; Andersen et al 2006, Rasmussen et al 2006, Svennson et al 2006, 2008). The mid-point of climate transitions common to both the marine and ice core was used as tie-points by which the well dated NGRIP GICC05 timescale was translated to MD04-2822 (e.g. Shackleton et al 2000) (Table 5.1, Figure 5.3). In addition, one calibrated radiocarbon date of monospecific *G. bulloides* was used to determine the age of the core top. The conventional age was calibrated using the Marine09 calibration curve (Reimer et al 2009) using OxCal (version 4.1; Bronk Ramsey 2009). No additional local marine reservoir correction (ΔR) was applied prior to calibration other than the global values included in the calibration curve (chapter 3).

This age model differs from that in chapter 3 where the surface proxies for the last glacial were tuned to the NGRIP $\delta^{18}\text{O}$ on the ss09sea timescale (NGRIP members 2004). No age model has been attempted for the corresponding gravity core +56-12/15 CS; faunal and IRD analyses were only undertaken on the piston core MD04-2822. A linear sedimentation rate was then calculated for MD04-2822 and used in the calculation of IRD flux.

Figure 5.2: GEOTEK magnetic susceptibility records for the piston core MD04-2822 (top) and the gravity core +56-12/15 CS. Black filled triangles denote age control tie-points for the piston core MD04-2822, example correlation between the two cores are given by dashed lines.

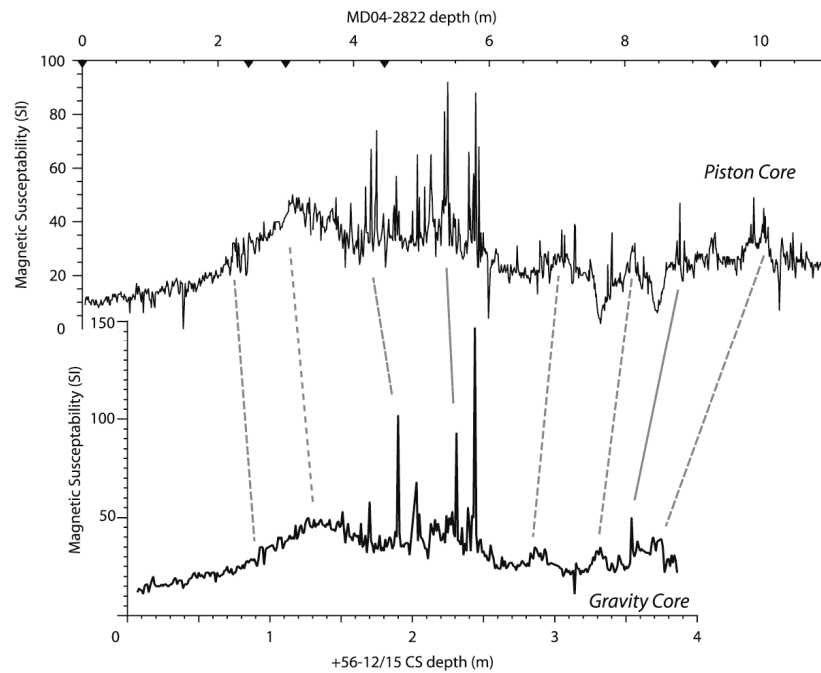


Figure 5.3: NGRIP $\delta^{18}\text{O}$ record on the GICC05 timescale (top) and the age model determined for MD04-2822 (bottom). Chronostratigraphic tie-points are: black filled triangles denote tuning of surface proxies to NGRIP $\delta^{18}\text{O}$ (GICC05 timescale, Andersen et al 2006, Rasmussen et al 2006, Svensson et al 2006, 2008) whilst open triangle gives the position of the core-top radiocarbon date. Grey vertical bars highlight the Greenland Interstadial events 2, 3 and 4 (mid-point of transition in and out) as well as the transition into Greenland Interstadial 1e and the Younger Dryas (GS1).

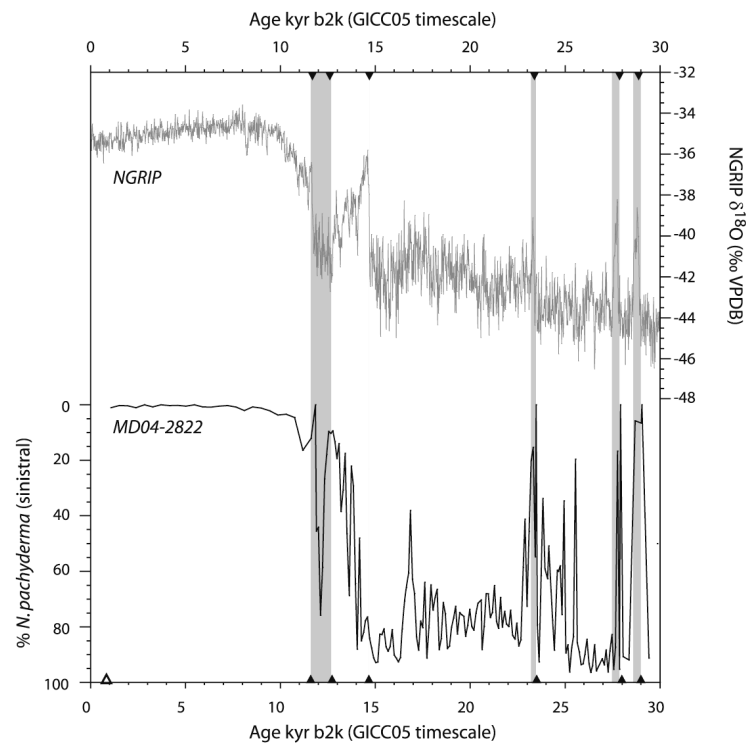


Table 5.1: Chronostratigraphical tie-points (GICC05 timescale; Andersen et al 2006, Rasmussen et al 2006, Svensson et al 2006, 2008) used in the construction of the MD04-2822 age model for this chapter (*note* only the upper ~13 m of MD04-2822 is used). Calibration of the radiocarbon date was via the Marine09 calibration curve (Reimer et al 2009) using OxCal 4.1 (Bronk Ramsey 2009); no additional local marine correction was applied prior to calibration.

Event	Depth in MD04-2822 (cm)	Cal. ¹⁴ C Age (b2k)	NGRIP GICC05 Age (b2k)	GICC05 counting (yrs)*	Max. error	Reference
Core top		930 ± 92	n/a	n/a		n/a
Younger Dryas/Preboreal transition	245.5	n/a	11,703	99		Lowe et al 2008/Svensson et al 2008
Transition into Younger Dryas (GS1)	300.5	n/a	12,896	138		Lowe et al 2008
Transition into GIS 1e	440.5	n/a	14,692	186		Lowe et al 2008
Transition into GIS 2	1325.5	n/a	23,340	596		Lowe et al 2008

* Maximum counting error is an quantified index of the discrepancies in layer counting (operator differences)

5. MD04-2822 IRD flux record, the over-sampling problem and correction using gravity core +56-1215 CS

When IRD flux was calculated for the upper 10 m of core MD04-2822, using the age model outlined above and the dimensions of the core, a conspicuous feature was a large peak in IRD flux during the Younger Dryas/GS 1 interval that was greater than for the LGM in the same core. This seems counter-intuitive; reconstructions of the BIS Younger Dryas (e.g. Golledge et al 2008) propose far less extensive ice margins than for the LGM BIS (e.g. Hubbard et al 2009) and is thought unlikely for a core proximal to this ice sheet. The large IRD flux calculated results from an erroneous estimation of sedimentation rate due to coring disturbance i.e. over-sampling, although alternative explanations are considered (section 6, this chapter). This ‘anomalous’ feature amply demonstrates the difficulties of relying solely on piston core dimensions to derive sedimentation rates.

In response, a ‘spliced’ sedimentation rate has been created using a combination of gravity and piston cores (following the recommendation of Skinner and McCave (2003)), mindful of the associated problems of each. This theoretical construct has then been used to ‘correct’ the sedimentation rate derived solely from the piston core MD04-2822.

5.1. Creation of a ‘spliced’ linear sedimentation rate

The gravity core is assumed to be a facsimile of the piston core and the close correspondence between the two records of magnetic susceptibility has been used to correlate one core to the other (Figure 5.2). This allows equivalent depths to be determined for the chronostratigraphic tie-points in MD04-2822. An ‘independent’ age model³ was obtained for the gravity core using these age-depth tie-points. From

³ *Note* the stratigraphic position of the MD04-2822 chronology tie-points within the gravity core was achieved via the correlation of the two records using their magnetic susceptibility records (Figure 5.2).

this, dimensional sedimentation rates for the gravity core were established, assuming uniform sedimentation between tie-points (Table 5.2).

Table 5.2: Piston core MD04-2822 depth and age of chronological tie points with linear sedimentation rate (LSR) calculated from these tie-points. Equivalent gravity core +56-12/15 CS depths for the MD04-2822 chronological tie-points and calculated LSR.

Event	MD04-2822 (Piston Core)			+56-12/15 CS (Gravity Core)	
	Depth (cm)	LSR (cm kyr ⁻¹)	Age (b2k (GICC05 timescale))	Depth (cm)	LSR (cm kyr ⁻¹)
Core top	0.5		930 ± 92	<i>Correlation problematic</i>	
		↓ 22.74			(10.63)
Younger Dryas/Preboreal transition	245.5		11,703	104.25	
		↓ 46.10			↓ 15.91
Transition into Younger Dryas (GS1)	300.5		12,896	123.23	
		↓ 77.95			↓ 35.78
Transition into GIS 1e	440.5		14,692	187.5	
		↓ 102.34			(36.62)
Transition into GIS 2	1325.5		23,340	<i>Insufficient core recovered</i>	

When plotted on age, the magnetic susceptibility records of both the piston (MD04-2822) and gravity core (+56-12/15CS) exhibit subtle differences (Figure 5.4). This suggests that the assumption of linear sedimentation between tie-points may not necessarily hold true for all portions of the cores. In addition, the upper sections of the cores were difficult to correlate visually; this may account for the differences between the two cores for the portions younger than ca. 10 kyr.

The linear sedimentation rate estimated for the gravity core (using the chronology of the piston core) is assumed to be devoid of any 'over-sampling' effects (cf. Skinner and McCave 2003). As such the gravity core LSR was transferred to the piston core (MD04-2822) ensuring that variations in the LSR calculated between the tie-points for the gravity core related to the same tie-points in the piston core.

The application of the gravity core derived LSR to MD04-2822 enabled the piston core sedimentation rates to be 'corrected'. This 'spliced' linear sedimentation rate was then used to re-calculate IRD flux for MD04-2822 (piston core) circumventing the over-sampled sedimentation rates initially used. Both the initial over-sampled influenced IRD flux, and 'corrected' IRD flux using the 'spliced' LSR, are presented in Figure 5.5. Both IRD flux determinations are presented on the same vertical scale; a clear reduction in IRD flux to the core site during the GS 1/Younger Dryas interval is produced for the gravity core corrected calculation compared to the original.

Using the age tie-points, an assessment of the degree of over-sampling may be made; the dimensions of the piston core are approximately twice those of the gravity core whilst the sedimentation rate calculated for the Younger Dryas (GS 1) from the piston core are three times that derived using the gravity core (Table 5.2, Figure 5.5).

Figure 5.4: Magnetic Susceptibility records for piston core MD04-2822 (black) and gravity core +56-12/15 CS (grey) plotted on their respective ages (using the tie-point originally derived for the piston core MD04-2822, black filled triangles). Inset, the resulting age-depth model and linear sedimentation rate (LSR) between tie-point for both cores (black original piston only; grey ‘spliced’).

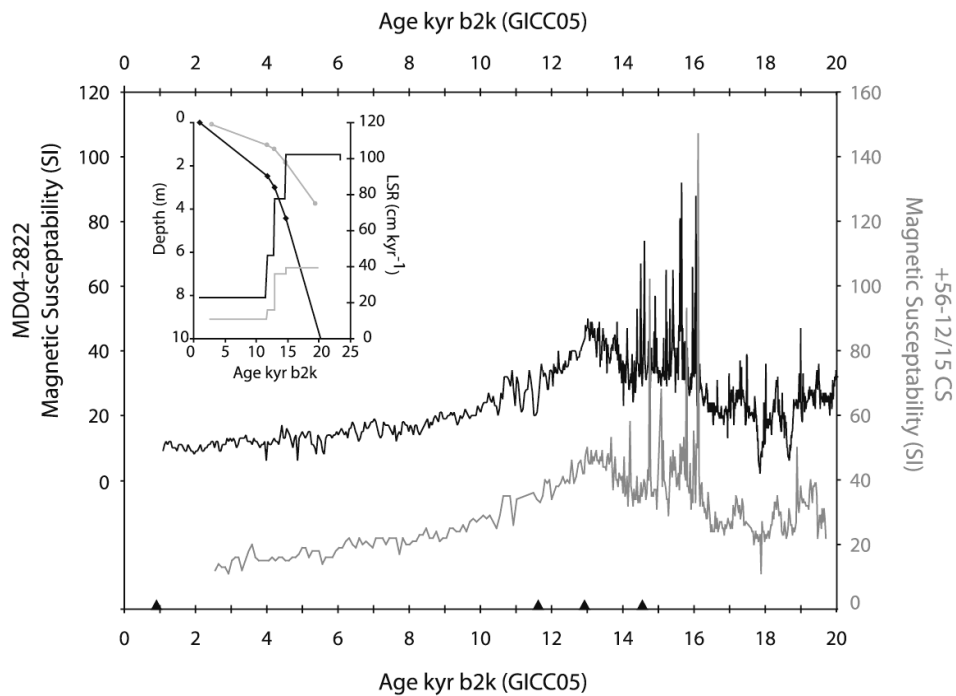
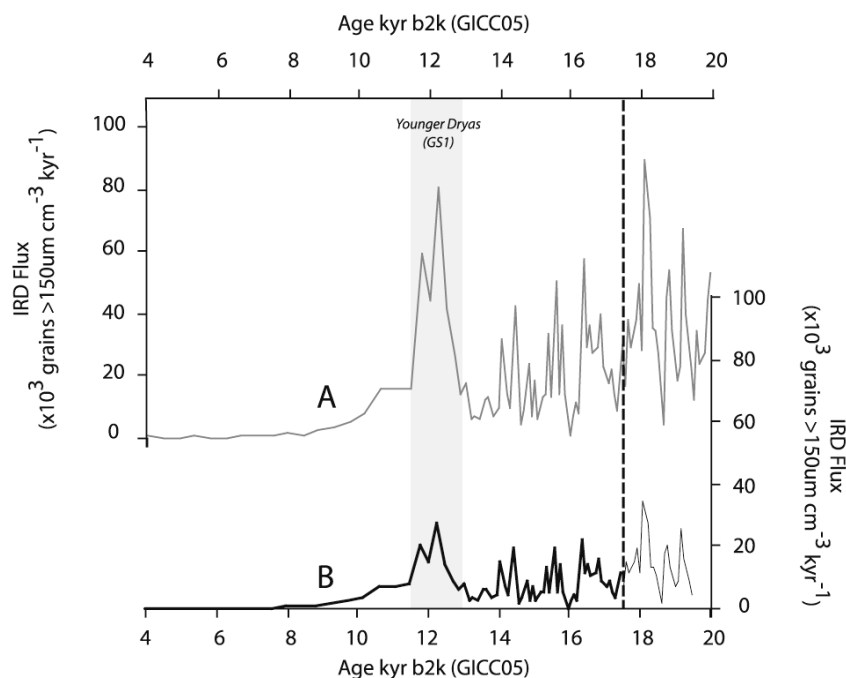


Figure 5.5: Calculated IRD flux for MD0-2822: A (grey line) original piston core MD04-2822 derived sedimentation rate and; B (black line) ‘spliced’ (piston and gravity core) determined sedimentation rates. Vertical grey bar gives denotes the Younger Dryas (GS1) interval, vertical dashed line indicates approximate position of 3 m in the gravity core i.e. the predicted lower limit for which gravity coring exhibits ideal behaviour (cf. Skinner and McCave 2003).



The dashed vertical line in Figure 5.5 denotes the approximate 3 m depth for the gravity core; this is the lower limit for which ideal behaviour is predicted for gravity coring (section 2, this chapter, Skinner and McCave 2003). Below this depth, gravity cores tend to produce under-sampled sediments. As such, any sedimentation rate determined from the gravity core below this 3 m point could result in an erroneous IRD flux estimation. 'Ideal' behaviour tends to occur at depths greater than 10 m in piston cores (Skinner and McCave 2003). Unfortunately, this does not 'overlap' with the upper 'ideal coring' depths of the gravity core (i.e. <3 m core depth). The dashed vertical line in Figure 5.5 marks the approximate position of the gravity core 3 m depth. Based upon the correlation of the magnetic susceptibility records, this would correspond to ~7.5 m core depth in the piston core, which lies above the proposed minimum depth at which over-sampling is thought to no longer occur i.e. ~10 m. Caution should therefore be exercised in interpreting any proxy records dependent upon dimensionally derived sedimentation rates, i.e. IRD flux, for this portion of MD04-2822.

The IRD flux for MD04-2822 calculated using the 'spliced' LSR is used throughout this study; IRD flux is however uncertain for ca. 17 to 20 kyr due to possible erroneous LSRs resulting from assumed coring artefacts for both the piston and gravity core (see chapter 6, section 4.1.1.).

6. The Younger Dryas (GS 1) enhanced IRD flux to the core site compared to the LGM: possible explanations

Section 5, above, demonstrated the value of Skinner and McCave's (2003) recommendation to use complimentary coring techniques in order to minimise any dimensional distortions during coring. An anomalously high Younger Dryas IRD flux is a conspicuous feature of the MD04-2822 record when only the piston core sedimentation rate is used to derive IRD fluxes. The 'spliced' sedimentation rate results in a threefold reduction in IRD flux for the Younger Dryas interval (Figure 5.5). Although 'over-sampling' of the piston core is proposed as the most likely cause of the anomalously high IRD flux during the Younger Dryas, the following section outlines alternative explanations considered i.e. the varying nature of sediment deposition at the site.

The Younger Dryas (GS 1) in this region of the NE Atlantic is characterised by: the (re)advance/growth of British ice (e.g. see review by Golledge 2009); cooling of surface water conditions (e.g. Kroon et al 1997, Elliot et al 2002 estimate cooling of ~4°C for the Rockall Plateau and an increase in IRD coeval with a decrease in $\delta^{13}\text{C}_{\text{Cib}}$); a reduction in bottom currents (McIntyre and Howe 2009) coincident with ice rafting; and cool sea surface temperatures (SSTs) (Austin and Kroon 2001) coupled with the migration of the polar front south and a weakening of the formation of North Atlantic Deep Water (NADW) (e.g. Keigwin and Boyle 1999, Elliot et al 2002).

Possible scenarios that may account for an increase in IRD deposited at the MD04-2822 site during the Younger Dryas in comparison to the LGM are:

1. The dilution of the LGM IRD signal by fin-grained terrigenous inputs (<150 μm)
2. Surface water conditions preventing the melting of icebergs during the LGM
3. Elevated calving and therefore IRD fluxes during the Younger Dryas compared to the LGM
4. A catastrophic failure of the Younger Dryas ice sheets
5. IRD of non BIS origin i.e. farfield sources
6. Increased contribution from the wider Rockall Basin possibly due to increased bottom current vigour during the Younger Dryas
7. The winnowing of fines during the Younger Drays
8. Reduced accumulation of IRD during the LGM compared to the Younger Dryas (due to e.g. scenarios 1 to 7 above)
9. Younger Dryas IRD flux represents slope failure within the basin e.g. turbidite emplacement

Each of these propositions has been discounted; Table 5.3 outlines each proposition and reason(s) for rejection in brief.

Table 5.3: Possible scenarios that may account for increased IRD input during the Younger Dryas compared to the LGM and reasons for discounting these in favour of ‘over-sampling’

Scenario	Likelihood	Reasons for discounting
1	<i>Possible</i>	<ul style="list-style-type: none"> • During the LGM, the MD04-2822 IRD concentration signal may be ‘diluted’ due to high inputs of fine-grained terrigenous material (< 150 μm); these inputs may have diminished during the Younger Dryas. The percentage (by mass) of material > 63 μm does increase during the Younger Dryas to approximately 7.5 % from an average of 2 to 4.5 % during the glacial. Whilst absolute inputs of IRD (> 150 μm) may have been higher during the glacial, their percentage contribution to the sediments (by mass) was reduced compared to the Younger Dryas. However, IRD flux is calculated to order to negate such ‘dilution’ effects (e.g. Ruddiman 1977).
2	<i>Possible but unlikely</i>	<ul style="list-style-type: none"> • There is currently limited evidence for the presence/absence of sea ice at the MD04-2822 site for the Younger Dryas, although ostracode assemblages suggest sea ice in the Rockall Trough during MIS 2 (Cornin et al 2010, Didić and Bauch 2000). Extensive sea ice might have restricted the transport of icebergs and the melting of those icebergs. • Significant sea ice expansion has been inferred for the North Atlantic during both intervals (e.g. Ruddiman and McIntyre 1981, Glidor and Tziperman 2003, CLIMAP 1976, 1981, EPILOG; Mix et al 2001, MARGO Project members 2009), although seasonally ice free conditions are thought to have occurred during the both the LGM and Younger Dryas within the NE Atlantic (Meland et al 2005, MARGO members 2009)). As such, the transport of icebergs is thought not to have been sufficiently impeded during the LGM to account for a lower IRD flux to the site than during the Younger Dryas. • Meltwater, i.e. cold surface conditions, are not thought to impede iceberg melting at more proximal site (MD95-2006) during the LGM (e.g. Wilson et al 2002); similar conditions are expected at MD04-2822 core site. • Alternatively, enhanced melting of icebergs during the Younger Dryas could account of increased fluxes. Summer surface water conditions for the LGM are estimated to be approximately 5 to 6 $^{\circ}\text{C}$ for the Rockall Plateau compared to ~ 8 $^{\circ}\text{C}$ for the Younger Dryas (Elliot et al 2002) therefore enhanced melting of icebergs might be expected during the Younger Dryas (GS 1) compared to the LGM at this latitude. However, a more extensive ice front (e.g. the model of Hubbard et al 2009) with increased calving rates (e.g. Marshall and Koutnick 2006) is proposed for the LGM possibly ‘balancing’ the effect of reduced SSTs on IRD inputs to MD04-2822.
3	<i>Very unlikely</i>	<ul style="list-style-type: none"> • Ice volumes during the LGM were significantly greater than those for the Younger Dryas (a proxy for global ice volumes, $\delta^{18}\text{O}_{\text{Cib}}$ indicates an approximate 2.5 % difference between the LGM and Younger Dryas in MD04-2822). In addition, modelled calving rates for the LGM, circum-Atlantic ice sheets, exceeds that for the Younger Dryas interval (e.g. Marshall and Koutnick 2006). • For the last BIS, the modelled and geologically mapped limits of the Younger Dryas (e.g. Golledge et al 2008) fall within those of the BIS at its maximum extent (e.g. Bowen et al 2002, Sejrup et al 2005, Boulton and Hagdorn 2006). • In addition, the modelled and reconstructed marine margins for the Younger Dryas are very restricted, therefore restricting iceberg calving and thus supply of debris laden icebergs from the local BIS, to the core site • Sea level changes may have acted to destabilise the marine margins of the Younger Dryas BIS, increasing calving and the delivery of icebergs into the Rockall Trough. However even if a destabilisation of the marine margins occurred, it is thought unlikely to be able to account for such increased IRD flux due the very restricted extent of those ice margins during the Younger Dryas.
4	<i>Very unlikely</i>	<ul style="list-style-type: none"> • The BIS Younger Dryas ice sheet is generally thought to have been a thick but restricted ice cap early within the Younger Dryas/GS 1 stadial which under increasingly continental conditions and aridity (e.g. Benn et al 1992) instigated deglaciation via thinning and eventually marginal recession (Golledge 2010). • The highly restricted marine margins are unlikely to be unduly affected by any increase in sea level that may precipitate ice sheet decay for ice sheets with extensive marine margins (e.g. the BIS at the LGM) nor produce sufficient debris laden icebergs to account solely for such a large input of IRD during the Younger Dryas

5	<i>Possible but thought unlikely - insufficient evidence</i>	<ul style="list-style-type: none"> • The source of IRD within the Younger Dryas interval has not yet been determined i.e. no detailed lithological description as yet for MD04-2822. However, the neighbouring core MD95-2006 has had some limited lithological characterisation for this interval. These samples contain grains of basalt that have previously been used to infer BIS dynamics (Knutz et al 2001) suggesting a local component to the IRD flux. An increase in fine-grained terrigenous material at MD04-2822 during the Younger Dryas also suggests that at least some of the material was derived from the BIS. Such fine-grained material is not thought to be transported vast distances from the source (Dowdeswell et al 2010). In addition, the ‘bulk’ IRD flux to sites proximal to ice sheets with marine margins is, in general, inferred to be local in origin (Scourse et al 2009, Peck et al 2007). • However, a far-field source cannot be ruled out; for example, the Scandinavian ice sheet had retreated from the shelf edge during the Younger Dryas but it did have far more extensive marine margins than the BIS (e.g. Knies et al 2007, Lohne et al 2007). The ‘diagnostic’ BIS lithics (cf. Knutz et al 2001) may also have derived from rock below the Scandinavian or Greenland ice sheets (Hibbert et al 2010, Scourse et al 2009). In addition, a sea ice mechanism has also been invoked for the transport of tephra (e.g. the Vedde Ash; Austin et al 1995); therefore icebergs or sea ice from higher latitudes may have been transported to the site. The contribution of far-field sites remains undetermined for MD04-2822.
6 and 7	<i>Very unlikely</i>	<ul style="list-style-type: none"> • Evidence suggests the opposite occurred during the Younger Dryas interval. A decrease in bottom current vigour is inferred from cores in the vicinity i.e. palaeoflow speeds decreased during the Younger Dryas within the Rockall Trough (McIntyre and Howe 2009, Austin and Kroon 2001). A reduction in current speed would reduce the potential for sand transport and for the winnowing of fines. • Basal ‘freeze-on’ of material from the Rockall Bank may have occurred during the LGM (M. Stoker, <i>pers. comm.</i>) when sea level was ~ 120m lower than present (e.g. Peltier and Fairbanks 2006). However, sea level during the Younger Dryas interval is far closer to modern values than the LGM and therefore basal ‘freeze-on’ of material from the Rockall Plateau is thought less likely.
8	<i>Very unlikely</i>	<ul style="list-style-type: none"> • High IRD inputs are seen for neighbouring core MD95-2006, a site more proximal to the marine margins of the last BIS, during the LGM (e.g. Wilson et al 2002); similar high IRD concentrations would be expected at core MD04-2822. • The marine calving margins for last BIS far more extensive during the LGM than the Younger Dryas (e.g. Gollledge et al 2009); greater iceberg calving from the BIS during the LGM than the Younger Dryas proposed (e.g. Marshall and Koutnick 2006).
9	<i>Unlikely</i>	<ul style="list-style-type: none"> • It is possible that some of the IRD inputs during the Younger Dryas could be a result of slope failure, however this is thought highly unlikely as no graded sediments were evident during lithological logging. However, the recognition that very distal turbidites is difficult but these are unlikely to account for such a large IRD input.

The large IRD concentration and IRD flux to the MD04-2822 core site during the Younger Dryas (GS 1) is therefore attributed to a combination of coring artefacts producing over-sampled sediments in the upper ~ 10 m, with some contribution of varying inputs of primarily fine terrigenous material ‘diluting’ the IRD signal during the LGM (although the calculation of IRD flux reduces this effect; Ruddiman 1977).

Other cores in the region also display very high IRD concentrations during the Younger Dryas and glacial periods (e.g. Knutz et al 2001, 2002, 2007, Elliot et al 2002). Indeed, in core DAPC2 (Rosemary Bank) the flux of IRD >250 µm is also greater during the Younger Dryas than during the LGM, whilst NA87-22 (Rockall Plateau) IRD concentrations during the Younger Dryas are very similar to episodes of enhanced IRD inputs inferred to be Heinrich Events 1 to 5 (Elliot et al 2002). These are giant piston cores and some degree of ‘over-sampling’ could account for the very high IRD inputs documented at these cores during the Younger Dryas.

The use of paired coring therefore, provides not only a means by which coring artefacts may be detected, but also a method for 'correcting' any over-sampling problems.

7. Summary and Conclusions

Using paired coring techniques, as recommended by Skinner and McCave (2003), a 'spliced' sedimentation rate was created for site in the Rockall Trough based upon both a piston and a gravity core. The surface proxy record of the piston core (MD04-2822) was the means by which a (tuned) chronology was obtained. This chronology was then transferred, using the close correspondence of the magnetic susceptibility records, to the gravity core (+56-12/15CS) providing a means of deriving linear sedimentation from the dimensions of a core unaffected by over-sampling. The over-sampling of the piston core necessitated the 'correction' of the upper section of MD04-2822 as the imperfect coring resulted in an erroneous depth-age relationship. This error in determining the LSR was propagated in the initial IRD flux calculations prior to the creation of a 'spliced' LSR record. The 'corrected' sedimentation rate reduced IRD flux estimates within the Younger Dryas threefold compared to the original calculations.

The distortion of the MD04-2822 sediments due to over-sampling was not evident from core logging; if left 'un-corrected' this would have given rise to spurious age-depth relationships for the upper portion of the core. Such relationships are essential in determining depositional processes such as IRD flux and thus over-sampling may distort any cyclic phenomena with the proxy records for those sediments. Therefore palaeoenvironmental reconstructions based upon piston cores, should endeavour to combine piston and gravity cores from the same location, in order to maintain the stratigraphic and dimensional integrity of the sediments.

CHAPTER 6¹: The Last and Penultimate Glacial Cycles in the MD04-2822 record

The MD04-2822 record contains the entirety of the last glacial cycle - from the last interglacial (MIS 5e) to the current (Holocene), as well as the majority of the penultimate glaciation. This allows for direct comparison between the Devensian/Weichselian and the Saalian glaciations from the same core.

This chapter outlines and discusses the overall trends of deposition and hydrological conditions at the MD04-2822 site for the last ~175 kyr, with a focus on the last and penultimate glaciations. IRD deposition to the MD04-2822 site is evaluated and 'first order' ice sheet dynamics for the NW portion of the BIS is attempted. Subsequent chapters (chapters 7 and 8) consider in detail the MD04-2822 IRD record for MIS 5 and MIS 4 and the inception of the last glacial period.

MD04-2822 presents a unique opportunity to address questions regarding the dynamics of the last two BIS; MD04-2822 is currently the only high resolution sediment core proximal to the last BIS containing the entirety of the last glacial cycle. Most high resolution cores extend only to ca. 60 kyr (e.g. Knutz et al 2001, Wilson et al 2002, Peck et al 2006), whilst cores with greater temporal range (e.g. ODP 980, McManus et al 2002) have much reduced resolution in comparison to MD04-2822. This core therefore contains evidence of the early history of the last BIS, which may be masked or removed by the subsequent ice sheet oscillations on land, as well as documenting the majority of the penultimate glacial for which there exists scant evidence for the NW sector of the ice sheet.

In the absence of a high resolution core (and thus detailed glacial record) such as MD04-2822, no direct evidence for a MIS 6 glaciation is available. Whilst an extensive glaciation of the Hebridean margin seems likely, little evidence is available to support this proposal. The following discussion presents the first evidence confirming an extensive glaciation of the Hebridean margin during MIS 6.

Orbitally driven variations in climate have been documented throughout the Quaternary (e.g. Broecker and van Donk 1970) with millennial scale climate variability a prominent feature of the last glacial period, most notably the D/O cycles (e.g. Dansgaard et al 1982, Bond et al 1993, 1997b). Such variability is thought to have persisted within the Holocene (e.g. Bond et al 2001, 1997a, b). The high resolution MD04-2822 record enables the investigation of the degree to which such sub-orbital climate variability was present within the North East Atlantic during the MIS 6 glacial period, at a resolution comparable to that of the last glacial.

These matters, amongst others, were investigated via analysis of MD04-2822 and demonstrate the importance of this high resolution sediment core in unravelling the NW European glacial history during the Late Quaternary.

¹ This chapter underpins *Hibbert FD*, Austin WEN, Leng MJ and Gatliff RW 2010. British Ice Sheet dynamics inferred from North Atlantic ice-rafted debris records spanning the last 175, 000 years. *Journal of Quaternary Science* 25(4): 461–482 doi. 10.1002/jqs.1331. All material in this chapter is the sole work of F. Hibbert.

1. Methods

This chapter utilises proxies for prevailing hydrological conditions and terrigenous inputs (details of which may be found within chapter 2). The proxies are presented on their age scale and the compound age model (chapter 3, *Chronostratigraphy*) is used throughout this chapter². The benthic $\delta^{18}\text{O}$ isotopes provide both age control (see chapter 3, *Chronostratigraphy*) and an indicator of global ice volume³, whilst the % *N. pachyderma* (sinistral) record allows tuning to the Greenland ice cores and is a semi-quantitative measure of sea surface temperature.

The interaction between variations in northern hemisphere insolation and sea level upon ice sheet oscillations, may account for variations in IRD delivered to the site (although the difficulties in dating, implicit and explicit assumptions used in the reconstruction of global sea level and associated uncertainty estimates preclude definitive correlation (see e.g. Caputo 2007)). For example, an increase in insolation is thought to have prompted the demise of the penultimate glaciation, resulting in enhanced iceberg calving and delivery of IRD (H11 is clearly evident at the end of the penultimate glaciation within MD04-2822). Similarly, an increase in sea level may destabilise the marine margins of ice sheets, prompting enhanced calving and delivery of IRD. As such, the MD04-2822 IRD record is compared to a reconstruction of global sea level. The Red Sea reconstruction of Siddall et al (2003, data Siddall et al 2006b) is used as this provides: a fairly high resolution record (centennial scale from 70 to 25 kyr BP) spanning the last 180 kyr; reproducible and favourable comparison to fossil reef estimates; and the incorporation of an uncertainty estimate (± 12 m for the last 125 kyr).

2. Climatic and IRD Events at the MD04-2822 site during the last 175 kyr

2.1. Ice-rafted deposition over the last 175 kyr

The incorporation of IRD within the sediments at the MD04-2822 site has been variable through time (Figure 6.1). The Last Glacial Maximum (LGM)⁴ is clearly evident, as an extended period of high IRD flux. The penultimate glaciation (MIS 6, Saalian) also contains episodes of elevated IRD fluxes, although the magnitude of these is less than those during MIS 2.

Additional, smaller IRD episodes (i.e. those $> 20,000$ grains ($> 150 \mu\text{m}$) $\text{cm}^{-2} \text{kyr}^{-1}$) are seen at ca. 60 to 70 kyr (MIS 4) and 40 kyr (MIS 3). This latter increase in IRD

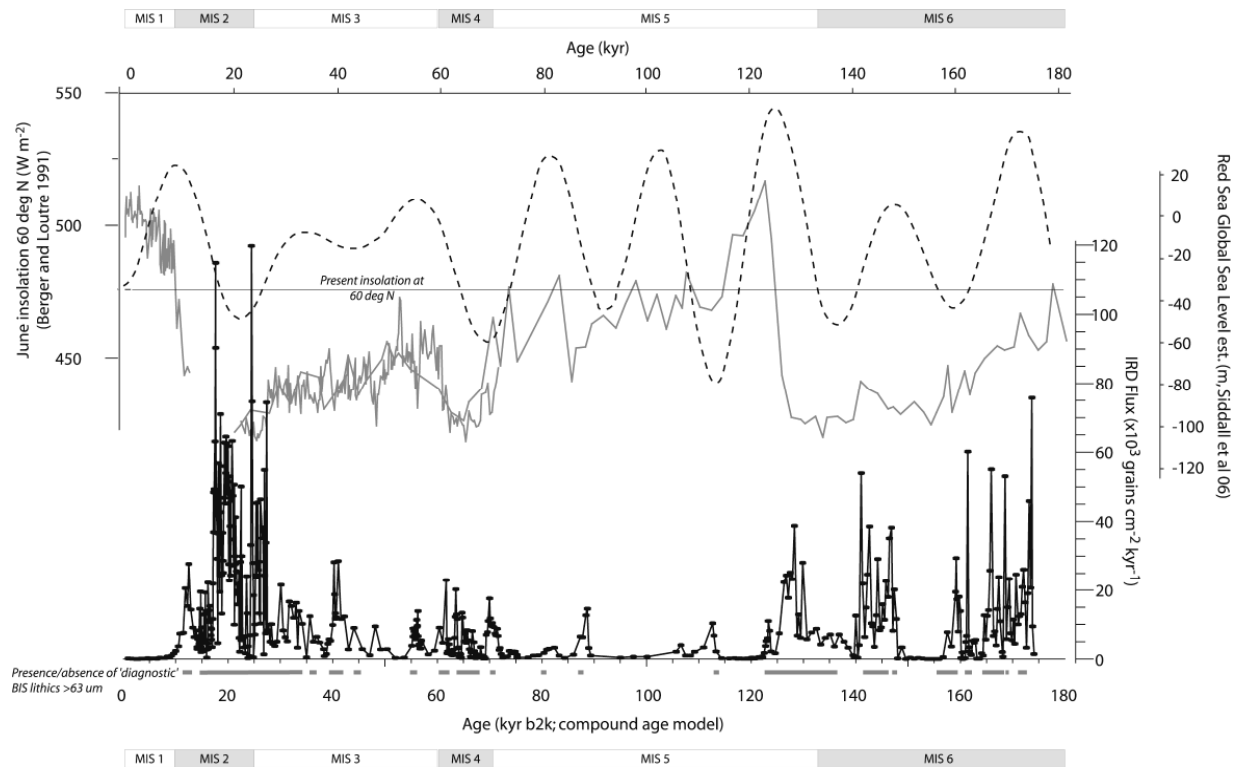
² Ages for MD04-2822 are quoted as kyr b2k (before 2000) unless otherwise stated

³ Global ice volumes are not the sole influence upon benthic $\delta^{18}\text{O}$, the reader is directed to chapter 3 (*Chronostratigraphy*) for a full discussion of benthic $\delta^{18}\text{O}$.

⁴ This term is used variably within the literature for example referring to ca. 19-23 kyr (EPILOG, Mix et al 2001); whilst the BIS LGM has been placed at 18-24 kyr (Boulton et al 1991, Bowen et al 2002) while others have used the term to denote the period 25- 35 kyr (Sejrup et al 2005, Carr et al 2006, Bradwell et al 2008); or alternatively in reference to the global ice volume maximum at 30- 22 kyr determined from sea-level curves (e.g. Peltier and Fairbanks 2006). The LGM occurs within MIS 2 and is part of the Devensian/Weichselian glaciation on land.

has also been noted for sediment cores proximal to the last BIS and may be associated with HE 4; cf. MD95-2006 (e.g. Knutz et al 2001, Peters et al 2008) and MD01-2461 (Peck et al 2007, 2008).

Figure 6.1: MD04-2822 IRD flux (grains > 150 μm), grey bar below gives the presence/absence of 'diagnostic' BIS lithics (>63 μm), June insolation at 60 °N (Berger and Loutre 1991) and reconstruction of global sea level (Siddall et al 2003, 2006). Note – all records shown on their own age scales. MIS designations after Imbrie et al (1984).

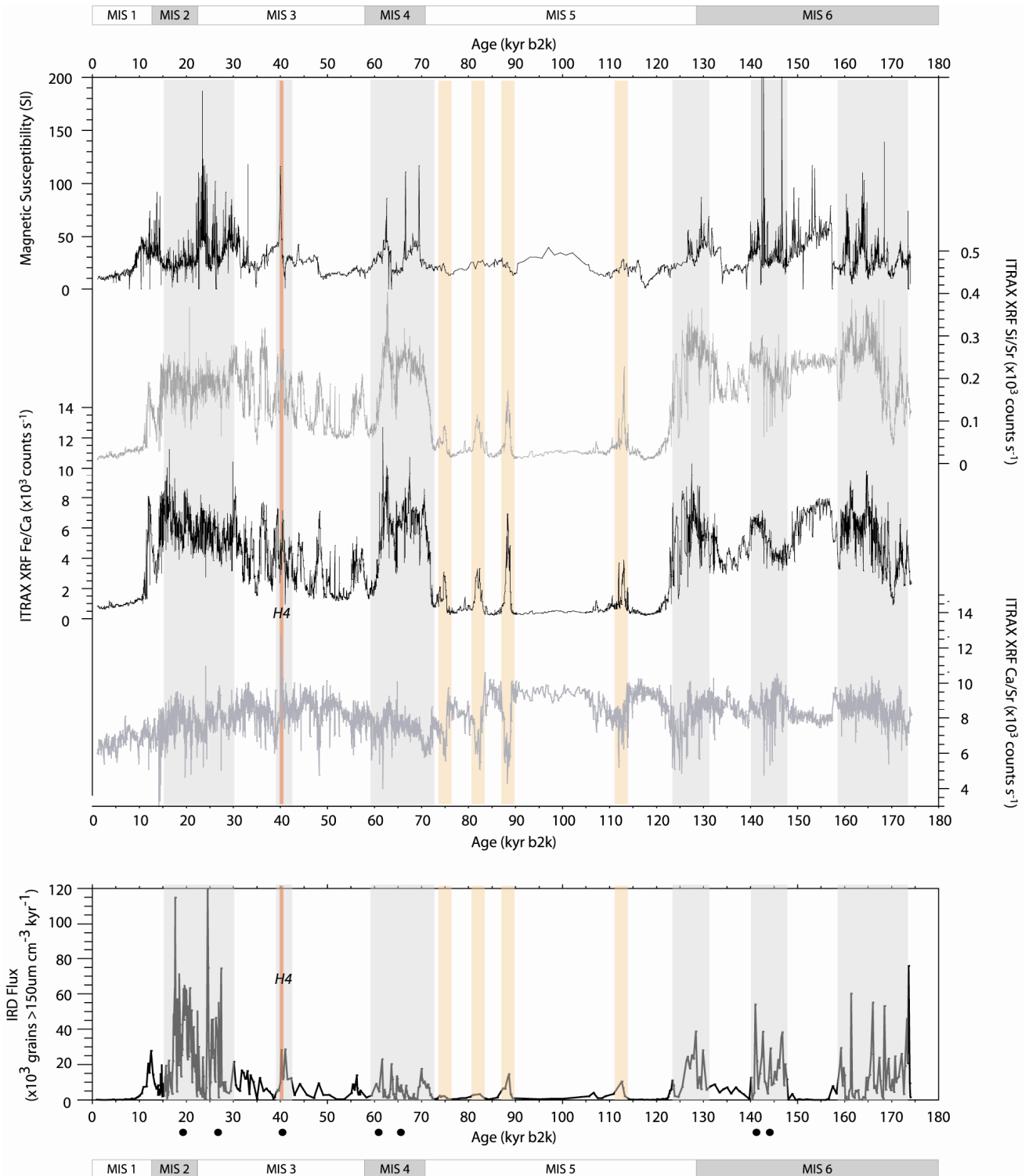


The clearest examples of insolation and sea level interaction are at ~40 kyr (H4), ~60 kyr (chapter 8) and ~130 kyr (H11) (this chapter) within the MD04-2822 record. In the latter two examples, insolation and sea level changes are offset, with both IRD events occurring on the rising limb of June insolation. This offset is unsurprising: northern hemisphere ice sheets respond to integrated warming on centennial scales rather than instantaneous temperature changes (Rohling et al 2009).

This pattern of IRD delivery to the MD04-2822 site is reflected in the proxies for terrigenous inputs (Figure 6.2). Episodes of high magnetic susceptibility are clearly discernable within both MIS 6 and MIS 2 with further peaks in MIS 4. Similarly, both the Si/Sr and Fe/Ca records display peaks in each of these intervals. Unsurprisingly, these two proxy records mirror one another for the entire 175 kyr record, reflecting terrigenous inputs to the MD04-2822 sediment core.

CHAPTER 6:
The Last and Penultimate Glacial Cycles in the MD04-2822 record

Figure 6.2: Terrigenous proxies for MD04-2822 (top to bottom): ship board magnetic susceptibility, XRF core scanning Si/Sr record, XRF core scanning Fe/Ca record, XRF core scanning Ca/Sr record and IRD flux (>150 μm). Vertical grey bars indicate inferred increases in terrigenous inputs (and IRD); vertical orange bars highlight enhanced episodes of Si/Sr and Fe/Ca during MIS 5 (co-incident with minor IRD events). Vertical red bar gives the position of HE 4 (peak in Ca/Sr); subsequently confirmed lithologically. Black dots give the approximate position of pebble sized (mostly 0.5 to 2 cm diameter) IRD grains seen at the cut surface of both the archive and working sections of MD04-2822. MIS designations after Imbrie et al (1984).



The large IRD fluxes, proximity of the core to the BIS and pebble-sized⁵ dropstones found within MIS 6 and MIS 4 to 2 (inclusive), could suggest a British origin for the majority of the IRD (Hibbert et al 2010). In addition, the presence of ‘diagnostic BIS’ lithics⁶ (cf. Knutz et al 2001) within all these IRD peaks (Figure 6.1) is also highly suggestive of a British origin (Hibbert et al 2010). It should be remembered that such grains may also derive from other sources (e.g. Rockall Bank, Greenland etc).

Minor IRD events are evident within MIS 5 (Figure 6.1); these are correlated to the amphi-Atlantic SST cooling and IRD events C24, C23, C21 and C20, based upon stratigraphic position (cf. Chapman and Shackleton 1999) (see chapter 8). The occurrence of these IRD peaks during cool surface conditions at the MD04-2822 site may indicate that this IRD is primarily of non-local origin; the excursion of polar waters would have brought debris-laden icebergs to the site, where surface water conditions would have prompted melting and incorporation of IRD into the MD04-2822 sediments. The majority of IRD peaks outside MIS 5 are associated with a surface warming. Such sea surface warming could have destabilised the marine margins of the BIS, leading to enhanced iceberg calving and melting.

Conspicuous within the record are three intervals of near zero IRD flux (<100 grains $>150 \mu\text{m cm}^{-2} \text{ kyr}^{-1}$) at ca. 150 to 155 kyr (MIS 6), 115 to 120 kyr (MIS 5e) and <10 kyr (MIS 1, Holocene); the interval ~ 90 to 100 kyr also experiences very limited IRD flux (<400 grains $>150 \mu\text{m cm}^{-2} \text{ kyr}^{-1}$) to the MD04-2822 site. MIS 5e and MIS 1 are periods of interglacial climate with global ice volumes similar (or smaller) than present. However, the MIS 6 interval of little or no IRD inputs, but continuing high magnetic susceptibility and XRF Si/Sr and Fe/Ca, occurs during a period of insolation greater than present and levels experienced during the build up to the LGM (at 60°N ; Berger and Loutre 1991), (Figure 6.1).

The terrigenous proxy records (magnetic susceptibility, Si/Sr and Fe/Sr) vary slightly between the MIS 6/Saalian and Devensian/Weichselian glaciations (Figure 6.2). Broad peaks in Si/Sr and Fe/Ca are evident within MIS 6, however, these proxies seem to have a quasi-cyclic appearance within the last glacial. This may mark the response of the BIS to the D/O events that are conspicuous during the last glacial as noted for the neighbouring core MD95-2006 (Knutz et al 2001, Wilson and Austin 2002, Wilson et al 2002). Alternatively this feature may be related to the biogenic inputs associated with the D/O cycles. These proxies also continue to record high values within the MIS 6 IRD minima (ca. 150 to 165 kyr) in contrast to the interglacial IRD minima. Intervals of high magnetic susceptibility are more numerous within MIS 6 and may be connected to slight coarsening of sediments noted during lithological description (see chapter 2). These coarser layers are thought to be the distal manifestations of turbidites. The peaks in Si/Sr and Fe/Ca within MIS 5 differ from those during the glaciials; peaks in both terrigenous proxies are coincident with lows in the Ca/Sr records, suggestive of decreased biogenic inputs.

⁵ Most dropstones observed on the surface of the cut sediments are ~ 0.5 cm (maximum dimension), however, at 2029-30 cm a 2 cm dropstone was recorded. Pebbles are defined as being 4 to 64 mm in diameter (Udden-Wentworth grain size scale)

⁶ Visual identification of dark finely crystalline volcanic grains (basalt); assumed British Tertiary Igneous Province origin

The Heinrich (H) Events discernable within other North Atlantic cores (e.g. Heinrich 1988, Bond et al 1992, 1993) are less obvious within the MD04-2822 IRD record. Large IRD events, which may be connected with HE 1, 2 and 11 (and possibly H6) based upon their timing (ca. 16.8, 24, 60 kyr respectively for H1, 2 and 6; Hemming 2004), have not been investigated lithologically. Therefore these cannot be confirmed as Heinrich Events until such lithological characterisation has been undertaken i.e. by the presence of characteristic detrital carbonate (cf. Bond et al 1992).

Large peaks in IRD (often used to indicate the position of Heinrich Events; see above) may not be discernable from the MD04-2822 IRD record due in part to the current sampling resolution (predominately every 10 cm); the events may be present, but could have been 'missed' during sampling. As such, XRF core scanning (e.g. Hodell et al 2008) was used to detect Heinrich Events within sediments using the ratio of calcium to strontium (Ca/Sr) (see chapter 2, *Materials and Methods*), however, only at ~ 2015.5 cm is there a clear peak in Ca/Sr. Subsequent lithological characterisation confirms this as Heinrich Event 4 (see chapter 4).

2.2. Hydrological conditions – Surface waters

The distinctive D/O events that characterise the last glacial interval in both the Greenland ice core and North Atlantic marine record are clearly evident within MD04-2822. These punctuations of low % *N. pachyderma* (sinistral) abundances are also a feature of the penultimate glacial. They reflect the northward migration of the polar front relative to the core site resulting in the MD04-2822 site being bathed with warmer surface waters. Such warming of surface waters provides a potential moisture source for ice sheet growth; however, such a warming may also act to destabilise a marine margin, thereby enhancing both the rate of iceberg calving and the rate of melting of those icebergs.

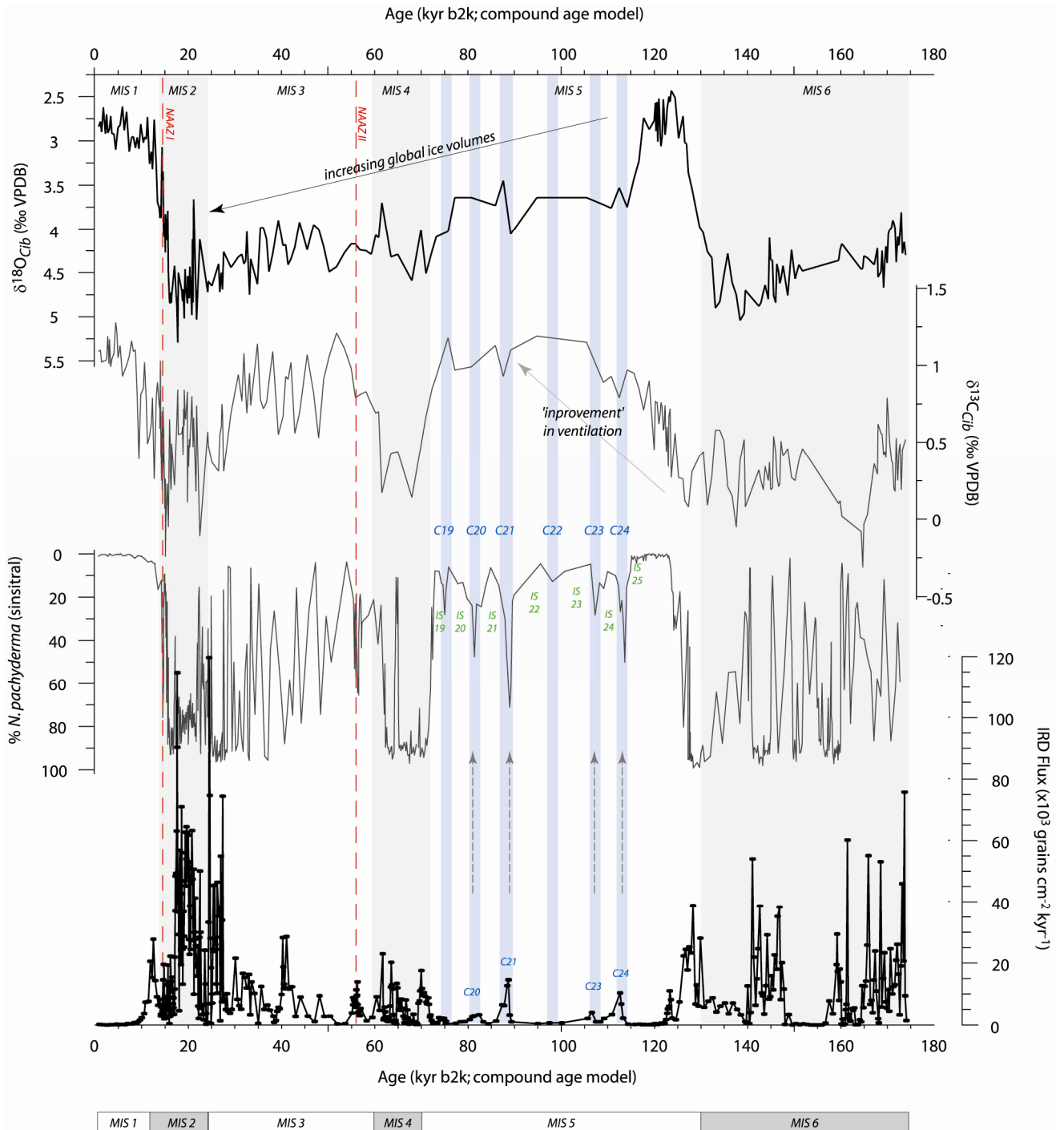
The converse, i.e. enhanced IRD delivery during cooling, is illustrated within MIS 5 (Figure 6.3). An expansion of polar waters during MIS 5 facilitated iceberg migration into the wider North Atlantic, resulting in increased IRD deposition (e.g. the cooling 'C' events within MIS 5 cf. Chapman and Shackleton 1999, Oppo et al 2006). The C events within MIS 5 are discussed further within chapter 8.

The MD04-2822 planktonic isotope record (*N. pachyderma* (sinistral) and *G. bulloides*) is incomplete; MIS 5 in particular is very patchy. Despite this, inferences regarding surface water conditions (e.g. temperature and salinity) and the degree of stratification may be attempted. These are presented where appropriate in the sections below.

2.3. Hydrological conditions – Bottom waters

The benthic $\delta^{18}\text{O}$ may be used as a qualitative measure of global ice volumes (it should be remembered that the benthic $\delta^{18}\text{O}$ signal may not scale with global ice volumes and there may be some degree of local 'over-printing' due to changes in bottom water temperature or salinity – the reader is directed to chapter 3, *Chronostratigraphy*, for a full discussion of these influences upon the benthic $\delta^{18}\text{O}$ signal).

Figure 6.3: Proxy records for MD04-2822 (from top to bottom) $\delta^{18}\text{O}_{\text{Cib}}$, $\delta^{13}\text{C}_{\text{Cib}}$, % *N. pachyderma* (sinistral) and IRD flux (grains >150 μm). All proxies are plotted on the compound age model (see chapter 3) in kyr b2k. MIS designations after Imbrie et al (1984). Red vertical red dashed lines give the stratigraphical positions of NAAZ I and II. Blue shaded bars highlight surface cooling within MIS 5 (the C events cf. Chapman and Shackleton 1999, McManus et al 2002; labelled C19 to C24 in blue). Green labels are the Greenland Interstadial designations for MIS 5. Vertical dashed grey arrows highlight the association of minor IRD events within MIS 5 and increases in the abundance of *N. pachyderma* (sinistral).



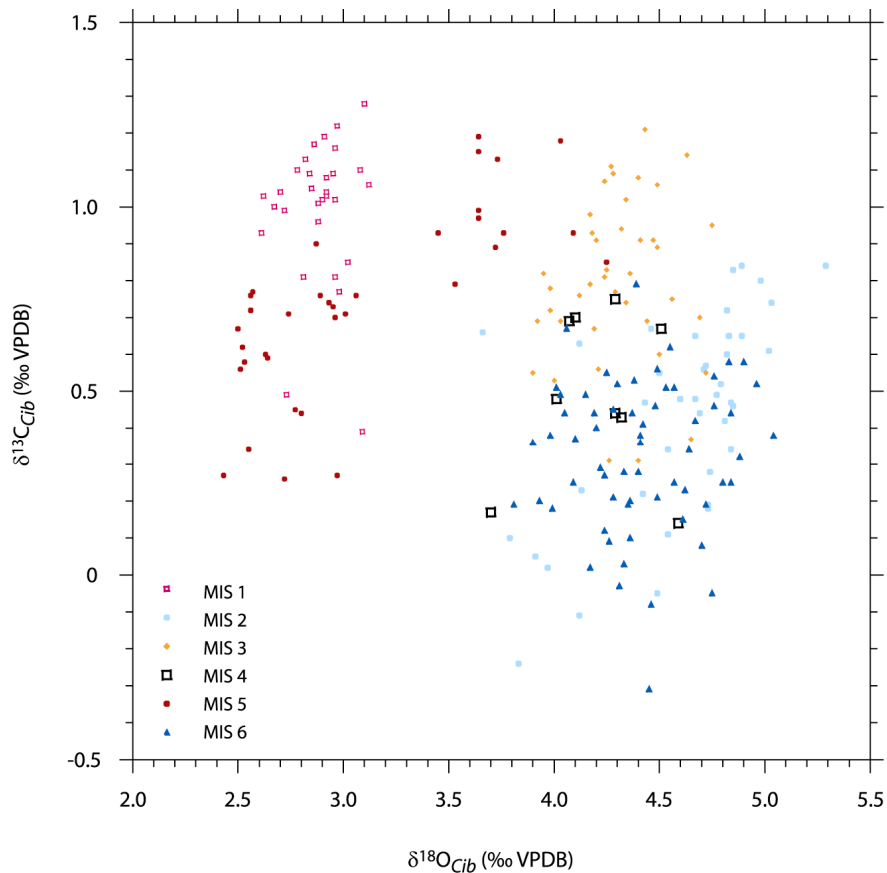
The interglacials (MIS 1 and MIS 5e) can be clearly discerned within the record by their light (more negative) $\delta^{18}\text{O}$ values (Figure 6.3, Figure 6.4). Similarly the LGM can be recognised by the heavy (more positive) $\delta^{18}\text{O}$ values. A long-term increase in values from the MIS 5e to the LGM reflects the initiation and development of the last glacial. The maximum benthic $\delta^{18}\text{O}$ (correlated to the benthic stack feature of Pisias et al 1984) for the entire record is 5.29 ‰ (no correction for disequilibrium effects e.g. Shackleton and Updyke 1973, has been applied to the MD04-2822 values); however this is just one data point. Several intervals record benthic $\delta^{18}\text{O}$ values of ~ 5 ‰ within MIS 2. In comparison, the isotopic maximum obtained during MIS 6 is 5.04 ‰ and there are several intervals with $\delta^{18}\text{O}$ values ~ 4.8 ‰. The benthic $\delta^{18}\text{O}$ signal is variable, with some millennial-scale variations evident. An increase in the current low resolution (10 cm) may reveal further surface hydrological variations.

The $\delta^{18}\text{O}$ and $\delta^{13}\text{C}$ values for both MIS 2 and MIS 6 are similar (Figure 6.4) suggesting that deep water hydrological conditions were similar for both intervals, although conditions were not static through these time periods. Similarly, both MIS 1 and MIS 5 plot within the same field. There is a notable two field structure to the MIS 5 values reflecting the build up of Northern hemisphere ice with the progression of the isotope stage. The penetration of low $\delta^{13}\text{C}$ waters of southern origin or derived from brine rejection in the Nordic Seas (Vidal et al 1998, Dokken and Fronval 1999, Dokken and Jansen 1999, Meland 2008) was not limited to MIS 2 and 6, but is also evident in MIS 5, 4 and 3 to a lesser extent. The presence of low salinity deep-water brines has been inferred within MIS 3 for the proximal core MD95-2006 (Dickson et al 2008) and is thought to reflect seasonal sea ice formation in the Nordic Seas and brine formation (although a locally derived brines may also have formed) and their outflow into the North Atlantic. The expansion of sea ice in the Nordic Seas during the stadial intervals is thought to contribute to D/O warming by initiating a weak AMOC (Dokken and Jansen 1999, van Kreveld et al 2000) and thus destabilising the build-up of warm saline waters in the sub-tropics (Schmidt et al 2004, 2006).

The benthic $\delta^{13}\text{C}$ also displays millennial-scale variability throughout the last 175 kyr (Figure 6.3). This proxy may be used to monitor the intensity of AMOC (e.g. Kroopnik 1985, Lehman and Keigwin 1992). During vigorous overturning, more positive $\delta^{13}\text{C}$ waters bathe the MD04-2822 site, whilst during reductions in AMOC, southern sourced waters (AABW), with low $\delta^{13}\text{C}$ values are able to penetrate into the Rockall Trough. The most negative $\delta^{13}\text{C}$ value is seen within MIS 6 (-0.31 ‰), although other low or negative values are evident within MIS 4, 3 and 2.

During glacial intervals, the site of convection in the North Atlantic was located to the south compared to present; cold surface waters became more buoyant as evaporation reduced (Duplessy et al 1988) and the resulting water mass (GNAIW) was of insufficient density to sink into the deep North Atlantic, instead this water bathed depths of 1000 to 2000 m (Venz et al 1999). Other studies suggest that GNAIW sank to depths of ~ 2.3 km (Boyle and Keigwin 1987, Zahn et al 1987, Oppo and Lehman 1993), or assert the presence of an additional water mass at intermediate depths (2-3 km), i.e. not GNAIW or glacial Antarctic (AABW), nor a mixing of the two, but water mass derived from sustained formation of a deep water component in the Norwegian-Greenland Seas (Yu et al 2008).

Figure 6.4: MD04-2822 benthic (*C. wuellerstorfi*) $\delta^{18}\text{O}$ and $\delta^{13}\text{C}$ (note – last deglacial values are not shown)



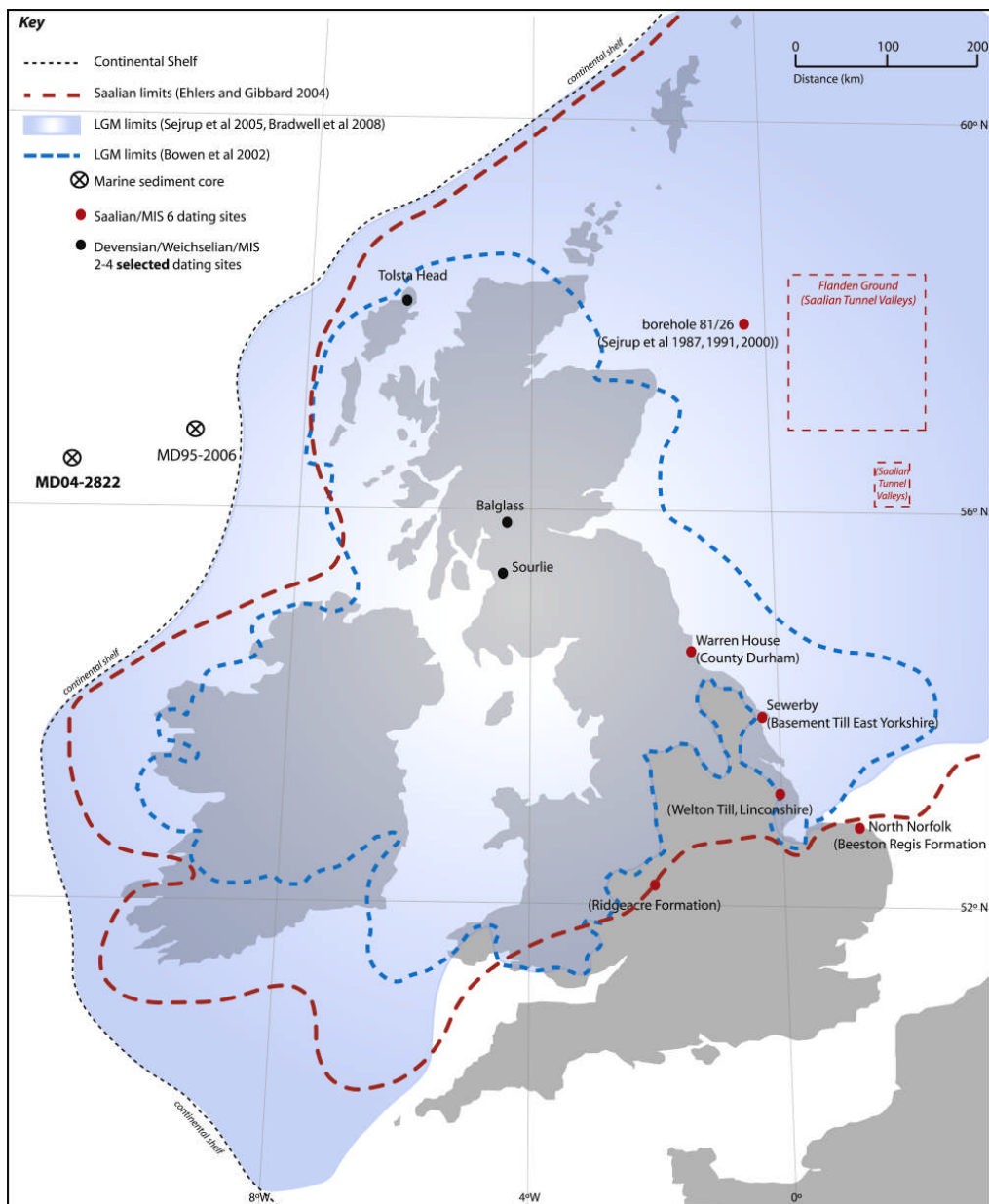
In contrast to the two glacials, the present interglacial (MIS 1, Holocene), portions of MIS 3 and much of MIS 5 display fairly positive $\delta^{13}\text{C}$ values. The last interglacial (MIS 5e), although recording a general increase in $\delta^{13}\text{C}$ values, does not display very positive $\delta^{13}\text{C}$ values (similar to the present interglacial) until around 106 kyr (MIS 5c). It is proposed that this offset in the benthic $\delta^{18}\text{O}$ and $\delta^{13}\text{C}$ is a result of large meltwater influences from the decay of the Saalian ice sheets, impeding the formation of deep water within the Nordic Seas and thus overflow into the Rockall Trough (the reader is directed to chapter 7 for a full discussion).

In very broad terms, the $\delta^{13}\text{C}$ signal is similar to the % *N. pachyderma* (sinistral) record; this may reflect the close association between the advection of warm, saline waters into the Nordic Sea (and thus over the MD04-2822 site) and the formation of deep water within the Nordic Seas. Any reduction in deep water formation would result in a ‘slowdown’ in the transport of warmer waters northwards. This is evident within MIS 5, where relatively small reductions in $\delta^{13}\text{C}$ are accompanied by increases in the % abundance of *N. pachyderma* (sinistral) and small increases in IRD. The decrease in AMOC would have facilitated the expansion of polar waters (and consequently icebergs) into the wider North Atlantic and where surface conditions permitted, these icebergs would have melted depositing any entrained IRD.

3. Discussion - Comparison between the last (Devensian/Weichselian) and penultimate (Saalian) glaciations within MD04-2822

This section discusses the IRD deposition at the MD04-2822 site within the context of the regional evidence for ice sheet dynamics and the last two BIS (Figure 6.5). An evaluation of the last two glacial periods and deglacial events recorded within the same sediment core is offered; the nature of sedimentation for both intervals and in particular IRD deposition is investigated.

Figure 6.5: Location map with core and site locations mentioned in the text. Shelf edge LGM BIS limits are after Sejrup et al 2005 and Bradwell et al 2008), LGM limit of Bowen et al (2002) also shown (dashed blue line). MIS 6/Saalian maximum extent of Ehlers and Gibbard (2004) (dashed red line) and dating sites (red dots).



3.1. BIS dynamics inferred from MD04-2822 within a regional context

3.1.1. MD04-2822 MIS 6 IRD record

The NW UK margin is characterised by distinctive sediment architecture⁷ indicative of multiple Pleistocene shelf glaciations of the BIS (Stoker 1997); seismic data also confirms MIS 6 shelf edge glaciations for the North Sea Fan and the Norwegian margin (King et al 1996, 1998b, Nygård et al 2005, Dahlgren et al 2002, Heinrich and Baumann 1994) as well as bore hole data from the North Sea (e.g. Sejrup et al 1987, Ekman 1998, Carr 2004). In addition, fragmentary terrestrial evidence for the pre-Weichselian is available (e.g. Ehlers and Gibbard 2004), however sediments from older glaciations have often been eroded and correlation between terrestrial sites and the marine record is problematic, which coupled with chronological uncertainties, currently hamper understanding of the long-term dynamics of the pre-Weichselian/Devensian BIS (Lee et al 2010). The precise configuration of the Saalian BIS is poorly understood with several different scenarios proposed (e.g. Long et al 1988, Rappol et al 1989, Ehlers and Gibbard 2004; Figure 6.5).

From this fragmentary evidence, glaciation curves for the penultimate BIS have been constructed with tentative Hebridean and Shetland shelf edge glaciation within MIS 6 (Sejrup et al 2005); however, evidence for this is insecure and the expansion of the BIS during MIS 6 on the Hebridean margin is inferred from long-range correlation of seismic data with the North Sea succession (Holmes 1997). Within the recovered MIS 6 interval, four major episodes of enhanced ice rafting to the MD04-2822 site are evident (Figure 6.1 Figure 6.3); these intervals of elevated IRD flux are centred about ca. 173–166 kyr, 160 kyr, 147–141 kyr and 128 kyr. An interval of minimal IRD flux is seen at 157–150 kyr. The presence of ‘diagnostic BIS’ lithics within these IRD peaks provides the first evidence for the presence of a BIS, of sufficient size and with a marine margin (presumably grounded on the Hebridean shelf), to deliver IRD to the core site during MIS 6 (Hibbert et al 2010).

The Saalian glaciation in Europe has traditionally been subdivided into a primary advance phase: the Drenthe (175– 160 kyr); and a second re-advance: the Warthe glaciation (150– 140 kyr). The Drenthe glaciation resulted in the continental ice advances in Russia, Scandinavia and the British Isles (Ehlers 1990, Ehlers et al 2004, Clark et al 2004a, Mangerud 2004, Svendsen et al 2004), with the subsequent Warthe glaciation within the limits of the Drenthe glaciation. The timing of these advances corresponds favourably with the two primary phases of increased IRD flux to the MD04-2822 site, which are separated at ca. 157–150 kyr by a period of limited IRD flux.

Several records note large environmental changes ca. 175 kyr; a northward migration in the ITCZ (Malaizé et al 2006, Tisseraud et al 2009); increased rainfall in the Mediterranean recorded in the $\delta^{18}\text{O}$ of stalagmites (Bard et al 2002, Ayalon et al 2002); increased North Atlantic surface winds (Masson et al 2000) and; an increase in productivity of the surface waters of the Bay of Biscay (Penaud et al 2009). The increase in precipitation within the mid-latitudes may have contributed to the growth of the

⁷ Extensive stacked tills that interdigitate with sediments that form the slope apron.

European ice sheets, with some 'threshold' reached at ca. 170-160 kyr, precipitating a partial ice sheet collapse and intensification of the 'Fleuve Manche' palaeoriver discharge (Penaud et al 2009).

A pronounced 'collapse' of European ice sheets has also been proposed ca.150 kyr from laminated sediments within cores from the Bay of Biscay, produced by increased 'Fleuve Manche' palaeoriver discharge. This in turn has been linked to increasing insolation (Toucanne et al 2009, Penaud et al 2009). The sharp decrease in Northern Hemisphere summer insolation between 150 and 140 kyr may then have favoured a period of re-growth of European ice sheets in the latter portion of MIS 6 (Toucanne et al 2009).

In the North Sea, two phases of glaciation are proposed for the Saalian (Ehlers 1990, Carr 2004), with much of the North Sea Basin covered by ice during the Late Saalian. An extensive Late Saalian till containing Scottish origin fragments was identified from a central North Sea borehole (Sejrup et al 1987, 1991, 2000, Ekman 1998) and the tip of East Anglia is thought to have been ice covered (Clark et al 2004) (Figure 6.5). However, the position of ice cover over Britain during the Saalian remains unclear (Svendsen et al 2004) with the correlation of offshore and bounding terrestrial evidence highly ambiguous (Lee et al 2010).

The coalescence of the British and Fennoscandian ice sheets (estimated to have been established at ~150 kyr) has been proposed by Penaud et al (2009) based upon the relative timing of laminated facies, reworked tracer species and global sea level: a reduced sea level during the latter stages of MIS 6, in conjunction with an ice barrier would have resulted in the diversion of lowland Europe meltwater via the palaeo 'Fleuve Manche' river system, into the Bay of Biscay, giving rise to these distinctive sediments. In addition, Busschers et al (2008) speculate that a reconfiguration of ice flows and the connection of ice sheets within the North Sea contributed to the formation of the present Dover Strait. However the configuration of the BIS and Scandinavian ice in the southern N. Sea is unclear (Carr 2004) and there is no direct evidence for grounded BIS ice, instead glacio-lacustrine sedimentation (Clever Bank Formation) has been identified in both the UK and Dutch sectors (Cameron et al 1992, Busschers et al 2008).

The coalescence of the BIS and Scandinavian ice remains somewhat speculative. However the tills in County Durham, east Yorkshire and east Lincolnshire (Basement Till, Ash Gill Member/Warren House Till) as well as outwash sands and gravels in East Anglia have been interpreted as Scandinavian in origin (Lewis and Rose 1991, Catt 2007, Gibbard et al 2009) but precise age control for these sediments remains elusive⁸ (Clark et al 2004b). Subsequent research suggests a BIS origin for these

⁸ The Sewerby deposits of east Yorkshire are found below biostratigraphically and luminescence dated MIS 5e deposits (Catt and Penny 1966, Bateman and Catt 1996, Briant 2002). Other dating is derived from the comparison of glacial sequences to those of mainland Europe (e.g. the landforms of Norfolk and the Netherlands; Ehlers et al 1984). The correlation of eastern England landforms with those of the Netherlands and Germany suggests a Scandinavian source; this is the only time this is known to have occurred in Britain (Clark et al 2004b). However, Lee et al (2002, 2004) demonstrate that these MIS 6

sediments, that Scandinavian erratics are rare and may represent reworking of older deposits in the North Sea (Hoare and Connell 2005, Lee et al 2005). Terrestrial evidence for the expansion of the BIS during MIS 6 remains ambiguous (Lee et al 2010) with differing chronological and stratigraphic interpretations of the same data (Lewis and Rose 1991, Gibbard et al 1992, 2009, Hamblin et al 2005, Pawley et al 2008).

Glacio-lacustrine deposits in the southern North Sea prompted some (e.g. Clark et al 2004b, Gibbard 2007, Busschers et al 2008) to speculate that an ice dammed lake between the North Sea ice margin and the chalk ridge between Northern France and Dover was likely and may have contributed to the final breaching of the Dover Straits. Indeed, Gupta et al (2007) cannot resolve the timing of the catastrophic flooding event(s) in the Straits of Dover, as revealed by high resolution (sonar) bathymetric survey. A catastrophic flood from a pro-glacial lake in the North Sea basin has been speculated as the cause of these large valley systems in the floor of the English Channel (e.g. Smith 1985, Gibbard 1995). An MIS 12 (Anglian/Elsterian) age was initially proposed for the draining of a southern North Sea lake (Gibbard 1995) but a Saalian/Wolstonian (MIS 10 to 6) has also been suggested (Meijer and Preece 1995, Clark et al 2004b). Whilst age constraint is as yet insufficient, the Dover Strait was certainly open by MIS 5e (Keen 1995).

As such, many glaciation curves for the region envisage shelf edge glaciations for most of the northwestern European margin during MIS 6 (Stoker 1990, Sejrup et al 2000, 2005, Dahlgren et al 2002, Hjelstuen et al 2005, Nygård et al 2005). The two phases of increased IRD flux (and fine grained terrigenous inputs i.e. Si/Sr) to MD04-2822, potentially corresponding to continental (Drenthe and Warthe) glacial phases, provide the first firm evidence for the presence of a BIS ice sheet with an actively calving margin during MIS 6.

The period of very low IRD deposition (157–150 kyr) within MIS 6 is accompanied by high values for terrigenous inputs⁹ (magnetic susceptibility, Si/Sr, Fe/Ca). This may suggest that whilst IRD inputs decreased, perhaps due to retreat of the ice sheet from the edge of the continental shelf, large inputs of material continued to be delivered to the site, possibly via meltwater plumes, from a proximal ice sheet. Sedimentation rates (estimated from core dimensions) are very similar during this interval, to those during ~ 130 to 140 kyr (and those during MIS 4 and portions of MIS 3) where IRD inputs are elevated above background levels (Figure 6.6).

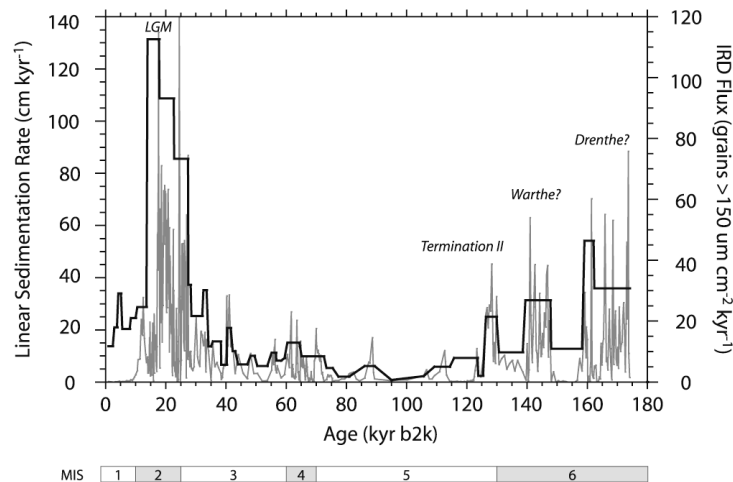
Millennial-scale D/O and Bond cycle type behaviour recorded by the percentage abundance of the polar foraminifera *N. pachyderma* (sinistral), pre-eminent during the last glacial, is also a striking feature of the penultimate glacial record of MD04-MD04-2822 (Figure 6.3). All intervals of increased IRD within MIS 6 are preceded by an abrupt warming in surface waters at the site. The combination of rapid northward retreat in the position of the oceanic polar front at the MD04-2822 site and rising sea level (e.g. Shackleton et al 2000, Siddall et al

age deposits are of BIS derivation with ice flow down the east coast incorporating distinctive lithologies unique to the UK.

⁹ Measured on bulk sediment samples via core scanning; ship board magnetic susceptibility and ITRAX XRF core scanning.

2003) may have acted to destabilise a BIS with a marine calving margin, prompting an increase in IRD flux to the core site during MIS 6.

Figure 6.6: Linear sedimentation rate (black line) and IRD flux (grey line) for MD04-2822. MIS designations after Imbrie et al (1984).



Direct evidence of the penultimate BIS remains somewhat limited; MD04-2822 presents the first evidence for a shelf-edge glaciation of NW Britain for this interval. However, the IRD signal recorded in marine sediments may represent both ice sheet advance and decay. Further work remains to unravel the history of the MIS 6 glaciation, for this sector of the penultimate BIS.

3.1.2. *The MIS 2/3 IRD record at the MD04-2822 core site*

Nearly continuous IRD flux to the MD04-2822 core site is seen throughout MIS 3 (Figure 6.2 and Figure 6.3), with a pulse at ca. 41 kyr and a step change increase in flux at ca. 27.4 kyr. The general pattern of IRD delivery agrees well with the IRD record for the neighbouring core MD95-2006 (Knutz et al 2001, Wilson et al 2002).

Knutz et al (2001) demonstrate BIS-derived IRD fluxes to the MD95-2006 site, corresponded to the D/O stadial cycles of MIS 2 and 3. In addition, an increase in the concentration of presumed British Tertiary Igneous Province basalt at ca. 30 kyr coincides with global cooling at the MIS 3/2 transition. This pattern was confirmed from the sediment lightness record of Wilson and Austin (2002) and recently by the environmental magnetic provenance work of Peters et al (2008). Utilising a magnetic unmixing model, Peters et al (2008) propose a large BIS component within the MD95-2006 record at the end of Greenland Stadial 9, ca. 38.5 kyr, and limited BIS IRD through the early part of MIS 3.

BIS 'diagnostic' lithics are also present within the MD04-2822 record at the step change in IRD flux (ca. 27.4 kyr), suggesting either an expansion of the BIS onto the outer continental shelf or the destabilisation of an already established marine margin by, for example, an increase in global sea level.

While it is well established that global sea level fell towards the LGM as global ice volume increased, emerging evidence suggests multi-millennial scale oscillations (Siddall et al 2003, Arz et al 2007, Siddall et al 2008) superimposed on this long-term fall in sea level throughout MIS 3, with a periodicity longer than that of the D/O cycles themselves (Figure 6.1). The driving mechanisms of these sea-level changes are poorly understood, although Antarctic warmth is thought to play a contributory role. There is sufficient ambiguity in both the timing and the magnitude of sea-level change associated with and pre-dating Heinrich Event 2, to preclude unequivocal attribution of the increase in contemporaneous IRD flux to a short period of global sea-level rise during a major phase of BIS expansion onto the continental shelf. The step change in IRD flux may be a circum-Atlantic phenomenon at ca. 27 kyr (Peck et al 2007), which may initially be synchronised in response to a short-lived phase of sea-level rise.

During the last glacial period, a near neighbour of the BIS was the Irish Ice Sheet (IIS), and IRD from this ice sheet may also be incorporated into the IRD of MD04-2822. The IIS for the last 45 kyr is speculated to have been a dynamic system with several ice margin fluctuations comparable to the LGM event (McCabe et al 1986, 1998, 2005, McCabe and Clark, 1998, 2003; Bowen et al 2002). A thick ice mass over Ireland is inferred to have existed from ca. 25.3 to 28.3 kyr and glacial and marine sediments record an expansion of the IIS onto the continental shelf ca. 28 kyr (McCabe et al 2007); this is comparable to the onset of enhanced IRD flux to the MD04-2822 site. In the southern Norwegian Sea between 40 and 20 kyr, enhanced IRD inputs originating from the southern Fennoscandian Ice Sheet are recorded with an increase at ca. 25 kyr, reflecting the maximum extension of the ice sheets and increased heat flux to the Nordic Seas (Lekens et al 2006). In the North Sea, the Flandern/Witch Ground Basin experienced its most extensive glaciation in this region at 29–25 kyr (Sejrup et al 2009), with an ice margin extending from Ireland to Spitsbergen (Sejrup et al 2005). During the last glacial, the IRD record of MD04-2822 compares favourably, *sensu lato*, to other marine sediment cores in the near vicinity (e.g. Scourse et al 2009); the Barra Fan (Knutz et al 2001); the Rosemary Bank Seamount (Knutz et al 2007); the Porcupine Seabight (Peck et al 2006, 2007, van Rooij et al 2007), Goban Spur and Meriadzek Terrace (Auffret et al 2002) and the wider northeast Atlantic (McManus et al 1994, Oppo et al 2006, Alvarez Zarikian et al 2009). This reflects the expansion of the Northern Hemisphere ice sheets towards their LGM configurations.

Within MIS 2, IRD fluxes for MD04-2822 remain high and contain abundant 'characteristic BIS' lithic grains, confirming the presence of a proximal calving BIS margin on the western Hebridean shelf. Terrigenous proxies remain high throughout much of MIS 2 (Figure 6.2) While the step-like increase in IRD flux at ca. 27.4 kyr may be a regionally synchronised feature, arising from partial ice sheet collapse/surging propagated by an increase in global sea levels; the subsequent period of high IRD fluxes represents the (re)advance of the BIS to its LGM margins, with a series of deglacial IRD events during the oscillations from fully glacial to BIS-free conditions. The GS1/Younger Dryas interval IRD flux may result from an oceanic control on IRD deposition linked to the changing position of the oceanic polar front, with warm surface water incursions into the Nordic Seas triggering the final phases of ice sheet disintegration (Austin and Kroon 2001). The deglacial signals are discussed more fully in section 4, this chapter.

3.2. Comparison of the last two glacial intervals within MD04-2822

The depositional record for the last two glacials within the MD04-2822 record, while bearing similarities, does exhibit subtle differences. These may arise from differing climatic forcing, BIS geometries and glacial regimes (i.e. ice streaming). The exact geometry of the last two BIS cannot be inferred from the MD04-2822 record (unfortunately most terrestrial evidence has been removed or masked by subsequent ice sheet oscillations for the penultimate BIS; the geometry of the last BIS on the other hand, is more secure due to the increased amount of evidence preserved, see for example the recent review by Chiverrell and Thomas 2010) however the timing of IRD inputs allows the dynamics of ice sheet oscillations to be attempted. The main control on sediment delivery to marine basins (and thus to sediment cores such as MD04-2822) is the intensity of the glaciation i.e. the changing dimensions and dynamics of the ice sheet operating at both orbital and millennial timescales (Dowdeswell et al 2010).

Differences between the lithology of the MD04-2822 sediments of the last and penultimate glacial, with a greater frequency of distal turbidites during MIS 6 (recognised as thin silt laminae; see chapter 2, section 2), could result from a greater lateral extension onto the shelf. A more extensive ice sheet could have destabilised sediments on the shelf from previous glaciation (e.g. the extensive Anglian glaciation, MIS 12; Ehlers and Gibbard 2004) and this may account for the increased occurrence of what have been interpreted as distal turbidites within MIS 6, compared to MIS 3 and 2. The prograding of sediments out into the Rockall Trough along a considerable lateral extension also suggests that this region was receiving sediments from an extensive ice sheet margin during the Quaternary (Figure 6.7).

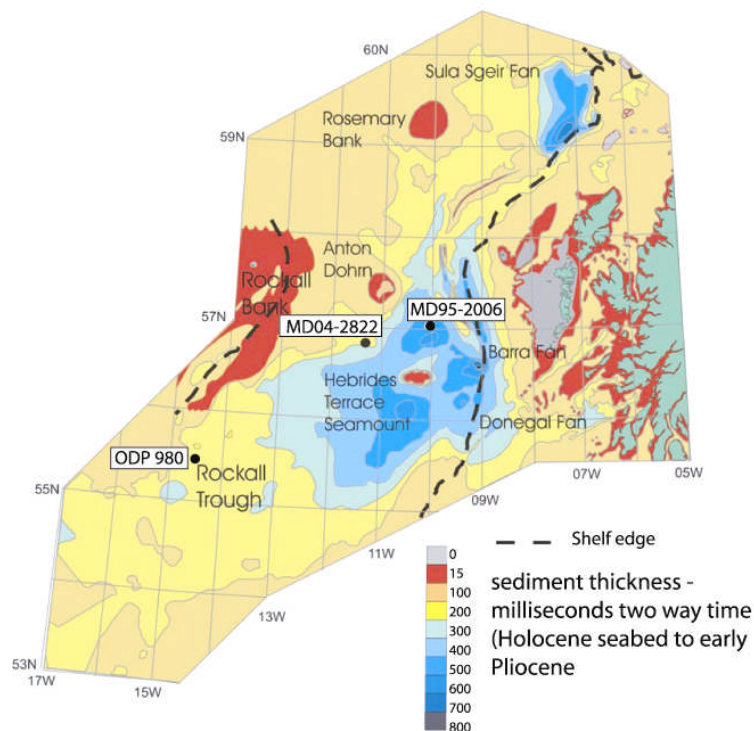
A larger MIS 6 BIS is highly speculative but could account for the variation in the sediments between these two glacial intervals. Penaud et al (2009) suggest that fluvial discharges into the Bay of Biscay, which was draining European glaciated systems including the BIS¹⁰, was greater during MIS 6 than MIS 2 and Termination I. These authors suggest that this is due to the greater extent of the European MIS 6 ice sheets. Geological evidence (e.g. moraines) suggest that the European ice sheets had a greater extent during the Saalian compared to the Weichselian (e.g. Svendsen et al 2004, Ehlers et al 2004).

Toucanne et al (2009) have correlated the MIS 6 sediments within the Bay of Biscay to the Saalian glaciation which has been demonstrated to be one of the most extensive European glaciations of the last 160 kyr (Svendsen et al 2004). However, Penaud et al (2009) rely upon a restricted model of the BIS and IIS extent during MIS 2. This view of the LGM configuration is at odds with new and emerging data highly suggestive of a shelf edge LGM glaciation (e.g. Bradwell et al 2008, Ballantyne 2010, Chiverrell and Thomas 2010). For the NW sector of the former BIS, however, the maximum extent of the BIS onto the continental shelf is primarily controlled by the edge of the continental shelf itself. It seems unlikely therefore, that the Saalian ice sheet was more

¹⁰ Note that the discharge from the NW sector of the BIS, thought to be the source of IRD to the MD04-2822 site, would not drain via the Bay of Biscay. Indeed, the dynamics of these two areas of the BIS may be very different, especially with ice streaming behaviour. Indeed, not all sectors of the last two BIS reached their maximum extent at the same time.

extensive than the Weichselian for the *NW sector* of the BIS, as lateral extent is limited by deep water beyond the shelf; where water depth exceeds a few hundred meters, the ice front generally floats, and further expansion is limited by calving processes.

Figure 6.7: Isopach map of Rockall Trough sediment thickness in milliseconds of two-way travel time. Approximate locations of MD04-2822, MD95-2006 and ODP 980 are given. Note – only the British portion of the Rockall Trough is shown (figure courtesy of the British Geological Survey)



During the last glacial, IRD and proxy records of terrigenous input display a gradual ‘build-up’ to their LGM peak, whereas the penultimate glacial has consistently high inputs of terrigenous material; although not a continually high IRD flux (Figure 6.2). The last glacial is characterised by periodically high Si/Sr and Fe/Ca inputs with generally low magnetic susceptibilities until very high values during MIS 2. MIS 6, on the other hand, displays an initial gradual increase with oscillation similar to the last glacial, followed by consistently high input with some longer-term fluctuations. This might be a consequence of differing BIS dynamics, although the earliest portion of the penultimate glacial was not recovered by MD04-2822. The earliest dynamics of the penultimate BIS recorded within MIS 6 more closely resemble MIS 2 and 3 and may reflect the growth of the MIS 6/Saalian BIS and extension onto the continental shelf during the Drenthe primary advance phase (~175 to 160 kyr). The near continuous high terrigenous inputs and magnetic susceptibility may reflect an ice front for the penultimate BIS that was close to or at the edge of the continental shelf, for longer periods during MIS 6 than for the last glaciation.

The increase in June insolation at 60 °N (beginning ca. 160 kyr) prompted the retreat of the penultimate BIS; IRD inputs continue after this point due to the relatively long

response times for the large ice sheet to climatic forcing (e.g. Rohling et al 2009). Melting and enhanced iceberg calving (and thus IRD inputs) continued as the ice front retreated from the shelf edge; much of the deposition to the MD04-2822 was now via meltwater plumes resulting in low IRD fluxes but continuing high fine grained terrigenous inputs. This retreat was sufficiently close to the shelf edge to facilitate continued inputs of this terrigenous material to the MD04-2822. Relatively little catchment derived material is thought to have bypassed the Barra-Donegal Trough Mouth Fan (and hence MD04-2822) as icebergs, based upon comparison with the Fennoscandian Ice Sheet (cf. Dowdeswell et al 2010).

The subsequent decrease in insolation, combined with the advection of warm waters to high latitudes (as seen by low abundances of the polar foraminifera *N. pachyderma* (sinistral)) provided a moisture source, which could have enabled the re-advance of the BIS (as speculated for other European ice sheets e.g. Ehlers et al 2004, Toucanne et al 2009) and hence deposition of IRD to the MD04-2822 site. The gradual decrease in SSTs (increased % *N. pachyderma* (sinistral)) may have inhibited calving or the melting of those icebergs and so IRD flux to the site was again diminished despite the increase in insolation. The final large pulse of elevated IRD fluxes within MIS 6 is associated with the decay of the MIS 6/Saalian ice sheets (Termination II), prompted by an increase in Northern Hemisphere insolation (Figure 6.1).

For the last glacial, MIS 3 and 2 display a gradual increase in IRD (in contrast to MIS 6, although the earliest portion of MIS 6 is not present in MD04-2822) and insolation changes through this interval display a more gradual decline towards a minima ca. 20 kyr (Berger and Loutre 1991). This is reflected in the benthic $\delta^{18}\text{O}$, which may be taken on longer timescales, as a proxy for global ice volumes. Northern hemisphere insolation differed between the two periods and may account for some differences in the deposition at MD04-2822; for most of MIS 3, insolation was greater than present whilst within MIS 6, similar insolation levels below present levels occur for a far shorter time (Figure 6.1).

Both glacials are characterised by high IRD inputs with amelioration in surface conditions (increases in the % *N. pachyderma* (sinistral)) and occasional IRD fluxes that are not driven by SST changes. The destabilisation of the ice sheet and/or enhanced melting of any resulting icebergs produced may have been triggered by an increase in global sea levels which would destabilise ice sheet marine margins. The clearest example of this within MD04-2822 is the rise in sea level associated with H4 but there appears to be a possible sea level cause for the increase in IRD during MIS 6 ca. 175 and 160 kyr (Figure 6.1). Again, the difficulties of unambiguously assigning a sea level cause due to dating uncertainties should be remembered.

There is evidence for D/O events within both the last and penultimate glacial cycle. The pacing of these events within MIS 6 is millennial to multi-millennial, although the sampling resolution may mean that some of these oscillations are 'missing' from the record. The Atlantic quasi-1,500 yr cycle that persisted through the last glacial and into the Holocene, also appears to have been a persistent and prevalent feature of MIS 6. ODP 980 also records the late MIS 6 decrease in SSTs (as recorded by the % *N. pachyderma* (sinistral)) (Oppo et al 2006), however much of this record remains at low resolution in comparison to MD04-2822.

4. Comparison of the Last and Penultimate Deglaciations (Terminations I and II) within MD04-2822

MD04-2822 contains sediments deposited during the last two deglacial events – Terminations I (after Broecker and van Donk 1970) and Termination II. Terminations are thought to be triggered by changes in insolation (e.g. Raymo 1997, Imbrie et al 1993, Imbrie et al 1992) with precession (Huybers and Wunsch 2003) or obliquity (Huybers and Wunsch 2005, Drysdale et al 2009) playing a major role. These changes in the Earth's orbit are also associated during terminations with a number of associated feedback mechanisms (e.g. Alley and Clark 1999, Ruddiman and McIntyre 1981, Johnson 1991, Peltier and Marshall 1995). The end of the termination is marked by a rapid increase in atmospheric methane (documented in ice cores) which is thought to be related to the resumption of AMOC (Petit et al 1999, Loulergue et al 2008). The following section outlines events recorded at the MD04-2822 sites within the context of the BIS (NW Scotland in particular) and then compares the two terminations.

In the following section, the last deglacial for MD04-2822 is placed upon the GICC05 timescale (Andersen et al 2006, Rasmussen et al 2006, Svensson et al 2006, 2008, Vinther et al 2006) as this chronology provides 'significantly improved temporal resolution and precision' and the ss09sea chronology is 'relatively imprecise for the Last Termination' (Lowe et al 2008, Svensson et al 2006)¹¹. The construction of the NGRIP GICC05 timescale MD04-2822 tuned chronology followed the same procedure as that documented within chapter 3 (*Chronostratigraphy*); details of the tie-points used can be found within Appendix C₂. The penultimate deglacial (Termination II) is placed upon the compound chronology outlined in chapter 3 (*Chronostratigraphy*).

4.1. Deglacial history

4.1.1. *Termination I*

Major changes in the configuration of the BIS ca. 24 kyr are proposed by Bradwell et al (2008) as a result of rapid changes in sea level, probably induced by glacio-isostatic loading and linked to H₂, leading to the break up of the BIS and FIS into independent ice sheets. The final deglaciation of the BIS is associated with thinning and increased topographical control with the invigoration of several nearshore ice streams and ice marginal oscillations in eastern and western Scotland. Post-H₁ (ca. 16 kyr), Bradwell et al (2008) place a stable BIS margin at the present-day shoreline in northwestern Scotland with subsequent retreat primarily driven by ice sheet melting rather than by calving. The southern Irish Sea Basin was deglaciated by 19 to 18 kyr, with extensive deglaciation of low ground in Ireland and NE Scotland prior to 14.5 kyr. However in NW Scotland, ice cover persisted in low ground after ca. 14 kyr in 'favourable locations' (Ballantyne 2010).

¹¹ The ss09sea timescale (NGRIP members 2004) was used for the age model detailed in chapter 3 as it remains the sole timescale extending to ca. 123 kyr

The persistence of ice cover in NW Scotland is suggested by cosmogenic isotope (^{10}Be or ^{36}Cl) ages from several locations; for example, an average exposure age of 14.1 ± 1.3 kyr from N. and S. Harris (Stone and Ballantyne 2006) and ^{10}Be ages from Wester Ross (Stone et al 1998, Bradwell et al 2008a, Ballantyne et al 2009b). As a consequence, Bradwell et al (2008a) suggested ‘substantial ice caps’ persisted through the first half GIS 1 (~14.7 to 12.9 kyr b2k; GICC05 timescale). This statement implies that any remnants of BIS survived the rapid warming associated with GIS 1 and into the period of oscillating climate that followed (c.f. Brooks and Birks 2000, Watson et al 2010, Lowe et al 2008, Svensson et al 2008).

The retreat of the last BIS was interrupted by several retreat features identified from Northern Scotland (e.g. Robinson and Ballantyne 1979, Ballantyne 2009, Bradwell et al 2008a) and the continental shelf (Bradwell et al 2008); the most prominent of these is the Wester Ross Read Vance (ca. 13.5 to 14.0 kyr; Ballantyne 2010), probably coincident with GIS 1d (Older Dryas; 14.1 to 14 kyr b2k) although a later response to climatic forcing or a stabilisation and read Vance following rapid calving cannot be discounted (Ballantyne et al 2009b). Bradwell et al (2008a) infer a more extensive ice cover for the Wester Ross region of NW Scotland during the Older Dryas (GIS1d, ca. 14.1 to 14.0 kyr b2k; GICC05 timescale) than during the Younger Dryas (GS1, Loch Lomond Stadial, ca. 12.9 to 11.7 kyr b2k; GICC05 timescale). Ballantyne (2010) questions this interpretation due to prevailing climatic conditions; the proposed ‘shrinking’ of glaciers during GS1 (cf. Bradwell et al 2008a) occurs in an interval in which summer temperatures were lower than any portion of the preceding GIS 1 (cf. Brooks and Birks 2000, Bedford et al 2004, Watson et al 2010, Kroon et al 1997, Svensson et al 2008). An alternative interpretation offered by Ballantyne (2010) for the limited extent of Younger Dryas glaciation in NW Scotland, is that it reflects growth from ‘complete or near complete deglaciation’ prior to cooling with the onset of the Younger Dryas (GS1, Loch Lomond Readvance) (Ballantyne et al 2009b). It must be borne in mind that modelling studies have demonstrated that the removal of ice requires warmer conditions than those that inhibit initial ice build-up (e.g. Oelermans 1982, Crowley and Baum 1995).

By using the marine record, including MD04-2822, a record of the last deglaciation may be unravelled. However, as the ice retreated from the edge of the continental shelf, the distance travelled by BIS origin icebergs to the MD04-2822 site would increase, thereby increasing the potential for melting or overturning of icebergs prior to reaching the core site. As retreat continued, the extent of the marine margins would reduce, thus reducing the number of icebergs calved. In addition, the deglacial section of the MD04-2822 sediment core was subjected to ‘oversampling’ during extraction (chapter 5); whilst this has been corrected using the gravity core +56-12/15CS, there remains a small portion of the piston core for which there is no gravity core facsimile¹². This may lead to an unreliable estimation of linear sedimentation rates and consequently erroneous IRD flux calculations. With these potential limitations in mind: is there any evidence for ice sheet activity within GIS 1 within the MD04-2822

¹² Piston cores > 10 m core depth tend towards ‘ideal’ behaviour, whilst gravity cores > 3 m tend to ‘undersample’ sediments (Skinner and McCave 2003). These two limits do not overlap within the core studied (MD04-2822 and +56-12/15CS) i.e. there is a small portion (~2.5 m; 17.5 to 20 kyr b2k GICC05 timescale) of the piston core for which the suspected ‘oversampling’ cannot be corrected using the gravity core. The reader is directed to chapter 5 for a full discussion.

record and how does this compare to both the GS2 and GS1 intervals? Is there any offshore evidence of the Wester Ross Readvance?

A dramatic change in IRD deposition to the MD04-2822 site is evident at ca. 25 to 24 kyr (Figure 6.2, Figure 6.8 and Figure 6.9); whilst this large peak in IRD has not been lithologically characterised, a peak in Ca/Sr as well as the magnitude and timing of the event suggest that this may be H2. Bradwell et al (2008) propose a major reorganisation of the BIS post H2 and the pattern of IRD deposition to the MD04-2822 site appears to confirm this. IRD fluxes continue to remain high until ca. 17.5 kyr. At this time, there is another very large influx of IRD to the MD04-2822 site. The magnitude of the flux is as great as H2, although IRD flux calculations remain uncertain within this interval due to potential coring artefacts (~20-17.5 kyr, see above); the event is also older than H1 in other cores proximal to the last BIS (cf. Knutz et al 2002b, Peck et al 2007, Haapaniemi et al 2010).

A differential response of the circum-Atlantic ice sheets between H1 and H2 has been suggested from provenance studies (e.g. the ‘precursor events’ of Grousset et al 2000, Scourse et al 2000). Such events are, however, neither ‘uniquely nor mechanistically’ linked to Heinrich events (Haapaniemi et al 2010). Instead, during this interval, marine sediment cores indicate millennial scale IRD fluxes for ice streams draining the last BIS (Knutz et al 2002, Wilson and Austin 2002, Jullien et al 2006, Peck et al 2006, 2007, Scourse et al 2009). The aforementioned dramatic change in IRD deposition may instead be associated with the invigoration of several nearshore ice streams and ice marginal oscillations in eastern and western Scotland after H2 (e.g. Bradwell et al 2008), giving rise to continuing high terrigenous inputs to MD04-2822.

IRD levels post the ca.17.5 kyr event reduce markedly but also demonstrate several minor IRD events (Figure 6.8, Figure 6.9); each IRD event is associated with sharp surface $\delta^{18}\text{O}$ depletions suggesting that these are local discharge events. These minor IRD events occur within GS2 at roughly the same time as the inferred retreat of the BIS to the present day shoreline (completed ~16 kyr, Bradwell et al 2008). The ‘muted’ IRD record of MD04-2822 appears to confirm this and the Bradwell et al (2008) proposal that the post ~16 kyr mass loss from the BIS was predominately via melting rather than iceberg calving.

The second of the minor pulses of IRD (~15.5 kyr) may be associated with H1; although the IRD has not been lithologically characterised¹³, it is coincident with a severe reduction in benthic $\delta^{13}\text{C}$ values and a major decrease (lightening) of planktonic $\delta^{18}\text{O}$, consistent with large freshwater inputs perturbing AMOC (e.g. Clark et al 2002a, Flückiger et al 2006). Although IRD inputs are much reduced during this interval (i.e. after ~17 kyr, GS2a), terrigenous inputs (XRF Si/Sr and Fe/Ca) remain at their LGM levels until ~14.4 kyr (within GIS1e), when there is a dramatic reduction followed by a small increase ca 14.4 to 13.8 kyr.

This relatively small increase in terrigenous proxies is accompanied by surface meltwater (low planktonic $\delta^{18}\text{O}$) and a reduction in SSTs (decreased % *N*.

¹³ i.e. only bulk IRD count were undertaken without differentiation into e.g. detrital carbonate (used to define a Heinrich event), haematite stained quartz etc.

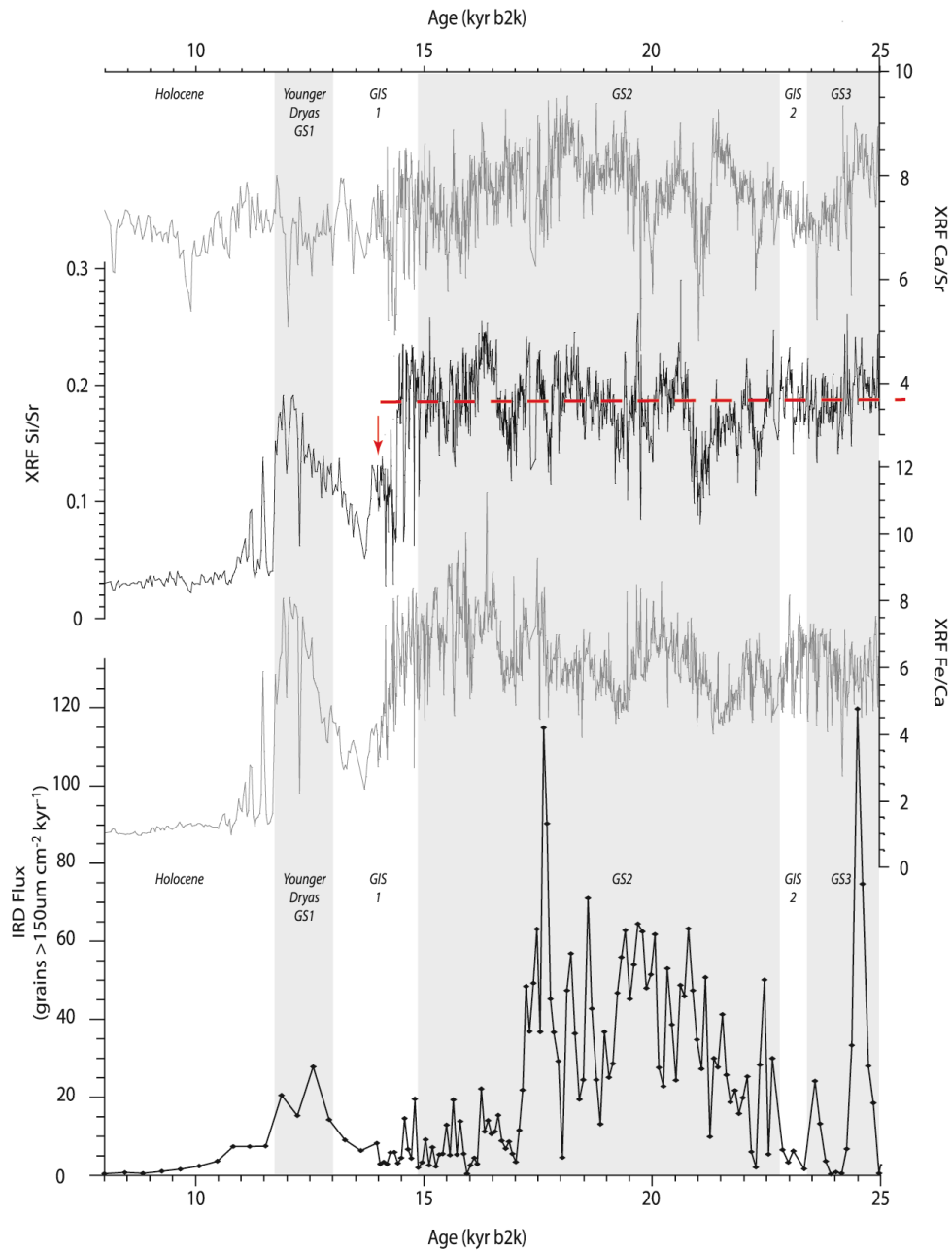
pachyderma (sinistral)). The MD04-2822 age model places this SST reduction within the second half of GIS 1e (labelled event (C) in Figure 6.9). A series of short lived meltwater events during the deglacial have also been recorded at a site on the South Iceland Rise, including one during the early deglacial, relating to meltwater from the decay of the LIS (Thornalley et al 2010). The low SST event within GIS 1e in MD04-2822, however, is believed to be a local feature prompted by the continuing input of meltwater from the decaying BIS; fine grained terrigenous inputs are high with some IRD input and there is no reduction in benthic $\delta^{13}\text{C}$. The increase in terrigenous inputs during this SST cooling (Figure 6.8 and Figure 6.9), may have been prompted by a readvance of the BIS prior to GIS 1d.

By contrast, the subsequent SST reduction (labelled (B) in Figure 6.9), is associated with a reduction in benthic $\delta^{13}\text{C}$ (of a similar magnitude to that experienced at the MD04-2822 site during the Younger Dryas). This is correlated to the SST cooling of the Older Dryas (GIS1d). The Older Dryas coincides with meltwater pulse 1a¹⁴ (Stanford et al 2006, Thornalley et al 2010) and an increase in sea level may have prompted destabilisation of the marine margins of the BIS, resulting in a small increase in IRD at the MD04-2822 site and the local meltwater surface $\delta^{18}\text{O}$ anomaly. The marine margins are assumed to be restricted due to the very low input of IRD to the site at this time; alternatively the IRD may originate from sources other than the BIS, as the SST decrease and inferred southward migration of the polar front enabled the transport of icebergs to the MD04-2822 site. In Scotland, the prominent glacial moraines (Wester Ross Readvance) region has been correlated to the Older Dryas/GIS1d (Ballantyne et al 2009) although this correlation remain speculative due to the large error¹⁵; however in the MD04-2822 record, the Older Dryas/GIS1d is associated with minimal IRD inputs and very low Si/Sr and Fe/Ca. As surface water conditions warmed after the Older Dryas (Figure 6.9, event B; Kroon et al 1997), a gradual increase in terrigenous proxies is seen, mirrored by an increase in IRD with peak values obtained during the Younger Dryas.

¹⁴ Meltwater pulse 1a (Fairbanks 1989) is one of a series of rapid sea level rises documented during the last deglaciation, a rise of ~20 m over a period of ~500 years (Peltier and Fairbanks 2006). The source of this meltwater remains debated (e.g. Clark et al 1996, Peltier 2005) with both the Antarctic (Clark et al 2002b, Bassett et al 2005) and Laurentide (Keigwin et al 1991, Peltier 1994) ice sheets proposed.

¹⁵ The ¹⁰Be error encompasses the entirety of GIS 1, therefore surface exposure dating cannot unambiguously identify such a centennial scale event.

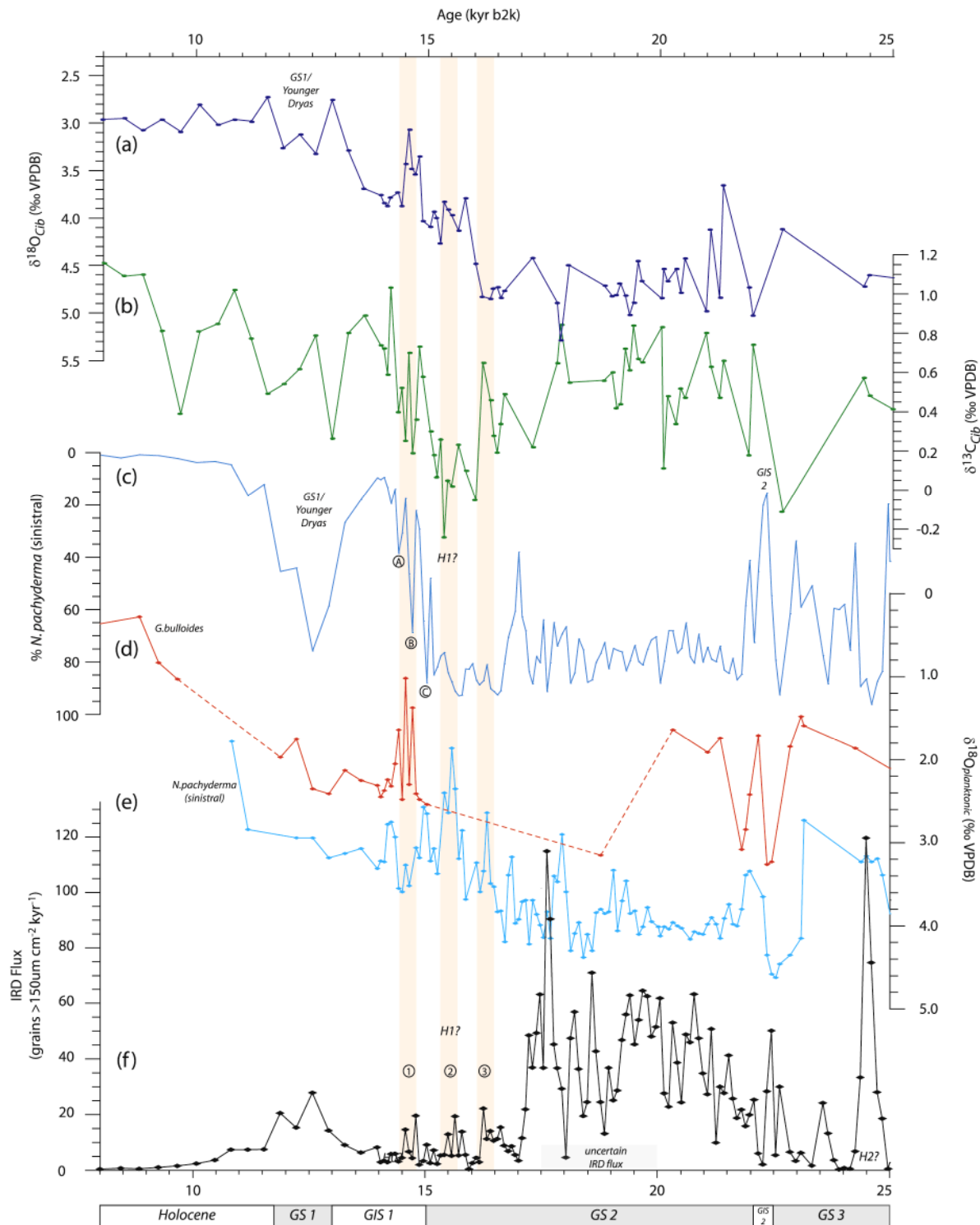
Figure 6.8: MD04-2822 terrigenous proxies (ITRAX XRF Ca/Sr, Si/Sr and Fe/Ca) and IRD flux. All proxies are on the GICC05 timescale (Andersen et al 2006, Rasmussen et al 2006, Svensson et al 2006, 2008, Vinther et al 2006); stadial (GS) and interstadial (GIS) designations are after Lowe et al (2008). Red dashed line is indicative of detrital silicate input to the site during the LGM. Red arrow indicates a possible reinvigoration of terrigenous input during GIS 1.



CHAPTER 6:

The Last and Penultimate Glacial Cycles in the MD04-2822 record

Figure 6.9: MD04-2822 (a,b) benthic $\delta^{18}\text{O}$ and $\delta^{13}\text{C}$ isotopes; (c) % *N. pachyderma* (sinistral); (d) *G. bulloides* $\delta^{18}\text{O}$; (e) *N. pachyderma* (sinistral) $\delta^{18}\text{O}$ and; (f) IRD flux for the end of the last glaciation and deglaciation. All proxies are present ed on the GICC05 timescale (Andersen et al 2006, Rasmussen et al 2006, Svensson et al 2006, 2008, Vinther et al 2006); stadial (GS) and interstadial (GIS) designations after Lowe et al (2008). Orange vertical bars highlight minor IRD events (labelled 1 to 3). SST cooling events experienced at the MD04-2822 site during the deglaciation are labelled A, B and C.



The Younger Dryas (GS 1)

The transition between glacial and interglacial conditions at the last termination was most notably punctuated by a return to cold conditions, the Younger Dryas (12.9 to 11.7 kyr b2k; GICC05 timescale), throughout the Atlantic region (e.g. Broecker 2003, Mayewski et al 1994, Maslin et al 1995) during a period of atmospheric cooling in the Northern Hemisphere almost equalled that experienced during the coldest portions of the Late Devensian/Weichselian (Stuvier et al 1995). Fresh water forcing and the disruption of thermohaline circulation in the North Atlantic, is widely accepted as the trigger for the event (e.g. Broecker 2006, Golledge 2010). A sudden outburst from the ice-dammed Lake Agassiz¹⁶ has been proposed (Broecker et al 1989, Teller 1990, Teller et al 2002) although the chronology, exact source and routing of waters remains elusive (Teller et al 2002, 2005, Lowell et al 2005, Fisher and Smith 1994). Alternative explanations include: sub-ice escape of waters from Lake Agassiz¹⁷ (Teller and Thorleifson 1983); an 'armada' of icebergs (Andrews et al 1994a,b, 1995); freshening of the Arctic Ocean by meltwater (Peltier et al 2006, Spielhagen et al 2005, Tarasov and Peltier 2006); a tropical temperature anomaly that triggered a shift in wind patterns over the Northern Atlantic, allowing the formation of sea ice and the inhibition of thermohaline circulation (Seager and Battisti 2005) and; an extraterrestrial impact at ca. 12.9 kyr (Firestone et al 2007).

The mean annual temperatures in Scotland decreased by ~8 to 10 °C (Hubbard 1999, Isarin and Renssen 1999) which was key to the rapid growth of ice in much of Scotland (Clapperton 1997, Alley 2000, Lie and Paasche 2006) with much increased seasonality than present (e.g. Atkinson et al 1987, Denton et al 2005, Golledge et al 2009). During the summer months, mean temperatures are estimated at 6 to 8 °C cooler than present but perhaps as much as 30 °C cooler during the winter (Golledge 2010). A sea ice 'curtain pulled down to the British Isles' has been invoked to explain such seasonality (Gildor and Tziperman 2003) but the sea ice requires melting each summer; this presents dynamical modelling problems (Lie and Paasche 2006, Seager and Battisti 2005). Denton et al (2005) propose a maximum seasonality of ~20 °C, whereas a reassessment of the data by Lie and Paasche (2006) reduces this to ~10 °C, thereby reducing the amount of sea ice present and consequently the amount of atmospheric or oceanic heat required to melt it.

The Younger Dryas in Britain and Ireland is therefore characterised, in general, by enhanced continentality and aridity forced by the presence of sea ice, leading to very cold winters but only moderately cooler summers (Ballantyne and Harris 1994, Brooks and Birks 2000, Watson et al 2010).

The growth of glacier ice in Scotland (and elsewhere) is coeval with an expansion of polar waters in the North Atlantic (e.g. Ruddiman and McIntyre 1981; Figure 6.9) and the formation of sea ice (e.g. Mayewski et al 1994, Clapperton et al 1997, Lie and Paasche 2006). This may have given rise to more vigorous atmospheric circulation resulting in increased precipitation in western Scotland (Ballantyne 2002). The main

¹⁶ Lake Agassiz was an ice-dammed lake formed during the retreat of the Laurentide Ice Sheet, during the last deglaciation.

¹⁷ A similar scenario has been invoked as an explanation of the 8.2 kyr cold event in the North Atlantic (Barber et al 1999).

ice cap was linear in form, stretching from Loch Lomond to Wester Ross (e.g. see modelling by Golledge et al 2008, Figure 6.10) with glaciation of the islands of Skye, Lewis, Mull and an active ice field on Arran (Gray and Brooks 1972, Ballantyne 1989, 2002, 2006, 2007). Debate continues as to whether the Younger Dryas ice masses grew from remnants of the LGM BIS that survived the climate amelioration of GIS 1 (e.g. Bradwell et al 2008a, Ballantyne et al 2009b, Ballantyne 2010, see discussion above). Decay of the Younger Dryas ice masses was initially slow, prompted by a decrease in precipitation (Benn et al 1992) leading to active recession with numerous stillstands and minor readvances (e.g. Benn et al 1992, Golledge 2007). Subsequent decay was much more rapid, triggered by rapid climate warming (Dansgaard et al 1989, Benn et al 1992, Dix and Duck 2000).

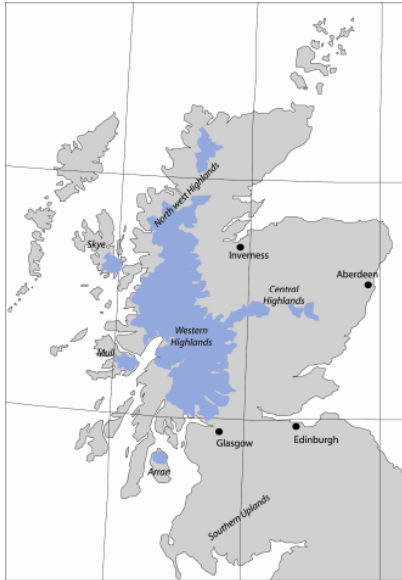
Reconstructions of the extent of the Younger Dryas in Scotland (e.g. Golledge et al 2008, Golledge 2010, Figure 6.10) propose very restricted marine margins and yet the IRD flux to the MD04-2822 site is greater than 20,000 grains $\text{cm}^{-2} \text{kyr}^{-1}$ at its peak (Figure 6.8 and Figure 6.9), which is similar to that seen at ca. 40 kyr (H4^{18} , Figure 6.1) and greater than at ~ 16 kyr, when the BIS is positioned at the present day shoreline (Bradwell et al 2008). Similarly, terrigenous proxies (XRF Si/Sr and Fe/Ca) return to levels evident during the LGM (Figure 6.8). Ice sheet expansion may have been triggered by the increased precipitation in conjunction with cooling temperatures, as GIS1 proceeded (cf. Brooks and Birks 2000, Watson et al 2010, Kroon et al 1997). The cold surface water conditions during the Younger Dryas (Figure 6.9) may have enabled calved icebergs, and any entrained material, to 'survive' into the Rockall Trough and deliver IRD to the core site. As detailed lithological characterisation has not been undertaken for this interval, a far field source for the IRD seen in the MD04-2822 sediments cannot be ruled out and indeed may be the most likely source of IRD. For example, whilst the Scandinavian ice sheet during the Younger Dryas had retreated from the shelf edge, it did have more extensive marine margins (e.g. Knies et al 2007, Lohne et al 2007). The increase in fine grained terrigenous material (Figure 6.8) does however suggest, that at least some of the material delivered to the MD04-2822 site was of British origin (fine grained material is not transported significant distances from the source cf. Dowdeswell et al 2010).

In summary, the MD04-2822 sediment record indicates continuing high levels of terrigenous inputs (Si/Sr and Fe/Ca records) into GIS 1, although high levels of IRD fluxes cease after ~ 17 kyr. The input of terrigenous and IRD fluxes to the site varies through GIS 1 with coeval meltwater anomalies suggesting a local ice sheet source. IRD and terrigenous inputs increase during the Younger Dryas coincident with surface water cooling before declining to background levels ca. 9 to 10 kyr.

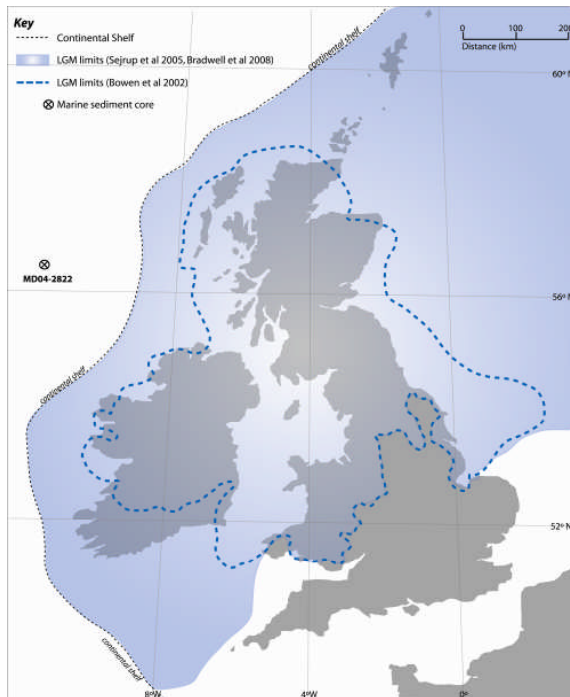
¹⁸ A significant input from the BIS towards the end of GS9 (~ 40 kyr) is inferred from a magnetic unmixing model of Peters et al (2008).

Figure 6.10: (a) Mapped and modelled limits for the Younger Dryas glaciation of Scotland (adapted from Gollidge 2010) with (b) proposed LGM limits of the last BIS (adapted from Sejrup et al 2005, Bradwell et al 2008, Bowen et al 2002).

(a)



(b)



4.1.2. *Termination II*

The increased flux of IRD at ca. 128 kyr (Figure 6.1, Figure 6.2, Figure 6.3 and Figure 6.11) is associated with a transition from glacial to interglacial conditions: Termination II. The decay of the penultimate northern hemisphere ice sheets is thought to be prompted by the increase in northern hemisphere insolation (Figure 6.1). Termination II is thought to be one of the most rapid and abrupt deglacial events of the Late Quaternary (e.g. Jouzel et al 2007, Lisecki and Raymo 2009, Lourantou et al 2010) and occurs during an interval of higher eccentricity and precession in the Earth's orbit than during Termination I (Imbrie et al 1984) resulting in a more intense Northern Hemisphere summer insolation maximum (Broecker and Henderson 1998, Schulz and Zeebe 2006). During Termination II, the sea level rise prior to peak June insolation at 65°N has been ascribed in part to the stronger summer insolation maximum (Waelbroeck et al 2008).

In the sub-polar North Atlantic, a climatic 'pause' has been identified from benthic $\delta^{18}\text{O}$ records (Lototskaya and Ganssen 1999) but this feature is not evident within the MD04-2822 record. This may be a reflection of current MD04-2822 sampling resolution rather than the absence of this feature.

Several northern hemisphere records also display a 'Younger Dryas' type event however, the magnitude of these climate reversals compared to the Younger Dryas is uncertain (e.g. Sánchez-Goni et al 1999, Cannariato and Kennett 2005; the C28 event of Oppo et al 2001, 2006) and indeed some authors have questioned the degree to which they may be thought of as analogous to the Younger Dryas (e.g. Carlson 2008). The Younger Dryas has been suggested as 'unique to the termination of the last glacial cycle' (Broecker 2006). Differences in the timing of the resumption of AMOC during the deglacials have been proposed as a means of accounting for the absence of a 'Younger Dryas type' feature (Carlson 2008). The absence of a reversal in methane concentrations within the Antarctic ice cores during the penultimate deglacial (as identified for Termination I; e.g. Brook et al 2000, Monnin et al 2001) is thought to be consequence of freshwater inputs into the North Atlantic from the decaying MIS 6 ice sheets occurring prior to the resumption of AMOC. Rather than suppressing an already 're-invigorated' AMOC (as during Termination I), these freshwater inputs further protracted AMOC suppression during Termination II, thereby accounting for the lack of a 'Younger Dryas type' feature (Carlson 2008). Such input of meltwater into the North Atlantic (with increased northern hemisphere insolation), despite cold surface conditions, have been previously suggested and may have suppressed AMOC until close to the end of the deglaciation (Oppo et al 1997, Carlson 2008, Lourantou et al 2010).

The transition from the penultimate glacial into the last interglacial is marked by large oscillations in sea level (e.g. Thompson and Goldstein 2005, Andrews et al 2007, Rohling et al 2008) and unlike Termination I, included an interval of significant reduction in sea level (e.g. Siddall et al 2006). However, the exact timing of these fluctuations remains elusive (Siddall et al 2006, Fujita et al 2010).

The deglaciation of the penultimate BIS is largely unknown. MD04-2822 presents an opportunity to investigate the demise of the MIS 6 ice sheet in considerable detail, due to the unusually high accumulation rate; Termination II occurs over approximately 2

m core depth at the site, current sampling resolution however is relatively low (10 cm). This portion of the record would yield unprecedented detail into the demise of the penultimate BIS and hydrologic conditions if sampling resolution were to be increased. In comparison, Termination I was also sampled at 10 cm intervals, however, ‘oversampling’ during the extraction of the core enabled a high resolution record to be constructed (see chapter 5).

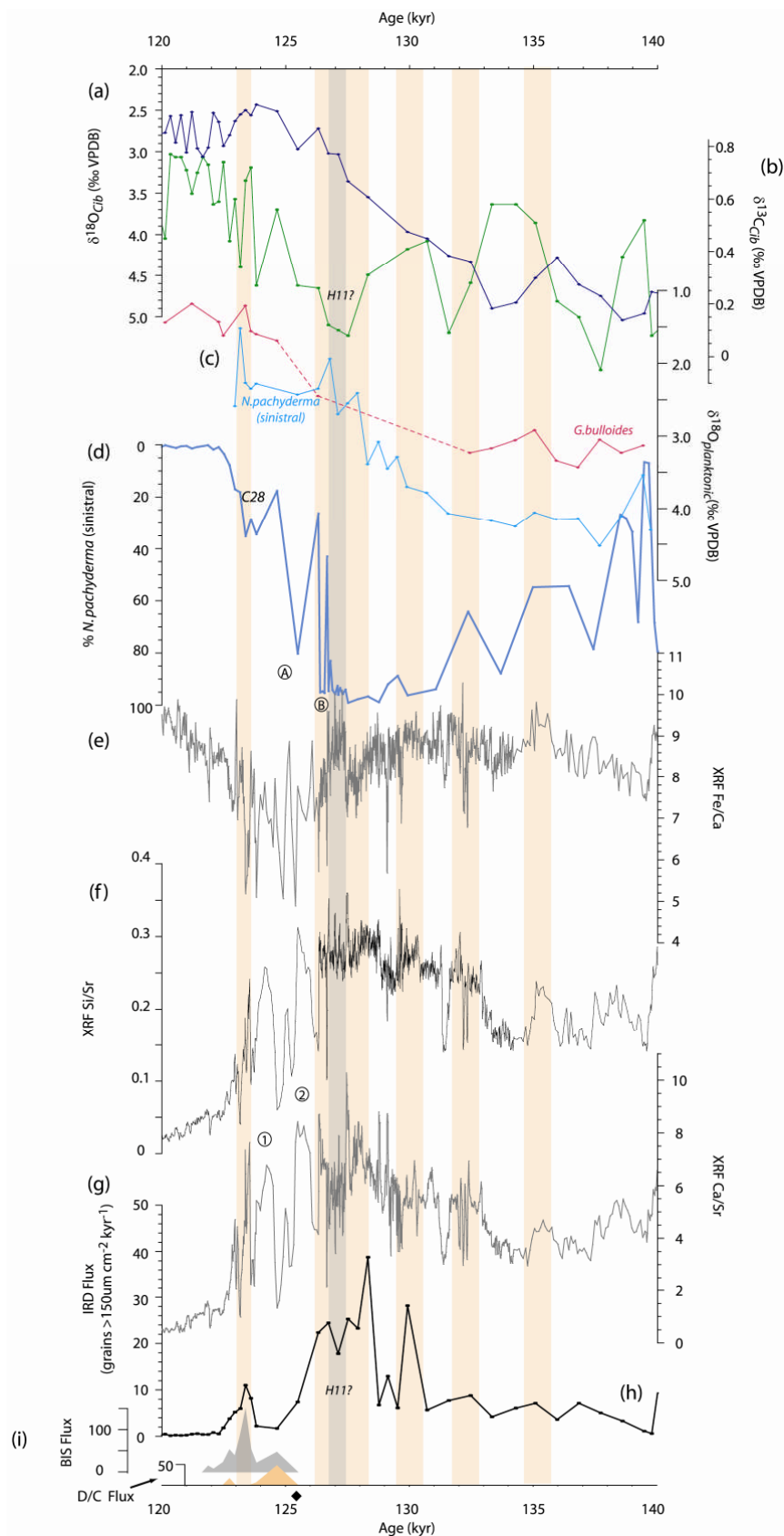
The disintegration of the Saalian ice sheets prompted the final episode of increased IRD flux to the MD04-2822 site during MIS 6. IRD inputs to the site are low for the period ca. 140 to 130 kyr but terrigenous proxies remain fairly high. This reflects the re-growth of European ice sheets during the Warthe glaciation (150– 140 kyr) within the limits of the previous Drenthe glaciation (Ehlers 1990, Ehlers et al 2004, Clark et al 2004, Mangerud 2004, Svendsen et al 2004). An increase in northern hemisphere insolation beginning ca 135 kyr (Berger and Loutre 1991) prompted an increase in terrigenous inputs and IRD. Meltwater $\delta^{18}\text{O}$ anomalies suggest that these inputs were local in origin (Figure 6.11).

The melting of European ice sheets and the input of large volumes of meltwater into the high latitudes may have led to a reduction in AMOC, seen as a low $\delta^{13}\text{C}$ event (ca. 132 kyr) in the MD04-2822 record. AMOC production, as inferred from the benthic $\delta^{13}\text{C}$ record, was variable though the termination possibly as a consequence of inputs of meltwater into the Nordic Seas, or due to brine rejection with the formation of sea ice. Surface conditions at MD04-2822 cooled for much of the duration of the termination until after H11 (ca. 127 kyr b2k), suggesting a southward migration of the polar front despite increasing insolation, perhaps coincident with seasonal sea ice.

A striking feature of the MD04-2822 record is the broad IRD peak at ca. 125 to 130 kyr (Figure 6.11). This period of enhanced IRD flux began close to the mid-point of the transition from the isotopic maxima to minima in the MD04-2822 benthic $\delta^{18}\text{O}$ record and ends with a return to very low levels of IRD before a minor IRD peak ca. 122 kyr. This feature has also been identified within the ODP 980 core (Feni Drift; Oppo et al 2006) as well as most North Atlantic marine sediment cores (e.g. Chapman and Shackleton 1998, 1999, Skinner and Shackleton 2006, Hodell et al 2008) and is correlated to H11 in these cores. This IRD feature has not been characterised lithologically but a peak in the XRF Ca/Sr in conjunction with low benthic $\delta^{13}\text{C}$, would suggest that H11 in MD04-2822 is centred about 127 kyr. The largest peak in IRD (ca. 128 kyr) making up this broad IRD feature is associated with a surface $\delta^{18}\text{O}$ anomaly and high terrigenous inputs suggesting a local ice sheet reconfiguration. The Heinrich event is tentatively placed at ca. 127 kyr with ‘bracketing’ BIS IRD and terrigenous inputs (all associated with meltwater ‘spikes’). The increase in sea level connected with H11 may have destabilised the marine margins of the penultimate BIS, prompting large inputs of IRD to the site.

CHAPTER 6:
The Last and Penultimate Glacial Cycles in the MD04-2822 record

Figure 6.11: MD04-2822 proxies for Termination II (all proxies presented on the compound age scale detailed in chapter 3, *Chronostratigraphy*). (a, b) benthic $\delta^{18}\text{O}$ and $\delta^{13}\text{C}$; (c) planktonic $\delta^{18}\text{O}$; (d) % *N. pachyderma* (sinistral); (e,f,g) XRF Fe/Ca, Si/Sr and Ca/Sr; (g) IRD flux and (h) flux of 'diagnostic' BIS and detrital carbonate grains. Orange vertical bars highlight IRD events, terrigenous inputs without IRD inputs are labelled 1 and 2. Local SST cooling events are labelled A and B. Black filled diamond gives the position of detrital carbonate $\delta^{18}\text{O}$ analyses.



Detrital carbonate has been visually identified at ~125.5 kyr (the approximate transition out of H11 based upon benthic $\delta^{13}\text{C}$) and isotopically analysed (D. Hodell, *pers.comm*; 2 analyses, Appendix B₅; position of sample denoted by filled diamond in Figure 6.11). A mean detrital carbonate $\delta^{18}\text{O}$ of -5.26 ± -1.7 ‰ for H11, from core T90-9P North Atlantic; (45°N, 25°W) was obtained by Lototskaya and Ganssen (1999) whilst an average (mean) oxygen isotope value for Heinrich events 1 to 6 (inclusive) of -5.5 ± 1.6 ‰ (n=166 grains) (Hodell and Curtis 2008) is consistent with material eroded from beneath the Laurentide ice sheet. Such values are characteristic of dolomitic limestone derived from the lower Palaeozoic basins in northern Canada. Whilst one of the MD04-2822 grains from this interval appears to have an isotopic signature consistent with a North American origin (-5.4 ‰), the other (3.1 ‰) is distinct from those obtained for Heinrich events 1 to 6 by Hodell and Curtis (2008), H4 within MD04-2822 (Appendix B₅) and MD95-2006 (WEN Austin, *unpublished data*). This very high value for one of the detrital carbonate grains suggests a very different source and may relate to carbonates derived from Ireland (cf. Knutz et al 2001, Sevastopulo 1981). Further investigation would be needed to identify an alternative source of carbonate transported to the MD04-2822 core site. The continuing presence of 'diagnostic' BIS lithics within this small peak suggests that this IRD peak represents the final demise of the penultimate BIS.

Immediately post H11, there is a very short lived increase in SSTs (decrease in % *N. pachyderma* (sinistral)) but the large input of meltwater from the proximal BIS may have dampened any surface warming, giving rise to the local SST cooling after H11 (labelled B in Figure 6.11). Warming of the surface waters resumed ca. 126 kyr but was again checked (event A; Figure 6.11) possibly as result of continued disintegration of the BIS and inputs of meltwater. During this SST oscillation, IRD flux is low but terrigenous proxies remain high, which may indicate that the penultimate BIS had retreated from the shelf edge and mass loss was primarily via melting rather than calving (cf. Termination I ca. 16 kyr; Bradwell et al 2008). This SST reversal is not accompanied by low benthic $\delta^{13}\text{C}$ values, lending confidence to the interpretation as a local event.

SSTs continued to increase (decreasing % *N. pachyderma* (sinistral)) as insolation increased, further enhancing the melting of the BIS which resulted in further episodes of terrigenous inputs to the MD04-2822 site. These episodes are coincident with very low IRD fluxes (Figure 6.11). Another brief temperature oscillation centred ca. 123.6 kyr, and lasting approximately 1.7 kyr, is evident during the deglacial and is correlated to the late deglacial oscillation C28 within the North Atlantic (cf. Oppo et al 2001, 2006, chapter 7). This is accompanied by a reduction in benthic $\delta^{13}\text{C}$. Continuing episodic terrigenous inputs and a final IRD peak (containing 'diagnostic' BIS lithics¹⁹), coincident with low *N. pachyderma* (sinistral) $\delta^{18}\text{O}$, suggests the continued and final decay of the BIS. Oppo et al (2006) also suggest a continued input of meltwaters to site ODP 980 based upon the observation of low planktonic $\delta^{18}\text{O}$ values. After ca. 122 kyr, it appears that deglaciation of the penultimate BIS was

¹⁹ A small interval surrounding this small IRD peak was examined further: lithological characterisation of the IRD was undertaken in order to investigate the provenance of this feature and in particular to determine if any 'diagnostic' BIS lithics were present. Unfortunately time restraints prevented a detailed lithological investigation of the entire penultimate deglacial.

complete as IRD flux and terrigenous inputs to the MD04-2822 site fall to background levels.

At ODP 980, low planktonic $\delta^{18}\text{O}$ values have been used to infer a continued input of low- $\delta^{18}\text{O}$ meltwater to the region and within the wider North Atlantic, the low benthic $\delta^{18}\text{O}$ coincident with C28 is thought to result from the incorporation of low $\delta^{18}\text{O}$ meltwaters into the deep ocean (e.g. Lehman et al 1993). The ODP 980 record (Oppo et al 2006) contains only the C28 SST oscillation, whereas MD04-2822 has three brief surface cooling events (including C28) of which two appear to be highly localised. The absence of these short lived SST cooling events may be due in part to differing sampling resolution and/or sedimentation rate between the two cores.

The final surface temperature oscillation (C28) is placed within MIS 5e rather than the termination itself (defined using the benthic $\delta^{18}\text{O}$ record). The offset between the benthic $\delta^{18}\text{O}$ and $\delta^{13}\text{C}$, as well as the % *N. pachyderma* (sinistral) record for MD04-2822, is one of the most conspicuous features of the deglaciation. This offset is also present within the ODP 980 record (Feni Drift; Oppo et al 2006), U1304, ODP 983, NEAP-18K (Gardar Drift; Hodell et al 2009, Channell et al 1997, Hall et al 1998 respectively) and the Norwegian Sea (Duplessy and Shackleton 1985, Oppo and Lehman 1995, Fronval and Jansen 1997, Bauch et al 2000).

The reduction or curtailment of Glacial North Atlantic Intermediate Water (GNAIW) or Labrador Sea Water (LSW) with meltwater fluxes into the high latitudes, and a greater penetration of southern sourced Antarctic Intermediate Water (AAIW) into the North Atlantic has been proposed during Termination II, to account for the persistence of low benthic $\delta^{13}\text{C}$ values into the early interglacial (e.g. Hodell et al 2009). Alternatively, low $\delta^{13}\text{C}$ waters originating in the Nordic Seas (e.g. Bauch et al 2000) possibly via brine rejection (Dokken and Jansen 1999, Bauch et al 2000) may also account for the low $\delta^{13}\text{C}$ signature evident during Termination II (further discussion of the offset in both benthic and surface proxies can be found in chapter 7).

Using the benthic $\delta^{18}\text{O}$ as a first order approximation of global ice volumes and benthic $\delta^{13}\text{C}$ as a proxy for the 'strength' of AMOC, Termination II may be seen as the interplay of disintegrating ice sheets, with large inputs of meltwater into high latitudes and the formation of deep water. An initial decrease in global ice volume ca. 138-136 kyr is accompanied by a decrease in $\delta^{13}\text{C}$, reflecting increased Northern Hemisphere insolation and the initiation of ice sheet decay. AMOC 'resumes' i.e. benthic $\delta^{13}\text{C}$ increases to levels reached during the MIS 5e plateau, before another reduction ca. 132 kyr followed by $\delta^{13}\text{C}$ increase, prior to a subsequent decrease associated with H11. These reductions in $\delta^{13}\text{C}$ and inferred reduction in AMOC, are probably linked to the inputs of large volumes of meltwater into the Nordic and Labrador Seas with the disintegration of Northern Hemisphere ice sheets impeding deep water formation. During these changes in $\delta^{13}\text{C}$, $\delta^{18}\text{O}$ continues to decrease in a fairly smooth fashion (this may reflect sampling resolution at MD04-2822; cf. Lototskaya and Ganssen 1999). Benthic $\delta^{13}\text{C}$ increases really only occur towards the end to the benthic $\delta^{18}\text{O}$ change and H11, although further oscillations in benthic $\delta^{13}\text{C}$ are evident.

4.2. Comparison of Terminations I and II within MD04-2822

Terminations I and II vary in their ‘boundary conditions’ i.e. variations in orbital parameters (e.g. Berger and Loutre 1999) and the configuration of the European ice sheets. Despite the obvious similarity, i.e. the disappearance of most, if not all, Northern Hemisphere ice sheets, the progression of each deglacial event varies within the same sediment core.

The magnitude of the IRD flux is different between both the glacial and deglacial events of the two glacial cycles, with Termination I recording far greater IRD inputs to the MD04-2822 core site. During Termination I, a step-like change is evident ca. 17 kyr (Figure 6.9) reflecting the retreat of the last BIS from the edge of the continental shelf. A similar pattern can be discerned for the penultimate deglacial; deglaciation appears to have progressed via pulses of terrigenous inputs following a sharp reduction in IRD inputs after H11 (Figure 6.11) as melting and retreat of the BIS from the shelf continued. The increased occurrence of discrete graded sediments (interpreted as distal turbidites) within the MIS 6 sediments is suggestive of a differing sediment supply regime and may indicate a more ‘massive’ penultimate BIS. Further work would help unravel the dynamics of the penultimate BIS, for which relatively little terrestrial evidence remains.

Both terminations are associated with localised SST cooling events, linked to the decay of the BIS and inputs of meltwater into the Rockall Trough. Additionally, both deglacial events contain a regional surface cooling (the Younger Dryas and C28) linked to changes in AMOC; although the magnitude and spatial extent of these events remains uncertain. Within MD04-2822, C28 is associated with an approximate 2 °C decrease in surface temperatures (estimate obtained from Mg/Ca analysis; see chapter 7 for further discussion) whilst the Younger Dryas is associated with an approximately 6 °C decrease (Kroon et al 1997). Therefore surface oscillations within the sub-polar North Atlantic were less pronounced during Termination II compared to Termination I i.e. reflecting a climatic ‘pause’ rather than a reversal such as the Younger Dryas (e.g. Lototskaya and Ganssen 1999). The Younger Dryas during Termination I is associated with ice sheet readvance; C28 however, probably reflects the terminal stages of deglaciation, with a minor southward migration of the polar front in response to high latitude meltwater inputs disrupting AMOC.

The lag between benthic and surface proxies is a conspicuous feature during Termination II. The ‘improvement’ in benthic $\delta^{18}\text{O}$ and $\delta^{13}\text{C}$ as well as % *N. pachyderma* (sinistral), is offset by ~ 6 kyr. Within Termination I, a similar offset is evident, but of ~1 kyr. Unlike Termination I, the penultimate deglacial does not display several step-changes in benthic $\delta^{18}\text{O}$, although sampling resolution remains low for Termination II. However, a series of benthic $\delta^{13}\text{C}$ oscillations are evident for both Terminations, reflecting the input of meltwater from the decaying Northern Hemisphere ice sheets into the high latitudes, impeding the formation of deep water (e.g. H1 and H11). Such cyclic variability in deep water production has previously been demonstrated for both terminations (Rasmussen et al 1999, Lototskaya and Ganssen 1999, Boyle and Keigwin 1987, Lehman and Keigwin 1992).

5. Conclusions

Both the last and penultimate glacial cycles are recorded within the MD04-2822 sediments, which allows the direct comparison of these two glacial (and deglacial) intervals from the same location. The marine record also provides a more 'complete' record of ice sheet dynamics, as it is a continuous record not subject to removal or obfuscation by later ice sheet oscillations. However, IRD flux and concentration are multifactorial records of ice sheet dynamics requiring caution in interpretation. While the difficulties in deciphering the IRD concentration record for sites proximal to an active calving margin are highlighted, this long sediment record provides the first continuous record of BIS expansion/contraction through a full glacial cycle as well as providing the first direct evidence of BIS activity during MIS 6. Whilst much of the evidence presented within this chapter is speculative in nature, the following firm conclusions may be drawn.

MD04-2822 provides the first direct evidence for BIS activity on the Hebridean margin during MIS 6 and the fluctuating nature of IRD delivery to the MD04-2822 site has been demonstrated for the last 175 kyr. IRD flux during MIS 6 containing distinctive 'BIS type' lithics confirms the earlier interpretation of seismic data (Holmes 1997, Stoker 1997), indicating an expansion of the BIS onto the continental shelf around northern Britain.

Sediment core MD04-2822 also allows an approximate determination of the timing of the first significant delivery of BIS-sourced IRD across the continental shelf to the core site. The first evidence of 'diagnostic' BIS lithics for the last glacial, i.e. the point at which the last BIS had reached a sufficient size to deliver IRD across the shelf edge to the core site, is seen within MIS 4 at around 70 kyr (see chapter 8 for further consideration of the early dynamics of the last BIS).

The pattern of BIS activity within MIS 3 and 2 (Kroon et al 2000, Knutz et al 2001, 2002, 2007, Wilson et al 2002) from the Barra Fan/Rockall Trough is replicated in core MD04-2822. 'Diagnostic' BIS lithic grains (dark basalts from the Tertiary volcanic provinces of northwestern Britain), first reported from MD95-2006 by Knutz et al (2001), are observed within the last glacial IRD record of MD04-2822. These 'diagnostic' lithologies suggest BIS expansion for each of the main glacial stages (MIS 2, 4, 6), with expansive shelf glaciation and marine calving margins. However, much ambiguity remains as to the exact origin of these 'diagnostic' lithics (e.g. Greenland, Rockall Bank etc.).

For portions of MIS 3, a BIS of sufficient size and with a marine margin was presumably established in order to deliver IRD to the MD04-2822 core site; the exact configuration, however, remains undetermined. Peak IRD fluxes at the MD04-2822 site are seen during MIS 2. This record is but one component in an ongoing attempt to reconstruct the initiation and dynamics of the last BIS (e.g. review of Scourse et al 2009, Haapaniemi et al 2010).

The last and penultimate glaciations for the NW sector of the BIS are limited by the continental shelf. The increased incidence of distal turbidites within MIS 6 (i.e. thin silt laminae; chapter 2, section 2) is highly suggestive of differing sediment delivery during the penultimate deglaciation, possibly due to a more extensive Saalian (MIS

6) European glaciation (e.g. Svendsen et al 2004, Ehlers et al 2004) than for the last glacial period. However, the lateral extent for the NW portion of the BIS is highly constrained by topography/bathymetry. A shelf edge glaciation is therefore envisaged for NW sector of both the Devensian/Weichselian (MIS 2/3; see review by Chiverrell and Thomas 2010) and Saalian (MIS 6; Hibbert 2010) BIS. Subtle variations in both IRD and terrigenous delivery to the MD04-2822 core site, during the last and penultimate glacial and deglacial events, reflect differences in orbital parameters, ice sheet configurations and the dynamics of the BIS.

CHAPTER 7:

Surface and deep water hydrography in the Rockall Trough (and wider NE Atlantic) during the last interglacial (MIS 5e)

This chapter focuses upon the hydrographic conditions recorded at the MD04-2822 core site in the Rockall Trough and the wider N.E. Atlantic during the last interglacial (MIS 5e). These changes are viewed within the context of ocean circulation; from full glacial to interglacial conditions (Termination II), MIS 5e and the initiation of the last glaciation (MIS 5d).

1. Background

The last interglacial (MIS 5e) has been defined in the marine record (Shackleton 1967, Pisias et al 1984, Martinson et al 1986) as commencing at the mid-point of the transition from glacial to interglacial benthic $\delta^{18}\text{O}$ and ending with increased benthic $\delta^{18}\text{O}$ as a consequence of increases in global ice volumes.

The last interglacial period is thought to be a period of elevated temperatures ($\sim + 2$ °C) and sea levels compared to the present interglacial (e.g. Otto-Bliesner et al 2006). Varying views of the 'climatic optimum' have been proposed: a prolonged period of relatively stable climate and thermohaline circulation in the North Atlantic (e.g. McManus et al 2002, Kukla et al 1997); or alternatively, episodes of major cooling within the MIS 5e evident in both the marine and terrestrial record (e.g. Cheddadi et al 1997, Oppo et al 2001). Additionally, both deep water and surface ocean variability has been documented during the transition into MIS 5d (e.g. Chapman and Shackleton 1999). The last interglacial (MIS 5e) varies subtly in timing between the marine and terrestrial record (e.g. Sánchez-Goñi et al 1999). The end of the terrestrial Eemian was diachronous, with cooling beginning at higher latitudes (e.g. Müller and Kukla 2004, Sánchez-Goñi et al 2005).

The disintegration of the MIS 6 (Saalian) ice sheets was initiated by increased insolation forced by orbital parameters, in particular an increase in Northern Hemisphere summer insolation (e.g. Berger 1978), with the rate of insolation change (especially at 65 °N) perhaps controlling the timing of transitions from glacial to interglacial (Ji et al 2006). The following interglacial (MIS 5e) was an interval of low global ice volumes and is thought to have been slightly warmer than the present interglacial; approximately 2 to 5 °C in the North Atlantic, Greenland and the Arctic (Cortijo et al 1999, NGRIP members 2004, Otto-Bliesner et al 2006).

Strong Northern Hemisphere summer insolation gradients may account for the increased European temperatures of the last interglacial compared to the Holocene (Overpeck et al 2006). In addition, the steepening of sea surface temperature gradients during MIS 5e may have been a response to shifts in latitudinal distribution of both summer and average insolation (e.g. Cortijo et al 1999). High insolation favours increased evaporation and could potentially create a large tropical moisture source, whilst increased latitudinal gradients would promote the transport and 'deposition' of this moisture northwards (Ruddiman et al 1980). Latitudinal temperature gradients may respond rapidly to insolation changes and drive changes in large-scale wind

fields. The influence of these altered conditions may include: changes in regional evaporation/precipitation patterns; the strength, physical properties and/or the position of the Gulf Stream; the temperature and salinity conditions in areas of deep water production (e.g. Gröger et al 2007).

Global sea levels during the last interglacial were several meters above present (mean sea level 4 to 6 m higher than modern, with fluctuations of up to 10 m about the mean) due to the partial melting of both the Greenland and Antarctic ice sheets, as well as the melting of the circum-Arctic/Atlantic ice sheets (e.g. Rohling et al 2008, Overpeck et al 2006, Otto-Bliesner et al 2006, Thompson and Goldstein 2005, Stirling et al 1998, Neumann and Hearty 1996). Up to 5 m of the interglacial sea level signal derived from a reduction in the Greenland ice sheet (Cuffey and Marshall 2000), with possible responses from Antarctica to the partial collapse of the Greenland ice sheet and to shallow ocean warming close to the continent (Overpeck et al 2006). Indeed, evidence for average centennial sea level change of approximately ± 1.6 m has been recorded throughout MIS 5e (e.g. Rohling et al 2008).

The North East Atlantic displays a regionally coherent climatic progression and millennial-scale oscillations in climate. For example, a series of surface ocean cooling (C) events associated with the southward migration of the polar front and their counterparts on land (e.g. McManus et al 1994), indicate that large scale climate variability is not just associated with the presence of large ice sheets in the Northern Hemisphere (McManus et al 1994, 2002, Oppo et al 2006, Chapman and Shackleton 1999). Sub-orbital variations (~1 to 3 kyr) in climate, well documented for the last glacial, are thought to have persisted into the Holocene (e.g. Bond et al 2001, Bianchi and McCave 1999). Variation in deepwater formation is one proposed mechanism for the 1-3 kyr variability observed (e.g. Broecker et al 1990).

For much of MIS 5e, the North Atlantic Current (NAC) is believed to have extended into much of the Nordic and Greenland Seas (e.g. see compilation by Müller and Kukla 2004). The Greenland and Norwegian Sea experienced a greater degree of climate variability during this interval, with a proposed migration of the polar front to the west of its present position during the warmest interval of MIS 5e (e.g. Fronval et al 1997) possibly facilitating the melting of the Greenland ice sheet (Otto-Bliesner et al 2006).

Elevated IRD concentrations are seen in the Greenland and Iceland Seas during the inferred MIS 5e climatic optimum. An additional two episodes of enhanced ice rafting in the Nordic Seas (Fronval and Jansen 1997) have been correlated to the subpolar cooling events (events C27a and b) identified in ODP 980 (Feni Drift, Rockall Trough; 55°29'N, 14°42'W, 2179 m; Oppo et al 2006). These increases in IRD deposition are thought to reflect the first instances of tidewater glaciers reaching the margins of the Nordic Seas (Fronval and Jansen 1997) and/or local ice caps on Arctic Islands, Canadian Arctic or north Greenland (Svendson et al 2004). These early MIS 5e climate instabilities, recognised at high latitudes (Fronval and Jansen 1997, Knudsen et al 2002, Seidenkrantz et al 1995), are also documented within the subpolar North Atlantic as a SST cooling events and episodic ice rafting (e.g. Bond et al 2001, Oppo et al 2006). Such cooling of the North Atlantic contributed to the climatic deterioration and vegetation changes recorded in Western Europe (e.g. Müller and Kukla 2004, Sánchez-Goñi et al 2005). The widespread North Atlantic surface cooling event (C26), occurring at the end of the benthic $\delta^{18}\text{O}$ plateau as

defined by Shackleton et al (2002), is thought to have precipitated the demise of the peak terrestrial interglacial climates in the North Atlantic region (Chapman and Shackleton 1999, Lehman et al 2002, Oppo et al 2001, 2006, Sánchez-Goñi et al 2005). An increase in the meridional SST gradient towards the end of MIS 5e has been proposed and linked to the cessation of warm waters penetrating into the Nordic Seas (e.g. Müller and Kukla 2004).

Oppo et al (2001) demonstrate persistent ~1-4 kyr periodicities for the subtropical planktonic $\delta^{18}\text{O}$ record throughout MIS 5. The amplitude of these sub-orbital variations is constant throughout, including MIS 5e. In contrast, the sub-orbital variations within MIS 5e documented by Cortijo et al (1999) are attributed to the strongly asymmetric variations (i.e. between high and low latitudes) in the insolation gradients forced by orbital changes, with some possible sea-ice/albedo feedbacks. Such forcings and feedbacks are also invoked for Holocene North Atlantic SST reconstruction at 6 kyr BP (Ruddiman and Mix 1993), where high latitude are warmer, low latitudes cooler, than present. Within the Nordic Seas, Bauch and Erlenkeuser (2008) document a warmer early Holocene than late Holocene. In addition, this region experienced warmer SSTs and land temperatures during MIS 5e than the Holocene (e.g. Bauch and Kandino 2007).

Deep ocean circulation underwent dramatic changes during the transition from glacial to interglacial conditions (i.e. Termination II); a return to high latitude deep ocean convection during the interglacial and the formation of deep water, re-establishing Atlantic Meridional Overturning Circulation (AMOC) and the production of North Atlantic Deep Water (NADW), with convection similar to present. This is in contrast to the penultimate glacial, which was characterised by reduced Nordic Sea deep water outflow and increased influence of southern sourced water in the North Atlantic and at the MD04-2822 core site (e.g. Chapman et al 2000, Hodell et al 2009, chapter 6). During terminations, the intermediate depth North Atlantic was poorly ventilated as Glacial North Atlantic Intermediate Water (GNAIW) ceased, due to freshwater inputs from icebergs and meltwater into the Nordic Seas and NE Atlantic. A return to interglacial NADW formation was delayed until full interglacial conditions were established in the Nordic and Labrador Seas (Venz et al 1999).

The location of MD04-2822 is sensitive to variations within the formation of NADW on both millennial and glacial-interglacial timescales and should therefore record changes in deep ocean temperature, salinity and ventilation. AMOC has also been implicated as a driver or amplifier of millennial scale climate changes via the redistribution of heat from low to high latitudes (Oppo et al 2006). The mechanism of the MIS 5e and MIS 5e/5d transition AMOC decreases, and the transport of minor IRD inputs may well reflect changes in surface circulation through this interval; millennial scale variations in IRD of a northerly source of detrital carbonates in core V29-191 (54 °16'N, 16 °47'W) have been interpreted as excursions of polar waters further to the south and west respectively, possibly in response to atmospheric circulation changes forced by orbital parameters (Bond et al 2001). The common association of AMOC reductions and increases in ice rafted debris in the North Atlantic may be explained in terms of reductions in AMOC contributing to surface cooling and increased ice rafting (McManus et al 1999).

One proposed mechanism by which the end of the last interglacial was brought about invokes a cooling of the Nordic Seas (and other high latitude seas) with lowered

summer insolation at high northern latitudes, which in turn provided snow and sea-ice feedbacks that accelerated cooling by freshening the surface ocean and thereby weakening AMOC (e.g. Imbrie et al 1992, Cortijo et al 1999). An alternative offered by Risebrobakken et al (2007), is an increase in the northern limb of AMOC towards the end of MIS 5e; initiation of Northern European glaciation is though to have occurred with dwindling insolation and thus lowered snow melting and increased precipitation (as previously suggested by McManus et al 1999).

Proxy data from MD04-2822 is presented for this interval and the stability, duration, as well as surface and deep water responses to climatic changes, of the last interglacial at the site evaluated.

2. The last interglacial as recorded within MD04-2822

A plateau in the benthic $\delta^{18}\text{O}$ has been used to define MIS 5e within the MD04-2822 record (after Shackleton et al 2002). Striking differences in the timing of events compared to the benthic $\delta^{18}\text{O}$ record are evident for both the benthic $\delta^{13}\text{C}$ and surface water proxies, e.g. the % *N. pachyderma* (sinistral) and XRF calcium records (Figure 7.1). Minimum values of benthic $\delta^{18}\text{O}$ (2554.5 cm) are reached prior to lowest % *N. pachyderma* (sinistral) i.e. warm sea surface temperatures (2540.5 to 2536.5 cm), suggesting global changes in ice volume (as recorded by $\delta^{18}\text{O}_{Cib}$) are manifested in the benthic proxy data at the MD04-2822 site prior to a surface water response.

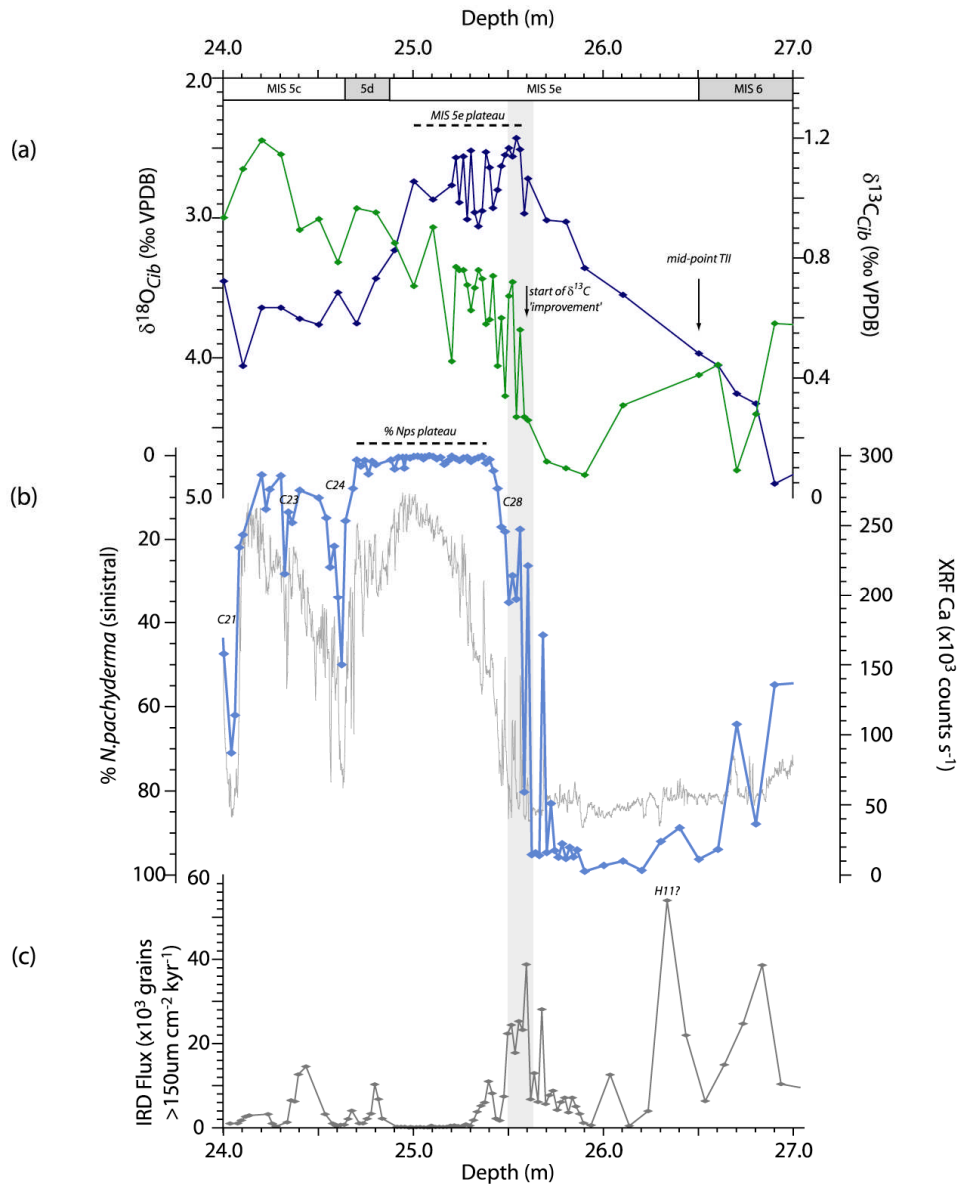
2.1. Termination II

The transition from MIS 6 (penultimate glacial) to MIS 5e (last interglacial) is conspicuous within the $\delta^{18}\text{O}_{Cib}$ record (Termination II) as changes in global ice volumes are a primary control on benthic $\delta^{18}\text{O}$ (Shackleton 1967) (Figure 7.1). The change from glacial to interglacial conditions and the melting of the MIS 6 (Saalian) ice sheets was prompted by increases in insolation due to orbital variations. The transition from $\delta^{18}\text{O}$ maxima to minima (Termination II) occurs over ~1.96 m (depths 2750.5 to 2554.5 cm) allowing this climatic event to be investigated in high resolution (please see chapter 6 for further discussion of Termination II).

Termination II is associated with a $\Delta\delta^{18}\text{O}$ of 2.61 ‰ for MD04-2822. The $\delta^{18}\text{O}$ of the mineral precipitated is a function of the $\delta^{18}\text{O}$ of the water in which the mineral is precipitated, the temperature of that water as well as local and vital effects (chapters 2 and 3). Therefore an estimate of the proportion of the MD04-2822 benthic $\delta^{18}\text{O}$ that is attributable to global ice volume (and hence global sea levels) at the penultimate termination should be possible. However, it will be remembered (chapters 2 and 3) that the relationship between global ice volumes and sea level is associated with several uncertainties; relative sea level (RSL) may not relate directly to global ice volumes at any measured locality due to: glacio-hydro-isostatic effects; uncertainties in the exact ice volume at the LGM¹; and the temporal variation of isotopic composition of the stored ice and its contribution through time.

¹ Fairbanks (1989) estimate LGM a 120 m drop in sea level global from Barbados corals, equating to an $\sim\delta^{18}\text{O}$ variation of ~ 1.3 ‰ therefore 0.011 ‰ m⁻¹. However, considerable debate remains as to the precise RSL, with estimates ranging from 113 to 135 m for the last glaciation (Peltier 2002, Clark and

Figure 7.1: MD04-2822 proxies on depth for the Termination II, MIS 5e and MIS 5d interval. (a) benthic $\delta^{18}\text{O}$ (black) and benthic $\delta^{13}\text{C}$ (grey); (b) surface proxies % *N. pachyderma* (sinistral) (black) and XRF Ca (light grey); and (c) IRD flux. MIS designations are after Imbrie et al (1984); the placement of these boundaries within MD04-2822 is based upon the benthic $\delta^{18}\text{O}$ record. Two episodes of elevated IRD fluxes are evident within Termination II; the grey shaded bar highlights one episode at the beginning of the MIS 5e benthic $\delta^{18}\text{O}$ plateau. The placement of H11 remains uncertain for the MD04-2822 record.



Mix 2002, Yokoyama et al 2000) and the proportion of the glacial-interglacial benthic $\delta^{18}\text{O}$ attributable to fluctuating ice volumes (estimates range from 1.7 ‰ (Broecker and Denton 1989) to 0.8 ‰ (Schrag et al 1996, Burns and Maslin 1999) with current 'best estimate' of 1 ± 0.1 ‰ (Schrag et al 2002, Waelbroeck et al 2002, Duplessy et al 2002).

This last effect is thought to be very small and does not fully explain the observed non-linearity between global ice volumes and sea level (Chappell and Shackleton 1986). In addition, benthic $\delta^{18}\text{O}$ has been shown to lead global ice volume changes across Terminations I and II (Skinner and Shackleton 2006, Waelbroeck et al 2008) with an ~ 4 kyr age uncertainty associated with using benthic $\delta^{18}\text{O}$ as a proxy for ice volumes during terminations (Lisiecki and Raymo 2009). Benthic $\delta^{18}\text{O}$ responses may vary at different depths within the same basin, with a rapid transmission of the signal to intermediate depths and a ~ 1.5 kyr delay to deep waters (Labeyrie et al 2005, Waelbroeck et al 2006).

Using the sea level estimates of Siddall et al (2003), an approximation of global sea level change for Termination II of 113 to 123 m is obtained (equating to 1.24 to 1.35 ‰, assuming a relationship of Fairbanks (1989) i.e. 0.011 ‰ m^{-1}). This leaves approximately 1.26 ‰ ‘unaccounted’ for by sea level estimates in the MD04-2822 benthic record, across the transition from fully glacial to fully interglacial conditions. Of course, from the above equation, changes in the bottom water temperatures and/or changes in the $\delta^{18}\text{O}$ of the bottom waters could also account for the discrepancy between the global ice volume signal and the observed $\delta^{18}\text{O}$ at the MD04-2822 core site. This could equate to an approximate $5 \text{ }^\circ\text{C}$ temperature change in bottom waters (assuming $1 \text{ ‰} \sim 4 \text{ }^\circ\text{C}$) or a 2.5 psu change in salinity (assuming $1 \text{ ‰} \sim 2 \text{ psu}$), or some combination of the two. In addition, the transfer of freshwater formerly stored within the ice sheets², alters the $\delta^{18}\text{O}_{\text{water}}$ ‘end member’ between glacial and interglacial periods (e.g. Duplessy et al 2002).

2.2. MIS 5e benthic $\delta^{18}\text{O}$ plateau

A flattening off in $\delta^{18}\text{O}$ values, the MIS 5e plateau, occurs between the depths of 2580.5 and 2500.5 cm (80 cm; average sedimentation rates of 6.7 cm kyr^{-1}) (Figure 7.1). The benthic $\delta^{18}\text{O}$ plateau is characterised by quasi-constant values of $\delta^{18}\text{O}_{\text{Cib}}$ with some variation in $\delta^{18}\text{O}$ values. This variation (MIS 5e mean = $2.75 \pm 0.21 \text{ ‰ } 1\sigma$, $n=25$) would equate to a temperature change in bottom waters during the MIS 5e plateau of $\sim 0.84 \text{ }^\circ\text{C}$ or 0.42 psu change in salinity or some combination of the two. However, the difference between maximum and minimum in $\delta^{18}\text{O}$ during the plateau is 0.63 ‰, equating to a temperature change of $2.5 \text{ }^\circ\text{C}$ or 1.26 psu or some combination of the two.

The mean Holocene $\delta^{18}\text{O}$ for MD04-2822 is $2.88 \pm 0.14 \text{ ‰}$ ($n=25$). When the mean values for the last interglacial are compared with those for the Holocene in the same core, a difference of $\sim 0.13 \text{ ‰}$ is found, which is not much greater than the measurement error of 0.08 ‰ . This difference in mean benthic $\delta^{18}\text{O}$ values could equate to deep water temperatures at the MD04-2822 site that were on average $0.5 \text{ }^\circ\text{C}$ higher during MIS 5e than those experienced during the Holocene. The difference between the mean benthic $\delta^{18}\text{O}$ values for these intervals compares favourably with cores in the North Atlantic and the Norwegian Sea (see Duplessy et al 2007), where such differences

² Duplessy et al (2002) provide evidence of the average isotopic composition of the major ice sheets at the LGM: Laurentide $\sim -28 \text{ ‰}$ to -34 ‰ ; Eurasian $\sim -16 \text{ ‰}$ to -40 ‰ ; Greenland $\sim -43 \text{ ‰}$, Antarctica $\sim -40 \text{ ‰}$ to -60 ‰ . These extremely low $\delta^{18}\text{O}$ values reflect the preferential sequestration of ^{16}O within the ice sheets towards the ‘end’ of the Rayleigh distillation process.

were attributed to the influx of low $\delta^{18}\text{O}$ water (as mentioned above), with the partial melting of both Greenland and Antarctic ice sheets, as well as a warming and an increase in the salinity of deep water.

2.3. Benthic $\delta^{13}\text{C}$ during the interglacial

One of the more striking features of the MD04-2822 record is the apparent decoupling of the benthic $\delta^{18}\text{O}$ and $\delta^{13}\text{C}$ signals; the benthic $\delta^{13}\text{C}$ record for MD04-2822 does not display a shift towards more positive values until the transition in benthic $\delta^{18}\text{O}$ from high glacial values to low interglacial values is nearly complete i.e. the co-registered benthic $\delta^{13}\text{C}$ record at MD04-2822 does not change coevally with the benthic $\delta^{18}\text{O}$ signal (Figure 7.1).

Benthic $\delta^{13}\text{C}$ has been demonstrated as being a sensitive proxy to changes in deep water ventilation and a measure of NADW productivity (e.g. Keigwin et al 1994). The change from very low $\delta^{13}\text{C}$ glacial values (~ 0.1 ‰) does not occur until ~ 2560.5 cm, 1.9 m after the start of the $\delta^{18}\text{O}$ transition and positioned at the beginning of the benthic $\delta^{18}\text{O}$ plateau. The highest values of $\delta^{13}\text{C}$ do not occur within the MIS 5e plateau, but within MIS 5c (see chapter 8). Again, as with the benthic $\delta^{18}\text{O}$ record, this is not a smooth improvement in ventilation at the site but has some degree of variability superimposed. Values of $\delta^{13}\text{C}$ continue to show a general trend towards greater values throughout the MIS 5e plateau, with oscillations of up to 0.38 ‰ during the MIS 5e plateau occurring on the same timescale as those seen within the benthic $\delta^{18}\text{O}$ record. Maximum benthic $\delta^{13}\text{C}$ values (~ 0.97 ‰) are achieved within MIS 5c rather than during the interglacial. These values are slightly lower than the mean experienced at the site during the Holocene (1.03 ± 0.17 ‰ $n=26$), however they are within the measurement error of the analyses (0.08 ‰). An increase in the ‘strength’ of AMOC through the MIS 5e to MIS 5c may account for the long-term increase in the benthic $\delta^{13}\text{C}$. Alternatively, the benthic $\delta^{13}\text{C}$ record may reflect a ‘shoaling’ of NADW through this interval; MD04-2822 is situated at a depth of 2,344 m and a shoaling of well ventilated deep waters may only bathe the site during MIS 5c and MIS 5c. These are discussed further in section 4.3 of this chapter.

2.4. Surface proxies

In addition to the offset of the benthic $\delta^{18}\text{O}$ and $\delta^{13}\text{C}$ records, there is an offset in the timing of the transition of the surface proxies, from values typical of glacial conditions to those of interglacial conditions, when compared to the benthic $\delta^{18}\text{O}$ record (Figure 7.1, Figure 7.2). The first instances of sustained very low percentages of *N. pachyderma* (sinistral) occur at a depth of 2540.5 to 2536.5 cm. The onset of very low percentages of *N. pachyderma* (sinistral) is offset with the onset of the benthic $\delta^{18}\text{O}$ plateau by approximately 40 cm. This occurs after the $\delta^{18}\text{O}$ isotopic minimum and during the flattening off of the benthic $\delta^{13}\text{C}$ values (i.e. reduced variability of $\delta^{13}\text{C}$). The migration of the polar front to the north of the core site, thereby resulting in low % *N. pachyderma* (sinistral), therefore took place after the $\delta^{18}\text{O}_{\text{Cib}}$ minimum. The interval of sustained low *N. pachyderma* (sinistral) percentages (< 5 %) persisted until 2470.5 cm (~ 30 cm) with a mean value of 1.1 ± 1 % ($n=36$). The corresponding mean Holocene value was 0.91 ± 0.2 % ($n=20$). The plateau in % *N. pachyderma* (sinistral) corresponds to sustained levels of high planktonic

foraminifera concentrations, but peak concentrations are not achieved until well into MIS 5 (~24m, MIS 5c).

Peak values of XRF calcium, primarily controlled by surface water productivity, do not occur until ~2500 cm depth, suggesting that whilst the polar front was situated to the north of the core site, the most productive surface water conditions did not occur until the end of the benthic $\delta^{18}\text{O}$ plateau and late within the % *N. pachyderma* (sinistral) plateau. Values of calcium remain fairly high until the transition into MIS 5d, but a stepwise drop in values is observed at ~2485 cm (Figure 7.1).

Whilst the planktonic isotope records for both *N. pachyderma* (sinistral) and *G. bulloides* are incomplete through the Termination II-MIS 5e interval, they do enable some inferences of surface water conditions to be made. In Figure 7.2 the $\delta^{18}\text{O}_{Nps}$ signal follows that of the benthic $\delta^{18}\text{O}$ through the transition from glacial to interglacial, whilst the $\delta^{18}\text{O}_{Gb}$ follows the benthic $\delta^{18}\text{O}$ through MIS 5e and into MIS 5d. Increased $\delta^{18}\text{O}_{Nps}$ values can be detected ~2570.5 to 5246.5 cm; these correspond to fluctuating percentages of *N. pachyderma* (sinistral) and a prolonged reversal in the % *N. pachyderma* (sinistral) trend at 2556.5 to 2448.5 cm.

This gradual 'improvement' in surface water conditions, hinted at in the calcium record, is reflected in palaeotemperature reconstructions derived from Mg/Ca analyses on *G. bulloides* (300 to 355 μm mesh size). The maximum values in sea surface temperatures obtained from Mg/Ca reconstructions (~14 °C), occur at a depth of 2470.5 cm, the very end of the % *N. pachyderma* (sinistral) plateau and over 80 cm from the benthic $\delta^{18}\text{O}$ minima (i.e. 'peak' MIS 5e) (Figure 7.2). The palaeotemperature reconstructions show a general warming trend through MIS 5e but with some degree of variability superimposed; oscillations greater than 1.5 °C (Mg/Ca error estimates of ± 1 °C) occur on top of a 5 °C warming through the MIS 5e interval. The mean surface water palaeotemperature for the benthic $\delta^{18}\text{O}$ plateau is 11.0 ± 0.9 °C (n=26), whilst for the whole interval sampled (i.e. MIS 5e) the mean is 11.4 ± 1.2 °C (n=32). This compares to a late Holocene mean of 11.8 ± 0.6 °C (n=11). Holliday et al (2000), Holiday (2003) demonstrate an approximate temperature variation in modern surface waters in the Rockall Trough of ± 0.5 °C and ± 0.05 psu for a recent 26 year period (1975-1998) which is comparable with the standard deviation of the MD04-2822 late Holocene palaeotemperature estimates.

The $\delta^{18}\text{O}$ of the surface waters in which the *G. bulloides* shell was precipitated, can be estimated using the paired Mg/Ca and stable isotope analyses, by solving for $\delta^{18}\text{O}_w$ in the palaeotemperature equation of Shackleton (1974) (Figure 7.3), although the large (~1 °C) error associated with the palaeotemperature should be remembered.

$$T = 16.9 - 4.38(\delta_m - \delta_w) + 0.1(\delta_m - \delta_w)^2$$

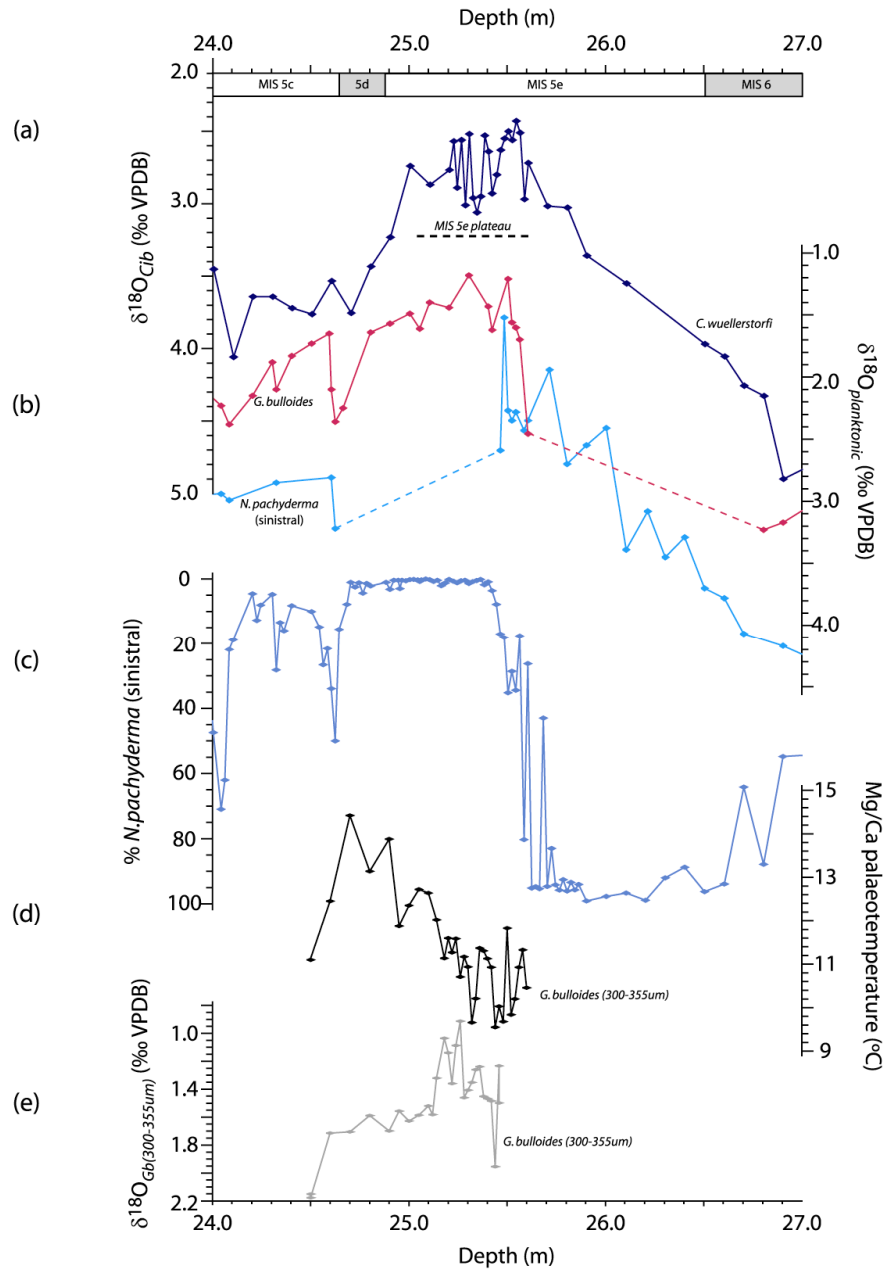
where;

T is temperature,

δ_m is the $\delta^{18}\text{O}$ of the mineral precipitated,

δ_w is the $\delta^{18}\text{O}$ of the water in which the mineral is precipitated

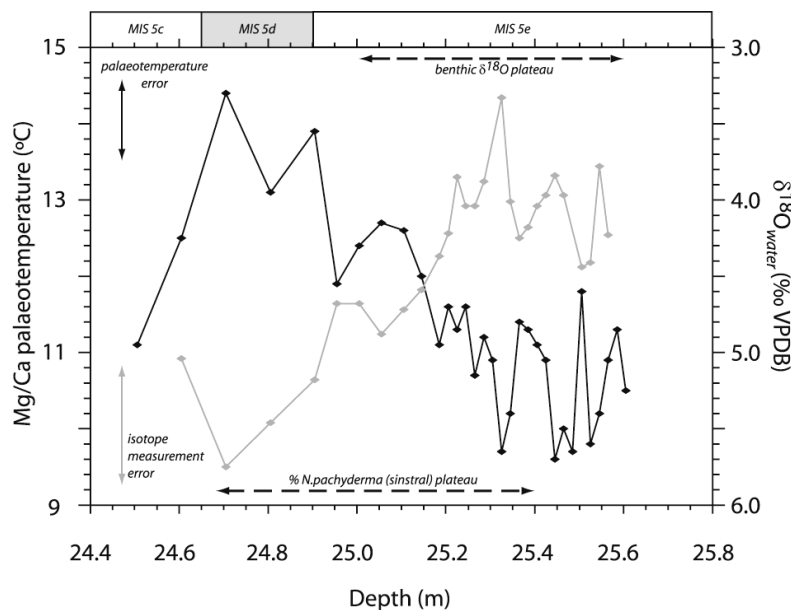
Figure 7.2: MD04-2822 surface proxies with benthic $\delta^{18}\text{O}$ (a) benthic $\delta^{18}\text{O}$; (b) planktonic $\delta^{18}\text{O}$, *G. bulloides* (light grey), *N. pachyderma* (sinistral) (dark grey); (c) % *N. pachyderma* (sinistral); (d) Mg/Ca palaeotemperature reconstruction ($\pm 2\sigma \sim 1^\circ\text{C}$) and (e) paired *G. bulloides* $\delta^{18}\text{O}$ (carried out on same size fraction as the Mg/Ca analyses).



The seawater $\delta^{18}\text{O}$ reconstruction comprises changes in palaeosalinities and variations in global ice volumes (vital effects are assumed to be minimal due to the constant and narrow size range used for all paired analyses). It must be remembered that fluctuations of up to ± 10 m about the MIS 5e mean are present in fossil coral reefs (e.g. Thompson and Goldstein 2005) during this interval. Palaeosalinity reconstructions have not been attempted due to the inherent difficulties resulting from the propagation of errors; *inter alia* the relatively large errors associated with palaeotemperature reconstructions, errors in the calculation of sea level change, calculation of mean ocean salinity estimates (and their relationship to global ice volume) and the estimation of the freshwater end-members (Schmidt 1999, Rohling 2000).

However, the surface seawater $\delta^{18}\text{O}$ (displays a general increasing trend from ~ 25.3 m. This coincides with the general warming trend of the surface waters derived from Mg/Ca analyses. Several oscillations in the $\delta^{18}\text{O}$ of the surface waters (~ 1 ‰) are evident within early MIS 5e, the first of which coincides with a pronounced increase in the % *N. pachyderma* (sinistral) and decrease in temperature, suggesting that the ‘flickering’ of the position of the polar front in the region was linked to changes in the surface conditions. The calculated surface water $\delta^{18}\text{O}$ record follows that of the surface temperatures; as temperatures increase, there is in general an increase in the $\delta^{18}\text{O}$ of the surface waters at the MD04-2822 core site.

Figure 7.3: Reconstructed SSTs and seawater $\delta^{18}\text{O}$ derived from paired Mg/Ca and stable isotope measurements on *G. bulloides* (300-355 μm). A general warming trend as well as an increase in surface water $\delta^{18}\text{O}$ is seen through the MIS 5e plateau and into MIS 5d. The stratigraphic position of MIS designations (after Imbrie et al 1984) and benthic $\delta^{18}\text{O}$ plateau (after Shackleton et al 2002) based upon the MD04-2822 benthic $\delta^{18}\text{O}$ record.



3. Age Control for the last interglacial

MIS designations have been used to create a global stratigraphic framework for marine sediment cores (e.g. SPECMAP, LR04 stacks of $\delta^{18}\text{O}$), but concerns include: the assumption of a smooth response to changing insolation (Shackleton et al 2002), record resolution (e.g. Shackleton et al 2003), the timing of key events such as Termination II compared to U/Th dated coral terraces (e.g. Thompson and Goldstein 2006), and changes in local hydrographic conditions (Skinner and Shackleton 2005)³. Skinner and Shackleton (2005) question our ability to use the benthic $\delta^{18}\text{O}$ stratigraphy at sub-orbital timescales and highlight that benthic $\delta^{18}\text{O}$ need not scale consistently with sea level change.

Accordingly, for MD04-2822 ages were assigned utilising the approach of Shackleton et al (2002, 2003) for MD95-2042 (Iberian margin), whereby radiometrically determined ages of sea level stillstands in coral terraces are assigned to benthic $\delta^{18}\text{O}$ plateaus (Figure 7.4). The following age tie-points were used (from Shackleton et al 2002, 2003): the mid-point of Termination II (2652.5 cm), an age of 132 kyr; the start (2580.5 cm) and end (2500.5 cm) of the MIS 5e plateau, 128 and 116 kyr respectively; and the mid-point of the transition into MIS 5d (2485.5 cm) an age of 115 kyr. Based upon these age-tie points, the variability in the benthic $\delta^{18}\text{O}$ occurs at approximately millennial or sub-millennial timescales.

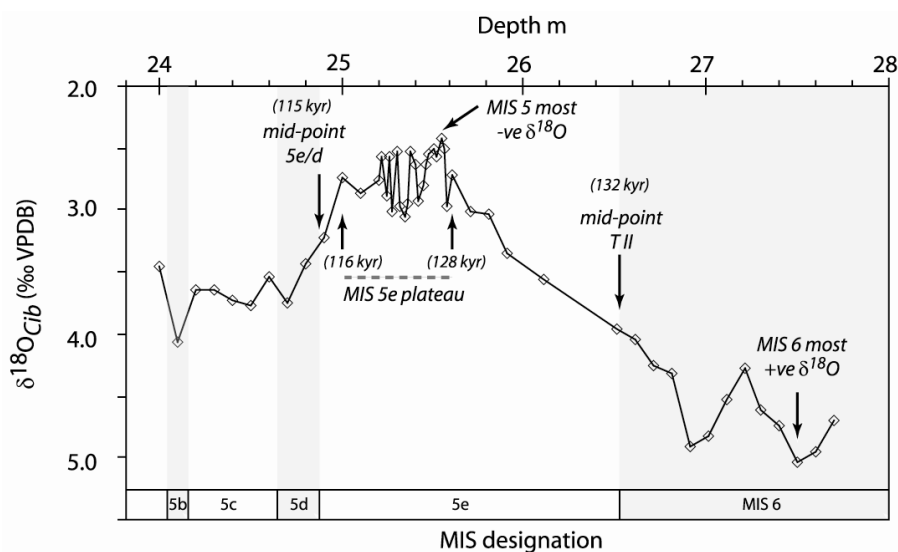
For MD95-2042 (Shackleton et al 2002, 2003), little variability in benthic $\delta^{18}\text{O}$ is documented, beyond that associated with measurement errors, during the MIS 5e plateau (Shackleton et al 2003). This is in contrast to MD04-2822, where the standard deviation of the mean MIS 5e $\delta^{18}\text{O}$ is $\pm 0.21 \text{‰}$ ⁴. This may be a reflection of the geographical position of the two cores; MD04-2822 is much more proximal to the Nordic Seas than the Iberian margin and therefore more susceptible to any changes in the characteristics (e.g. temperature/salinity) of overflow water derived from the Nordic Sea.

The relatively low resolution (10 cm) of the benthic $\delta^{18}\text{O}$ record outside of the MIS 5e plateau (where sampling is every 2 cm) precludes utilising the approach of Shackleton et al (2003) in assigning other sea level stillstands to other plateaus in the benthic $\delta^{18}\text{O}$ record and thus providing additional age control points.

³ The reader is directed to chapter 3, Chronostratigraphy, for a full discussion of the influences upon benthic $\delta^{18}\text{O}$.

⁴ Measurement error (2σ) for benthic $\delta^{18}\text{O}$ is $\pm 0.08 \text{‰}$

Figure 7.4: Age control for the MIS 5e portion of MD04-2822 (after Shackleton et al 2002, 2003). Tie-point ages are given in brackets. MIS designations are after Imbrie et al (1984).



4. Discussion

4.1. Termination II

Across the transition from MIS 6 to MIS 5 (Termination II) MD04-2822 exhibits a $\Delta\delta^{18}\text{O}_{\text{Cib}}$ of 2.61 ‰, with 1.26 ‰ ‘unaccounted’ for when ‘corrected’ for global ice volume changes (see section 2.1, this chapter). A change in the $\delta^{18}\text{O}_{\text{water}}$ ‘end-member’ would also occur across this transition with inputs from the MIS 6/Saalian ice sheets (e.g. Duplessy et al 2002). The ‘unaccounted’ for MD04-2822 $\delta^{18}\text{O}$ could correspond to an increase of up to 5 °C in the temperature of bottom waters or a change in salinity of 2.5 psu, or a combination of the two⁵. The MD04-2822 estimate of bottom water temperature change from glacial to interglacial conditions compares favourably to the magnitude of temperature change of ~4.4 °C for the LGM to the Holocene, reconstructed by Adkins et al (2002) for ODP 981 (Feni Drift, 2184 m depth)⁶. At several North Atlantic sites, temperature and salinity changes account for more than half of the observed benthic $\delta^{18}\text{O}$ change across glacial-interglacial transitions (Schrag et al 1996, Adkins et al 2002).

Atlantic millennial scale hydrographic changes are thought to have contributed to age discrepancies between the Atlantic and the Pacific for Termination I (Skinner and

⁵ Assuming 1 ‰ ~ 4°C and 1 ‰ ~ 2 psu.

⁶ A maximum lower limit bottom water temperatures of ~ -1.5 °C is suggested for the present ODP 980 site (Feni Drift, Rockall Trough) with LGM bottom water temperatures calculated as -0.8 to -1.5 °C (Waelbroeck et al 2002). Estimates based upon pore water measurements for a neighbouring core (ODP 981, Feni Drift 2184 m) suggests LGM bottom water temperatures of approximately -1.2 ± 0.2 °C and a salinity of 36.10 ± 0.01 psu, with corresponding modern values of 3.25 ± 0.05 °C and 34.945 ± 0.008 psu. This would give a ΔT across Termination I of ~ 4.45 °C and ΔS of ~ 1.2 psu (Adkins et al 2002). However, there is a non-linear relationship between global ice volume and sea level changes; in addition, the accompanying benthic $\delta^{18}\text{O}$ amplitudes vary between glacial and deglacial regimes and also between terminations (Waelbroeck et al 2002).

Shackleton 2005). During the full glacial, the Rockall Trough may have experienced a greater degree of southern sourced waters (i.e. AABW) as convection changed from NADW formation to the production of GNAIW: during the LGM there was a significant northward expansion of AABW within the North Atlantic (e.g. Adkins et al 2002, Waelbroeck et al 2002, Marchitto and Broecker 2006). The retreat of southern sourced waters with the resumption of AMOC and NADW formation during Termination II, would have been accompanied by an increase in bottom water temperatures bathing the MD04-2822 site (as seen for Termination I e.g. Labeyrie et al 2005 and modelling studies e.g. Weaver et al 1993, Winton 1997).

Currently, it is only the deepest portions of the Trough where the more dense southern sourced waters are recognised⁷. Warming of deep water masses during Termination II may therefore account for at least some of the observed $\Delta\delta^{18}\text{O}$ not ascribed to changes in sea level during this interval. Therefore, local overprinting of the benthic $\delta^{18}\text{O}$ signal due to hydrological changes (e.g. Skinner and Shackleton 2005) may be responsible for the deviation of the MD04-2822 $\Delta\delta^{18}\text{O}$ from estimates of global ice volumes (of e.g. Siddall et al 2003) across Termination II.

Alternatively, a change in the $\delta^{18}\text{O}$ of the bottom waters may be accounted for by the incorporation of low $\delta^{18}\text{O}$ waters (e.g. from meltwater) to the deep ocean via sea-ice freezing and brine rejection (e.g. for the last glacial Dokken and Jansen 1999, Vidal et al 1998, Labeyrie et al 2005, Meland et al 2008, Dickson et al 2008⁸). A change from deep water regime whereby brine formation may locally overprint the $\delta^{18}\text{O}$ signal to full interglacial conditions may also account in part for the discrepancy between the $\Delta\delta^{18}\text{O}$ across a Termination at the MD04-2822 core site and that of the global $\delta^{18}\text{O}$ as estimated from sea level changes.

Therefore, oceanographic regime changes and their manifestation at the MD04-2822 core site, may account for the observed $\Delta\delta^{18}\text{O}$ from glacial to interglacial values; a switch from: a) increased influence of southern sourced waters (AABW) i.e. an admixture of both northern and southern source waters (Oppo and Lehmann 1993, McManus et al 1999) and/or b) the freezing of low salinity surface waters (brine rejection in the Nordic Seas) producing isotopically light brines (e.g. Dokken and Jansen 1999), to conditions similar to the present with AMOC and deep convection within the Greenland and Nordic Seas.

⁷ At present, overflow from the Norwegian Sea can be discerned in the Rockall Trough; at depths of 2,000 m to 3,500 m there is a mixing of NADW and southern source water i.e. AABW. NADW can be identified by a salinity maximum of 34.941 to 34.947 near 2,500 m (MD04-2822 is located at a depth 2,344 m) below which silicate concentrations reveal influence of AABW occupying the deepest portions of the basin and mixing with overlying NADW. Water masses are dominated by NADW at depths of 2,000 to 2,500 m whilst below 3,300 m waters are mainly derived from AABW. The influence of AABW becomes progressively less the further to the north in the Trough but a significant component derived from the AABW extends to 57 °N (New and Smythe-Wright 2001). The present temperature difference in the Rockall Trough between these southern sourced water and deep outflow from the Nordic Seas is approximately 0.6 °C (~0.15 ‰) and 1psu (~0.5 ‰) (Frew et al 2000).

⁸ Dickson et al (2008) demonstrate the influence of brines during MIS 3 for the core MD95-2006 (Barra Fan) and suggest that these result from seasonal sea ice formation in the Nordic Sea, although there may be a local Hebridean margin brine component (see chapter 6, section 2.2).

4.2. The MIS 5e benthic $\delta^{18}\text{O}$ plateau: Deep water temperature changes and Sea level fluctuations

The oscillations seen in benthic $\delta^{18}\text{O}$ through the MIS 5e plateau are a striking feature of this record and display greater variability than the measurement error (Figure 7.5). Such fluctuations in benthic $\delta^{18}\text{O}$ are primarily governed by global ice volumes (Shackleton 1974) but the utility of this proxy as a stratigraphic tool is questioned, due to possible 'over-printing' by local influences on the signal i.e. deep water temperature and salinity changes (e.g. Duplessy et al 2007, Skinner and Shackleton 2005).

Duplessy et al (2007) estimate that NADW was approximately 0.4 ± 0.2 °C warmer during the last interglacial than present, based upon the difference in the mean benthic $\delta^{18}\text{O}$ between the last interglacial and the Holocene (when corrected for ice volume changes). Utilising the same approach, MD04-2822 displays a $\delta^{18}\text{O}$ anomaly (last interglacial (LIG) minus Holocene) of ~ 0.9 ‰ assuming the same correction for ice volume (-0.045 ‰) of Duplessy et al (2007). This would equate to an average temperature increase in the deep water bathing the MD04-2822 core site of ~ 0.4 °C during the last interglacial compared to present. This compares favourably to the North Atlantic average determined by Duplessy et al (2007) as well as the means of the Norwegian Sea (0.58 °C) and Atlantic Ocean (0.37 °C).

These $\delta^{18}\text{O}$ anomalies are small and Duplessy et al (2007) infer that they represent only small divergence in conditions to those of the present interglacial; such small changes in properties tend to occur in water masses of constant density. Thus a warming of NADW of 0.37 ± 0.2 °C was compensated for by an increase in salinity of 0.04 psu and in the Norwegian Sea, a warming of deep waters by 0.57 ± 0.2 °C was balanced by a 0.07 psu increase in salinity. The benthic $\delta^{18}\text{O}$ anomaly for MD04-2822 falls between those of the Norwegian Sea (0.23 to 0.06 ‰) and those for cores in the northern North Atlantic (0.15 ‰).

The magnitude of deep water temperature changes has been shown to be much greater immediately prior and just after interglacial periods. For example, an approximate 2 °C temperature decrease has been recorded in the equatorial Atlantic and Pacific between MIS 5e and MIS 5c (Cutler et al 2003), with glacial-interglacial amplitudes in the Atlantic of 3 to 4 °C (Culter et al 2003, Dwyer et al 1995, Labeyrie et al 1987, Martin et al 2002).

Superimposed upon the mean MIS 5e deep water temperature increase (compared to mean Holocene) are shorter term (millennial scale or less) $\delta^{18}\text{O}$ (± 0.21 ‰ about the mean) variations and oscillations of up to 0.63 ‰. Whilst these may also be a result of changes in the temperature and salinity of the deep water overflow from the Nordic Seas (i.e. constant density maintained) they may be a product of variations in global sea level (Figure 7.5).

Global ice volumes are intimately tied to fluctuations in global sea levels; emerging evidence suggests that the MIS 5e plateau was not a period of static sea level but of sea level fluctuations (e.g. Thompson and Goldstein 2005, Hearty et al 2007a). When the oscillations in benthic $\delta^{18}\text{O}$ of MD04-2822 are compared to the sea level reconstructions (e.g. Riccio et al 2001 (Italy); Hearty 1986, 1987 (Mediterranean Basin); Hearty and Kindler 1995 (Bermuda and Bahamas); Stirling et al 1998

(Western Australia), Thompson and Goldstein 2005 (Barbados); Rohling et al 2008, 2009 (Red Sea)), features common to the coral and foraminifera sea level reconstructions, as well as the MD04-2822 benthic $\delta^{18}\text{O}$, are apparent and suggest that at least some of the observed variation in the MD04-2822 benthic $\delta^{18}\text{O}$ may be attributable to changes in global sea levels.

For example, the composite sea level curve based upon a large number of sites, both tectonically stable and areas of minor uplift, of Hearty et al (2007a) contains several fluctuations in sea level through the last interglacial (Table 7.1). The following sea level reconstruction for MIS 5e is proposed: an initial deglacial sea level rise to above present levels ca. 130 ± 2 kyr; a stabilisation early in MIS 5e lasting about 5 to 7 kyr from ca. 132-125 kyr, this prolonged higher than present sea level may be linked to the partial melting of the Greenland Ice Sheet; a short regression lasting only about 1,000 years ca. 125-124 kyr, possibly associated with incipient build up of polar ice, (although the magnitude of this fall remains uncertain); a second rise above present (~3m) ca. 124 to 121 kyr but this interval was poorly defined; the end of MIS 5e characterised by multiple sharp rises in sea level (+ 6 to 9 m) ca. 121 to 119 kyr, possibly linked to a disintegration of the Western Antarctic Ice Sheet; a final rapid retreat of sea level associated with MIS 5d, implying a rapid build-up of Northern Hemisphere and possibly Antarctic ice.

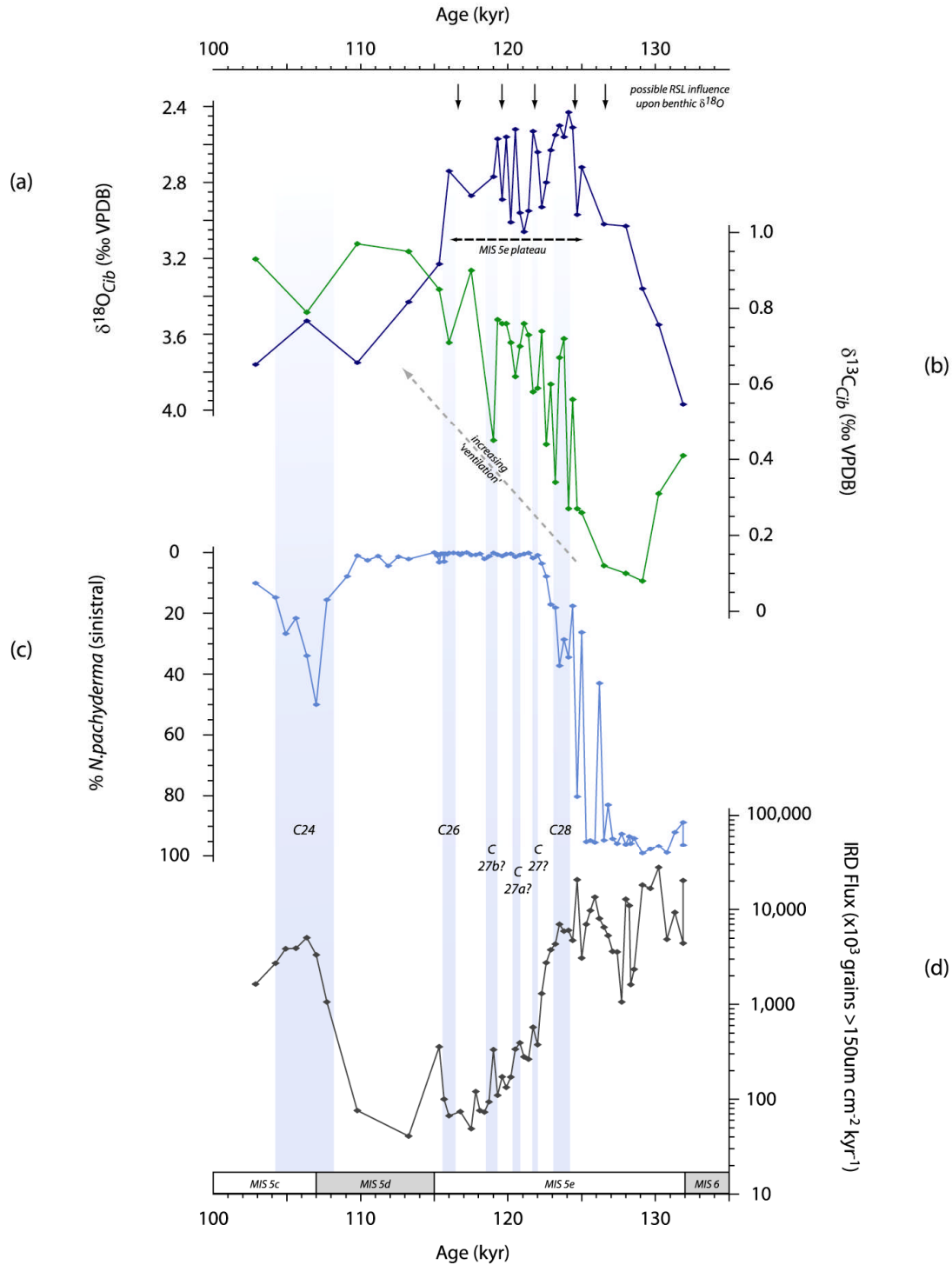
Table 7.1: Composite sea level reconstruction for the last interglacial of Hearty et al (2007a)

Sea level event	Est. Age (kyr)	Est. Magnitude (m)	Estimated age of possible correlating MD04-2822 benthic $\delta^{18}\text{O}$ event *
1) deglacial sea level rise	130 ± 2		
2) Sea level stabilisation	132 to 125	$+ 2.5 \pm 1$	128 to 125
3) Short lived regression	125 to 124		124.7
4) Second sea level rise	124 to 121	+ 3	~122
5) Multiple sharp rises in sea level	121 to 119	+ 6 to + 9	121.1 to 119
6) Rapid sea level retreat (onset MIS 5d)	120 to 118		116

* Age model based upon approach of Shackleton et al (2002, 2003) where mid-point of TII, start and end of the benthic $\delta^{18}\text{O}$ plateau and the mid-point of the MIS 5e/5d transition are assigned the following ages 132, 128, 116, 115 kyr derived from fossil coral reef evidence

CHAPTER 7:
Surface and Deep Water Hydrography during the Last Interglacial

Figure 7.5: MD04-2822 proxies on age (derived from radiometric age estimates – see section 1, this chapter). (a) benthic $\delta^{18}\text{O}$; (b) benthic $\delta^{13}\text{C}$; (c) % *N. pachyderma* (sinistral); and (d) IRD flux (on a logarithmic scale). Vertical blue bars give the positions of the North Atlantic C events (cf. Chapman and Shackleton 1998, 1999, McManus et al 2004, Oppo et al 2006), whilst black arrows in panel (a) highlight benthic $\delta^{18}\text{O}$ variations within the MIS 5e plateau that may be due to variations in global sea levels.



An alternative reconstruction, derived from foraminifera of the Red Sea (Rohling et al 2008, 2009), also contains several sea level fluctuations within the last interglacial; two sea level highstands, separated by a lowstand and a possible third highstand late in MIS 5e (Table 7.2). The intra-MIS 5e sea level oscillations documented by Rohling et al (2008) appear to be corroborated, with respect to both timing and magnitude, by coral and reef architecture data from localities surrounding the Red Sea, Barbados, Western Australia and the Bahamas (see references with the supplementary data for Rohling et al 2008 e.g. Orszag-Sperber et al 2001, Walter et al 2000, Thompson and Goldstein 2007). The authors suggest that the collective data is strongly suggestive of two highstands (at ca. 123 and 121.5 kyr), separated by a decrease in sea level (ca. 122.5 kyr) with possibly a minor highstand late within MIS 5e (ca. 119.5 kyr). Recent coral reef data from the Yucatán peninsula, Mexico, corroborates the timing of this highstand towards the demise to the last interglacial (ca. 121 kyr), but estimates a smaller amplitude (~2-3 m) (Blanchon et al 2009) than Rohling et al (2008, 2009).

Table 7.2: Estimated ages and magnitude of MIS 5e sea level events (Rohling et al 2008, 2009)

Sea level event	Est. Age (kyr) of mid-point (Rohling et al 2008)	Est. Age (kyr, b2k) transition (Rohling et al 2009)	Est. magnitude of event (m) (Rohling et al 2008, 2009)	Est. RSL Equivalent ‰ [§]	Est. age of possible MD04-2822 benthic $\delta^{18}\text{O}$ event *	$\Delta \delta^{18}\text{O}$ (‰) of MD04-2822 event
Rise into Initial MIS 5e highstand	123	129.4 to 128.5	11.55	~0.13	123.8	0.54
Fall to Intermediate lowstand	122.5	128.7 to 125.3	21.12	~ 0.23	121.6	0.63
Rise into Second MIS 5e highstand	121.5	125.3 to 123.9	9.7	~ 0.12	120.7	0.49
Rise into Minor MIS 5e highstand	119.5	120.8 to 120.4	7.6	~ 0.08	118	0.13

§ Assuming 0.011‰m^{-1}

* Age model based upon approach of Shackleton et al (2002, 2003) where mid-point of TII, start and end of the benthic $\delta^{18}\text{O}$ plateau and the mid-point of the MIS 5e/5d transition are assigned the following ages: 132, 128, 116, 115 kyr, derived from fossil coral reef evidence

The MD04-2822 benthic $\delta^{18}\text{O}$ record displays similar features to both these reconstructions (Figure 7.5) and indeed the timing of the $\delta^{18}\text{O}$ variations (age control is achieved via the coral radiometric ages, after Shackleton et al 2002, 2003, see section 1 of this chapter) compares favourably to that of Rohling et al (2008). This is unsurprising as both age models rely upon fitting to fossil coral radiometric ages⁹.

⁹ Rohling et al (2008) rely upon linearly matching the long term inverted U shape of their foraminiferally derived sea level record to the coral record of Thompson and Goldstein (2005); whilst only a very few age control points are used, the tightly constrained stratigraphy produces relative age estimates that are quoted as $\pm 1\text{kyr}$ uncertainty. The sea level record produced by Thompson and Goldstein (2005) has been criticised by some as being 'unlike any geologically derived MIS 5e sea level record' and that their 'corrected' of U/Th ages may be a product of 'systematic diagenetic shift' rather than a temporal correction (Hearty et al 2007a). Whilst the sea level history of MIS 5e derived by Rohling et al (2008) is not connected to the reconstruction of Thompson and Goldstein (2005), it is the basis of their age control.

Hearty et al (2007a) state that one challenge to high amplitude and frequency MIS 5e sea level reconstructions is that ‘such a record is not observed in the benthic $\delta^{18}\text{O}$ record’. By contrast, this study suggests that the benthic $\delta^{18}\text{O}$ record of MD04-2822 does show some degree of high frequency variations during MIS 5e, although some are documented only by a single data point.

Whilst there is a mechanism whereby global sea level change may be ‘imprinted’ upon the benthic $\delta^{18}\text{O}$ record, this is not the only influence upon the $\delta^{18}\text{O}$ signal (e.g. temperature, $\delta^{18}\text{O}$ of seawater) and indeed the relationship between sea level and global ice volumes contains several uncertainties (e.g. determination of exact RSL contribution, local glacio-hydro-isostatic effects, temporal variation of isotopic composition).

In addition, age comparisons between these sea level reconstructions are solely illustrative and the inherently difficult task of age control during this interval for the record is recognised. The age control tie-points used in the MD04-2822 MIS 5e age model (after Shackleton et al 2002, 2003) are derived from fossil reef terraces and the matching to sea level stillstands. The MD04-2822 benthic record is not as high resolution as that of Shackleton et al (2002, 2003), but key features are discernable that allow the transferral of these coral ages. Indeed, reef terraces are thought to be a better measure of sea level stability than sea level change but they are more amenable to dating (Hearty et al 2007b). Whilst controversy still surrounds some U/Th dating of corals (e.g. Thompson and Goldstein 2005), the comparison between the MD04-2822 benthic $\delta^{18}\text{O}$ record and the selected sea level records is sufficient to suggest some contribution of fluctuating global sea levels upon the MD04-2822 benthic $\delta^{18}\text{O}$ record.

These intra-MIS 5e sea level events do not account for the entirety of the $\Delta\delta^{18}\text{O}$ changes recorded at MD04-2822 (Table 7.2). Instead the ‘additional’ $\delta^{18}\text{O}$ observed is attributed to changing $\delta^{18}\text{O}$ characteristics of the water incorporated into deep water during convection. The sea level increases, possibly due to the partial melting of the Greenland Ice Sheet (e.g. Cuffey and Marshall 2000) and associated inputs of low $\delta^{18}\text{O}$ meltwater into high northern latitudes, would have altered the $\delta^{18}\text{O}$ signature of deep waters.

Indeed, for the inferred increases in global sea level, there is a coeval decrease in benthic $\delta^{13}\text{C}$. This might suggest a reduction in AMOC by inputs of large volumes of meltwater into the high northern latitudes, thereby inhibiting convection. Any reduction in the production of NADW would be recorded as a low benthic $\delta^{13}\text{C}$ excursion as the deep water signature of MD04-2822 would be influenced to a greater extent by southern sourced waters (see section 4.3 below) or by incorporation of low $\delta^{13}\text{C}$ meltwater into deep waters.

The age estimates for both data sets (Rohling et al 2008 and this study) do not unequivocally link the fluctuations in the benthic $\delta^{18}\text{O}$ with sea level changes through the MIS 5e plateau; they are however highly suggestive that at least some of the variability within the MD04-2822 $\delta^{18}\text{O}_{Cib}$ is attributable to global changes in sea

level¹⁰. Sea level increases are linked to changes in the position of the polar front in the Arctic (e.g. Rasmussen et al 2003), enabling a warming and reduction in the Greenland Ice Sheet (Otto-Bliesner et al 2006) with some contribution from Antarctica during the last interglacial (e.g. Overpeck et al 2006). Sea level decreases may be a result of increases in high latitude ice volumes; indeed the increased transport of warm waters to high northerly latitudes may have provided a moisture source for ice sheet growth as insolation declined through MIS 5e (McManus et al 2002) and as recorded by IRD inputs to the Nordic, Iceland and Greenland Seas (e.g. Fronval and Jansen 1997) (see chapter 8, *Glacial Inception*, for a full discussion).

4.3. Benthic $\delta^{13}\text{C}$ changes: reflections on changes to AMOC through the last interglacial

At present, the MD04-2822 core site is bathed predominately by NADW originating in the Nordic Seas, with some degree of mixing with southern sourced waters in the lower depths of the Rockall Trough. For the last interglacial period, an offset is evident between the co-registered benthic $\delta^{13}\text{C}$ and $\delta^{18}\text{O}$ records. The transition to well ventilated (i.e. high $\delta^{13}\text{C}$ values), similar to modern conditions in the Rockall Trough, does not occur until after the transition to interglacial benthic $\delta^{18}\text{O}$ values i.e. there is a decoupling of the benthic $\delta^{13}\text{C}$ and $\delta^{18}\text{O}$ signals.

Glacial values of $\delta^{13}\text{C}$ (~ 0 to 0.2 ‰) are experienced at the site within the benthic $\delta^{18}\text{O}$ plateau, with ‘improvement’ in the benthic $\delta^{13}\text{C}$ signal occurring only as the $\delta^{18}\text{O}$ isotopic minima is reached (Figure 7.1, Figure 7.5). This suggests subtly differing global versus local influences upon these proxies, with the benthic $\delta^{18}\text{O}$ dominated by global changes in ice volumes with some degree of local ‘overprinting’ (see sections 4.1, 4.2 of this chapter), whilst the MD04-2822 $\delta^{13}\text{C}$ represents variations in NADW formation and outflow from the Nordic Seas across the Wyville-Thomson Ridge. Benthic $\delta^{13}\text{C}$ is a well established proxy for monitoring variations in AMOC and NADW formation (e.g. Keigwin et al 1994) and the MD04-2822 core site is well placed to capture variations through this interval.

The decoupling of the benthic $\delta^{18}\text{O}$ and $\delta^{13}\text{C}$ records may be due to large inputs of meltwater into the Nordic Seas with decreasing global ice volumes, preventing convection of deep water as surface waters become significantly less dense. Overflow of NADW into the Rockall Trough continues to be suppressed despite the minima in global ice volumes. Indeed surface water amelioration at the MD04-2822 site (as

¹⁰ The sea level data set of Rohling (2009), which incorporates data from Rohling et al (2008), is tuned to Antarctic CO₂ concentrations (a proxy for global temperature changes) on the EDC 3 timescale in an approach similar to that undertaken for the portion of the MD04-2822 record older than Termination II (see chapter 3). However, the authors recognise the relatively imprecise nature of their age model. The tuning of the MD04-2822 surface proxies to this global temperature record is not undertaken for the last interglacial period as, unlike the Red Sea data, the MD04-2822 surface proxy data are highly sensitive to the disintegration of proximal ice sheets and the incorporation of large volumes of meltwater at high latitudes. This results in a damping of the changes caused by global temperature increases and a decoupling of the surface and deep water proxies at the MD04-2822 core site. Instead, the comparison between the MD04-2822 age model (after Shackleton et al 2002, 2003) and that of Rohling et al (2008), is thought sufficient to hint at the association of fluctuating sea levels through MIS 5e without the need for precise and absolute age control.

reflected in low percentages of *N. pachyderma* (sinistral)) is also seen after the benthic $\delta^{18}\text{O}$ minima (Figure 7.1, Figure 7.5).

Several marine sediment cores within the North Atlantic display low benthic $\delta^{13}\text{C}$ through Termination II, which in some cores extends into MIS 5e (Hodell et al 2009, Oppo et al 1997, 2001, 2006, Skinner and Shackleton 2006, Lototskaya and Ganssen 1999, Adkins et al 1997, Oppo and Lehman 1993, Zahn et al 1987). Skinner and Shackleton (2006) comment upon the 'drawn out appearance' of the deglaciation, where the benthic $\delta^{13}\text{C}$ lags the 'sharper' changes in benthic $\delta^{18}\text{O}$. Indeed, within the Rockall Trough (ODP 982, 57°30.8'N, 15°52.5'W; 1145m), low benthic $\delta^{13}\text{C}$ values are a common feature of late Pleistocene glaciations, including Termination II, where low values extend into MIS 5e (Venz et al 1999).

A change in deepwater formation regime has been invoked to explain this feature of many North Atlantic records: GNAIW ceased during Termination II with intermediate depths (~1,500 to 2,000 m) bathed in low $\delta^{13}\text{C}$ water mass of either a southern source (e.g. Hodell et al 2009) or Nordic Seas origin (Oppo et al 1997, Bauch et al 2000, Raymo et al 2004). Hodell et al (2009) suggest that reduced contributions of GNAIW, Labrador Sea Water (LSW) and Mediterranean Overflow Water (MOW) during Termination II and early in MIS 5 would have allowed a greater penetration of waters from the Southern Ocean into the North Atlantic (although ISOW is inferred to have formed within both Termination II and early MIS 5e). Enhanced penetration into the North Atlantic (to ~ 60 °N) of Antarctic Intermediate Water (AAIW) was inferred by Rickaby and Elderfield (2005) for the last deglaciation; these authors propose greater volumetric inputs of AAIW during the past than at present. Alternatively, the low $\delta^{13}\text{C}$ signal within Norwegian Seas cores during Termination II and into MIS 5e (e.g. Bauch et al 2000, Fronval and Jansen 1999, Oppo and Lehman 1995, Duplessy and Shackleton 1985) and the relatively infrequent incidence of high $\delta^{13}\text{C}$ values within the Nordic Seas¹¹ (Raymo et al 2004) could suggest a Nordic Seas origin for these low $\delta^{13}\text{C}$ waters (possibly formed through brine rejection under sea ice e.g. Dokken and Jansen 1999, Bauch et al 2000).

Several core sites within the Atlantic document variations in the convective intensity of the Nordic Seas during the interglacial: the Blake and Bahama Ridges (although at relatively low resolution) display variations in the Deep Western Boundary Current during MIS 5e attributed to small changes in the convective activity of the Nordic Seas, possibly due to changes in insolation affecting the latitudinal SST and salinity gradients in the North Atlantic (Bianchi et al 2001); weak thermohaline activity during early MIS 5e in the North Atlantic is also inferred by Cortijo et al (1999). Hodell et al (2009) propose a surface-deep water connection to explain the persistence of low $\delta^{13}\text{C}$ waters in the North Atlantic despite reduced global ice volumes and increased insolation.

The low benthic $\delta^{13}\text{C}$ and decreased current speeds recorded at the Gardar Drift (U1304 and NEAP18K) (Hodell et al 2009, Hall et al 1998, Chapman and Shackleton 1999) occur in conjunction with a minima in planktonic $\delta^{18}\text{O}$ suggesting a warming

¹¹ Raymo et al (2004) demonstrate that high benthic $\delta^{13}\text{C}$ values occur in the Nordic Seas only during 'extreme interglacials of the Late Pleistocene' and are relatively uncommon in the past.

and/or a reduction in salinity at these sites. This is coincident with increased Northern Hemisphere summer insolation, which is thought to have prompted a melting of continental ice. This increased input of freshwater (e.g. from melting of the Greenland Ice Sheet¹²) into the Nordic Seas thereby reduced the strength or density of outflow from the Nordic Seas and enabled an increased influence of southern sourced waters at intermediate depths. At the MD04-2822 core site, a reduction in benthic $\delta^{13}\text{C}$ is seen for each of the sea level rises documented with the fossil record (see section 4.2, this chapter) with a subsequent recovery in $\delta^{13}\text{C}$ values (i.e. increased deep convection). Thus at the MD04-2822 core site, the bottom waters may have been influenced to a greater degree by bottom waters derived in part from Antarctica (AABW)¹³. Melting of continental ice during the early portion of the last interglacial has been inferred from lower and more variable salinities off southern Greenland (de Vernal and Hillaire-Marcel 2008) as well as significant freshwater and IRD inputs within the Norwegian Seas (Bauch and Erlenkeuser 2008, van Nieuwenhove et al 2008).

An estimated 3.4 m sea level rise is attributed to melting in the Arctic during the initial stages of the interglacial (Greenland Ice Sheet and western Arctic icefields over ~3 kyr) by Otto-Bliesner et al (2006), translates to a freshwater forcing of the Atlantic of ~ 0.013 Sverdrup. In their model simulation, 1 Sv was added to a present Atlantic ocean over a period of 100 years; such injections of freshwater resulted in a reduction of 25 % in AMOC and a cooling of 1 to 2 °C over much of the Atlantic.

Surface cooling (of ~ 1.5 to 1.7 °C) and inferred reduction in AMOC (i.e. benthic $\delta^{13}\text{C}$ changes of ~ 0.29 and 0.14 ‰) are recorded at the MD04-2822 record for the two main inferred sea level highstands (Rohling et al 2008, 2009) and the postulated third highstand at the end of the interglacial (Figure 7.5). This is consistent with proposed AMOC and temperature decreases following injections of freshwater into the North Atlantic (Otto-Bliesner et al 2006). The reduction in $\delta^{13}\text{C}$ values is less for sea level changes associated with the second highstand of Rohling et al (2008, 2009), in accordance with the inferred lower absolute rise in sea level, but it is accompanied by a greater reduction in surface temperatures at the MD04-2822 core site. Whilst benthic $\delta^{13}\text{C}$ and SSTs are not expected to vary coevally (the former is a reflection of NADW formation in the Nordic Sea, whilst the latter is specific to the MD04-2822 core site) they are linked via AMOC and the advection of warm, saline waters over the MD04-2822 site into the Nordic Sea, where heat is lost to the atmosphere and water sinks to the deep ocean before spilling over into the deep Atlantic Ocean.

Low $\delta^{13}\text{C}$ conditions prevailed in the North Atlantic until a strengthened/more dense Iceland-Scotland Overflow Water (ISOW) was able to displace it later within MIS 5e; increased benthic $\delta^{13}\text{C}$ and current velocity at the Gardar Drift as well as more stable and increased salinities south of Greenland (Hillaire-Marcel et al 2001, de Vernal and

¹² The Greenland Ice Sheet is thought to be particularly sensitive to warm, early summer conditions and is likely to have a negative mass balance at the beginning of the last interglacial (Otto-Bliesner et al 2006).

¹³ The contribution of low $\delta^{13}\text{C}$ due brine formation is considered to be minimal for the interglacial; enhanced seasonal sea ice melting due to increased insolation and minimum LIG Arctic sea ice is modelled at 50 % less than present with a 50% summer coverage occurring only poleward of 80 °N (Otto-Bliesner et al 2006, supplementary data).

Hillaire-Marcel 2008) are thought to reflect the penetration of ISOW to depth > 3 km in the latter stages of MIS 5e (Hodell et al 2009). At MD04-2822 a large decrease in $\delta^{13}\text{C}$ at 2520.35 cm is coeval with a reduction in benthic $\delta^{18}\text{O}$ of ~ 0.2 ‰ at the end of the MIS 5e benthic $\delta^{18}\text{O}$ plateau. The cause of this reduction remains elusive (obscured in part due to a decrease in the resolution of the benthic record) although this decrease in benthic $\delta^{13}\text{C}$ is suggestive of greater influence of southern sourced waters in the Rockall Trough, or the incorporation of low $\delta^{13}\text{C}$ meltwater into the deep North Atlantic. This $\delta^{13}\text{C}$ decrease is co-incident with a slight increase in the concentration of IRD deposited at the site. As such, this event is tentatively correlated with C27 (Figure 7.5). This event marks the end of the benthic $\delta^{18}\text{O}$ plateau at ODP 980 (Feni Drift, Rockall Trough) and is a regional cooling event (Chapman and Shackleton 1998, 1999). The first significant input of IRD into the Norwegian Sea is tentatively correlated to C27 by Oppo et al (2006) and is thought to reflect the growth of tidewater glaciers (for a full discussion of the North Atlantic C events, the reader is directed to chapter 8, *Glacial Inception*).

Towards the end of the MIS 5e plateau (ca. 117 kyr), a decrease in salinities is documented for southern Greenland (de Vernal and Hillaire-Marcel 2008) as well as decreased current speeds and benthic $\delta^{13}\text{C}$ (with lowest values near the MIS 5e/d transition) which imply a reduction in ISOW and lowered surface salinities in the Labrador, Irminger and Nordic Seas (Hodell et al 2009). Other studies also document a brief but pronounced decrease in NADW formation at the end of MIS 5e (Adkins et al 1997, Lehman et al 2002). In contrast, enhanced NADW formation has been reconstructed for ODP 980 (McManus et al 2002), with enhanced AMOC implicated as a potential moisture source for glacial inception. At MD04-2822 benthic $\delta^{13}\text{C}$ values continue to increase throughout MIS 5, with peak values occurring within MIS 5c (Figure 7.5) (see chapter 8, *Glacial Inception*, for a full consideration of the C events).

4.4. Surface Conditions

Surface conditions at the MD04-2822 core site lagged the global changes in ice volumes. The increased insolation that initiated the demise of the penultimate glaciation and the input of large volumes of meltwater, especially at high latitudes, acted to dampen the surface water response, thereby producing an offset in the benthic $\delta^{18}\text{O}$ and $\delta^{13}\text{C}$ ratios, as well as the surface and deep water proxy records. This lag in surface ocean response to the benthic $\delta^{18}\text{O}$ change has also been documented in the Nordic Seas (e.g. Bauch and Erlenkeuser 2008) and the wider North Atlantic (e.g. Hodell et al 2009). The offset in benthic ratios may be associated with a lag in the initiation of AMOC and deep convection within the Nordic Seas, due to large influxes in meltwater at high latitudes derived from an initial MIS 5e sea level rise (as discussed previously).

4.4.1. *Early MIS 5e (Termination II):*

The polar front migrated to the north of the MD04-2822 core site (low % *N. pachyderma* (sinistral)) only after the benthic $\delta^{18}\text{O}$ minima has been attained i.e. after the MIS 5e global ice volume minima has been attained (Figure 7.2, Figure 7.5).

The position of the polar front oscillated across the MD04-2822 core location throughout the initial stages of MIS 5e; three episodes of increased % *N. pachyderma*

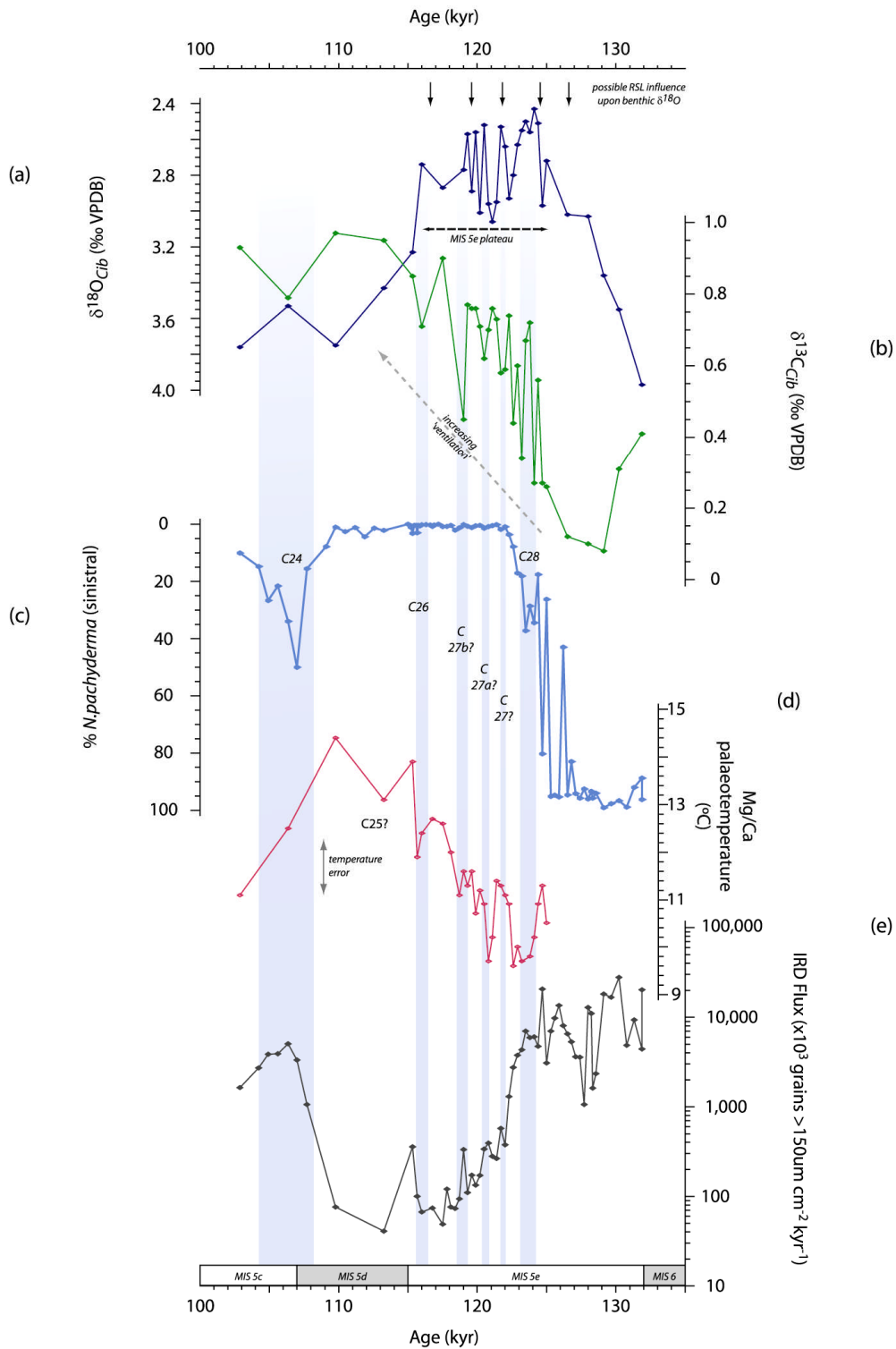
(sinistral) can be distinguished, each of which is associated with an increase in IRD concentration¹⁴ (Figure 7.6). The middle of the three (~ 2558.5 cm), whilst only captured by a single data point, does coincide with the maximum IRD concentration of the interval studied in this chapter. The last of the three ‘reversals’ appears to be of longest duration, with *N. pachyderma* (sinistral) values of ~ 25 % and is coincident with the attainment of the benthic isotopic minima. This cold SST event is correlated with the late deglacial oscillation C28 (cf. Oppo et al 1999, 2006) (Figure 7.6). As discussed in section 4.2 (of this chapter), this feature in the benthic record may be associated with a sea level rise and an initial MIS 5e highstand (e.g. Shackleton et al 2002, Rohling et al 2008).

On the basis of the forgoing, the following description of the first SST cooling event is proposed. The input of large volumes of meltwater into the North Atlantic dampened surface response to climate warming and reduced AMOC, thereby reducing the advection of warm, saline waters to high latitudes. The initial warming prior to C28 is accompanied by a reduction in the $\delta^{18}\text{O}$ of surface waters consistent with a ‘freshening’ (i.e. reduction in salinity), possibly in response to the input of large volumes of meltwater associated with the ~ 11.5 m increase in global sea levels (Rohling et al 2008, 2009) and/or the final destabilisation of the Saalian BIS. After C28, AMOC ‘strengthens’ thereby enabling SST and surface salinities to increase at the MD04-2822 site. An approximate warming of 2 °C out of C28 is consistent with that estimated by Oppo et al (2006) for core ODP 980 (Feni Drift, Rockall Trough). The low planktonic $\delta^{18}\text{O}$ during C28 (Figure 7.2) suggests the incorporation of local meltwaters from the decay of the penultimate BIS (Termination II and the BIS is considered in more detail in chapter 6).

¹⁴ IRD concentration records may be difficult to interpret for locations proximal to former ice sheets; often the IRD concentration signal may be distorted due to varying inputs of fine grained terrigenous material. IRD flux circumvents this problem to a degree but assumptions regarding sedimentation rates are implicit in its calculation. For simplicity, the proxies are shown on their depth scale in order to facilitate unambiguous phase relationships being discerned. The reader is directed to chapter 6 for a more full consideration of the IRD signal through Termination II.

CHAPTER 7:
Surface and Deep Water Hydrography during the Last Interglacial

Figure 7.6: MD04-2822 proxy record on age (*note* age control was achieved via the transfer of radiometric coral ages for sea level stillstands after Shackleton et al (2002, 2003) – please see section 1, this chapter, for further details. (a) benthic $\delta^{18}\text{O}$; (b) benthic $\delta^{13}\text{C}$; (c) % *N. pachyderma* (sinistral) with tentative correlations to the C events (Chapman and Shackleton 1998, 1999, McManus et al 2002, Oppo et al 2006) labelled and highlighted by vertical blue shaded bars; (d) SST derived from Mg/Ca analysis; and (e) IRD flux on a logarithmic scale.



4.4.2. *Surface water conditions - the N. pachyderma (sinistral) plateau*

Minimum percentages of *N. pachyderma* (sinistral) begin to be recorded only at depths less than ~2540.5 cm. Within the % *N. pachyderma* (sinistral) plateau, three additional episodes of surface cooling (~1 °C) are discernable in the Mg/Ca palaeotemperature estimates (against a background of warming through MIS 5e) (Figure 7.6). The relative insensitivity of the % *N. pachyderma* (sinistral) to changes in temperature at very low percentages should be remembered. Maximum surface temperatures are attained at the MD04-2822 site during MIS 5d; renewed warming of surface waters is also seen in the Vøring Plateau and the Fram Strait late in MIS 5e¹⁵ as Northern Hemisphere summer insolation approached its minima. Prevailing strong westerly winds may have provided enhanced warm water transport to the Arctic (Risebrobakken et al 2007) with a possible increase in Ekman transport into the Barents Sea, as a consequence of the increased westerly airflow. This effect is currently observed in the Barents Sea (Dickson et al 2000, Leong et al 1997) and is also suggested by the modelling study of Risebrobakken et al (2007).

The intra MIS 5e cooling events outlined by Oppo et al (2006) are also recorded as minor SST cooling events within the Mg/Ca record of MD04-2822 (Figure 7.6): C28 (~ 1.5 °C); a series of SST oscillations associated with the C27 events (the precise correlation of C27, C27a and C27b is unclear in the MD04-2822 record); ~ 2 °C warming out of C26; and an ~ 1 °C warming out of C25 (although the approximate error of ± 1 °C associated with Mg/Ca palaeotemperature method urges caution in the interpretation of this data). These oscillations are superimposed upon a general warming trend of ~ 4 °C through the % *N. pachyderma* (sinistral) plateau (the relatively large ~1 °C error associated with Mg/Ca palaeotemperature reconstructions should be remembered). The last of these events (C25) is outside the MIS 5e benthic δ¹⁸O plateau and whilst a muted (if any) SST changes is seen at the MD04-2822 site, this event represents the first widespread, substantial cooling of the wider North Atlantic (Chapman and Shackleton 1999). Chapter 8 (*Glacial Inception*) considers the North Atlantic C events in more detail.

Early in MIS 5e and within the Nordic Seas, sea surface warming at sites to the north of the Iceland-Scotland Ridge was delayed by ~ 3 kyr, when compared to a core located to the south. A temperature difference of at least 8 °C is inferred (Rasmussen et al 1999, 2003). Commensurate with SST warming to the south of the ridge, deep convection started in the Nordic Seas. Enhanced polar water influence is inferred for the initial phase of MIS 5e and the Iceland-Scotland Ridge is thought to mark the approximate position of the polar front. The strong east-west temperature gradient for this interval was caused by the spreading of meltwater in the western Atlantic whilst a narrow corridor of warm Atlantic waters penetrated into the Nordic Seas (Fronval and Jansen 1997, Fronval et al 1998, Rasmussen et al 2003).

¹⁵ NB age control for the Vøring Plateau and Fram Strait cores is based upon *planktonic* δ¹⁸O. At these high latitudes an offset in the planktonic and benthic δ¹⁸O signals would be expected due to the input of large volumes of meltwater (see section 4.1, this chapter). This effect would be most noticeable during the initial stages of MIS 5; nonetheless the conclusions of Risebrobakken et al (2007) are thought reasonable.

4.4.3. *Comparison to other North Atlantic Records:*

The long term SST warming and increase in surface $\delta^{18}\text{O}$ (inferred increasing surface salinities) in conjunction with a long-term increase in benthic $\delta^{13}\text{C}$ is suggestive of increased NAC influence at the MD04-2822 site. The data could also suggest an increase advection of warm, saline waters into the Nordic Sea enabled deep convection and the production of NADW, which bathed the MD04-2822 site. A similar long-term warming trend through MIS 5e is also seen at core K708-1 (50.0 °N, 23.44 °W, 4053 m) (Imbrie et al 1992). The MD04-2822 increasing temperature profile is more closely allied with the proposition of Risebrobakken et al (2007) of continued warmth at the end of MIS 5e.

This pattern of surface water temperature change (i.e. a warming through MIS 5e with maximum SSTs at the MIS 5e/d transition) does not appear to be replicated in other cores in the North Atlantic. For example, Cortijo et al (1999) in their study of eight cores from the North Atlantic note differing sea surface responses at high and low latitude sites during the MIS 5e benthic plateau: high latitude sites (72 to 52 °N) display a gradual decrease in SSTs and salinities during MIS 5e whilst low latitude sites (41 to 31 °N), SSTs and salinities were stable or increased during the interval i.e. meridional gradients in temperature and salinity increased as the last interglacial progressed. The MD04-2822 surface proxies might therefore be expected to follow the gradual cooling trend of the high latitude sites of Cortijo et al (1999). Counter-intuitively however, the Mg/Ca palaeotemperature record and surface water $\delta^{18}\text{O}$ of MD04-2822 most closely resembles that of the mid latitude sites CH69-K9 (41 °N, 47 °W) or SU90-03 (40 ° 30'N, 32 °03'W) of the Cortijo et al (1999) study; despite very low *N. pachyderma* (sinistral) percentages at the MD04-2822 site. The connection to lower latitudes may be due, in part, to the location of MD04-2822 within an 'arterial' route of NAC and thus the *G. bulloides* record may reflect the advection of this warmer water to the Nordic Seas.

Müller and Kukla (2004) also propose a declining influence of NAC upon high latitude marine cores (~ 73 to 66 °N, Nordic Seas) as the last interglacial progressed with vegetation changes in Northern Europe related to the changes in surface hydrography of the North Atlantic. However, the authors rely upon the percentage abundance of *N. pachyderma* (sinistral), which may not accurately capture all variations in SSTs at very low percentage abundances. Percentage *N. pachyderma* (sinistral) records do however offer clues as to the position of the polar front. Event C26, on the MIS 5e/d boundary, is thought by these authors to reflect a change in circulation, with NAC no longer penetrating into the Nordic Seas and a decline in NADW production, as recorded at the Bermuda rise (Lehman et al 2002), which brought about the end of high latitude warmth.

The XRF calcium record for MD04-2822, primarily governed by surface productivity, broadly follows this pattern for the demise of 'peak' interglacial conditions; an abrupt cooling (correlated to C26) brings about the end of high Ca values associated with the latter portion of MIS 5e at this site¹⁶. One possibility for this unexpected result is that the long term surface water temperature increases seen at MD04-2822 may be reflecting Müller and Kukla's (2004) proposed relocation of the NAC. The polar front

¹⁶ A 'climatic optimum' is difficult to resolve for this core based upon the available surface proxies.

remains to the north of the core site but the steepening thermal and salinity gradients at the demise of the last interglacial, in conjunction with continuing NAC, brought warmth and increased salinities to the MD04-2822 site. Whilst Müller and Kukla (2004) suggest that there was little penetration of the NAC into the Nordic Seas, the benthic $\delta^{13}\text{C}$ record for MD04-2822 continues to increase into MIS 5d, suggesting that whilst NADW water production varied through MIS 5e, deep convection was still taking place.

The neighbouring core, ODP 980 (Feni Drift) located to the west of MD04-2822, closely resembles the % *N. pachyderma* (sinistral) and benthic $\delta^{13}\text{C}$ profiles of MD04-2822, but displays the opposite trends in surface temperatures and salinities to MD04-2822 i.e. there is a general decline in SSTs at the ODP 980 site as MIS 5e progresses (Oppo et al 2006, Stolz and Baumann *in press*). This would accord with the suggestion of decreased penetration of the NAC to high latitudes (e.g. Cortijo et al 1999).

The benthic $\delta^{18}\text{O}$ and $\delta^{13}\text{C}$ records are consistent between the two cores and when placed upon the same age scale¹⁷, show remarkable similarities (Figure 7.7). These two cores should record variations in NADW (and intermediate water) outflow from the Nordic Seas and are presently bathed by the same deep water mass emanating from the Nordic Sea (e.g. Hansen and Østerhus 2000). Both records show a general increase in benthic $\delta^{13}\text{C}$ values, with low $\delta^{13}\text{C}$ events superimposed. This would point to continued deep water formation in the Nordic Seas throughout the interglacial and into MIS 5d with episodic low $\delta^{13}\text{C}$ events (McManus et al 2002, Oppo et al 2006). Both cores exhibit decoupled benthic $\delta^{18}\text{O}$ and $\delta^{13}\text{C}$ signals; the $\delta^{13}\text{C}$ signal lags that of $\delta^{18}\text{O}$. Similarly in both cores, the transition to low percentages of *N. pachyderma* (sinistral) is delayed with respect to the benthic $\delta^{18}\text{O}$. ODP 980 suggests decreasing SSTs through the last interglacial whereas MD04-2822 displays an increase in SSTs through this interval. However, the palaeotemperature record of MD04-2822 is based upon Mg/Ca and major shifts in oceanic conditions, such as those associated with a change from glacial to interglacial conditions, may have altered the seasonal preference of *G. bulloides* (e.g. Ganssen and Kroon 2000; at present, seasonal peak abundance is during the spring in NE Atlantic, Bauch and Kandiano 2007). If peak abundance altered to summertime during glacial inception, this change could account for the SST and isotopic variations recorded at MD04-2822.

Despite seemingly opposing SST records, the cooling events (C28 to C26) are recognisable in both cores, although the magnitude of change appears to be muted at MD04-2822. Of note however, is the differing position of C28 in the cores; the C28 cooling event (and associated benthic $\delta^{13}\text{C}$ minima) occurs much later in the MD04-2822 record¹⁸. C28 in MD04-2822 is associated with a large increase in IRD flux

¹⁷ Following the approach outlined in section 1 of this chapter i.e. using radiometrically determined coral ages for the start and end of the MIS 5e plateau (see Shackleton et al 2002, 2003) of 128 and 116 kyr respectively.

¹⁸ There are very few age control points used in the age models for these cores. The apparent age difference between the events however, appears not to be an artefact of the assumption of linear sedimentation between tie-points; the benthic $\delta^{13}\text{C}$ of both cores are similar but there are differences in the % *N. pachyderma* (sinistral).

which occurs at the start of the benthic $\delta^{18}\text{O}$ plateau¹⁹ (Figure 7.9). A similar feature has been recorded at two cores in the Labrador Sea (EW9302-2JPC, 48°47.70' N, 45°05.09' W, 1251 m and EW9302-1JPC, 49°14.30' N, 45°05.34' W, 2527 m; Rasmussen et al 2003b) and is attributed to the late deglaciation of the Laurentide ice sheet or a pro-glacial lake outburst. Also striking is that the discrepancy in the placement of C28 between MD04-2822 and ODP 980 is not recorded for event C26 (the C27 events of Oppo et al 2006 are difficult to unravel in MD04-2822 but the concomitant benthic $\delta^{13}\text{C}$ reductions of these events may be discerned).

MD04-2822 is further to the north than ODP 980 (the cores are ~ 240 km apart). One possibility that could account for the discrepancy between the timing of C28 within the cores is that the polar front migrated to the north of the ODP 980 site earlier than the MD04-2822 and that at the latter there was a greater influence of polar waters, possibly connected to the initial MIS 5e global sea level highstand (e.g. Rasmussen et al 2003). In addition, MD04-2822 is closer to the continental margin and therefore more proximal to the penultimate BIS. Any meltwater inputs associated with the decay of the Saalian BIS would be more likely recorded in MD04-2822 than the more open ocean site of ODP 980. Subsequent to the C28 cooling event, the polar front migrated to the north of both sites and low percentages of *N. pachyderma* (sinistral) are recorded.

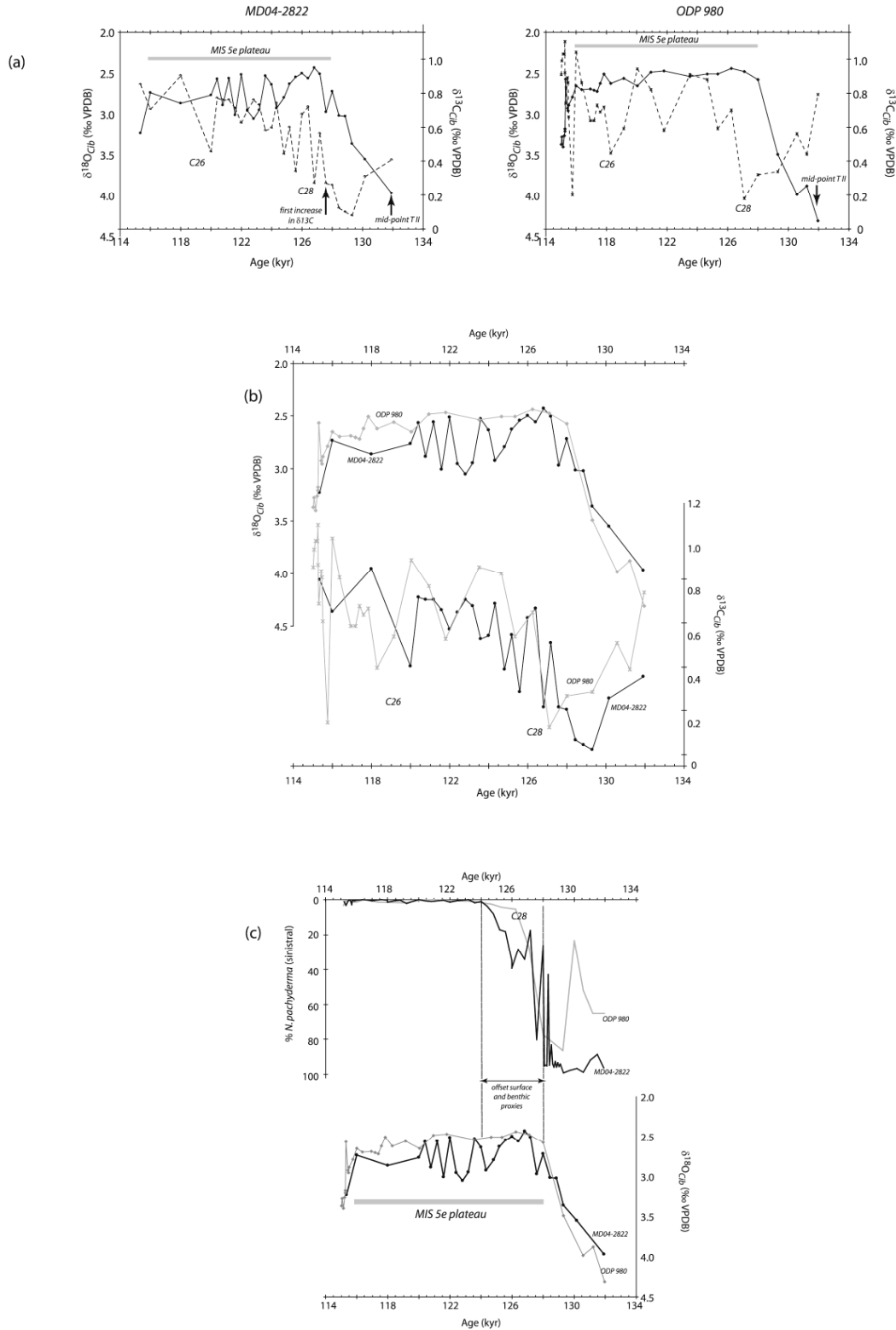
A greater influence of any large meltwater inputs at higher latitudes, and mixing of these waters with the surface waters over the MD04-2822 core site, may also account for the more muted temperature changes experienced at the site compared to ODP 980. Indeed, a greater than present influence of polar waters in the Nordic Seas during the initial stages of MIS 5e (Rasmussen et al 2003)²⁰ and early MIS 5e diatom peaks in cores ENAM33 (Witak and Kuijpers 2001) and MD95-2009 (Rasmussen et al 1999), either side of the Faeroe-Shetland Ridge, suggest just such a frontal zone where surface water mixing is intensive. Similarly, the occurrence of *G. quinqueloba*, associated with sharp surface water gradients²¹, is documented early in MIS 5e (Cortijo et al 1997) within cores in the subpolar Atlantic (south of Iceland) and hints that the position of a region of increased mixing of polar and subpolar waters was to the south of its present position, with a greater temperature gradient between the polar and subpolar Atlantic (Bauch et al 1999).

¹⁹ The benthic $\delta^{18}\text{O}$ plateau is associated with oscillations in global sea level of approximately ± 10 m (e.g. Overpeck et al 2006, Otto-Bliesner et al 2006, Rohling et al 2008); the significance of this high IRD input and association with global sea levels remains uncertain. Provenance of IRD remains undetermined; due to the relatively small size of the BIS and its maritime position, an early decay of this ice sheet might be expected.

²⁰ *NB* age control is based upon planktonic $\delta^{18}\text{O}$ and an offset between benthic and planktonic $\delta^{18}\text{O}$ would be expected for cores at this latitude.

²¹ Enhanced abundances of *G. quinqueloba* are found in modern waters proximal to the Arctic Front in the Norwegian, Greenland and Icelandic Seas (Johannessen et al 1994) and are an indicator of the past position of the Arctic Front (e.g. Fronval et al 1998). This may however, be an over-simplification (Bauch and Erlenkeuser 2008).

Figure 7.7: Comparison of benthic and surface proxies between MD04-2822 (2,344 m water depth) and ODP 980 (2,179 m water depth) (data McManus et al 1999, 2002, Oppo et al 2001, 2003 – note the Oppo et al 2006 data is currently unavailable) on the same age model (see section 1, this chapter). (a) benthic $\delta^{18}\text{O}$ (solid black line) and benthic $\delta^{13}\text{C}$ (dashed line) for both cores; (b) The same data plotted together: MD04-2822 (black line), ODP 980 (grey line); and (c) % *N. pachyderma* (sinistral) and benthic $\delta^{18}\text{O}$ for both cores: MD04-2822 (black line), ODP 980 (grey line).



It is proposed that whilst both ODP 980 and MD04-2822 are within the general flow of warm waters advected northwards (i.e. NAC), the influence of these waters was less during the initial phases of MIS 5e at the MD04-2822 site, due to increased mixing with polar waters (i.e. MD04-2822 was more proximal to this zone of mixing than the more southerly ODP 980); or due to increased local freshwater inputs (i.e. from the decay of the penultimate BIS). The SSTs recorded at the MD04-2822 site are therefore muted compared to the ODP 980, giving rise to the differing surface temperature and $\delta^{18}\text{O}$ records. The SST estimated at the end of MIS 5e is very similar for both (and to the present, Levitus 1982), at $\sim 14^\circ\text{C}$ (Cortijo et al 1999, Oppo et al 2006). As the interglacial progressed, NAC dominated surface water conditions at the MD04-2822 site as well as at ODP 980.

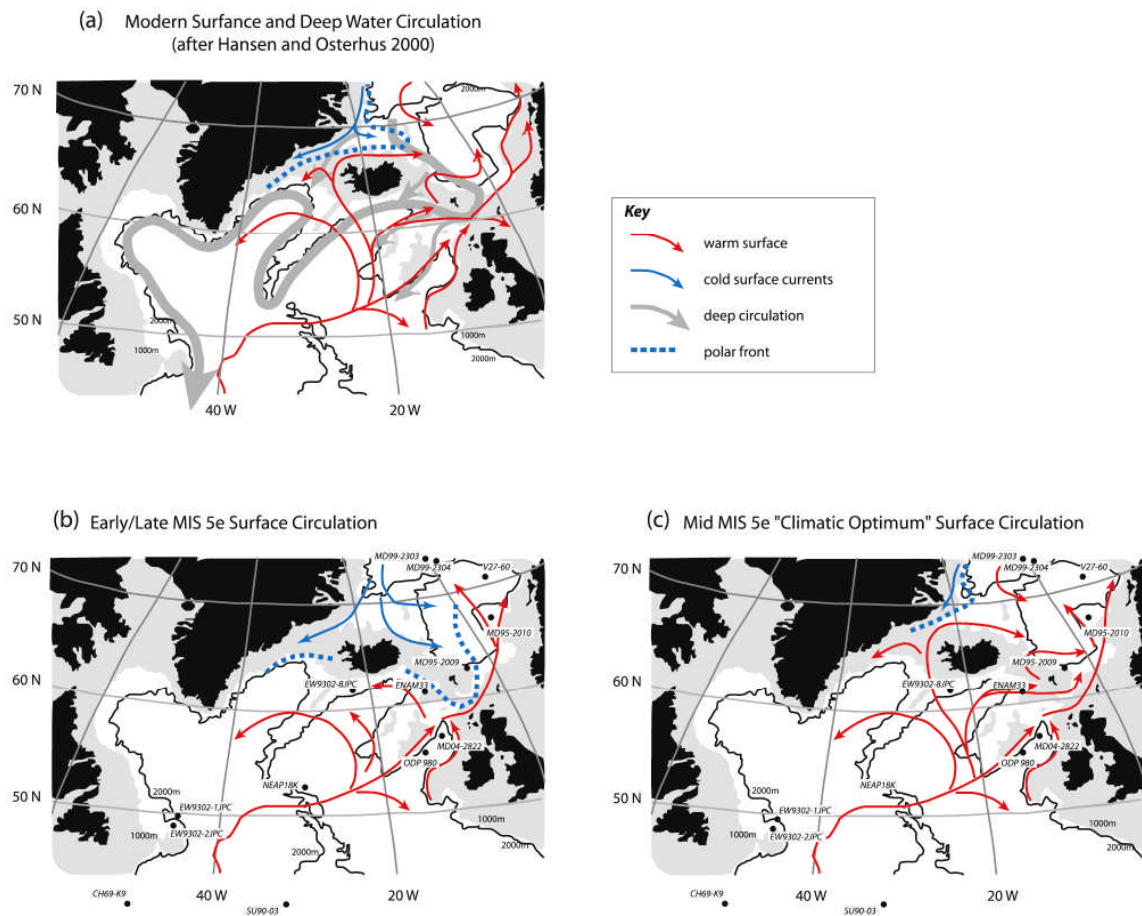
NADW formation, suggested by generally high benthic $\delta^{13}\text{C}$ values at both sites, would imply continued NAC penetration into the Nordic Seas. A stable outflow of Norwegian Sea Overflow Water (NSOW) has been documented during the last interglacial (~ 10 to 12 kyr) by Rasmussen et al (1999) based upon the benthic fauna of SE Norwegian Sea core; outflow only ceased at ca. 106 kyr during the latter stages of MIS 5d.

4.4.4. *Reconciling the Surface Hydrology of the Last Interglacial:*

The apparently contradictory proposals regarding the penetration of NAC to high latitudes during MIS 5e may be partially resolved by consideration of the modern circulation patterns of the North Atlantic, and the geographic positions of the cores studied (i.e. those detailed in: Chapman and Shackleton 1999, Cortijo et al 1999, McManus et al 1994, 2002, Müller and Kukla 2002, Oppo et al 1997, 2001, 2006, Risebrobakken et al 2007) (Figure 7.8). MD04-2822 is one of the more easterly cores of those detailed above and proximal to a former ice sheet. An initial restricted influx of warm waters into the Nordic Sea is clear from the % *N. pachyderma* (sinistral) records of these sites (e.g. Cortijo et al 1999) consistent with a more easterly position of the polar front, with large inputs of meltwater into the high latitudes. This would account for the decoupling of the surface and benthic $\delta^{18}\text{O}$ records seen at the more northerly latitudes. However, the 'climatic optimum' saw a retreat of the polar front to the west (e.g. Rasmussen et al 2003), facilitating the partial melting of the Greenland Ice Sheet and enhanced warm water transport in much of the Nordic and Greenland Seas.

A proposed decline in the penetration of NAC waters into high latitudes towards the end of the last interglacial may be inferred from decreases in the % *N. pachyderma* (sinistral), especially at the most westerly of the northern cores (e.g. Müller and Kukla 2004), and suggests a return of the polar front to a more easterly position. Where data is available, the benthic $\delta^{13}\text{C}$ records for cores throughout the North Atlantic display a general increasing trend into MIS 5d from MIS 6, strongly suggestive that deep water convection continued throughout the interglacial.

Figure 7.8: North Atlantic surface circulation. (a) modern circulation (modern hydrography after Hansen and Østerhaus 2000); (b) reconstructed surface circulation for the early and late MIS 5e (after Rasmussen et al 2003 and this study); (c) 'climatic optimum' surface circulation (after Rasmussen et al 2003 and this study).



The opposite view of continued NAC penetration at the end of the last interglacial (e.g. Risebrobakken et al 2007), as well as the apparently divergent views of AMOC drawn from *N. pachyderma* (sinistral) and benthic $\delta^{13}\text{C}$ records, may be reconciled if warm water inflow was highly restricted and limited to inflow to the eastern Nordic Sea (i.e. if the flow were confined to the Faeroe-Shetland Channel).

Warm water penetration initially occurred only within the eastern Norwegian Sea in early MIS 5e (Figure 7.8) (Fronval and Jansen 1997, Fronval et al 1998, Rasmussen et al 2003). Such a restricted inflow of warm waters may also account for the observed lower SSTs early in MIS 5e compared to mid-MIS 5e, for more northerly Atlantic core sites (Oppo et al 2001, 2006, Cortijo et al 1999). Changes in the latitudinal insolation anomalies through MIS 5e prompted greater summer warmth at lower latitudes and increased thermal gradients between the wider North Atlantic and the Nordic Seas.

The progressive decreases in % *N. pachyderma* (sinistral) within high latitude records during the last interglacial may be accounted for by a migration of the polar front eastwards, post the MIS 5e 'climatic optimum'. It is proposed that only a narrow 'corridor' of warm water was able to penetrate to high latitudes at the demise of MIS 5e. This influx of warm, dense water was sufficient to facilitate the continued production of deep water in the Nordic Seas. As this warm, dense water is confined to the eastern Nordic Seas, a decline in deep water production is conceivable in the Labrador Sea (Hillaire-Marcel et al 2001) and which would account for the apparent decreased NADW bathing the Bermuda Rise (Lehman et al 2002).

The advection of warm waters at the end of MIS 5e to high latitude sites was associated with warm SSTs and open-water masses in the Barents Sea and Fram Strait (Risebrobakken et al 2007). It contributed to the increased thermal and salinity gradients proposed by all authors, whilst also providing a moisture source for the growth of continental ice sheets (e.g. McManus et al 2002). Advection of warm NAC type waters past the MD04-2822 site and up into the Nordic Seas via AMOC during MIS 5e, also acted as a moisture source for the initiation of MIS 5d ice growth, with declining insolation (chapter 8). The increasing trend of SSTs at the MD04-2822 site may therefore be accounted for by: i) a suppression of the early North Atlantic MIS 5e warming by inputs of meltwater from a proximal penultimate BIS; and ii) the eventual mixing of this water with continued advection of NAC waters into the Nordic Seas, throughout MIS 5e and into MIS 5d. A major cooling of the North Atlantic and a migration of the polar front to the south of the MD04-2822 core site (C24) occurs only with increased global ice volumes during MIS 5d (see chapter 8, *Glacial Inception*).

5. Summary and Conclusions

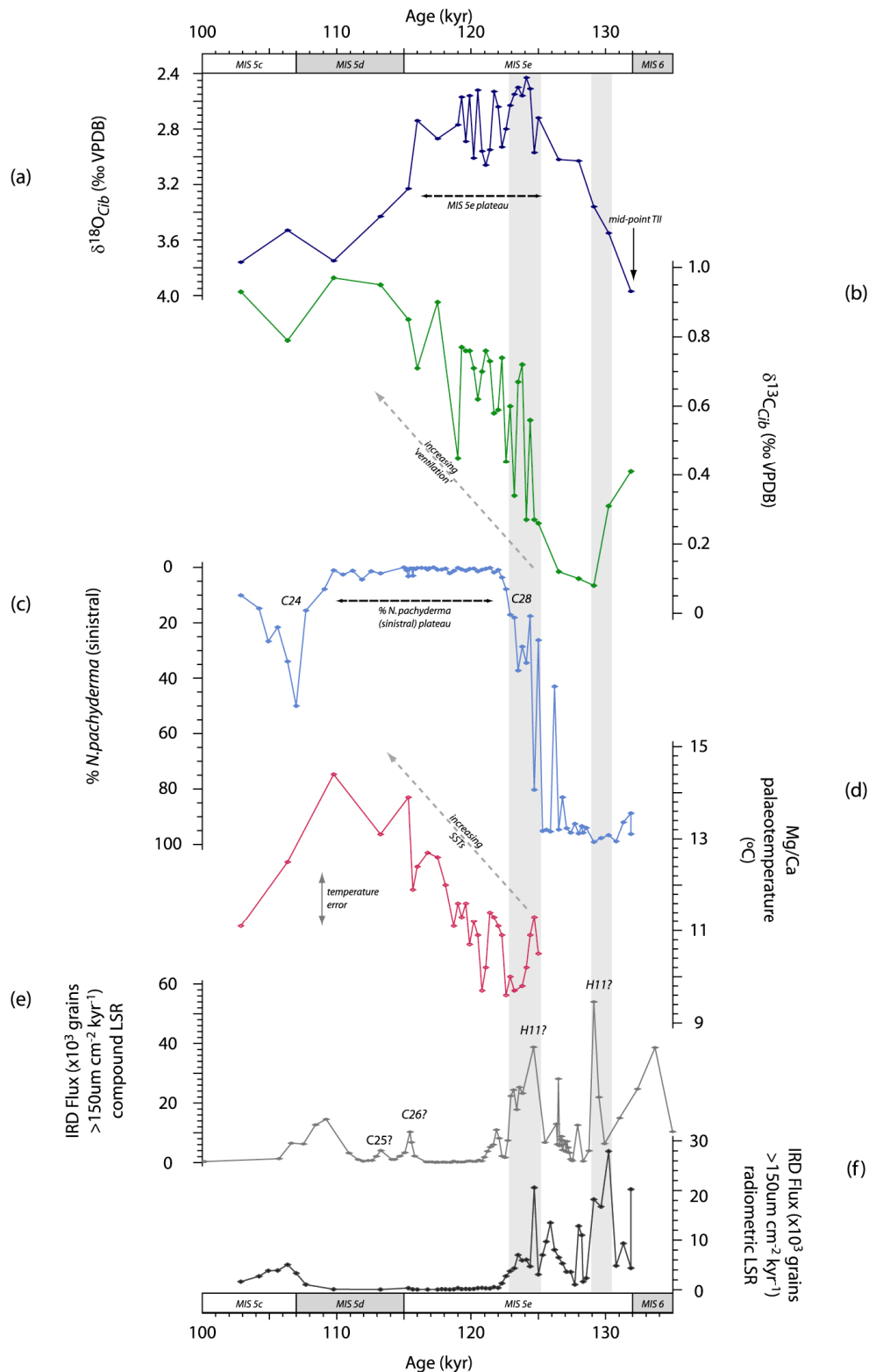
Millennial scale variability is a feature of both the surface and deep water hydrography at the MD04-2822 site, during the last interglacial (Figure 7.9). Variations in the benthic $\delta^{18}\text{O}$ record may reflect increased bottom water temperatures, changes in the $\delta^{18}\text{O}_{\text{water}}$ 'end-member' with inputs from the MIS 6 ice sheets and sea level changes through the MIS 5e plateau. Such changes in sea levels documented have been attributed, in part, to the negative mass balance of the Greenland Ice Sheet (e.g. Otto-Bliesner et al 2006) and to inputs of freshwater into the Nordic Seas. Such inputs reduced the deep convection in the Nordic Seas giving rise to the de-coupled benthic $\delta^{18}\text{O}$ and $\delta^{13}\text{C}$ records of many North Atlantic cores (e.g. Hodell et al 2009).

A decoupled benthic $\delta^{18}\text{O}$ and $\delta^{13}\text{C}$ record is also evident within the proxy records of MD04-2822 (Figure 7.9). In addition, there is an offset in the attainment of the benthic $\delta^{18}\text{O}$ minima and the lowest % of *N. pachyderma* (sinistral) for MD04-2822. Differences in global (i.e. the melting of Northern Hemisphere ice sheets during Termination II) and local (i.e. inputs of meltwater from the proximal MIS 6 BIS) is proposed. Of note during this interval, is an increase in IRD flux that occurs at the start of the benthic $\delta^{18}\text{O}$ plateau in MD04-2822. The provenance of material has yet to be ascertained; global sea level fluctuations of up to 10 m have been documented within the MIS 5e plateau (e.g. Hearty et al 2007a, Rohling et al 2008, 2009) although precise correlation to such sea level reconstruction remains problematic. The expanded nature of the MD04-2822 sediments during Termination II offers a unique opportunity to investigate this major climatic transition further, in particular the phasing of the decay of the circum-Atlantic ice sheets.

MD04-2822 displays an increase in SSTs through the MIS 5e benthic plateau and into MIS 5d, although some SST cooling events might be present, however the errors associated with the Mg/Ca palaeotemperature method are rather large ($\sim 1\text{ }^{\circ}\text{C}$). This is an unexpected and counterintuitive result; further testing e.g. via other SST proxies, is needed. This apparent disparity in the SST records of NE Atlantic cores (Cortijo et al 1999, Oppo et al 2001, 2006, this study) may be accounted for in the changing balance between local and regional influences. Inputs of meltwater derived from the decay of the penultimate BIS (prompted by increasing insolation during Termination II) are more likely to be recorded within the most proximal MD04-2822 record rather than the more open ocean site of ODP 980. As such, the NE Atlantic trend of SST increases associated with the transition from glacial (MIS 6) to interglacial (MIS 5e) are dampened at the MD04-2822 site (hence the difference in C28 between MD04-2822 and ODP 980). As warm, saline water continue to be advected into the Nordic Seas, and the polar front migrated northwards, surface temperatures at MD04-2822 continued to increase with peak temperatures occurring not within the benthic $\delta^{18}\text{O}$ plateau, but within MIS 5d. This is prior to a $>3\text{ }^{\circ}\text{C}$ decrease in SST into C24, which compares favourably to the $4\text{ }^{\circ}\text{C}$ SST reduction of Oppo et al (2006) for the neighbouring core ODP 980.

CHAPTER 7:
Surface and Deep Water Hydrography during the Last Interglacial

Figure 7.9: MD04-2822 Termination II and MIS 5e proxies on age (radiometric age assignment, see section 1 this chapter). (a) benthic $\delta^{18}\text{O}$; (b) benthic $\delta^{13}\text{C}$; (c) % *N. pachyderma* (sinistral); (d) Mg/Ca palaeotemperature reconstruction; (e) IRD flux (calculated using the compound age model LSR (chapter 3) but plotted on the radiometric age scale; and (f) IRD flux (calculated using the radiometric age model LSR). MIS designations after Imbrie et al (1984). Vertical grey shaded bars highlight elevated IRD events during the latter portion of Termination II.



The MD04-2822 benthic $\delta^{13}\text{C}$ record initially documents low values characteristic of glacial intervals with an increase in values occurring as the benthic $\delta^{18}\text{O}$ minima is achieved²². The benthic $\delta^{13}\text{C}$ values continue to increase throughout MIS 5e at the MD04-2822, with some millennial-scale variation evident. A shoaling of deep water could account for this long-term change; however this increase in benthic $\delta^{13}\text{C}$ values is evident for several cores within the North Atlantic and at varying depths (1 to > 3 km depth). It has been proposed that the formation of deep water was initially impeded by large volumes of meltwater within the Nordic Seas due to enhanced melting, promoted by increased summer insolation and enhanced penetration of the NAC to high latitudes (Hodell et al 2009, Risebrobakken et al 2007). Deep water continued to form throughout the MIS 5e plateau in the Norwegian-Greenland Sea (e.g. Rasmussen et al 1999, Hillaire-Marcel et al 2001, Hodell et al 2009) and also possibly within the Labrador Sea (e.g. Rasmussen et al 2003b). The continuing increases in benthic $\delta^{13}\text{C}$, recorded at MD04-2822 and other cores within the North Atlantic, suggest a 'change in production rate' or an increasing depth of NADW (Chapman and Shackleton 1998) as MIS 5 progressed.

IRD flux to the MD04-2822 site continued throughout the Termination. Indeed, a large event (20,000 to 40,000²³ grains cm^{-2} kyr^{-1}) occurs at the very start of the benthic $\delta^{18}\text{O}$ plateau. Global sea level variations have been documented with the benthic $\delta^{18}\text{O}$ plateau (e.g. Hearty et al 2007) with enhanced melting of the Greenland ice sheet proposed (e.g. Otto-Bliesner et al 2006). The provenance of this late Termination II IRD peak has not been determined but the high resolution of the MD04-2822 record may in future provide insights into the phasing of ice sheet decay.

²² Such initial low $\delta^{13}\text{C}$ values are evident in many North Atlantic cores; the input of large volumes of meltwater into the high latitudes, prior to the resumption of AMOC, is thought to have suppressed deep convection until the end of the deglaciation and may account for the lack of a 'Younger Dryas type' event during Termination II (e.g. Carlson et al 2008).

²³ The difference in IRD flux arises from the differing age model (and hence linear sedimentation rate) used in the calculation of this proxy (IRD flux = [IRD]*LSR*dry bulk density).

CHAPTER 8: Glacial Inception

The terrestrial records of the British Late Quaternary present a palimpsest of glacial oscillations, with much evidence obscured or removed; they provide an incomplete account that can be difficult to interpret. Whilst marine records afford a potentially uninterrupted record of ice sheet dynamics. Glacial initiation the definition of glacial initiation (i.e. the progression from mountain glaciation to subsequent ice cap) is often far from clear. The first input of IRD to a site may represent the first established marine calving front or the destabilisation of an already established ice front i.e. increased IRD flux may result from either ice sheet advance or decay (McCabe and Clark 1998, Clarke et al 1999) and is dependent upon the presence of a marine margin, the rate of iceberg calving, the debris content of icebergs, the rate of iceberg melting and the strength, direction and heat content of surface currents over the core site.

The MD04-2822 sediment record affords an unprecedented opportunity to begin unravelling the early history of the last BIS, as it is currently the only high resolution record extending beyond ca. 60 kyr (cf. Wilson et al 2002, Peck et al 2007, Scourse et al 2009). This chapter presents MD04-2822 proxy data from the last interglacial (MIS 5e) to the MIS 4/3 transition (ca. 60 kyr) within the context of both marine and terrestrial data for the initiation of Northern Hemisphere glaciation and the last BIS in particular. A multi-proxy approach is adopted in an attempt to resolve the early BIS dynamics. The first evidence for a BIS (presumed NW Scotland) during MIS 4 is presented.

This chapter outlines the regional record of glacial inception after the last interglacial with a focus on the NW European and North Atlantic records, followed by the evidence for a BIS pre-Devensian (MIS 2) glaciation. Section 3 (this chapter) details the hydrographic conditions and IRD inputs to the MD04-2822 core site since the last interglacial to the MIS 4/3 transition. Provenance indicators suggest a likely presence of a BIS during the latter stages of MIS 5 with enhanced input within MIS 4. This provides the first evidence for substantial NW British ice growth early within the last glacial cycle.

1. Background

The triggers and feedbacks invoked for the initiation of the last glacial include: decreased Northern Hemisphere insolation (e.g. Berger and Loutre 1991); a steepening of thermal gradients and increased moisture transport to high northern latitudes (and thus precipitation) (e.g. Risebrobakken et al 2007, Khodri et al 2001); changes in atmospheric freshwater transport (Gröger et al 2007) and increases in precipitation (e.g. Felis et al 2004); vegetation and albedo feedbacks (e.g. Khodri et al 2001, Crucifix and Loutre 2002).

Several ‘modes’ of glacial inception have been proposed including: ‘a highland origin and windward growth’ based upon North American observations (Flint 1943); initiation due to wind drift snow – the ‘leeside effect’ from observations in

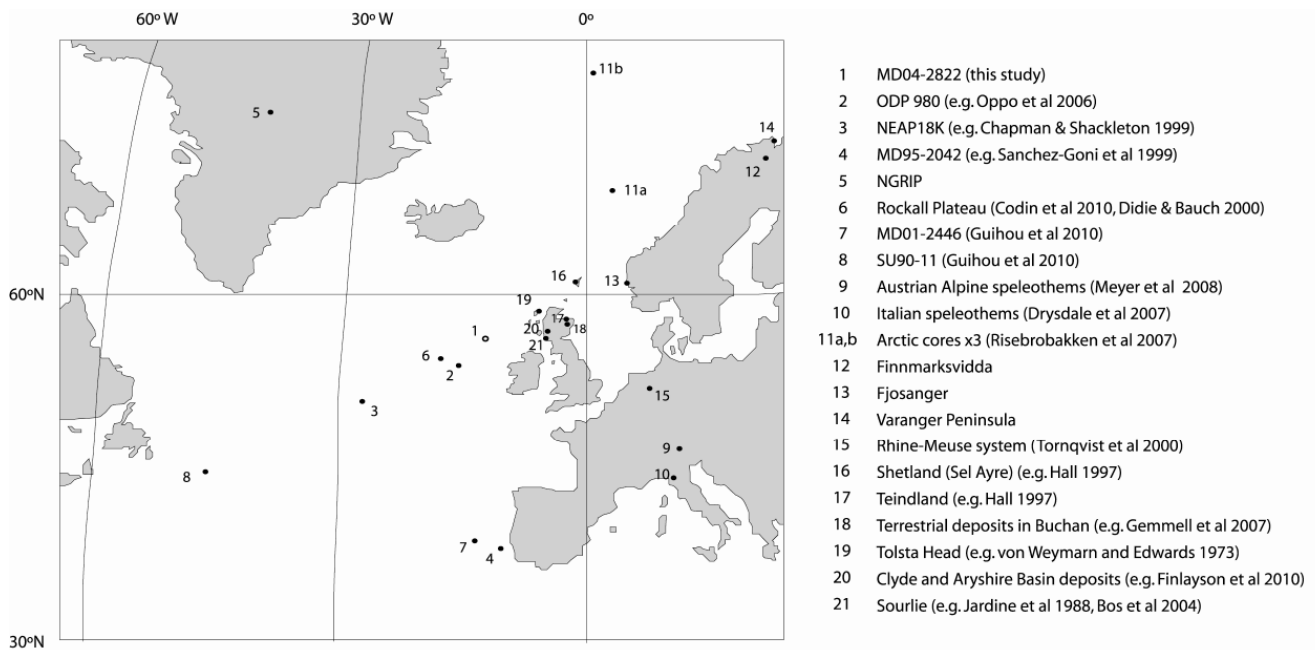
Scandinavia and Baffin Island (Enquist 1918, Andrews et al 1970); an albedo feedback mechanism whereby large polar plateaus produce ‘instantaneous glacierisation’ (Ives et al 1975); and topography acting as a strong feedback, resulting in accelerated glacier growth (Payne and Sugden 1990b) based upon a modelling study of Scotland. Glacial initiation appears to be a delicate balance of climate, topography and glacierisation (Fredin 2002).

The climatic optimum (Eemian/MIS 5e; chapter 7) was followed by a progressive climate deterioration towards glacial conditions within MIS 4 (Guihou et al 2010), with high/mid latitude marine and ice cores documenting an ‘unstable’ climate from the end of MIS 5e (e.g. McManus et al 1994, Chapman and Shackleton 1999, NGRIP members 2004).

2. Regional Evidence of Glacial Inception after the Last Interglacial

The following section outlines evidence of glacial inception with a particular focus on the NE Atlantic, and Scotland in particular. A map of locations mentioned in this chapter is given in Figure 8.1.

Figure 8.1: Principle locations mentioned in the text of this chapter.



2.1. North Atlantic records of ice sheet activity during MIS 5

The last interglacial period was punctuated by a series of IRD events, thought to reflect enhanced iceberg discharge as a result of decreasing temperatures (e.g. Bond et al 2001) with millennial scale climate variability thought an inherent feature of interglacial periods (Keigwin 1996) and demonstrated for the MD04-2822 core site (Chapter 7). During the MIS 5e plateau, Sánchez-Goñi et al (2005) demonstrate a $\sim 10^\circ$ southward migration of vegetation belts (including a southward displacement of the treeline between 60°N and 50°N as early as 120 kyr) within Western Europe. This supports the hypothesis that the changes in vegetation (and associated albedo change) at northern latitudes contributed to the initiation of glaciation (e.g. Crucifix and Loutre 2002)¹.

Amphi-Atlantic cooling episodes and enhanced IRD deposition, documented in North Atlantic marine sediment cores within MIS 5 (the cooling or 'C' events 19–27) (e.g. McManus et al 1994, Chapman and Shackleton 1999, Oppo et al 2006), mark the inception of Northern Hemisphere glaciation. However, the increase in ice volume was spatially variable and this is reflected in the spatial distribution and magnitude variations of the C events within the North Atlantic. These circulation changes within MIS 5 (surface cooling and increased ice-rafting, linked to reductions in AMOC; Oppo et al 2006) are thought to be rapid (Chapman et al 2000). The general sequence of climate deterioration evident within the North Atlantic is: little or no IRD input during MIS 5e; generally low IRD abundances until late within MIS 5d (C24); and a number of increased IRD depositional events within the remainder of MIS 5. These cooling events are discussed in detail below, with a focus on the NE Atlantic events documented in the ODP 980 core (Feni Drift, $55^\circ 29' \text{N}$, $14^\circ 42' \text{W}$; 2179 m water depth; McManus et al 1999, 2002, Oppo et al 2001, 2006) due to its relative proximity² to MD04-2822 (Feni Drift, Rockall Trough; number 2 within Figure 8.1).

Within the NE Atlantic (site ODP 980), Oppo et al (2006) document the end of the interglacial as a two step decrease in SST (Figure 8.2). The first initial step is a minor decrease in SSTs ($\sim 1^\circ\text{C}$) termed C27b, thought to be a regional episode of cooling from correlation with $\delta^{18}\text{O}$ feature in NEAP18K (Chapman and Shackleton 1998, 1999), occurring at the end of the MIS 5e benthic $\delta^{18}\text{O}$ plateau. The preceding C events C27 and C27a register as minimal ice rafting events in the NE Atlantic but are accompanied by a reduction in benthic $\delta^{13}\text{C}$. However, in the Greenland Seas, the first episode of increased IRD is tentatively correlated to C27 (Oppo et al 2006) and is thought to indicate the expansion of tidewater glaciers on the margins of the Nordic Seas (Fronval and Jansen 1997).

A second larger ($\sim 3^\circ\text{C}$) cooling in the NE Atlantic C26 (Chapman and Shackleton 1999, Oppo et al 2001, 2006, Lehman et al 2002) at the end of the MIS 5e marks the onset of a series of minor ice rafting events at ODP 980 and NEAP18K (Chapman and Shackleton 1998, 1999), with widespread cooling in the western Atlantic and parallel

¹ For example, the replacement of taiga by tundra acts as a positive feedback promoting perennial snow cover as snow covered tundra has a larger albedo than snow covered taiga (e.g. Crucifix and Loutre 2002, Sánchez-Goñi et al 2005)

² Site ODP 980 is approximately 240 km from the MD04-2822 core site; both cores are at a similar water depth (ODP 980 2,179 m; MD04-2822 2,344 m).

cooling in southern Europe and the Iberian Margin (Sánchez-Goñi et al 2005). As this cooling event occurred after the benthic $\delta^{18}\text{O}$ plateau, Oppo et al (2006) suggest that ice accumulation had already begun. Indeed the MIS 5e/5d transition is associated with a significant decrease in global sea levels with estimates ranging from 25 to 70 m (Lambeck and Chappell 2001, Lea et al 2002, Waelbroeck et al 2002, Siddall et al 2003). A rapid decrease in AMOC is inferred from two mid-latitude sites in the eastern and western North Atlantic³ at the MIS 5/4 transition (Guihou et al 2010). This does not appear to lag significantly Northern Hemisphere summer insolation and occurs in tandem with a large IRD event and decrease in sea level. As such Guihou et al (2010) conclude that Northern Hemisphere ice sheets had grown sufficiently large to release icebergs into the North Atlantic, thereby reducing AMOC. Within the Iceland basin, this event marks a step change in surface temperatures (Chapman and Shackleton 1998) whilst further south, the event is recorded as a brief cold excursion (Lehman et al 2002).

Figure 8.2: Proxy records for ODP 980 (after figure 2, Oppo et al 2006. Includes data from McManus et al 1999, 2002, Oppo et al 2001, 2003) (b) benthic $\delta^{18}\text{O}$; (c) planktonic $\delta^{18}\text{O}$; (d) benthic $\delta^{13}\text{C}$; (e) dissimilarity coefficients for SST estimates; (f) standard deviation of SST estimates; (g) SST estimates derived from modern analogue techniques; (h) lithic abundance, logarithmic scale; (i) % *N. pachyderma* (sinistral); (j) lithic abundance on linear scale.

IMAGE REMOVED - COPYRIGHT PROTECTED
(see original reference in caption above)

³ MD02-2246 (Iberian margin 39°03'N, 12°37'W; 3547 m water depth) and SU90-11 (Newfoundland margin 44°04'N, 40°01'W; 3645 m water depth).

Within the NW Atlantic, C25 is associated with a greater cooling than for the eastern North Atlantic (e.g. Cortijo et al 1999) and there is evidence for IRD deposition in the Greenland and Iceland Seas prior to this event (Fronval and Jansen 1997, Hald et al 2001). At ODP 980, surface temperatures remained cool for the remainder of MIS 5, with a series of SST oscillations: the greatest cooling at the ODP 980 site was during the C24 (end of MIS 5d) and C21 (end of MIS 5b) events. The C24 event brought about an approximate decrease of $\sim 4^{\circ}\text{C}$ in the Rockall Trough (Oppo et al 2006). This widespread North Atlantic cooling is believed to have triggered the cooling seen in many European pollen records, as the northern limb of the NAC ceased to penetrate into the Nordic Seas (Müller and Kukla 2004).

The prominent cooling associated with C23 and C24 is also documented within the NGRIP ice core (NGRIP members 2004), sub-tropical western North Atlantic (Heusser and Oppo 2003, Lehman et al 2002) and the Iberian margin records (Sánchez-Goñi et al 2005) suggesting widespread disruption of North Atlantic circulation. Drysdale et al (2007) radiometrically (U/Th) dated these two events using a speleothem from a cave⁴ in NW Italy to 105.1 ± 0.9 to 102.6 ± 0.8 kyr for C23 and 112.0 ± 0.8 to 108.8 ± 1.0 kyr for C24. These ages appear to be in “broad agreement” with the timing of GS25 (111.0 to 108.5 kyr⁵) and GS24 (106.0 to 104.5 kyr) for the NGRIP $\delta^{18}\text{O}$ record (Drysdale et al 2007) which have been previously correlated to C24 and C23 (McManus et al 1994, Shackleton et al 2002). Drysdale et al (2007) suggest that these ages ‘constitute new tuning points for the NGRIP record’, however the interpretation of speleothem records is far from straightforward (e.g. Fairchild et al 2006), and this also assumes the synchronicity of climatic events and ice sheet growth during glacial inception. This is difficult to reconcile with terrestrial evidence (e.g. Svendsen et al 2004, demonstrate the asymmetric growth of early Weichselian European ice sheets) and many marine records (latitudinal variations in the increases of IRD; for example, IRD events are recorded earlier in the Nordic and Greenland Seas than in the NE Atlantic). Whilst the precision of these ages⁶ certainly contributes to the emerging pattern of climate variability and ice sheet evolution, the latitudinal diachroneity evident within vegetation (Tzedakis 2003), landform (e.g. Svendsen et al 2004) and marine records (e.g. McManus et al 2002) cautions against aligning these events, particularly from different climate archives.

The larger IRD events during MIS 5 within the North Atlantic, are associated with a decrease in benthic $\delta^{13}\text{C}$ and, beginning with C24, reflect ice sheet instability (Broecker et al 1992, Chapman and Shackleton 1999) rather than changes in surface circulation as suggested for earlier events (Bond et al 2001). The most pronounced cooling events, that are accompanied by a significant increase in IRD i.e. C24, C23, C21⁷, C20 and C19, are all associated with reductions in benthic $\delta^{13}\text{C}$ suggestive of declining or reduced bottom water ventilation and a reduction in AMOC (e.g. McManus et al 2004, Oppo et al 2006).

⁴ Antro del Corchina (44°2’N, 10°17’E), stalagmite growth reported from ca. 118 to 96 kyr (late MIS 5e to MIS 5c).

⁵ Ages quoted are based upon the NGRIP $\delta^{18}\text{O}$ (NGRIP members 2004)

⁶ Age control for this interval can prove problematic; this interval is beyond the radiocarbon method and the relationship between benthic $\delta^{18}\text{O}$ and sea level/global ice volumes is not straightforward.

⁷ C21 is also labelled H7 within record of Chapman and Shackleton 1998, although C21 is preferred for the same event within Chapman and Shackleton 1999 and Chapman et al 2000.

Variations in AMOC, a major source of heat and moisture to the region, have also been implicated as a driver or amplifier of millennial-scale climate changes (Oppo et al 2006). Indeed, variation in the AMOC is proposed as a mechanism by which the warmth of the last interglacial was brought to an end (Adkins et al 1997, Hald et al 2001, Guihou et al 2010) and as a contributor to renewed warmth and moisture at high northern latitudes during MIS 5d glacial inception (McManus et al 2002). During the C events, the association of IRD, SST cooling and $\delta^{13}\text{C}$ decreases is consistent with surface conditions being affected by reductions in AMOC (Oppo et al 2006). A reduction in the penetration of warm waters into the northern North Atlantic and Nordic Seas, in conjunction with a decrease in insolation and the steepening of thermal gradients (and increased seasonality⁸) may therefore have provided the moisture source for the initiation and growth of the NW European ice sheets including the BIS.

2.2. Regional Evidence for the Evolution of Ice Sheet Growth after the Last Interglacial

An intensification of the AMOC in its northern limb has been proposed as a means of initiating high-latitude Northern Hemisphere glaciation (e.g. McManus et al 2002, Risebrobakken et al 2007, Bauch and Kandino 2007, Guihou et al 2010). Evidence from the Nordic Seas suggests that an intensification of AMOC at the end of the last interglacial (possibly as a result of strong prevailing westerlies) provided enhanced warm water transfer to the high latitudes, which was coupled with an increase in salinity due to a reduction in summer sea ice melting (Risebrobakken et al 2007). As a result of enhanced AMOC, a strong wintertime sea-land gradient was set up which, in conjunction with a strong wintertime latitudinal insolation gradient⁹, prompted an increase in moisture transport (and storminess) to the high northern European latitudes. The moist, maritime air-mass and the cold atmospheric temperatures prompted an excess of winter snow and reduced summer melting (Risebrobakken et al 2007, Ruddiman and McIntyre 1979). This scenario appears to be replicated by modelling studies (e.g. Cane et al 2006, Calov et al 2005a,b, Vettoretti and Peltier 2003) where as long as the site of deep convection for THC remains in a northerly position, moisture supply and ice sheet build up in high northern latitudes is highly effective. The earliest IRD inputs (C27, C27a, C27b within the Oppo et al 2006 scheme) have been documented within MIS 5e from Spitsbergen (Risebrobakken et al 2005; terrestrial evidence Mangerud et al 1998) prior to the major global increase in ice volumes. Early IRD inputs (prior to MIS 5d) have also been documented within the Nordic Seas (Fronval and Jansen 1997, Hald et al 2001, see above). The expansion

⁸ The role of seasonality during the Younger Dryas was emphasised by Denton et al (2005) with cooling principally a winter phenomenon without substantial changes in summer temperatures; this appears to be replicated for Scotland where winter cooling exceeded summer cooling (Golledge 2010). A widespread freezing of surface water of the North Atlantic during GS1, in response to AMOC reduction (Gildor and Tziperman 2003, Lie and Paasche 2003, Alley and Clark 1999, Alley 2000) has also been invoked for the increase in continentality in central Europe, during the cold intervals of MIS 5 (Alley 2000, Broecker 2006b).

⁹ Latitudinal moisture flux (from low to high) is a function of the latitudinal insolation gradient; an increased latitudinal insolation flux would result in enhanced transport of moisture to the high latitudes (e.g. Raymo and Nisancioglu 2003).

of warm waters into the high latitudes could explain the a-synchronicity in the evidence for the growth of these high latitude Northern Hemisphere ice sheets.

Geological evidence for the northwestern European ice sheet initiation indicates a southern progression in ice sheet loci during MIS 5. For example, the Barents–Kara Ice Sheets (BKIS) are thought to have become progressively smaller during successive MIS 5 stadials, whereas the dimensions of the Scandinavian Ice Sheets increased through time (Svendsen et al 2004). The early extent of the BKIS may be a consequence of the extension of warm SSTs within the Barents Seas with an increase in AMOC at the end of the last interglacial. The production of a strong thermal gradient between the land and ocean, in conjunction with wind forcing and wintertime latitudinal insolation gradients, provided excess precipitation in northern Russia that became perennial ice cover as insolation began to decrease. As the ice sheet advanced over the Barents Sea coupled with falling sea levels, the transport of warm waters into the Barents Sea would be curtailed therefore restricting moisture in northern Russia. As the Nordic Seas experienced more stable and perennial sea ice cover, such high latitude ice sheets would be cut off from their moisture source (Risebrobakken et al 2007) therefore displacing the locus of ice sheet growth southwards.

The NGRIP ice core is thought to contain ~123 kyr of undisturbed ice¹⁰ and using the $\delta^{18}\text{O}$ isotopic measurements of trapped air (nitrogen, oxygen and argon), Landis et al (2006) provide evidence for large climate variability associated with the inception of Northern Hemisphere glaciation. By comparing the $\delta^{18}\text{O}$ records of NGRIP to Vostok¹¹, polar temperatures in both hemispheres decrease prior to the end of the MIS 5e plateau (also described in Meyer et al 2008) with ‘the slow growth of ice sheets...in phase with or slightly lags the polar Atlantic temperature decrease’ mirroring the findings of Cortijo et al (1994, 1999). High CO_2 levels are still recorded by both ice cores for this interval. The initial ice sheet growth is instead attributed to the reduction in summer temperatures at high northern latitudes (Oerlemans 2001) as a consequence of decreased Northern Hemisphere insolation. The steepening of the insolation gradient between high and low latitudes would enhance moisture transport to the high northern latitudes (e.g. Khodri et al 2001) discussed previously.

The first rapid cooling event within the $\delta^{18}\text{O}$ of the NGRIP core (GS26) is recorded only in the Northern Hemisphere and is ‘triggered while the CO_2 and ice sheet size is intermediate between interglacial and full glacial values’ (Landis et al 2006). A temperature increase during GIS25 followed a period of large CO_2 decrease and the latter is not therefore thought responsible for driving global cooling, rather ice sheet growth was probably initiated by a decrease in Northern Hemisphere insolation and amplified by albedo effects of the growing ice sheets (e.g. Berger et al 1991, Khodri et al 2001, 2003).

¹⁰ The $\delta^{18}\text{O}$ of trapped air varies smoothly for the lowermost portions of the NGRIP core (in contrast to rapid excursions at the bottom of the GRIP core; Fuchs and Leuenberger 1996, Chappellaz et al 1997, Landis et al 2003) and was seen by Landis et al (2006) to confirm the integrity of the ice stratigraphy.

¹¹ The authors compared the two records by synchronising the $\delta^{18}\text{O}$ records and the rapid changes in methane evident in both records (NGRIP members; Caillon et al 2003). Both records were placed on the Vostok GT4 timescale (Petit et al 1999).

Increased precipitation and the invigoration of AMOC (e.g. Risebrobakken et al 2007) at high latitudes enabled the growth of ice at high latitudes (e.g. BKIS). The initial cooling documented in the ice cores (NGRIP and Vostok) is not associated with significant inputs of IRD or surface cooling within the Atlantic (although some ice-rafting is documented in the Nordic and Greenland Seas, e.g. Fronval and Jansen 1997, see discussion above). The first major atmospheric CO₂ decrease is recorded during this interval (GS26 and GIS 25) and THC was potentially unstable due to increased precipitation over the Nordic and Greenland Seas (Landis et al 2006). GIS24 and 23 exhibit characteristics of 'typical' interstadials i.e. a rapid temperature increase, and an Antarctic counterpart e.g. GIS24 compares favourably to GIS19 (Lang et al 1999, Landis et al 2004) (i.e. a rapid increase in temperature, up to +16 °C for GIS 24, Landis et al 2006, 2004). By contrast, GIS25 appears to be unique in having no southern counterpart, prompting Landis et al (2006) to propose a key role for the atmospheric hydrological cycle in glacial inception.

Speleothem records also provide an archive of climate variability during and at the conclusion of the last interglacial. Certainly, deposition of some Alpine speleothems appears to have begun at ca. 127 kyr (approximately the beginning of the last interglacial, MIS 5e plateau) (Spötl et al 2007). The Spannagel Cave speleothem records the end of interglacial warmth in the Alps at ca. 118-119 kyr (Spötl et al 2007), whereas lower altitude speleothems continued to grow until ca. 114 kyr (Meyer et al 2008). A marked climate deterioration is inferred post ca. 118-119 kyr in the Alps with strong cooling (mean ~10°C) at the cave sites and at least some vegetation and soil present within the catchment¹² (Meyer et al 2007). This is correlated to the North Atlantic marine cooling events¹³ and Greenland ice core GS25 by these authors. A similar cooler climate and high precipitation levels have been inferred from European pollen sequences (e.g. Sáchez-Goñi et al 1999) at the MIS 5e/5d transition. Alpine cave conditions remained relatively stable after the cave 'C26' event (cold winters, vegetated catchment) until calcite deposition ceases at ca. 114 kyr, which Meyer et al (2007) correlate to the C24 widespread cooling in the North Atlantic. The tree populations of southern Europe also disappear around this time (Tzedakis 2003, Müller and Kukla 2004).

2.2.1. *NW European evidence*

Evidence of the early history of the Weichselian NW European ice sheets has been documented within marine and terrestrial records of Scandinavia, the Netherlands and the Buchan area of NE Scotland. These are discussed in brief below.

At Fjøsanger¹⁴ in SW Norway, marine records suggest the expansion of ice directly after the Eemian interglacial i.e. within MIS 5d (Mangerud et al 1981a), with glaciers that were 'seeded' in the mountains reaching the coast soon after the interglacial.

¹² An increased flux of fine grained detrital material into the speleothem deposits (for example the speleothem deposit of Entriche Kirche) reflects the incorporation of into the cave system of detrital material with the breakdown of vegetation cover and solifluction processes (e.g. Haeberli 1983).

¹³ The authors correlate this reduction in mean cave temperatures with C26 on the MIS 5e/5d transition

¹⁴ The correlation of the Fjøsangerian Interglacial to the Eemian is well established (Mangerud 2004), however dating of the younger portion has proved more problematic and is based upon correlation with both western European terrestrial sequences and deep-sea stratigraphy.

Milder conditions are represented by a layer of gravels in this sediment sequence (Miller et al 1983), overlain by a till deposited in MIS 5b. Therefore, the ice front calving at Fjøsanger oscillated during MIS 5 and appears to have been sensitive to climatic change.

Early evidence for ice sheet growth after the interglacial is seen in northern Norway¹⁵ (Olsen 1988, Olsen et al 1996) and is thought to correlate to MIS 5d, with the next ice advance in this area correlated to MIS 4. This ice advance is significantly younger than associated Finnish and Swedish glacial stratigraphies (Hirvass 1991, Lundqvist 1992, Fredin 2002), however correlation between sites remains problematic as is robust age control. Notwithstanding this, Larsen et al (2000) propose that in southern Norway, two phases of significant growth within MIS 5 and MIS 4 formed an ice stream in the Norwegian Channel. A till within the Norwegian Channel is thought to be either Saalian or early Weichselian in age, with the latter preferred by Sejrup et al (2000). This till may represent the older of the ice streams described by Larsen et al (2000) (Mangerud 2004). In southern Norway, ice is therefore thought to have extended from the coast near Fjøsanger during MIS 5b and over the wider coastal area during MIS 4 and 3 (Mangerud 2004), even though the precise dating and correlation of events remain debated (e.g. Sejrup et al 2000, Mangerud 2004). The extension of Scandinavian ice into the North Sea is also proposed by Carr (2004) from sub-glacially deformed till and large infilled channels, thought to be tunnel valleys (Carr 1998, Johnson et al 1993, Skinner et al 1986; discussed further in section 2.2.2, this chapter). Sejrup et al (1994) also attribute a thick diamicton in the North Seas to glaciation within MIS 4.

However, ice free conditions in the early/ mid Weichselian have been proposed for parts of Norway (Olsen et al 1996, Mangerud et al 1981 a, b), Finland (Ukkonen et al 1999, Helmens et al 2000) and from Norwegian speleothem records (Lauritzen 1991, 1995) where growth continued until ~73 to 71 kyr. The continued growth of these speleothem records from the Eemian until the approximate end of MIS 5 is intriguing¹⁶ as these caves are situated in the Norwegian mountains, where favourable conditions for ice growth existed. For example, Fredin and Hättestrand (2002) document relict lateral moraines in the mountains of N. Sweden that were deposited prior to ca. 75 kyr, although the authors cannot rule out the possibility that these were formed prior to the Weichselian. Similarly, the speleothem records are difficult to reconcile with the proposed reconstructions of Lunqvist (1992) and Mangerud (2004).

MIS 4 (~59 to 71 kyr; SPECMAP, Imbrie and Imbrie 1980) marks an increase in global ice volumes and the growth of the northwestern European ice sheets. For example, an MIS 4/late MIS 5 (Karmøy Interstadial) episode of enhanced IRD input in the Norwegian Sea is thought to derive from the first major expansion of ice sheets

¹⁵ Hardangervidda and Varanger Peninsula (Olsen 1988, Olsen et al 1996)

¹⁶ Speleothems are an archive of palaeo-groundwater conditions that is primarily driven by climate but also other influences such as soil and vegetation dynamics, karst hydrology, cave ventilation and evaporation (e.g. Fairchild et al 2006). In the Norwegian caves, the assumption made is that speleothems only precipitate when not covered by an ice sheet (Lauritzen 1991, 1995) however, speleothems may continue to precipitate calcite in decreased temperatures as long as internal cave temperatures remain above freezing; instead changes in the $\delta^{18}\text{O}$ may reflect changes in seasonality (cf. Meyer et al 2008).

from central Norway (Sejrup et al 2000). Significant fluvial erosion in the Netherlands of the Rhine-Meuse system is also associated with the glacio-eustatic controlled MIS 4 sea level fall (Törnqvist et al 2000).

2.2.2. *British evidence for the early history of the Weichselian/Devensian BIS*

Early investigations of the early Weichselian/Devensian suggested two episodes of cool climate (within the interval ~117 to 74 kyr) with pollen sequences indicating the development of birch or pine-birch woodland in NE Scotland and heathland on Shetland; climatic conditions were thought to be more continental than present (Hall 1997).

Analysis of seismic reflection data from the outer Moray Firth and the Hebridean Shelf provide tentative evidence for a major ice advance between 75-60 kyr (Andrews et al 1990, Stoker et al 1993), as do till units at described at Teindland, NE Scotland (Hall 1997), although precise age control for these remain problematic.

Within the northern North Sea Basin, the glacially-deformed till forming the upper portion of the Ferder Formation and a number of large, infilled channels (~200 m depth) thought to be tunnel valleys (Carr 1998, Johnson et al 1993, Skinner et al 1986) are evidence for an early Weichselian glaciation. These deposits are thought to be MIS 4 in age and reflect the same glacial episode documented by Sejrup et al (1995) (Carr 2004). Firm age control remains elusive and is based primarily upon stratigraphy; these deposits overlie glacial and interglacial sediment and underlie the Middle Weichselian marine and glacio-marine sediments of the Cape Shore Formation (Skinner et al 1986). Carr (2004) suggests the confluence of British and Scandinavian sourced ice within the North Sea during MIS 4, but with uncertain southern limits¹⁷.

For western central Scotland (Clyde Basin and Ayrshire), Finlayson et al (2010) provide a (simplified) stratigraphy (after McMillan et al 2005, 2010) (Figure 8.3) for the early Weichselian (i.e. pre-Devensian) and Late Devensian. The Ballieston Till Formation (Clyde basin; Rose 1981, 1989, Browne and McMillan 1989) and the Littlestone Till Formation (the basal unit of the Sourlie stratigraphy; Jardine et al 1988, Sutherland 1999) 'pre-Devensian' till units, are recognised and may have been deposited during MIS 4 or by an older glacial advance-retreat cycle. The thin lenses (Sourlie Organic Silt Formation), rich in flora and fauna suggestive of treeless, low shrub-sedge moss tundra have an MIS 3 age¹⁸ (e.g. Bos et al 2004), and overlay the Lawthorn Diamicton Member (glaciogenic debris flow deposits: Jardine et al 1988, Finlayson et al 2010) of the Littlestone Till Formation. Similarly, the Ballieston Till

¹⁷ Carr (2004) speculates that for a confluent British (Scottish) and Scandinavian ice during MIS 4, the ice margin 'likely extended to the south for some considerable distance, probably to the Dogger Bank region at around 55 to 59 °N'.

¹⁸ The Sourlie (Jardine et al 1988, Bos et al 2004) organic deposits are seen as evidence of a largely ice free MIS 3 in Scotland (e.g. Hall et al 2003, Bradwell et al 2008) (other evidence includes organic deposits at Tolsta Head, North Lewis (von Weymarn and Edwards 1973, Whittington and Hall 2002) and Balglass Burn (Brown et al 2007)). Areas of Buchan have also previously been interpreted as ice free during MIS 3 (e.g. Bowen et al 2002), however Gemmel et al (2007) using OSL dating propose that parts of Buchan and Aberdeen were glaciated during MIS 4 (see later discussion).

Formation of the Clyde basin is related to a pre-Devensian ice advance in the area and is overlain by bedded bouldery sands of the Cadder Sand Formation, which include teeth of woolly rhinoceros (Rolfe 1966), and glaciolacustrine clays (Broomhill Clay Formation) prior to the deposition of the MIS 2 Wilderness Till Formation (Rose et al 1988). Both the Ballieston Till and Littlestone Till Formations may relate to MIS 4 glaciation of the region, however, age control is poor for these sediments and their deposition during an earlier phase of glaciation cannot be excluded.

Figure 8.3: Simplified lithostratigraphy for the Clyde and Argyshire Basins describing the Devensian ice sheet growth (Finlayson et al 2010).



Extensive areas of Buchan (northeastern Scotland) may have been glaciated earlier than previously believed (Gemmell et al 2007) and the presence of lake and deltaic deposits in the Ugie valley (Buchan) may also have resulted from damming by coastal ice during the equivalent to the Karmøy Interstadial (Mangerud 2004). This area was previously thought to be ice free during the Devensian glaciation (e.g. Hall et al 2003). Dating from Nigg Bay, Buchan, provide the ‘first directly dated onshore evidence for extensive glacial activity over Scotland in MIS 4’ (Gemmell et al 2007). The maximum age for the deposition of this till of 63 ± 7 kyr (*ibid.*) would support the suggested coalescence of the Scandinavian and British origin ice within the North Sea during the Ferder glacial of MIS 4 (Sejrup et al 1995, 2000, Carr 2004). Similarly, ice sheet activity in eastern Scotland during MIS 4 or 3 is suggested by a date of 74 ± 6 kyr for Oldmill site in central Buchan. Gemmell et al (2007) propose an extensive glaciation for this area of NE Scotland during MIS 4 or 3, with ice withdrawing from some portions of Buchan prior to the advance of coastal ice streams from the south and the Moray Firth during MIS 2. These authors also moot the possibility of lake and deltaic sediments in the Ugie Valley during MIS 5; this is compatible with the valley being dammed by significant coastal ice within the Karmøy Interstadial or MIS 4 (e.g. Mangerud 2004, Sejrup et al 2000). These dates indicate that portions of Buchan were ice free, but on a much more restricted scale than previously outlined.

Indirect evidence of glacial activity has been recorded within the Rockall Trough. Sea ice cover during MIS 4 (as well as MIS 2 and 6) has been inferred from ostracode assemblages, suggest that perennial sea ice cover extended far beyond the Arctic

during ‘peak glacial climates’ (Cronin et al 2010). Similarly Didié and Bauch (2000) propose icebergs or sea ice during MIS 2, 4 and 6 from the ostracode assemblages, coupled with increased IRD inputs for a core from the southern Rockall Plateau (M23414-9; 2196 m water depth).

The initiation of the last BIS within MIS 4 is predicted by some models (e.g. Siegert et al 2001, Marshall and Koutnik 2006, van der Berg et al 2007, Hubbard et al 2009¹⁹) with modelled ice volume for the Eurasian ice sheets (including the BIS) peaking ca. 60 kyr (Siegert et al 2001). Payne and Sugden (1990a) highlight the importance of sufficient moisture supply during cooling episodes to enable the initiation of an ice sheet in Scotland. In addition, the importance of topography is stressed for Scottish ice sheet growth. Payne and Sugden (1990b) demonstrate a very pronounced bifurcation due to topography where a very small temperature decrease (~0.125 °C) results in the switching from a steady state to a rapidly growing ice cap, enabling higher areas to start glaciation which subsequently expands to lower levels. Such non-linear behaviour has been observed for the present Patagonian ice fields. Glaciation is readily achieved through a modest lowering in the snowline but deglaciation requires far greater temperatures and/or a drier climate (e.g. Oelermans 1982, Crowley and Baum 1995).

2.3. Summary

In summary, glacial inception of the Northern Hemisphere following the last interglacial, was brought about by a combination of cool northern latitudes (due to decreased N. Hemisphere insolation) and enhanced northward moisture transport by both the ocean and atmosphere, thereby enhancing winter snowfall in high northern latitudes. The decreasing Northern Hemisphere insolation also decreased the rate of ablation and facilitated perennial snow accumulation. The growth of high latitude glaciers prompted a reduction in the penetration of the northern limb of the NAC into the high Arctic, thereby ‘starving’ the highest latitude ice sheet (e.g. BKIS) of moisture but enabling the growth of more southerly ice sheets (e.g. Fennoscandian). A series of IRD and benthic $\delta^{13}\text{C}$ events within the marine record document the growth of these ice sheets, however the terrestrial record remains fragmentary. Scant evidence available for the early history of the BIS due to erosion or obfuscation by subsequent ice sheet oscillations. Recent revaluation of deposits within Buchan, NE Scotland tentatively suggests major glaciation within MIS 4, an interval of sea level reduction (e.g. Siddall et al 2003), temperature minima in Greenland (although not as severe as MIS 2) (e.g. Alley et al 2010) and substantial growth of European ice sheets (e.g. Scandinavian and Barents-Kara ice sheet; Svendsen et al 2004 and references therein) (Figure 8.4).

¹⁹ Although the model of Hubbard et al (2009) focuses on the last BIS, the model is artificially initiated from ‘as near ice free conditions as can be identified’. The authors have chosen the Tolsta Interstadial 38 to 31 ka BP (within MIS 3) (Whittington and Hall 2002) based upon the Tolsta Head (Whittington and Hall 2002), Balglass (Brown et al 2007) and Sourlie (Bos et al 2004) radiocarbon ages, as a start point due to computational restrictions. Very little calving is proposed for MIS 3, with modest calving flux at ca. 30 yr before a series of large calving events beginning ca. 24 kyr. A large increase in IRD flux to the MD04-2822 site is seen at 40 kyr associated with H4, followed by a steady increase until MIS 2 where IRD fluxes are significantly higher than MIS 3 or 4 (for further discussion of the last glacial IRD inputs to MD04-2822, the reader is directed to chapter 6).

Figure 8.4: Reconstruction of the European Weichselian ice sheets extent from geologic evidence (left panel) and modelled ice thickness based upon those observations (right panel) for the periods (a) ca. 90 ka; (b) ca. 60 ka; and (c) ca. 20 ka (Svendsen et al 2004 and references therein). Note the southward progression of ice sheet growth. Not all sectors of all ice sheets are shown e.g. the authors suggest a glaciated continental shelf between Scandinavia and the UK at ca. 60 ka (b) (based upon Carr 2004) however, the ice sheet configuration is uncertain and therefore not plotted or modelled.

IMAGE REMOVED - COPYRIGHT PROTECTED
(see original reference in caption above)

3. Events recorded at the MD04-2822 core site

The above brief review of evidence for the early history of the European Weichselian ice sheets demonstrates the difficulties in the reconstruction of ice sheet inception: fragmentary evidence which may be modified, obscured or removed by later ice sheet oscillations and potentially problematic age control. Sediment core MD04-2822 provides an uninterrupted record of the climatic changes experienced at the site during the transition from MIS 5 to 4. Additionally, the robust age model achieved for the MD04-2822 record (Chapter 3, *Chronostratigraphy*) may help unravel the timing of both climatic changes and ice sheet dynamics.

3.1. MIS 5 and MIS 4 – Glacial Inception

The increase in global ice volume through MIS 5 and into MIS 4 is documented by the increase in the benthic $\delta^{18}\text{O}$ ²⁰. Similarly the prominent SST oscillations (C events) recorded at many North Atlantic sites (Chapman and Shackleton 1999, Oppo et al 2006) are also present within the MD04-2822 % *N. pachyderma* (sinistral) record. D/O cycles 19 (GIS19 and GS19) and 18 (GIS 18 and GS 18) are also clearly evident within this record, with very high % *N. pachyderma* (sinistral) values (≥ 80 %) during stadial events punctuated by very low values (< 30 %) during the interstadials (Figure 8.6).

The geographical range of these (C event) cooling excursions is documented in the contrasting IRD events between the western and eastern Atlantic (Figure 8.5; McManus et al 2002, Chapman and Shackleton 1999²¹). The IRD record of MD04-2822 conforms to the geographic expression of IRD events within the North Atlantic proposed by Chapman and Shackleton. However, based upon the % *N. pachyderma* (sinistral) records, these same cooling events have a wider expression (McManus et al 2002). McManus et al (2002) propose that cores in a similar location to MD04-2822 would ‘experience’ only C23 and C24. However, using the same criteria as these authors²², MD04-2822 records all events C19 to C24 except for C22. The MD04-2822 record closely resembles that of Oppo et al (2006) for ODP 980 (this is considered by McManus et al (2002) but prior to the increase in resolution by Oppo et al (2006), which may account for the apparent discrepancy.

The pattern of SST cooling during MIS 5 mirrors that documented for ODP 980, although the magnitude of the cooling (as determined by the % *N. pachyderma* (sinistral)²³) differs between the cores, with MD04-2822 experiencing a greater

²⁰ The benthic $\delta^{18}\text{O}$ does not scale directly with global ice volume and may also consist of local ‘overprinting’ e.g. due to changes in the temperature of bottom waters (see chapter 3, *Chronostratigraphy* for a full discussion of the influences upon the benthic $\delta^{18}\text{O}$ signal).

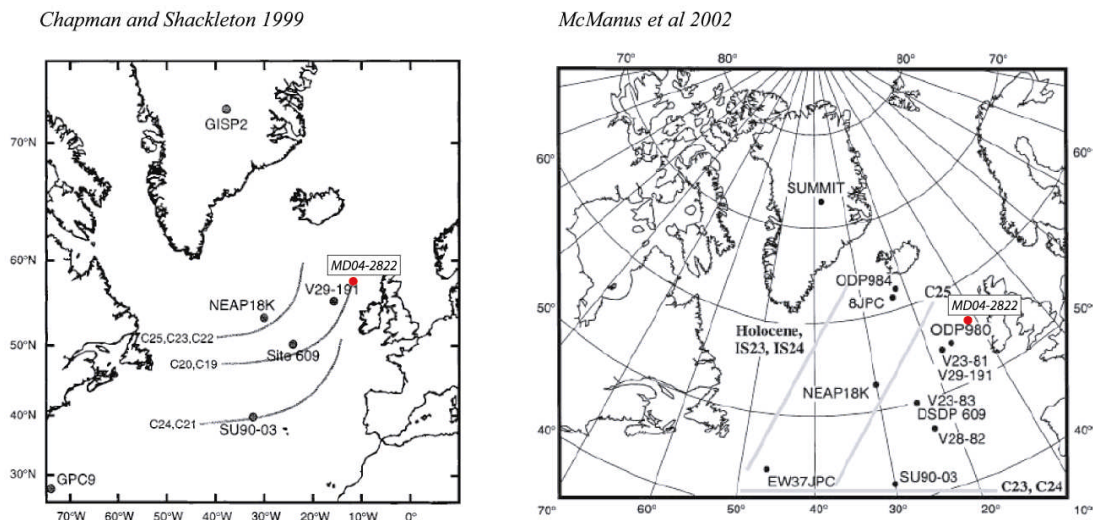
²¹ NB Chapman and Shackleton (1999) define the geographic coverage of the C events within the North Atlantic using IRD from 4 cores whilst McManus et al (2002) use the % *N. pachyderma* (sinistral) records of 9 cores (abundances > 10 to 20 %)

²² McManus et al (2002) employ a 10 to 20 % *N. pachyderma* (sinistral) abundance as their ‘threshold’.

²³ No quantitative SST proxy is available for this portion of the core.

change in this proxy²⁴. In MD04-2822, each of the C events is characterised by an increase in IRD and a marked decrease in % *N. pachyderma* (sinistral), they are also accompanied by low benthic $\delta^{13}\text{C}$ values. An additional benthic $\delta^{13}\text{C}$ low is evident at ~ 24.9 m. This might be C26, although it is accompanied by little or no terrigenous inputs. However, the decrease in benthic $\delta^{13}\text{C}$ and a decrease in XRF Ca (which is dominated by biogenic inputs and productivity) is evident. Oppo et al (2006) reconstruct a ~ 4 °C SST decrease during C26; such a decrease may have reduced productivity at the MD04-2822 site but not increased the % *N. pachyderma* (sinistral)²⁵. Each reduction in the benthic $\delta^{13}\text{C}$ flux occurs with an increase in IRD, when plotted on a log scale (cf. Oppo et al 2006) (Figure 8.7). However, these reductions in benthic $\delta^{13}\text{C}$ occur against a general trend of increasing values through MIS 5.

Figure 8.5: Spatial distribution of C events (adapted from Chapman and Shackleton 1999 and McManus et al 2002). Filled red dot gives the approximate position of MD04-2822. In map of Chapman and Shackleton (1999), the grey lines indicate the maximum limits of IRD deposition during the C events. In the map of McManus et al (2002) the grey lines indicate ‘portions of the region affected by...climate events’.



²⁴ The C24, 21 and 20 events record much lower percentages at MD04-2822 than ODP 980: ~50, 70 and 50 % respectively for MD04-2822 and ~25, 60 and 20 % at ODP 980.

²⁵ An approximate 1 °C SST decrease has been reconstructed from Mg/Ca analyses (see chapter 6).

CHAPTER 8:
Glacial Inception

Figure 8.6: Interglacial-glacial transition for MD04-2822. (a,b) benthic $\delta^{18}\text{O}$ and $\delta^{13}\text{C}$; (c) % *N. pachyderma* (sinistral); (d) XRF Ca; (e) IRD flux; (f) XRF Si/Sr; (g) % 'diagnostic' BIS lithics; (h) linear sedimentation rate and % (by mass) of sediments greater the $>63\ \mu\text{m}$.

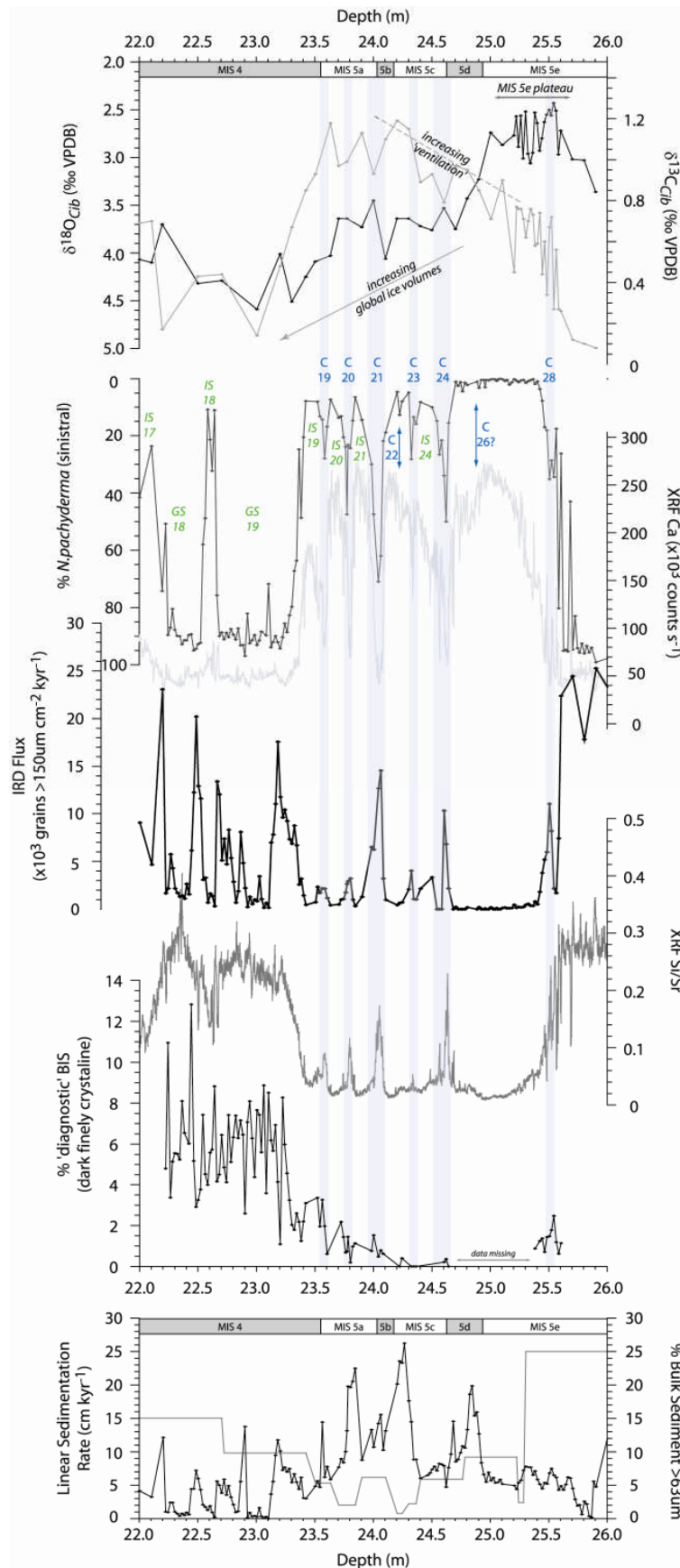
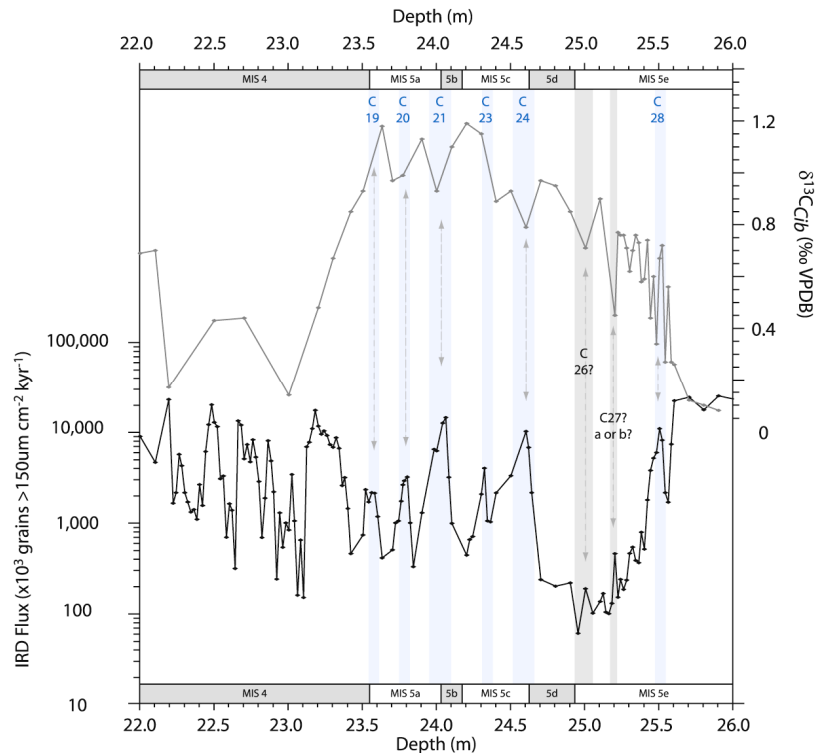


Figure 8.7: Benthic $\delta^{13}\text{C}$ and IRD flux (on a logarithmic scale) records for MD04-2822 during MIS 5 and MIS 4. Note both proxies are plotted on their depth scale in order illustrate any correlation, leads or lags more clearly.



The prominent increase in benthic $\delta^{18}\text{O}$ at 2377.5 cm marks the beginning of the transition into MIS 4 with isotopic maximum attained at 23.5 m (ca. 68 kyr) (Figure 8.6). The transition from generally low percentages of *N. pachyderma* (sinistral) and high XRF Ca counts, to high percentages of *N. pachyderma* (sinistral) and low Ca values is a conspicuous feature of the MD04-2822 record. The local deterioration in surface conditions again lags the MD04-2822 benthic record, suggesting that high-latitude climates had deteriorated before the mid-latitude surface ocean cooled significantly.

The C events (Figure 8.6) in MD04-2822 are all associated with peaks in Si/Sr (indicative of terrigenous detrital silicate inputs; Hodell et al 2008). Within MIS 4, IRD input continues to be episodic in character but of increased frequency and magnitude. A step change in deposition and proxies occurs at this point (transition into GS19) with increases in both Si/Sr and the % abundance of ‘diagnostic’ BIS lithics (cf. Knutz et al 2001). Inputs of Si/Sr are no longer episodic but are instead continuous, with levels similar to those during Termination II (Figure 8.6). LSR also increases gradually during MIS 4; in MIS 5 accumulation rates increase only during interstadials, with increased productivity and biogenic inputs being the probable driver. The % (by mass) of the sediments also changes through MIS 5 into MIS 4; sediments in MIS 4 are dominated by particles less the 63 μm (i.e. clays and silts comprise ~90 % or more of the MD04-2822 sediments) (Figure 8.6).

The proxy data outlined above and presented in Figure 8.6, document sustained inputs of fine grained material, high Si/Sr inputs and episodic IRD which is increasingly comprised of ‘diagnostic’ BIS lithics. This reflects both the increase in Northern Hemisphere ice after the last interglacial and, in the latter portion of MIS 5, the probable growth of ‘local’ ice i.e. growth of an ice sheet in NW Scotland at the MIS 5/4 transition. Prior to ~23.5 m, the IRD flux to the MD04-2822 site is sporadic, whilst after this time the IRD flux is fairly continuous. The expansion of polar waters associated with decreased AMOC, brought IRD laden icebergs from high latitude ice sheets to the MD04-2822 core site during MIS 5 (the C events). In contrast, IRD increases within MIS 4 occur against a background of cold SSTs (high % *N. pachyderma* (sinistral)) suggesting a reduced hydrographic influence on IRD inputs at MD04-2822 at this time.

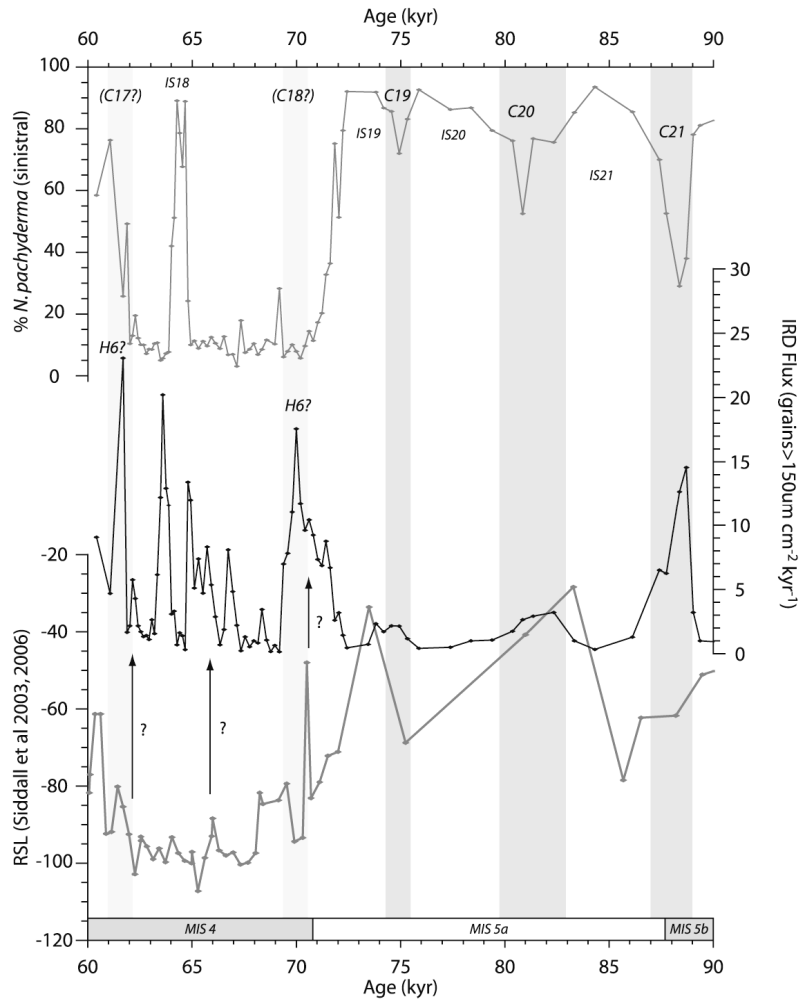
In addition, the decay in circum-Atlantic ice sheets may have influenced MD04-2822 IRD inputs through changes in sea level; such changes would have destabilised the marine margins of any BIS present. Difficulties remain in unambiguously assigning a direct relationship between IRD inputs and sea level changes in this interval, due to chronological concerns and the degree to which they represent a global sea level signal; however, the pulse of IRD after GIS18 occurs during a time of oscillating sea levels (e.g. Thompson and Goldstein 2005, Arz et al 2007). The high resolution RSL record of Siddall et al (2003, 2006) also suggests a sea level influence on IRD deposition, although the alignment with the MD04-2822 record is uncertain²⁶ (Figure 8.8).

The qualitative lithological investigation of MD04-2822 IRD suggests a build-up of British ice during MIS 4; ‘diagnostic’ BIS lithics are present and abundant within this interval. The presence of these lithic grains suggests BIS activity during this interval of significant global cooling and ice volume increases. The warm SSTs during MIS 5, coupled with cooling climate, enabled the expansion of the BIS and the development of a marine calving margin, thereby supplying IRD-laden icebergs to MD04-2822. This proposition accords with Marshall and Koutnik’s (2006) model prediction of iceberg flux for the BIS, as well as the modelled iceberg calving of Siegert et al (2001) and Forsström and Greve (2004) for the Eurasian ice sheets.

The following section attempts to unravel in greater detail the provenance of IRD supplied to MD04-2822 during the MIS 5/4 transition and MIS 5.

²⁶ The sea level reconstruction of Siddall et al (2003, 2006) pertains strictly to the Strait of Bab el Mandab in the Red Sea/Gulf of Aden and these may deviate from the global sea level change due to uplift and isostatic effects; although the authors consider these effects to be negligible and within the error of the method. The age model for the portion of the sea level record shown in Figure 8.8 was constructed via tuning of the planktonic $\delta^{18}\text{O}$ to the Byrd $\delta^{18}\text{O}$ ice core record (Siddall et al 2003).

Figure 8.8: Relative sea level reconstruction of Siddall et al (2003, 2006) and the % *N. pachyderma* (sinistral) and IRD flux for MD04-2822 presented on their own age scales. Grey bars indicate C events, pale grey bars give possible positions of C19 and C18 after Chapman et al (2000). Arrows indicate possible correlation of RSL and increases in MD04-2822 IRD flux. Note that some ambiguity surrounds the position of H6 (e.g. Manighetti et al 1995) with some authors positioning the event within GS 19 (C18) (e.g. Bond et al 1992), others within GS 18 (C17).



3.2. Early Dynamics of the BIS (provenance of material delivered to MD04-2822)

The large increase in IRD inputs and the XRF Si/Sr content of bulk sediment at ~22 to 24 m is suggestive of a possible contribution from a local ice sheet i.e. the NW sector of the BIS. This portion of the MD04-2822 record was investigated further, in order to determine the likely provenance of the IRD increases as well as the contribution, if any, of the BIS during the early Weichselian. Detailed lithological characterisations were undertaken, which in conjunction with Sr, Nd and Pb analyses of bulk sediment and the product of a magnetic un-mixing model (C. Peters, *unpublished data*) enabled possible contributions from the likely source regions to be assigned.

3.2.1. IRD lithological characterisations

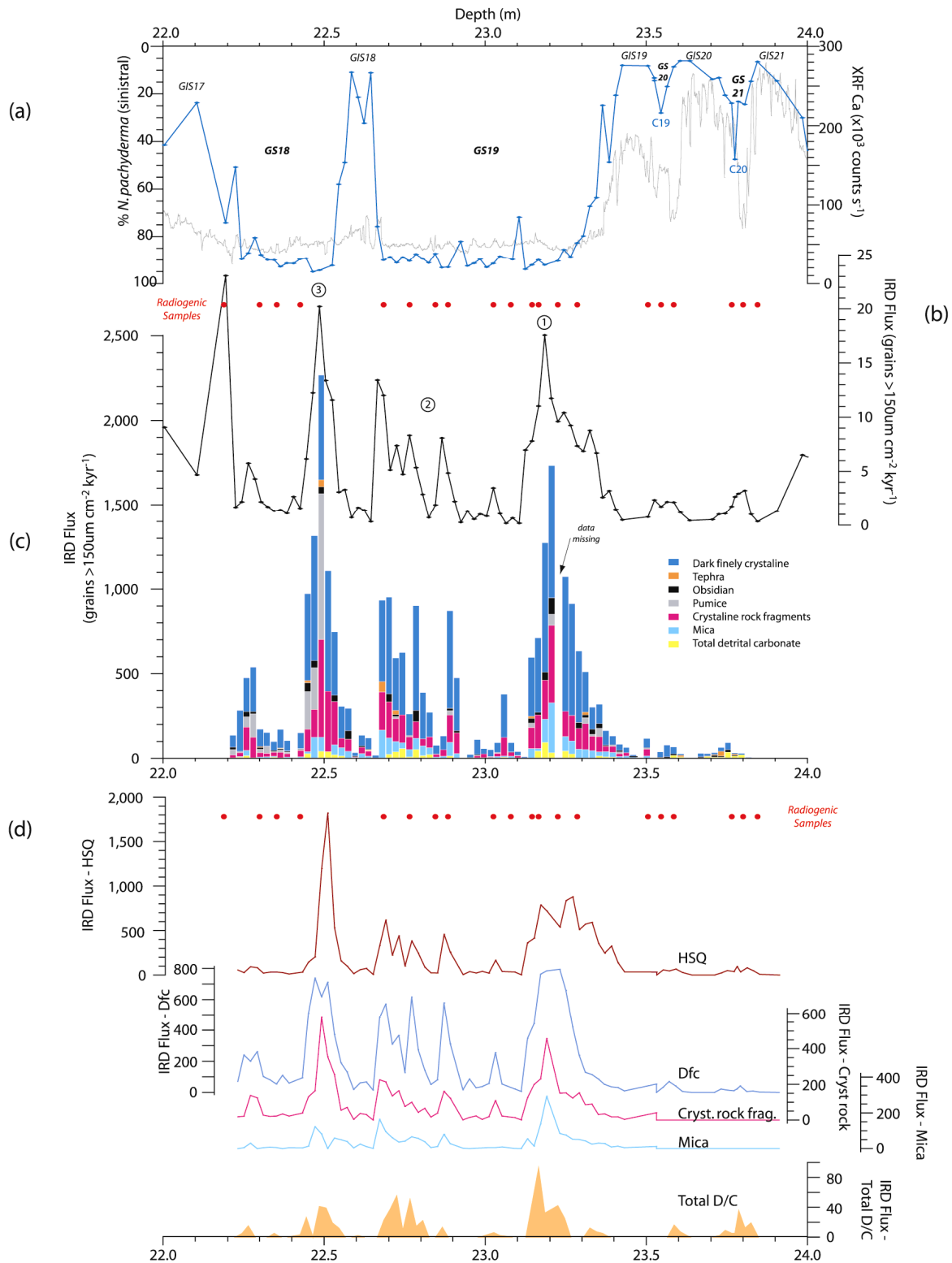
IRD grains were sub-divided into the following lithological components: quartz, haematite stained quartz, dark finely crystalline grains, tephra, obsidian, pumice, crystalline rock fragments, mica and detrital carbonate grains (further sub-divided into 'sugary', grey and 'chalky'). Selected profiles are presented in Figure 8.9.

The IRD peaks within MIS 4 are characterised by an increase in the 'diagnostic' BIS grains (labelled Dfc in panel (c) of Figure 8.9) as well as increases in mica and crystalline rock fragments. The rise in these components is preceded by an increase in haematite stained quartz. The MD04-2822 IRD (>150 µm) is dominated by quartz grains, with the percentage of the 'diagnostic' BIS lithics comprising only ~6 to 8 %, with occasional peaks of ~12 % (Figure 8.6). Detrital carbonate is a very small proportion of the total IRD flux for this portion and indeed throughout the core, with the exception of H4²⁷ (inferred as the largest of the Heinrich events by Hemming (2004)).

In Figure 8.9 panel (d), the dark finely crystalline grains (primarily basalt of presumed BTIP origin; Knutz et al 2001), crystalline rock fragments and mica (of presumed Scottish metamorphic provinces; Scourse et al 2000, Peck et al 2007) are thought to represent a northwestern source 'BIS IRD assemblage'. These components closely mirror one another through this interval and are believed to derive from areas underneath the NW sector of the last BIS. Haematite stained quartz may also derive from Britain (Peck et al 2007) although these grains have also been used to infer the dynamics of the Greenland Ice Sheet (Bond and Lotti 1995) and ice derived from the Gulf of St Lawrence (van Kreveld et al 2000, St John et al 2004). Whilst haematite stained quartz seems to vary with the 'BIS IRD assemblage' in IRD peaks labelled 2 and 3 (Figure 8.9), it increases before these grains in IRD peak 1.

²⁷ Detrital carbonate ('sugary' in appearance) constitutes ~ 10.7% of the IRD >150 µm for the peak of H4 (determined as the maximum abundance of detrital carbonate) whereas the maximum total carbonate ('sugary', 'grey' and 'chalky') during MIS 4 is ~2 % of total IRD >150 µm.

Figure 8.9: (a) Hydrological conditions; % *N. pachyderma* (sinistral) and XRF Ca; (b) IRD flux; (c) stacked bar graph of IRD lithological characterisations; (d) lithological component flux: haematite stained quartz (HSQ), dark finely crystalline (Dfc), crystalline rock fragments (cryt. rock frag.), mica and total detrital carbonate (D/C). Also indicated are Greenland interstadials (GIS) and stadials (GS) as well as C events 20 and 21. The stratigraphic position of radiogenic isotope (Sr, Nd and Pb) analyses are indicated by red filled dots.



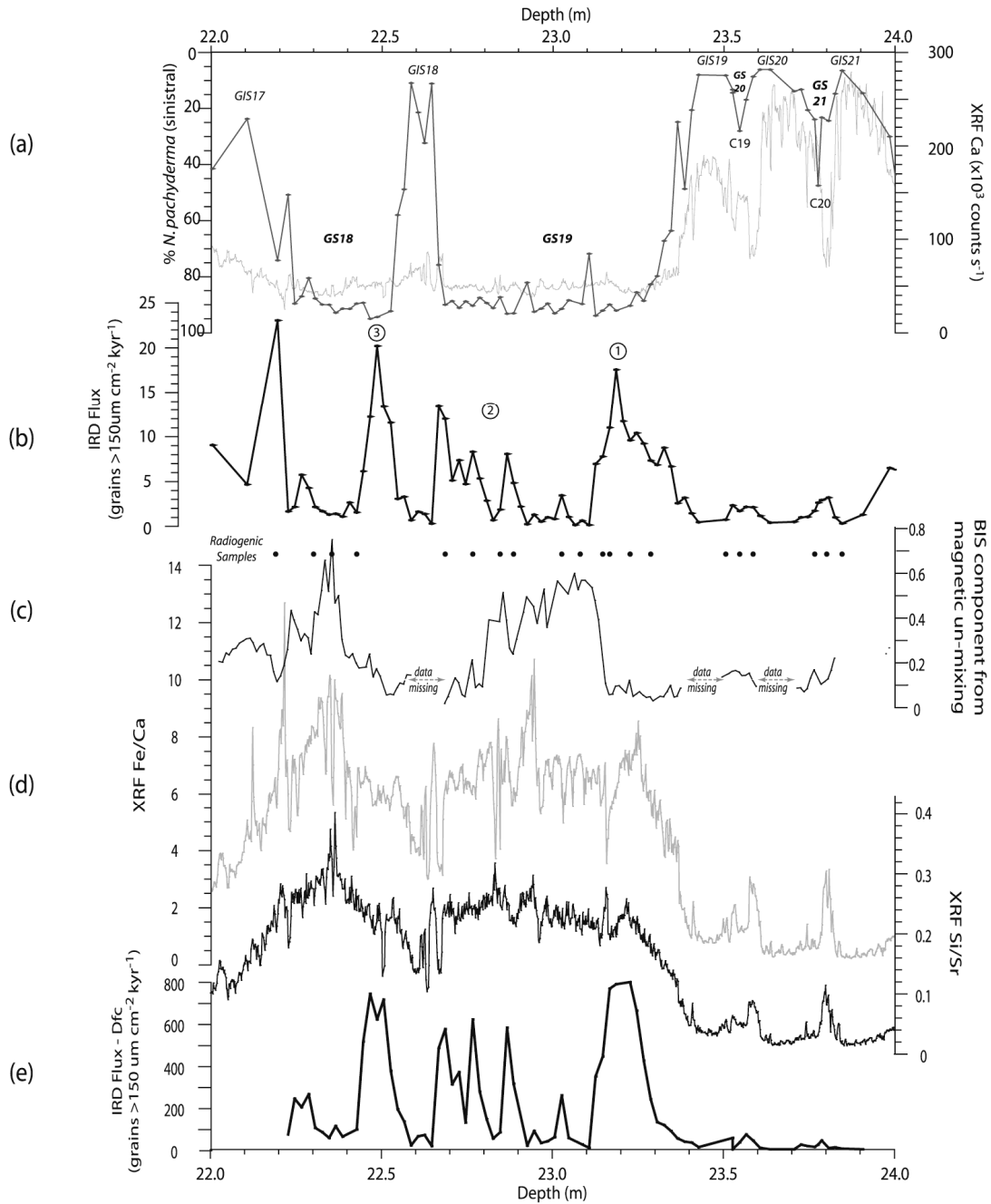
The very similar geological history of the circum-Atlantic regions means that assigning provenance by lithological characterisation alone may be difficult. Several locations may be represented by the same lithic grain types within the IRD record (e.g. haematite stained quartz, see above). Visual lithological characterisation is somewhat subjective and remains a qualitative rather than quantitative indicator of provenance. 'Diagnostic' BIS lithic grains (i.e. basalts) may in fact have been supplied by a number of eroding ice sheets e.g. the BIS, the Fennoscandian or the Greenland Ice Sheet. Additionally, the Rockall Bank may be a source of these grains during intervals of reduced sea levels, through basal 'freeze-on' (M. Stoker, *pers. comm.* Hibbert et al 2010, Scourse et al 2009). The sea level reconstruction of Siddall et al (2003, 2006) estimates a reduction of 80 to 100 m during MIS 4 (Figure 8.8); this would have resulted in the exposure of some portions of the Rockall Bank. Sea ice has been inferred for the Rockall Trough during MIS 4 (Cronin et al 2010, Didié and Bauch 2000) and therefore the contribution of basalt from western sources such as the Rockall Bank cannot be excluded.

Notwithstanding the above, the majority of IRD delivered to a marine site proximal to the location of an ice stream is presumed to be delivered by that ice stream (Scourse et al 2000, Peck et al 2007). Significantly, Clark (1987) demonstrate that the transport of distinctive lithological grains decreases exponentially over a 'characteristic half-distance' of a few tens of kilometres.

When viewed in conjunction with the XRF Si/Sr and Fe/Ca profiles, the lithological characterisations may allow a BIS 'signal' to be more clearly resolved. The increase in 'diagnostic' BIS lithics at the MIS 5/4 transition is accompanied by an increase in XRF Fe/Ca and Si/Sr (Figure 8.10), indicative of increased input of fine grained terrigenous material to the MD04-2822 core site (cf. MIS 6 and MIS 2, chapter 6). The inputs of both Fe/Ca and Si/Sr are episodic during MIS 5 and occur only with the IRD increases associated with the C events. However, at ~ 23.4 m, inputs rise rapidly and remain at high levels until the end of MIS 4. The values of these proxies are similar to those experienced during both Termination II and the last glacial maximum (see chapter 6). The increased input of fine grained terrigenous material is also suggestive of a proximal ice sheet, with sediment delivery via meltwater plumes and melting icebergs.

A British source for both the increased IRD and fine grained terrigenous material is also suggested from an un-mixing model, based upon magnetic parameters of bulk sediments (C. Peters, *unpublished data*; see Peters et al 2008, Walden et al 2007 for details of methodology) (panel (c) in Figure 8.10). Whilst broad similarities exist, this model output differs subtly from both the 'diagnostic' BIS lithic grain type and bulk sediment XRF profiles, the former due in part to analyses on differing size fractions (IRD >150 µm whilst the magnetic analyses are based upon bulk sediments). This may express our inability to resolve the BIS from other potential sources using these proxies, due to the possible contribution of the same material from other regions. The use of these proxies in parallel may reduce the number of potential source areas, although it is not a definitive provenance determination.

Figure 8.10: (a) % *N. pachyderma* (sinistral) and XRF Ca; (b) total IRD flux; (c) BIS source proportions (C. Peters, unpublished data) derived from an un-mixing based upon bulk sediment magnetic parameters (Peters et al 2008); (d) XRF Fe/Ca and Si/Sr; (e) flux of dark finely crystalline grains ('diagnostic' BIS; Knutz et al 2001). Also labelled are Greenland interstadials (GIS) and stadials (GS) as well as C events 20 and 21. The stratigraphic position of radiogenic isotope (Sr, Nd and Pb) analyses are indicated by black filled dots.



3.2.2. *Radiogenic isotope analysis of MD04-2822 bulk sediment*

The provenance indicators presented above were complemented by radiogenic analyses of bulk sediments (the stratigraphic position of these analyses are indicated by the filled dots in Figure 8.9 and Figure 8.10, all analyses are detailed in Appendix B₄). Bulk sediment was analysed as this is thought to represent the integrated erosional signature of ice proximal sediments in areas of former ice streams (e.g. Clark et al 1999, Farmer et al 2003, Jenadel et al 2007). However, within the marine environment, fine grained material may be deposited (or removed) by a variety of processes including the winnowing or scavenging of fine grained material by increased bottom current vigour (e.g. McCave and Hall 2006). The <63 μm fraction may, nonetheless, be the most representative of glaciogenic sediments due to the dominance of the silt and clay fraction within bulk sediments (Andrews 2000).

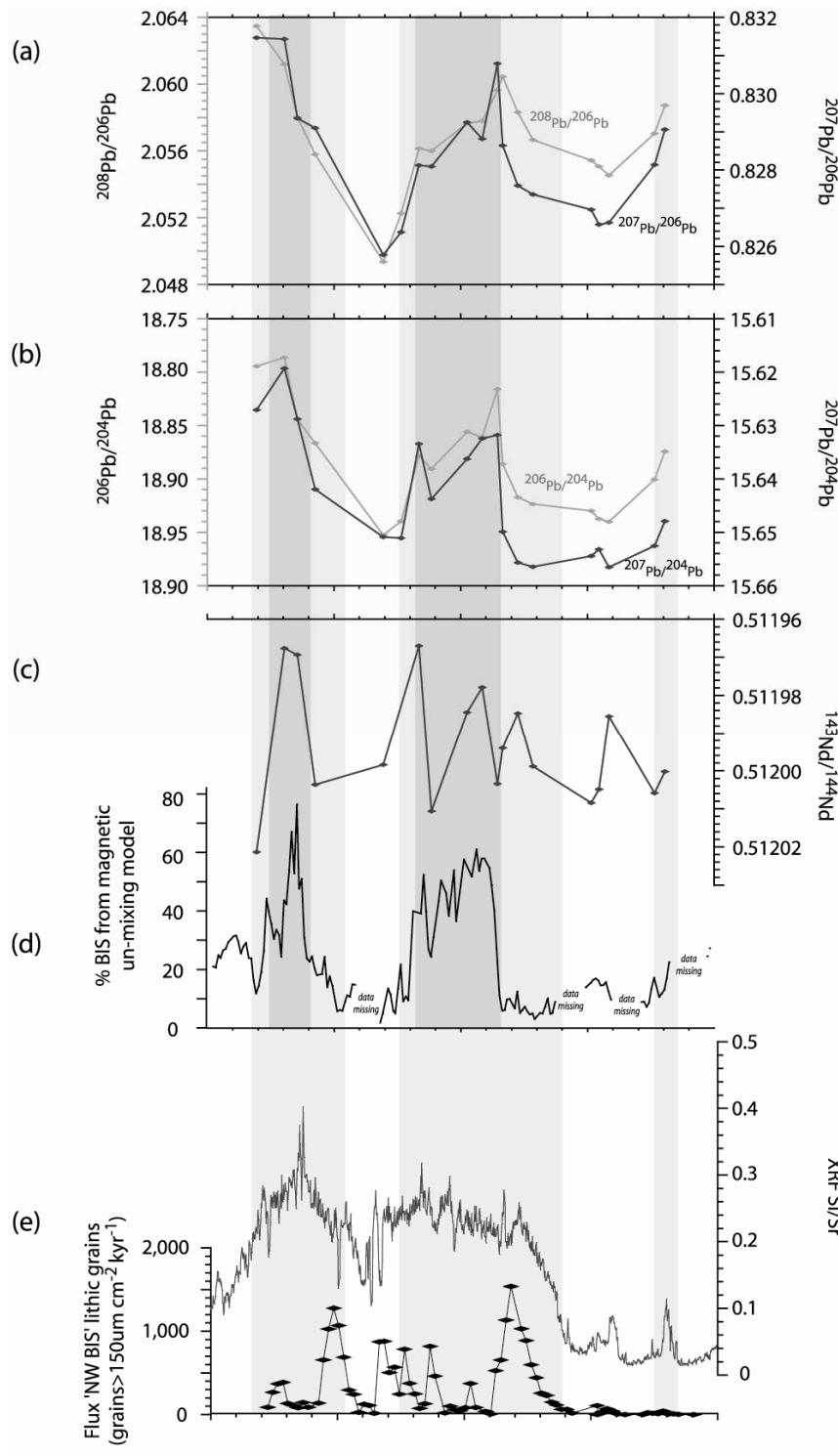
The Sr, Nd and Pb analyses enable the relative source contributions to be determined via the matching of unknown sample analyses to source 'fields' derived from isotopic inventories (e.g. Grousset et al 1993, 2001, Jeandel et al 2007). Often bulk sediment samples plot amongst several fields and thus a single source cannot be determined; instead the 'dominant' source may be identified (Revel et al 1996) i.e. the relative change in source contribution.

The variation within the radiogenic isotopes (Pb, Nd and Sr) is fairly subtle, but there is a strong correspondence between the Pb and Nd isotopes with the proposed BIS component determined from a magnetic un-mixing model (C. Peters, *unpublished data*) (Figure 8.11).

The variation in the Pb isotopes may be accounted for by a very small increase in 'old' crust or volcanic material e.g. from the Rockall Trough. The lithic characterisations (Figure 8.9) could suggest a combination of the two. Similarly, the variation in the Nd isotopes may result from a very small increase in old crustal material but both signals are rather muted.

There are also similarities between the Si/Sr data and the Pb isotopes; this is thought to reflect a change from 'background' hemipelagic deposition (low radiogenic) to increased terrigenous input (increased radiogenic).

Figure 8.11: Bulk sediment analyses for MD04-2822 - radiogenic isotopes and modelled BIS source component (magnetic un-mixing, C. Peters, *unpublished data*). (a) $^{208}\text{Pb}/^{206}\text{Pb}$ and $^{207}\text{Pb}/^{206}\text{Pb}$; (b) $^{206}\text{Pb}/^{204}\text{Pb}$ and $^{207}\text{Pb}/^{204}\text{Pb}$; (c) $^{143}\text{Nd}/^{144}\text{Nd}$; (d) % BIS component from magnetic un-mixing model; and (e) XRF Si/Sr and flux of 'NW sector BIS' lithic grains ($>150\ \mu\text{m}$). Vertical pale green bars highlight correspondence between fine-grained terrigenous inputs and the radiogenic Pb isotopes; grey bars highlight correspondence of radiogenic isotopes with BIS component derived from magnetic un-mixing model.



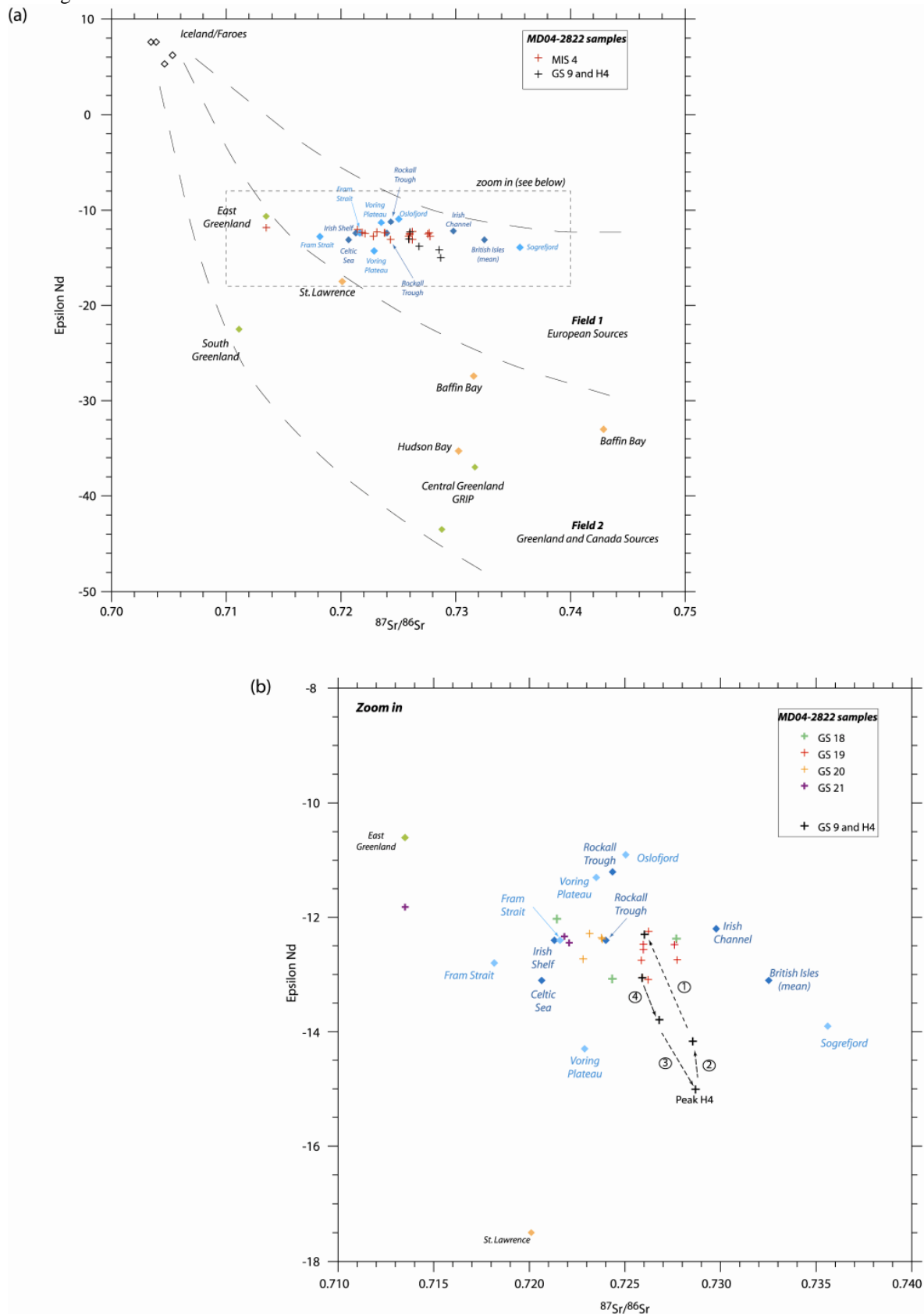
IRD provenance studies of Heinrich events often use radiogenic isotopes (particularly Sr and Nd) to discriminate source regions (e.g. Peck et al 2007, Gwiazda et al 1996). The MD04-2822 samples are compared to the IRD (>63 μm) data of material proximal to the former circum-Atlantic ice sheets (Grousset et al 2001). From Figure 8.12(a), all the MD04-2822 samples plot within the European source field identified by Grousset et al (2001), including a sample from the peak occurrence of detrital carbonate of H4 (Figure 8.12b). However, on the expanded scale, the relative increase in a Canadian/Greenland source (after Grousset et al 2001) during H4 may be discerned as a shift to more negative epsilon Nd ($\epsilon_{\text{Nd}}(0)$) values with a small change in $^{87}\text{Sr}/^{86}\text{Sr}$ values. The MD04-2822 samples plot amongst >63 μm data for the Fram Strait, Vøring Plateau, Oslofjord, Irish shelf and Rockall Trough (Grousset et al 2001), except for one data point which lies close to the East Greenland end member.

When the MIS 4 data is plotted according to stadial designation (Figure 8.12b), there is a progression to increased $^{87}\text{Sr}/^{86}\text{Sr}$ values through GS21, 20 and 19. Stadials 20 and 19 values are clustered, whilst those for GS 21 and GS 18 are more dispersed. In addition, the GS19 samples plot amongst the GS9 and H4 samples. Subtle variations in the contributions of these sources may account for some of the variation observed within the MD04-2822 MIS 4 radiogenic isotopes. However, the variation within the data is insufficient to be able to plot vectors towards potential source components, indeed all of the observed variation could be accounted for with British sources, without recourse to a Laurentide source (Ian Millar, *pers comm.*).

The Sr and Nd isotopes were plotted against the inverse of the concentration of Sr or Nd in order to investigate further any potential mixing of components as mixing trends on plot as straight lines (Figure 8.13). The GS9 and H4 Nd data plot along a vertical line reflecting mixing between 'normal' sedimentation and incorporation of an 'older' component. Lithological characterisation confirms the presence of detrital carbonate ('sugary' in appearance) which is thought to have been eroded from below the Laurentide ice sheet (confirmed by $\delta^{18}\text{O}$ of individual carbonate grains; Appendix B₅). For the MIS 4 data, most display the same vertical trend, although samples from stadials 20 and 21 lie upon a trend to the right. It is proposed that for the MIS 4 interval, there is a mixing between two sources. The same trends are also apparent within the Sr data, although the trends are less clear (Figure 8.13b).

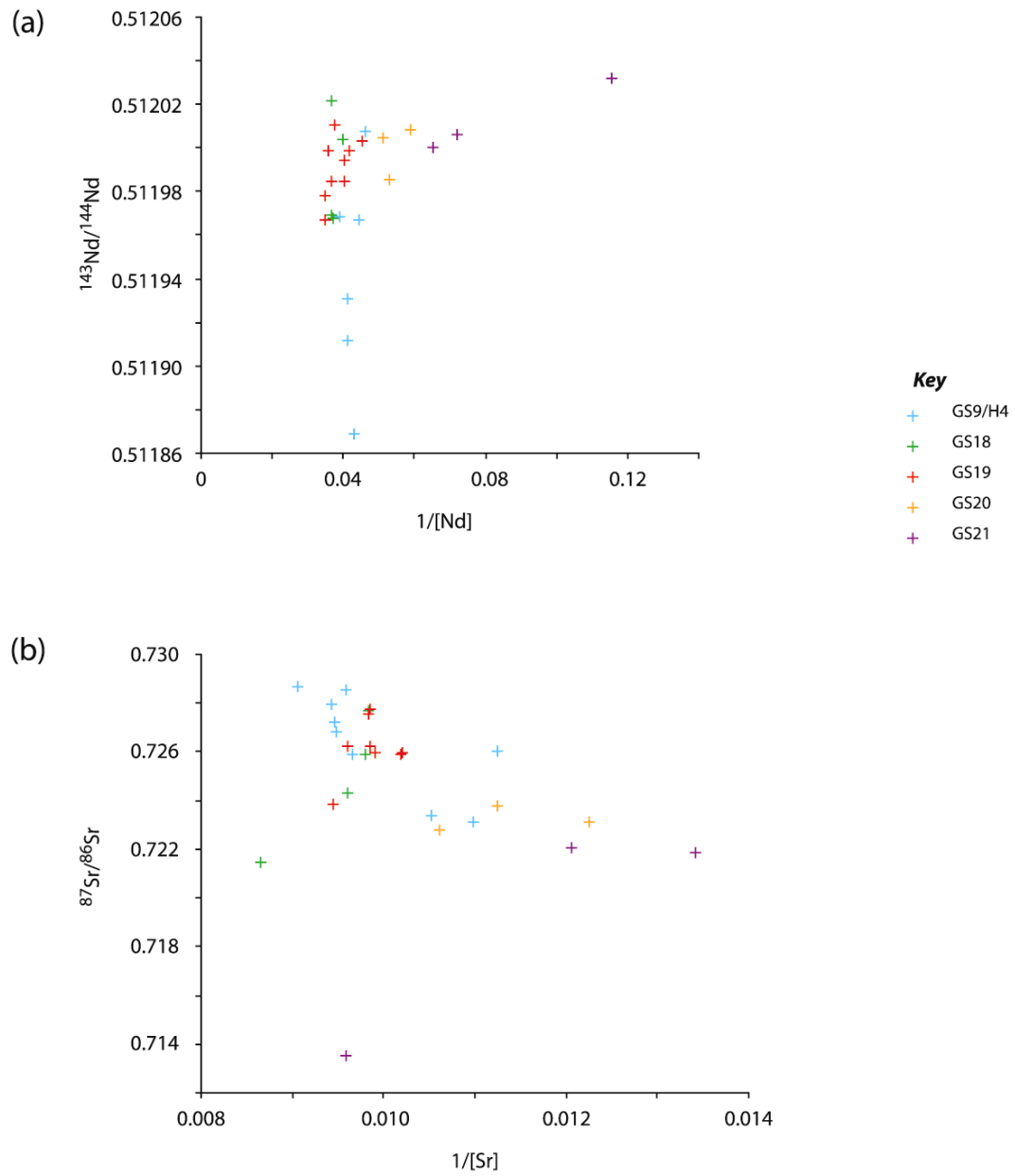
Whilst the radiogenic isotope data alone does not allow unequivocal discrimination of sources, this data, in conjunction with increased fine-grained terrigenous inputs, increased IRD and an increase in the BIS component of bulk sediments predicted by a magnetic unmixing model (C. Peters, *unpublished data*) suggest a change from hemipelagic dominated sedimentation, to episodes of increased terrigenous inputs. Within this, there appears to be a change in source of material as MIS progresses, with isotope values more closely resembling those obtained for GS9 and Heinrich event 4. As such, we have used the GS9 sub-set as analogous to a 'small' BIS. This is discussed further in the following section.

Figure 8.12: Sr and $\epsilon_{Nd}(0)$ analyses for MD04-2822 (MIS 4 red crosses; GS9 and H4 black crosses) plotted within the fields of Grousset et al (2001) ($\epsilon_{Nd}(0)$, $2\sigma \pm 0.3$; $^{87}Sr/^{86}Sr$ $2\sigma \pm 3$ to 6×10^{-6}) (a). Data from Grousset et al (2001) was obtained from material $> 63 \mu m$, MD04-2822 data is for bulk sediment. (b) zoom in of dashed grey box in (a); note the MIS 4 MD04-2822 samples are now plotted according to their stadial designation.



CHAPTER 8:
Glacial Inception

Figure 8.13: (a) $^{143}\text{Nd}/^{144}\text{Nd}$ versus $1/[\text{Nd}]$ and (b) $^{87}\text{Sr}/^{86}\text{Sr}$ versus $1/[\text{Sr}]$. Note the data is plotted according to stadial designation (same colour scheme as Figure 8.12).



H4 analogy

Peters et al (2008) suggest BIS growth post H4, from bulk sediment magnetic parameters (interpreted using an un-mixing model) for core MD95-2006 (57° 01.82'N, 10° 03.48'W). Prior to H4, the low BIS source proportions are thought to indicate that the BIS was delivering only limited amounts of material to the Rockall Trough (Peters et al 2008). This appears to be confirmed by lithological characterisation of IRD within MD95-2006 and Sr and Nd isotope analyses (Leigh 2006). The analyses undertaken for MD95-2006 have been reproduced from MD04-2822 (Figure 8.14). The GS9 interval is therefore thought to represent a 'small' BIS, analogous to a nascent Weichselian BIS.

The first and last GS9 samples (Figure 8.12) have very similar $^{87}\text{Sr}/^{86}\text{Sr}$ values; there is a shift towards more negative $\epsilon_{\text{Nd}}(0)$ values and increased $^{87}\text{Sr}/^{86}\text{Sr}$ into (1 and 2 in Figure 8.12) and out of (3, Figure 8.12) the H4 peak, towards the Baffin Bay/Hudson Bay end-members of Grousset et al (2001) with a subsequent return values similar to early within GS9 (4, Figure 8.12). The low $\delta^{18}\text{O}$ values of individual carbonate grains, analysed from the peak interval of H4²⁸ within both cores (D. Hodell, *unpublished data*, Appendix B₅) are also indicative of a Hudson Bay or Baffin Bay origin (Hodell and Curtis 2008, Andrews 1988, Andrews and Tredesco 1992, Parnell et al 2007). The first and last GS9 samples analysed are inferred to be primarily BIS, with the latter representing an increased contribution of BIS material, due to the destabilisation of the marine margins by the sea level increase associated with H4. In addition, high values of $^{206}\text{Pb}/^{204}\text{Pb}$ are associated with increased BIS inputs.

Using the H4 data as representative of a 'small/immature' BIS, the progression through the stadials of MIS 4 may be thought of in terms of increasing BIS inputs to the MD04-2822 site. This is in agreement with the proposed expansion of the BIS at the GIS/GS 19 transition, based upon both the fine grained terrigenous and lithic grain counts (Figure 8.15).

Within Figure 8.12, values for GS21 samples cover a relatively wide range, possibly because this material is derived from a number of different sources (e.g. East Greenland and the Fram Strait). GS20 values are clustered but of increased $^{87}\text{Sr}/^{86}\text{Sr}$, perhaps indicative of the increasing contribution of BIS inputs. GS19 samples are again clustered (Figure 8.12), lying within the GS9/H4 'window' and are presumed to be dominated by a supply of material from NW BIS ice streams. The close correspondence of these samples suggests the dominance of a single source i.e. a dominance of BIS material, with some additional inputs from other sources accounting for the observed variations. These variations are relatively small and thus inhibit further attempts to attribute source regions. However, increased Laurentide derived material is predicted by the magnetic un-mixing model (C. Peters, *unpublished data*) and a slight increase in detrital carbonate with IRD >150 μm (Figure 8.15, Figure 8.16). GS18 is again widely distributed, with decreasing $^{87}\text{Sr}/^{86}\text{Sr}$ as the stadal progresses, which may suggest a decreasing influence of BIS material and the incorporation of material from other sources. The decreased inputs from the BIS could be a consequence of its retreat, prompted by melting and/or destabilisation of the marine calving margins with increased SSTs (GIS17).

²⁸ as defined by the peak concentration in detrital carbonate grains within IRD > 150 μm

CHAPTER 8:
Glacial Inception

Figure 8.14: Greenland Stadial 9 and H4 in MD95-2006 and MD04-2822 (a) % *N. pachyderma* (sinistral);(b) lithic grain counts - % Dfc (weathered volcanics) (black line) and % detrital carbonate (grey line); (c) magnetic source proportions from an un-mixing model BIS (black line), LIS (grey line); and (d) $^{206}\text{Pb}/^{204}\text{Pb}$ (open diamonds) and $\epsilon_{\text{Nd}}(0)$ (black filled squares).

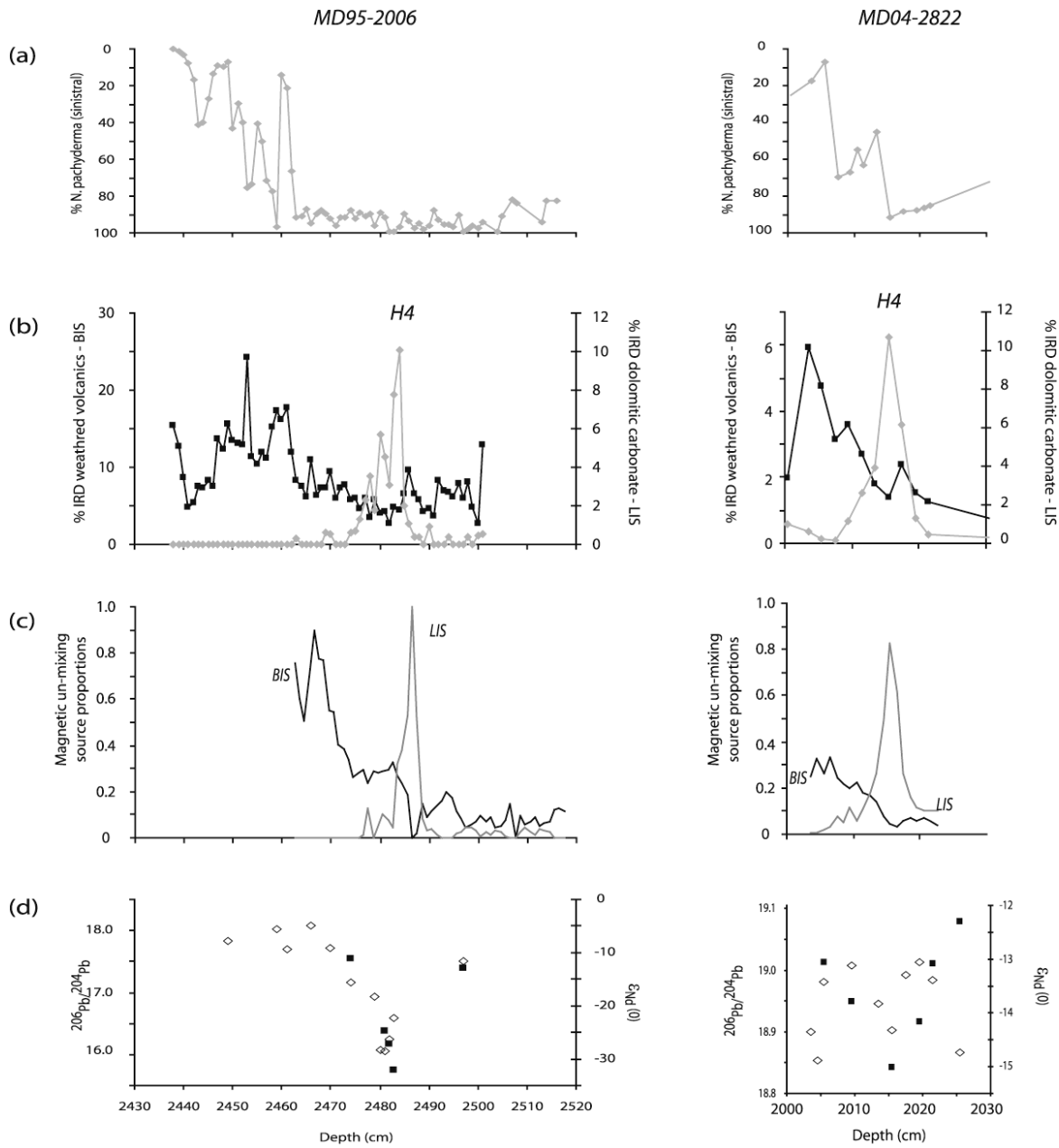
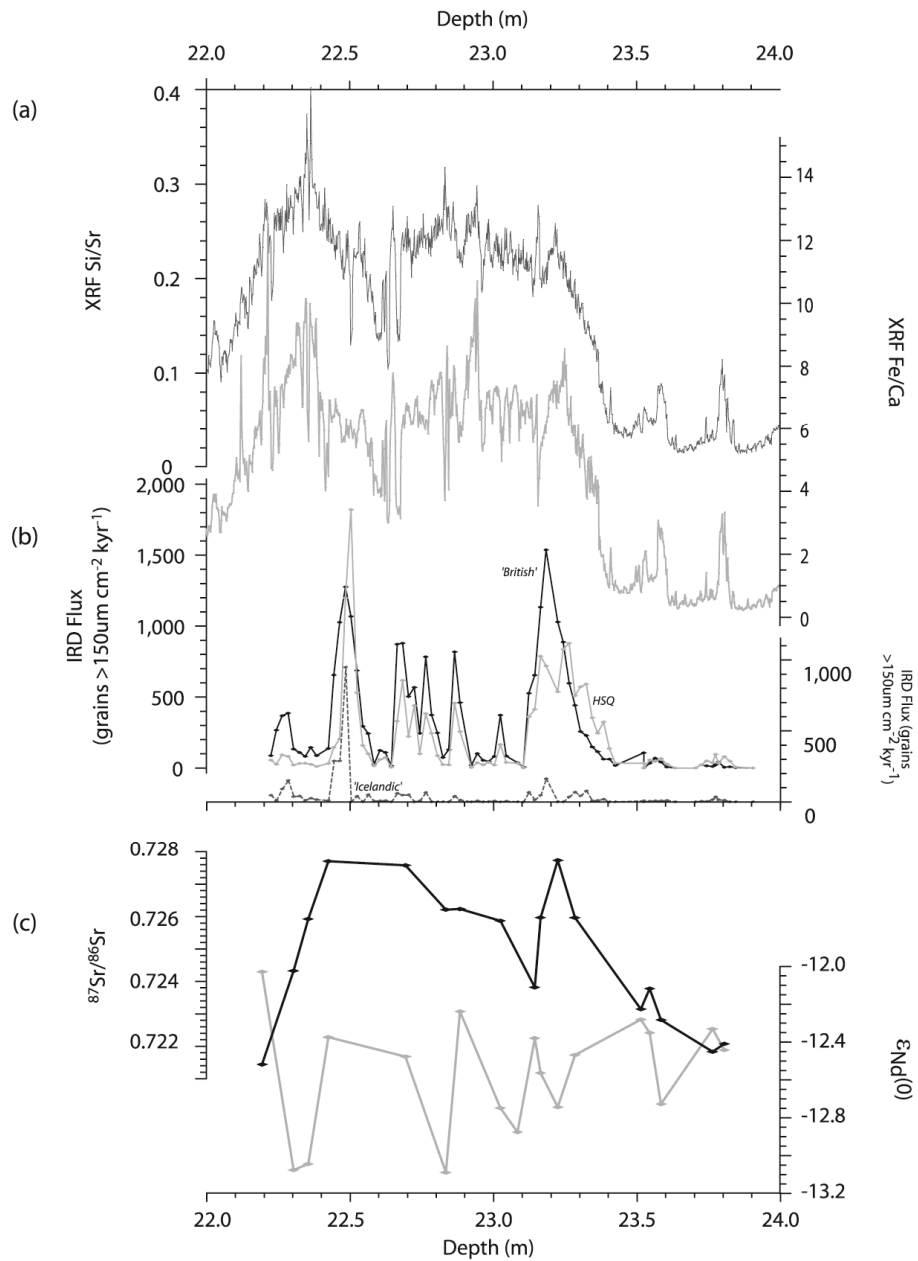
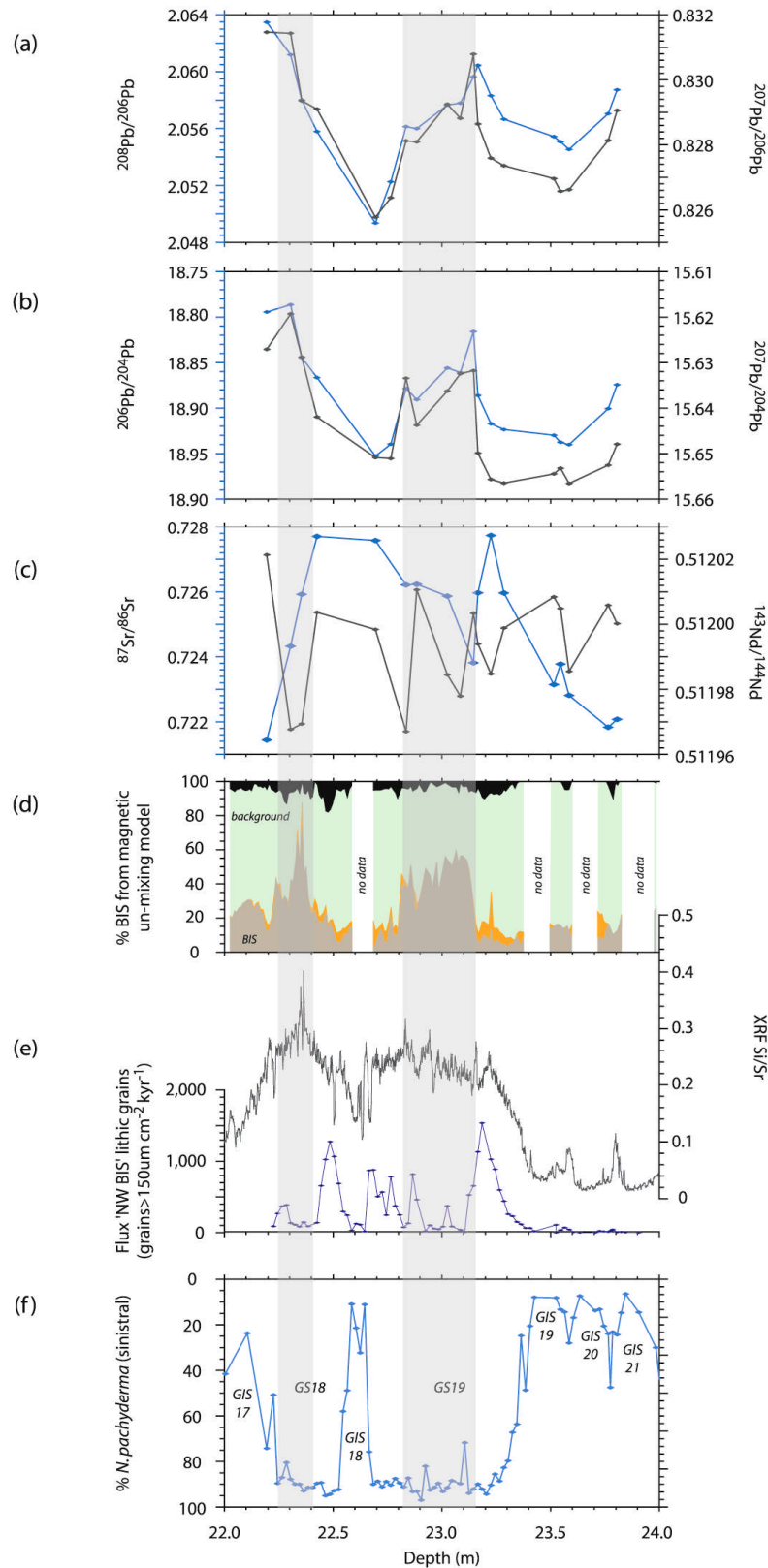


Figure 8.15: Terrigenous inputs to MD04-2822 (a) Fine grained terrigenous proxies XRF Si/Sr and Fe/Ca; (b) Lithic flux (grains >150 μm) 'British' includes dark finely crystalline, crystalline rock fragments and mica; HSQ is haematite stained quartz, 'Icelandic' includes tephra, pumice and obsidian; (c) $\epsilon_{\text{Nd}}(0)$ and $^{87}\text{Sr}/^{86}\text{Sr}$ analyses (bulk sediment).



CHAPTER 8:
Glacial Inception

Figure 8.16: Provenance indicators and surface hydrography for MD04-2822 (a) $^{208}\text{Pb}/^{206}\text{Pb}$ and $^{207}\text{Pb}/^{206}\text{Pb}$; (b) $^{206}\text{Pb}/^{204}\text{Pb}$ and $^{207}\text{Pb}/^{204}\text{Pb}$; (c) $^{87}\text{Sr}/^{86}\text{Sr}$ and $^{143}\text{Nd}/^{144}\text{Nd}$; (d) percentage contribution from the BIS (dark grey), LIS (orange), IIS (black) and background (green) derived from a magnetic un-mixing model (C. Peters, unpublished data); (e) XRF Si/Sr and flux of 'NW sector BIS' lithic grains ($>150\ \mu\text{m}$) and; (f) % *N. pachyderma* (sinistral), stadial (GS) and interstadial (GIS) designations. Vertical orange bars highlight the increase in BIS predicted by the magnetic un-mixing model and coincident increase in Pb isotopes.



3.2.3. *Age estimate for the early Weichselian BIS expansion*

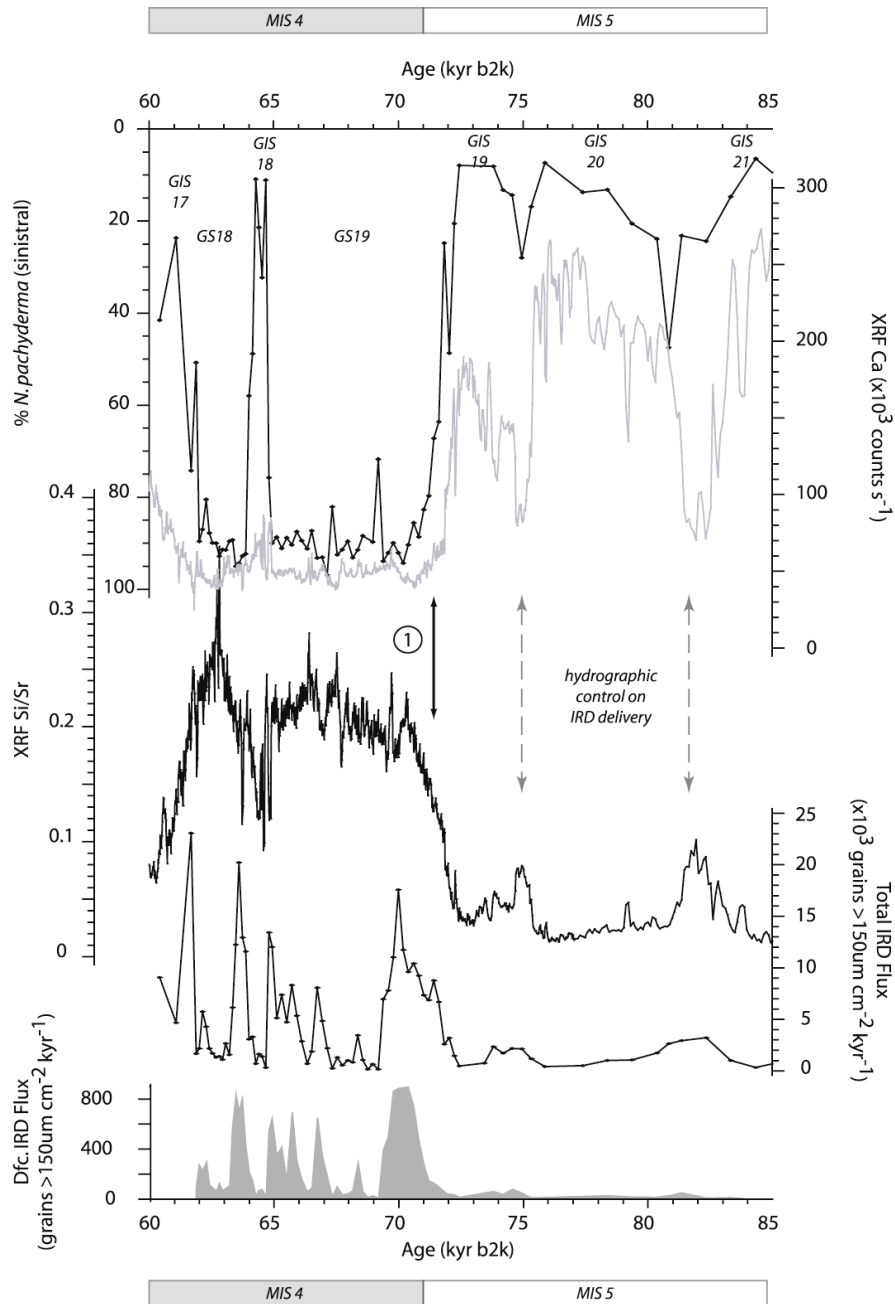
Excursions of polar waters (peaking at ca. 81 and 75 kyr; C20 and 19 respectively) would probably have increased the delivery of icebergs to the MD04-2822, resulting in minor increase in IRD inputs, shown in Figure 8.17. This IRD comprises very few 'diagnostic' BIS grains and from radiogenic isotope analysis of bulk samples, the dominant source of this material was is not thought to be the BIS. These minor IRD events within MIS 5 instead reflect the growth of more northerly ice sheets, although a very restricted BIS (i.e. mountain glaciation) cannot be ruled out. Cooling global temperatures and the steepening of thermal gradients, coupled with a moisture source (i.e. warm surface waters) and topographic highs may have promoted ice growth; however, this very early BIS glacial history would be missing from the MD04-2822 marine sediment record, due to its restricted size and the lack of marine calving margin.

The sustained delivery of IRD and fine grained terrigenous material to the MD04-2822 site started at ca. 72 kyr (labelled 1 in Figure 8.17) and remained until SST warming at the MIS 4/3 transition. A decrease in IRD and Si/Sr inputs at ca. 65 kyr was prompted by the warming into GIS18. This warming destabilised the marine margins, leading to a retreat and a brief episode of low IRD inputs. During this episode of warm SSTs, an increase in IRD within GIS18 attests to its potential as moisture source and BIS re-growth. The final peak of IRD seen at 61.5 kyr may be linked to H6 but as this peak has not been lithologically described, thus provenance for this IRD cannot be determined. Some ambiguity remains as to the positioning of this event with MIS 4 (e.g. Manighetti et al 1995). Increasing insolation and increased melting may account for the reduction in XRF Si/Sr from ca. 63 kyr, as the ice retreated.

Within MIS 4, the nascent Weichselian BIS had grown sufficiently to obtain a marine margin. This ice was very sensitive to climatic (and possible sea level) variations. IRD inputs are sustained but episodic prior to a significant retreat at the MIS 4/3 transition, as northern hemisphere insolation continued to increase. The presence of a BIS within MIS 4 need not contradict terrestrial evidence of a largely ice free MIS 3 prior to the Devensian LGM maximum (e.g. Hall et al 2003), if this ice had retreated significantly or decayed at the MIS 4/3 transition.

CHAPTER 8:
Glacial Inception

Figure 8.17: MD04-2822 hydrological proxies and terrigenous inputs presented on age. MIS designations after Imbrie et al (1984); Greenland stadial (GS) and interstadial (GIS) are labelled. Dashed arrows highlight the hydrographic control on IRD delivery to the MD04-2822 site during MIS 5; arrow labelled 1 indicates the start of sustained inputs of both IRD and fine grained material to the core site.



3.3. Summary and Conclusions: palaeoceanographic and climatic influences on IRD delivery to MD04-2822 and expansion of the BIS after the last interglacial

The SST cooling and IRD events (C events; e.g. Chapman and Shackleton 1999, McManus et al 2002) that characterised North Atlantic marine records after the demise of the last interglacial, are also present within the MD04-2822 record. All the C events (except C25 and C22) are present in this record, however they are not necessarily seen as a reduction in the % *N. pachyderma* (sinistral); rather some are only identified by a decrease in benthic $\delta^{13}\text{C}$ (i.e. reduction in AMOC) and a very small increase in IRD. This confirms the spatial distribution of IRD associated with the C events proposed by Chapman and Shackleton (1999) except for C23 where this event appears to have a greater geographic extent with increased IRD transported to both MD04-2822 (this study) and ODP 980 core sites (Oppo et al 2006), although these IRD inputs are modest (Figure 8.5, Figure 8.6). The geographic expression of the C events based upon % *N. pachyderma* (sinistral) (i.e. greater than 10 to 20 %) used by McManus et al (2002) to map the position of the C events is also corroborated by the MD04-2822 data.

The increased IRD with each of the C events, especially C24, 23, 21, 20 and 19, suggest hydrography exerted a strong influence on IRD delivery to the MD04-2822 site during MIS 5. The variation in AMOC associated with the C events reflects the inputs of freshwater into the Nordic Seas from incipient high latitude ice sheets. The geographically extensive C24 and C21 events may have been forced by increased melting of early Northern Hemisphere ice sheets with increased insolation.

The MD04-2822 record compares favourably to that of ODP 980 (Oppo et al 2006), with most C events documented in both records. The influence of high latitude ice sheet oscillations therefore extends to the NE Atlantic via a reduction in AMOC, often accompanied by widespread expansion of polar waters and an increase in IRD inputs. Some of the more pronounced C events (e.g. C24, 21 and 20) in these records are characterised as a greater decrease in the % *N. pachyderma* (sinistral) at the MD04-2822 site compared to ODP 980. This may reflect the closer proximity of the MD04-2822 core to the polar front during these intervals.

A long-term increase in benthic $\delta^{13}\text{C}$ throughout MIS 5 is evident in the MD04-2822 record. This trend is also seen within ODP 980 (e.g. McManus et al 2002, Oppo et al 2006) and other benthic $\delta^{13}\text{C}$ records throughout the North Atlantic (e.g. Chapman and Shackleton 1998, Chapman et al 2001, Oppo and Lehman 1995) and the eastern Atlantic Pa/Th record of Guihou et al (2010). AMOC therefore continued throughout MIS 5, with some variations forced by meltwater inputs derived from Northern Hemisphere ice sheets.

The penetration of NAC into the high latitudes at the end of the last interglacial and enhanced AMOC (with increased salinities) facilitated ice sheet growth (e.g. Risebrobakken et al 2007). As MIS 5 progressed, the extension of the NAC into the far northern Nordic Seas was curtailed as ice sheets grew and sea levels decreased. The Nordic Seas increasingly experienced stable and perennial sea ice cover with decreasing temperatures. The combination of continuing transport of saline waters into the Nordic Seas coupled with decreased temperatures promoted/enhanced deep

convection. This may explain the continuing 'improvement' in the benthic $\delta^{13}\text{C}$ signal of many North Atlantic deep sea cores through the MIS 5 interval. The increasing 'vigour' of AMOC, with both a salinity and temperature component, could account for the 'change in production rate' or increasing depth of NADW proposed by Chapman and Shackleton (1998). MD04-2822 $\delta^{13}\text{C}$ values attained during MIS 5c to MIS 5a are similar to those recorded during episodes of MIS 3 and MIS 1. It is only at the MIS 5/4 transition (although the benthic $\delta^{13}\text{C}$ record lags benthic $\delta^{18}\text{O}$) that deep circulation switches to another mode more akin to the formation of GNAIW and the polar front migrates far to the south of the MD04-2822 core site.

Early within MIS 4, inputs of IRD to MD04-2822 are primarily controlled by hydrography, specifically the expansion of polar water masses during GS 21 and 20 enabled icebergs and IRD from other circum-Atlantic ice sheets (e.g. Fennoscandian) to be delivered to the site, with a possible small contribution from a nascent BIS. The warm surface conditions (low % N. pachyderma (sinistral)) during GIS 21, 20 and 19 provided a moisture source for the build up of the BIS, which expanded to achieve a marine calving margin at the transition into GS19.

Elevated terrigenous inputs (both IRD and fine grained material) appear to occur in two pulses (recorded as, for example, increased Pb isotopes and Si/Sr). The first pulse occurs during GS19 (ca. 72 kyr b2k) and is thought to be primarily derived from BIS sources. This age corresponds favourably to the ages of MIS 4 ice sheet activity in eastern Scotland (e.g. Oldmill and Ungie Valley sites; Gemmel et al 2007) and the inferred expansion of British ice into the North Sea during MIS 4 (e.g. Carr 2004) (section 2.2.2, this chapter). A second pulse of terrigenous material occurs within GS18, with BIS inputs decreasing through the stadial. The decreased inputs from the BIS could be a consequence of its retreat, prompted by melting and/or destabilisation of the marine calving margins with increased SSTs (GIS17) with major decay/retreat of the BIS prompted by increased insolation at the MIS4/3 transition.

The similar geological history of the circum-Atlantic continents complicates the determination of sediment provenance at the MD04-2822 core site (especially lithological characterisation and radiogenic isotopes). However, the results from these techniques, in parallel with the bulk IRD counts, appear to corroborate the hypothesis of increased BIS inputs to the MD04-2822 site during MIS 4. Sustained BIS origin inputs occur during GS19 before reducing as the ice sheet retreated. The early BIS therefore appears to be highly sensitive to prevailing climatic conditions, with warm surface waters providing a moisture source for growth during global cooling.

4. Overview

The penetration of warm waters into the high Nordic Seas provided a moisture source for the formation of the early Weichselian ice sheets, as Northern Hemisphere insolation decreased and climate cooled at the end of the last interglacial. MD04-2822 documents the growth of these high northern latitude ice sheets as a series of amphiatlantic SST cooling events during MIS 5, which are associated with the advance of the polar front into the North Atlantic, increases in IRD and a reduction in AMOC

(reductions in benthic $\delta^{13}\text{C}$). These reductions may have been forced by input of freshwater (icebergs/meltwater) from the existent Northern Hemisphere ice sheets (e.g. Oppo et al 2006).

A progressive southward locus of ice sheet growth is documented within the terrestrial and marine records (e.g. Svendsen et al 2004, Mangerud et al 1981a) because the northern limb of the NAC was unable to penetrate into the high latitudes as MIS 5 progressed. At the MD04-2822 site, however, surface conditions appear to be relatively clement with low values of % *N. pachyderma* (sinistral) through MIS 5 and early into MIS 4.

At the MIS 5/4 transition, local deterioration in surface conditions lags the MD04-2822 benthic record, suggesting that high-latitude climates (and ice volume) had deteriorated (increased) before the mid-latitude surface ocean cooled significantly (e.g. Figure 8.6). This period marks an increase in global ice volumes and the growth of the northwestern European ice sheets. An expansion of British ice within MIS 4 has been suggested within the North Sea (e.g. Carr 2004) and NE Scotland (Gemmel et al 2007), although evidence from the Hebridean margin is currently based upon long-range correlation of North Sea seismic profiles (Holmes 1997) although terrestrial glacial deposits younger than the last interglacial but older than MIS 4 have been documented in western Scotland (e.g. stratigraphy of Finlayson et al 2010). MD04-2822 provides the first tentative evidence for an expansive glaciation in NW Scotland during MIS 4 at ca. 72 kyr (b2k)²⁹.

Increases in both 'diagnostic' lithics and XRF terrigenous proxies at the transition into GS19 suggest an expansion of ice (presumably 'seeded' at altitude and subsequently expanded to the coast) and a BIS of a significant size, in order to supply a sustained and significant input of IRD and fine grained material to the MD04-2822 site, during MIS 4. Of course, the very earliest history of the Weichselian ice sheet would not have been captured within the MD04-2822 record; without a marine calving margin, no BIS sourced IRD would be transported to the site. During GS19 therefore, the BIS in NW Scotland was sufficiently large to reach the coast and calve icebergs, but the ice sheet is presumed to have existed prior to this time.

²⁹ The MD04-2822 data provides a minimum age estimate for the expansion of the early BIS to the coast of NW Scotland. This expansion is inferred at ~72 kyr (b2k). The early history of the BIS is fragmentary and age control difficult for many sites. The data presented from MD04-2822 is however underpinned by a robust chronology. Whilst the timing of events is secure, provenance designations are indicative rather than unequivocal.

CHAPTER 9: Conclusions and Future Prospects

This study presents a stratigraphic investigation of the marine sediment core MD04-2822 from the Rockall Trough. This core is currently the only available high resolution record available for the British margin, for the calibration of Late Quaternary sedimentary sequences of the Hebridean margin. It therefore offers an unprecedented archive of changing sedimentological and climatological conditions for the last 175,000 years. The high resolution, multi-proxy records have enabled surface and deep water conditions within the Rockall Trough to be reconstructed. In addition, the fluctuating nature of IRD inputs to the MD04-2822 site allowed a first order attempt of BIS dynamics for the entirety of the last glacial period (i.e. from the demise of the last interglacial to the decay of the Devensian/Weichselian ice sheet) as well as the majority of the penultimate glaciation.

The temporal span of the MD04-2822 record has enabled an uninterrupted record of changing climatic conditions for the North East Atlantic to be determined. The following section summaries the principle scientific findings from the study, within the context of the original aims and objectives (chapter 1) as well as the wider corpus of Late Quaternary glacial and climatological change.

1. Chronology

A principle objective of this study was the derivation of a robust chronology for the MD04-2822 sediment core. This was achieved by utilising an event stratigraphy approach and by combining several ‘tuning targets’ (i.e. benthic $\delta^{18}\text{O}$ stacks, the Greenland ice core (NGRIP) $\delta^{18}\text{O}$ and the Antarctic EPICA Dome C methane record) tested with AMS ^{14}C dating and tephra isochrons (Chapter 3).

The relatively few age control points used to tie the MD04-2822 benthic $\delta^{18}\text{O}$ to the global benthic $\delta^{18}\text{O}$ stacks (SPECMAP and LR04) is a function, in part, of the potential alternative correlations in addition to concerns regarding the reliability of the benthic $\delta^{18}\text{O}$ stratigraphy on millennial timescales (e.g. Skinner and Shackleton 2005), arising from influences upon the benthic $\delta^{18}\text{O}$ other than changes in global ice volumes (e.g. intra basin offsets in the timing of terminations, local hydrographic ‘overprinting’) (Chapter 3). However, benthic $\delta^{18}\text{O}$ remains a valuable means by which age control on very long time periods may be applied to marine proxy records.

Similarly, the assumption of the synchronicity of SST changes in the North Atlantic and air temperatures over Greenland (cf. Shackleton et al 2000) appears to be reasonable; although relatively few intervals have tested the assumption of synchronicity (e.g. the stratigraphic occurrence of tephra layers (NAAZ II); Austin et al 2004, this study). The INTIMATE protocol offers some promise in untangling the degree to which the climatic events within the North Atlantic during the last glacial were synchronous, and facilitates both the correlation of records and an evaluation of leads or lags within the climate system. Problems remain in obtaining independent (i.e. non-tuned) age control of marine sediments using radiocarbon dating (e.g. the poorly constrained spatial and temporal variation in the marine reservoir effect) and

tephrochronology (due primarily to the relatively few well characterised events for the last glacial period).

Notwithstanding these concerns, the value of a diligent approach to stratigraphy has been highlighted by this study. For example, following the event stratigraphy approach the spatial extent of features may be discerned including the previously unrecorded warming event within the NE Atlantic during GS3 (NEA-GS-3b) (Chapter 4).

The formation of a robust chronology is paramount in the assessment of the timing and pacing of events. However, Skinner (2008) cautions that the chronologies of the 'tuning targets' are rarely 'absolute' and that 'a given chronostratigraphy is best viewed as a hypothesis'. The application of this chronology to palaeoclimatological reconstruction is reliant upon the 'end-user' being aware of its limitations; for example the prevalent application of linear interpolation, which whilst practicable may not accurately model 'true' sedimentation at the site.

1.1. Correction of Coring Artefacts

Once a chronology had been obtained for the MD04-2822 core, IRD flux could be calculated for the last ~175 kyr. Upon calculating IRD fluxes for the last deglacial (the Younger Dryas in particular), the strong probability that the upper portions of the core were affected by 'over-sampling' was highlighted. The maintenance of stratigraphic 'truth' is essential in investigating depositional processes. This study (Chapter 5) demonstrated the value of paired coring i.e. using both piston and gravity coring at the same site, as advocated by Skinner and McCave (2003). The availability of a gravity core from the same location enabled the correction of 'over-sampling', which appeared to suggest far greater IRD fluxes during the Younger Dryas (GS1) than for the LGM, a period in which the BIS ice extent was far greater. This corrected IRD flux was then used to reconstruct IRD input to the site during the last deglaciation.

The recovery of both piston and gravity cores from the same location may be vital in retaining the stratigraphical and dimensional 'truth' of marine sediments. The preservation of sediment dimensions is essential for the calculation of mass fluxes and hence many depositional processes such as IRD flux.

2. British Ice Sheet Activity

The MD04-2822 marine record is well placed to reconstruct Late Quaternary BIS glacial history, and climatic influences, in that it is continuous and more than doubles the current temporal range of high resolution cores for the British margin (cf. synthesis by Scourse et al 2009). In addition, the record is less susceptible than terrestrial records to the removal or obfuscation of evidence by subsequent ice sheet oscillations. The availability of a robust chronology also provides the first temporal constraint of older glacial episodes that are often problematic for many of the (fragmentary) terrestrial records.

A primary objective of this study was the calculation of IRD flux to the MD04-2822 site during the entirety of the last glacial cycle and most of the penultimate glacial. Elevated IRD and fine grained terrigenous inputs (inferred from XRF Si/Sr and Fe/Ca profiles) with MIS 2, 4 and 6 show an increase in glacially derived materials delivered to the MD04-2822, in line with seismic reflection data for this margin (Stoker 1993). Furthermore the resolution and robust chronology derived for the core enabled each glacial interval to be discerned and the timing of events determined. The fluctuating nature of IRD delivery to the MD04-2822 site has therefore been demonstrated for the last 175 kyr and the sensitivity of the BIS to climatic forcing is highlighted.

IRD records provide an important archive of glacial activity on adjacent landmasses and a means by which ice sheet dynamics may be attempted. However, this record is far from straightforward to interpret as it reflects both ice advance and decay (e.g. McCabe and Clark 1998, Clarke et al 1999). IRD flux and concentration are multifactorial records of ice sheet dynamics, requiring caution in interpretation. While the difficulties in deciphering IRD concentration for sites proximal to an active calving margin are highlighted i.e. the possible dilution of IRD by fine grained terrigenous material, the MD04-2822 core provides the first continuous record of glacial expansion and contraction through a full glacial cycle.

Whilst some of the inferences within this study are somewhat speculative, based as they are on proxies from one marine core correlated/compared to often fragmentary terrestrial evidence, the main scientific findings are summarised below.

2.1. MIS 6

Elevated IRD flux and fine grained terrigenous inputs during MIS 6 provide the first direct evidence for the expansion of an ice sheet onto the Hebridean margin (Chapter 6). This confirms the long-range correlation of seismic data, indicating an expansion of the BIS onto the continental shelf around northern Britain. The presence of IRD implies that this MIS 6 BIS had a marine margin and the two phases of IRD input may correspond to the two phases of glaciation proposed for the North Sea (Carr 2004) and the wider European ice sheets (i.e. the Drenthe and Warthe).

Distinct, sub-orbital SST and IRD variability is documented for the penultimate glacial period. Millennial or multi-millennial scale inputs of IRD to the MD04-2822 site occur during MIS 6 and are often associated with variations in surface hydrographic conditions. This suggests that the MIS 6/Saalian BIS, as well as the Devensian/Weichselian BIS, was a dynamic ice sheet sensitive to climatic changes, possibly due to its maritime position (e.g. Boulton 1990).

2.2. Termination II

The penultimate deglaciation history of the BIS was hitherto unknown. The MD04-2822 sediments are particularly expanded during this interval and thus provide the first high resolution evaluation of the dynamics of the BIS and prevailing hydrographic conditions during Termination II. The offset of benthic $\delta^{18}\text{O}$ and $\delta^{13}\text{C}$ records during this period is a striking feature of the MD04-2822 record. This suggests a decoupling of these proxies, reflecting the interplay of large volumes of

meltwater into the North Atlantic (with the disintegration of the Saalian ice sheets) and the location and 'strength' of deep convection (Chapters 6 and 7).

In addition, the benthic $\delta^{18}\text{O}$ and surface proxies are also offset at MD04-2822. A series of surface 'pauses' in the general warming trend into the last interglacial (MIS 5e) are recorded at the MD04-2822 site. These reductions in SST (increased % *N. pachyderma* (sinistral)) are evident for both deglacial episodes at MD04-2822 and are linked to inputs of freshwater from the decay of the proximal BIS. In addition, a regional SST cooling feature (C28) was documented within Termination II, linked to changes in the strength of AMOC. This event is perhaps not directly analogous to the Younger Dryas (GS1), as no 'pause' in benthic $\delta^{18}\text{O}$ is evident within the MD04-2822 record¹ and freshwater inputs to the high latitude North Atlantic are inferred to have occurred prior to the re-establishment of AMOC (Chapter 6).

2.3. Early history of the BIS after the Last Interglacial

The amphi-Atlantic SST cooling (C) events widely documented within MIS 5 are also present within the % *N. pachyderma* (sinistral) record of MD04-2822. These are coincident with episodic decreases in benthic $\delta^{13}\text{C}$ (inferred decrease in the strength of AMOC) and increases in IRD. Sustained inputs of IRD are evident at the MIS 4/5 transition. This is suggested as the first significant delivery of IRD across the continental shelf to the core site, from the British source during the last glacial cycle. It appears that the BIS had reached a sufficient size at around 72 kyr to deliver IRD across the shelf edge to the core site (Chapter 8).

Unequivocal provenance determination remains difficult despite a multi-proxy approach; instead, the proximity of the core, the significant and sustained inputs of both IRD and fine grained terrigenous material, lithological composition that may originate from NW British sources and radiogenic isotopes are, in conjunction, all highly suggestive of a British source for this material.

2.4. MIS 3 and MIS 2

The pattern of BIS activity within MIS 3 and 2 (Kroon et al 2000, Knutz et al 2001, 2002, 2007, Wilson et al 2002) from the Barra Fan and wider Rockall Trough is replicated in core MD04-2822 (Chapter 6). Whilst the marine records for the last glacial period (from ~ 60 kyr onwards) are remarkably consistent² (e.g. Scourse et al 2009), the marine and terrestrial records for this interval appear incompatible. The reconciliation of marine and terrestrial records for the dynamics of the last BIS during MIS 3 remains elusive. The IRD and XRF Si/Sr records for MD04-2822 suggest continued inputs of terrigenous material, although low levels and episodic, throughout MIS 3; the provenance of IRD remains undetermined and alternative, far-field sources of IRD cannot be ruled out.

¹ However, this may be due to the resolution of the MD04-2822 record rather than the absence of this feature (cf. Lototskaya and Ganssen 1999).

² Note ice streaming and the dynamic nature of the last BIS produces slight variations in IRD inputs.

3. Millennial-scale variability of hydrographic conditions

Millennial scale climate variability is documented within the MD04-2822 % *N. pachyderma* (sinistral) during not only the last glacial period but also the last interglacial and the penultimate glacial. In addition, during MIS 5e, the MD04-2822 benthic $\delta^{18}\text{O}$ and $\delta^{13}\text{C}$ records display sub-orbital variations that are thought to relate to global sea level and hydrographic changes. Millennial scale variability therefore appears to be an intrinsic feature of both NE Atlantic surface and deep water circulation for the last 175 kyr.

The last interglacial (MIS 5e) at the MD04-2822 site was characterised by increasing SSTs (with possible regional cooling events superimposed). This is contradictory to some North Atlantic records where a decrease in surface temperatures is seen across the last interglacial. This may be reconciled, in part, if advection of surface waters into the Nordic Seas was confined during the initial and final stages of MIS 5e. However, the SST reconstruction used is based upon Mg/Ca, which is subject to fairly large errors.

4. Provenance

This study has highlighted concerns regarding the use (in isolation), of lithological characterisation, as an indicator of IRD provenance. This is especially important for sites in the North East Atlantic and Nordic Seas due to the similar geological histories of rocks eroded by the circum-Atlantic ice sheets. Such lithological characterisations may prove difficult to interpret or indeed unreliable. For example, detrital carbonates (used to define Heinrich events) could also have been transported from icebergs calving from the Greenland and Irish ice sheets. Similarly, the 'diagnostic' BIS lithics (i.e. basalts of inferred BTIP origin) first used by Knutz et al (2001) to infer a British origin, may also derive from beneath the Scandinavian and Greenland ice sheets or from the Rockall Bank.

However, if this technique is used in conjunction with others, e.g. bulk IRD and fine grained inputs, radiogenic isotopes etc, and each are consistent with one another, then the proxies in tandem may be highly suggestive of a local (i.e. BIS) source for material (e.g. an expansion of the BIS during MIS 4; Chapter 8). An alternative hypothesis may not account for the consistency of such findings, even though alternative sources for most 'diagnostic' grain types may be offered. Therefore, a multi-proxy approach to considering sediment provenance, may reduce the potential source regions and offer tentative solutions.

5. Reflections on the future potential of the MD04-2822 archive

BIS dynamics:

The dynamics of the BIS through the last 175 kyr could be further investigated as follows:

- i) increasing the sampling resolution of the MD04-2822 record, especially within MIS 6, would further help unravel the dynamics of the BIS as well as ice-ocean-climate interactions;

- ii) replication of the older portion of the MD04-2822 record may enable local (i.e. BIS meltwater inputs) and regional influences to be discerned using an event stratigraphy approach;
- iii) extending a multi-proxy provenance study to key intervals (e.g. Termination II), in conjunction with rigorous age control, may elucidate the phasing of ice sheet interactions within the North Atlantic and assist in determining causal mechanisms for ice sheet oscillations i.e. external versus internal forcing;
- iv) An extension of multi-proxy IRD provenance studies to MIS 3 for cores proximal to the former BIS ice streams may help to reconcile the disparate terrestrial and marine records;
- v) and the application of an event stratigraphy approach across the continental shelf to the deep ocean would allow the investigation of IRD deposition with increasing distance from a marine margins (for a given time-slice). This would increase our understanding of the transport of material from glaciated margins to the deep ocean.

Chronostratigraphy:

Some reflections on chronology, in general, include:

- i) the use of automated graphic correlation algorithm programmes (e.g. the Match protocol; Lisiecki and Lisiecki, 2002) may reduce *some* of the subjectivity of visual alignment, in that ‘wiggles’ would be matched in the same way today as tomorrow or in a months time. The appropriateness of the algorithm would have to be established;
- ii) the MD04-2822 chronology remains a ‘hypothesis to be tested’ (Skinner 2008), especially the MIS 6 portion. One technique that may provide some insight in the future is relative palaeointensity. This technique offers a measurable proxy that is global in nature and devoid of environmental influences. Such an independent marine chronology could eventually eliminate difficulties inherent in oxygen isotope stratigraphy (Channell et al 2008, 2009);
- iii) the assumption of synchronicity between North Atlantic SST and Greenland air temperatures requires further testing as this is the basis of many marine chronologies; tephrochronology offers one means by which this could be achieved;
- iv) with continued improvements in our understanding of the temporal and spatial variability of the marine reservoir effect, an independent (i.e. non-tuned) age model may be derived for MD04-2822 for the last ~ 50 kyr. This would allow an assessment of any leads and lags between palaeoclimate archives to be determined and aid our understanding of the mechanisms of abrupt climate change. The consistency of mid latitude NE Atlantic, interstadial radiocarbon ages (i.e. MD04-2822 and MD95-2006) may provide a means by which the calibration curve may be ‘calibrated’ within the mid-latitudes. In addition, a similar study dating each stadial event could then be compared to the interstadial ages; this may offer some insights into the temporal variability of the marine reservoir effect for this location;
- v) the extension of the GICC05 timescale may help to reduce *some* of the uncertainty associated with the glaciologically modelled chronology of the NGRIP ss09sea timescale used for this study. In addition, the possibility of undisturbed ice from the last interglacial period (e.g. the ongoing NEEM

project³) may offer further insights into mechanisms of climate change and provide further temporal constraint within tuned age models.

Multi-proxy studies:

The value of a multi-proxy approach to palaeoenvironmental investigations (e.g. IRD provenance) has been demonstrated. In addition, the following complimentary analyses may further strengthen some of the tentative inferences within the present study:

- i) The Mg/Ca palaeotemperature method used within chapter 7 is associated with relatively large errors. The coupling of this proxy with an alternative SST determination (e.g. modern analogue technique MAT, alkenones) may improve our understanding of palaeoenvironmental conditions at the site and the degree to which changes in seasonal preference/depth habitat may account for the observed Mg/Ca changes. Additional replicate analyses would also aid interpretation.
- ii) Grain size determinations (and thus current velocities) (or alternatively Pa/Th analysis) may further corroborate the inference of increased AMOC ‘strength’ from the long-term increase in benthic $\delta^{13}\text{C}$ at the MD04-2822 site (and other North Atlantic locations) during MIS 5.

Modelling studies: The proxy data obtained by this study could also be used to constrain models of BIS dynamics (and calving) as well as the interaction of AMOC, surface hydrography and sea level change upon ice sheet dynamics.

³ North Greenland Eemian Ice Drilling, <http://neem.nbi.ku.dk>

6. Publications

The thesis has been written in a style that allows an easier translation of material from this study, to publications. Published and submitted works arising from this study are listed and potential publications outlined.

Published:

- **Hibbert FD**, Austin WEN, Leng MJ, Gatliff RW. 2010. British Ice Sheet Dynamics inferred from North Atlantic ice-rafted debris records spanning the last 175,000 years. *Journal of Quaternary Science* 25(4): 461–482 DOI: 10.1002/jqs.1331
(material derived from Chapters 3 and 6)
- Peters C, Austin WEN, Walden J, **Hibbert FD**. 2010. Magnetic characterisation and correlation of a Younger Dryas tephra in North Atlantic marine sediments. *Journal of Quaternary Science* 25: 339–347.
(% *N. pachyderma* (sinistral) record of MD04-2822 used)

Submitted, accepted or in preparation:

- Austin WEN, **Hibbert FD**, Rasmussen SO, Peters C, Abbott PM, Bryant CL (*Accepted*) The synchronisation of palaeoclimatic events in the North Atlantic region during Greenland Stadial 3. *Quaternary Science Reviews*
(the GS3 local event stratigraphy developed for Chapter 4)
- Austin WEN, **Hibbert FD**. (*in preparation.*) Tracing Time in the Ocean: A brief review of chronological constraints in marine event-based stratigraphies. (*Quaternary Science Reviews*)
(Chapter 3, *Chronostratigraphy* and comments on event stratigraphy, Chapter 4)

Potential manuscripts arising from this study:

- Correction of core ‘over-sampling’: an example from the Rockall Trough (Chapter 5)
- Comparison of last and penultimate glacial BIS (Chapter 6)
- Termination II (Chapter 6 and 7)
- Early glacial history of the last BIS (Chapter 8)

A: Sedimentological and Lithological

- A₁: Detailed core logs for each section of MD04-2822
- A₂: Physical Properties of MD04-2822 (determined onboard ship)
- A₃: Sediment photographs

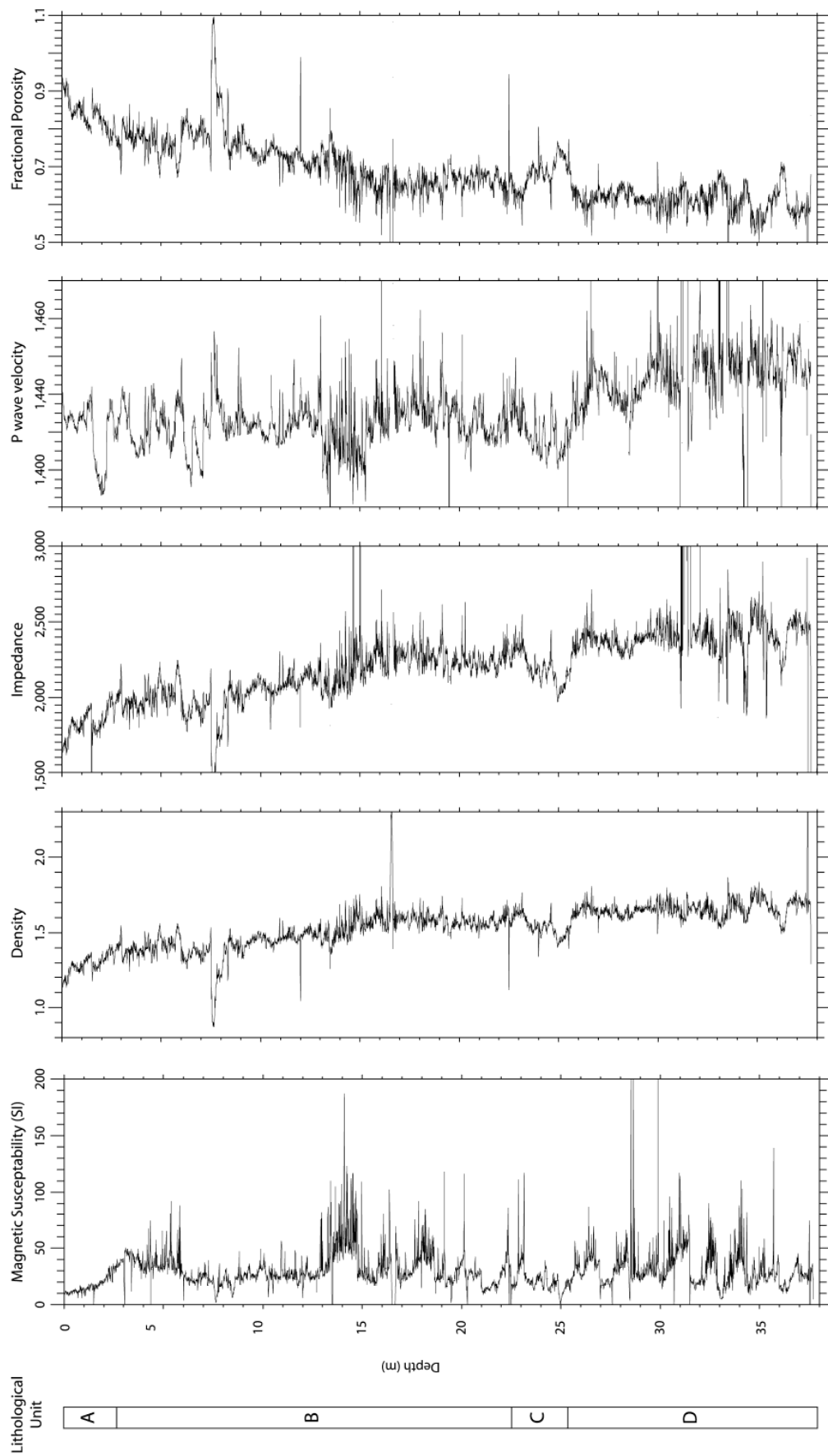
B: Analytical

- B₁: Repeat stable isotope analyses ($\delta^{18}\text{O}$ and $\delta^{13}\text{C}$) (NIGL and FEEA)
- B₂: Paired stable isotope and Mg/Ca analyses *G. bulloides* (University of East Anglia)
- B₃: Major element geochemistry of tephra horizons (FEEA)
- B₄: Radiogenic isotope analyses (NIGL)
- B₅: Stable isotope determinations for individual carbonate grains from Heinrich events within MD04-2822 and MD95-2006 (University of Cambridge)

C: Chronostratigraphical

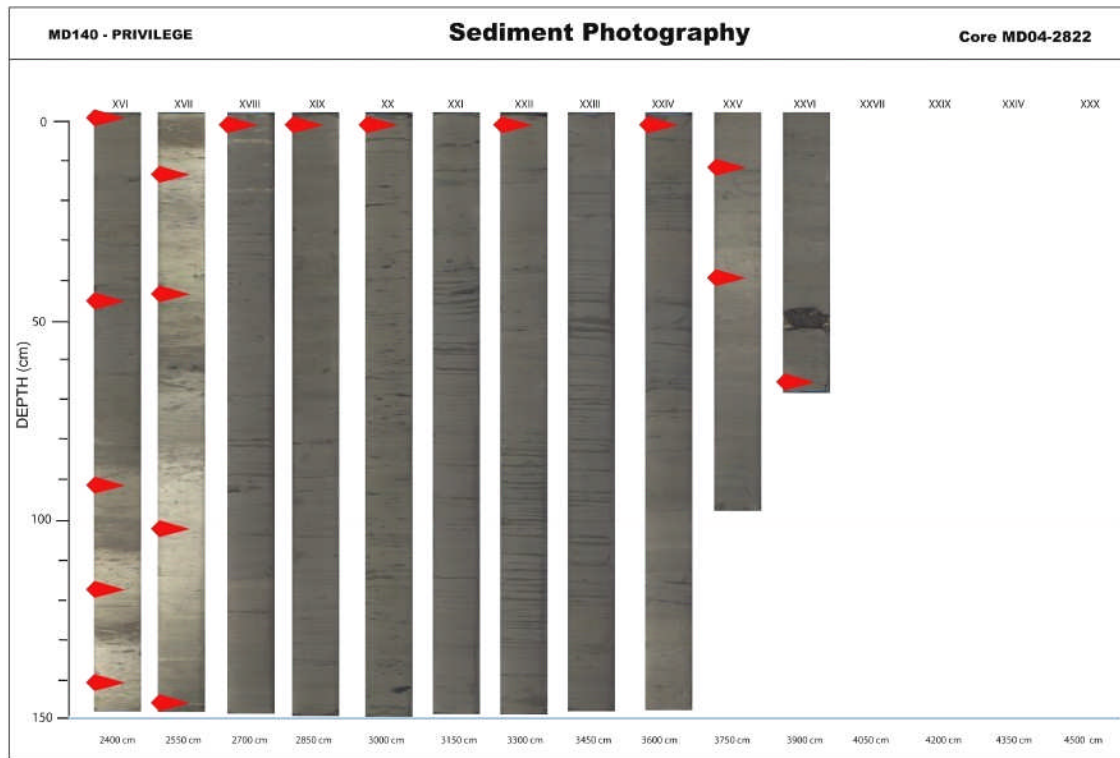
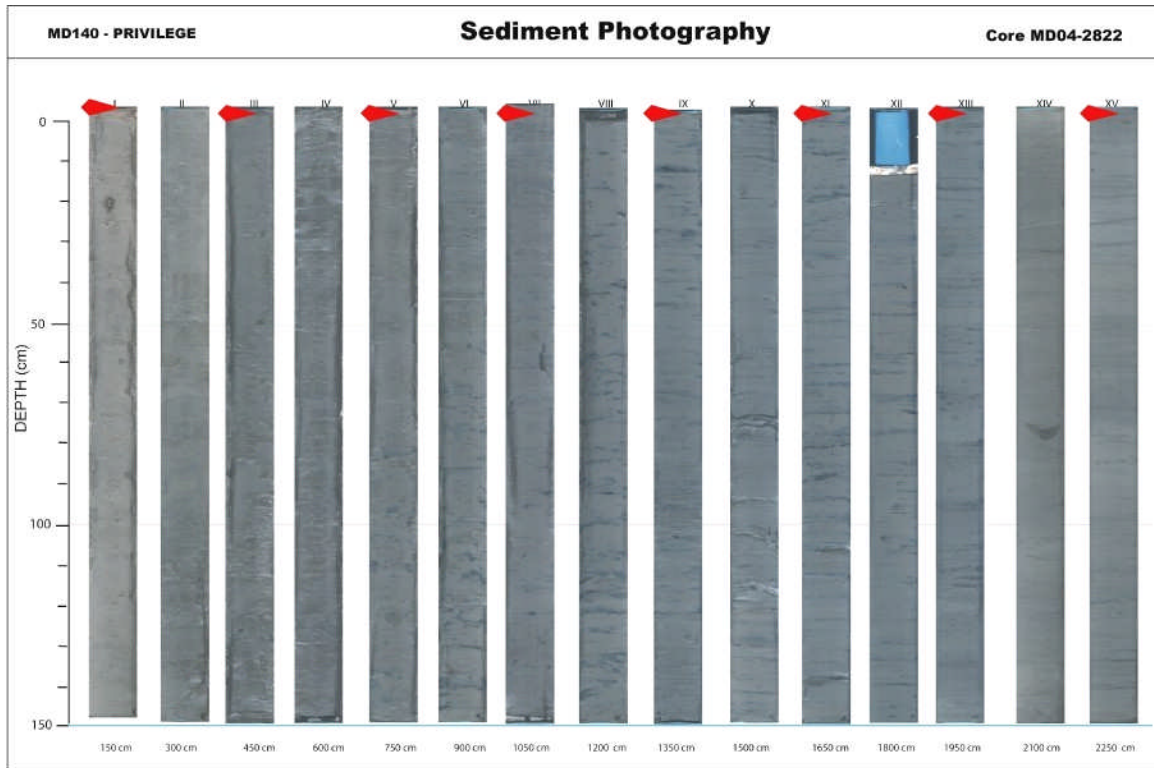
- C₁: Tuning tie-points for MD04-2822 to $\delta^{18}\text{O}$ stacks (SPECMAP and LR04)
- C₂: Tuning tie-points for MD04-2822 to NGRIP $\delta^{18}\text{O}$ on both the ss09sea and GICC05 timescale
- C₃: GS3 tuning tie-points (NGRIP, GICC05) and radiocarbon age determinations

Appendix A₂: Physical Properties of MD04-2822



Appendix A₃: Sediment photographs.

Red arrows indicate stratigraphic position of shipboard nannofossil sampling. *Note* the difference in colour is an artefact; the sediments are very similar in colour.



Appendix B₁: Repeat stable isotope analyses ($\delta^{18}\text{O}$ and $\delta^{13}\text{C}$) (NIGL and FEEA)

Replicate stable isotope analyses of planktonic foraminifera (*G. bulloides* and *N.pachyderma* (sinistral)) - NIGL

	Depth (cm)	$\delta^{13}\text{C}$				Mean $\delta^{13}\text{C}$ ‰	$\delta^{13}\text{C}$	$\delta^{18}\text{O}$			
		‰	‰	‰	‰			s.d.1 σ (2dp)	% error (2dp)	Mean ‰	s.d.1 σ (2dp)
Gb	2670.5	-0.76	+3.23	-1.00	+3.45	-0.88	0.17	19.41	+3.34	0.15	4.57
	2690.5	-1.09	+3.23	-1.00	+3.45	-1.04	0.07	6.39	+3.34	0.16	4.77
	2750.5	-0.87	+3.09	-0.84	+3.01	-0.86	0.03	3.07	+3.05	0.06	1.89
	2770.5	-0.84	+3.13	-0.84	+3.01	-0.84	0.00	0.09	+3.07	0.08	2.75
	2990.5	-1.19	+3.11	-0.96	+3.21	-1.07	0.16	15.34	+3.16	0.07	2.22
	3000.5	-0.88	+3.22	-0.96	+3.21	-0.92	0.05	5.98	+3.22	0.01	0.28
	3170.5	-0.56	+2.82	-1.48	+2.35	-1.02	0.65	63.25	+2.58	0.33	12.68
	3190.5	-0.70	+3.00	-1.48	+2.35	-1.09	0.55	50.46	+2.67	0.46	17.06
	3553.5	-0.62	+2.76	-1.00	+2.84	-0.81	0.27	33.17	+2.80	0.06	2.00
	3601.5	-0.69	+3.40	-0.59	+3.13	-0.64	0.07	11.65	+3.27	0.19	5.73
	3620.5	-0.95	+3.18	-0.59	+3.13	-0.77	0.26	33.29	+3.16	0.03	1.07
	3747.5	-1.11	+3.23	-1.02	+2.85	-1.07	0.06	5.78	+3.04	0.26	8.69
	3761.5	-0.89	+2.83	-1.02	+2.85	-0.96	0.09	9.79	+2.84	0.01	0.52
	Average error								19.82		4.94
	Np(s)	2560.5	-0.42	+4.11	-0.69	+4.11	-0.56	0.19	34.51	+4.11	0.01
2701.5		-0.27	+4.26	-0.62	+4.08	-0.45	0.25	55.13	+4.17	0.13	3.12
2720.5		-0.61	+4.06	-0.62	+4.08	-0.61	0.01	1.64	+4.07	0.01	0.33
2780.5		-0.57	+4.30	-0.69	+4.11	-0.63	0.09	14.08	+4.20	0.14	3.28
2910.5		-0.67	+3.85	-1.02	+4.14	-0.85	0.25	29.57	+4.00	0.20	5.02
2930.5		-0.74	+4.10	-1.02	+4.14	-0.88	0.20	22.88	+4.12	0.03	0.71
2970.5		-1.39	+3.97	-0.86	+3.96	-1.12	0.37	33.34	+3.97	0.00	0.12
2990.5		-0.77	+3.84	-0.86	+3.96	-0.81	0.06	7.65	+3.90	0.09	2.33
3170.5		-1.13	+3.67	-0.61	+3.96	-0.87	0.37	42.81	+3.82	0.21	5.39
3190.5		-0.68	+3.51	-0.61	+3.96	-0.64	0.05	8.09	+3.74	0.32	8.50
3420.5		-0.19	+4.00	-0.13	+4.08	-0.16	0.04	22.98	+4.04	0.06	1.42
3530.5		-0.48	+4.18	-0.36	+3.38	-0.42	0.09	20.75	+3.78	0.57	14.94
3554.5		-0.35	+3.73	-0.36	+3.38	-0.35	0.00	0.93	+3.56	0.24	6.88
3601.5		-1.23	+3.94	-0.86	+3.78	-1.04	0.26	25.29	+3.86	0.11	2.81
3620.5		-1.57	+3.59	-0.86	+3.78	-1.21	0.50	41.49	+3.68	0.14	3.81
3747.5		-0.90	+3.69	-0.31	+3.94	-0.61	0.42	68.31	+3.82	0.18	4.61
3761.5		-1.25	+3.76	-0.31	+3.94	-0.78	0.66	84.66	+3.85	0.13	3.38
Average error								36.28		3.78	

cont.

Replicate stable isotope analyses of planktonic foraminifera (*G. bulloides* and *N. pachyderma* (sinistral)) – St Andrews

	Depth (cm)					Mean $\delta^{13}\text{C}$ ‰	$\delta^{13}\text{C}$	$\delta^{13}\text{C}$ s.d.1 σ (2dp)	% error (2dp)				
		$\delta^{13}\text{C}$ ‰	$\delta^{18}\text{O}$ ‰	$\delta^{13}\text{C}$ ‰	$\delta^{18}\text{O}$ ‰					Mean $\delta^{18}\text{O}$ ‰	$\delta^{18}\text{O}$ s.d.1 σ (2dp)	%error (2dp)	
Gb	1310.5	-1.82	+3.26	-1.78	+3.25	-1.80	0.03	1.67	+3.26	0.01	0.24		
	1970.5	-1.74	+3.04	-1.77	+3.15	-1.75	0.02	1.14	+3.09	0.08	2.70		
	2250.5	-0.74	+2.89	-0.99	+2.93	-0.87	0.18	20.69	+2.91	0.03	0.99		
	2342.5	-0.47	+2.33	-0.61	+2.33	-0.54	0.07	12.96	+2.39	0.10	4.26		
						Average error		9.12			2.05		

	Depth (cm)					Mean $\delta^{13}\text{C}$ ‰	$\delta^{13}\text{C}$	$\delta^{13}\text{C}$ s.d.1 σ (2dp)	% error (2dp)				
		$\delta^{13}\text{C}$ ‰	$\delta^{18}\text{O}$ ‰	$\delta^{13}\text{C}$ ‰	$\delta^{18}\text{O}$ ‰					Mean $\delta^{18}\text{O}$ ‰	$\delta^{18}\text{O}$ s.d.1 σ (2dp)	%error (2dp)	
Nps	1000.5	-1.04	+3.84	-0.94	+3.81	-0.99	0.07	7.07	+3.82	0.02	0.51		
	1270.5	+0.10	+3.04	-0.14	+3.06	-0.06	0.14	233.33	+3.34	0.50	14.82		
	1310.5	-1.75	+4.37	-1.76	+4.33	-1.76	0.01	0.57	+4.35	0.02	0.54		
	1340.5	-1.77	+4.39	-1.77	+4.54	-1.77	0.004	0.23	+4.46	0.11	2.43		
	1500.5	-0.28	+3.23	-0.26	+3.22	-0.27	0.01	3.70	+3.23	0.01	0.23		
	1960.5	-1.76	+3.86	-1.74	+3.95	-1.09	1.15	105.50	+3.91	0.05	1.21		
	2000.5	-1.72	+3.65	-1.70	+3.55	-1.71	0.01	0.58	+3.60	0.07	2.04		
	2112.5	-0.30	+3.35	-0.52	+3.27	-0.41	0.15	36.59	+3.31	0.05	1.63		
	2250.5	-1.38	+3.62	-1.50	+3.58	-1.44	0.09	6.25	+3.60	0.03	0.86		
	2276.5	-11.5	+3.07	-10.4	+2.76	-10.95	0.82	7.49	+3.02	0.08	2.52		
	2294.5	-8.55	+3.08	-6.0	+2.97	-7.28	1.81	24.86	+3.03	0.08	2.59		
	2312.5	-10.4	+3.05	-10.4	+2.99	-10.43	0.03	0.29	+3.02	0.04	1.44		
	2326.5	-0.83	+2.95	-0.72	+2.85	-0.78	0.07	8.97	+2.90	0.08	2.65		
						Average error		33.49			2.58		

Replicate stable isotope determinations for *G. bulloides* (300-350 μm) (“paired Mg/Ca-stable isotope”) – NIGL (only)

Depth (cm)					Mean $\delta^{13}\text{C}$ ‰	$\delta^{13}\text{C}$	$\delta^{13}\text{C}$ s.d.1 σ (2dp)	% error (2dp)				
	$\delta^{13}\text{C}$ ‰	$\delta^{18}\text{O}$ ‰	$\delta^{13}\text{C}$ ‰	$\delta^{18}\text{O}$ ‰					Mean $\delta^{18}\text{O}$ ‰	$\delta^{18}\text{O}$ s.d.1 σ (2dp)	%error (2dp)	
0.5	-0.10	+1.39	-0.01	+1.40	-0.05	0.06	117.77	+1.39	0.01	0.65		
50.5	+0.24	+1.47	+0.00	+1.40	+0.12	0.17	136.41	+1.43	0.06	3.87		
2520.5	-0.78	+1.29	-0.47	+1.34	-0.62	0.22	35.02	+1.32	0.03	2.31		
2540.5	-0.94	+1.22	-0.73	+1.30	-0.84	0.15	17.62	+1.26	0.06	4.58		
						Average error		8.50		2.85		

cont.

Replicate stable isotope analyses of *C. wuellerstorfi* (>250 µm) – NIGL

Depth (cm)	$\delta^{13}\text{C}$ ‰	$\delta^{18}\text{O}$ ‰	Mean $\delta^{13}\text{C}$ ‰	$\delta^{13}\text{C}$ s.d.1 σ (2dp)	% error (2dp)	Mean $\delta^{18}\text{O}$ ‰	$\delta^{18}\text{O}$ s.d.1 σ (2dp)	% error (2dp)						
25.5	+1.12	+2.70	+0.96	+2.70					+1.04	0.11	10.86	+2.70	0.00	0.01
35.5	+1.01	+2.83	+1.00	+2.92					+1.01	0.01	0.83	+2.88	0.06	2.24
45.5	+0.91	+2.56	+1.07	+2.88					+0.99	0.11	11.30	+2.72	0.22	8.26
1760.5	+0.42	+3.94	+0.62	+4.07					+0.52	0.15	28.10	+4.00	0.09	2.22
2370.5	+0.90	+3.60	+1.04	+3.69					+0.97	0.10	10.48	+3.64	0.06	1.75
2524.5	+0.70	+2.94	+0.81	+2.84					+0.75	0.08	10.32	+2.89	0.06	2.25
2542.5	+0.80	+2.71	+0.71	+3.07	+0.69	+2.94	+0.76	+2.99	+0.74	0.05	6.68	+2.93	0.15	5.23
2558.5	+0.20	+2.69	+0.34	+3.25					+0.27	0.10	35.71	+2.97	0.39	13.27
2720.5	+0.44	+4.48	+0.46	+4.62					+0.45	0.02	3.61	+4.55	0.09	2.07
Average Error											13.10			

Comparison of stable isotope analyses for differing size fractions (from the same depth interval) of *G. bulloides* – NIGL and St Andrews

Depth (cm)	250-300 µm		300-355 µm						Difference ‰ $\delta^{13}\text{C}$ (larger_smaller)	Difference ‰ $\delta^{18}\text{O}$ (larger_smaller)
	$\delta^{13}\text{C}$ ‰	$\delta^{18}\text{O}$ ‰	$\delta^{13}\text{C}$ ‰	$\delta^{18}\text{O}$ ‰	$\delta^{13}\text{C}$ ‰	$\delta^{18}\text{O}$ ‰	mean $\delta^{13}\text{C}$	mean $\delta^{18}\text{O}$		
0.5	-0.60	1.27	-0.10	+1.39	-0.01	+1.40	-0.05	1.39	0.5	0.12
5.5			-0.02	+1.35						
10.5	-0.36	1.62	-0.03	+1.18					0.33	-0.44
15.5			-0.34	+1.52						
20.5	0.09	1.12	+0.08	+1.46					-0.01	0.34
25.5			+0.03	+1.33						
30.5	-0.16	1.06	-0.11	+0.75					0.05	-0.31
35.5			+0.19	+1.58						
40.5	-0.38	0.46	-0.11	+1.15					0.27	0.69
45.5			+0.05	+1.55						
50.5	0.05	1.09	+0.24	+1.47	+0.00	+1.40	0.12	1.43	0.07	0.34
2520.5	-0.20	+1.15	-0.78	+1.29	-0.47	+1.34	-0.62	1.32	-0.42	0.17
2522.5			-0.70	+1.44						
2524.5			-0.49	+1.04						
2526.5			-0.39	+1.14						
2528.5			-0.34	+1.36						
2530.5	-0.90	+1.09	-0.62	+0.92					0.28	-0.17
2532.5			-0.88	+1.18						
2534.5			-0.69	+0.91						
2536.5			-0.75	+1.46						
2538.5			-0.93	+1.41						
2540.5	-0.85	+1.43	-0.94	+1.22	-0.73	+1.30	-0.84	1.26	0.01	-0.17
2542.5	-0.98*	+1.62*	-0.79	+1.43						
2544.5			-1.29	+1.24						
2546.5			-1.11	+1.45						
2548.5			failed to run							
2550.5	-1.02	+1.49	-1.01	+1.23					0.01	-0.26
2552.5	-1.30*	+1.56*	-1.43	+1.21					-0.13	-0.35
2554.5	-1.23*	+1.60*	-0.76	+1.95					0.47	0.35
2556.5	-1.11*	+1.69*	-1.26	+1.23					-0.15	-0.46
2558.5			-1.08	+1.50						
2560.5	-0.88	+1.60	-1.00	+1.04					-0.12	-0.56

Bold* = FEEA, University of St Andrews values

Appendix B₂: Paired stable isotope (NIGL) and Mg/Ca analyses *G. bulloides* (University of East Anglia)

Mg/Ca analyses ($2\sigma = 1.2$ °C); Stable isotope analyses ($2\sigma = 0.08$ ‰)

Depth	Temperature °C	$\delta^{13}\text{C}$ VPDB)	(‰ $\delta^{18}\text{O}$ VPDB)	(‰
0.5	11.50	-0.05*	1.39*	
5.5	12.50	-0.02	1.35	
10.5	11.00	-0.03	1.18	
15.5	12.00	-0.34	1.52	
20.5	11.80	0.08	1.46	
25.5	11.60	0.03	1.33	
30.5	10.90	-0.11	0.75	
35.5	12.00	0.19	1.58	
40.5	12.50	-0.11	1.15	
45.5	12.50	0.05	1.55	
50.5	11.40	0.12*	1.43*	
2450.5	11.14	-1.02	2.00	
2460.5	12.45	-1.16	1.93	
2470.5	14.42	-0.80	2.15	
2480.5	13.14	-0.95	2.18	
2490.5	13.88	-0.92	1.71	
2495.5	11.88	-0.82	1.70	
2500.5	12.35	-1.01	1.59	
2505.5	12.72	-0.82	1.70	
2510.5	12.64	-1.07	1.56	
2514.5	12.02	-0.93	1.63	
2518.5	11.14	-0.93	1.58	
2520.5	11.60	-0.62	1.32	
2522.5	11.27	-0.49	1.04	
2524.5	11.59	-0.39	1.14	
2526.5	10.71	-0.34	1.36	
2528.5	11.17	-0.90	1.09	
2530.5	10.94	failed	failed	
2532.5	9.66	-0.69	0.91	
2534.5	10.21	-0.75	1.46	
2536.5	11.37	-0.93	1.41	
2538.5	11.31	-0.85	1.35	
2540.5	11.13	-0.84	1.26	
2542.5	10.93	-1.29	1.24	
2544.5	9.55	-1.11	1.45	
2546.5	10.03	-1.21	1.47	
2548.5	9.68	failed	failed	
2550.5	11.83	-1.38	1.48	
2552.5	9.84	-0.76	1.95	
2554.5	10.20	-1.26	1.23	
2556.5	10.93	-1.08	1.50	
2558.5	11.33	failed	failed	
2560.5	10.46	failed	failed	

Appendix B₃: Major element geochemistry of tephra horizons (FEEA)

MD04-2822 NAAZ II rhyolitic shards

Major element geochemical data for **NAAZ II rhyolitic shards from MD04-2822**. All analyses undertaken at FEEA, University of St Andrews; only analytical totals > 95 % shown. Number of shards = 21; number analyses = 27

	Id. No.	Core depth cm	Ox%(Na)	Ox%(Mg)	Ox%(Al)	Ox%(Si)	Ox%(K)	Ox%(Ca)	Ox%(Ti)	Ox%(Mn)	Ox%(Fe)	SUM	Population
M2164b1	120	2264-2465	3.00	0.09	11.72	73.53	4.27	0.23	0.19	0.16	2.29	95.47	II-Rhy-1
M2164f1	128	2264-2465	5.20	0.00	11.39	71.16	4.54	0.27	0.26	0.00	2.72	95.53	II-Rhy-1
M2164g2	131	2264-2465	3.33	0.00	11.94	73.41	4.38	0.35	0.16	0.16	2.17	95.90	II-Rhy-1
M2164i2	141	2264-2465	3.38	0.00	11.61	73.05	4.26	0.36	0.20	0.07	2.69	95.61	II-Rhy-1
M2164j1	142	2264-2465	3.76	0.04	12.04	75.48	4.53	0.35	0.17	0.08	2.44	98.89	II-Rhy-1
M2164j2	143	2264-2465	4.49	0.00	12.25	75.44	4.50	0.35	0.17	0.09	2.75	100.05	II-Rhy-1
M2164o3	152	2264-2465	2.57	0.08	11.55	73.75	4.14	0.27	0.18	0.05	2.51	95.10	II-Rhy-1
M2163d2	44	2163-2164	5.09	0.00	11.23	72.46	4.18	0.34	0.18	0.06	2.22	95.76	II-Rhy-1
M2163h1	57	2163-2164	3.23	0.00	11.87	73.93	4.09	0.38	0.26	0.00	2.21	95.98	II-Rhy-1
M2163k1	64	2163-2164	3.32	0.05	11.94	73.92	4.20	0.34	0.14	0.05	2.56	96.53	II-Rhy-1
M2163k2	65	2163-2164	5.22	0.00	11.14	71.60	4.36	0.33	0.13	0.07	2.17	95.02	II-Rhy-1
M2163m2	68	2163-2164	2.92	0.00	11.85	73.31	3.98	0.32	0.18	0.17	2.68	95.42	II-Rhy-1
M2163n2	70	2163-2164	3.00	0.00	11.80	73.69	4.11	0.42	0.16	0.11	2.60	95.90	II-Rhy-1
M2163o1	71	2163-2164	2.53	0.08	11.49	73.50	4.12	0.32	0.20	0.09	2.34	94.68	II-Rhy-1
M2163o2	72	2163-2164	2.66	0.00	11.68	73.86	3.96	0.32	0.23	0.13	2.70	95.53	II-Rhy-1
M2163q2	76	2163-2164	3.25	0.00	11.68	72.86	4.31	0.37	0.18	0.01	2.58	95.23	II-Rhy-1
M2163s1	79	2163-2164	3.31	0.07	11.56	73.88	4.14	0.38	0.14	0.13	2.51	96.12	II-Rhy-1
M2162B1	62	2162-2163	4.66	0.00	11.17	71.66	4.35	0.36	0.23	0.16	2.68	95.25	II-Rhy-1
M2162C1	65	2162-2163	3.04	0.00	11.63	74.32	4.25	0.33	0.18	0.09	2.54	96.38	II-Rhy-1
M2162C2	66	2162-2163	3.54	0.05	12.19	75.72	4.46	0.37	0.14	0.04	2.94	99.45	II-Rhy-1
M2162E1	69	2162-2163	2.60	0.28	11.63	74.52	3.98	0.32	0.18	0.09	2.26	95.87	II-Rhy-1
M2162E2	70	2162-2163	2.63	0.03	11.59	74.28	4.44	0.35	0.23	0.12	2.30	95.97	II-Rhy-1
M2162F1	71	2162-2163	2.74	0.00	11.70	74.30	3.86	0.35	0.24	0.12	2.58	95.88	II-Rhy-1
M2162F2	72	2162-2163	2.53	0.22	11.34	73.66	4.16	0.39	0.26	0.06	2.84	95.48	II-Rhy-1
M2162G1	74	2162-2163	2.94	0.00	11.38	73.98	4.09	0.31	0.20	0.00	2.51	95.40	II-Rhy-1
M2162Q2	101	2162-2163	3.72	0.00	11.72	75.18	4.53	0.33	0.26	0.03	2.10	97.86	II-Rhy-1
M2162Q3	102	2162-2163	4.07	0.00	11.97	76.07	4.58	0.37	0.09	0.13	2.74	100.03	II-Rhy-1

MD01-2461 NAAZ II rhyolitic shards

Major element geochemical data for **NAAZ II rhyolitic shards from MD01-2461**. All analyses undertaken at FEEA, University of St Andrews; only analytical totals > 95 % shown. Number of shards = 11; number analyses = 16

Identifier	Id. No.	Core depth cm	Ox%(Na)	Ox%(Mg)	Ox%(Al)	Ox%(Si)	Ox%(K)	Ox%(Ca)	Ox%(Ti)	Ox%(Mn)	Ox%(Fe)	SUM	Population
2461A1	74	948-949	4.94	0.01	11.64	73.43	4.34	0.37	0.12	0.09	2.35	97.28	II-Rhy-1
2461A2	75	948-949	4.35	0.00	11.34	73.32	4.34	0.15	0.39	0.07	2.37	96.32	II-Rhy-1
2461B1	77	948-949	2.21	0.00	11.58	74.32	4.18	0.29	0.14	0.15	2.41	95.28	II-Rhy-1
2461D2	82	948-949	4.60	0.09	11.36	72.48	4.32	0.32	0.14	0.05	2.57	95.91	II-Rhy-1
2461E1	83	948-949	4.16	0.09	12.41	70.98	4.27	0.64	0.07	0.32	2.19	95.14	II-Rhy-1
2461J3	87	948-949	2.54	0.00	11.68	74.33	4.31	0.32	0.23	0.14	2.70	96.24	II-Rhy-1
2461J4	88	948-949	2.59	0.00	11.56	74.01	4.13	0.31	0.18	0.01	2.46	95.26	II-Rhy-1
2461N1	94	948-949	3.23	0.27	11.68	74.00	4.07	0.36	0.16	0.00	2.50	96.26	II-Rhy-1
2461N2	95	948-949	2.48	0.04	11.72	74.68	4.21	0.31	0.18	0.02	2.44	96.08	II-Rhy-1
2461P2	104	948-949	2.69	0.00	11.48	73.95	3.99	0.32	0.17	0.00	2.42	95.01	II-Rhy-1
2461P3	105	948-949	2.76	0.00	11.79	73.58	3.98	0.33	0.15	0.14	2.36	95.10	II-Rhy-1
2461R3	31	948-949	2.83	0.00	11.50	73.67	3.88	0.34	0.26	0.00	2.66	95.14	II-Rhy-1
2461S6	39	948-949	4.33	0.00	11.94	72.13	4.55	0.30	0.17	0.00	2.48	95.91	II-Rhy-1
2461T2	41	948-949	2.69	0.00	11.42	73.59	4.54	0.42	0.17	0.08	2.47	95.37	II-Rhy-1
2461U1	42	948-949	2.80	0.01	11.54	74.80	4.23	0.30	0.18	0.25	2.28	96.39	II-Rhy-1
2461U2	43	948-949	4.81	0.00	11.29	72.18	4.32	0.37	0.19	0.08	2.42	95.66	II-Rhy-1

cont.

MD04-2822 NAAZ II basaltic shards:

Major element geochemical data for **NAAZ II basaltic shards from MD04-2822**. All analyses undertaken at FEEA, University of St Andrews; only analytical totals > 95 % shown. Number of shards = 7; number analyses = 16

Identifier	Id. No.	Core depth cm	Ox%(Na)	Ox%(Mg)	Ox%(Al)	Ox%(Si)	Ox%(K)	Ox%(Ca)	Ox%(Ti)	Ox%(Mn)	Ox%(Fe)	SUM	Population
M2164B1	89	2164-2165	2.44	6.83	13.50	48.43	0.21	11.04	1.54	0.15	11.82	95.96	II-THOL-1
M2164B2	90	2164-2165	2.37	6.97	13.51	49.11	0.21	11.39	1.54	0.13	12.63	97.87	II-THOL-1
M2164B3	91	2164-2165	2.64	6.94	13.36	48.37	0.21	11.18	1.56	0.32	11.76	96.32	II-THOL-1
M2164C1	92	2164-2165	2.22	6.91	13.67	49.21	0.21	11.44	1.50	0.22	12.00	97.38	II-THOL-1
M2164C2	93	2164-2165	2.34	7.14	13.70	49.39	0.29	11.14	1.37	0.28	11.54	97.17	II-THOL-1
M2164t1	158	2164-2165	2.35	6.94	13.42	48.46	0.21	11.15	1.46	0.29	11.89	96.17	II-THOL-1
M2164t2	159	2164-2165	2.18	6.97	13.35	48.55	0.18	11.17	1.48	0.23	11.82	95.93	II-THOL-1
M2164t3	160	2164-2165	2.39	6.87	13.35	47.88	0.27	11.25	1.55	0.26	11.67	95.49	II-THOL-1
M2164u1	161	2164-2165	2.22	6.96	13.38	48.16	0.17	11.21	1.60	0.15	11.80	95.66	II-THOL-1
M2164u2	162	2164-2165	2.69	6.91	13.63	48.47	0.15	11.38	1.41	0.23	11.88	96.75	II-THOL-1
M2164v1	163	2164-2165	2.38	7.10	13.31	48.25	0.21	11.33	1.37	0.29	11.81	96.06	II-THOL-1
M2164v2	164	2164-2165	2.25	6.97	13.41	50.08	0.19	10.81	1.34	0.07	11.03	96.14	II-THOL-1
M2164w1	165	2164-2165	2.28	6.75	13.44	49.39	0.18	11.41	1.74	0.32	11.33	96.84	II-THOL-1
M2164w2	166	2164-2165	2.13	6.86	13.29	48.65	0.21	11.33	1.55	0.12	12.14	96.28	II-THOL-1
M2164w3	167	2164-2165	2.61	7.01	13.81	49.37	0.20	10.86	1.50	0.24	11.30	96.92	II-THOL-1
M2162O1	97	2162-2163	2.72	5.94	13.12	49.37	0.35	10.68	2.56	0.19	13.51	98.44	II-THOL-2

MD04-2822 MIS 6 rhyolitic shards

Major element geochemical data for **MIS 6 rhyolitic shards from MD04-2822**. All analyses undertaken at FEEA, University of St Andrews; only analytical totals > 95 % shown. Number of shards = 8; number analyses = 12

Identifier	Id. No.	Core depth cm	Ox%(Na)	Ox%(Mg)	Ox%(Al)	Ox%(Si)	Ox%(K)	Ox%(Ca)	Ox%(Ti)	Ox%(Mn)	Ox%(Fe)	SUM	Population
MIS6A2	37	3060-3061	4.21	0.09	12.31	71.80	4.11	0.63	0.18	0.00	2.28	95.61	unknown
MIS6D2	46	3060-3061	4.12	0.02	12.23	71.53	4.22	0.65	0.12	0.02	2.12	95.03	unknown
MIS6E1	47	3060-3061	5.90	0.72	13.00	70.78	4.35	0.70	0.20	0.03	2.05	97.73	unknown
MIS6E2	48	3060-3061	4.26	0.02	12.69	72.31	4.26	0.63	0.21	0.09	2.41	96.87	unknown
MIS6F1	49	3060-3061	4.13	0.05	12.59	71.37	4.16	0.63	0.21	0.05	2.18	95.37	unknown
MIS6H2	53	3060-3061	5.20	0.13	12.44	71.84	4.22	0.60	0.09	0.09	2.34	96.95	unknown
MIS6I2	56	3060-3061	4.16	0.02	12.41	71.43	4.22	0.68	0.18	0.00	2.16	95.26	unknown
MIS6J1	57	3060-3061	5.42	0.10	12.25	70.55	4.27	0.64	0.22	0.00	2.29	95.73	unknown
MIS6J2	58	3060-3061	3.03	0.09	12.90	74.07	4.29	0.60	0.19	0.05	2.13	97.36	unknown
MIS6J3	59	3060-3061	2.05	0.13	12.78	73.51	4.27	0.74	0.21	0.02	2.46	96.17	unknown
MIS6K1	60	3060-3061	2.05	0.03	12.58	73.43	4.30	0.65	0.20	0.06	2.26	95.55	unknown
MIS6K2	61	3060-3061	2.37	0.16	12.80	73.03	3.95	0.71	0.15	0.04	2.49	95.71	unknown
		Mean	3.91	0.13	12.58	72.14	4.22	0.66	0.18	0.04	2.26		
		1 st. dev.	1.29	0.19	0.26	1.13	0.11	0.04	0.04	0.03	0.14		

cont.

Published and average data for Lipari rhyolitic glass standard over 6 days of analyses at FEEA, University of St Andrews n = 73

Ox%(Na)	Ox%(Mg)	Ox%(Al)	Ox%(Si)	Ox%(K)	Ox%(Ca)	Ox%(Ti)	Ox%(Mn)	Ox%(Fe)	Total
4.1066	0.0162	12.0248	69.7126	5.6742	0.59	0.076	0	1.5003	93.7
4.236	0	12.2182	67.1361	5.3479	0.6282	0.086	0.1089	1.4014	91.2
4.3945	0.0463	12.4797	72.8466	5.6367	0.662	0.0428	0.0099	1.6095	97.7
4.2025	0	12.393	72.1114	5.2958	0.7068	0.05	0.0789	1.5162	96.4
4.1204	0.023	12.5843	72.6688	5.2848	0.7849	0	0.079	1.4835	97.0
4.1373	0	12.6029	72.465	5.4603	0.5781	0.0557	0.0494	1.5861	96.9
8.5703	0.0027	12.8342	72.7456	5.5292	0.6816	0.0607	0.0488	1.4151	101.9
4.182	0	12.5961	71.5946	5.503	0.6965	0.0413	0	1.5917	96.2
4.1282	0	12.7547	70.9435	5.4421	0.6158	0.0586	0	1.616	95.6
4.1574	0.0927	12.5293	71.5212	5.5888	0.6636	0.0228	0.0498	1.3671	96.0
4.3487	0	12.7602	72.8974	5.6848	0.6395	0.1452	0	1.348	97.8
3.9612	0.0325	12.4766	69.8848	5.4483	0.6127	0.0931	0.1678	1.577	94.3
4.16	0	12.9124	72.5375	5.7633	0.7037	0.0445	0.0502	1.368	97.5
4.1998	0.0867	12.8076	73.1707	5.5864	0.6155	0.2223	0	1.5697	98.3
4.0065	0	12.3818	70.6485	5.6779	0.7121	0.0665	0.0494	1.7071	95.2
4.6306	0.0163	12.5574	72.1258	5.5968	0.6901	0.1643	0.0693	1.5732	97.4
4.1823	0	12.4923	71.8966	5.5097	0.658	0.0774	0.179	1.4158	96.4
4.2078	0.0816	12.8964	72.4729	5.4181	0.6743	0.0463	0.078	1.5927	97.5
4.0976	0.0067	12.9843	72.7909	5.5365	0.6022	0.004	0.0488	1.3645	97.4
4.3032	0.0244	12.9871	72.6507	5.5791	0.666	0.0103	0	1.4506	97.7
4.2232	0.019	12.7648	72.1894	5.4616	0.7113	0	0.0888	1.68	97.1
4.1561	0.0453	12.8398	74.0513	5.5568	0.6679	0.2449	0.0497	1.4944	99.1
3.7219	0	12.3652	69.6453	5.5052	0.5956	0.225	0.0793	1.4288	93.6
3.9868	0	12.842	71.9644	5.3805	0.5546	0	0.0297	1.4727	96.2
3.9078	0.0288	12.5649	73.2725	5.4478	0.6911	0.0175	0.0497	1.5454	97.5
7.7469	0	12.8239	73.8292	5.5215	0.6179	0.1743	0.0594	1.6364	102.4
3.8834	0.0246	12.5984	73.3959	5.5204	0.718	0.197	0.1188	1.5839	98.0
3.8205	0.0368	12.6526	72.7497	5.5248	0.5794	0	0.1782	1.497	97.0
6.1454	0.061	12.7437	72.8858	5.5424	0.736	0.1328	0	1.4719	99.7
4.3021	0.0906	12.1656	67.414	5.7437	0.7377	0.0971	0.0989	1.5222	92.2
4.3008	0.0205	12.82	74.0046	5.5455	0.721	0.0857	0.0396	1.4378	99.0
3.7016	0.1351	12.7829	73.6189	5.4216	0.5826	0.1105	0.0595	1.4743	97.9
3.6966	0	12.3132	71.6198	5.3743	0.658	0.0243	0.1295	1.2789	95.1
3.925	0.066	12.8316	73.4086	5.5074	0.7361	0.0452	0	1.8121	98.3
3.8341	0.0774	12.8438	74.1492	5.5605	0.6635	0.0788	0.0346	1.4828	98.7
3.7442	0	12.9789	74.2629	5.4977	0.6904	0.0511	0.1647	1.28	98.7
3.7645	0	12.9352	74.1211	5.5509	0.591	0.1265	0.0864	1.5497	98.7
3.6853	0	12.8308	73.8424	5.6246	0.4941	0.005	0.0519	1.4665	98.0
3.5586	0	12.4041	71.8083	5.6632	0.7162	0.1009	0.0173	1.3297	95.6
4.0171	0.0048	11.9364	66.737	5.3329	0.6084	0.0681	0.0173	1.6264	90.3
3.7739	0.0795	12.6587	71.6513	5.4618	0.6888	0.1547	0.0198	1.558	96.0
4.03	0	12.3911	73.0513	5.5024	0.65	0.0663	0.0197	1.4929	97.2
3.8551	0	12.2514	71.7803	5.5248	0.638	0.1294	0.1579	1.5011	95.8
4.0022	0.0376	12.7698	72.7502	5.5778	0.6194	0.0883	0	1.5889	97.4
4.2052	0.0515	12.5388	73.3831	5.6577	0.498	0.0339	0.0401	1.4553	97.9
4.0348	0.0247	12.443	71.8267	5.3888	0.7236	0.0715	0.089	1.2699	95.9
4.0825	0.0301	12.3981	72.7339	5.5976	0.6024	0.1568	0.1286	1.2785	97.0
3.9708	0.022	12.6909	72.3346	5.4771	0.5941	0.0585	0.257	1.66	97.1
4.1143	0	12.4953	73.2719	5.2098	0.7919	0.0198	0.0395	1.6749	97.6
4.2121	0.0492	12.658	73.2349	5.4652	0.8004	0	0.1284	1.1634	97.7
3.8508	0.0246	12.3725	71.577	5.4159	0.6412	0.1055	0.1479	1.5343	95.7
4.148	0	12.7491	73.1622	5.7027	0.6646	0.1023	0.0795	1.7749	98.4
4.162	0.0097	12.7863	73.5516	5.4709	0.6295	0.1173	0.1095	1.3562	98.2
4.1066	0.0162	12.0248	69.7126	5.6742	0.59	0.076	0	1.5003	93.7
4.236	0	12.2182	67.1361	5.3479	0.6282	0.086	0.1089	1.4014	91.2
4.3945	0.0463	12.4797	72.8466	5.6367	0.662	0.0428	0.0099	1.6095	97.7
4.2025	0	12.393	72.1114	5.2958	0.7068	0.05	0.0789	1.5162	96.4
4.1204	0.023	12.5843	72.6688	5.2848	0.7849	0	0.079	1.4835	97.0
4.1373	0	12.6029	72.465	5.4603	0.5781	0.0557	0.0494	1.5861	96.9
8.5703	0.0027	12.8342	72.7456	5.5292	0.6816	0.0607	0.0488	1.4151	101.9
4.182	0	12.5961	71.5946	5.503	0.6965	0.0413	0	1.5917	96.2
4.1282	0	12.7547	70.9435	5.4421	0.6158	0.0586	0	1.616	95.6
4.1574	0.0927	12.5293	71.5212	5.5888	0.6636	0.0228	0.0498	1.3671	96.0
4.3487	0	12.7602	72.8974	5.6848	0.6395	0.1452	0	1.348	97.8
3.9612	0.0325	12.4766	69.8848	5.4483	0.6127	0.0931	0.1678	1.577	94.3
4.16	0	12.9124	72.5375	5.7633	0.7037	0.0445	0.0502	1.368	97.5
4.1998	0.0867	12.8076	73.1707	5.5864	0.6155	0.2223	0	1.5697	98.3
4.0065	0	12.3818	70.6485	5.6779	0.7121	0.0665	0.0494	1.7071	95.2
4.6306	0.0163	12.5574	72.1258	5.5968	0.6901	0.1643	0.0693	1.5732	97.4
4.1823	0	12.4923	71.8966	5.5097	0.658	0.0774	0.179	1.4158	96.4
4.2078	0.0816	12.8964	72.4729	5.4181	0.6743	0.0463	0.078	1.5927	97.5
4.0976	0.0067	12.9843	72.7909	5.5365	0.6022	0.004	0.0488	1.3645	97.4
4.3032	0.0244	12.9871	72.6507	5.5791	0.666	0.0103	0	1.4506	97.7
4.2232	0.019	12.7648	72.1894	5.4616	0.7113	0	0.0888	1.68	97.1
Mean	4.29	0.02	12.62	72.10	5.52	0.66	0.08	0.06	1.50
1 St. Dev.	0.89	0.03	0.25	1.61	0.12	0.06	0.06	0.06	0.13
XRF Mean conc. (Hunt and Hill 1996)	4.06	0.03	13.04	73.72	5.06	0.76	n/a	n/a	1.75
Mean 184 analyses (Hunt and Hill 1993)	3.93	0.05	12.87	74.35	5.11	0.74	n/a	0.07	1.51

cont.

Published and average data for TB1G basaltic glass standard over 6 days of analyses at FEEA, n = 88

Ox%(Na)	Ox%(Mg)	Ox%(Al)	Ox%(Si)	Ox%(K)	Ox%(Ca)	Ox%(Ti)	Ox%(Mn)	Ox%(Fe)	Total
3.389	3.4682	15.7562	51.9615	4.7872	6.6235	0.9066	0.2615	7.5155	94.7
3.296	3.698	15.992	52.0972	4.7884	6.7275	0.7822	0.2684	7.9687	95.6
3.5353	3.605	15.8744	52.7034	4.7016	6.7051	1.0169	0.2045	7.762	96.1
3.4358	3.5726	15.563	49.9039	4.9335	6.635	1.0171	0.0877	8.019	93.2
3.4545	3.4671	16.314	53.9155	4.9854	6.759	0.9938	0.1268	8.2647	98.3
3.4829	3.5296	15.1481	50.1844	4.8733	6.3932	0.9237	0.1057	8.4651	93.1
3.1323	3.3955	15.6875	51.5103	4.5544	6.5707	0.8876	0.1539	7.8883	93.8
3.3616	3.361	15.2396	49.4889	4.6632	6.4913	0.9718	0.1827	7.8354	91.6
3.2471	3.2977	15.4735	50.3006	4.7003	6.5681	0.8023	0.2403	8.0512	92.7
3.3283	5.4933	15.3989	51.8927	4.7923	6.5038	0.8356	0.1641	8.4425	96.9
3.9998	3.6548	15.86	52.1693	4.5719	6.5591	0.9665	0.184	8.3072	96.3
3.4254	3.4154	15.9179	51.767	4.6847	6.4616	0.9959	0.2617	8.7893	95.7
3.2699	3.4881	15.6426	51.9697	4.9523	6.8032	0.7062	0.2784	7.7862	94.9
3.4184	3.4421	15.2606	49.2243	4.71	6.7659	0.8672	0.1744	8.4383	92.3
3.4743	3.6467	16.3073	52.6172	4.7006	6.7429	0.9151	0.0385	8.6665	97.1
3.571	3.4759	16.0592	52.526	4.7596	6.6282	1.0076	0.0577	7.9128	96.0
3.4693	3.6212	15.9889	51.8551	4.7789	6.6773	0.915	0.1757	8.0704	95.6
3.4757	3.5168	15.7573	51.1522	4.8323	6.7566	0.833	0.1862	8.1185	94.6
3.3986	3.1867	15.7909	51.4194	4.8235	6.7585	0.8648	0.2462	8.1583	94.6
3.1044	3.3022	15.7355	51.9609	4.8399	6.649	0.6896	0.3322	8.3615	95.0
3.4168	3.417	15.203	48.9828	4.6742	6.6198	0.8661	0.1842	8.6051	92.0
3.1138	3.441	15.592	50.5316	4.7674	6.6353	0.8576	0.0586	8.4486	93.4
3.6858	3.4247	16.0675	53.1223	4.8758	6.5484	0.8873	0.107	7.9648	96.7
3.1874	3.6116	15.6784	50.0434	4.7105	6.6453	1.0118	0.0684	8.4644	93.4
3.4076	3.4174	15.8605	52.9378	4.7522	6.4732	0.9113	0.1653	8.2746	96.2
3.4408	3.6738	16.2523	52.8698	4.6666	6.5599	0.9398	0.1558	8.0817	96.6
3.6077	3.3975	16.054	52.9118	4.6796	6.6359	0.9616	0.2045	7.9131	96.4
3.3978	3.6309	16.1856	52.4116	4.7875	6.5571	0.8635	0.0866	7.7235	95.6
3.5544	3.6882	16.2338	53.0317	4.7828	6.5499	0.9615	0.0876	8.2662	97.2
3.1035	3.543	16.111	52.8548	4.6151	6.6852	0.8642	0.3215	7.9988	96.1
3.649	3.7087	15.9422	53.1848	4.8865	6.6564	0.9192	0.357	8.7711	98.1
3.1383	3.6717	14.4451	52.0769	4.7509	6.6277	0.9064	0.2338	7.7703	93.6
3.1437	3.6178	16.117	52.6976	4.7148	6.6851	0.9957	0.117	8.2289	96.3
2.838	3.5722	15.2944	49.6624	4.6708	6.6637	0.9116	0.2733	8.1056	92.0
2.7471	3.5782	16.0915	51.8031	4.7446	6.672	1.0014	0.314	8.343	95.3
2.6257	3.4013	15.762	51.9838	4.8329	6.7569	0.8045	0.2464	8.6097	95.0
2.7485	3.2873	14.9928	47.6706	4.6318	6.6986	0.8399	0.0099	8.1442	89.0
3.2093	3.4297	16.717	54.3187	4.7646	7.032	1.0165	0.1985	8.4545	99.1
2.6865	3.5703	16.1227	53.4546	4.8302	6.8603	0.8112	0.2581	8.4206	97.0
3.1129	4.5782	14.3825	52.0965	5.0278	6.9378	0.8329	0.2082	8.3248	95.5
3.5275	3.6501	16.2141	54.0134	4.7397	6.7309	1.0244	0.1954	8.2274	98.3
3.0364	3.5729	15.6591	52.662	4.6898	6.7134	0.8654	0.0085	8.0859	95.3
3.2171	3.5952	16.0966	53.0379	4.7677	6.7288	0.7772	0.1191	8.0768	96.4
3.2385	3.4726	14.9319	47.5003	4.7562	6.6191	0.7787	0.2809	8.3948	90.0
3.8444	3.6188	16.5216	53.4548	4.7545	6.6711	0.8592	0.1454	8.7273	98.6
3.1723	3.5588	16.2028	53.6106	4.8177	6.9389	0.9383	0.2662	8.3978	97.9
3.1745	3.2585	14.6898	47.7458	4.675	6.7764	0.9434	0.1655	7.5967	89.0
3.4027	3.4225	15.927	53.382	4.7186	6.7861	0.7753	0.2241	7.9914	96.6
3.1159	3.6186	16.0614	53.2294	4.8807	6.6166	0.9599	0.0973	8.3232	96.9
3.3316	3.4139	16.0561	53.2973	4.6159	6.7153	0.826	0.1459	8.3916	96.8
3.2881	3.4609	15.3367	48.4361	4.6449	6.8356	1.0607	0.0693	7.7973	90.9
3.4395	3.6308	16.0991	53.1338	4.8699	6.7883	0.7334	0.0791	8.4052	97.2
3.3031	3.5009	16.1517	53.8679	4.8098	6.6403	0.9165	0.1362	9.0092	98.3
3.3144	3.3626	15.0369	49.541	4.818	6.6221	0.8327	0.0487	7.8028	91.4
3.2007	3.618	16.1448	53.4584	4.6325	6.6995	0.9441	0.1949	8.4752	97.4
3.2444	3.4907	16.0489	53.4609	4.7846	7.0229	0.8338	0.2926	8.0742	97.3
3.4407	3.3502	15.8688	53.0426	4.6435	6.5993	0.7346	0	8.656	96.3
3.1135	3.5313	16.3089	53.522	4.6026	6.746	0.813	0.0097	8.4197	97.1
3.1894	3.3574	15.9744	52.1518	4.8916	6.5817	0.876	0.0388	8.1635	95.2
3.286	3.4402	16.0514	53.3856	4.7485	6.9249	0.7497	0.039	7.9257	96.6
3.389	3.4682	15.7562	51.9615	4.7872	6.6235	0.9066	0.2615	7.5155	94.7
3.296	3.698	15.992	52.0972	4.7884	6.7275	0.7822	0.2684	7.9687	95.6
3.5353	3.605	15.8744	52.7034	4.7016	6.7051	1.0169	0.2045	7.762	96.1
3.4358	3.5726	15.563	49.9039	4.9335	6.635	1.0171	0.0877	8.019	93.2
3.4545	3.4671	16.314	53.9155	4.9854	6.759	0.9938	0.1268	8.2647	98.3
3.4829	3.5296	15.1481	50.1844	4.8733	6.3932	0.9237	0.1057	8.4651	93.1
3.1323	3.3955	15.6875	51.5103	4.5544	6.5707	0.8876	0.1539	7.8883	93.8
3.3616	3.361	15.2396	49.4889	4.6632	6.4913	0.9718	0.1827	7.8354	91.6
3.2471	3.2977	15.4735	50.3006	4.7003	6.5681	0.8023	0.2403	8.0512	92.7
3.3283	5.4933	15.3989	51.8927	4.7923	6.5038	0.8356	0.1641	8.4425	96.9
3.9998	3.6548	15.86	52.1693	4.5719	6.5591	0.9665	0.184	8.3072	96.3
3.4254	3.4154	15.9179	51.767	4.6847	6.4616	0.9959	0.2617	8.7893	95.7
3.2699	3.4881	15.6426	51.9697	4.9523	6.8032	0.7062	0.2784	7.7862	94.9
3.4184	3.4421	15.2606	49.2243	4.71	6.7659	0.8672	0.1744	8.4383	92.3
3.4743	3.6467	16.3073	52.6172	4.7006	6.7429	0.9151	0.0385	8.6665	97.1
3.571	3.4759	16.0592	52.526	4.7596	6.6282	1.0076	0.0577	7.9128	96.0
3.4693	3.6212	15.9889	51.8551	4.7789	6.6773	0.915	0.1757	8.0704	95.6
3.4757	3.5168	15.7573	51.1522	4.8323	6.7566	0.833	0.1862	8.1185	94.6
3.3986	3.1867	15.7909	51.4194	4.8235	6.7585	0.8648	0.2462	8.1583	94.6
3.1044	3.3022	15.7355	51.9609	4.8399	6.649	0.6896	0.3322	8.3615	95.0
3.4168	3.417	15.203	48.9828	4.6742	6.6198	0.8661	0.1842	8.6051	92.0
3.1138	3.441	15.592	50.5316	4.7674	6.6353	0.8576	0.0586	8.4486	93.4
3.6858	3.4247	16.0675	53.1223	4.8758	6.5484	0.8873	0.107	7.9648	96.7
3.1874	3.6116	15.6784	50.0434	4.7105	6.6453	1.0118	0.0684	8.4644	93.4
3.4076	3.4174	15.8605	52.9378	4.7522	6.4732	0.9113	0.1653	8.2746	96.2
3.4408	3.6738	16.2523	52.8698	4.6666	6.5599	0.9398	0.1558	8.0817	96.6
3.6077	3.3975	16.054	52.9118	4.6796	6.6359	0.9616	0.2045	7.9131	96.4
3.3978	3.6309	16.1856	52.4116	4.7875	6.5571	0.8635	0.0866	7.7235	95.6
3.5544	3.6882	16.2338	53.0317	4.7828	6.5499	0.9615	0.0876	8.2662	97.2
Mean	3.34	3.56	15.79	51.83	4.76	6.66	0.89	0.17	8.19
1 st. dev.	0.24	0.34	0.44	1.58	0.10	0.12	0.09	0.09	0.31
Assigned value (Potts et al 2002)	3.20	3.64	16.68	54.22	4.37	6.87	0.845	0.183	9.05
Target precision	0.11	0.12	0.44	1.19	0.14	0.21	0.035	0.009	0.26

Appendix B₄: Radiogenic isotope analyses (NIGL)

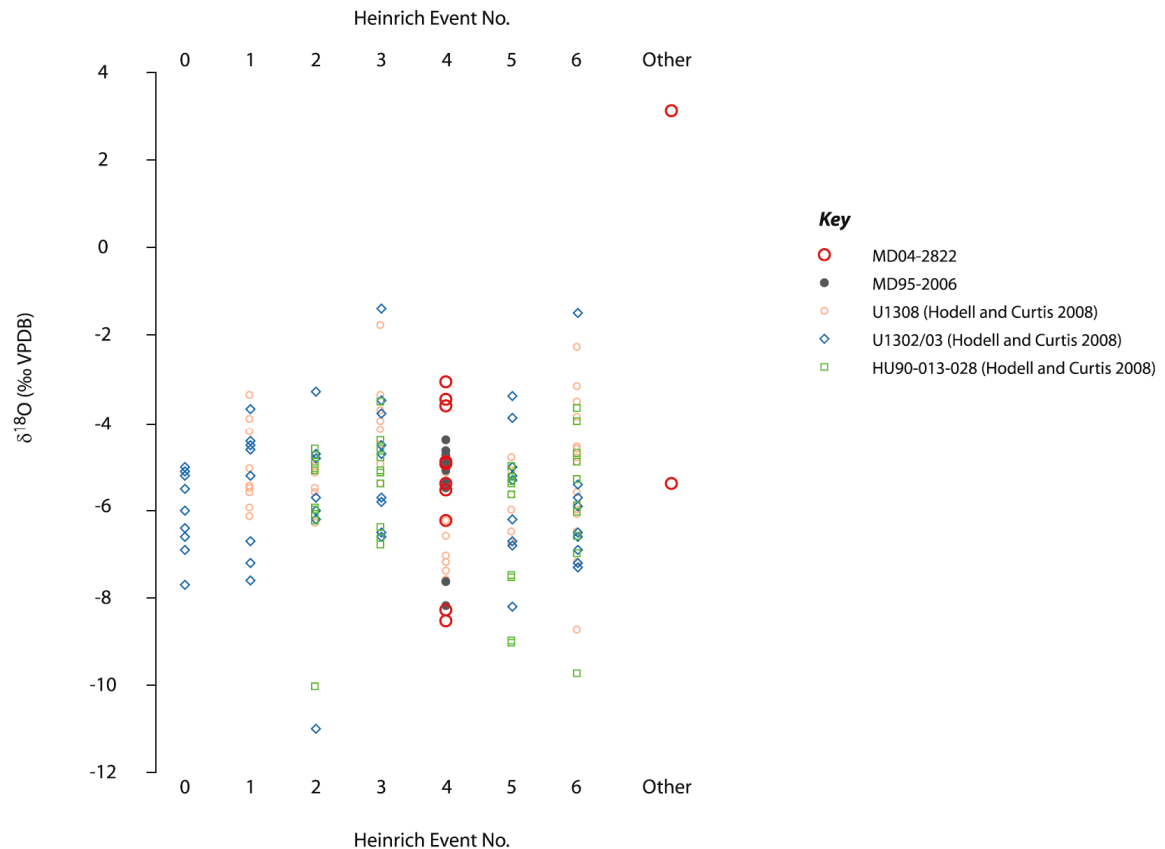
Radiogenic isotope (Sr, Nd and Pb) analyses for bulk samples within Greenland Stadial 9 and MIS 4 windows. All samples run at NIGL

Interval	Depth cm	$^{87}\text{Sr}/^{86}\text{Sr} \pm 2\sigma$	$^{143}\text{Nd}/^{144}\text{Nd} \pm 2\sigma$	Epsilon Nd	$^{206}\text{Pb}/^{204}\text{Pb} \pm 2\sigma$	$^{207}\text{Pb}/^{204}\text{Pb} \pm 2\sigma$	$^{208}\text{Pb}/^{204}\text{Pb} \pm 2\sigma$	$^{206}\text{Pb}/^{206}\text{Pb} \pm 2\sigma$	$^{208}\text{Pb}/^{206}\text{Pb} \pm 2\sigma$						
post-H4	2003.5	0.723093	0.000004	-	18.900102	0.002232	15.648121	0.001795	38.8339961	0.005382	0.827955	0.000083	2.055084	0.000272	
post-H4	2004.5	0.723394	0.000005	-	18.853482	0.002265	15.643332	0.001821	38.808483	0.005440	0.829720	0.000083	2.058431	0.000273	
post-H4	2005.5	0.725903	0.000004	0.511969	0.000006	-13.055334	0.002254	15.651939	0.001793	38.888696	0.005451	0.824647	0.000083	2.048882	0.000272
post-H4	2009.5	0.726800	0.000005	0.511931	0.000007	-13.791209	0.002245	15.655284	0.001772	38.898710	0.005303	0.823621	0.000082	2.046442	0.000271
post-H4	2013.5	0.727198	0.000005	-	18.945865	0.002225	15.652788	0.001809	38.901543	0.005486	0.826172	0.000083	2.053319	0.000274	
peak H4	2015.5	0.728697	0.000004	0.511869	0.000007	-15.006098	0.002220	15.654272	0.001784	38.881775	0.005329	0.828152	0.000083	2.056965	0.000273
pre-H4	2017.5	0.727977	0.000004	-	18.992683	0.002231	15.658134	0.001772	38.948065	0.005338	0.824437	0.000082	2.050746	0.000271	
pre-H4	2019.5	0.728552	0.000005	0.511912	0.000009	-14.167083	0.002299	15.660217	0.001836	38.952380	0.005460	0.823669	0.000083	2.048769	0.000273
pre-H4	2021.5	-	-	0.511967	0.000007	-13.085179	0.002254	15.665390	0.001797	38.926224	0.005425	0.825188	0.000082	2.050494	0.000272
pre-H4	2025.5	0.726017	0.000004	0.512008	0.000006	-12.294931	0.002194	15.646682	0.001749	38.804773	0.005213	0.829295	0.000083	2.056727	0.000271
GS18	2219.5	0.721440	0.000004	0.512021	0.000006	-12.028464	0.002334	15.627103	0.002047	38.780895	0.004908	0.831467	0.000026	2.063485	0.000136
GS18	2230.5	0.724328	0.000004	0.511968	0.000007	-13.075770	0.002244	15.619311	0.001832	38.720933	0.005428	0.831433	0.000083	2.061194	0.000273
GS18	2235.5	0.725928	0.000005	0.511969	0.000006	-13.044271	0.002192	15.628794	0.001736	38.781090	0.005210	0.829355	0.000083	2.058009	0.000272
GS18	2242.5	0.727702	0.000007	0.512004	0.000007	-12.374028	0.002453	15.641934	0.002109	38.785076	0.005048	0.829100	0.000027	2.055788	0.000136
GS19	2269.5	0.727580	0.000005	0.511998	0.000009	-12.476260	0.002326	15.650881	0.002009	38.842268	0.004741	0.825771	0.000026	2.049358	0.000133
GS19	2276.5	-	-	-	18.939522	0.002312	15.651091	0.001971	38.868891	0.004622	0.826372	0.000024	2.052252	0.000130	
GS19	2283.5	0.726210	0.000005	0.511967	0.000009	-13.088993	0.001918	15.633446	0.002038	38.815341	0.005893	0.828121	0.000028	2.056137	0.000122
GS19	2288.5	0.726230	0.000003	0.512011	0.000009	-12.238376	0.002518	15.643745	0.001985	38.839675	0.005129	0.828090	0.000035	2.055998	0.000097
GS19	2302.5	0.725866	0.000005	0.511984	0.000008	-12.748287	0.001932	15.636252	0.002002	38.798254	0.005661	0.829250	0.000028	2.057659	0.000116
GS19	2308.5	-	-	0.511978	0.000007	-12.875971	0.002060	15.632439	0.002170	38.812295	0.006332	0.828818	0.000029	2.057797	0.000127
GS19	2314.5	0.723815	0.000006	0.512003	0.000008	-12.378556	0.001961	15.631779	0.002093	38.753490	0.005994	0.830789	0.000029	2.059652	0.000125
GS19	2316.5	0.725967	0.000004	0.511994	0.000007	-12.562846	0.002530	15.649909	0.002013	38.913753	0.005218	0.828644	0.000034	2.060441	0.000092
GS19	2322.5	0.727734	0.000005	0.511985	0.000010	-12.742860	0.002008	15.655647	0.002096	38.936674	0.006023	0.827390	0.000029	2.058307	0.000122
GS19	2328.5	0.725962	0.000004	0.511999	0.000006	-12.468330	0.002364	15.656461	0.002037	38.919132	0.004880	0.827357	0.000025	2.056655	0.000134
GS20	2351.5	0.723144	0.000006	0.512008	0.000009	-12.280796	0.002365	15.654441	0.002111	38.910226	0.005161	0.826958	0.000028	2.055442	0.000140
GS20	2354.5	0.723778	0.000006	0.512005	0.000008	-12.350768	0.002029	15.653216	0.002111	38.917304	0.006098	0.826572	0.000029	2.055068	0.000130
GS20	2358.5	0.722817	0.000007	0.511986	0.000006	-12.727560	0.002412	15.656521	0.002111	38.913324	0.005211	0.826621	0.000026	2.054531	0.000142
GS21	2376.5	0.721834	0.000004	0.512006	0.000007	-12.330613	0.002646	15.652532	0.002134	38.879432	0.005564	0.828134	0.000036	2.057043	0.000103
GS21	2380.5	0.722078	0.000005	0.512000	0.000009	-12.441768	0.002344	15.647906	0.002050	38.856393	0.005057	0.829060	0.000026	2.058721	0.000136
GS21	2384.5	0.713495	0.000004	0.512032	0.000009	-11.818659	0.002482	15.661913	0.002144	38.972533	0.005170	0.826197	0.000028	2.055878	0.000138

Appendix B₅: Stable isotope determinations for individual carbonate grains from Heinrich events within MD04-2822 and MD95-2006 (University of Cambridge)

Stable isotope analysis ($\delta^{18}\text{O}$ and $\delta^{13}\text{C}$) of detrital carbonate grains from minor IRD peak (ca. 125.5 kyr) during Termination II from core MD04-2822. Analyses of Heinrich Event 4 from MD04-2822 and MD95-2006. All analyses carried out by D. Hodell (University of Cambridge). Plot of $\delta^{18}\text{O}$ of detrital carbonate grains from MD04-2822 and MD95-2006 as well as those reported within Hodell and Curtis (2008).

Core	IRD Event	Analysis	Core Depth (cm)	$\delta^{18}\text{O}$ (‰ VPDB)	$\delta^{13}\text{C}$ (‰ VPDB)
MD04-2822	Minor peak end TII	A	2558.5	3.10	1.41
		B	2558.5	-5.40	3.11
MD04-2822	H4	A	2015.5	-6.27	-1.08
		B	2015.5	-0.34	-0.34
		C	2015.5	-3.47	0.78
		D	2015.5	-8.54	-0.55
		E	2015.5	-8.31	1.22
		F	2015.5	-5.42	0.24
		G	2015.5	-3.64	1.77
		H	2015.5	-5.55	4.22
		I	2015.5	-4.94	0.78
		J	2015.5	-3.06	0.14
			Mean		-5.42
MD95-2006	H4	A	2460.5	-4.77	0.47
		B	2460.5	-8.20	0.19
		C	2460.5	-5.13	-0.91
		D	2460.5	-4.67	1.43
		E	2460.5	-5.38	1.36
		F	2460.5	-7.66	1.00
		G	2460.5	-5.52	-1.00
		H	2460.5	-4.40	2.31
		I	2460.5	-4.91	1.94
		J	2460.5	-5.45	0.13
			Mean		-5.61



Appendix C₁: Tuning tie-points for MD04-2822 to $\delta^{18}\text{O}$ stacks (SPECMAP and LR04)

Correlation of MD04-2822 benthic $\delta^{18}\text{O}$ record to the stack of Pisias et al (1984) and the age model of Martinson et al (1987). Thompson and Goldstein (2006) radiometric age for isotopic feature of Pisias et al (1984).

MD04-2822 depth (cm)	Isotope Pisias et al (1984)	taxonomy	Age (yr) Martinson et al 1987	Error (yr)	Age (yr, $\pm 2\sigma$ error) Thompson and Goldstein (2006)
820.5	2.2		17,850	1,370	23,100 \pm 500
2220.5	3.31		55,450	5,030	52,200 \pm 600
2300.5	4.22		64,090	6,350	
2320.5	4.23		68,830	4,200	67,700 \pm 1,700
2330.5	4.24		70,820	3,950	
2400.5	5.1		79,250	3,580	80,500 \pm 900
2410.5	5.2		90,950	6,830	91,300 \pm 8,000
2450.5	5.4		110,790	6,280	110,100 \pm 800
2554.5	5.5		123,820	2,620	
2652.5	6.0		129,840	3,050	129,300 \pm 1,000
2750.5	6.2		135,100	4,240	
2930.5	6.3		142,280	5,280	
3740.5	6.5		175,050	9,840	172,900 \pm 1,700

Correlation of MD04-2822 benthic $\delta^{18}\text{O}$ record to the stack LR04 (Lisiecki and Raymo 2005). Equivalent isotopic feature of Pisias et al (1984) and age difference between the two tuning targets (SPECMAP, age model Martinson et al 1987 minus LR04). Depths in brackets indicate that alternative correlations are possible.

MD04-2822 depth (cm)	LR04 age (yrs)	Age difference (yrs) (SPECMAP – LR04)
240.5	9,000	
820.5	18,000	-150
(1170.5)	38,000	
(1340.5)	45,000	
(1760.6)	50,000	
(1900.5)	52,000	
2220.5	55,000	
2300.5	62,000	2090
2320.5	64,000	4830
2330.5	66,000	4820
2400.5	82,000	-2750
2410.5	87,000	3950
2460.5	105,000	
2470.5	109,000	1790
2500.5	120,000	
2554.5	123,000	820
2652.5	130,000	-160
2690.5	135,000	
2750.5	140,000	-4900
2930.5	155,000	-12720
2970.5	156,000	
3670.5	167,000	
3700.5	171,000	
3740.5	174,000	1050

Appendix C₂: Tuning tie-points for MD04-2822 to NGRIP $\delta^{18}\text{O}$ on both the ss09sea and GICC05 timescale

MD04-2822 surface proxies tuned to the NGRIP $\delta^{18}\text{O}$ record using both the ss09sea (NGRIP members 2004) and GICC05 timescales (Andersen et al 2006, Rasmussen et al 2006, Svensson et al 2006, 2008).

NGRIP ss09sea timescale				NGRIP GICC05 timescale				
GIS number (transition in)	ss09sea (yrs b2k)	Age	MD04-2822 depth (cm)	GIS number (transition in)	GICC05 (yrs b2k)	Age	Maximum counting error (yrs)	MD04-2822 depth (cm)
-	8,225		95.005	YD/PB trans	11703		50	245.5
-	9,225		153.904	into YD (GS1)	12896		138	300.5
-	10,825		195.904	into GIS 1e	14692		186	440.5
-	11,325		238.905	1	14692		93	Not identified
-	12,775		261.905	2	23340		596	1325.5
-	15,575		357.905	3	27780		832	1766.509
2	22,675		1344.905	4	28900		898	1801.457
3	27,375		1747.009	5	32500		1132	1888.905
4	28,475		1788.900	6	33740		1286	1932.905
5	32,300		1884.905	7	35480		1321	1956.905
6	33,650		1932.405	8	38220		1449	2002.905
7	35,450		1956.905	9	40160		1580	2025.905
8	38,400		2002.905	10	41460		1633	2045.405
9	40,375		2015.905	11	43340		1736	2067.405
10	41,800		2045.405	12	46920		1915	2092.905
11	43,650		2067.405	13	49280		2031	2116.904
12	47,450		2092.905	14	54220		1150	2148.408
13	49,850		2116.904	NAAZ II	55380		1184	2163.500
14	54,950		2148.404	15	55800		1196	2166.905
15	56,600		2166.905	16	58280		1256	2187.405
16	59,100		2187.405					
17	60,250		2197.905					
18	65,000		2269.404					
19	73,050		2348.405					
20	77,100		2369.905					
21	85,350		2386.905					
22	90,400		2416.904					
23	104,550		2427.904					
24	108,600		2436.904					
25	115,400		2476.905					

Appendix C₃: GS3 tuning tie-points (NGRIP, GICC05) and radiocarbon age determinations

Tie-points for the tuning of the *N. pachyderma* (sinistral) records of the four cores to NGRIP $\delta^{18}\text{O}$ (GICC05 timescale, b2k). Maximum counting error for NGRIP $\delta^{18}\text{O}$ for the transitions into interstadials 2, 3, and 4 are given (Svensson et al 2008), as well as the age uncertainty derived for the Fugloyarbanki tephra layer (Davies et al 2008). Estimates for the duration of GIS are from Wolff et al (2009).

GIS no.	Transition	Age yrs b2k GICC05 timescale	max counting error GICC05	Est. GIS duration yrs Wolff et al (2009) (age estimate for transition)	MD04-2882 depth (cm)	MD95-2006 depth (cm)	LINK 17 depth (cm)	MD01-2461 depth (cm)
<hr/>								
Warming post GIS 2	n/a	22960 +			1270.5	1615.0	411.0	445.5
2	Out	22,900		(23240 ^a)	1290.5	1619.5	426.25	474.5
2	In	23340 *		100	1325.5	1634.5	441.75	502.5
Fugloyarbanki	n/a	26740 ± 390	596		n/a	1930.0	633.0	n/a
3	Out	27,540 *		(27480 ^a)	1745.5	2002.0	672.5	635.5
3	In	27,780 *	832	300	1755.5	2020.0	693.5	659.5
4	Out	28,600 *		(28600 ^a)	1785.5	2054.0	744.0	671.5
4	In	28,900 *	300	300	1805.5	2076.0	761.75	678.5

* age derived from the mid point of the $\delta^{18}\text{O}$ transition in combined NGRIP, GRIP and GISP2 records following the approach of Andersen et al 2006. Uncertainty up to 40 years (Lowe et al 2008);

Conventional and calibrated radiocarbon dates for cores MD04-2822, MD95-2006, LINK 17 and MD01-2461. All radiocarbon dates calibrated using the Marine09 calibration curve (Reimer et al 2009) using the OxCal programme (version 4.1; Bronk Ramsey 2009). Calibrated ages are given according to their 68 and 95 % probability distributions. ACalibration was also undertaken using a deposition model (Bronk Ramsey 2008).

Core	Depth (cm)	Species	Conventional Age (yrs BP \pm 1 σ)	Calibrated ¹⁴ C Age (yrs b2k) stratigraphic model used		no Calibrated ¹⁴ C Age (yrs b2k) Ramsey 2008) used in calibration		Deposition model (Bronk 2008)				
				68% Probability	95% Probability	68% Probability	95% Probability		Comment			
MD04-2822	1270.5	G. bulloides	19635 \pm 85	23142	22620	23370	22512	22546	22421	22596	22335	poor agreement
	1310.5	G. bulloides	19830 \pm 62	23440	22980	23510	22665	23079	22970	23122	22897	
	1490.5	<i>N. pachyderma</i> (sinistral)	21015 \pm 70	24780	24440	24946	24340	25495	25451	25498	25416	poor agreement
	1750.5	G. bulloides	24639 \pm 109	29326	28837	29435	28575	29068	28941	29155	28895	
	1790.5	G. bulloides	25495 \pm 100	30198	29756	30262	29558	29619	29476	29721	29421	poor agreement
	1800.5	G. bulloides	25225 \pm 108	29843	29445	30162	29413	29759	29611	29864	29554	
MD95-2006	1591.5	<i>N. pachyderma</i> (sinistral)	20390 \pm 150	24152	23666	24331	23437	23871	23445	24171	23229	
	1914.5	<i>N. pachyderma</i> (sinistral)	22720 \pm 130	27534	26356	27629	26255	27880	27691	27972	27611	poor agreement
	2010.5	G. bulloides	24571 \pm 185	29270	28717	29441	28499	29095	28909	29217	28843	
	2020.5		24710 \pm 280	29440	28780	29661	28411	29223	29034	29352	28967	
	2060	G. bulloides	25734 \pm 218	30401	29760	30591	29559	29737	29528	29883	29451	poor agreement
	LINK 17	436.5	<i>N. pachyderma</i> (sinistral)	20330 \pm 190	24057	23514	24351	29251	24353	23828	24748	23647
496.5		<i>N. pachyderma</i> (sinistral)	22300 \pm 220	26661	25985	27015	27982	25566	25168	25744	25056	poor agreement
633		<i>N. pachyderma</i> (sinistral)	24250 \pm 350	29176	28330	29439	25515	28464	28108	28662	27919	
718.5		<i>N. pachyderma</i> (sinistral)	25350 \pm 300	30170	29545	30444	23336	30370	29846	30655	29545	
478		G. bulloides	20193 \pm 118	23835	23480	24015	23248	22759	22650	22900	22413	poor agreement
MD01-2461	528.5	<i>N. pachyderma</i> (sinistral)	20931 \pm 129	24752	24313	24975	24113	24501	24402	24621	24326	
	570.5	<i>N. pachyderma</i> (sinistral)	21565 \pm 128	25484	25035	25791	24904	25955	25842	26057	25772	poor agreement
	602.5	<i>N. pachyderma</i> (sinistral)	22234 \pm 147	26590	25923	26791	25763	27071	26937	27201	26863	poor agreement
	648.5	<i>N. pachyderma</i> (sinistral)	24074 \pm 168	28628	28164	28952	27940	28697	28516	28855	28430	
	674	<i>N. pachyderma</i> (sinistral)	25312 \pm 195	30160	29519	30264	29413	29603	29395	29777	29291	

- de Abreu L, Shackleton NJ, Schönfeld J, Hall M, Chapman M. 2003. Millennial-scale oceanic climate variability off the Iberian Margin during the last two glacial periods. *Marine Geology* 196: 1-20
- Adkins JF, McIntyre K, Schrag DP. 2002. The salinity, temperature and $\delta^{18}\text{O}$ of the glacial deep ocean. *Science* 298: 1769–1773.
- Adkins JF, Boyle EA, Keigwin L, Cortijo E. 1997. Variability of the North Atlantic thermohaline circulation during the last interglacial period. *Nature* 390: 154–156.
- Ahn J, Brook EJ. 2008. Atmospheric CO_2 and climate on millennial time scales during the last glacial period. *Science* 322: 83-85.
- Ahn J, Brook EJ. 2007. Atmospheric CO_2 and climate from 65 to 30 ka B.P. *Geophysical Research Letters* 34: L10703. doi.10.1029/2007GL029551.
- Alley BA, Andrews JT, Brigham-Grette J, Clarke GKC, Cuffey KM, Fitzpatrick JJ, Funder S, Marshall SJ, Miller GH, Mitrovic JX, Muhs DR, Otto-Bliesner BL, Polyak I, White JWC. 2010. History of the Greenland Ice Sheet: paleoclimatic insights. *Quaternary Science Reviews* 29: 1728-1756.
- Alley BR. 2000. *Ice-core evidence of abrupt climate changes*. Proceedings of the National Academy of Sciences of the United States of America, vol 97, pp. 1331–1334.
- Alley RB. 2003. Raising Paleooceanography. *Paleoceanography* 18: 1085.
- Alley RB, Clark PU. 1999. The deglaciation of the northern hemisphere: a global perspective. *Annual Review of Global and Planetary Sciences* 27: 149–1182.
- Alley RB, Anandakrishnan S, Jung P. 2001. Stochastic resonance in the North Atlantic. *Paleoceanography* 16: 190-198.
- Alley RBS, Anandakrishnan S, Jung P, Clough A. 2001b. Stochastic resonance in the North Atlantic: Further insights In Seidov D, Maslin M, Haupt BJ (Eds) *The Oceans and Rapid Climate Change: Past, Present and Future, Geophysical Monograph Series* vol. 126. AGU, Washington D.C. p 57-68
- Alley RB, Clark PU, Keigwin LD, Webb RS. 1999. Making sense of millennial-scale change. In Clark PU, Webb RS, Keigwin LD (Eds) *Mechanisms of Global Climate Change at Millennial Time Scales*. American Geophysical Union, Geophysical Monograph 112: 385-394. Washington DC.
- Alley RB, Gow AJ, Johnsen SJ, Kipfstuhl J, Meese DA, Thorsteinsson TH. 1995. Comparison of deep ice cores. *Nature* 373: 393–394.
- Alvarez Zarikian CA, Stepanova AY, Gruñtznern J. 2009. Glacial–interglacial variability in deep sea ostracod assemblage composition at IODP Site U1 314 in the subpolar North Atlantic. *Marine Geology* 258: 69–87.
- Andersen KK, Svensson A, Johnsen SJ, Rasmussen SO, Bigler M, Röthlisberger R, Ruth R, Siggaard-Andersen M-L, Steffensen JP, Dahl-Jensen D, Vinther BM, Clausen HB. 2006. The Greenland Ice Core Chronology 2005, 15–42 ka. Part 1: Constructing the time- scale. *Quaternary Science Reviews* 25: 3246–3257.
- Andrews IJ, Long D, Richards PC, Thomson AR, Brown S, Chesher JA, McCormac M. 1990. *United Kingdom Offshore Regional Report: the Geology of the Moray Firth*. HMSO for the British Geological Survey, London.
- Andrews JE, Portman C, Rowe PJ, Leeder MR, Kramers JD. 2007. Suborbital sea-level change in early MIS 5e: new evidence from the Gulf of Corinth, Greece. *Earth and Planetary Science Letters* 259: 457– 468.
- Andrews JT. 2000. Icebergs and iceberg rafted debris (IRD) in the North Atlantic: facts and assumptions. *Oceanography* 13: 100-108.

- Andrews JT. 1988. Abrupt changes (Heinrich events) in Late Quaternary North Atlantic marine environments: a history and review of data and concepts. *Journal of Quaternary Science* 13: 3–16.
- Andrews JT, Tedesco K. 1992. Detrital carbonate-rich sediments, northwestern Labrador Sea: implications for ice-sheet dynamics and iceberg rafting (Heinrich) events in the North Atlantic. *Geology* 20: 1087–1090.
- Andrews JT, Jennings AE, Kerwin M, Kirby M, Manley W, Miller GH, Bond G, Maclean B. 1995. A Heinrich-like event, H-0 (DC-0) - source(s) for detrital carbonate in the North-Atlantic during the Younger Dryas chronozone. *Paleoceanography* 10: 943-952.
- Andrews JT, Erlenkeuser H, Tedesco K, Aksu AE, Jull AJT. 1994a. Late Quaternary (Stage-2 And Stage-3) Meltwater and Heinrich Events, Northwest Labrador Sea. *Quaternary Research* 41: 26-34.
- Andrews JT, Tedesco K, Briggs WM, Evans LW. 1994b. Sediments, Sedimentation-Rates, and Environments, Southeast Baffin Shelf and Northwest Labrador Sea, 8-26 Ka *Canadian Journal of Earth Science* 31: 90-103.
- Andrews JT, Barry RG, Drapier L. 1970. An inventory of the present and past glacierization of Home Bay and Okoa Bay, east Baffin Island, NWT, Canada, and some climatic and paleoclimatic considerations. *Journal of Glaciology* 9: 337-362.
- Armishaw JE, Holmes RW, Stow DA. 2000. The Barra Fan: a bottom- current reworked, glacially-fed submarine fan system. *Marine and Petroleum Geology* 17: 219–238.
- Arz HW, Lamy F, Ganopolski A, Nowaczyk N, Pätzold J. 2007. Dominant Northern Hemisphere climate control over millennial- scale glacial sea-level variability. *Quaternary Science Reviews* 26: 312–321.
- Ascough PL, Cook GT, Dugmore AJ, Scott EM. 2007. The North Atlantic marine reservoir effect in the Early Holocene: Implication for defining and understanding MRE values. *Nuclear Instruments and Methods in Physics Research B* 259: 438-447.
- Atkinson TC, Briffa KR, Coope GR. 1987. Seasonal temperatures in Britain during the past 22,000 years, reconstructed using beetle remains. *Nature* 365: 587-592.
- Auffret G, Zaragosi S, Dennielou B, Cortijo E, van Rooij D, Grousset F, Pujol C, Eynaud F, Seigert M. 2002. Terrigenous fluxes at the Celtic margin during the last glacial cycle. *Marine Geology* 188: 79–108.
- Austin WEN. 1994. Disturbed foraminiferal stratigraphies – a cautionary “tail” *Cushman Foundation Special Publication* 32: 155-159.
- Austin WEN, Abbott PM. 2010. Comment: Where last glacial climate event simultaneous between Greenland and France? A quantitative comparison using non-tuned chronologies. *Journal of Quaternary Science* doi 10.1002/jqs.1366.
- Austin WEN, Kroon D. 2001. Deep sea ventilation of the northeastern Atlantic during the last 15,000 years. *Global and Planetary Change* 30: 13–31.
- Austin WEN, Kroon D. 1996. Late glacial sedimentology, foraminifera and stable isotope stratigraphy of the Hebridean Continental Shelf, northwest Scotland. *Geological Society Special Publication Issue* 111: 187-213.
- Austin WEN, Wilson LJ, Hunt JB. 2004. The age and chronostratigraphic significance of North Atlantic Ash Zone II. *Journal of Quaternary Science* 19: 1 37–146.

- Austin WEN, Bard E, Hunt JB, Kroon D, Peacock JD. 1995. The ^{14}C age of the Icelandic Vedde Ash – Implications for Younger Dryas marine reservoir age corrections. *Radiocarbon* 37: 53-62.
- Ayalon A, Bar-Matthews M, Kaufman A. 2002. Climatic conditions during marine oxygen isotope stage 6 in the eastern Mediterranean region from the isotopic composition of speleothems of Soreq Cave, Israel. *Geology* 30: 303-306.
- Balbon E. 2000. Variabilité Climatique et Circulation Thermohaline dans l’Océan Atlantique Nord et en Mer Norwege au cours du Quaternaire Supérieur. PhD Thesis, University of Paris.
- Ballantyne CK. 2010. Extent and deglacial history of the last British-Irish Ice Sheet: implications of exposure dating using cosmogenic isotopes. *Journal of Quaternary Science* 25: 515-534 doi: 10.1002/jqs.1310.
- Ballantyne CK. 2007. Loch Lomond Stadial glaciers in North Harris, Outer Hebrides, North-West Scotland: glacier reconstruction and palaeoclimatic implications. *Journal of Quaternary Science* 26: 3134–3149.
- Ballantyne CK. 2006. Loch Lomond Stadial Glaciers in the Uig Hills, Western Lewis, Scotland. *Scottish Geographical Journal* 122: 256– 273.
- Ballantyne CK. 2002. The Loch Lomond Readvance on the Isle of Mull, Scotland: glacier reconstruction and palaeoclimate implications. *Journal of Quaternary Science* 4: 95-108.
- Ballantyne CK. 1989. The Loch Lomond Readvance on the Isle of Skye, Scotland: glacier reconstruction and palaeoclimatic implications. *Journal of Quaternary Science* 4: 95–108.
- Ballantyne CK, Harris C. 1994. *The Periglaciation of Great Britain*. Cambridge University Press: Cambridge, UK.
- Ballantyne CK, Schnabel C, Xu S. 2009b. Readvance of the last British-Irish Ice Sheet during Greenland Interstage 1 (GI-1): the Wester Ross Readvance, NW Scotland. *Quaternary Science Reviews* 28: 783-789.
- Ballantyne CK, Stone JO, McCarroll D. 2008. Dimensions and chronology of the last ice sheet in western Ireland. *Quaternary Science Reviews* 27: 185–200.
- Ballantyne CK, McCarroll D, Stone JO. 2007. The Donegal ice dome, NW Ireland: dimensions and chronology. *Journal of Quaternary Science* 22: 773–783.
- Bamber JL, Vaughan DG, Joughin I. 2000. Widespread complex flow in the interior of the Antarctic ice sheet. *Science* 287: 1248-1250.
- Barber DC, Dyke A, Hillaire-Marcel C, Jennings AE, Andrews JT, Kerwin MW, Bilodeau G, McNeely R, Southon J, Morehead MD, Gagnon JM . 1994. Forcing of the cold event of 8,200 years ago by catastrophic drainage of Laurentide lakes. *Nature* 400: 344-348.
- Bard E, Ménot-Combes G, Rostek F. 2004a. Present status of radiocarbon calibration and comparison records based on Polynesian corals and Iberian Margin sediments. *Radiocarbon* 46(3):1189–1202.
- Bard E, Rostek F, Ménot-Combes G. 2004b. A better radiocarbon clock. *Science* 303(5655):178–179.
- Bard E, Rostek F, Ménot-Combes G. 2004c. Radiocarbon calibration beyond 20,000 ^{14}C yr B.P. by means of planktonic foraminifera of the Iberian Margin. *Quaternary Research* 61(2):204–214.
- Bard E, Delaygue G, Rostek F, Antonioli F, Silenzi S, Shrag DP. 2002. Hydrological conditions over the western Mediterranean basin during the deposition of the cold Sapropel 6 (ca. 175 kyr B.P.). *Earth and Planetary Science Letters* 202: 481-494.

- Bard E, Arnold M, Hamelin B, Tisnerat-Laborde N, Cabioch G. 1998. Radiocarbon calibration by means of mass spectrometric $^{230}\text{Th}/^{234}\text{U}$ and ^{14}C ages of corals: an updated database including samples from Barbados, Mururoa and Tahiti. *Radiocarbon* 40(3):1085–1092.
- Bard E, Hamelin B, Fairbanks RG, Zindler A. 1990. Calibration of the ^{14}C timescale over the past 30,000 years using mass spectrometric U-Th ages from Barbados corals. *Nature* 345(6274):405–410.
- Bard E, Hamelin B, Fairbanks RG. 1990. U–Th ages obtained by mass spectrometry in corals from Barbados: sea level during the past 130,000 years. *Nature* 346: 456–458.
- Bard E, Arnold M, Duprat J, Moyes J, Duplessy JC. 1987. Reconstruction of the last deglaciation: deconvolved records of $\delta^{18}\text{O}$ profiles, micropaleontological variations and accelerator mass spectrometric ^{14}C dating. *Climate Dynamics* 1: 101-112.
- Barker S, Elderfield H. 2002. Foraminiferal calcification response to glacial-interglacial changes in atmospheric CO_2 . *Science* 297: 833-836.
- Barker S, Diz P, Vautravers MJ, Pike J, Knorr G, Hall IR, Broecker WS. 2009. Interhemispheric Atlantic seesaw response during the last glaciation. *Nature* 457: 1097-1103
- Barker S, Cacho I, Benway H, Tachikawa K. 2005. Planktonic foraminiferal Mg/Ca as a proxy for past oceanic temperatures: A methodological overview and data compilation for the Last Glacial Maximum. *Quaternary Science Reviews* 24: 821-834.
- Barker S, Greaves M, Elderfield H. 2003. A study of cleaning procedures used for foraminiferal Mg/Ca paleothermometry. *Geochemistry, Geophysics, Geosystems* 4(9): 8407 doi: 10.1029/2003GC000559.
- Bassett SE, Milne GA, Mitrovica JX, Clark PU. 2005. Ice sheet and solid Earth influences on far-field sea level histories. *Science* 309: 925-928.
- Bateman MD, Catt JA. 1996. An absolute chronology for the raised beach and associated deposits at Sewerby, East Yorkshire, England. *Journal of Quaternary Science* 11: 389-395.
- Bauch HA, Erlenkeuser H. 2008. A “critical” climatic evaluation of last interglacial (MIS 5e) records from the Norwegian Sea. *Polar Research* 27: 135–151.
- Bauch HA, Kandiano ES. 2007. Evidence for early warming and cooling in North Atlantic surface waters during the last interglacial. *Paleoceanography* 22, PA1201, doi: 10.1029/2005PA001252.
- Bauch HA, Erlenkeuser H, Jung SJA, Thiede J. 2000. Surface and deep water changes in the subpolar North Atlantic during Termination II and the last interglaciation. *Paleoceanography* 15: 76–84.
- Bauch HA, Erlenkeuser H, Fahl K, Spielhagen RF, Weinelt MS, Andruleit H, Henrich R. 1999. Evidence for a steeper Eemian than Holocene sea surface temperature gradient between Arctic and sub-Arctic regions. *Palaeogeography, Palaeoclimatology, Palaeoecology* 145: 95–117.
- Bauch D, Carstens J, Wefer G. 1997. Oxygen isotope composition of living *Neogloboquadrina pachyderma* (sin.) in the Arctic Ocean. *Earth and Planetary Science Letters* 146: 47-58, doi:10.1016/S0012-821X(96)00211-7.
- Bedford A, Jones RT, Lang B, Brooks S, Marshall JD. 2004. A Lateglacial chironomid record from Hawes Water, northwest England. *Journal of Quaternary Science* 19: 281–290.
- Bé AW. 1980. Gametogenic Calcification in a Spinose Planktonic Foraminifer, *Globigerinoides-Sacculifer* (Brady) *Marine Micropaleontology* 5: 283-310.
- Bé AW. 1977. Forams. *Science* 198:

- Bé AW, Tolderlund DS. 1971. Seasonal Distribution of Planktonic Foraminifera in the Western North Atlantic. In Funnel BM, Riedel WR (Eds) *The Micropaleontology of the Oceans*. Cambridge Univ. Press, Cambridge, pp 105–149.
- Bennett MR. 1994. Morphological evidence as a guide to deglaciation following the Loch Lomond Readvance – A review of Research Approaches and Models. *Scottish Geographical Magazine* 110: 24–32.
- Bemis EB, Spero HJ, Bijma J, Lea DW. 1998. Reevaluation of the oxygen isotopic composition of planktonic foraminifera: Experimental results and revised paleotemperature equation. *Paleoceanography* 13: 150–160, doi:10.1029/98PA00070.
- Benn DI, Lowe JJ, Walker MJC. 1992. Glacier response to climatic change during the Loch Lomond Stadial and early Flandrian: geomorphological and palynological evidence from the Isle of Skye, Scotland. *Journal of Quaternary Science* 7: 125–144.
- Berger AL. 1978. Long term variations of daily insolation and Quaternary climatic changes. *Journal of Atmospheric Science* 35: 2362–2367.
- Berger A, Loutre MF. 1991. Insolation values for the climate of the last 10000000 years. *Quaternary Science Reviews* 10: 297–317.
- Berger A, Galleé H, Li XS, Dutrieux A, Loutre MF. 1996. Ice sheet growth and high-latitude sea-surface temperature. *Climate Dynamics* 12: 441–448.
- Bertram CJ, Elderfield H, Shackleton NJ, MacDonald JA. 1995. Cadmium/calcium and carbon isotope reconstructions of the glacial northeast Atlantic Ocean. *Paleoceanography* 10: 563–578
- Bentley CR, Giovinetto MB. 1991. Mass balance of Antarctica and sea level change. In Weller G, Wilson CL, Sevberin BAB. (Eds) *International Conference on the Role of the Polar Regions in Global Change: Proceedings of a conference held June 11–15, 1990 at the University of Alaska, Fairbanks*. Vol III. Geophysical Institute/Centre for Global Change and Arctic Systems Research, Fairbanks. pp 481–488.
- Bianchi GG, Vautravers M, Shackleton NJ. 2001. Deep flow variability under apparently stable North Atlantic Deep Water production during the last interglacial of the subtropical NW Atlantic. *Paleoceanography* 16: 306–316.
- Bianchi GG, McCave IN. 1999. Holocene periodicity in North Atlantic climate and deep ocean flow south of Iceland. *Nature* 365: 143–147.
- Bigg GR, Wadley MR, Stevens DP, Johnson JA. 1997. Modelling the dynamics and thermodynamics of icebergs. *Cold Regions Science and Technology* 26: 113–135.
- Bigg GR, Wadley MR, Stevens DP, Johnson JA. 1996. Prediction of iceberg trajectories for the North Atlantic and Arctic Oceans. *Geophysical Research Letters* 23: 3587–3590.
- Bijma J, Spero HJ, Lea DW. 1999. Reassessing Foraminiferal Stable Isotope Geochemistry: Impact of the Oceanic Carbonate System (Experimental Results). In Fischer G, Weffer G. (Eds). *Use of proxies in paleoceanography: examples from the South Atlantic*. Springer, Berlin.
- Birks HH, Gulliksen S, Hafliðason H, Mangerud J, Possnert G. 1996. New Radiocarbon Dates for the Vedde Ash and the Saksunarvatn Ash from Western Norway. *Quaternary Research* 45: 119–127.
- Björck S, Walker MJC, Cwynar L, Johnsen SJ, Knudsen KL, Lowe JJ, Wohlfarth B, INTIMATE members. 1998. An event stratigraphy for the Last Termination in the North Atlantic region based upon the Greenland Ice Core record: a proposal by the INTIMATE group. *Journal of Quaternary Science* 13: 283–292.

- Blaauw M, Wohlfarth B, Christen JA, Ample L, Veres D, Hughen KA, Preusser F, Svensson A. 2010. Were last glacial climate events simultaneous between Greenland and France? A quantitative comparison using non-tuned chronologies. *Journal of Quaternary Science* 25(3): 387-394.
- Blanchon P, Eisenhauer A, Fietzke J, Liebetrau V. 2009. Rapid sea-level rise and reef back-stepping at the close of the last interglacial highstand. *Nature* 458: 881-885.
- Blockley S, Lowe JJ, Walker MJC, Asioli A, Trincardi F, Coope GR, Donahue RE, Pollard AM. 2004. Bayesian analysis of radiocarbon chronologies: examples from the European Lateglacial. *Journal of Quaternary Science* 19:159-175.
- Blomqvist S 1985. Reliability of core sampling of soft bottom sediment - an *in situ* study. *Sedimentology* 32: 605-612.
- Blunier T, Brook EJ. 2001. Timing of millennial-scale climate change in Antarctic and Greenland during the last glacial period. *Science* 291: 109-112.
- Blunier T, Spahni R, Barnola JM, Chappellaz J, Loulergue L, Schwander J. 2007. Synchronisation of ice core records via atmospheric gases. *Climate of the Past* 3: 325-330.
- Blunier T, Chappellaz J, Schwander J, Dällenbach A, Stauffer B, Stocker TF, Raynaud D, Jouzel J, Clausen HB, Hammer CU, Johnsen SJ. 1998. Asynchrony of Antarctic and Greenland climate change during the last glacial period. *Nature* 394: 739-743.
- Bond G, Lotti R. 1995. Iceberg discharges into the North Atlantic on millennial time scales during the last glaciation. *Science* 267: 1005-1010.
- Bond G, Kromer B, Beer J, Muscheler R, Evans MN, Showers W, Hoffmann S, Lotti-Bond R, Hajdas I, Bonani G. 2001. Persistent solar influence on North Atlantic climate during the Holocene. *Science* 294: 2130-2136.
- Bond G, Showers W, Cheseby M, Lotti R, Almasi P, deMenocal P, Priore P, Cullen H, Hajdas I, Bonani G. 1997a. A pervasive millennial-scale cycle in North Atlantic Holocene and glacial climates. *Science* 278: 1257-1266.
- Bond G, Showers W, Elliot M, Evans M, Lotti R, Hajdas I, Bonani G, Johnson S. 1997b. The North Atlantic's 1-2 kyr climate rhythm: relation to Heinrich events, Dansgaard/Oeschger cycle and the Little Ice Age. In *Mechanisms of Global Climate Change at Millennial Time Scales*, Clark P, Webb R, Keigwin L (eds). Geophysical Monograph Series 112. American Geophysical Union: Washington, DC; 35-58.
- Bond G, Broecker W, Johnsen S, McManus J, Labeyrie L, Jouzel J, Bonani G. 1993. Correlations between climate records from North Atlantic sediments and Greenland ice. *Nature* 365: 143-147.
- Bond G, Heinrich H, Broecker W, Labeyrie L, McManus J, Andrews J, Huon S, Jantschik R, Clasen S, Simet C, Tedesco K, Klas M, Bonani G, Ivy S. 1992. Evidence for massive discharges of icebergs into the North Atlantic ocean during the last glacial period. *Nature* 360: 245-249.
- Bos JAA, Dickson JH, Coope GR, Jardine WG. 2004. Flora, fauna and climate during the Weichselian Middle Pleniglacial: palynological, macrofossil and coleopteran investigations. *Palaeogeography, Palaeoclimatology, Palaeoecology* 204: 65-100.
- Boulton GS. 1990. Sedimentary and sea level changes during glacial cycles and their control on glaciomarine facies architecture. In *Glaciomarine Environments: Processes and Sediments*, Dowdeswell JA, Scourse JD (Eds). Special Publication 53. Geological Society: London; 15-52.
- Boulton G, Hagdorn M. 2006. Glaciology of the British Isles Ice Sheet during the last glacial cycle: form, flow, streams and lobes. *Quaternary Science Reviews* 25: 3359-3390.

- Boulton GS, Peacock JD, Sutherland DG. 1991. Quaternary. In *Geology of Scotland*, (4th edition), Craig GY (ed.). Geological Society: London; 503–543.
- Bouma AH, Boerma JAK 1968. Vertical disturbances in piston cores. *Marine Geology* 6: 231-241.
- Bowen DQ, Philips FM, McCabe AM, Knutz PC, Sykes GA. 2002. New data for the Last Glacial Maximum in Great Britain and Ireland. *Quaternary Science Reviews* 21: 89–101.
- Boyle EA, Keigwin L. 1987. North Atlantic thermohaline circulation during the last 20,000 years linked to high-latitude surface temperature. *Nature* 330: 35-40.
- Bradwell T, Stoker MS, Golledge NR, Wilson CK, Merritt JW, Long D, Everest JD, Hestvik OB, Stevenson AG, Hubbard AL, Finlayson AG, Mathers HE. 2008. The northern sector of the last British Ice Sheet: maximum extent and demise. *Earth Science Reviews* 88: 207– 226.
- Bradwell T, Fabel D, Stoker M, Mathers H, McHargue L, Howe J. 2008a. Ice caps existed throughout the Lateglacial Interstadial in northern Scotland. *Journal of Quaternary Science* 23: 401–407.
- Bradwell T, Stoker M, Larter R. 2007. Geomorphological signature and flow dynamics of the Minch palaeo-ice stream, northwest Scotland. *Journal of Quaternary Science* 22: 609–617.
- Braun H, Ditlevsen PD, Kurths J, Mudlesee M. 2010. Limitations in red noise in analysing Dansgaard-Oeschger events. *Climate of the Past* 6: 85-92.
- Braun H, Christl M, Rahmstorf S, Ganopolski A, Mangini A, Kubatzki C, Roth K, Kromer B. 2005. Possible solar origin of the 1,470-year glacial climate cycle demonstrated in a coupled model. *Nature* 438: 208-211.
- Briant B. 2002. The Quaternary of east Yorkshire and north Lincolnshire. Report on QRA Short Field Meeting, 13-16th September 2001. *Quaternary Newsletter* 96: 38-42.
- Broecker WS. 2006. Was the Younger Dryas Triggered by Flood? *Science* 312: 1146-1148.
- Broecker WS. 2006b. Abrupt climate change revisited. *Global and Planetary Change* 54: 211–215.
- Broecker WS. 2003. Does the trigger for abrupt climate change reside in the ocean or the atmosphere? *Science* 300: 1519-1522.
- Broecker WS. 2000. Abrupt climate change: causal constraints provided by the paleoclimate record. *Earth-Science Reviews* 51: 137-154.
- Broecker W. 1999. Climate change prediction. *Science* 283: 179.
- Broecker WS. 1994. Massive iceberg discharges as triggers for global climate change. *Nature* 368: 421.
- Broecker WS. 1991. The Great Oceanic Conveyor. *Oceanography* 4: 79-89.
- Broecker WS, Henderson GM. 1998. The sequence of events surrounding termination II and their implications for the cause of glacial-interglacial CO₂ changes. *Paleoceanography* 13: 352-364.
- Broecker WS, Denton GH. 1989. The role of ocean-atmosphere reorganisation in glacial cycles. *Geochimica Cosmochimica Acta* 53: 2465-2500.
- Broecker WS, van Donk JV. 1970. Insolation changes, ice volumes and the ¹⁸O record in deep-sea cores. *Review of Geophysics* 8: 169-198.
- Broecker WS, Bond G, Klas M, Clark E, McManus J. 1992. Origin of the northern Atlantic's Heinrich events. *Climate Dynamics* 6: 265–273.

- Broecker W, Bond G, McManus J. 1992. Heinrich events: triggers of ocean circulation change? *Global Environmental Change* 12: 161–166.
- Broecker WS, Bond G, Klas M. 1990. A salt oscillator in the North Atlantic?: 1, The concept. *Paleoceanography* 5: 469-477.
- Broecker WS, Kennett JP, Flower BP, Teller JT, Trumbore S, Bonani G, Woli W. 1989. Routing of meltwater from the Laurentide Ice-Sheet during the Younger Dryas cold episode. *Nature* 341: 318–321.
- Broecker WS, Peteet DM, Rind D. 1985. Does the ocean-atmosphere system have more than one stable mode of operation? *Nature* 315:21–26.
- Bronk Ramsey C. 2009. Bayesian analysis of radiocarbon dates. *Radiocarbon* 51: 337-360.
- Bronk Ramsey C. 2008. Deposition models for chronological records. *Quaternary Science Reviews* 27: 42-60.
- Bronk Ramsey C. 2001. Development of the radiocarbon calibration program. *Radiocarbon* 43: 355-363.
- Bronk Ramsey C. 1995. Radiocarbon calibration and analysis of stratigraphy: the OxCal program. *Radiocarbon* 37: 425-430.
- Brook EJ, Harder S, Severinghaus J, Steig EJ, Sucher CM. 2000. On the origin and timing of rapid changes in atmospheric methane during the last glacial period. *Global Biogeochemical Cycles* 14: 559–572.
- Brooks SJ, Birks HJB. 2000. Chironomid-inferred Late-glacial air temperatures at Whitrig Bog, southeast Scotland. *Journal of Quaternary Science* 15: 759-764.
- Brown EJ, Rose J, Coope R, Lowe JJ. 2007. An MIS 3 age organic deposit from Balglass Burn, central Scotland: palaeoenvironmental significance and implications for the timing of the onset of the LGM ice sheet in the vicinity of the British Isles. *Journal of Quaternary Science* 22: 295–308.
- Brown L, Cook G T, Mackenzie AB, Naysmith P, Anderson R, Thomson J, Nixon S. 2000. Characterisation of differential mixing of foraminifera and bulk carbonate in NE Atlantic sediments *Nuclear Instruments and Methods in Physics Research B* 172: 490-494.
- Browne MAE, McMillan AA. 1989. Quaternary Geology of the Clyde Valley. British Geological Survey Research Report SA/89/1.
- Buck CE, Kenworthy JB, Litton CD, Smith AFM. 1991. Combining archaeological and radiocarbon information: a Bayesian approach to calibration. *Antiquity* 65: 808-821.
- Buckley DE, MacKinnon WG, Cranston RE, Christian HA 1994. Problems with piston core sampling: Mechanical and geochemical diagnosis. *Marine Geology* 117: 95-106.
- Burr GS, Galang C, Taylor FW, Gallup CD, Edwards RL, Cutler KB, Quirk B. 2004. Radiocarbon results from a 13-kyr BP coral from the Huon Peninsula, Papua New Guinea. *Radiocarbon* 46(3):1211–1224.
- Burr GS, Beck JW, Taylor FW, Récy J, Edwards RL, Cabioch G, Corrège T, Donahue DJ, O'Malley JM. 1998. A high-resolution radiocarbon calibration between 11,700 and 12,400 calendar years BP derived from ²³⁰Th ages of corals from Espiritu Santo Island, Vanuatu. *Radiocarbon* 40(3):1093–1105.

- Burns S, Maslin MA. 1999. Composition and circulation of bottom water in the Western Atlantic Ocean during the last glacial based upon pore water analyses from the Amazon Fan. *Geology* 27: 1011-1014.
- Busschers FS, van Balen RT, Cohen KM, Kasse C, Weerts HJT, Wallinga J, Bunnik FPM. 2008. Response of the Rhine-Meuse fluvial system to Saalian ice-sheet dynamics. *Boreas* 37: 377-398.
- Caillon N, Jouzel J, Severinghaus JP, Chappellaz J, Blunier T. 2003. A novel method to study the phase relationship between Antarctic and Greenland climates. *Geophysical Research Letters* 30(17): doi: 10.1029/2003GL017838.
- Calov R, Ganopolski A, Claussen M, Petoukhov V, Greve R. 2005a. Transient simulation of the last glacial inception. Part I: Glacial inception as a bifurcation in the climate system. *Climate Dynamics* 24: 545–561.
- Calov R, Ganopolski A, Claussen M, Petoukhov V, Greve R. 2005b. Transient simulation of last glacial inception. Part II: Sensitivity and feedback analysis. *Climate Dynamics* 24: 562–576.
- Cameron TDJ, Crosby A, Balson PS, Jeffrey DH, Lott JK, Bulat J, Harrison DJ. 1992. *The Geology of the Southern North Sea*. United Kingdom Offshore Regional Report, British Geological Survey. HMSO, London.
- Cameron TDJ, Stoker MS, Long D. 1987. The history of Quaternary sedimentation in the UK sector of the North Sea Basin. *Journal of the Geological Society of London* 144: 43–58.
- Cane MA, Braconnot P, Clement A, Gildor H, Joussaume S, Kageyama M, Khodri M, Paillard D, Tett S, Zorita E. 2006. Progress in paleoclimate modelling. *Journal of Climate* 19: 5031–5057.
- Cannariato KG, Kennett JP. 2005. Structure of the penultimate deglaciation along the California margin and implications for Milankovitch theory. *Geology* 33: 157-160
- Caputo R. 2007. Sea-level curves: Perplexities of an end-user in morphotectonic applications. *Global and Planetary Change* 57: 417-423.
- Carlson AE. 2008. Why there was not a Younger Dryas-like event during the Penultimate Deglaciation. *Quaternary Science Reviews* 27: 882-887.
- Carr SJ. 2004. The North Sea Basin. In *Quaternary Glaciations - Extent and Chronology*, Ehlers J, Gibbard PL (eds). Elsevier; 261–270.
- Carr SJ. 1998. *The last glaciation of the North Sea Basin*. PhD thesis, University of London.
- Carr SJ, Holmes R, van der Meer JJM, Rose J. 2006. The Last Glacial Maximum in the North Sea Basin: micromorphological evidence of extensive glaciation. *Journal of Quaternary Science* 21: 131– 153.
- Carstens J, Hebbeln D, Wefer G. 1997. Distribution of planktic foraminifera at the ice margin in the Arctic (Fram Strait). *Marine Micropaleontology* 29: 257-269.
- Catt JA. 2007. The Pleistocene glaciations of eastern Yorkshire: a review. *Proceedings of the Yorkshire Geological Society* 56: 177-207.
- Catt JA, Penny LF. 1966. The Pleistocene deposits of Holderness, East Yorkshire. *Proceedings of the Yorkshire Geological Society* 35: 375-420.
- Channell JET, Raymo ME. 2003. Paleomagnetic record at ODP 980 (Feni Drift, Rockall) for the past 1.2 Myrs. *Geochemistry, Geophysics, Geosystems* 4: 1033 doi: 13.1029/2002GC000440.
- Channell JET, Xuan C, Hodell DA. 2009. Stacking paleointensity and oxygen isotope data for the last 1.5 Myr (PISO-1500). *Earth and Planetary Science Letters* 283: 14-23.

- Channell JET, Hodell DA, Xuan C, Mazaud A, Stoner JS. 2008. Age calibrated relative paleointensity for the last 1.5 Myr at IODP Site U1308 (North Atlantic). *Earth and Planetary Science Letters* 274: 59-71.
- Channell JET, Hodell DA, Lehman B. 1997. Relative geomagnetic paleointensity and $\delta^{18}\text{O}$ at ODP Site 983 (Gardar Drift, North Atlantic) since 350 ka. *Earth and Planetary Science Letters* 153: 103–118.
- Chapman MR. 2010. Seasonal production patterns of planktonic foraminifera in the NE Atlantic Ocean: Implications for paleotemperature and hydrographic reconstructions. *Paleoceanography* 25: PA1101, doi: 10.1029/2008PA001708.
- Chapman MR, Shackleton NJ. 1999. Global ice-volume fluctuations, North Atlantic ice-rafting events and deep-ocean circulation changes between 130 and 70 ka. *Geology* 27: 795-798.
- Chapman MR, Shackleton NJ. 1998. Millennial-scale fluctuations in North Atlantic heat flux during the last 150,000 years. *Earth and Planetary Science Letters* 159: 57-70.
- Chapman MR, Shackleton, NJ, Duplessey JC. 2000. Sea surface temperature variability during the last glacial-interglacial cycle: assessing the magnitude and pattern of climatic change in the North Atlantic. *Palaeogeography, Palaeoclimatology, Palaeoecology* 157: 1-25.
- Chappell J, Shackleton NJ. 1986. Oxygen isotopes and sea level. *Nature* 324: 137-140.
- Chappellaz J, Brook E, Blunier T, Malaize B. 1997. CH_4 and $\delta^{18}\text{O}$ of O_2 records from Greenland ice: a clue for stratigraphic disturbance in the bottom part of the Greenland Ice Core Project and the Greenland Ice Sheet Project 2 ice-cores. *Journal of Geophysical Research* 102(C12): 26547–26557.
- Charlesworth JK. 1957. *The Quaternary Era*. Arnold: London.
- Charlesworth JK. 1929. The South Wales end moraine. *Quarterly Journal of the Geological Society of London* 85: 335–358.
- Charlesworth JK. 1928. The glacial retreat from central and southern Ireland. *Quarterly Journal of the Geological Society of London* 84: 293–344.
- Cheddadi R, Mamkova K, Guiot J, de Beaulieu JL, Reille M, Andrieu V, Granoszewski W, Peyron O. 1997. Was the climate of the Eemian stable? A quantitative climate reconstruction from seven European pollen records. *Palaeogeography, Palaeoclimatology, Palaeoecology* 143: 73-85.
- Chiverrell RC, Thomas GSP. 2010. Extent and timing of the Last Glacial Maximum (LGM) in Britain and Ireland: a review. *Journal of Quaternary Science* 25: 535-549.
- Christen JA, Claymo RS, Litton CD. 1995. A Bayesian approach to the use of ^{14}C dates in the estimation of the age of peat. *Radiocarbon* 37: 431-441.
- Clapperton CM. 1997. Greenland ice cores and North Atlantic sediments: implications for the last glaciation in Scotland. In Gordon JE (Ed) *Reflections on the Ice Age in Scotland: An Update on Quaternary Studies*. Scottish Association of Geography Teachers and Scottish Natural Heritage, Edinburgh
- Clark CD, Evans DJA, Khatwa A, Bradwell T, Jordan CJ, Marsh SH, Mitchell WA, Bateman MD. 2004. BRITICE: map and GIS database of landforms and features related to the last British Ice Sheet. *Boreas* 33: 359–375.

- Clark CD, Gibbard PL, Rose J. 2004b. Pleistocene glacial limits in England, Scotland and Wales. In Ehlers and Gibbard (Eds) *Quaternary Glaciations – Extent and Chronology Part I: Europe*. Elsevier, London.
- Clark PU. 1987. Subglacial sediment dispersal and till composition. *Journal of Geology* 95: 527-541.
- Clark PU, Mix AC. 2002. Ice sheets and sea level of the Last Glacial Period. *Quaternary Science Reviews* 21: 1-8.
- Clark PU, Pisias NG, Stocker TF, Weaver AJ. 2002a. The role of the thermohaline circulation in abrupt climate change. *Nature* 415: 863–869.
- Clark PU, Mitrovica JX, Milne GA, Tamisiea ME. 2002b. Sea-level fingerprinting as a direct test for the source of global meltwater 1A. *Science* 295: 2438-2441.
- Clark PU, Alley RB, Keigwin LD, Licciardi JM, Johnson SJ, Wang H. 1996. Origin of the first global meltwater pulse following the Last Glacial Maximum. *Paleoceanography* 11: 563-577.
- Clarke GKC, Marshall SJ, Hilliare-Marcel C, Bilodeau G, Veiga-Pires C. 1999. A glaciological perspective on Heinrich events. In *Mechanisms of Global Climate Change at Millennial Time Scales*, Clark PU, Webb RS, Keigwin LD (eds) Geophysical Monograph, Vol. 112 AGU: Washington, DC; 243–262.
- Cleroux C, Cortijo E, Anand P, Labeyrie L, Bassinot F, Caillon N, Duplessy JC. 2008. Mg/Ca and Sr/Ca ratios in planktonic foraminifera: Proxies for upper water column temperature reconstruction. *Paleoceanography* 23: PA3214 doi: 10.1029/2007PA001505.
- CLIMAP Project. 1981. Seasonal reconstructions of the Earth's surface at the last glacial maximum. Technical Report MC-36, Geological Society of America.
- CLIMAP Project Members. 1976. The surface of the ice-age Earth. *Science* 191: 1131–1137.
- Coope GR, Lemdahl G, Lowe JJ, Walkling A. 1998. Temperature Gradients in Northern Europe during the Last Glacial-Interglacial Transition (14-9 ¹⁴C ka BP) interpreted from Coleopteran Assemblages. *Journal of Quaternary Science* 13: 419–433.
- Cortijo E, Lehman S, Keigwin L, Chapman M, Palliard D, Labeyrie L. 1999. Changes in the meridional temperature and salinity gradients in the North Atlantic Ocean (30 °-72°) during the last interglacial period. *Paleoceanography* 14: 23-33.
- Cortijo E, Duplessy JC, Labeyrie L, Leclair HL, Duprat J, van Weering TCE. 1994. Eemian cooling in the Norwegian Sea and North Atlantic Ocean preceding continental ice sheet growth. *Nature* 372: 446-449.
- Craig H, Gordon LI. 1965. Deuterium and oxygen 18 variations in the ocean and marine atmosphere. *Stable Isotopes in Oceanographic Studies and Paleotemperatures*. Consiglio Nazionale della Ricerche, Laboratorio di Geologica Nucleare. Pisa pp 9-130.
- Croll J. 1864. Climate and Time. *Philosophical Magazine* 28: 121–137.
- Cronin TM, Gemery L, Briggs Jnr WM, Jakobsson M, Brouwers EM. 2010. Quaternary sea-ice history in the Arctic Ocean based on a new Ostracode sea-ice proxy. *Quaternary Science Reviews* doi: 10.1016/j.quatscirev.2010.05.024.
- Crowdace IW, Rindby A, Rothwell RG. 2006. ITRAX: description and evaluation of a new multi-function X-ray core scanner. In *New Techniques in Sediment Core Analysis*, Rothwell RG (ed.). Special Publication 267, Geological Society: London; 51–63.
- Crowley TJ. 1992. North Atlantic Deep Water cools the Southern Hemisphere. *Paleoceanography* 7: 489-497.

- Crowley TJ, Baum SK. 1995. Is the Greenland Ice Sheet bistable? *Paleoceanography* 10: 357–363.
- Crucifix M, Loutre MF. 2002. Transient simulations over the last interglacial period (126–115 kyr BP): feedback and forcing analysis. *Climate Dynamics* 19: 417–433.
- Cuffey KM, Marshall SJ. 2000. Substantial contribution to sea-level rise during the last interglacial from the Greenland ice sheet. *Nature* 404: 591–594.
- Curry WB, Oppo DW. 2005. Glacial water mass geometry and the distribution of $\delta^{13}\text{C}$ of ΣCO_2 in the western Atlantic Ocean. *Paleoceanography* 20: PA1017, doi:10.1029/2004PA001021.
- Curry WB, Oppo DW. 1998. Glacial water mass geometry and the distribution of $\delta^{13}\text{C}$ of ΣCO_2 in the western Atlantic Ocean. *Paleoceanography* 20: PA1017, doi:10.1029/2004PA001021.
- Curry WB, Duplessy JC, Labeyrie LD, Shackleton NJ. 1998. Changes in the distribution of $\delta^{13}\text{C}$ of deep water ΣCO_2 between the last glaciation and the Holocene. *Paleoceanography* 3: 327–337.
- Cutler KB, Edwards RL, Taylor FW, Cheng H, Adkins J, Gallup CD, Cutler PM, Burr GS, Bloom AL. 2003. Rapid sea-level fall and deep-ocean temperature change since the last interglacial period. *Earth and Planetary Science Letters* 206: 253–271.
- Cutler KB, Gray SC, Burr GS, Edwards RL, Taylor FW, Cabioch G, Beck JW, Cheng H, Moore J. 2004. Radiocarbon calibration to 50 kyr BP with paired ^{14}C and ^{230}Th dating of corals from Vanuatu and Papua New Guinea. *Radiocarbon* 46(3):1127–1160.
- Dahlgren KIT, Vorren TO, Laberg JS. 2002. Late Quaternary glacial development of the mid-Norwegian margin –65 to 68°N. *Marine and Petroleum Geology* 19: 1089–1113.
- Dansgaard W, Johnsen SJ, Clausen H B, Dahl-Jensen D, Gundestrup NS, Hammer CU, Hvidberg CS, Steffensen JP, Sveinbjörnsdóttir AE, Jouzel J, Bond G. 1993. Evidence for general instability of past climate from a 250 kyr ice-core record. *Nature* 364: 218–220.
- Dansgaard W, White JW, Johnsen SJ. 1989. The abrupt termination of the Younger Dryas climate event. *Nature* 339: 532–534.
- Dansgaard W, Clausen HB, Gundestrup N, Hammer CU, Johnsen SF, Kristindóttir PM, Reeh N. 1982. A new Greenland deep ice core. *Science* 218: 1273–1277.
- Davies SM, Wastegård S, Rasmussen TL, Svensson A, Johnsen SJ, Steffensen JP, Andersen KK. 2008. Identification of the Fugloyarbanki tephra in the NGRIP ice core: a key tie-point for marine and ice-core sequences during the last glacial period. *Journal of Quaternary Science* 23: 409–414.
- de Vernal A, Hillaire-Marcel C. 2008. Natural variability of Greenland climate, vegetation, and ice volume during the past million years. *Science* 320: 1622–1625.
- Death R, Seigert MJ, Bigg GR, Wadley MR. 2006. Modelling iceberg trajectories, sedimentation rates and meltwater input to the ocean from the Eurasian Ice Sheet at the Last Glacial Maximum. *Paleogeography, Palaeoclimatology, Palaeoecology* 236: 135–150.
- Delmotte M, Chappellaz J, Brook E, Yiou P, Barnola JM, Goujon C, Raynaud D, Lipenkov VI. 2004. Atmospheric methane during the last four glacial–interglacial cycles: rapid changes and their link with Antarctic temperature. *Journal of Geophysical Research* 109: 12104.
- Denton GH, Alley RB, Comer GC, Broecker WS. 2005. The role of seasonality in abrupt climate change. *Quaternary Science Reviews* 24: 1159–1182.
- Denton GH, Karlen W. 1973. Holocene climatic variations—their pattern and possible cause. *Quaternary Research* 3:155–205.

- Dickson AJ, Austin WEN, Hall IR, Maslin MA, Kucera M. 2008. Centennial-scale evolution of Dansgaard–Oeschger events in the northeast Atlantic Ocean between 39.5 and 56.5 ka BP. *Paleoceanography* 23: PA3206.
- Dickson R, Kidd RB. 1986. Circulation in the Southern Rockall Trough, oceanographic setting of site 601. *Initial Report Deep Sea Diving Project XC IV*: 1061–1074.
- Didié C, Bauch HA. 2000. Species composition and glacial-interglacial variations in ostracode fauna of the northeast Atlantic during the past 200,000 years. *Marine Micropaleontology* 40: 105–129.
- Ditlevsen PD, Andersen KK, Svensson A. 2007. The DO-climate events are probably noise induced: statistical investigation of the claimed 1470 years cycle. *Climate of the Past* 3: 129–134.
- Ditlevsen PD, Kristensen MS, Andersen AA. 2005. The recurrence time of Dansgaard-Oeschger events and limits on the possible periodic component. *Journal of Climate* 18: 2594–2603.
- Dix JK, Duck RW. 2000. A high-resolution seismic stratigraphy from a Scottish sea loch and its implications for Loch Lomond Stadial deglaciation. *Journal of Quaternary Science* 15: 645–656.
- Dokken TN, Jansen E. 1999. Rapid changes in the mechanism in ocean convection during the last glacial period. *Nature* 401: 458–44461.
- Domack EW, Taviani M, Rodriguez A. 1999. Recent sediment remolding on a deep shelf, Ross Sea: implications for radiocarbon dating of Antarctic marine sediments. *Quaternary Science Reviews* 18: 1445–1451.
- Dowdeswell JA. 1986. The distribution and character of sediments in a tidewater glacier, Southern Baffin Island, N.W.T., Canada. *Arctic and Alpine Research* 18: 45–56.
- Dowdeswell JA. 1987. Processes of glacial marine sedimentation. *Progress in Physical Geography* 11: 52–90.
- Dowdeswell JA, Dowdeswell EK. 1989. Debris in icebergs and rates of glacial marine sedimentation: observations from Spitsbergen and a simple model. *Journal of Geology* 97: 221–231.
- Dowdeswell JA, Murray T. 1990. Modelling rates of sedimentation from icebergs. In Dowdeswell J, Scourse J. (Eds.) *Glacial Marine Environments: Processes and Sediments*. Geological Society of London Special Publication vol. 53: 121–137.
- Dowdeswell JA, Ottensen D, Rise L. 2010. Rates of sediment delivery from the Fennoscandian Ice Sheet through and ice age. *Geology* 38: 3–6 doi: 10.1130/G25523.1
- Dowdeswell JA, Elverhøi A, Spielhagen R. 1998. Glacial marine sedimentary processes and facies on the polar North Atlantic Margins. *Quaternary Science Reviews* 17: 234–272.
- Dowdeswell JA, Maslin MA, Andrews JT, McCave IN. 1995. Iceberg production, debris rafting and the extent and thickness of Heinrich layers (H-1, H-2) in North Atlantic sediments. *Geology* 23: 301–304.
- Dowdeswell JA, Whittington RJ, Marienfeld P. 1994. The origin of massive diamicton facies by iceberg rafting and scouring, Scoresby Sund, East Greenland. *Sedimentology* 41: 21–35.
- Drewry D. 1986. *Glaciological Geologic Processes*. Edward Arnold, London.
- Drysdale RN, Hellstrom JC, Zanchetta G, Fallick AE, Sanchez-Göni MF, Couchoud I, McDonald J, Maas R, Lohmann G, Isola I. 2009. Evidence for obliquity forcing of glacial termination II. *Science* 325: 1527–1531.

- Drysdale RN, Zanchetta G, Hellstrom JC, Fallick AE, McDonald J, Cartwright I. 2007. Stalagmite evidence for the precise timing of North Atlantic cold events during the early last glacial. *Geology* 35: 77-80.
- Duplessy JC, Shackleton NJ. 1985. Response of global deep-water circulation to the earth's climatic change 135,000–107,000 years ago. *Nature* 316: 500–507.
- Duplessy JC, Roche DM, Kageyama M. 2007. The deep ocean during the last interglacial period. *Science* 316: 89-91.
- Duplessy JC, Labeyrie L, Waelbroeck C. 2002. Constraints on the ocean oxygen isotopic enrichment between the Last Glacial Maximum and the Holocene. *Quaternary Science Reviews* 21: 315-330.
- Duplessy J, Cobra E, Arnold M, Shackleton NJ, Duprat J, Labeyrie L. 1991. How fast did the ocean-atmosphere system run during the last deglaciation? *Earth and Planetary Science Letters* 103: 27-40.
- Duplessy JC, Shackleton NJ, Fairbanks RG, Labeyrie L, Oppo DW, Kallel N. 1988. Deep water source variations during the last climatic cycle and their impact on global deepwater circulation. *Paleoceanography* 3: 343-360.
- Duplessy JC, Shackleton NJ, Matthews RK, Prell W, Ruddiman WF, Caralp M, Hendy CH. 1984. ^{13}C Record of benthic foraminifera in the last interglacial ocean: Implications for the carbon cycle and the global deep water circulation. *Quaternary Research* 21: 225-243.
- Dwyer GS, Cronin TM, Baker PA, Raymo ME, Buzas JS, Corregge T. 1995. North Atlantic deepwater temperature change during late Pliocene and late Quaternary climatic cycles. *Science* 270: 1347-1351.
- Edwards RL, Beck JW, Burr GS, Donahue DJ, Chappell JMA, Bloom AL, Druffel ERM, Taylor FW. 1993. A large drop in atmospheric $^{14}\text{C}/^{12}\text{C}$ and reduced melting in the Younger Dryas, documented with ^{230}Th ages of corals. *Science* 260(5110):962–968.
- Ehlers J. 1990. Reconstructing the dynamics of the North-West European Pleistocene ice sheets. *Quaternary Science Reviews* 9: 71–83.
- Ehlers J, Gibbard PL. 2008. Extent and chronology of Quaternary glaciation. *Episodes* 31: 211-218.
- Ehlers J, Eissmann L, Lippstreu L, Stephan HJ, Wansa S. 2004. Pleistocene glaciations of North Germany. In *Developments in Quaternary Science*, Ehlers J, Gibbard PL (eds). Elsevier: 135–146.
- Ekman SR. 1998. Middle Pleistocene pollen biostratigraphy in the central North Sea. *Quaternary Science Reviews* 17: 931-944.
- Elderfield H, Ganssen G. 2000. Past temperature and $\delta^{18}\text{O}$ of surface ocean waters inferred from foraminiferal Mg/Ca ratios. *Nature* 405: 442-445.
- Ellett DJ, Roberts DG. 1973. The overflow of Norwegian Sea Deep Water across the Wyville-Thomson Ridge. *Deep-Sea Research* 20: 819–835.
- Elliot M, Labeyrie L, Duplessy JC. 2002. Changes in North Atlantic deepwater formation associated with the Dansgaard-Oeschger temperature oscillations (60-10 ka). *Quaternary Science Reviews* 21: 1153-1165.
- Elliot M, Labeyrie L, Bond G, Cortijo E, Turon JL, Tisnerat N, Duplessy JC. 1998. Millennial-scale iceberg discharges in the Irminger Basin during the last glacial period, relationship with the Heinrich events and environmental settings. *Paleoceanography* 13: 433–446.

- Emery KO, Dietz RS 1941. Gravity coring instrument and mechanics of sediment coring. *Bulletin of the Geological Society of America* 52: 1685- 1714.
- Emery KO, Hülsemann J 1964. Shortening of sediment cores collected in open barrel gravity corers. *Sedimentology* 3: 144-154.
- Emiliani C. 1971. The amplitude of Pleistocene climatic cycles at low latitudes and the isotopic composition of glacial ice. In Turehian KK (Ed). *The late Cenozoic glacial ages*. Yale University, New Haven, Connecticut. Pp 183-197.
- Emiliani C. 1955. Pleistocene temperatures. *Journal of Geology* 63: 538-578.
- Enquist F. 1918. Die glaziale entwicklungsgeschichte Nordwes Skandinaviens. *Sveriges Geologiska Undersökning C* 285: 142.
- EPICA members. 2006. One-to-one coupling of glacial climate variability in Greenland and Antarctica. *Nature* 444: 195–198.
- Epstein S, Buchsbaum R, Lowenstam HA, Urey HC.1953. Revised carbonate-water isotopic temperature scale. *Geological Society of America Bulletin* 64: 1315-1325.
- Ericson DB. 1959. Coiling direction of *Globigerina pachyderma* as a climatic index. *Science* 130: 219–220.
- Eiriksson J, Larsen G, Krudsen KL, Heinemeier J, Simonarson LA 2004. Marine reservoir variability and water mass distribution in the Iceland Sea. *Quaternary Science Reviews* 23: 2247-2268
- Evans HB 1965. GRAPE- a devise for continuous determination of material density and porosity. In *Transactions of the 6th Annual SPWLA Logging Symposium B*: 1-25 <http://www.spwla.org/cgi-bin/shop.pl?choice=display;itemid=82>
- Eyles N, McCabe AM. 1989. The Late Devensian (<22,000 BP) Irish Sea Basin: the sedimentary record of a collapsed ice sheet margin. *Quaternary Science Reviews* 8: 307–351.
- Fairbanks RG. 1989. A 17,00 year glacio-eustatic sea level record: Influence of glacial melting on the Younger Dryas event and deep-ocean circulation. *Nature* 342: 637-642.
- Fairbanks RG. 1982. The Origin of Continental-Shelf and Slope Water in the New-York Bight And Gulf of Maine - Evidence From H218o/H216o Ratio Measurements *Journal of Geophysical Research* 87: 5796-808
- Fairbanks RG, Mortlock RA, Chiu TC, Cao L, Kaplan A, Guilderson TP, Fairbanks TW, Bloom AL, Grootes PM, Nadeau MJ. 2005. Radiocarbon calibration curve spanning 0 to 50,000 years BP based upon paired $^{230}\text{Th}/^{234}\text{U}/^{238}\text{U}$ and ^{14}C dates on pristine corals. *Quaternary Science Reviews* 24: 1781-1796.
- Fairchild IJ, Smith CL, Baker A, Fuller LM, Spötl C, Matthey D, McDermott F. 2006. Modification and preservation of environmental signals in speleothems. *Earth-Science Reviews* 75: 105–153.
- Farmer GL, Barber D, Andrews J. 2003. Provenance of Late Quaternary ice-proximal sediments in the North Atlantic: Nd, Sr and Pb isotopic evidence. *Earth and Planetary Science Letters* 209: 227-243.
- Felis T, Lohmann G, Kuhnert H, Lorenz SJ, Scholz D, Patzold J, Al-Rousan SA, Al-Moghrabi SM. 2004. Increased seasonality in Middle East temperatures during the last interglacial period. *Nature* 429: 164–168.
- Finlayson A, Merritt J, Browne J, McMillan A, Whitbred K. 2010. Ice sheet advance, dynamics and decay configurations: evidence from west central Scotland. *Quaternary Science Reviews* 29: 969-988.

- Firestone RB, West A, Kennett JP, Becker L, Bunch TE, Revay ZS, Schultz PH, Belgia T, Kennett DJ, Erlandson JM, Dickenson OJ, Goodyear AC, Harris RS, Howard GA, Kloosterman JB, Lechler P, Mayewski PA, Montgomery J, Poreda R, Darrah T, Que Hee SS, Smith AR, Stich A, Topping W, Wittke JH, Wolbach WS. 2007. Evidence for an extraterrestrial impact 12,900 years ago that contributed to the megafaunal extinctions and the Younger Dryas cooling. *Proceedings of the National Academy of Sciences* 104: 16016–16021.
- Fisher TG, Smith DG. 1994. Glacial Lake Agassiz: its northwest maximum extent and outlet in Saskatchewan (Emerson Phase). *Quaternary Science Reviews* 13: 845–858.
- Flint RF. 1943. Growth of the North American ice sheet during the Wisconsinian age. *Bulletin of the Geological Society of America* 54: 325-362.
- Flower BP, Oppo DW, McManus JF, Venz KA, Cullen JL, Hodell DA 2000. North Atlantic intermediate to deep water circulation and chemical stratification during the past 1 Myr. *Paleoceanography* 15: 388-403.
- Flückiger J, Knutti R, White JWC. 2006: Oceanic processes as potential trigger and amplifying mechanisms for Heinrich events. *Paleoceanography* 21: PA2014, doi: 10.1029/2005PA001204.
- Forsström P-L, Greve R. 2004. Simulation of the Eurasian ice sheet dynamics during the last glaciation. *Global and Planetary Change* 42: 59–81.
- Fratantoni DM. 2001. North Atlantic Surface Circulation during the 1990's Observed with Satalite_Tracked Drifters. *Journal of Geophysical Research* 102: 22067-22093.
- Fredin O. 2002. Glacial inception and Quaternary mountain glaciations in Fennoscandia. *Quaternary International* 95-96: 99-112.
- Fredin O, Hättestrand C. 2002. Relict lateral moraines in northern Sweden – evidence for an early mountain centred ice sheet. *Sedimentary Geology* 149: 145-156.
- Frew RD, Dennis PF, Heywood KJ, Meredith MP, Boswell SM. 2000. The oxygen isotope composition of water masses in the northern North Atlantic. *Deep-Sea Research I* 47: 2265-2268.
- Frew RD, Heywood KJ, Dennis PF. 1995. Oxygen-Isotope Study of Water Masses In The Princess-Elizabeth Trough, Antarctica. *Marine Chemistry* 49: 141-153.
- Fronval T, Jansen E. 1997. Eemian and early Weichselian (140-60 ka) *Paleoceanography* and paleoclimate in the Nordic seas with comparisons to Holocene conditions. *Paleoceanography* 12: 443–462.
- Fronval T, Jansen E, Haflidason H, Sejrup HP. 1998. Variability in surface and deep water conditions in the Nordic Seas during the last interglacial period. *Quaternary Science Reviews* 17: 963-985.
- Fronval T, Jansen E, Bloemendal J, Johnsen S. 1995. Oceanic evidence for coherent fluctuations in Fennoscandian and Laurentide ice sheets on millennium timescales. *Nature* 6521: 443.
- Fuchs A, Leuenberger MC. 1996. $\delta^{18}\text{O}$ of atmospheric oxygen measured on the GRIP ice core document stratigraphic disturbances in the lowest 10% of the core. *Geophysical Research Letters* 23(9):1049–1052.
- Fujita K, Omori A, Yokoyama Y, Sakai S, Iryu Y. 2010. Sea-level rise during Termination II inferred from large benthic foraminifers: IODP Expedition 310, Tahiti Sea Level. *Marine Geology* 271: 149-155.
- Fyfe JA, Long D, Evans D. 1993. *United Kingdom Offshore Regional Report: the Geology of the Malin-Hebrides Sea Area*. HMSO for the British Geological Survey, London.

- Gallup CD, Cheng H, Taylor FW, Edwards RL. 2002. Direct determination of the timing of sea level change during Termination II. *Science* 295: 310–313.
- Gallup CD, Edwards RL, Johnson RG. 1994. The timing of high sea levels over the past 200,000 years. *Science* 263: 796–800.
- Gammaitoni L, Hanggi P, Jung P, Marchesoni F. 1998. Stochastic resonance. *Review of Mod. Physics* 70: 223–287.
- Ganopolski A, Rahmstorf S. 2002. Abrupt glacial climate changes due to stochastic resonance. *Physics Review Letters* 88: 038501 doi: 10.1103/PhysRevB.88.038501.
- Ganopolski A, Rahmstorf S. 2001a. Rapid changes of glacial climate simulated in a coupled climate model *Nature* 392: 59.
- Ganopolski A, Rahmstorf S. 2001b. Rapid changes of glacial climate simulated in a coupled climate model. *Nature* 409: 153–158.
- Ganssen GM, Kroon D. 2000. The isotopic signature of planktonic foraminifera from NE Atlantic surface sediments: Implications for the reconstruction of past oceanic conditions. *Journal of the Geological Society of London* 157: 693–699.
- Gatliff RW, Richards PC, Smith K, Graham CC, McCormac M, Smith NJP, Jeffery D, Long D, Cameron TDJ, Evans D, Stevenson AG, Bulat J, Ritchie JD. 1994. *British Geological Survey: United Kingdom Offshore Regional Report: the Geology of the Central North Sea*. HMSO: London.
- Geldsetzer HHJ, Nowland GS. 1993. Event markers in Earth's history, Special Issue. *Palaeogeography, Palaeoclimatology, Palaeoecology* 104: 1–286.
- Gemmell AMD, Murray AS, Connell ER. 2007. Devensian glacial events in Buchan (NE Scotland): a progress report on new OSL dates and their implications. *Quaternary Geochronology* 2: 237–242.
- Gibbard PL. 2007. Palaeogeography: Europe cut adrift. *Nature* 448: 259–260.
- Gibbard PL. 1995. title *In* Preece RC (Ed) *Island Britain: a Quaternary perspective*. Geological Society Special Publication, London.
- Gibbard PL, Pasanen AH, West RG, Lunkka JP, Boreham S, Cohen K, Rolfe C. 2009. Late Middle Pleistocene glaciation in East Anglia, England. *Boreas* 38: 504–528.
- Gibbard PL, West RG, Andrew R, Pettit M. 1992. The margin of a Middle Pleistocene ice advance at Tottenhill, Norfolk, England. *Geological Magazine* 129: 59–76.
- Glidor H, Tziperman E. 2003. Sea-ice switches and abrupt climate change. *Philosophical Transactions of the Royal Society of London A* 361: 1935–1942.
- Golledge NR. 2010. Glaciation of Scotland during the Younger Dryas stadial: a review. *Quaternary Science Reviews* 25: 550–566.
- Golledge NR. 2007. Sedimentology, stratigraphy, and glacier dynamics, western Scottish Highlands. *Quaternary Research* 68: 79–95 (see also 'Corrigendum', *Quaternary Research* 68: 456–457).
- Golledge NR, Stoker M. 2006. A palaeo-ice stream of the British Ice Sheet in eastern Scotland. *Boreas* 35: 231–243.
- Golledge N, Hubbard A, Bradwell T. 2009. Influence of seasonality on glacier mass balance and implications for palaeoclimate reconstructions. *Climate Dynamics* doi: 10.1007/s00382-009-0616-6.

- Golledge NR, Hubbard A, Sugden DE. 2008. High-resolution numerical simulation of Younger Dryas glaciation in Scotland. *Quaternary Science Reviews* 27: 888–904.
- Gordon JE, Sutherland DG. 1993. *Quaternary of Scotland*. Chapman and Hall, London. pp. 695.
- Graham AGC, Lonergan L, Stoker MS. 2007. Evidence for Late Pleistocene ice stream activity in the Witch Ground Basin, central North Sea, from 3D seismic reflection data. *Quaternary Science Reviews* 26: 627–643.
- Gray JM, Brooks CL. 1972. The Loch Lomond Readvance moraines of Mull and Menteith. *Scottish Journal of Geology* 8: 95–103.
- Grootes PM, Stuvier M. 1997. Oxygen 18/16 variability in Greenland snow and ice with 10-3 and 10-5 year time resolution. *Journal of Geophysical Research* 102(C12): 26455-26470.
- Gröger M, Maier-Reimer E, Mikolajewicz U, Schurgers G, Vizcaíno M, Winguth A. 2007. Changes in the hydrological cycle, ocean circulation and carbon nutrient cycling during the last interglacial and glacial transition. *Paleoceanography* 22: PA4205, doi: 10.1029/2006PA001375.
- Grönvold K, Oskarsson N, Johnson SJ, Clausen HB, Hammer CU, Bond Bard E. 1995. Ash layers from Iceland in the Greenland GRIP ice core correlated with oceanic and land sediments. *Earth and Planetary Science Letters* 135: 149–155.
- Grossman EL. 1987. Stable isotopes in modern benthic foraminifera – a study of vital effect. *Journal of Foraminiferal Research* 17: 48-61.
- Grousset FE, Cortijo E, Huon S, Hervé L, Richter T, Burdloff D, Duprat J, Weber O. 2001. Zooming in on Heinrich layers. *Paleoceanography* 16: 240-259.
- Grousset FE, Pujol C, Labeyrie L, Auffret G, Boelaert A. 2000. Were the North Atlantic Heinrich events triggered by the behavior of the European ice sheets? *Geology* 28: 123-126.
- Grousset FE, Labeyrie L, Sinko JA, Cremer M, Bond G, Duprat J, Cortijo E, Huon S. 1993. Patterns of ice-rafted debris in the glacial North Atlantic (40–55°N). *Paleoceanography* 8: 175–192.
- Guihou A, Pichat S, Nave S, Govin A, Labeyrie L, Michel E, Waelbroeck C. 2010. Late slowdown of the Atlantic Meridional Overturning Circulation during the Last Glacial Inception: New constraint from sedimentary ($^{231}\text{Pa}/^{230}\text{Th}$). *Earth and Planetary Science Letters* 289: 520-529.
- Gulliksen S, Thomsen M. 1992. Examination of background contamination levels for gas counting and AMS target preparation in Trondheim. In Long A, Kra RS (Eds), Proceedings of the 14th International ^{14}C Conference. *Radiocarbon* 34: 312-317.
- Gupta S, Collier JS, Palmer-Felgate A, Potter G. 2007. Catastrophic flooding origin of shelf valley systems in the English Channel. *Nature* 448: 342-346.
- Gwiazda RH, Hemming SR, Broecker WS. 1996. Provenance of icebergs during Heinrich Event 3 and contrasts in their sources during other Heinrich episodes. *Paleoceanography* 11: 371-378.
- Haapaniemi AI, Scourse JD, Peck VL, Kennedy H, Kennedy P, Hemming SR, Furze MFA, Pienkowski AJ, Austin WEN, Walden J, Wadsworth E, Hall IR. 2010. Source, timing, frequency and flux of ice-rafted detritus to the Northeast Atlantic margin, 30-12 ka: testing the Heinrich precursor hypothesis. *Boreas* 39: 576-591.
- Haeberli W., 1983. Permafrost–glacier relationships in the Swiss Alps today and in the past. In *Proceedings of the Permafrost: fourth international conference on permafrost*, pp. 415–420.
- Haflidason H, Eiriksson J, van Kreveld S. 2000. The tephrochronology of Iceland and the North Atlantic region during the Middle and Late Quaternary: a review. *Journal of Quaternary Science* 15: 3-22.

- Hajdas I, Bonani G, Thut J, Leone G, Pfenninger R and Maden C. 2004. A report on sample preparation at the ETH/PSI AMS facility in Zurich *Nuclear Instruments and Method in Physics Research B* 223-224: 267-271.
- Hald M, Dokken T, Mikalsen G. 2001. Abrupt climatic change during the last interglacial–glacial cycle in the polar North Atlantic. *Marine Geology* 176: 121–137.
- Hall AM. 1997. Quaternary Stratigraphy: the Terrestrial Record. In Gordon (ed) *Reflections on the Ice Age in Scotland: An Update on Quaternary Studies*, Scottish Association of Geography Teachers and Scottish Natural Heritage: Glasgow; 59–71.
- Hall AM, Peacock JD, Connell ER. 2003. New data for the Last Glacial Maximum in Great Britain and Ireland: a Scottish perspective on the paper by Bowen et al. (2002). *Quaternary Science Reviews* 22: 1551–1556.
- Hall IR, McCave IN, Chapman MR, Shackleton NJ. 1998. Coherent deep flow variation in the Iceland and American basins during the last interglacial. *Earth and Planetary Science Letters* 164: 15–21.
- Hamblin RJO, Moorlock BSP, Rose J, Lee JR, Riding JB, Booth SJ, Pawley SM. 2005. Revised pre-Devensian glacial stratigraphy in Norfolk, England, based on mapping and till provenance. *Geologie en Mijnbouw* 84: 77-85.
- Hansen B, Østerhus S. 2000. North Atlantic-Nordic Seas exchanges. *Progress in Oceanography* 45: 109-208.
- Haug GH, Haughey KA, Sigman DM, Peterson LC and Röhl U 2001 Southward Migration of the Intertropical Convergence Zone through the Holocene. *Science* 293: 1304-1308.
- Hays JD, Imbrie J, Shackleton NJ. 1976. Variations in the Earth's orbit: pacemaker of the ice ages. *Science* 194: 1121–1132.
- Hearty PJ. 1987. New data on the Pleistocene of Mallorca. *Quaternary Science Reviews* 6: 245-257.
- Hearty PJ. 1986. An inventory of Last Interglacial (sl) age deposits from the Mediterranean basin: a study in isoleucine epimerization and U/Th dating. *Zeitschrift für Geomorphologie (Supplement Band)* 62: 51-69.
- Hearty PJ, Kindler P. 1995. Sea-level highstand chronology from stable carbonate platforms (Bermuda and Bahamas). *Journal of Coastal Research* 11: 675-689.
- Hearty PJ, Hollin JT, Neumann AC, O'Leary MJ, McCulloch M. 2007a. Global sea-level fluctuations during the Last Interglaciation (MIS 5e). *Quaternary Science Reviews* 26: 2090-2112.
- Hearty PJ, O'Leary MJ, Neumann AC. 2007b. Comment on "Record of MIS 5e sea-level highstands based upon U/Th dated coral terraces of Haiti" Dumas B, Hoang CT, Raffy J. 2006. *Quaternary International* 145-146: 106-118, *Quaternary International* 162-163: 205-208.
- Hebbeln D, Dokken T, Andersen ES, Hald M, Elverhoi. 1994. Moisture supply for northern ice sheet growth during the last glacial maximum. *Nature* 370: 357-359.
- Heinrich H. 1988. Origin and consequences of cyclic ice rafting in the northeast Atlantic ocean during the past 130,000 years. *Quaternary Research* 29: 142–152.
- Henrich R, Baumann K-H. 1994. Evolution of the Norwegian current and the Scandinavian ice sheets during the past 2.6 m.y.: evidence from ODP leg 104 biogenic carbonate and terrigenous records. *Paleogeography, Paleoclimatology Paleocology* 108: 75-94.

- Helmens KF, Räsänen ME, Johansson PW, Jungner H, Korjonen K. 2000. The last interglacial-glacial cycle in NE Fennoscandia: a nearly continuous record from Sokli (Finnish Lapland). *Quaternary Science Reviews* 19: 1605-1623.
- Hemming SR. 2004. Heinrich events: Late Pleistocene detritus layers of the North Atlantic and their global climate imprint. *Review of Geophysics* 42: RG1 005.
- Hemming SR, Broecker WS, Sharp WD, Bond GC, Gwiazda RH, McManus JF, Klas M, Hajdas I. 1998. Provenance of Heinrich layers in core V28-82, northeastern Atlantic: $^{40}\text{Ar}/^{39}\text{Ar}$ ages of ice-rafted hornblende, Pb isotopes in feldspar grains and Nd-Sr-Pb isotopes in the fine fraction. *Earth and Planetary Science Letters* 164: 317-333.
- Henderson GM, Slowey NC. 2000. Evidence from U–Th dating against Northern Hemisphere forcing of the penultimate deglaciation. *Nature* 6773: 61-65.
- Hesse R, Khodabakhsh S. 2006. Significance of fine-grained sediment lofting from melt-water generated turbidity currents for the timing of glaciomarine sediment transport to the deep sea. *Sedimentary Geology* 186: 1-11.
- Hesse R, Khodabakhsh S, Klauke I, Ryan WBF. 1997. Asymmetrical turbid surface-plume deposition near ice-outlets of the Pleistocene Laurentide ice sheet in the Labrador Sea. *Geo-Marine Letters* 17: 179-187.
- Heusser L, Oppo D. 2003. Millennial-and orbital-scale climate variability in southeastern United States and in the subtropical Atlantic during Marine Isotope Stage 5: Evidence from pollen and isotopes in ODP Site 1059. *Earth and Planetary Science Letters* 214: 483–490.
- Hibbert FD, Austin WEN, Leng MJ, Gatliff RW. 2010. British Ice Sheet dynamics inferred from North Atlantic ice-rafted debris records spanning the last 175,000 years. *Journal of Quaternary Science* 25(4): 461–482 doi: 10.1002/jqs.1331.
- Hillaire-Marcel C, Bilodeau G. 2000. Instabilities in the Labrador Sea water mass structure during the last climatic cycle. *Canadian Journal of Earth Sciences* 37: 795-809.
- Hillaire-Marcel, C, de Vernal A, Bilodeau G, Weaver AJ. 2001. Absence of deep-water formation in the Labrador Sea during the last interglacial period. *Nature* 410: 1073–1077.
- Hillaire-Marcel C, de Vernal AK, Bilodeau G, Wu G. 1994. Isotope stratigraphy, sedimentation rates, deep circulation and carbonate events in the Labrador Sea during the last ~200 ka. *Canadian Journal of Earth Science* 31: 68–89.
- Hirvas, H. 1991. *Pleistocene stratigraphy of Finish Lapland*. Geological Survey of Finland Bulletin vol. 354, pp 123.
- Hjelstuen BO, Sejrup HP, Haflidason H, Nygård A, Cermicola S, Bryn P. 2005. Late Cenozoic glacial history and evolution of the Storegga Slide area and adjacent slide flank regions, Norwegian continental margin. *Marine and Petroleum Geology* 22: 57–69.
- Hoare PG, Gale SJ, Robinson RAJ, Connell ER, Larkin NR. 2009. Marine Isotope Stage 7-6 transition age for beach sediments at Morston, north Norfolk, UK: implications for Pleistocene chronology, stratigraphy and tectonics. *Journal of Quaternary Science* 24: 311-316.
- Hoek WZ, Bohncke SJP. 2001. Oxygen-isotope wiggle matching as a tool for synchronising ice-core and terrestrial records over Termination I. *Quaternary Science Reviews* 20: 1251-1264.
- Hodell DA, Curtis JH. 2008. Oxygen and carbon isotopes of detrital carbonate in North Atlantic Heinrich Events. *Marine Geology* 256: 30-35.

- Hodell DA, Minth EK, Curtis JH, McCave IN, Hall IR, Channell JET, Xuan C. 2009. Surface and deep-water hydrography on Gardar Drift (Iceland Basin) during the last interglacial period. *Earth and Planetary Science Letters* 288: 10-19.
- Hodell DA, Channell JET, Curtis JH, Romero OE, Röhl U. 2008. Onset of "Hudson Strait" Heinrich events in the eastern North Atlantic at the end of the middle Pleistocene transition (~640 ka)? *Paleoceanography* 23: PA4218, doi: 10.1029/2008PA001591.
- Holliday NP. 2003. Air-sea interaction and circulation changes in the northeast Atlantic. *Journal of Geophysical Research* 108: 3259 doi: 10.1029/2002JC001344.
- Holliday NP, Pollard RT, Read JF, Leach H. 2000. Water mass properties and fluxes in the Rockall Trough, 1975-1998. *Deep-Sea Research I* 47: 1302-1332.
- Holmes R. 1997. Quaternary stratigraphy: the offshore record. In *Reflections on the Ice Age in Scotland: An Update on Quaternary Studies*, Gordon JE (ed.). Scottish Association of Geography Teachers and Scottish Natural Heritage: Glasgow; 72-94.
- Howe JA. 1995. Sediment transport processes and variations in slope-current activity during the last Glacial-Interglacial episode on the Hebridean Slope, northern Rockall Trough, North Atlantic Ocean. *Sedimentary Geology* 96: 201-230.
- Hua Q, Jacobsen G E, Zoppi U, Lawson E M, Williams A A, Smith A M and McGann M J. 2001. Progress in Radiocarbon Target Preparation at the ANTARES AMS Centre *Radiocarbon* 43: 275-282.
- Hubbard A. 1999. High-resolution modeling of the advance of the younger dryas ice sheet and its climate in Scotland. *Quaternary Research* 52: 27-43.
- Hubbard A, Bradwell T, Golledge N, Hall A, Patton, Sugdon D, Cooper R, Stoker M. 2009. Dynamic ice cycles, ice streams and their impact on the extent, chronology and deglaciation of the British-Irish ice sheet. *Quaternary Science Reviews* 28: 758-776.
- Hughen K, Southon J, Lehman S, Bertrand C, Turnbull J. 2006. Marine-derived ^{14}C calibration and activity record for the past 50,000 years updated from the Cariaco Basin. *Quaternary Science Reviews* 25(23-24):3216-3227.
- Hughen KA, Lehman S, Southon J, Overpeck J, Marchal O, Herring C, Turnbull J. 2004a. ^{14}C activity and global carbon cycle changes over the past 50,000 years. *Science* 303(5655):202-207.
- Hughen KA, Baillie MGL, Bard E, Beck JW, Bertrand CJH, Blackwell PG, Buck CE, Burr GS, Cutler B, Damon PE, Edwards RL, Fairbanks RG, Friedrich M, Guilderson TP, Kromer B, McCormac G, Manning S, Ramsey CB, Reimer PJ, Reimer RW, Remmele S, Southon JR, Stuiver M, Talamo S, Taylor FW, van der Plicht J, Weyhenmeyer CE. 2004b. Marine04 marine radiocarbon age calibration, 0-26 cal kyr BP. *Radiocarbon* 46(3):1059-86.
- Hughen KA, Southon JR, Bertrand CJH, Frantz B, Zerbeño P. 2004c. Cariaco Basin calibration update: revisions to calendar and ^{14}C chronologies for core PL07-58PC. *Radiocarbon* 46(3):1161-1187.
- Hughen KA, Southon JR, Lehman SJ, Overpeck JT. 2000. Synchronous radiocarbon and climate shifts during the last deglaciation. *Science* 290(5498):1951-1954.
- Hughen, KA, Overpeck JT, Lehman SJ, Kashgarian M, Southon J, Peterson LC. 1998b. A new ^{14}C calibration data set for the Last Deglaciation based on marine varves. *Radiocarbon* 40, 483-494.
- Hunt JB, Hill PG. 1996. An inter-laboratory comparison of the electron probe microanalysis of glass geochemistry. *Quaternary International* 34-36: 229-241.

- Hunt JB, Hill PG. 1993. Tephra geochemistry: a discussion of some persistent analytical problems. *The Holocene* 3: 271–278.
- Hunt JB, Fannin NGT, Hill PG, Peacock JD. 1995. The tephrochronology and radiocarbon dating of North Atlantic, Late-Quaternary sediments: an example from the St Kilda Basin. In *The Tectonics, Sedimentation and Palaeoceanography of the North Atlantic Region*. Scrutton RA, Stoker MS, Shimmield GB, Tudhope AW (Eds). Geological Society of London Special Publication No. 90. Bath pp 227-248.
- Huybers P, Wunsch C. 2005. Obliquity pacing of the late Pleistocene glacial terminations. *Nature* 434: 491-494.
- Huybers P, Wunsch C. 2004. A depth derived Pleistocene age model: uncertainty estimates, sedimentation variability and non-linear climate change. *Paleoceanography* 19: PA1028.
- Huybers P, Wunsch C. 2003. Rectification and precession signals in the climate system. *Geophysical Research Letters* 30: 2011, doi: 10.1029/2003GL017875.
- Hvorslev MJ 1949. Subsurface sampling and sampling of soils for civil engineering purposes. Tech. Rep. U.S. Corps Engrs. Waterways Expt. Sta 521 In Ross DA, Riedel WR 1967. Comparison of upper parts of some piston cores with simultaneously collected open-barrel cores. *Deep-Sea Research* 14: 285-294.
- Imbrie J, Imbrie JZ. 1980. Modelling the climatic response to orbital variations. *Science* 207: 943–953.
- Imbrie J, Berger A, Boyle EA, Clemens SC, Duffy A, Howard WR, Kukla G, Kutzbach J, Martinson DG, McIntyre A, Mix AC, Molfino B, Morley JJ, Peterson LC, Shackleton NJ, Toggweiler JR. 1993. On the structure and origin of major glacial cycles: 2. The 100,000 year cycle. *Paleoceanography* 8: 699-735.
- Imbrie J, Boyle EA, Clemens SC, Duffy A, Howard WR, Kukla G, Kutzbach J, Martinson DG, McIntyre A, Mix AC, Molfino B, Morley JJ, Peterson LC, Pisias NG, Prell WL, Raymo ME, Shackleton NJ, Toggweiler JR. 1992. On the structure and origin of major glacial cycles: 1. Linear responses to Milankovitch forcing. *Paleoceanography* 7: 701-738.
- Imbrie J, Hays JD, Martinson DG, McIntyre A, Mix AC, Morley JJ, Pisias NG, Prell WL, Shackleton NJ. 1984. The orbital theory of Pleistocene climate: support from a revised chronology of the marine $\delta^{18}\text{O}$ record. In Berger A, Imbrie J, Hays H, Kukla G, Saltzman B. (Eds) *Milankovitch and Climate: Understanding the Response to Astronomical Forcing*, Proceedings of the NATO Advanced Research Workshop held 30 November-4 December, 1982 in Palisades, NY. D. Reidel Publishing, Dordrecht.
- Imbrie J, Hays JD, Martinson DG, McIntyre A, Mix AC, Morely JJ, Pisias NG, Prell WL, Shackleton NJ. 1984. The orbital theory of Pleistocene climate: support from a revised chronology of the marine $\delta^{18}\text{O}$ record. In *Milankovitch and Climate*, Vol. 1, Berger AL (ed.). D. Reidel: Dordrecht; 269–305.
- Isarin RFB, Renssen H. 1999. Reconstructing and modelling Late Weichselian climates: the Younger Dryas in Europe as a case study. *Earth Science Reviews* 48: 1-38.
- Ives JD, Andrews JT, Barry RG. 1975. Growth and decay of the Laurentide ice sheet and comparisons with Fenno-Scandia. *Naturwissenschaften* 62: 118-125.
- Jardine WG, Dickson JH, Haughton PDW, Harkness DD, Bowen DQ, Sykes GA. 1988. A late Middle Devensian interstadial site at Sourlie, near Irvine, Strathclyde. *Scottish Journal of Geology* 24: 288–295.
- Jeandel C, Arsouze T, Lacan F, Téchiné P, Dutay JC. 2007. Isotopic Nd compositions and concentrations of the lithogenic inputs into the ocean: A compilation, with an emphasis on the margins. *Chemical Geology* 239: 156-164.

- Ji J, Balsam W, Chen X, Chen J, Chen Y, Wang H. 2006. Rate of solar insolation change and the glacial/interglacial transition. *Geophysical Research Letters* 33: L04706, doi:10.1029/2005GL025401.
- Johannessen T, Jansen E, Flatøy A, Ravelo AC. 1994. The relationship between surface water masses, oceanographic fronts and paleoclimatic proxies in surface sediments of Greenland, Iceland, Norwegian Seas. In *Carbon Cycling in the Glacial Ocean: Constraints on the Oceans Role in Global Change: Quantitative Approaches in Paleoceanography*, Zahn R, Pedersen TF, Kaminski MA, Labeyrie L (eds). NATO ASI series I, vol. 17. Springer: New York.
- Johnson H, Richards PC, Long D, Graham CC. 1993. *United Kingdom Offshore Regional Report: the geology of the Northern North Sea*. HMSO for the British Geological Survey, London.
- Johnson RG. 1991. Major Northern Hemisphere deglaciation caused by moisture deficit 140 ka. *Geology* 19: 686-689.
- Johnsen SJ, Dahl-Jensen D, Grundstrup N, Steffensen JP, Clausen HB, Miller H, Masson-Delmotte V, Sveinbjörnsdóttir AE, White J. 2001. Oxygen isotope and palaeotemperature records from six Greenland ice-core stations: Camp Century, Dye-3, GRIP, GISP2, Renland and NorthGRIP. *Journal of Quaternary Science* 16: 299-307.
- Johnsen SJ, Clausen HB, Dansgaard W, Gundestrup NS, Hammer CU, Tauber H. 1995. The Eem Stable-Isotope Record Along The Grip Ice Core And Its Interpretation. *Quaternary Research* 43: 117-124.
- Jouzel J, Stiévenard M, Johnsen SJ, Landis A, Masson-Delmotte V, Sveinbjörnsdóttir A, Vimeux F, von Grafenstein U, White JWC. 2007. The GRIP deuterium-excess record. *Quaternary Science Reviews* 26: 1-17.
- Jouzel J, Masson-Delmotte V, Cattani O, Dreyfus G, Falourd S, Hoffmann G, Minster B, Nouet J, Barnola JM, Chappellaz J, Fischer H, Gallet JC, Johnsen S, Leuenberger M, Loulergue L, Luethi D, Oerter G, Parrenin F, Raisbeck G, Raynaud D, Schilt A, Schwander J, Selmo E, Souchez R, Spahni R, Stauffer B, Steffensen JP, Stenni B, Stocker TF, Tison JL, Werner M, Wolff EW. 2007. Orbital and millennial Antarctic Climate Variability over the past 800,000 years. *Science* 317: 793-796.
- Jouzel J, Masson-Delmotte S, Stiévenard M, Landis A, Vimeux F, Johnsen SJ, Sveinbjörnsdóttir A, White JWC. 2005. Rapid deuterium excess changes in Greenland ice cores: a link between the ocean and the atmosphere. *CRAS Géosciences* 337: 957-969.
- Jouzel J, Vimeux F, Caillon N, Delaygue G, Hoffmann G, Masson-Delmotte V, Parrenin F. 2003. Magnitude of isotope/temperature scaling for the interpretation of central Antarctic ice cores. *Journal of Geophysical Research* 108(D12): 4361
- Jullien E, Grousset FE, Hemming SR, Peck VL, Hall IR, Jeantet C, Billy I. 2006: Contrasting conditions preceding MIS3 and MIS2 Heinrich events. *Global and Planetary Change* 54: 225-238.
- Karner DB, Levine J, Medeiros BP, Muller RA. 2002. Constructing a stacked benthic $d^{18}O$ record. *Paleoceanography* 17: 1030.
- Keigwin LD. 1996. The Little Ice Age and Medieval warm period in the Sargasso Sea. *Science* 274: 1504-1508.
- Keigwin LD, Boyle EA. 1999. Surface and deep ocean variability in the northern Sargasso Sea during marine isotope stage 3. *Paleoceanography* 14: 164-170.
- Keigwin LD, Curry WB, Lehman SJ, Johnsen S. 1994. The role of the deep ocean in North Atlantic climate changes between 70 and 130 kyr ago. *Nature* 371: 323-325.

- Keigwin LD, Jones GA, Lehman SJ, Boyle EA. 1991. Deglacial meltwater discharge, North Atlantic deep circulation and abrupt climate change. *Journal of Geophysical Research* 96(C9): 16811-16826.
- Kellogg TB. 1980. Paleoclimatology and paleoceanography of the Norwegian and Greenland Seas: Glacial-interglacial contrasts. *Boreas* 9: 115-136.
- Khodri M, Ramstein G, Paillard D, Duplessy JC, Kageyama M, Ganopolski A. 2003. Modelling the climate evolution from the last interglacial to the start of the last glaciation: the role of Arctic Ocean freshwater budget. *Geophysical Research Letters* 30: doi: 10.1029/2003GL017108.
- Khodri M, Leclainche Y, Ramstein G, Braconnot P, Marti O, Cortijo E. 2001. Simulating the amplification of orbital forcing by ocean feedbacks in the last glaciation. *Nature* 410: 570-574.
- King AL, Howard WR. 2005. $\delta^{18}\text{O}$ seasonality of planktonic foraminifera from Southern Ocean sediment traps: Latitudinal gradients and implications for paleoclimate reconstructions. *Marine Micropaleontology* 56: 1-24, doi:10.1016/j.marmicro.2005.02.008.
- King EL, Hafliðason H, Sejrup HP. 1998. *End moraines on the northwest Irish continental shelf*. Abstract 3rd ENAM II Workshop, Scotland.
- King EL, Hafliðason H, Sejrup HP, Lovlie R. 1998b. Glacigenic debris flows on the North Sea Trough Mouth Fan during ice stream maxima. *Marine Geology* 152: 217-246.
- King EL, Sejrup HP, Hafliðason H, Elverhøi A, Aarseth I. 1996. Quaternary seismic stratigraphy of the North Sea Fan: glacially fed gravity flow aprons, hemipelagic sediments, and large submarine slides. *Marine Geology* 130: 293-315.
- Kipphut GW. 1990. Glacial Meltwater Input to the Alaska Coastal Current: Evidence from Oxygen Isotope Measurements. *Journal of Geophysical Research* 95: 5177-5181.
- Kissel C. 2005. Magnetic signature of rapid climatic variations in glacial North Atlantic, a review. *C. R. Geosciences* 337: 908-918, doi:10.1016/j.crte.2005.04.009.
- Knies J, Vogt C, Matthiessen J, Nam S, Ottesen D, Rise L, Bargel T, Eilertsen RS. 2007. Re-advance of the Fennoscandian Ice Sheet during Heinrich Event 1. *Marine Geology* 240: 1-18.
- Knight J. 2003. Evaluating controls on ice sheet dynamics in the north-east Atlantic using an event stratigraphy approach. *Quaternary International* 99-100: 45-57.
- Knudsen KL, Seidenkrantz MS, Kristensen P. 2002. Last Interglacial and Early Glacial Circulation in the Northern North Atlantic. *Quaternary Research* 58: 22-26.
- Knutz PC, Zahn R, Hall IR. 2007. Centennial-scale variability of the British Ice Sheet: implications for climate forcing and meridional overturning circulation during the last glaciation. *Paleoceanography* 22: PA1 207.
- Knutz PC, Jones EJ, Austin WE, van Weering TC. 2002. Glacimarine slope sedimentation, contourite drifts and bottom current pathways on the Barra Fan, UK North Atlantic margin. *Marine Geology* 188: 129-146.
- Knutz PC, Hall IR, Zahn R, Rasmussen TL, Kuijpers A, Moros M, Shackleton NJ. 2002b. Multidecadal ocean variability and NW European ice sheet surges during the last deglaciation. *Geochemistry, Geophysics, Geosystems* 3: 1077 doi: 10.1029/2002GC00351.
- Knutz PC, Austin WEN, Jones EJW. 2001. Millennial-scale depositional cycles related to British Ice Sheet variability and North Atlantic paleocirculation since 45 kyr BP, Barra Fan, UK margin. *Paleoceanography* 16: 53-64.

- Kovanen DJ, Easterbrook DJ. 2002. Paleodeviations of radiocarbon marine reservoir values for the northeast Pacific. *Geology* 30: 243-246.
- Krinner G and Werner M. 2003. Impact of precipitation seasonality changes on isotopic signals in polar ice cores: a multi-model analysis. *Earth and Planetary Science Letters* 216: 525-538.
- Kroon D, Darling K. 1995. Size and Upwelling Control of the Stable-Isotope Composition of *Neogloboquadrina-dutertrei* (Dorbigny), *Globigerinoides-ruber* (Dorbigny) And *Globigerina-bulloides* Dorbigny - Examples From The Panama Basin And Arabian Sea. *Journal of Foraminiferal Research* 25: 39-52.
- Kroon D, Shimmield G, Austin WEN, Derrick S, Knutz P, Shimmieald T. 2000. Century to millennial-scale sedimentological geochemical records of glacial-Holocene sediment variations from the Barra Fan (NE Atlantic). *Journal of the Geological Society of London* 157: 643-653.
- Kroon D, Austin WEN, Chapman MR, Ganssen GM. 1997. Deglacial surface circulation changes in the northeastern Atlantic: Temperature and salinity records off NW Scotland on a century scale. *Paleoceanography* 12: 755-763.
- Kroopnik PM. 1985. The distribution of ^{13}C of total CO_2 in the worlds oceans. *Deep Sea Research* 32: 57-77.
- Kuhlmann H, Freudenthal T, Helmke P and Meggers H 2004 Reconstruction of Paleoceanography off NW Africa during the last 40,000 years: influence of local and regional factors on sediment accumulation. *Marine Geology* 207: 209-224.
- Kukla G, McManus JF, Rousseau DD, Chuine I. 1997. How land and stable was the last interglacial? *Quaternary Science Reviews* 16: 605-612.
- Kvamme T, Mangerud J, Furnes H, Ruddiman WF. 1989. Geochemistry of Pleistocene ash zones in cores from the North Atlantic. *Norsk Geologisk Tidsskrift* 69: 251-272.
- Labeyrie L, Waelbroeck C, Cortijo E, Michel E, Duplessy JC. 2005. Changes in deep water hydrology during the last deglaciation. *Comptes Rendus Geoscience* 337: 919-927.
- Labeyrie LD, Duplessy JC, Blanc PL. 1987. Variations in mode of formation and temperature of oceanic deep waters over the past 125,000 years. *Nature* 327: 477-482.
- Lacasse, C Garbe-Schonberg CD. 2001. Explosive silicic volcanism in Iceland and the Jan Mayen area during the last 6 Ma: sources and timing of major eruptions. *Journal of Volcanology and Geothermal Research* 107: 113-147.
- Lacasse C, Sigurdsson H, Carey S, Paterne M, Guichard F. 1996. North Atlantic deep sea sedimentation of late Quaternary tephra from the Iceland hotspot. *Marine Geology* 129: 207-235.
- Lackschewitz KS, Wallrabe-Adams HJ. 1997. Composition and origin of volcanic ash zones in Last Quaternary sediments from the Reykjanes Ridge: evidence for ash fallout and ice-rafting. *Marine Geology* 136: 209-224.
- Lackschewitz KSK, Baumann K, Gehrke B, Wallrabe-Adams H, Thiede J, Bonani G, Endler R, Erenkeuser H, Heinemeier J. 1998. North Atlantic ice sheet fluctuations 10,000 – 70,000 yr ago as inferred from deposits on the Reykjanes Ridge, southeast of Greenland. *Quaternary Research* 49: 171-182, doi:10.1006/qres.1997.1948.
- Laj C, Kissel C, Beer J, 2004. High resolution global paleointensity stack since 75 kyr (GLOPIS-75) calibrated to absolute values. In Channell JET, Kent DV, Lowrie W, Meert JG. (Eds) *Timescales of the Paleomagnetic Field*. Geophysical Monograph vol. 145. American Geophysical Union, Washington DC, USA.

- Laj C, Kissel C, Mazaud A, Channell JET, Beer J. 2000. North Atlantic palaeointensity stack since 75 ka (NAPIS-75) and the duration of the Laschamp event. *Philosophical Transactions of the Royal Society of London A*: 1009–1025.
- Lambeck K, Chappell J. 2001. Sea level change through the Last Glacial Cycle. *Science* 292: 679–686.
- Lamy F, Kaiser J, Ninnemann U, Hebbeln D, Arz HW and Stoner J 2004 Antarctic timing of Surface Water changes off Chile and Patagonian Ice Sheet Response. *Science* 304: 1959-1962.
- Landis A, Masson-Delmotte V, Jouzel J, Raynaud D, Johnsen S, Huber C, Leuenberger M, Schwander J, Minster B. 2006. The glacial inception as recorded in the NorthGRIP Greenland ice core: timing, structure and associated abrupt temperature changes. *Climate Dynamics* 26: 273-284.
- Landis A, Jouzel J, Masson-Delmotte V, Caillon N. 2005. Large temperature variations over rapid climate events in Greenland: a method based upon air isotope measurements. *CRAS Géosciences* 337: 947-956.
- Landais A, Barnola J-M, Masson-Delmotte V, Jouzel J, Chappellaz J, Caillon N, Huber C, Leuenberger M, Johnsen S. 2004. A continuous record of temperature evolution over a whole sequence of Dansgaard-Oeschger during Marine Isotopic Stage 4 (76 to 62 kyr BP). *Geophysical Research Letters* 31: L22211 doi: 10.1029/2004GL021193.
- Landais A, Chappellaz J, Delmotte MJ, Jouzel J, Blunier T, Bourg C, Caillon C, Cherrier S, Malaize B, Masson-Delmotte V, Raynaud D, Schwander J, Steffensen JP. 2003. A tentative reconstruction of the last interglacial and glacial inception in Greenland based on new gas measurements in the Greenland Ice Core Project (GRIP) ice core. *Journal of Geophysical Research* 108(D18): doi: 10.1029/2002JD003147.
- Lane GA, Doyle M. 1956. Fractionation of oxygen isotopes during respiration. *Science* 123: 574
- Lang C, Leuenberger M, Schwander J, Johnsen S. 1999. 16 °C rapid temperature variation in central Greenland 70,000 years ago. *Science* 286: 934–937.
- Larsen E, Sejrup HP, Janocko J, Landvik JY, Stalsberg K, Steinsund PI. 2000. Recurrent interaction between the Norwegian Channel Ice Stream and terrestrial based ice across southwest Norway. *Boreas* 29:185-203.
- Lauritzen SE. 1995. High-resolution palaeotemperature proxy records from the last interglacial based upon Norwegian speleothems. *Quaternary Research* 43: 133-146.
- Lauritzen SE. 1991. Uranium series dating of speleothems: a glacial chronology for Nordland, Norway, for the last 600 ka. *Striae* 34: 127-133.
- Lea DW, Martin PA, Pak DK, Spero HJ. 2002. Reconstructing a 350 ky history of sea level using planktonic Mg/Ca and oxygen isotope records from a Cocos Ridge core. *Quaternary Science Reviews* 21: 283–293.
- Lea DW, Mashiotta TA, Spero HJ. 1999. Control on magnesium and strontium uptake in planktic foraminifera determined by live culturing. *Geochimica et Cosmochimica Acta* 63: 2369-2379
- Lebel J, Silverberg N, Sundby B 1982. Gravity core shortening and pore water gradients. *Deep-Sea Research* 29: 1365-1372
- Lee A, Ellett DJ. 1965. On the contribution of overflow water from the Norwegian Sea to the hydrographic structure of the North Atlantic Ocean. *Deep-Sea Research* 12: 129–142.
- Lee JR, Busschers FS, Sejrup HP. 2010. Pre-Weichselian Quaternary glaciations of the British Isles, The Netherlands, Norway and adjacent marine areas south of 58 °N: implications for the long-term ice sheet development in northern Europe. *Quaternary Science Reviews* (in press): doi: 10.1016/j.quatres.2010.02.027

- Lee JR, Moorlock BSP, Rose J, Hamblin RJO, Pawley SM, Riding JB, Jarrow AM, Booth SJ, Palmer A, Morigi AN, Kessler H. 2005. A reply to the paper by Hoare and Connell. "The first appearance of Scandinavian indicators in East Anglia's glacial record". *Bulletin of the Geological Society of Norfolk* 55: 43-62.
- Lee JR, Booth SJ, Hamblin RJO, Jarrow AM, Kessler H, Moorlock BSP, Morigi AN, Palmer A, Pawley SM, Riding JB, Rose J. 2004. A new stratigraphy for the glacial deposits around Lowestoft, Great Yarmouth, North Walsham and Cromer, East Anglia, UK. *Bulletin of the Geological Society of Norfolk* 53: 3-60.
- Lee JR, Rose J, Riding JB, Hamblin RJO, Moorlock BSP. 2002. Testing the case for a Middle Pleistocene Scandinavian glaciation in Eastern England: evidence for a Scottish ice source for tills within the Corton formation of East Anglia, UK. *Boreas* 31: 345-355.
- Lehman SJ, Keigwin LD. 1992. Sudden changes in North Atlantic circulation during the last deglaciation. *Nature* 356: 757-762.
- Lehman S, Sachs J, Croxwell A, Keigwin L, Boyle E. 2002. Relation of subtropical Atlantic temperature, high latitude ice rafting, deep water formation and European climate 130,000-60,000 years ago. *Quaternary Science Reviews* 21: 1917-1924.
- Leigh SNB. 2005. A study of the dynamics of the British Ice Sheet during Marine Isotope Stages 2 and 3 focusing on Heinrich Events 2 and 4 and their relationship to the North Atlantic glaciological and climatological conditions. *MPhil Thesis*, University of St Andrews.
- Lekens WAH, Sejrup HP, Haflidason H, Knies J, Richter T. 2006. Meltwater and ice rafting in the southern Norwegian Sea between 20 and 40 calendar kyr BP: implications for Fennoscandian Heinrich events. *Paleoceanography* 21: PA3013.
- Levitus S. 1982. *Climatological Atlas of the World Ocean*. NOAA Prof. Pap. 13: 173 In Cortijo et al 1999. *Paleoceanography* 14: 23-33.
- Lewis SG, Rose J. 1991. Tottenhill, Norfolk (TF 639 120). In Lewis SG, Whiteman CA, Bridgland DR (Eds) *Central East Anglia and the Fen Basin, Field Guide*. Quaternary Research Association, London, pp. 145-148.
- Libes SM. 2009. *Introduction to Marine Biogeochemistry* (2nd Edition). Elsevier, London pp 351-372.
- Lie Ø, Paasche Ø. 2006. How extreme was northern hemisphere seasonality during the Younger Dryas? *Quaternary Science Reviews* 25: 404-407.
- Lisiecki LE and Raymo ME. 2010 (online advance proofs, *Submitted*). Diachronous $\delta^{18}\text{O}$ responses during Late Pleistocene terminations. *Paleoceanography*
- Lisiecki LE, Raymo M. 2009. Diachronous benthic $\delta^{18}\text{O}$ responses during last Pleistocene terminations. *Paleoceanography* 24: PA3210, doi: 10.1029/PA001732.
- Lisiecki LE, Raymo ME. 2005. A Pliocene–Pleistocene stack of 57 globally distributed benthic $\delta^{18}\text{O}$ records. *Paleoceanography* 20: PA1003.
- Lisiecki LE, Lisiecki PA. 2002. Application of dynamic programming to the correlation of paleoclimate records. *Paleoceanography* 17: 1049. doi:10.1029/2001PA000733.
- Lohne ØS, Bondevik S, Mangerud J, Svendsen JJ. 2007. Sea-level fluctuations imply that the Younger Dryas ice-sheet expansion in western Norway commenced during the Allerød. *Quaternary Science Reviews* 26: 2128-2151.
- Long D, Laban C, Streif H, Cameron TDJ, Schüttenhelm RTE. 1988. The sedimentary record of climatic variation in the southern North Sea. *Philosophical Transactions of the Royal Society of London B* 318: 523-537.

- Lototskaya A, Ganssen GM. 1999. The structure of Termination II (penultimate deglaciation and Eemian) in the North Atlantic. *Quaternary Science Reviews* 18: 1641-1654.
- Loulergue L, Schilt A, Spahni R, Masson-Delmotte V, Blunier T, Lemieux B, Barnola JM, Raynaud D, Stocker T, Chappellaz J. 2008. Orbital and millennial-scale features of atmospheric CH₄ over the past 800,000 years. *Nature* 453: 383–386.
- Lourantou A, Chappellaz J, Barnola JM, Masson-Delmotte V, Raynaud D. 2010. Changes in atmospheric CO₂ and its carbon isotopic ratio during the penultimate deglaciation. *Quaternary Science Reviews* 29: 1983-1992.
- Loving JL, Vallis GK. 2005. Mechanisms for climate variability during glacial and interglacial periods. *Paleoceanography* 20: PA4024 doi: 10.1029/2004PA001113.
- Lowe JJ, Walker MJC. 2000. Radiocarbon dating the last glacial-interglacial transition (ca 14-9 14C ka BP) in terrestrial and marine records: The need for new quality assurance protocols *Radiocarbon* 42: 53-68.
- Lowe JJ, Rasmussen SO, Björck S, Hoek WZ, Steffensen JP, Walker MJC, Yu ZC, the INTIMATE group 2008. Synchronisation of palaeoenvironmental events in the North Atlantic region during the Last Termination: a revised protocol recommended by the INTIMATE group. *Quaternary Science Reviews* 27: 6-17.
- Lowe JJ, Blockley S, Trincardi F, Asioli A, Cattaneo A, Matthews IP, Pollard M, Wulf S. 2007. Age modelling of late Quaternary marine sequences in the Adriatic: towards improved precision and accuracy using volcanic event stratigraphy. *Continental Shelf Research* 27: 560–582.
- Lowe JJ, Hoek WZ, INTIMATE group. 2001. Inter-regional correlation of palaeoclimatic records for the Last Glacial-Interglacial Transition: a protocol for improved precision recommended by the INTIMATE group. *Quaternary Science Reviews* 20: 1175-1187.
- Lowell TV, Fisher TG, Comer GC, Hajdas I, Waterson N, Glover K, Loope HM, Schaefer JM, Rinterknecht VR, Broecker WS, Denton GH, Teller JT. 2005. Testing the Lake Agassiz meltwater trigger for the Younger Dryas. *Eos* 86: 365-372.
- Lownestam H, Weiner S. 1989. *On biomineralisation* Oxford University Press
- In Nadeau MJ, Grootes P, Voelker A, Bruhn F, Duhr A, Oriwall A. 2001. Carbonate ¹⁴C background: Does it have multiple personalities? *Radiocarbon* 43(2A): 169-176.
- Lundqvist J 1992. Glacial stratigraphy in Sweden. *Geological Survey of Finland Special Paper* 15: 43-59.
- Lynch-Stieglitz J, Adkins JF, Curry WB, Dokken T, Hall IR, Herguera JC, Hirschi JJM, Ivanova EV, Kissel C, Marchal O, Marchitto TM, McCave IN, McManus JF, Mulitza S, Ninnemann U, Peeters F, Yu EF, Zahn R. 2007. Atlantic meridional overturning circulation during the Last Glacial Maximum. *Science* 316: 66–69, doi:10.1126/science.1137127.
- Mackensen A. 2008. On the use of benthic foraminiferal $\delta^{13}\text{C}$ in palaeoceanography: constraints from primary proxy relationships. In Austin WEN, James RH (Eds). *Biogeochemical Controls on Palaeoceanographic Environmental Proxies*. Special Publication of the Geological Society, London 303: 121-133.
- Mackensen A, Bickert T. 1999. Stable carbon isotopes in benthic foraminifera: Proxies for deep and bottom water circulation and new production. In Fischer G, Wefer G (Eds) *Use of Proxies in Paleoceanography: Examples From the South Atlantic*, Springer, Berlin.
- Mackensen A, Schumacher S, Radke J, Schmidt DN. 2001. Microhabitat preferences and stable carbon isotopes of endobenthic foraminifera: clue to quantitative reconstruction of oceanic new production? *Marine Micropaleontology* 40: 233-258.

- Malaizé B, Joly C, Vénec-Peyré MT, Bassinot F, Caillon N, Charlier K. 2006. Phase lag between Intertropical Convergence Zone migration and subtropical monsoons onset over northwestern Indian Ocean during Marine Isotopic Substage 6.5 (MIS 6.5). *Geochemistry, Geophysics, Geosystems* 8: doi : 10.1029/2006GC001496.
- Mangerud J. 2004. Ice sheet limits on Norway and the Norwegian continental shelf. In *Quaternary Glaciations: Extent and Chronology. Vol. 1: Europe*, Ehler J, Gibbard PL (eds). Elsevier: Amsterdam; 271– 294.
- Mangerud J. 2000. Was Hardangerfjorden, western Norway, glaciated during the Younger Dryas? *Norsk Geologisk Tidsskrift* 80: 229-234.
- Mangerud J, Dokken T, Hebbeln D, Heggen B, Ingólfsson Ó, Landvik JY, Mejdahl V, Svendsen JI, Vorren TO. 1998. Fluctuations of the Svalbard-Barents Sea ice sheet during the last 150,000 years. *Quaternary Science Reviews* 17: 11-42.
- Mangerud J, Sønstergaard E, Sejrup HP, Haldorsen S. 1981a. A continuous Eemian-Early Weichselian sequence containing pollen and marine fossils at Fjøsanger, western Norway. *Boreas* 10: 137-208.
- Mangerud J, Gulliksen S, Larsen E, Longva O, Müller GH,. 1981b. A Middle Weichselian ice-free period in western Norway: the Ålesund Interstadial. *Boreas* 10: 447-462.
- Manighetti B, McCave IN, Maslin MA, Shackleton NJ. 1995. Chronology for climate change: Developing age models for the Biogeochemical Ocean Flux Study cores. *Paleoceanography* 10: 513–525.
- Marchitto TM, Broecker WS. 2006. Deep water mass geometry in the glacial Atlantic Ocean: A review of constraints from the paleonutrient proxy Cd/Ca. *Geochemistry Geophysics Geosystems* 7(12): Q1203 doi: 10.1029/2006GC001323.
- MARGO Project Members. 2009. Constraints on the magnitude and patterns of ocean cooling at the Last Glacial Maximum. *Nature Geoscience* 2: doi: 10.1038/NGEO411.
- Marshall SJ, Koutnik MR. 2006. Ice sheet action versus reaction: distinguishing between Heinrich events and Dansgaard–Oeschger cycles in the North Atlantic. *Paleoceanography* 21: PA2021.
- Martin PA, Lea DW, Rosenthal Y, Shackleton NJ, Sarnthein M, Papenfuss T. 2002. Quaternary deep sea temperature histories derived from benthic foraminiferal Mg/Ca. *Earth and Planetary Science Letters* 198: 193-209.
- Martinson DG, Pisias NG, Hays JD, Imbrie J, Moore TC Jr, Shackleton NJ. 1987. Age dating and the orbital theory of the ice ages: development of a high resolution 0 to 300,000-year chronostratigraphy. *Quaternary Research* 27: 1–29.
- Maslin M, Shackleton NJ, Pflaumann U. 1995. Surface water temperature, salinity and density changes in the northeast Atlantic during the last 45,000 years: Heinrich events, deep water formation and climatic rebounds. *Paleoceanography* 10: 527-544.
- Masson V, Baconnot P, Jouzel J, de Noblet N, Cheddadi R, Marchal O. 2000. Simulation of intense monsoons under glacial conditions. *Geophysical Research Letters* 27: 1747-1750.
- Mayewski PA, Meeker LD, Whitlow S, Twickler MS, Morrison MC, Bloomfield P, Bond GC, Alley RB, Gow AJ, Meese DA, Grootes PM, Ram M, Taylor KC, Wumkes W. 1994. Changes in atmospheric circulation and ocean ice cover over the North Atlantic during the last 41,000 years. *Science* 263: 1747–1751.
- McCabe AM. 2008. *Glacial Geology and Geomorphology: The Landscapes of Ireland*. Dunedin Press: Edinburgh.

- McCabe AM, Clark PU. 2003. Deglacial chronology from County Donegal, Ireland: implications for deglaciation of the British–Irish ice sheet. *Journal of the Geological Society of London* 160: 847–855.
- McCabe AM, Clark PU. 1998. Ice sheet variability around the North Atlantic Ocean during the last deglaciation. *Nature* 392: 373–377.
- McCabe AM, Clark PU, Clark J. 2007. Radiocarbon constraints on the history of the western Irish ice sheet prior to the Last Glacial Maximum. *Geology* 35: 147–150.
- McCabe AM, Clark PU, Clark J. 2005. AMS ^{14}C dating of deglacial events in the Irish Sea Basin and other sectors of the British–Irish ice sheet. *Quaternary Science Reviews* 24: 1673–1690.
- McCabe AM, Knight J, McCarron SG. 1998. Evidence for Heinrich event 1 in the British Isles. *Journal of Quaternary Science* 13: 549–568.
- McCabe AM, Haynes JR, Macmillan NF. 1986. Late Pleistocene tidewater glaciers and glaciomarine sequences from north County Mayo, Republic of Ireland. *Journal of Quaternary Science* 1: 73–84.
- McCarroll D, Stone SO, Ballantyne CK, Scourse JD, Hiemstra JF, Evans DJA, Fifield LK, Rhodes E. 2010. Exposure-age constraints on the extent, timing and rate of retreat of the last Irish Sea ice stream. *Quaternary Science Reviews* 29: 1844–1852.
- McCartney MS. 1992. Recirculating components of the deep boundary current of the northern North Atlantic. *Progress in Oceanography* 29: 283–383.
- McCave IN. 1972. Transport and escape of fine-grained sediment from shelf areas. In Swift DJP (Ed) Shelf Sediment Transport: Processes and Pattern. Dowden, Hitchen and Ross, Stroudsburg. pp 225–248.
- McCave IN, Hall IR. 2006. Size sorting in marine muds: Processes, pitfalls and prospects for paleoflow-speed proxies. *Geochemistry, Geophysics, Geosystems* 7: Q10N05, doi: 10.1029/2006GC001284.
- McCave IN, Manighetti B, Robinson SG. 1995. Sortable silt and fine sediment size/composition slicing: Parameters for paleocurrent speed and paleoceanography. *Paleoceanography* 10: 593–610.
- McCoy FW 1985. Photographic analysis of coring. *Marine Geology* 38: 263–282.
- McIntyre KL and Howe JA 2009. Bottom-current variability during the last glacial-deglacial transition, Northern Rockall Trough and Faeroe Bank Channel, NE Atlantic. *Scottish Journal of Geology* 45: 43–57.
- McManus JF, Francois R, Gherardi JM, Keigwin LD, Brown-Leger S. 2004. Collapse and rapid resumption of Atlantic meridional circulation linked to deglacial climate changes. *Nature* 428: 834–837, doi:10.1038/nature02494.
- McManus JF, Oppo DW, Keigwin LD, Cullen JL, Bond GC. 2002. Thermohaline Circulation and Prolonged Interglacial Warmth in the North Atlantic. *Quaternary Research* 58: 17–21.
- McManus JF, Oppo DW, Cullen JL. 2001. ODP 980 Isotope and IRD data. IGBP PAGES/World Data Centre A for Paleoclimatology. Data Contribution Series #2001-065. NOAA Paleoclimatology Programme, Boulder CO, USA.
- McManus JF, Oppo DW, Cullen JL. 1999. 0.5 Million years of millennial-scale climate variability in the North Atlantic. *Science* 283: 971–975.

- McManus JF, Bond GC, Broecker WS, Johnsen S, Labeyrie L, Higgins S. 1994. High-resolution climate records from the North Atlantic during the last interglacial. *Nature* 371: 326–329.
- McMillan AA, Hamblin RJO, Merritt JW. 2010. A lithostratigraphical framework for onshore Quaternary and Neogene (Tertiary) superficial deposits of Great Britain and the Isle of Man. British Geological Survey Research Report, RR/10/03, pp 367.
- McMillan AA, Hamblin RJO, Merritt JW. 2005. An overview of the lithostratigraphical framework for the Quaternary and Neogene deposits of Great Britain (Onshore). British Geological Survey Research Report RR/04/04 pp 38.
- McNichol AP, Jull AJT, Burr GS. 2001. Converting AMS data to radiocarbon values: considerations and conventions. *Radiocarbon* 43: 313-320.
- Meese DA, Gow AJ, Alley RB, Zielinski GA, Grootes PM, Ram M, Taylor KC, Mayewski PA, Bolzan JF. 1997. The Greenland Ice Sheet Project 2 depth-age scale: Methods and results. *Journal of Geophysical Research* 102(C12): 26411-26423.
- Meijer T, Preece RC. 1995 title *In Preece RC (Ed) Island Britain: a Quaternary perspective*. Geological Society Special Publication, London.
- Meland MY, Dokken TM, Jansen E, Hevrøy K. 2008. Water mass properties and exchanges between the Nordic seas and the northern North Atlantic during the period 23-6 ka: Benthic oxygen isotope evidence. *Paleoceanography* 23: PA 1210 doi: 10.1029/2007PA001416.
- Meland MY, Jansen E, Elderfield H. 2005. Constraints on SST estimates for the northern North Atlantic/Nordic Seas during the LGM. *Quaternary Science Reviews* 24: 835-852.
- Merlivat L, Memery L. 1983. Gas exchange across an air-water interface: Experimental results and modelling of bubble contribution to transfer. *Journal of Geophysical Research* 88 (C1): 707
- Merlivat L, Jouzel J. 1979. Global climatic interpretation of the deuterium-oxygen 18 relationship for precipitation. *Journal of Geophysical Research* 84: 5029-2033.
- Merritt JW, Auton CA, Connell ER, Hall AM, Peacock JD. 2003. *Cainozoic geology and landscape evolution of north-east Scotland*. British Geological Survey, Edinburgh. pp 178.
- Meyer MC, Spötl C, Mangini A. 2008. The demise of the Last Interglacial recorded in isotopically dated speleothems from the Alps. *Quaternary Science Reviews* 27: 476-496.
- Milankovitch MM. 1941. Canon of insolation and the ice age problem. *Koniglich Serbische Akademie, Beograd* 133 (English translation by the Israel Programme for Scientific Translations, Jerusalem 1969).
- Miller GH, Sejrup HP, Mangerud J, Andersen BG. 1983. Amino acid ratios in Quaternary molluscs and foraminifera from western Norway: correlation, geochronology and paleotemperature estimates. *Boreas* 12: 107-124.
- Mix AC, Bard E, Schneider R. 2001. Environmental Processes of the Ice Age: Land, Oceans, Glaciers (EPILOG). *Quaternary Science Reviews* 20: 627–658.
- Monges Soares AM. 1993. The ¹⁴C content of marine shells: evidence for variability in coast upwelling off Portugal during the Holocene. *In Isotope Techniques in the study of Past and Current Environmental Changes in the Hydrosphere and Atmosphere*. Proceedings IAEA-SM-329/49, Vienna p 471-485.
- Monnin E, Indermühle A, Dällenbach A, Flückiger J, Stauffer B, Stocker TF, Raynaud D, Barnola J.-M. 2001. Atmospheric CO₂ concentrations over the Last Glacial Termination. *Science* 291: 112-114.

- Muscheler R, Beer J. 2006. Solar forced Dansgaard/Oeschger events? *Geophysical Research Letters* 33: L20706 doi: 10.1029/2006GL026779.
- Müller UC, Kukla GJ. 2004. North Atlantic Current and European environments during the declining stage of the last interglacial. *Geology* 32: 1009-1012.
- Nadeau MJ, Grootes P, Voelker A, Bruhn F, Duhr A, Oriwall A. 2001. Carbonate ^{14}C background: Does it have multiple personalities? *Radiocarbon* 43(2A): 169-176.
- Nadeau MJ, Grootes PM, Schleicher M, Hasselberg P, Rieck A, Bitterling M. 1998. Sample throughput and data quality at the Leibniz-Labor AMS facility. *Radiocarbon* 40: 239-245.
- Nadeau M-J, Schleicher M, Grootes PM, Erlenkeuser H, Gott dang A, Mous DJW, Sarnthein JM, Willkomm H. 1997 The Leibniz-Labor AMS facility at the Christian-Albrechts-University, Kiel, Germany. *Nuclear Instruments and Methods in Physics Research B*123: 22-30.
- Neumann AC, Hearty PJ. 1996. Rapid sea-level changes at the close of the last interglacial (substage 5e) recorded in Bahamian island geology. *Geology* 24: 775-778
- New AL, Smythe-Wright D. 2001. Aspects of the circulation in the Rockall Trough. *Continental Shelf Research* 21: 777-810
- NGRIP members. 2004. High resolution record of Northern Hemisphere climate extending into the last interglacial period. *Nature* 431: 147-151.
- Nielsen T, Rasmussen TL, Ceramicola S, Kuijpers A. 2000. Mapping and sampling glacial and post-glacial sediments on the Faeroe Shelf and slope areas, GEUS Rep. 2000/69, pp. 1 – 23, Geological Survey of Denmark and Greenland, Copenhagen.
- Nürnberg D, Wollenburg I, Dethleff D, Eicken H, Kassens H, Letzig T, Reimnitz E, Thiede J. 1994. Sediments in Arctic sea ice: implications for entrainment, transport and release. *Marine Geology* 119: 185-214.
- Nygård A, Sejrup HP, Haflidason H, Bryn P. 2005. The glacial North Sea fan, southern Norwegian Margin: architecture and evolution from the continental slope to the deepsea basin. *Marine and Petroleum Geology* 22: 71-84.
- Oerlemans J. 2001. *Glaciers and Climate Change*. Balkema Publishers, Amsterdam
- Oerlemans J. 1982. A model of the Antarctic ice sheet. *Nature* 297: 550-553.
- Oeschger H, Siegenthaler U, Schotterer U, Gugelmann A. 1975. A box diffusion model to study the carbon dioxide exchange in nature. *Tellus* 27:168-92.
- Ohkouchi N, Eglinton TI, Hughen K, Roosen E and Keigwin L 2005. Radiocarbon dating of alkenones from marine sediments: III Influence of solvent extraction procedures on ^{14}C measurements of foraminifera *Radiocarbon* 47(3): 425-432.
- Olsen L. 1988. Stadials and interstadials during the Weichselian glaciation on Finnmarksvidda, northern Norway. *Boreas* 17: 517-541.
- Olsen L, Mejdal V, Selvik SF. 1996 Middle and Late Pleistocene stratigraphy, chronology and glacial history in Finnmark, North Norway. *Norges Geologiske Undersøkelse Bulletin* 429: 1-111.
- Oppo DW, Lehman SJ. 1995. Suborbital timescale variability of North Atlantic deep water during the past 200,000 years. *Paleoceanography* 10: 901-910.
- Oppo DW, Lehmann SJ. 1993. Mid-depth circulation of the subpolar North Atlantic during the Last Glacial Maximum. *Science* 259: 1148-1152.

- Oppo DW, McManus JF, Cullen JL. 2006. Evolution and demise of the Last Interglacial warmth in the subpolar North Atlantic. *Quaternary Science Reviews* 25: 3268–3277.
- Oppo DW, Keigwin LD, McManus JF, Cullen JL. 2001. Persistent suborbital climate variability in marine isotope stage 5 and Termination II. *Paleoceanography* 16: 280-292.
- Oppo DW, Horowitz M, Lehman SJ. 1997. Marine core evidence for reduced deep water production during Termination II followed by a relatively stable substage 5e (Eemian). *Paleoceanography* 12: 51–63.
- Orvik KA, Niiler P. 2002. Major pathways of Atlantic water in the northern North Atlantic and Nordic Seas toward Arctic. *Geophysical Research Letters* 29: 1896, doi:10.1029/2002GL015002.
- Orszag-Sperber F, Plaziat JC, Baltzer F, Purser BH. 2001. Gypsum salina-coral reef relationships during the Last Interglacial (Marine Isotopic Stage 5e) on the Egyptian Red Sea coast: a Quaternary analogue for Neogene marginal evaporites? *Sedimentary Geology* 140: 61-85.
- Otterå OH, Drange H. 2004. Effects of solar irradiance forcing on the ocean circulation of the North Atlantic in an isopycnic coordinate OGCM. *Dynamic Meteorology and Oceanography Tellus Series A* 56: 154-166.
- Otto-Bliesner et al 2006. Simulating Arctic climate warmth and icefield retreat in the last interglaciation. *Science* 311: 1751-1753.
- Overpeck JT, Otto-Bliesner BL, Miller GH, Muhs DR, Alley RB, Kiehl JT. 2006. Paleoclimatic Evidence for Future Ice-Sheet Instability and Rapid Sea-Level Rise. *Science* 311: 1747-1750.
- Parnell J, Bowden S, Andrews JT, Colin T. 2007. Bioindicator determination as a provenance tool for detrital carbonate events (Heinrich events?): fingerprinting Quaternary glacial sources into Baffin Bay. *Earth and Planetary Science Letters* 257: 71-82.
- Parren JG, Potter JR. 1984. Isotopic Tracers in Polar Seas and Glacier Ice. *Journal of Geophysical Research* 89: 749-750.
- Parrenin, F, Paillard D. 2003. Amplitude and phase of glacial cycles from a conceptual model. *Earth and Planetary Science Letters* 214: 243-250.
- Parrenin F, Barnola JM, Beer J, Blunier T, Castellano E, Chappellaz J, Dreyfus G, Fischer H, Fujita S, Jouzel J, Kawamura K, Lemieux-Dudon B, Loulergue L, Masson-Delmotte V, Narcisi B, Petit JR, Raisbeck G, Raynaud D, Ruth U, Schwander J, Severi M, Spahni R, Steffensen JP, Svensson A, Udisti R, Waelbroeck C, Wolff E. 2007. The EDC3 chronology for the EPICA Dome C ice core. *Climate of the Past* 3: 485–497.
- Paterson WSB. 1994. *The Physics of Glaciers*, 3rd edition. Pergamon, Oxford.
- Pawley SM, Bailey RJJ, Moorlock BSP, Hamblin RJO, Booth SJ, Lee JR. 2008. Age limits on Middle Pleistocene glacial sediments from OSL dating, North Norfolk, UK. *Quaternary Science Reviews* 27: 1363-1377.
- Payne A, Sugden D. 1990a. Climate and the initiation of maritime ice sheets. *Annals of Glaciology* 14: 232-237.
- Payne A, Sugden D. 1990b. Topography and ice sheet growth. *Earth Surface Processes and Landforms* 15: 625-639.
- Peck VL. 2006. Millennial-scale ice-ocean-climate variability during the last glacial: High-resolution records from the NE Atlantic. *PhD Thesis*, Cardiff University.

- Peck VL, Hall IR, Zahn R, Grousset F, Hemming SR, Scourse JD. 2007. The relationship of Heinrich events and their European precursors over the past 60ka BP: a multi-proxy ice rafted debris provenance study in the North East Atlantic. *Quaternary Science Reviews* 26: 862–875.
- Peck VL, Hall IR, Elderfield H, Grousset F, Hemming SR, Scourse JD. 2006. High resolution evidence for linkages between NW European ice sheet instability and Atlantic Meridional Overturning Circulation. *Earth and Planetary Science Letters* 243: 476–488.
- Peltier WR. 2005. On the hemispheric origins of meltwater pulse 1A. *Quaternary Science Reviews* 24: 1655–1671.
- Peltier WR. 2002. On eustatic sea level history: Last Glacial Maximum to the Holocene. *Quaternary Science Reviews* 21: 1–8.
- Peltier WR. 1994. Ice age paleotopography. *Science* 265: 195–201.
- Peltier WR, Fairbanks RG. 2006. Global glacial ice volume and Last Glacial Maximum duration from an extended Barbados sea level record. *Quaternary Science Reviews* 25: 3322–3337.
- Peltier WR, Marshall S. 1995. Coupled energy-balance/ice-sheet model simulations of the glacial cycle: a possible connection between terminations and terrigenous dust. *Journal of Geophysical Research* 100(D7): 14269–14289.
- Peltier WR, Vettoretti G, Stastna M. 2006. Atlantic meridional overturning and climate response to Arctic Ocean freshening. *Geophysical Research Letters* 33: L06713 doi: 10.1029/2005GL025251.
- Penaud A, Eynaud F, Turon JL, Zaragosi S, Malizé B, Toucanne S, Bourillet JF. 2009. What forced the collapse of European ice sheets during the last two glacial periods (150 ka B.P. and 18 ka cal. B.P.)? Palynological evidence. *Palaeogeography, Palaeoclimatology, Palaeoecology* 281: 66–78.
- Peters C, Austin WEN, Walden J, Hibbert FD. 2010. Magnetic characterisation and correlation of a Younger Dryas tephra in North Atlantic marine sediments. *Journal of Quaternary Science* 25: 339–347.
- Peters C, Walden J, Austin WEN. 2008. Magnetic signature of European margin sediments: Provenance of ice-rafted debris and the climatic response of the British ice sheet during Marine Isotope Stages 2 and 3. *Journal of Geophysical Research* 113: F03007 doi:10.1029/2007JF000836.
- Petit JR, Jouzel J, Raynaud D, Barkov NI, Barnola JM, Basile I, Bender M, Chappellaz J, Davis M, Delaygue G, Delmotte M, Kotlyakov VM, Legrand M, Lipenkov VY, Lorius C, Pepin L, Ritz C, Saltzman E, Stievenard M. 1999. Climate and atmospheric history of the past 420,000 years from the Vostok ice core, Antarctica. *Nature* 399: 429–436.
- Pflaumann U, Sarnthein M, Chapman MR, d'Abreu L, Funnell B, Huels M, Kiefer T, Maslin M, Schulz H, Swallow J, van Kreveland S, Vautravers M, Vogelsang E, Weinelt M. 2003. Glacial North Atlantic: sea-surface conditions reconstructed by GLAMAP 2000. *Paleoceanography* 18(3): 1065, doi:10.1029/2002PA000774.
- Pflaumann U, Duprat J, Pujol C, Labryrie LD. 1996. SIMMAX: A modern analogue technique to deduce Atlantic sea surface temperatures from planktonic foraminifera in deep-sea sediments. *Paleoceanography* 11: 15–35.
- Pisais NG, Martinson DG, Moore TC Jr, Shackleton NJ, Prell W, Hays J, Boden G. 1984. High resolution stratigraphic correlation of benthic oxygen isotopic records spanning the last 300,000 years. *Marine Geology* 56: 119–136.

- Potts PJ, Thompson M, Wilson S. 2002. G-Probe-1: an international proficiency test for microprobe laboratories – report on round 1: February 2002 (TB-1 Basaltic Glass). *Geostandards Newsletter: Journal of Geostandards and Geoanalysis* 26: 197–235.
- Powell RD. 1984. Glacimarine processes and inductive lithofacies modelling of ice shelf and tidewater glacier sediments based on Quaternary examples. *Marine Geology* 57: 1-52.
- Powell RD. 1981. A model for sedimentation by tidewater glaciers. *Annals of glaciology* 2: 129-134.
- Pratje O 1952. Die Erfahrungen bei der Gewinnung von rezenten, marinen sedimenten in den letzten 25 jahren. Mitt. Geogr. Ges. Hamb. 1:118-197 In Ross DA, Riedel WR 1967. Comparison of upper parts of some piston cores with simultaneously collected open-barrel cores. *Deep-Sea Research* 14: 285-294.
- Rahmstorf S. 2003. Timing of abrupt climate change: a precise clock. *Geophysical Research Letters* 30: 1510.
- Rahmstorf S. 1994. Rapid climate transitions in a couple ocean atmosphere model. *Nature* 372:82–85.
- Rappol M, Haldorsen S, Jørgensen P, van der Meer JJM, Stoltenberg HMP. 1989. Composition and origin of petrographically-stratified thick till in the Northern Netherlands and a Saalian glaciation model for the North Sea basin. *Mededelingen van de Werkgroep voor Tertiaire en Kwartaire Geologie* 26: 31-64.
- Rasmussen SO, Seierstad IK, Andersen KK, Bigler M, Dahl-Jensen D, Johnsen SJ. 2008. Synchronisation of the NGRIP, GRIP and GISP2 ice cores across MIS 2 and Palaeoclimatic implications. *Quaternary Science Reviews* 27: 18-28.
- Rasmussen SO, Andersen KK, Svensson AM, Steffensen JP, Vinther BM, Clausen HB, Siggaard-Andersen M-L, Johnsen SJ, Larsen LB, Dahl-Jensen D, Bigler M, Röthlisberger R, Fischer H, Goto-Azuma K, Hansson ME, Ruth U. 2006. A new Greenland ice core chronology for the last glacial termination, *Journal of Geophysical Research* 111: D06102, doi:10.1029/2005JD006079.
- Rasmussen TL, Wastegård S, Kuijpers A, van Weering TCE, Heinemeier J, Thomsen E. 2003. Stratigraphy and distribution of tephra layers in marine sediment cores from the Faeroe Islands, North Atlantic. *Marine Geology* 199: 263 – 277.
- Rasmussen TL, Thomsen E. 2008. Warm Atlantic surface water inflow to the Nordic seas 34-10 calibrated ka B.P. *Paleoceanography* 23: PA1201, doi:10.1029/2007PA001453.
- Rasmussen TL, Thomsen E, Kuijpers A, Wastegård S. 2003. Late warming and early cooling of the sea surface in the Nordic seas during MIS 5e (Eemian Interglacial). *Quaternary Science Reviews* 22: 809-821.
- Rasmussen TL, Oppo DW, Thomsen E, Lehman SJ. 2003b. Deep sea records from the southeast Labrador Sea: Ocean circulation changes and ice-rafting events during the last 160,000 years. *Paleoceanography* 18: 1018 doi: 10.1029/2001PA000736.
- Rasmussen TL, Balbon E, Thomsen E, Labeyrie L, van Weering TCE. 1999. Climate records and changes in deep outflow from the Norwegian Sea ~150-155 ka. *Terra Nova* 11: 60-61.
- Raymo ME. 1997. The timing of major climate transitions. *Paleoceanography* 12: 577-585.
- Raymo ME, Nisancioglu K. 2003. The 41 kyr world: Milankovitch's other unsolved mystery. *Paleoceanography* 18: 1011.
- Raymo ME, Oppo DW, Flower BP, Hodell DA, McManus JF, Venz KA, Kleiven KF, McIntyre K. 2004. Stability of North Atlantic water masses in face of pronounced climate variability during the Pleistocene. *Paleoceanography* 19, PA2008. doi:10.1029/2003PA000921.

- Reeh N. 1968. On the calving of ice from floating glaciers and ice shelves. *Journal of Glaciology* 7: 215–232.
- Reimer P, Reimer R. 2010. Marine Reservoir Correction database. www.radiocarbon.pa.qub.ac.uk.
- Reimer PJ, Baillie MGL, Bard E, Bayliss A, Beck JW, Blackwell PG, Bronk Ramsey C, Buck CE, Burr GS, Edwards RL, Friedrich M, Grootes PM, Guilderson TP, Hajdas I, Heaton TJ, Hogg AG, Hughen KA, Kaiser KF, Kromer B, McCormac FG, Manning SW, Reimer RW, Richards DA, Southon JR, Talamo S, Turney CSM, van der Plicht J, Weyhenmeyer CE. 2009. IntCal09 and Marine09 Radiocarbon age calibration curve, 0-50,000 years cal BP. *Radiocarbon* 51: 1111-1150.
- Revel M, Sinko JA, Grousset FE, Biscaye PE. 1996. Sr and Nd isotopes as tracers of North Atlantic lithic particles: Paleoclimatic implications. *Paleoceanography* 11: 95-113.
- Reynolds LA, Thunell RC. 1986. Seasonal production and morphologic variation of *Neogloboquadrina pachyderma* (Ehrenberg) in the northeast Pacific. *Micropalaeontology* 32: 1-18, doi:10.2307/1485696.
- Riccio A, Riggio F, Romano P. 2001. Sea level fluctuations during Oxygen Isotope Stage 5: new data from fossil shorelines in the Sorrento Peninsula (Southern Italy). *Zeitschrift für Geomorphologie* 45: 121-137.
- Richards AF 1961. Investigations of deep-sea sediment cores: 1. Shear strength, bearing capacity and consolidation. *Technical Report of Hydrographic Office, Washington* 63: 70 In Ross DA, Riedel WR 1967. Comparison of upper parts of some piston cores with simultaneously collected open-barrel cores. *Deep-Sea Research* 14: 285-294.
- Rickaby REM, Elderfield H. 2005. Evidence from the high-latitude North Atlantic for variations in Antarctic Intermediate water flow during the last deglaciation. *Geochemistry Geophysics Geosystems* 6: Q05001. doi:10.1029/2004GC000858.
- Rignot E. 1996. Tidal motion, ice velocity and melt rate of Petermann Gletscher, Greenland, measured from radar interferometry. *Journal of Glaciology* 42(142): 476-485.
- Risebrobakken BR, Dokken T, Otterå OH, Jansen E, Gao Y, Drange H. 2007. Inception of the Northern European ice sheet due to contrasting ocean and insolation forcing. *Quaternary Research* 67: 128– 1135.
- Risebrobakken BR, Dokken T, Jansen E. 2005. The extent and variability of the meridional Atlantic circulation in the Nordic Seas during marine isotope stage 5 and its influence upon the inception of the last glacial. In Drange H, Dokken T, Furevik T, Gerdes R, Berger WH (Eds) *The Nordic Seas: An Integrated Perspective*. AGU Geophysical Monograph 158, pp 323-339.
- Robinson M, Ballantyne CK. 1979. Evidence for a glacial readvance pre-dating the Loch Lomond Advance in Wester Ross. *Scottish Journal of Geology* 15, 271–277.
- Roche D, Paillard D. 2005. Modelling the oxygen-18 and rapid glacial climatic events: a data-model comparison. *CRAS Géosciences* 337: 928-934.
- Rohling EJ. 2000. Paleosalinity: confidence limits and future applications. *Marine Geology* 163: 1-11.
- Rohling EJ, Bigg GR. 1998. Paleosalinity and $\delta^{18}\text{O}$: A critical assessment. *Journal of Geophysical Research C: Oceans* 103: 1307-1318.
- Rohling EJ, Grant K, Bolshaw M, Roberts AP, Siddall M, Hemleben C, Kucera M. 2009. Antarctic temperature and global sea level closely coupled over the past five glacial cycles. *Nature Geoscience* 2: doi: 10.1038/NGEO0557.

- Rohling EJ, Grant K, Hemleben Ch, Siddal M, Hoogakker BAA, Bolshaw M, Kucera M. 2008. High rates of sea-level rise during the last interglacial period. *Nature GeoScience* 1: 38–42.
- Rolfe WDI. 1966. Woolly rhinoceros from the Scottish Pleistocene. *Scottish Journal of Geology* 2: 253–258.
- Rose J. 1989. Stadial type sections in the British Quaternary. In Rose J, Schlüchter C. (Eds). *Quaternary Type Sections: Imagination or Reality?* Balkema, Rotterdam.
- Rose J. 1981. Field guide to the Quaternary geology of the south-eastern part of the Loch Lomond basin. *Proceedings of the Geological Society of Glasgow* 122/123: 12–28.
- Rose J, Lowe JJ, Switsur R. 1988. A radiocarbon date on plant detritus beneath till from the type area of the Loch Lomond Readvance. *Scottish Journal of Geology* 24: 113–124.
- Rothwell RG 2006 *New Techniques in Sediment Core Analysis*. Geological Society, London, *Special Publications* 267: 51-63.
- Rothwell RG, Hoogakker B, Thomson J, Crowdace IW, Frenz M. 2006. Turbidite emplacement on the southern Balearic Abyssal Plain (western Mediterranean Sea) during Marine Isotope Stages 1–3: an application of ITRAX XRF scanning of sediment cores to lithostratigraphic analysis. In *New Techniques in Sediment Core Analysis*, Rothwell RG (ed.). Special Publication 267, Geological Society: London; 78–98.
- Ruddiman WF. 1977. Late Quaternary deposition of ice rafted sand in the sub-polar North Atlantic (lat 40° to 65°). *Geological Society of America Bulletin* 88: 1813–1821.
- Ruddiman WF, Glover LK. 1982. Mixing of volcanic ash zones in subpolar North Atlantic sediments. In *The Ocean Floor*, Scutton RA, Talwani M (eds). John Wiley & Sons Ltd.: 37–61.
- Ruddiman WF, Glover LK. 1972. Vertical mixing of ice -rafted volcanic ash in North Atlantic sediments. *Geological Society American Bulletin* 83: 2817–2836.
- Ruddiman WF, McIntyre A. 1981. The North Atlantic Ocean during the last deglaciation. *Palaeogeography, Palaeoclimatology, Palaeoecology* 35: 145-214.
- Ruddiman WF, McIntyre A. 1979. Warmth of the sub-polar North-Atlantic ocean during northern hemisphere ice-sheet growth. *Science* 204: 173-175.
- Ruddiman WF, Mix AC. 1993. The North and Equatorial Atlantic at 9000 and 6000 yr BP In *Global Climates Since the Last Glacial Maximum* Wright HEJ (ed) University of Minneapolis Press, Minneapolis.
- Ruddiman WF, Wright HE. 1987. North America and adjacent oceans during the last deglaciation. *The geology of North America*, vol. K-3, Geological Society of America.
- Ruddiman, WF, Molfino B, Esmay A, Pokras E. 1980. Evidence bearing on the mechanism of rapid deglaciation. *Climate Change* 3: 65-87.
- Sánchez-Goñi MF, Loutre MF, Crucifix M, Peyron O, Santol L, Duprat J, Malaizé, Turon JL, Peyrouquet JP. 2005. Increasing vegetation and climate gradient in Western Europe over the last glacial inception (122-110 ka): data model comparison. *Earth and Planetary Science Letters* 231: 111-130.
- Sánchez-Goñi MF, Eynaud F, Turon JL, Shackleton NJ. 1999. High resolution palynological record off the Iberian margin: direct land-sea correlation for the Last Interglacial complex. *Earth and Planetary Science Letters* 171: 123-137.

- Sarnthein M, Grootes PM, Kennett JP, Nadeau MJ. 2007. ^{14}C reservoir ages show deglacial changes in ocean currents and carbon cycle. In Schmittner A, Chiang J, Hemming S (eds) *Ocean Circulation: Mechanisms and Impacts*. American Geophysical Union. p175-196.
- Schmidt GA. 1999. Error analysis of palaeosalinity calculations. *Paleoceanography* 3: 307-334.
- Schrag DP, Adkins JF, McIntyre K, Alexander JL, Hodell DA, Charles CD, McManus JF. 2002. The oxygen isotope composition of seawater during the Last Glacial Maximum. *Quaternary Science Reviews* 21: 331-342.
- Schrag DP, Hampt G, Murray DW. 1996. Pore fluid constraints on the temperature and oxygen isotopic composition of the glacial ocean. *Science* 272: 1930-1932.
- Schiebel R, Bijma J, Hemleben C. 1997. Population dynamics of the planktic foraminifer *Globigerina bulloides* from the eastern North Atlantic. *Deep-Sea Research* 44: 1701-1713.
- Schleicher M, Grootes PM, Nadeau MJ and Schoon A 1998 The Carbonate ^{14}C background and its components at the Leibniz AMS Facility *Radiocarbon* 40(1): 85-93.
- Schmidt GA, Mulitza S. 2002. Global calibration of ecological models for planktic foraminifera from coretop carbonate oxygen-18. *Marine Micropaleontology* 44: 125-140.
- Schmidt MW, Vautravers MJ, Spero HJ. 2006. Rapid subtropical North Atlantic salinity oscillations across Dansgaard-Oeschger cycles. *Nature* 443: 561-564 doi:10.1038/nature05121.
- Schmidt MW, Spero HJ, Lea DW. 2004. Links between salinity variation in the Caribbean and North Atlantic circulation. *Nature* 428: 160-163, doi:10.1038/nature02346.
- Schulz KG, Zeebe RE. 2006. Pleistocene glacial terminations triggered by synchronous changes in Southern and Northern Hemisphere insolation: the insolation canon hypothesis. *Earth and Planetary Science Letters* 249: 326-336.
- Schwander J, Sowers T, Barnola JM, Blunier T, Fuchs A, Malaize B. 1997. Age scale of the air in the summit ice: Implication for glacial-interglacial temperature change. *Journal of Geophysics* 102: 19483-19493
- Scourse JD, Haapaniemi AI, Colmenero-Hidalgo E, Peck VL, Hall IR, Austin WEN, Knutz PC, Zahn R. 2009. Growth, dynamics and deglaciation of the last British-Irish ice sheet: the deep sea ice-rafted debris record. *Quaternary Science Reviews* 28: 3066-3084
- Scourse JD, Hall IR, McCave IN, Young JR, Sugdon C. 2000. The origin of Heinrich layers: evidence from H₂ for European precursor events. *Earth and Planetary Science Letters* 182: 187-195.
- Seager R, Battisti DS. 2005. Challenges to our understanding of the general circulation: abrupt climate change. In Schneider T, Sobel A (Eds). *The General Circulation of the Atmosphere*. Princeton University Press.
- Seidenkrantz MS, Kristensen P, Knudsen KL. 1995. Marine evidence for climate instability during the last interglacial in shelf records from northwest Europe. *Journal of Quaternary Science* 10: 77-82.
- Sejrup HP, Nygård A, Hall AM, Haflidason H. 2009. Middle and Late Weichselian (Devensian) glaciation history of south-western Norway, North Sea and eastern UK. *Quaternary Science Reviews* 28: 370-380.
- Sejrup HP, Hjelstuen BO, Dahlgren KIT, Haflidason H, Kuijpers A, Nygård A, Praeg D, Stoker MS, Vorren TO. 2005. Pleistocene glacial history of the NW European continental margin. *Marine and Petroleum Geology* 22: 1111-1129.

- Sejrup HP, Larsen E, Landvik J, King EL, Hafliðason H, Nesje A. 2000. Quaternary glaciations in southern Fennoscandia: evidence from southwestern Norway and the northern North Sea region. *Quaternary Science Reviews* 19: 667–685.
- Sejrup HP, Aarseth I, Hafliðason H, Løvlie R, Bratten A, Tjostheim G, Forsberg CF, Ellingsen KL. 1995. Quaternary of the Norwegian Channel: glaciation history and palaeoceanography. *Norges Geologiske Tidsskrift* 75: 1-28.
- Sejrup HP, Hafliðason H, Aarseth I, Forsberg CF, King E, Long D, Rokoegen K. 1994. Late Weichselian glaciation history of the northern North Sea. *Boreas* 23: 1–13.
- Sejrup HP, Aarseth I, Hafliðason H. 1991. The Quaternary succession in the northern North Sea. *Marine Geology* 101: 103–111.
- Sejrup HP, Aarseth KL, Ellingsen KL, Reither E, Jansen E, Løvlie R, Bent A, Brigham-Grette J, Larsen E, Stoker MS. 1987. Quaternary Stratigraphy of the Fladen area, central North Sea: a multidisciplinary study. *Journal of Quaternary Science* 2: 35–58.
- Seilacher A. 1991. Events and their signatures – an overview. In Einsele G, Ricken W, Seilacher A (Eds) *Cycles and Events in Stratigraphy*. Springer, Berlin pp 222-226.
- Sevastopulo GD. 1981. Lower Carboniferous In Holland CH (ed) *A Geology of Ireland*, Scottish Academy, Edinburgh, UK. pp147-171.
- Shackleton NJ. 1995. New data on the evolution of Pliocene climate variability. In Paleoclimate and Evolution, with Emphasis on Human Origins, Virba ES, Denton GH, Partridge TC, Burckle LH (eds). Yale University Press: 242–248.
- Shackleton NJ. 1977. Oxygen Isotope Stratigraphic Record of Late Pleistocene. *Philosophical Transactions of The Royal Society Of London Series B* 280: 169-182.
- Shackleton NJ. 1974. Attainment of isotopic equilibrium between ocean water and benthonic foraminifera genus *Uvigerina*: isotopic changes in the ocean during the last glacial. In Les Methodes Quaintitatives d'Etude des Variations du Climat au Cours du Pleistocene, Centre National de la Rech Scientific, Gif-sur-Yvette. Pp 203-209.
- Shackleton NJ. 1967. Oxygen isotope analysis and Pleistocene temperature reassessed. *Nature* 215: 15-17.
- Shackleton NJ, Opdyke ND. 1973. Oxygen isotope and palaeomagnetic stratigraphy of equatorial Pacific core V28-238: oxygen isotope temperature and global ice volumes on a 10^5 year and 10^6 year scale. *Quaternary Research* 3: 39–55.
- Shackleton NJ, Fairbanks RG, Chiu TC, Parrenin F. 2004. Absolute calibration of the Greenland time scale: implications for Antarctic time scales and for $\Delta^{14}\text{C}$. *Quaternary Science Reviews* 23: 1513-1522.
- Shackleton NJ, Sánchez-Goñi MF, Paillet D, Lancelot Y. 2003. Marine Isotope Substage 5e and the Eemian Interglacial. *Global and Planetary Change* 36: 151-155.
- Shackleton NJ, Chapman M, Sanchez-Goni MF, Paillet D, Lancelot Y. 2002. The classic marine isotope stage substage 5e. *Quaternary Research* 58: 14–16.
- Shackleton NJ, Hall MA, Vincent E. 2000. Phase relationships between millennial scale events 64,000 to 24,000 years ago. *Paleoceanography* 15: 565–569.
- Shin SI, Liu Z, Otto-Bliesner B, Brady EC, Kutzbach JE, Harrison SP. 2003. A Simulation of the Last Glacial Maximum climate using the NCAR-CCSM. *Climate Dynamics* 20: 127-151.

- Shulz M. 2002. On the 1,470-year pacing of Dansgaard-Oeschger warm events. *Paleoceanography* 17: 1014, doi 10.1029/2000PA000571.
- Shulz KG, Zeebe RE. 2006. Pleistocene glacial terminations triggered by synchronous changes in Southern and Northern Hemisphere insolation: The insolation canon hypothesis. *Earth and Planetary Science Letters* 249: 326-336.
- Siddall M, Rohling EJ, Thompson WG, Waelbroeck C. 2008. MIS 3 sea level fluctuations: data synthesis and new outlook. *Review of Geophysics* 46: RG4003.
- Siddall M, Bard E, Rohling EJ, Hemleben C. 2006. Sea-level reversal during Termination II. *Geology* 34: 817-820.
- Siddall M, Rohling EJ, Almogi-Labin A, Hemleben C, Meischner D, Schmelzer I, Smeed DA. 2006b. Red Sea Level Reconstruction. IGBP PAGES/World Data Centre for Paleoclimatology. Data Contribution Series ~2006-063. NOAA/NCDC Paleoclimatology Program, Boulder, Colorado, USA.
- Siddall M, Rohling EJ, Almogi-Labin A, Hemleben C, Meischner D, Schmelzer I, Smeed DA. 2003. Sea-level fluctuations during the last glacial cycle. *Nature* 422: 853-857.
- Sigurdsson H, McIntosh WC, Dunbar N, Lacasse C, Carey SN. 1998. Thørmörk ignimbrite in Iceland: Possible source of North Atlantic Ash Zone 2. EOS transactions, AGU, Spring meeting supplement. 79: S377.
- Siegert MJ, Dowdeswell JA, Hald M, Svendsen JI. 2001. Modelling the Eurasian Ice Sheet through a full (Weichselian) glacial cycle. *Global and Planetary Change* 31: 367-385.
- Singarayer JS, Richards DA, Ridgwell A, Valdes PJ, Austin WEN, Beck JW. 2008. An oceanic origin for the increase of atmospheric radiocarbon during the Younger Dryas. *Geophysical Research Letters* 35: L14707, doi: 10.1029/2008GL034074.
- Singer BS, Guillou H, Jicha BR, Laj C, Kissel C, Beard BL, Johnson CM. 2009. $^{40}\text{Ar}/^{39}\text{Ar}$, K-Ar and ^{230}Th - ^{238}U dating of the Laschamp excursion: a radioisotopic tie-point for ice core and climate chronologies. *Earth and Planetary Science Letters* 286(1-2): 80-88.
- Skinner AC, McElvanney E, Ruckley N, Rise L, Rokoengen K. 1986. *1:250,000 Offshore Regional Geology Maps: Cormorant: Quaternary*. HMSO for the British Geological Survey, London.
- Skinner LC. 2008. Revisiting the absolute calibration of the Greenland ice-core age-scales *Climate of the Past* 4: 295-302.
- Skinner LC, Shackleton NJ. 2006. Deconstructing Terminations I and II: Revisiting the glacioeustatic paradigm based on deep-water temperature estimates. *Quaternary Science Reviews* 25: 3312-3321.
- Skinner LC, Shackleton N.J. 2005. An Atlantic lead over Pacific deep-water change across Termination I: Implications for the application of the marine isotope stage stratigraphy. *Quaternary Science Reviews* 24: 571-580.
- Skinner LC, McCave IN. 2003. Analysis and modelling of gravity and piston coring based on soil mechanics. *Marine Geology* 199: 181-204.
- Slatt RM, Eyles N. 1981. Petrology of glacial sand: implications for the origin and mechanical durability of lithic fragments. *Sedimentology* 28: 171-183.
- Smith AJ. 1985. A catastrophic origin for the paleovalley system of the eastern English Channel. *Marine Geology* 64: 65-75.

- Snoeckx H, Grousset FE, Revel M, Boelaert A. 1999. European contribution of ice-rafted sand to Heinrich layers H3 and H4. *Marine Geology* 158: 197-208.
- Southon J. 2004. A radiocarbon perspective on Greenland ice-core chronologies: Can we use ice cores for ^{14}C calibration? *Radiocarbon* 46; 1239-1259.
- Spahni R, Chappellaz J, Stocker TF, Loulergue L, Hausammann G, Kawamura K, Flückiger J, Schwander J, Raynaud D, Masson-Delmotte V, Jouzel J. 2005. Atmospheric methane and nitrous oxide of the Late Pleistocene from Antarctic ice cores. *Science* 310: 1317– 1321.
- Spero HJ, Lee DL. 1996. Experimental determination of stable isotope variability in *Globigerina bulloides*: implications for paleoceanographic reconstructions. *Marine Micropaleontology* 28: 231-246.
- Spero HJ, Lee DL. 1993. Intraspecific stable isotope variability in the planktic foraminifera *Globigerinoides sacculifer*: Results from laboratory experiments. *Marine Micropaleontology* 22: 221-234.
- Spero HJ, Bijma J, Lea DL, Bemis BE. 1997. Effect of seawater carbonate concentration on foraminiferal carbon and oxygen isotopes. *Nature* 390: 497-500.
- Spielhagen RF, Erlenkheuser H, Siegert C. 2005. History of freshwater runoff across the Laptev Sea (Arctic) during the last deglaciation. *Global Planetary Change* 48: 187-207.
- Spötl C, Holzschläger S, Mangini A. 2007. The Last and the Penultimate Interglacial as recorded by speleothems from a climatically sensitive high-elevation cave site in the Alps. In Sirocko F, Claussen M, Litt T, Sánchez-Goni MF(Eds) *The Climate of Past-Interglacials*. Developments in Quaternary Science Series, Elsevier, vol 7, pp. 471–491.
- St John K, Flower BP, Krissek L. 2004. Evolution of iceberg melting, biological productivity and the record of Icelandic volcanism in the Irminger Basin since 630 ka. *Marine Geology* 212: 133-152.
- Stanford JD, Rohling EJ, Huntr SE, Roberts AP, Rasmussen SO, Bard E, McManus J, Fairbanks RG. 2006. Timing of meltwater pulse 1a and climate responses to meltwater injections. *Paleoceanography* 21: PA4123, doi: 10.1029/2006PA001340.
- Steig EJ. 2006. Climate change: The south-north connection. *Nature* 444: 152-153.
- Stein M, Wasserburg GJ, Aharon P, Chen JH, Zhu ZR, Bloom A, Chappell J. 1993. TIMS U-series dating and stable isotopes of the last interglacial event in Papua New Guinea. *Geochimica et Cosmochimica Acta* 57: 2541–2554.
- Stirling Ch, Esat TM, Lambeck K, McCulloch MT. 1998. Timing and duration of the Last Interglacial: evidence for a restricted interval of widespread coral reef growth. *Earth and Planetary Science Letters* 160: 745-762.
- Stirling CH, Esat TM, McCulloch MT, Lambeck K. 1995. High-precision U-series dating of corals from Western Australia and implications for the timing and duration of the Late Interglacial. *Earth and Planetary Science Letters* 135: 115–130.
- Stocker TF, Johnsen SJ. 2003. A minimum thermodynamic model for the bipolar seesaw. *Paleoceanography* 18:1087 doi:10.1029/2003PA000920.
- Stocker TF, Wright DG. 1998. The effect of a succession of ocean ventilation changes on ^{14}C . *Radiocarbon* 40: 359-366.
- Stoker MS. 1997. Mid- to late Cenozoic sedimentation on the continental margin off NW Britain. *Journal of the Geological Society of London* 154: 509-515.

- Stoker MS. 1995. The influence of glacial sedimentation on slope-apron development on the continental margin off Northwest Britain. *Journal of the Geological Society of London* 90: 159–177.
- Stoker MS. 1990. Glacially-influenced sedimentation of the Hebridean slope, northwestern United Kingdom continental margin. In *Glacio-marine Environments: Processes and Sediments*, Dowdeswell JA, Scourse JD (eds). Special Publication 53. Geological Society: London; 349–362.
- Stoker MS, Bradwell T. 2005. The Minch palaeo-ice stream, NW sector of the British–Irish Ice Sheet. *Journal of the Geological Society of London* 162: 425–428.
- Stoker MS, Leslie AB, Scott WD, Briden JC. 1994. A record of late Cenozoic stratigraphy, sedimentation and climatic change from the Hebrides Slope, NE Atlantic Ocean. *Journal of the Geological Society, London* 151: 235–249.
- Stoker MS, Hitchen K, Graham CC. 1993. United Kingdom Offshore Report: *The Geology of the Hebrides and West Shetland Shelves and Adjacent Deep-water Areas*. HMSO for the British Geological Survey, London.
- Stolz K, Baumann K-H. 2010 (in press). Changes in palaeoceanography and palaeoecology during Marine Isotope Stage (MIS) 5 in the eastern North Atlantic (ODP Site 980) deduced from calcareous nannoplankton observation., *Palaeogeography* doi: 10.1016/j.palaeo.2010.04.002.
- Stone JO, Ballantyne CK. 2006. Dimensions and deglacial chronology of the Outer Hebrides Ice Cap, northwest Scotland: implications of cosmic ray exposure dating. *Journal of Quaternary Science* 21: 75–84.
- Stone JO, Ballantyne CK, Fifield LK. 1998. Exposure dating and validation of periglacial weathering limits, northwest Scotland. *Geology* 26: 587–590.
- Strain PM, Tan FC 1993. Seasonal Evolution of Oxygen Isotope-Salinity Relationships in High-Latitude Surface Waters *Journal of Geophysical Research* 98: 14589–14598.
- Stuiver M, Braziunas TF. 1993. Modelling atmospheric ^{14}C influences and ^{14}C ages of marine samples to 10,000 BC. *Radiocarbon* 35(1):137–89.
- Stuiver M, Grootes PM, Braziunas TF. 1995. The GISP2 $\delta^{18}\text{O}$ climate record of the past 16,500 years and the role of the sun, ocean and volcanoes. *Quaternary Research* 44: 341–354.
- Stow DAV, Bowen AJ. 1980. A physical model for the transport and sorting of fine-grained sediments by turbidity currents. *Sedimentology* 27: 31–46.
- Sutcliffe AJ. 1995. title In Preece RC (Ed) *Island Britain: a Quaternary perspective*. Geological Society Special Publication, London.
- Sutherland DG. 1999. Scotland. In Bowen DQ (Ed). *A Revised Correlation of Quaternary Deposits in the British Isles*. Geological Society Special Report No. 23. The Geological Society, Bath, pp. 99–114.
- Svendsen J I, Alexanderson H, Astakhov VI, Demidov I, Dowdeswell JA, Funder S, Gataullin V, Henriksen M, Hjort C, Houmark-Nielsen M, Hubberten HW, Ingólfsson O´, Kakobsson M, Kjær KH, Larsen E, Lokrantz H, Lunkka JP, Lysa´ A, Mangerud J, Matiouchkov A, Murray A, Möller P, Niessen F, Nikolskaya O, Polyak L, Saarnisto M, Siegert C, Siegert MJ, Spielagen RF, Stein R. 2004. Late Quaternary ice sheet history of northern Eurasia. *Quaternary Science Reviews* 23: 1229–1271.
- Svensson, A., Andersen, K.K., Bigler, M., Clausen, H.B., Dahl-Jensen, D., Davies, S.M., Johnsen, S.J., Muscheler, R., Parrenin, F., Rasmussen, S.O., Röthlisberger, R., Seierstad, I., Steffensen, J.P.,

- Vinther, B.M., 2008. A 60,000 year Greenland stratigraphic ice core chronology. *Climate of the Past* 4: 47-57.
- Svensson, A., Andersen, K.K., Bigler, M., Clausen, H.B., Dahl-Jensen, D., Davies, S.M., Johnsen, S.J., Muscheler, R., Rasmussen, S.O., Röthlisberger, R., Steffensen, J.P., Vinther, B.M., 2006. The Greenland Ice Core Chronology 2006, 15–42 kyr. Part 2: comparison to other records. *Quaternary Science Reviews* 25: 3258–3267.
- Syvitski JPM, Andres JT, Dowdeswell JA. 1996. Sediment deposition in an iceberg-dominated glaciomarine environment, East Greenland: basin fill implications. *Global and Planetary Change* 12: 251-270.
- Syvitski JPM, Burrell DC, Skei JM. 1987. *Fjords: Processes and Products*. Springer, New York.
- Székely N, Bassinot F, Balut Y, Labeyrie L, Pagel M 2004. Oversampling of sedimentary series collected by giant piston corer: Evidence and corrections based on 3.5-kHz chirp profiles. *Paleoceanography* 19: PA1005, doi:10.1029/2002PA000795.
- Tarasov L, Peltier WR. 2006. A calibrated deglacial drainage chronology for the North American continent: evidence of an Arctic trigger for the Younger Dryas. *Quaternary Science Reviews* 25: 659-688.
- Telford RJ, Heegaard E, Birks HJB. 2004a. The intercept is a poor estimate of a calibrated radiocarbon age. *The Holocene* 14: 296-298.
- Telford RJ, Heegaard E, Birks HJB. 2004b. All age-depth models are wrong: but how badly? *Quaternary Science Reviews* 23: 1-5.
- Teller JT. 1990. Volume and routing of Late-Glacial runoff from the southern Laurentide Ice-Sheet. *Quaternary Research* 34: 12–23.
- Teller and Thorleifson 1983. In Teller JT, Clayton L. (Eds). *Glacial Lake Agassiz*. Geological Association of Canada, Newfoundland.
- Teller JT, Boyd M, Yang ZR, Kor PSG, Fard AM. 2005. Alternative routing of Lake Agassiz overflow during the Younger Dryas: new dates, paleotopography, and a re-evaluation. *Quaternary Science Reviews* 24: 1890–1905.
- Teller JT, Leverington DW, Mann JD. 2002. Freshwater outbursts to the oceans from glacial Lake Agassiz and their role in climate change during the last deglaciation. *Quaternary Science Reviews* 21: 879–887.
- Thirlwall MF. 2000. Inter-laboratory and other errors in Pb-isotope analyses investigated using a $^{207}\text{Pb}/^{204}\text{Pb}$ double spike. *Chemical Geology* 163: 299-322.
- Thomas GSP, Chiverrell RC. 2006. A model of subaqueous sedimentation at the retreating margin of the Late Midlandian Irish Ice Sheet, Connemara, Republic of Ireland, and its implications for possible regionally high isostatic sea-levels. *Quaternary Science Reviews* 25: 2868–2893.
- Thomson J, Croudace IW, Rothwell RG. 2006. A geochemical application of the ITRAX core scanner to a sediment core containing eastern Mediterranean sapropel units. In *New Techniques in Sediment Core Analysis*, Rothwell RG (ed.). Special Publication 267. Geological Society: London; 65–77.
- Thompson WG, Goldstein SL. 2006. A radiometric calibration of the SPECMAP timescale. *Quaternary Science Reviews* 25: 3207–3215.
- Thompson WG, Goldstein SL. 2005. Open-system coral ages reveal persistent suborbital sea-level cycles. *Science* 308: 401–404.

- Thornalley DJR, Elderfield H, McCave IN. 2010. Intermediate and deep water paleoceanography of the northern North Atlantic over the past 21,000 years. *Paleoceanography* 25: PA1211.
- Thornalley DJR, McCave IN, Elderfield H. 2010. Freshwater input and abrupt deglacial climate change in the North Atlantic. *Paleoceanography* 25: PA1201, doi: 10.1029/2009PA001772.
- Thornalley DJR, Elderfield H, McCave IN. 2009. Holocene oscillations in temperature and salinity of the surface subpolar North Atlantic. *Nature* 457: 711-714 .
- Tisseraud A, Malaizé B, Jullien E, Zaragosi S, Charlier K, Grousset F. 2009. African monsoon enhancement during the penultimate glacial period (MIS 6.5 – 170 ka) and its atmospheric impact. *Paleoceanography* 24: PA2202. doi: 10.1029/2008PA001630.
- Törnqvist TE, Wallinga J, Murray AS, de Wolf H, Cleveringa P, de Gans W. 2000. Response of the Rhine-Meuse system (west-central Netherlands) to the last Quaternary glacio-eustatic cycles: a first assessment. *Global and Planetary Change* 27: 89-111.
- Toucanne S, Zaragosi S, Bourillet JF, Cremer M, Eynaud F, van VlietLanoë B, Penaud A, Fontanier C, Turon JL, Cortijo E, Gibbard PL. 2009. Timing of massive “Fleuve Manche” discharges over the last 350 kyr: insights into the European drainage network from MIS 10 to 2. *Quaternary Science Reviews* 28: 1238–1256.
- Troggweiler JR, Lee DW. 2010. Temperature differences between the hemisphere and ice age variability. *Paleoceanography* 25: PA2212, doi: 10.1029/2009PA001758.
- Turney CSM, Lowe JJ, Davies SW, Hall V, Lowe DJ, Wastegård S, Hoek WZ, Alloway B, SCOTAV and INTIMATE members. 2004. Tephrochronology of the Last Termination Sequences in Europe: a protocol for improved analytical precision and robust correlation procedures (a joint SCOTAV and INTIMATE proposal). *Journal of Quaternary Science* 19: 111-120.
- Tzedakis PC. 2003. Timing and duration of Last Interglacial conditions in Europe: a chronicle of a changing chronology. *Quaternary Science Reviews* 22: 763–768.
- Ukkonen P, Lunkka JP, Jungner H, Donner J. 1999. New radiocarbon dates from mammoths indicating large ice free areas in Fennoscandia during the Middle Weichselian. *Journal of Quaternary Science* 14: 711-714.
- van Aken HM. 2000. The hydrography of the mid-latitude northeast Atlantic Ocean. I: The deep water masses. *Deep Sea Research* 47: 757–788.
- van den Berg J, van de Wal R, Oerlemans H. 2007. A mass balance model for the Eurasian Ice Sheet for the last 120,000 years. *Global and Planetary Change* 61: 194–208.
- van der Veen CJ. 2002. Calving glaciers. *Progress in Physical Geography* 26: 96-122.
- van Kreveld S, Sarnthein M, Erlenkeuser H, Grootes P, Jung S, Nadeau MJ, Pflaumann U, Voelker A. 2000. Potential links between surging ice sheets, circulation changes, and the Dansgaard–Oeschger cycles in the Irminger Sea, 60-18kyr. *Paleoceanography* 15: 425–442.
- van Nieuwenhove N, Bauch HA, Matthiessen J. 2008. Last interglacial surface water conditions in the eastern Nordic Seas inferred from dinocyst and foraminiferal assemblages. *Marine Micropaleontology* 66: 247–263. doi:10.1016/j.marmicro.2007.10.004.
- van Rooij D, Blamart D, Richter T, Wheeler A, Kozachenko M, Henriët JP. 2007. Quaternary sediment dynamics in the Belgica mound province, Porcupine Seabight: ice-rafting events and contour current processes. *International Journal of Earth Sciences* 96: 121–140.
- Venz KA, Hodell DA, Stanton C, Warnke DA. 1999. A 1.0 Myr record of Glacial North Atlantic Intermediate Water variability from ODP site 982 in the northeast Atlantic. *Paleoceanography* 14: 42-52.

- Vettoretti G, Peltier WR. 2003. Post-Eemian glacial inception. Part I: The impact of summer seasonal temperature bias. *Journal of Climate* 16: 889–911.
- Vidal L, Labeyrie L, van Weering TCE. 1998. Benthic $\delta^{18}\text{O}$ records in the North Atlantic over the last glacial period (60-10 kyr): Evidence for brine formation. *Paleoceanography* 13: 245-251.
- Vinther BM, Clausen HB, Johnsen SJ, Rasmussen SO, Andersen KK, Buchardt SL, Dahl-Jensen D, Seierstad IK, Siggaard-Andersen ML, Steffensen JP, Svensson A, Olsen J, Heinemeier J. 2006. A synchronized dating of three Greenland ice cores throughout the Holocene. *Journal of Geophysical Research – Atmospheres* 111: D13102.
- Voelker AHL. 2002. Global distribution of centennial-scale records for marine isotope stage (MIS) 3: a database. *Quaternary Science Reviews* 21: 1185–1214.
- Volker AHL, Grootes PM, Nadeau MJ, Sarnthein M. 2000. Radiocarbon levels in the Iceland Sea from 23-53 kyr and their link to the Earth's magnetic field intensity. *Radiocarbon* 42: 437-452.
- Voelker AHL, Sarnthein M, Grootes PM, Erlenkeuser H, Jaj C, Mazaud A, Nadeau M-J, Schleicher M. 1998. Correlation of marine ^{14}C ages from the Nordic Seas with the GISP2 Isotope record: Implications for ^{14}C calibration beyond 25 ka BP. *Radiocarbon* 40: 517-534.
- Vogel JS, Nelson DE, Southon JR. 1987. ^{14}C Background levels in and accelerator mass spectrometry system *Radiocarbon* 29(3): 323-329 In Schleicher M, Grootes PM, Nadeau MJ and Schoon A 1998 The Carbonate ^{14}C background and its components at the Leibniz AMS Facility *Radiocarbon* 40(1): 85-93.
- Vogel JS, Nelson DE and Southon JR 1987 ^{14}C Background levels in and accelerator mass spectrometry system *Radiocarbon* 29(3): 323-329 In Schleicher M, Grootes PM, Nadeau MJ and Schoon A 1998 The Carbonate ^{14}C background and its components at the Leibniz AMS Facility *Radiocarbon* 40(1): 85-93
- von Weyman J, Edwards KJ. 1973. Interstadial site on the island of Lewis, Scotland. *Nature* 246: 473–474.
- Waelbroeck C, Frank N, Jouzel J, Parrenin F, Masson-Delmotte V, Genty D. 2008. Transferring radiometric dating of the last interglacial sea level high stand to marine and ice core records. *Earth and Planetary Science Letters* 265: 183-194.
- Waelbroeck C, Levi C, Duplessy JC, Labeyrie L, Michel E, Cortijo E, Bassinot F, Guichard F. 2006. Distant origin of circulation changes in the Indian Ocean during the last deglaciation. *Earth and Planetary Science Letters* 243: 244-251.
- Waelbroeck C, Labeyrie L, Michel E, Duplessy JC, McManus JF, Lambeck K, Balbon E, Labracherie M. 2002. Sea level and deep water temperature changes derived from benthic foraminifera isotopic records. *Quaternary Science Reviews* 21: 295-305.
- Waelbroeck C, Duplessy JC, Michel L, Labyrinth L, Paillard D, Duprat J. 2001. The timing of the last deglaciation in North Atlantic climate records. *Nature* 412: 724–727.
- Walden J, Wadsworth ER, Austin WEN, Peters C, Scourse JD, Hall IR. 2007. Compositional variability of ice-rafted debris in Heinrich layers 1 and 2 on the northwest European continental slope identified by environmental magnetic analyses. *Journal of Quaternary Science* 22: 163-172, doi:10.1002/jqs.1020.
- Walker MJC, Björck S, Lowe JJ, Cwynar LC, Johnsen S, Knudsen KL, Wolfforth B, INTIMATE members. 1999. Isotopic 'events' in the GRIP ice core: a stereotype for the Late Pleistocene. *Quaternary Science Reviews* 18: 1143-1150.
- Walter RC, et al. 2000. Early human occupation of the Red Sea coast of Eritrea during the last interglacial. *Nature* 405: 65-69.

- Wang YJ, Cheng H, Edwards RL, An ZS, Wu JY, Sheen CC, Doral JA. 2001. A high-resolution absolute-dated late Pleistocene monsoon record from Hulu Cave, China. *Science* 294: 2345–2348.
- Wang X, Aulter AS, Edwards RL, Cheng H, Ito E, Solheid M. 2006. Interhemispheric anti-phasing of rainfall during the last glacial period. *Quaternary Science Reviews* 25: 3391-3403.
- Warren WP. 1991. Fenitian (Midlandian) glacial deposits and glaciation in Ireland and the adjacent offshore regions. In Ehlers J, Gibbard PL, Rose J (Eds). *Glacial Deposits of Great Britain and Ireland*. Balkema: Rotterdam pp 79–88.
- Wastegård S, Rasmussen TL, Kuijpers A, Nielsen T, van Weering TCE. 2006. Composition and origin of ash zones from Marine Isotope Stages 3 and 2 in the North Atlantic. *Quaternary Science Reviews* 25: 2409-2419.
- Watson JE, Brooks SJ, Whitehouse NJ, Reimer PJ, Birks HJB, Turney C. 2010. Chironomid-inferred late-glacial summer air temperatures from Lough Nadourcan, Co. Donegal, Ireland. *Journal of Quaternary Science*: doi: 10.1002/jqs.1399.
- Weaver AJJ, Marotzke J, Cummins PF, Sarachik ES 1993. Stability and variability of the thermohaline circulation. *Journal of Physical Oceanography* 23: 39-60.
- Weinelt, M., E. Vogelsang, M. Kucera, U. Pflaumann, M. Sarnthein, A. Voelker, H. Erlenkeuser, and B. A. Malmgren (2003), Variability of North Atlantic heat transfer during MIS 2. *Paleoceanography* 18: 1071, doi:10.1029/2002PA000772.
- Weiss RF, Ostlund HG, Craig H. 1979. Geochemical Studies of the Weddell Sea *Deep Sea Research* 26A: 1093-1120.
- White M, Scott B, Ashton N. 2006. The Early Middle Palaeolithic in Britain: archaeology, settlement history and human behaviour. *Journal of Quaternary Science* 21: 525-541.
- Whittington G, Hall AM. 2002. The Tolsta Interstadial, Scotland: correlation to D-O cycles GI-8 to GI-5. *Quaternary Science Reviews* 21: 901–915.
- Wilson LJ, Austin WEN. 2002. Millennial and sub-millennial-scale variability in sediment colour from the Barra Fan, NW Scotland: implications for British ice sheet dynamics. *Journal of the Geological Society of London* 203: 349–366.
- Wilson LJ, Austin WEN, Jansen E. 2002. The last British Ice Sheet: growth, maximum extent and deglaciation. *Polar Research* 21: 243– 250.
- Winograd IJ, Coplen TB, Landwehr JM, Riggs AC. 1992. Continuous 500,000-year climate record from vein calcite in Devils Hole, Nevada. *Science* 5080: 255–260.
- Winton M. 1997. The effect of cold climate upon North Atlantic Deep Water formation in a simple ocean-atmosphere model. *Journal of Climatology* 39: 37-51.
- Witak M, Kuijpers A. 2001. Diatom records of Northeast Atlantic circulation changes in Marine Isotope Stages 1 and 5. *Oceanological Studies* 30: 21-38.
- Wohlfarth B, Veres D, Ampel L, Lacourse T, Blaauw M, Preusser F, Andrieu-Ponel V, Ke´ravis D, Lallier-Vergès E, Björck S, Davies SM, de Beaulieu J-L, Risberg J, Hormes A, Kasper HU, Possnert G, Reille M, Thouveny N, Zander A. 2008. Rapid ecosystem response to abrupt climate changes during the last glacial period in western Europe, 40–16 ka. *Geology* 36: 407–410.
- Wohlfarth B, Björck S, Possnert E, Lemdahl G, Brunnberg L, Ising J, Olsson S, Svensson NO. 1993. AMS dating Swedish varved clays of the last glacial/interglacial transition and the potential/difficulties of calibrating Late Weichselian absolute chronologies. *Boreas* 22: 113-128.

- Woillard GM. 1978. Grande Pile peat bog: A continuous pollen record for the last 140,000 years. *Quaternary Research* 9: 1–21.
- Wolff EW, Chappellaz J, Blunier T, Rasmussen SO, Svennson A. 2009. Millennial-scale variability during the last glacial: The ice core record. *Quaternary Science Reviews*: (in press- online) doi:10.1016/j.quatscirev.2009.10.013.
- Wright LD, Wisema WJ, Bornhold BD, Prior DB, Suhayda JN, Keller GH, Yang ZS, Fan YB. 1998. Marine dispersal and deposition of Yellow River silts by gravity driven underflows. *Nature* 332: 629-632.
- Wright WB. 1937. *The Quaternary Ice Age*. Macmillan: London.
- Wright WB. 1914. *The Quaternary Ice Age*. 1st edition. Macmillan. London.
- Wunsch, C., 2006. Abrupt climate change: an alternative view. *Quaternary Research* 65: 191–203.
- Wunsch C, Heimbach P. 2008. How long to oceanic tracer and proxy equilibrium? *Quaternary Science Reviews* 27: 637-651.
- Yokoyama Y, Lambeck K de Decker PPJ, Fitfield LK. 2000. Timing of the last glacial maximum from observed sea level minima. *Nature* 406: 713-716.
- Yu J, Elderfield H, Piotrowski AM. 2008. Seawater carbonate ion- $\delta^{13}\text{C}$ systematics and application to glacial-interglacial North Atlantic circulation. *Earth and Planetary Science Letters* 271: 209-220.
- Zahn R, Mix AC. 1991. Benthic foraminiferal $\delta^{18}\text{O}$ in the ocean's temperature-salinity-density field: Constraints on ice age thermohaline circulation. *Paleoceanography* 6: 1-20.
- Zahn R, Sarnthein M, Erlenkeuser H. 1987. Benthic isotope evidence for changes of the Mediterranean outflow during the late Quaternary. *Paleoceanography* 2: 543–559.
- Zielinski GA, Mayewski PA, Meeker LD, Grönvold K, Germani MS, Whitlow S, Twickler MS, Taylor K. 1997. Volcanic aerosol records and tephrochronology of the Summit, Greenland ice cores. *Journal of Geophysical Research* 102: 26625–2664.